ARISTOTLE UNIVERSITY OF THESSALONIKI
FACULTY OF SCIENCES
SCHOOL OF GEOLOGY

PAVLOS I. PISKOULIS
MSc Geologist

QUATERNARY CHIROPTERA (MAMMALIA) FROM LOUTRA ALMOPIAS CAVE A (PELLA, MACEDONIA, GREECE) – SYSTEMATICS, PHYLOGENETIC RELATIONSHIPS, BIOGEOGRAPHY, PALAEOENVIRONMENT

DISSERTATION THESIS

This research is co-financed by Greece and the European Union (European Social Fund-ESF) through the Operational Programme «Human Resources Development, Education and Lifelong Learning» in the context of the project "Strengthening Human Resources Research Potential via Doctorate Research" (MIS-5000432), implemented by the State Scholarships Foundation (IKY)

Ευρωπαϊκή Ένωση
European Social Fund

Operational Programme
Human Resources Development,
Education and Lifelong Learning
Co-financed by Greece and the European Union

ΕΣΠΑ
2014-2020
ανάπτυξη - εργασία - αλληλεγγύη

THESSALONIKI
2021

ΑΡΙΣΤΟΤΕΛΕΙΟ ΠΑΝΕΠΙΣΤΗΜΙΟ ΘΕΣΣΑΛΟΝΙΚΗΣ
ΣΧΟΛΗ ΘΕΤΙΚΩΝ ΕΠΙΣΤΗΜΩΝ
ΤΜΗΜΑ ΓΕΩΛΟΓΙΑΣ

ΠΑΥΛΟΣ Η. ΠΙΣΚΟΥΛΗΣ
MSc Γεωλόγος

ΤΑ ΤΕΤΑΡΤΟΓΕΝΗ ΧΕΙΡΟΠΤΕΡΑ (ΘΗΛΑΣΤΙΚΑ) ΤΟΥ ΣΠΗΛΑΙΟΥ Α ΤΩΝ ΛΟΥΤΡΩΝ ΑΛΜΩΠΙΑΣ (ΠΕΛΛΑ, ΜΑΚΕΔΟΝΙΑ, ΕΛΛΑΔΑ) – ΣΥΣΤΗΜΑΤΙΚΗ, ΦΥΛΟΓΕΝΕΤΙΚΕΣ ΣΧΕΣΕΙΣ, ΒΙΟΓΕΩΓΡΑΦΙΑ, ΠΑΛΑΙΟΠΕΡΙΒΑΛΛΟΝ

ΔΙΔΑΚΤΟΡΙΚΗ ΔΙΑΤΡΙΒΗ

Το έργο συγχρηματοδοτείται από την Ελλάδα και την Ευρωπαϊκή Ένωση (Ευρωπαϊκό Κοινωνικό Ταμείο) μέσω του Επιχειρησιακού Προγράμματος «Ανάπτυξη Ανθρώπινου Δυναμικού, Εκπαίδευση και Διά Βίου Μάθηση», στο πλαίσιο της Πράξης «Ενίσχυση του ανθρώπινου ερευνητικού δυναμικού μέσω της υλοποίησης διδακτορικής έρευνας» (MIS-5000432), που υλοποιεί το Ίδρυμα Κρατικών Υποτροφιών (ΙΚΥ)

Ευρωπαϊκή Ένωση
Ευρωπαϊκό Κοινωνικό Ταμείο

Επιχειρησιακό Πρόγραμμα
Ανάπτυξη Ανθρώπινου Δυναμικού,
Εκπαίδευση και Διά Βίου Μάθηση
Με τη συγχρηματοδότηση της Ελλάδας και της Ευρωπαϊκής Ένωσης

ΕΣΠΑ 2014-2020
ανάπτυξη - εργασία - αλληλεγγύη

ΘΕΣΣΑΛΟΝΙΚΗ
2021

PAVLOS I. PISKOULIS
MSc Geologist

QUATERNARY CHIROPTERA (MAMMALIA) FROM LOUTRA ALMOPIAS CAVE A (PELLA, MACEDONIA, GREECE) – SYSTEMATICS, PHYLOGENETIC RELATIONSHIPS, BIOGEOGRAPHY, PALAEOENVIRONMENT

Prepared at the Department of Geology of the School of Geology of A.U.Th.
Submitted at the School of Geology of A.U.Th. on June 2021

Date of Oral Examination: 28/05/2021

Annex Number of the Scientific Annals of the School of Geology A.U.Th. N°: 217

Three-member Advisory Committee

Professor Evangelia Tsoukala, Supervisor
Professor Dimitrios Kostopoulos, Member of the Three-member Advisory Committee
Professor Paloma Sevilla, Member of the Three-member Advisory Committee

Examination Committee

Professor Evangelia Tsoukala
Professor Dimitrios S. Kostopoulos
Associate Professor María Paloma Sevilla García
Professor Dionisios Youlatos
Associate Professor George Iliopoulos
Professor Emeritus Jelle W. F. Reumer
Assistant Professor Wilma Wessels

QUATERNARY CHIROPTERA (MAMMALIA) FROM LOUTRA ALMOPIAS CAVE A (PELLA, MACEDONIA, GREECE) – SYSTEMATICS, PHYLOGENETIC RELATIONSHIPS, BIOGEOGRAPHY, PALAEOENVIRONMENT. – *Ph.D. Thesis*

ΤΑ ΤΕΤΑΡΤΟΓΕΝΗ ΧΕΙΡΟΠΤΕΡΑ (ΘΗΛΑΣΤΙΚΑ) ΤΟΥ ΣΠΗΛΑΙΟΥ Α ΤΩΝ ΛΟΥΤΡΩΝ ΑΛΜΩΠΙΑΣ (ΠΕΛΛΑ, ΜΑΚΕΔΟΝΙΑ, ΕΛΛΑΔΑ) – ΣΥΣΤΗΜΑΤΙΚΗ, ΦΥΛΟΓΕΝΕΤΙΚΕΣ ΣΧΕΣΕΙΣ, ΒΙΟΓΕΩΓΡΑΦΙΑ, ΠΑΛΑΙΟΠΕΡΙΒΑΛΛΟΝ. – *Διδακτορική Διατριβή*

Citation:
Piskoulis P. I., 2021. – Quaternary Chiroptera (Mammalia) from Loutra Almopias Cave A (Pella, Macedonia, Greece) – Systematics, phylogenetic relationships, biogeography, palaeoenvironment. Ph.D. Thesis, School of Geology, Aristotle University of Thessaloniki, Annex Number of Scientific Annals of the School of Geology No 217, 300 pp.
Πισκούλης Π. Η., 2021. – Τα Τεταρτογενή Χειρόπτερα (Θηλαστικά) του Σπηλαίου Α των Λουτρών Αλμωπίας (Πέλλα, Μακεδονία, Ελλάδα) – Συστηματική, φυλογενετικές σχέσεις, βιογεωγραφία, παλαιοπεριβάλλον. Διδακτορική Διατριβή, Τμήμα Γεωλογίας Α.Π.Θ., Αριθμός Παραρτήματος Επιστημονικής Επετηρίδας Τμ. Γεωλογίας Νο 217, 300 σελ.

Cover Image:

PREFACE

The aim of the present PhD Thesis is the thorough examination of the rich chiropteran collection from Loutra Almopias Cave A, which will contribute to the knowledge of the Quaternary bats of the Greek region and the Balkan Peninsula.

This was achieved by a comprehensive systematic taxonomy (descriptions, measurements and illustrations) and phenetic analysis of a fossil chiropteran fauna, the correlation of the studied specimens with the two chronologically different faunal assemblages of the cave site and other modern and fossil faunal assemblages from the Greek region and the broader region of the Balkan Peninsula (biogeography) and with a palaeoclimatological/palaeoecological approach, based on the bats' biocoenosis. All these are expected to inaugurate more scientists to further investigate this relatively unexplored topic aiming to better understand the evolutionary trends of Quaternary Chiroptera and the mechanisms that led to their dispersal in the Greek region.

ACKNOWLEDGEMENTS

First of all, I would like to express my gratitude to Prof. E. Tsoukala, who not only gave me the opportunity to work on the material from Loutra Almopias Cave A, one of the most important localities in Greece, but also supervised me at her best on many levels. Her advisory was always to the point and she gave me the support needed to grow my knowledge and skills in palaeontology.

I would also like to thank Prof. D. S. Kostopoulos, member of my three-member committee, for his continuous support during my PhD years and for his invaluable comments on my PhD Thesis.

I would also like to thank Assoc. Prof. P. Sevilla, also member of my three-member committee, who generously offered her expertise whenever I asked, for her invaluable comments on my PhD Thesis and her hospitality during my stay at Madrid.

Moreover, I am greatly indebted to Prof. D. Youlatos, Assoc. Prof. G. Iliopoulos, Prof. Emer. J.W.F. Reumer and Asst. Prof. W. Wessels, whose comments helped me to improve the manuscript of my PhD Thesis.

I would also like to thank Dr. Panagiotis Georgiakakis from the Natural History Museum of Crete for hosting me and giving me access to comparative material from the collections of the institution. Additionally, I would like to thank Prof. P. Stoev, Prof.

N. Spassov and MSc zoologist V. Zhelyazkova from Sofia's National Museum of Natural History for hosting me and giving me access to comparative material from the collections of the institution.

I would also like to thank Dr. Katerina Chatzopoulou (co-author) and Dr. Evangelos Vlachos (editor) for their collaboration that resulted in the publication of a chapter in a massive work accomplished by numerous Greek palaeontologists.

Thanks also due to Mr. P. Theodoroudis for his help with all the necessary documents regarding the dating of material, as well as Prof. C. Papazachos, Prof. K. Voudouris and Ass. Prof. N. Kantiranis.

Moreover, I would like to thank Nancy, Panagiotis and Raul for their hospitality during my stay at Heraklion, Milena and John for their hospitality during my stay at Madrid and Dimitar, Stojan and Vladislav for their hospitality during my stay at Sofia.

I would also like to dedicate this work to the late palaeontologist K. Vasileiadou, an inspirational and committed scientist, passionate for palaeontology and eager to pass her knowledge.

Furthermore, I would like to thank my parents, Anastasia and Ilias, who have supported me over the years in many levels and my family and friends for their compassion. Last but not least, I would like to express my gratitude to my partner in life, MSc Rural and Surveying Engineer C. Dadala, for her continuous support and inspiration throughout all these years.

Table of Contents

CHAPTER 1. INTRODUCTION

1.1 CHIROPTERA

The mammalian order Chiroptera (Bats) is the most diverse group after rodents, as with more than 1100 extant species they currently comprise approximately 20% of the world's mammal species and their distribution is almost global, with bats occupying every corner of the Earth apart from the poles and some isolated islands (Simmons 2005a, 2005b). Bats are unique because of their ability to echolocate and to perform self-powered flight. More specifically, "laryngeal echolocation" is the bats' ability to perceive their surroundings with a mechanism that has been developed after several auditory adaptations and thus navigate in their environment without the need of visual perception (Simmons 2005a, 2005b, Gunnel and Simmons 2005, Dietz et al. 2009, etc.). Furthermore, bats achieved self-powered flight due to adaptations of their forelimbs and other structural elements (e.g. axial skeleton, hind limbs, etc.) (Gunnel and Simmons 2005 and references therein).

Bats' appearance in the fossil record is global and it seems to be an isochronous event (Smith et al. 2007), with the earliest fossils coming from the Early Eocene of all continents, apart from Antarctica (Tabuce et al. 2009, Simmons et al. 2008, Tejedor et al. 2005, Ravel et al. 2011, Hand et al. 1994, Smith et al. 2007). The earliest occurrence of chiropteran fossils in:

- Europe, – and the world's earliest chiropteran fossil (Palaeocene/Eocene boundary) – is *Archaeonycteris*? *praecursor* from Silveirinha, Coimbra District, Portugal (Tabuce et al. 2009);
- North America, is *Onychonycteris finneyi* from Green River Formation, Wyoming, U.S.A. (Simmons et al. 2008);

- South America, is an indeterminate taxon from Laguna Fría, Chubut, Argentina (Tejedor et al. 2005);
- Africa, is an indeterminate taxon from the suborder of Eochiroptera from El Kohol, Algeria (Ravel et al. 2011);
- Oceania, is *Australonycteris clarkae* from Murgon, Queensland, Australia (Hand et al. 1994);
- Asia, is the bat fauna from Vastan Mine, Gujarat, India, which includes seven species (*Icaronycteris sigei*, *Protonycteris gunnelli*, *Archaeonycteris*? *storchi*, *Hassianycteris kumari*, *Cambaya complexus*, *Microchiropteryx folieae*, *Jaegeria cambayensis*) (Smith et al. 2007).

Hence, it is believed that the origin of bats should have occurred at about 64.00 Ma (at the Cretaceous-Tertiary boundary) and onwards, when crown bats shared their last common ancestor (Teeling et al. 2005).

In Greece, recent zoological studies recorded 36[1] extant chiropteran species: *Rhinolophus ferrumequinum*, *Rhinolophus mehelyi*, *Rhinolophus blasii*, *Rhinolophus euryale, Rhinolophus hipposideros, Myotis myotis*, *Myotis blythii*, *Myotis bechsteinii*, *Myotis emarginatus*, *Myotis capaccinii*, *Myotis nattereri*, *Myotis aurascens, Myotis alcathoe*, *Myotis brandtii*, *Myotis daubentonii*, *Myotis mystacinus*, *Nyctalus lasiopterus*, *Nyctalus noctula*, *Nyctalus leisleri*, *Pipistrellus pipistrellus*, *Pipistrellus pygmaeus*, *Pipistrellus kuhlii*, *Pipistrellus nathusii*, *Pipistrellus hanaki*, *Hypsugo savii*, *Vespertilio murinus*, *Eptesicus serotinus*, *Eptesicus bottae*, *Plecotus auritus*, *Plecotus austriacus*, *Plecotus kolombatovici*, *Plecotus macrobullaris*, *Barbastella barbastellus*, *Miniopterus schreibersii*, *Tadarida teniotis* and *Rousettus aegyptiacus* (Hanák et al. 2001, Simmons 2005a, Sfougaris 2009, Strachinis et al. 2018).

In respect of the chiropteran fossil record from Greece, even though it is sparse, there are 23 localities were Chiroptera have been documented and span from Early Miocene to Early/Middle Holocene (Piskoulis and Chatzopoulou in press). Those localities (Figure 1.1) and their respective chiropteran fauna are summarised in Table 1.1.

[1] The Egyptian Fruit Bat, *Rousettus aegyptiacus*, has been recorded only on the island of Kastellorizo and it is still not known whether it roosts on the island or it travels from the Turkish mainland – given the short distance – to forage (Strachinis et al. 2018).

Figure 1.1 Map with the Greek localities where Chiroptera have been recorded. **1.** Lapsarna, Lesvos, **2.** Antonios, Chalkidiki, **3.** Elaiochoria 2, Chalkidiki, **4.** Mytilinii, Samos, **5.** Nea Silata, Chalkidiki, **6.** Maramena, Serres, **7.** Tourkobounia 1, Attiki, **8.** Tourkobounia 2, 3, 5, Attiki, **9.** Vathy, Kalymnos, **10.** Latomi 1, Chios, **11.** Petralona Cave, Chalkidiki, **12.** Varkiza 1, 2, Attiki, **13.** Kalamakia Cave, Lakonia, **14.** Loutra Almopias Cave, Pella, **15.** Naxos, Cyclades, **16.** Kharoumes 5, Lasithi, **17.** Liko, Chania, **18.** Bate Cave, Rethymno, **19.** Franchthi Cave, Argolis, **20.** Anonymous Cave of Schisto at Keratsini, Piraeus, **21.** Charkadio Cave, Tilos, **22.** Vraona Cave, Attiki, **23.** Sarakenos Cave, Boeotia. Modified after Piskoulis and Chatzopoulou (in press).

Most research on fossil Chiroptera from Greece was focused on basic systematic palaeontology, with a few exceptions (i.e. Petralona Cave, Charkadio Cave, Sarakenos Cave, etc.). Nevertheless, albeit the Greek chiropteran fossil record is not quite rich, it is quite informative. It is worth mentioning the occurrence of Megadermatidae (cf. Megadermatidae gen. and sp. indet.) in the Early/Middle Miocene locality of Antonios, Chalkidiki (Vasileiadou and Koufos 2005), the occurrence of Rhinopomatidae

(*Rhinopoma* aff. *hardwickii*) in the Late Miocene locality of Elaiochoria 2, Chalkidiki, which is unique at a European scale (Horáček 1991, Hulva et al. 2007, Sigé et al. 2014), the occurrence of the monotypic taxon *Samonycteris majori* from the Late Miocene locality of Mytilinii, Samos (Revilliod 1922) and the richest – prior to this research – bat fauna in Greece from the Middle Pleistocene locality of Petralona Cave, Chalkidiki, with the presence of 19 taxa (Sickenberg 1964, 1971, Kretzoi 1977, Kretzoi and Poulianos 1981, Horacek and Poulianos 1988, Tsoukala 1989).

Table 1.1 List of fossiliferous localities with Chiroptera in Greece.

Locality	**Age**	**Taxa**
Lapsarna, Lesvos[1]	Early Miocene (MN4)	Chiroptera indet.
Antonios, Chalkidiki[2]	Early/Middle Miocene (MN4/5)	cf. Megadermatidae gen. and sp. indet.
Elaiochoria 2, Chalkidiki[3]	Late Miocene (MN10/11)	*Rhinolophus* gr. *delphinensis* *Rhinopoma* aff. *Hardwickii* cf. *Myotis* (small-sized)
Mytilinii, Samos[4]	Late Miocene (MN12)	*Samonycteris majori*
Nea Silata, Chalkidiki[5]	Miocene/Pliocene (MN13/14)	Vespertilionidae sp.1 Vespertilionidae sp.2
Maramena, Serres[6]	Miocene/Pliocene (MN13/14)	Chiroptera indet.
Tourkobounia 1, Attiki[7]	Late Pliocene (MN16)	Chiroptera indet.
Tourkobounia 2, 3, 5, Attiki[8]	Early Pleistocene (MNQ19)	Chiroptera indet.
Vathy, Kalymnos[9]	Early Pleistocene	*Miniopterus schreibersii* Chiroptera indet.
Latomi 1, Chios[10]	Middle Pleistocene	Chiroptera indet.
Petralona Cave, Chalkidiki[11]	Middle Pleistocene	*Rhinolophus ferrumequinum topali* *Rhinolophus* cf. *hipposideros* *Rhinolophus* cf. *mehelyi* *Rhinolophus* sp. I (euryale group) *Rhinolophus* sp. II *Rhinolophus* sp. III *Myotis myotis* *Myotis blythii* *Myotis blythii oxygnathus* *Myotis emarginatus* *Myotis* cf. *daubentonii* *Myotis* sp. I *Myotis* sp. II *Nyctalus* cf. *noctula* *Pipistrellus*? sp. *Hypsugo savii* *Vespertilio murinus* *Eptesicus* sp. *Miniopterus schreibersii*

Varkiza 1, 2, Attiki[12]	Late/Middle Pleistocene	Chiroptera indet.
Kalamakia Cave, Lakonia[13]	Late Pleistocene	*Myotis* cf. *blythii* *Pipistrellus* sp. *Rhinolophus* sp.
Loutra Almopias Cave A, Pella[14, *]	Late Pleistocene (MNQ26)	*Rhinolophus* sp. *Myotis* sp. *Miniopterus* sp.
Naxos, Cyclades[15]	Late Pleistocene	Chiroptera indet.
Kharoumes 5, Lasithi[16]	Late Pleistocene	Chiroptera indet.
Liko, Chania[17]	Late Pleistocene	Chiroptera indet.
Bate Cave, Rethymno[18]	Late Pleistocene	Chiroptera indet.
Franchthi Cave, Argolis[19]	Late Pleistocene/Early Holocene	Chiroptera indet.
Anonymous Cave of Schisto at Keratsini, Piraeus[20]	Late Pleistocene/Early Holocene	Chiroptera indet.
Charkadio Cave, Tilos[21]	Holocene	*Rhinolophus hipposideros* *Rhinolophus blasii* *Myotis blythii* *Myotis* sp. *Plecotus austriacus*
Vraona Cave, Attiki[22]	Holocene	*Myotis* sp.
Sarakenos Cave, Boeotia[23]	Early/Middle Holocene	*Rhinolophus ferrumequinum* *Rhinolophus hipposideros* *Myotis blythii* *Myotis myotis*/*blythii* *Nyctalus noctula* *Eptesicus serotinus*

[1]Vasileiadou and Zouros 2012, Vasileiadou et al. 2017, [2]Vasileiadou and Koufos 2005, [3]Horáček 1991, Hulva et al. 2007, Sigé et al. 2014, [4]Revilliod 1922, [5]Vasileiadou et al. 2003, [6]Schmidt-Kittler et al. 1995, [7]Reumer and Doukas 1985, [8]Reumer and Doukas 1985, [9]Kuss 1973, Kotsakis et al. 1979, [10]Storch 1975, Kotsakis et al. 1979, [11]Sickenberg 1964, 1971, Kretzoi 1977, Kretzoi and Poulianos 1981, Horacek and Poulianos 1988, Tsoukala 1989, [12]van de Weerd 1973, [13]Harvati et al. 2013, Darlas and Psathi 2016, Kolendrianou et al. 2020, [14]Chatzopoulou et al. 2001, Chatzopoulou 2003, 2005b, Tsoukala et al. 2006, [15]van der Geer et al. 2014, [16]Kuss 1970, Dermitzakis 1977, Mayhew 1977, Doukas and Papayianni 2016, [17]Dermitzakis 1977, Mayhew 1977, Doukas and Papayianni 2016, [18]Kotsakis et al. 1976, [19]Stiner and Munro 2011, [20]Mavridis et al. 2013, [21]Symeonidis et al. 1973, Kotsakis et al. 1979, [22]Symeonidis et al. 1980, [23]Pereswiet-Soltan 2016. [*]Loutra Almopias Cave A bat fauna prior to this research and its respective outcomes (viz. Piskoulis 2018, 2019, 2020, Piskoulis and Chatzopoulou in press).

1.2 PHYLOGENETIC INFORMATION

Bats have evolved several anatomical characteristics in their axial skeleton and pectoral girdle – which allow them to perform self-powered flight – and hind limbs – which allow them to rest in an upside-down position (Gunnell and Simmons 2005, Simmons 2005b, Teeling et al. 2005). Moreover, Chiroptera (all chiropteran families apart from Old World fruit bats, Pteropodidae) has also evolved “laryngeal echolocation" – a biosonar-like feature – due to several adaptations in their middle and inner ear, which allows them to perceive their surroundings and navigate in their environment without the need of visual perception (Simmons 2005a, 2005b, Gunnel and Simmons 2005, Dietz et al. 2009, etc.). All these features unambiguously distinguish Chiroptera from other mammalian taxonomic groups (Gunnell and Simmons 2005, Simmons 2005b, Teeling et al. 2005).

With Chiroptera being the only known mammalian taxonomic group with these characteristics, until the late 1980s it was assumed that it is a monophyletic group with a common (flying) ancestor for all the taxa included (Gunnell and Simmons 2005, Teeling et al. 2005). More specifically, Chiroptera was traditionally divided into the sub-orders of Megachiroptera, which includes the non-echolocating family of Pteropodidae and Microchiroptera, which includes the rest of the 19 extant families of echolocating bats[2] (Table 1.2) (Gunnell and Simmons 2005, Simmons 2005b). However, several workers on the specific topic suggested that Chiroptera is diphyletic (Gunnell and Simmons 2005 and references therein), which led to an intensification of research related to this topic and, consequently, the acquirement of plethora of data (morphological, DNA hybridization and nucleotide sequence data) that further supports the initial hypothesis that Chiroptera is a monophyletic group (Simmons 1994, Murphy et al. 2001, Gunnell and Simmons 2005, Teeling et al. 2005).

Table 1.2 All chiropteran families, extinct and extant. As classification above the family level is still a matter of dispute, only the most widely accepted distinct families are presented (modified after Gunnell and Simmons 2005, Simmons et al. 2008). The chiropteran families present in the fossil record of Greece are underlined. * Here are followed the suggestions by Miller-Butterworth et al. (2007) and Lack et al. (2010) that Miniopteridae and Cistugidae are distinct families.

Extinct Families	**Extant Families**		
Icaronycteridae	Pteropodidae	Emballonuridae	Furipteridae
Archaeonycteridae	<u>Rhinolophidae</u>	Myzopodidae	Natalidae
Palaeochiropterygidae	Hipposideridae	Mystacinidae	Molossidae
Hassianycteridae	<u>Megadermatidae</u>	Phyllostomidae	<u>Vespertilionidae</u>
Tanzanycteridae	<u>Rhinopomatidae</u>	Mormoopidae	<u>Miniopteridae</u>*
Philisidae	Craseonycteridae	Noctilionidae	Cistugidae*
Onychonycteridae	Nycteridae	Thyropteridae	

[2] Here are followed the suggestions by Miller-Butterworth et al. (2007) and Lack et al. (2010) that Miniopteridae and Cistugidae are distinct families.

Nevertheless, the disputed monophyly/diphyly of Chiroptera led to the conclusion that Rhinolophoidea (Rhinolophidae, Hipposideridae, Megadermatidae, Craseonycteridae and Rhinopomatidae) have a closer relationship to Megachiroptera (viz. Pteropodidae) rather than to Microchiroptera (Gunnell and Simmons 2005, Teeling et al. 2005, Simmons 2005b). Considering all the above mentioned and taking into account the earlier suggestion by Springer et al. (2001) for the creation of a new suborder, Yinpterochiroptera, which will include Pteropodidae and Rhinolophoidea (Gunnell and Simmons 2005), this gained ground and is nowadays widely accepted, with the remaining chiropteran families being placed within the Yangochiroptera suborder (Gunnell and Simmons 2005).

Another topic regarding chiropteran phylogeny that has not yet been resolved is the status of Miniopteridae and Cistugidae and whether they are distinct families or included in Vespertilionidae. Gunnell and Simmons (2005), Simmons (2005b) and Fracasso et al. (2011) suggest that Miniopteridae and Cistugidae are not separate families and they should be included in the Vespertilionidae family again. However, Hoofer and Van Den Bussche (2003) and Miller-Butterworth et al. (2007) follow the suggestion by Mein and Tupinier (1977) and characterise Miniopteridae as a distinct family. Similarly, Lack et al. (2010) found evidence that allowed them to raise *Cistugo* from being a genus within the Vespertilionidae family to a separate family, Cistugidae.

One question that still needs to be answered is whether Chiroptera evolved laryngeal echolocation once, with Pteropodidae losing it at a later stage or multiple times and separately for each chiropteran taxonomic group (Teeling et al. 2005, Simmons 2005b). The earliest chiropteran fossils, dating back to the Early Eocene, have features which indicate they had already developed both their ability to fly and to echolocate, developments that date the origin of Chiroptera prior to the Early Eocene (Gunnell and Simmons 2005, Teeling et al. 2005). Nevertheless, the most recent data regarding the phylogenetic origin of bats indicate that Onychonycteridae is the basal family of the order and the rest of the extinct and extant families are sister groups (Simmons et al. 2008). In addition, there is evidence that Onychonycteridae evolved their ability to fly ("flight-first" hypothesis) prior to their ability to echolocate ("echolocation-first" hypothesis) (Simmons et al. 2008, 2010). Although, recent works on the specific topic validate the "echolocation-first" hypothesis (Carter and Adams

2015, 2016)[3]. Moreover, it is worth mentioning that Eulipotyphla was found to be the sister group of Chiroptera, whereas no direct relationship was found with Primates, Dermoptera and Scandentia (Murphy et al. 2001).

1.3 HISTORICAL OVERVIEW OF THE RESEARCH AT LOUTRA ALMOPIAS CAVE A AND THE BROADER REGION

The research in the Loutra Almopias Cave A started in 1990 and the systematic excavations in 1992. More specific, the 1st Panhellenic Speleological Research was organised at Loutra Almopias, in 1990, by the late speleologist K. Ataktidis. His motivation was initiated by some photographs that were taken by E. Baltakis. Attendees of this meeting were the Aristotle University of Thessaloniki (AUTh), the Hellenic Survey of Geology and Mineral Exploration (HSGME), with Dr. P. Tsamantouridis in charge, the National Centre for Scientific Research "Demokritos" (NCSR "Demokritos"), with Dr. Y. Bassiakos in charge, the Ephorate of Palaeoanthropology and Speleology (EPS), Ministry of Culture, the Hellenic Speleological Society (HSC) and the Speleological Team of Kavala (STK). During this meeting the first detailed recording of several caves from the broader region took place and the results of the research were published in a relevant volume (Figure 1.2). In 1990, the late speleologist I. Ioannou founded the first speleological park in Greece, the "Almopia Speleopark", because of the great scientific interest and natural beauty of the region.

The first palaeontological excavation started in 1992 after information given by K. Ataktidis regarding the presence of fossils that were brought to light after extensive illicit diggings in the caves. According to the "APX/A3/40604/392/31-8-92" decision of the Ministry of Culture, the excavation was carried out by AUTh with Prof. E. Tsoukala (School of Geology), the late Emer. Prof. G. Chourmouziadis (School of History and Archaeology) and the late Prof. E. Tchernov (Department of Evolution, Systematics and Ecology, Hebrew University of Jerusalem) in charge, under the supervision of EPS. The excavations were continued in 1993-1994 in cooperation with EPS (Dr. E. Kabouroglou), 1996 and 1999-2006. Since 1996, the palaeontological

[3] Recent studies on tree and terrestrial shrews and on the Vietnamese Pygmy Dormouse, *Typhlomys chapensis*, have shown their ability to navigate with the use of echolocation and therefore support the hypothesis that bats evolved their ability to echolocate prior to their ability for self-powered flight (Adams and Carter 2017 and references therein, Youlatos et al. 2020, Granatosky et al. 2021).

research has been carried out in co-operation with the School of History and Archaeology (AUTh) (Prof. K. Kotsakis), the Department of Palaeontology of the University of Vienna and the Austrian Academy of Sciences, with Prof. G. Rabeder in charge. From 1996 till 2000, the late Prof. S. Verginis from the Department of Geography and Regional Research of the University of Vienna participated in the excavation. On behalf of EPS, Dr. A. Athanasiou and MSc geologist D. Bouzas participated from 1999 till 2005. In 1997, EPS's topographer T. Chatzitheodorou designed the ground plan (horizontal alignment) of Loutra Almopias Cave A.

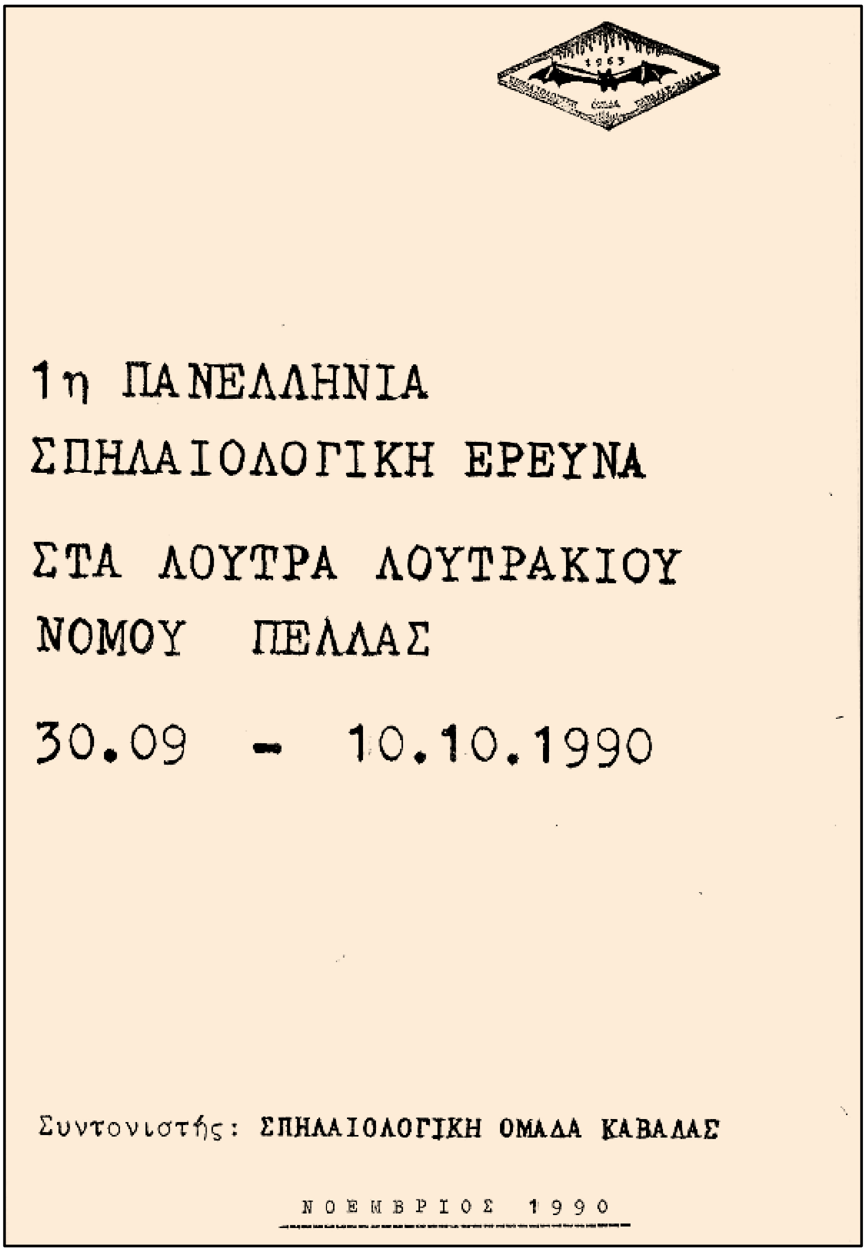
1η ΠΑΝΕΛΛΗΝΙΑ
ΣΠΗΛΑΙΟΛΟΓΙΚΗ ΕΡΕΥΝΑ
ΣΤΑ ΛΟΥΤΡΑ ΛΟΥΤΡΑΚΙΟΥ
ΝΟΜΟΥ ΠΕΛΛΑΣ
30.09 - 10.10.1990

Συντονιστής: ΣΠΗΛΑΙΟΛΟΓΙΚΗ ΟΜΑΔΑ ΚΑΒΑΛΑΣ

ΝΟΕΜΒΡΙΟΣ 1990

Figure 1.2 Cover of the volume from the 1st Panhellenic Speleological Research (translation: 1st Panhellenic Speleological Research at Loutra Loutrakiou, Prefecture of Pella, 30.09-10.10.1990, Coordinator: Speleological Team of Kavala, November 1990).

The research in the region lasted more than 15 years, with 12 excavational phases, 36 excavated squares, 211 layers and the participation of over 100 people (researchers, students and associates). This research brought to light over 50000 fossils of Late Pleistocene age. Part of the rich fossil record was displayed in the physiographical museum of Almopia (founded in 1992) and the Municipal Museum of Aridea (founded in 2002). In 2006, the 12th International Cave Bear Symposium took place in Aridea and the broader region of Loutra Almopias.

The extensive and thorough research that followed the excavations at the Loutra Almopias Cave A – which is still ongoing – has brought to light thousands of fossils, with most of the specimens belonging to the Gamssulzen Cave Bear, *Ursus ingressus* Rabeder et al., 2004 (Tsoukala et al. 2006). Additionally, a rich and diverse fauna of large and small mammals, birds, amphibia and reptilia was also recovered:

- The large mammals are represented by 18 taxa of Carnivora and Artiodactyla (for species representation per chamber see Table A.1): *Ursus ingressus*, *Mustela nivalis*, *Mustela* (*Putorius*) *putorius*, *Martes foina*, *Martes martes*, *Martes* sp., *Meles meles*, Mustelidae indet., *Canis lupus*, *Vulpes vulpes*, *Felis silvestris* aff. *catus*, *Panthera pardus*, *Crocuta crocuta spelaea*, *Capra ibex*, *Rupicapra rupicapra*, *Cervus elaphus*, *Dama dama*, *Bos primigenius* (Tsoukala et al. 2006, Nagel et al. 2019);
- The small mammals faunal list includes 28 taxa of Eulipotyphla, Rodentia and Lagomorpha (for species representation per chamber see Table A.1): *Erinaceus* cf. *europaeus*, *Talpa europaea*, *Talpa* sp. (*minor*), *Sorex araneus*, *Sorex minutus*, *Neomys* sp., *Crocidura leucodon*, *Crocidura suaveolens*, *Spermophilus citellus*, *Apodemus mystacinus epimelas*, *Apodemus sylvaticus*/*flavicollis*, *Apodemus uralensis*, *Mus spicilegus*, *Cricetulus migratorius*, *Mesocricetus newtoni*, *Arvicola terrestris*, *Microtus arvalis*/*agrestis*, *Microtus* (*Chionomys*) *nivalis*, *Microtus* (*Pitymys*) cf. *subterraneus*, *Clethrionomys glareolus*, *Dryomys nitedula*, *Glis glis*, *Muscardinus avellanarius*, *Sicista subtilis*, *Spalax leucodon*, *Ochotona pusilla*, *Lepus timidus*, *Lepus europaeus* (Chatzopoulou 2014);
- The avifauna is represented by 68 taxa of Galliformes, Columbiformes, Caprimulgiformes, Accipitriformes, Falconiformes, Strigiformes, Piciformes and Passeriformes (for species representation per chamber see Table A.2): *Perdix perdix*, *Perdix* sp., *Alectoris graeca*, *Alectoris* sp., *Francolinus francolinus*,

Francolinus sp., *Alectoris*/*Francolinus*, *Perdix*/*Francolinus*, Perdicinae gen., *Tetrao tetrix*, *Lagopus* cf. *lagopus*, aff. *Lagopus* sp., cf. *Bonasa bonasia*, *Bonasa bonasia*/*Lagopus muta*, *Columba livia*, *Columba palumbus*, ?*Caprimulgus* sp., *Buteo* sp. cf. *B. lagopus*, *Falco* sp. cf. *F. peregrinus*, *Falco* sp. ex gr. *F. cherrug*, *Falco* sp. cf. *tinnunculus*, *Falco* sp. cf. *vespertinus*, *Falco* sp. ex gr. *tinnunculus*, *Bubo bubo*, *Athene noctua*, cf. *Otus scops*, cf. *Dryocopus martius*, cf. *Picidae*, *Galerida* sp. cf. *G. cristata*, *Melanocorhypha calandra*, *Melanocorhypha* sp., *Alauda* sp., *Lulula arborea*, cf. *Hirundo* sp., *Riparia*/*Ptyonoprogne*, *Anthus* sp., *Bombicylla garrulous*, *Cinclus cinclus*, *Turdus* sp. cf. *T. vuscivorus*, *Turdus* sp., *Sylvia* sp. cf. *S. borin*, *Phoenicurus* sp. cf. *P. ochruros*, *Erithacus*/*Luscinia*, *Parus major*, *Sitta* cf. *europaea*, *Sitta* sp., *Garrulus glandarius*, *Pica pica*, *Pica* sp., *Pyrrhocorax graculus*, *Pyrrhocorax* cf. *pyrrhocorax*, *Pyrrhocorax* sp. (*P. graculus*/*pyrrhocorax*), Corvidae gen. -1, Corvidae gen. -2, cf. Corvidae gen., *Sturnus* sp. cf. *S. vulgaris*, *Fringilla* sp. cf. *F. coelebs*, *Carduelis* sp. cf. *C. carduelis*, cf. *Chloris chloris*, *Carduelis* sp., *Loxia curvirostra*, *Coccothraustes coccothraustes*, *Pyrrhula pyrrhula*, Fringillidae gen., *Emberiza calandra*, cf. *Plectrophenax nivalis*, *Emberiza* sp. cf. *E. cirlus*, Emberizidae gen., Oscines Non-Corvidae indet., Non-Passeriformes indet. (Boev and Tsoukala 2019);

- The amphibia are represented by 6 taxa of Anura (for species representation per chamber see Table A.3): *Bufo bufo*, *Pseudepidalea viridis*, *Bombina variegata*, *Pelobates syriacus*, *Hyla arborea*, *Rana temporaria* (Rauscher, K. L. pers. comm. to Tsoukala, E.);
- The reptilia are represented by 11 taxa of Squamata (for species representation per chamber see Table A.4): *Anguis fragilis*, *Pseudopus apodus*, Varanidae indet., *Lacerta agilis*, *Lacerta vivipara*, *Lacerta trilineata*, *Lacerta viridis*, *Ophisops elegans*, *Podarcis muralis*, *Coronella austriaca*, Scincidae indet. (Rauscher, K. L. pers. comm. to Tsoukala, E.).

Even though Loutra Almopias Cave A has been extensively excavated and researched over the past years, Chiroptera were not thoroughly studied. In the previous works of Chatzopoulou et al. (2001), Chatzopoulou (2003, 2005b) and Tsoukala et al. (2006) *Rhinolophus* sp., *Myotis* sp. and *Miniopterus* sp. are included. This chiropteran faunal list was later enriched by Piskoulis (2018, 2019) and Piskoulis and Chatzopoulou (in press) with preliminary results (Table A.5).

1.4 RESEARCH AIMS AND OBJECTIVES

The aim of the present doctoral research is the in depth study of the rich chiropteran collection from Loutra Almopias Cave A, in order to contribute to the knowledge of the Quaternary bats of the Greek region and the Balkan Peninsula. This will be accomplished by detailed systematic taxonomy, phenetic analysis, correlation of the chiropteran specimens with the two chronologically different faunas of the cave site and other Greek faunas (modern and fossil), but also with the broader region (biogeography) and with a palaeoclimatological/palaeoecological approach, based on the bats' biocoenosis. It is expected that this research will act as a solid background for the initiation of further studies in the Greek region, aiming to better understand the evolutionary trends of Quaternary Chiroptera and the mechanisms that led to their universal distribution.

CHAPTER 2. GEOLOGY AND STRATIGRAPHY

2.1 GEOLOGY

The “Almopia Speleopark” – and thus the Loutra Almopias Cave A – is developed at the boundary between the Pelagonian zone (west) and Almopias subzone (east) (Figure 2.1) (Georgiadis et al. 2019). The latter, together with the subzones of Peonias and Paikon, comprise the Axios Zone (a.k.a. Vardar Zone) (Mercier 1968), “a unique oceanic area of Jurassic age” (Mountrakis 1986 and references therein). More specifically, the subzones of Peonias (east) and Almopias (west) were both deep water oceans, separated by a shallower ocean, the Paikon subzone (Mercier 1966). Consequently, the Paikon subzone was an island-arc, whilst the Peonias subzone a back-arc basin (Mercier et al. 1975). The Peonias subzone is characterized by nappe tectonics and is mostly comprised of Jurassic deep sea clay sediments and hornfels (Mercier 1966); the Paikon subzone is characterized by a thick neritic limestone series of Jurassic age (Mercier 1966) and the Almopias subzone is characterized by ophiolites and is mostly comprised of Jurassic deep oceanic sediments, Upper Cretaceous transgressive deposits and metamorphosed pre-ophiolitic sediments (Mercier 1966).

The Almopias subzone is comprised of twelve units (distinct nappes), with the Unit of Loutra Almopias (Pozar) being one of them (Figure 2.2). It is composed of a Palaeozoic-Triassic metamorphic basement with phyllites, sericitic schists, greenschists, amphibolitic schists, gneisses, marbles, cipolines and ophiolitic rocks, the Lower Cretaceous limestone of Diasselo and the Upper Cretaceous clastic formation of Mariam (Georgiadis et al. 2019).

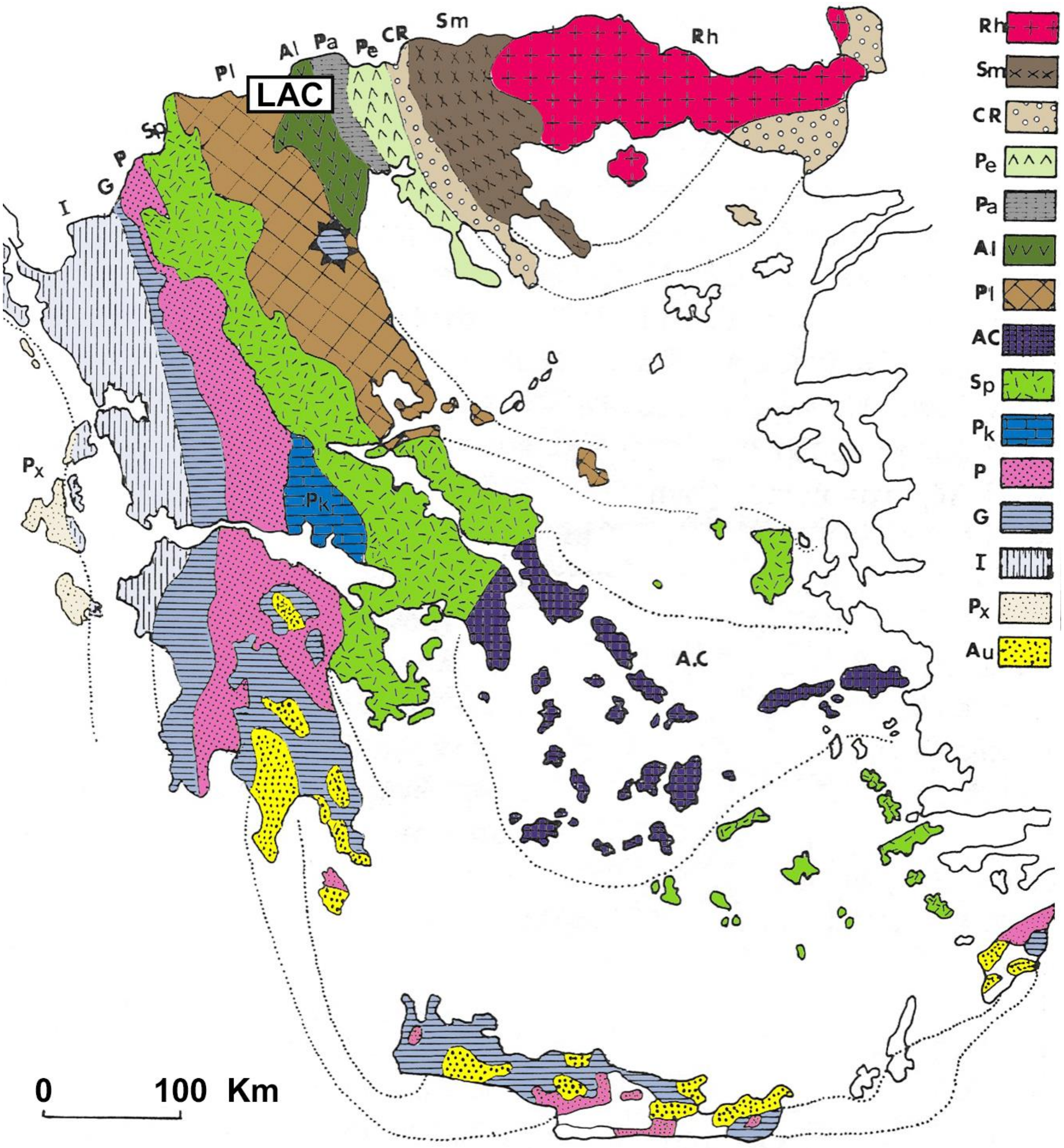

Figure 2.1 Simplified geologic map of Greece. **LAC:** Loutra Almopias Cave A, **Rh:** Rhodope Massif, **Sm:** Serbomacedonian Massif, **CR:** Circum Rhodope Belt, (**Pe:** Peonias subzone, **Pa:** Paikon subzone, **A1:** Almopias subzone): Axios Zone, **Pl:** Pelagonian Zone, **AC:** Attico-Cycladic Massif, **Sp:** Subpelagonian Zone, **Pk:** Parnasos Zone, **P:** Pindos Zone, **G:** Gavrovo-Tripolis Zone, **I:** Ionian Zone, **Px:** Paxos Zone, **Au:** Plattenkalk-Talea Ori. Modified after Mountrakis (2010).

The Pelagonian Zone (Figure 2.2), which used to be a Cimmerian fragment that separated the Neo- from the Palaeo-Tethys (Mountrakis 1986), is characterized by the presence of two Triassic-Jurassic carbonate covers (marbles and dolomitic/micaceous marbles) deposited on both of its margins (east and west) (Mountrakis 1986, Georgiadis et al. 2019), of transgressional limestones of Upper Cretaceous (Maastrichtian and Campanian-Santonian) age and of flysch of Upper Cretaceous-Lower Palaeocene age (Georgiadis et al. 2019). The unit of Loutra Almopias (Pozar) is positioned on top of the Pelagonian Zone, because of a west-moving thrust fault (Figure 2.2) (Mountrakis 1976, Georgiadis et al. 2019). The northern parts of the Pelagonian Massif have been uplifted at higher rates than its southern parts (Lazaridis 2006). The caves of the "Almopia Speleopark" are developed in the Maastrichtian limestone – an over 100 m dark grey homogeneous limestone that is rich in the foraminifer *Orbitoides media* – which sits on top of an underlying light grey Campanian-Santonian limestone, with both limestones being highly fragmented and karstified (Chatzopoulou 2014).

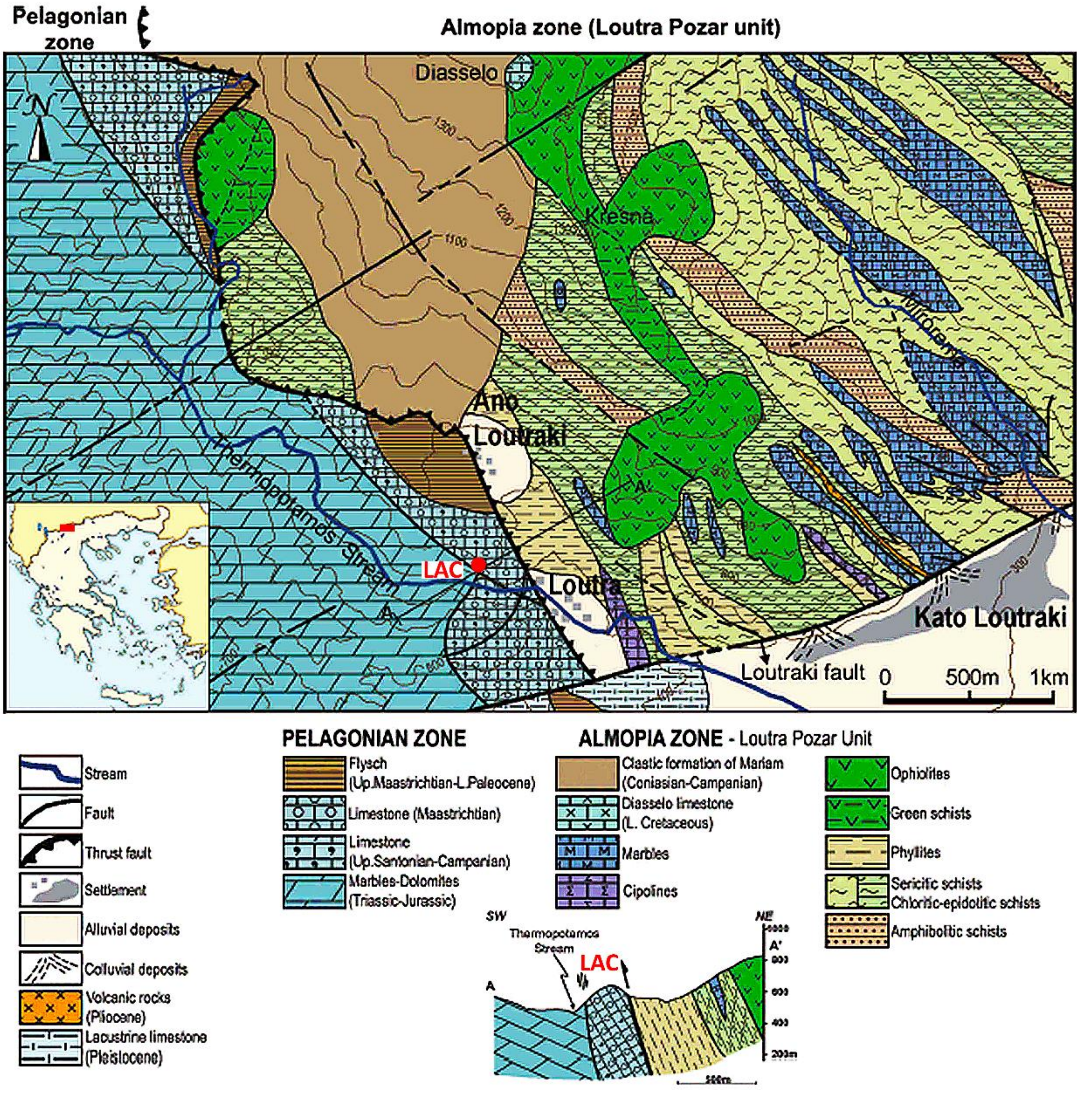

Figure 2.2 Geological map of Loutra Almopias Cave A (LAC) and the broader region (Georgiadis et al. 2019).

During Upper Pliocene, the Almopias subzone, was subject to volcanism, due to the (re)activation of faults within the area of study, which resulted in the upwelling of magmas (Eleftheriadis 2006). The volcanic centres occur in the northern region of the subzone (Mount Voras) and the volcaniclastic sediments occur in the southern region of the subzone (Almopia Plain) (Eleftheriadis 1977).

The tensile forces that acted in the area of study during the Upper Pliocene and resulted in the formation of the Almopia basin, were also responsible, together with the Upper Pliocene volcanism, for the appearance of numerous hot (and cold) springs (Mountrakis 1976, Patras 1990, Vougioukalakis 2002, Eleftheriadis 2006). These springs resulted in the extensive deposition of travertine, which can be found both in the “Almopia Speleopark” and the broader region of Almopia (Mountrakis 1976, Eleftheriadis 2006). These travertine depositions are characterized by their clearance, fine crystallization and absence of xenoliths (Eleftheriadis 2006).

2.2 LOUTRA ALMOPIAS CAVE A

The entrance of Loutra Almopias Cave A (a.k.a. Loutra Arideas Cave and/or Bear Cave) is located on the northern slope of the Nikolaou Rema gorge at an altitude of 540 m and coordinates: N40°58'23.7", E21°54'31.3" (Figure 2.3). The broader region of the “Almopia Speleopark” is located in an intra-mountainous basin, which is surrounded by Voras Mountain Range (2524 m) to the north and Paiko Mountain (1950 m) to the east. To the south, the area is surrounded by the low mountainous region of Edessa. The differences in elevation observed between the plain and the mountainous regions are greater than 1500 m and therefore, the broader region of the “Almopia Speleopark” is characterized by intense relief. Almopeos River (a.k.a. Moglenitsas River) – the main river of the region – runs through the basin and it is fed by 13 streams. On the NW side of the basin occurs the Nikolaou Rema gorge, which is crossed by the Thermopotamos River, which is later connected with the Aspropotamos River.

Neotectonic activity that has been generated by the ENE-WSW Loutraki fault resulted in the uplift of Voras Mountain and, thus, the “Almopia Speleopark”, which in turn led to a severe vertical erosion of the Thermopotamos River and the formation of the V-shaped Nikolaou Rema gorge (Lazaridis 2006). Consequently, the caves of the “Almopia Speleopark” were uplifted from the phreatic to the vadose zone (Lazaridis 2006).

Loutra Almopias Cave A (Figure 2.4) can be reached by a narrow path with steep steps, which begins from Loutra Almopias (a.k.a. Loutra Pozar, Loutra Loutrakiou and/or Loutra Arideas) and leads to the entrance of the cave (Tsirambides 2006, Tsoukala et al. 2006). The total area of the cave is 875 m^2 (Tsirambides 2006) and it was mapped (horizontal alignment) in 1997 by EPS's topographer T. Chatzitheodorou and his team (Kabouroglou and Chatzitheodorou 1999). A simplified ground plan of the Loutra Almopias Cave A can be seen in Figure 2.5.

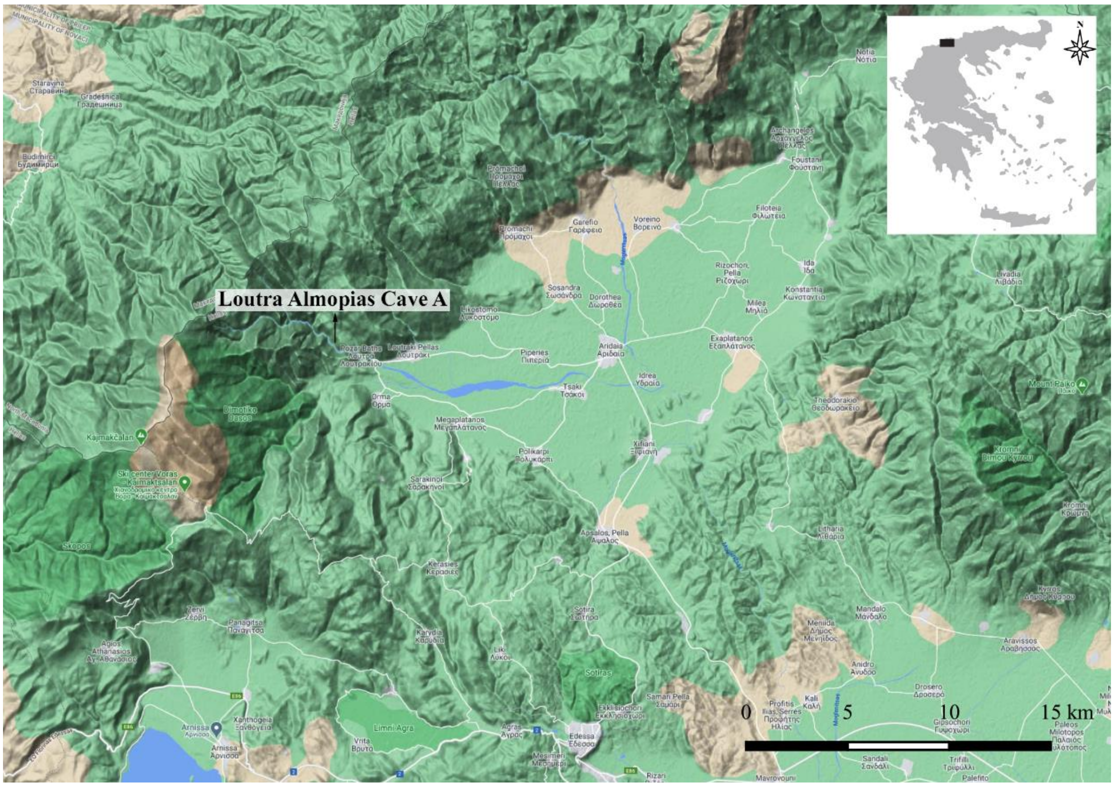

Figure 2.3 Loutra Almopias Cave A and the broader region of the "Almopia Speleopark". Map generated using Google Maps (Google Terrain).

The entrance of Loutra Almopias Cave A is SE oriented and its 2.50 x 1.50 m opening is partly covered by a large polished boulder[4] (see CHAPTER 3, Figure 3.1a-b). Next to the entrance is located a 10 m long, narrow, ENE-WSW passage with a wooden staircase, which leads to LAC I – the first and largest chamber of the cave – where the main excavation occurred, with 13 excavated squares (Figure 2.5). LAC I is 1.50 m higher than the narrow passage and its maximum height reaches 10 m. A small karstic basin filled with water (Agiasma: Holy Water in Greek, Figure 2.5) is located at the NW part of LAC I, where pottery and glass remains from the Neolithic/Byzantine era till present occur and they are related to religious customs (Tsoukala et al. 2006).

[4] Several European caves that used to be occupied by cave bears present similar polished surfaces on narrow paths and passages. This possibly occurs because cave bears were rubbing on such surfaces or because of chemical weathering (Kurtén 1976, Tsoukala et al. 2006).

The floor of LAC I is covered by clastic sediments and there are plenty of illegal excavations which led to the discovery of the *Ursus ingressus* fossils (Tsoukala 1994, Tsoukala and Rabeder 2005, Tsoukala et al. 1998, 2001, 2006). Moreover, potholes occur at several spots, where the sediments have been washed out and the fossils are found stuck on the calcareous crust. The floor of this chamber is covered by guano, even though no bats currently inhabit the cave (Paragamian 2021).

Figure 2.4 The Nikolaou Rema gorge with the entrance of Loutra Almopias Cave A depicted. Photograph by Dr. M. Vaxevanopoulos.

East of LAC I a small, slippery and inclined surface occurs that leads to chamber LAC Ia – the smallest chamber of the cave – approximately 5 m higher than the floor (Figure 3.1c). LAC Ia was excavated in 1996. The sediment supply of this chamber seems to have a different origin than the rest of the cave and additionally, its fauna is of different age than the cave’s floor (Tsoukala et al. 2006).

LAC Ib is located at the SE side of LAC I and it has been extensively excavated (nine squares), due to its numerous large mammal fossils, both in absolute numbers and variety (Chatzopoulou 2014). The fossiliferous layer bears also a large amount of large-sized cobbles. The walls of LAC Ib are covered with botryoidal calcareous debris 1.50 m below the cave's floor. West of LAC Ib many fallen boulders are present, which are partly covered by clastic sediments.

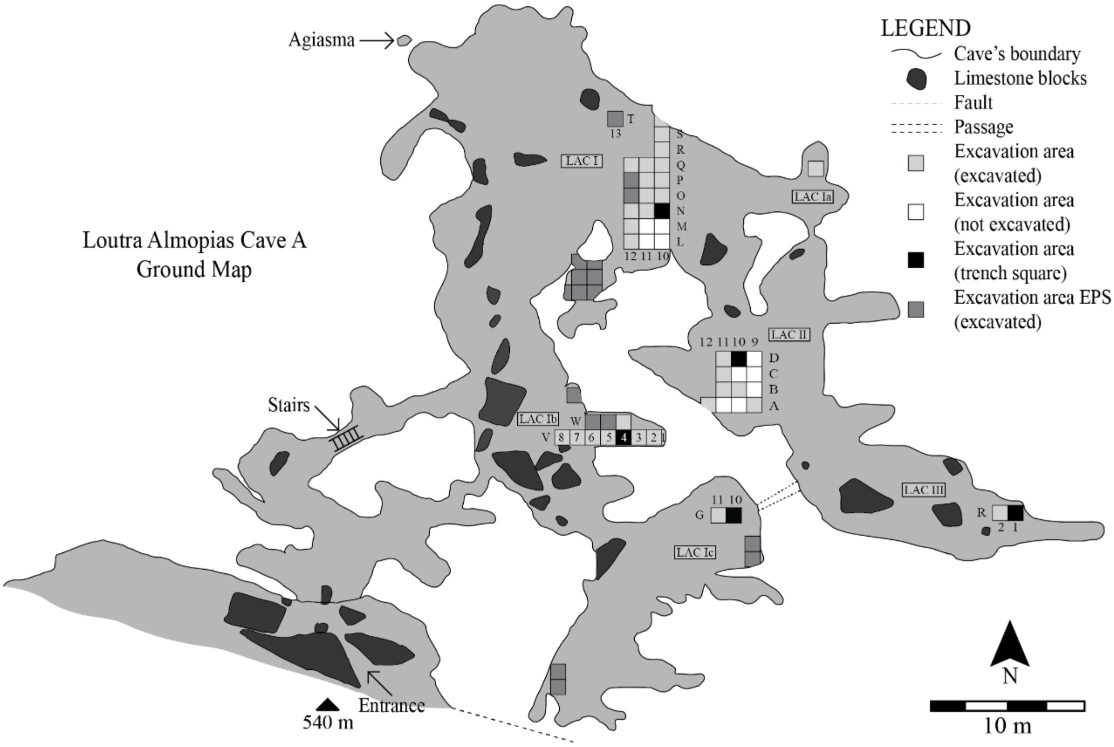

Figure 2.5 Simplified ground plan of the Loutra Almopias Cave A (a.k.a. Loutra Arideas Cave and/or Bear Cave) with the excavating block of squares of the various chambers (LAC I, LAC Ib, LAC Ic, LAC II, LAC III and LAC Ia) (1992-2006), based on the topographic plan of Kabouroglou and Chatzitheodorou 1999 (modified by G. Withalm).

Chamber LAC Ic is located south of LAC I and LAC Ib and it has a great resemblance to the slope of the gorge outside the cave. In fact, the root system of a tree can be observed at the southern part of the chamber and plant roots can be found in all the sediments of the cave. Another entrance for the cave was possibly present in LAC Ic, which is, however, blocked by fallen boulders nowadays. The floor of the chamber is covered with gours. The fossiliferous layer (two squares excavated) bears a large amount of large-sized cobbles, too (Chatzopoulou 2014). The walls of LAC Ic are also covered with botryoidal calcareous debris. The eastern side of LAC Ic is possibly connected with LAC III via a very narrow passage.

The entrance – which is not taller than 0.70 m – that leads to LAC II and LAC III is located on the ESE side of LAC I. The floor of LAC II is developed in two levels.

The only form of speleothem present in this chamber is a 3 m-tall, eroded stalagmite at the NE side. Six squares have been excavated in this chamber. Moreover, the datum point was fixed here (just south of A10 square).

LAC III is well-connected with LAC II. This chamber is elongated (WNW-ESE orientation) and it is the deepest of all. Many fallen boulders are also present, which are partly covered by clastic sediments. No speleothems are present in LAC III and apart from the two excavated squares, there are also extensive illicit excavations.

Loutra Almopias Cave A is developed horizontally and its orientation is NW-SE and ENE-WSW. Large joints and fractures also occur on the walls and the ceiling of the cave. The orientation corresponds to the Pliocene/Quaternary faults' stretch field. The narrow corridors and chambers of the cave are controlled by a neotectonic joint system with large dip angles (80^o-90^o) (Chatzopoulou 2014).

2.3 STRATIGRAPHY

The decoration of Loutra Almopias Cave A is not rich, but it holds a plethora of different elements with the main speleothems being stalactites, stalagmites, curtains, flowstones, gours, cave pearls and coralloids, with flow deposits prevailing over drip deposits (Chatzopoulou 2014). Cave deposits can hold data about their composition, their formation and their depositional environment, consequently their study provides crucial information on the evolution of a cave, the climate and environment of the region at a certain time frame and the taphonomy, when fossils have been discovered (Tsoukala et al. 2006).

The stratigraphy of Loutra Almopias Cave A has been extensively described by Tsirambides (1998), Chatzopoulou et al. (2001), Chatzopoulou (2003, 2005a, 2005b, 2014), Tsoukala et al. (2006) and Georgiadis et al. (2019). For that reason, the stratigraphy of the cave will be briefly described.

One trench square (see CHAPTER 3) was excavated in each chamber, with those being N10 (LAC I), V4 (LAC Ib), G10 (LAC Ic), D10 (LAC II) and R1 (LAC III) and the lithostratigraphic columns (Figure 2.6-10) are N-S/E-W oriented, apart from LAC Ia (Figure 2.11) which is N-S oriented (Chatzopoulou 2014).

In chamber LAC I (Figure 2.6) the excavation of trench square N10 reached a depth of approximately 200 cm and revealed 15 strata. N10 is dominated by clastic material with five thin interpolated calcite crusts and the sediments are mainly brownish clay and silt (Tsoukala et al. 2006). Below 250 cm (from the datum point) occurs a sandy layer with many pebbles, which seems to be the deepest layer of the cave. The fossiliferous layer is <20 cm from the surface, it is thin (approximately 25 cm) and its uppermost beds are integrated with the overlaying calcite crust.

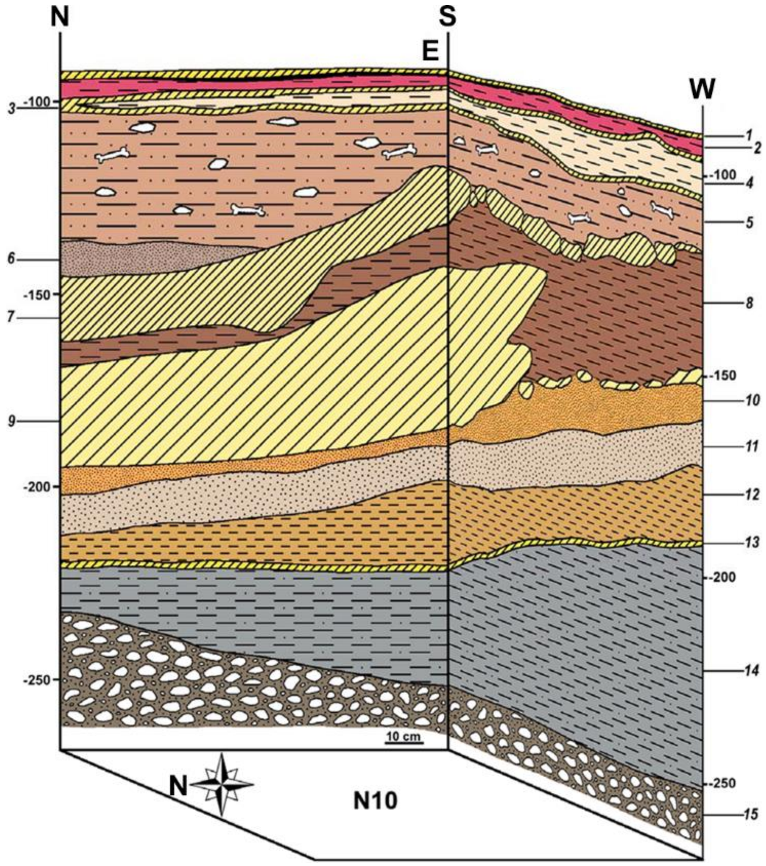

Figure 2.6 LAC I (N10 square) stratigraphic column. **1.** Calcite crust, **2.** Clay layer, **3.** Calcite crust, **4.** Clay, **5.** Fossiliferous clay stratum, **6.** Fine grained sand stratum, **7.** Calcite crust, **8.** Clay stratum, **9.** Calcite crust, **10.** Sandy stratum, **11.** Sandy stratum, **12.** Clay stratum, **13.** Calcite crust, **14.** Sandy silt, **15.** Conglomerate stratum. Modified after Chatzopoulou (2014).

In chamber LAC Ib (Figure 2.7) the excavation of trench square V4 reached a depth of approx. 100 cm and revealed 7 strata. V4 is dominated by clastic material and all strata reach their maximum thickness at V4 square and they are wedging out towards the walls of the cave and towards LAC I (Tsoukala et al. 2006). The clay and sandy strata overlaying the fossiliferous stratum show similarities to square G10 (LAC Ic) (Tsoukala et al. 2006). The relatively thin (approx. 40 cm) fossiliferous stratum bears large pebbles and stones on its uppermost beds (in V4), which are of different lithological composition and a thick (>130 cm) sterile sand is underlying the fossiliferous stratum (Tsoukala et al. 2006).

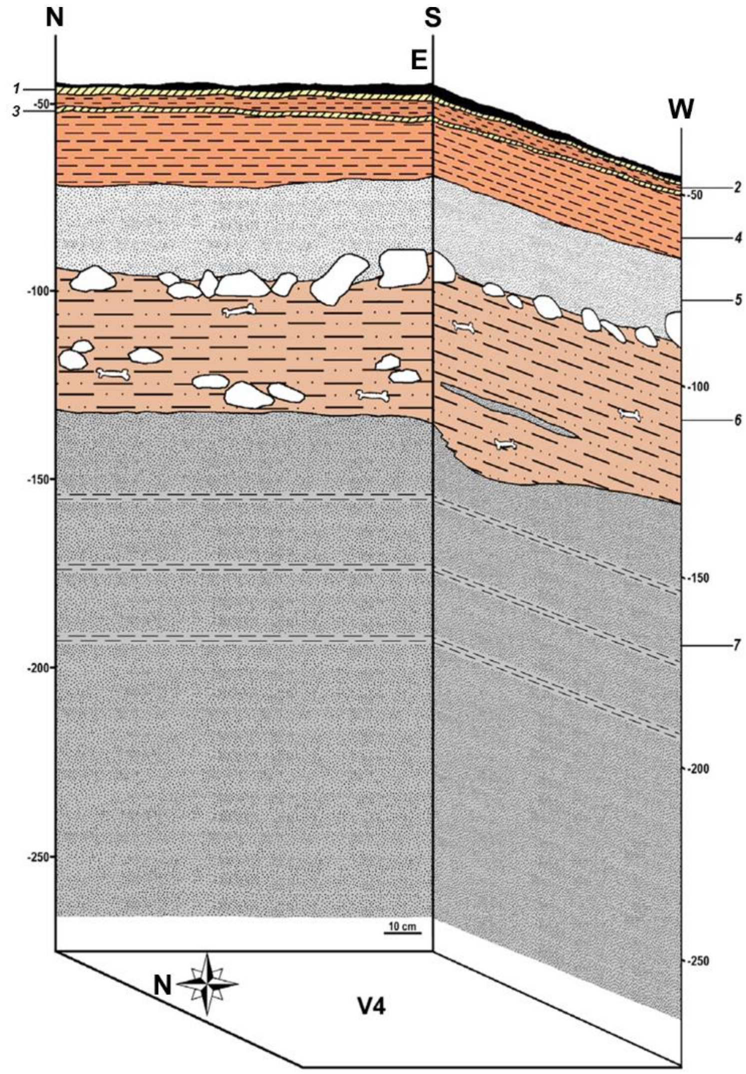

Figure 2.7 LAC Ib (V4 square) stratigraphic column. **1.** Calcite crust, **2.** Clay stratum, **3.** Calcite crust, **4.** Clay stratum, **5.** Sandy stratum, **6.** Fossiliferous clay stratum, **7.** Sandy stratum. Modified after Chatzopoulou (2014).

In chamber LAC Ic (Figure 2.8) the excavation of trench square G10 reached a depth of approximately 190 cm and revealed five strata. The floor is covered with gours and the sterile soaked clay and sandy strata are overlaying the fossiliferous beds. Even though the fossiliferous stratum reaches its maximum thickness (approximately 140 cm) in the cave, the fossil material is relatively scarce (Tsoukala et al. 2006). The fossiliferous stratum is clearly full in medium-sized pebbles and it sits on top of an underlying calcite crust (Tsoukala et al. 2006). All strata have a SW inclination towards the central part of the chamber. It is also worth to note that the top 100 cm of the sediments are penetrated by plant roots (Tsoukala et al. 2006, Chatzopoulou 2014). Apart from this, a tree trunk root is also present at the SW wall of LAC Ic chamber, indicating that this chamber could have acted as another natural entrance in the past.

This is further supported by the absence of sediments at the narrow passage with the stairs (near today's entrance) (Chatzopoulou 2014).

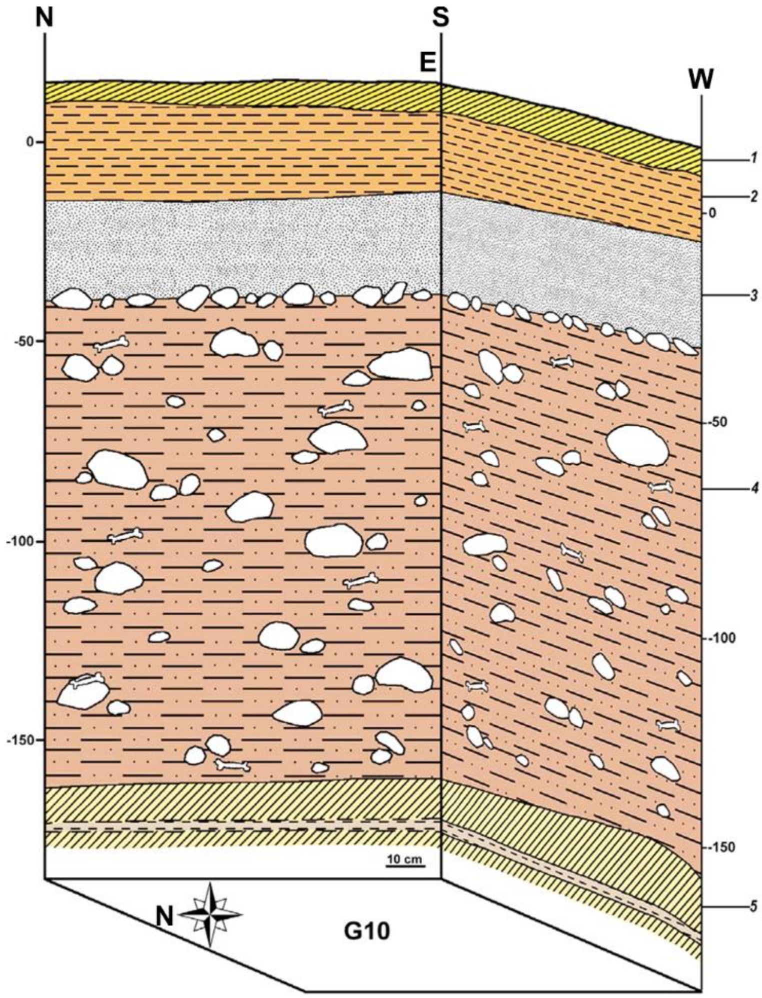

Figure 2.8 LAC Ic (G10 square) stratigraphic column. **1.** Calcite crust, **2.** Soaked clay stratum, **3.** Sandy stratum, **4.** Fossiliferous clay stratum, **5.** Calcite crust. Modified after Chatzopoulou (2014).

In chamber LAC II (Figure 2.9) the excavation of trench square D10 reached a depth of approximately 210 cm and revealed eleven strata. It is evident that clastic and chemical sediments are alternating in D10 (Tsoukala et al. 2016). The calcite crusts were deposited during warm and humid climatic conditions, whereas the clastic sediments (sand, clay and silt) were deposited during colder climatic conditions (Tsirambides 1998). Additionally, the small grain size of the clastic sediments on the floor of LAC II indicates a depositional environment with slow water flow, which resulted from increased water mass surface in Loutra Almopias Cave A, in addition to a probable climate change from wet to dry conditions (Tsirambides 2006).

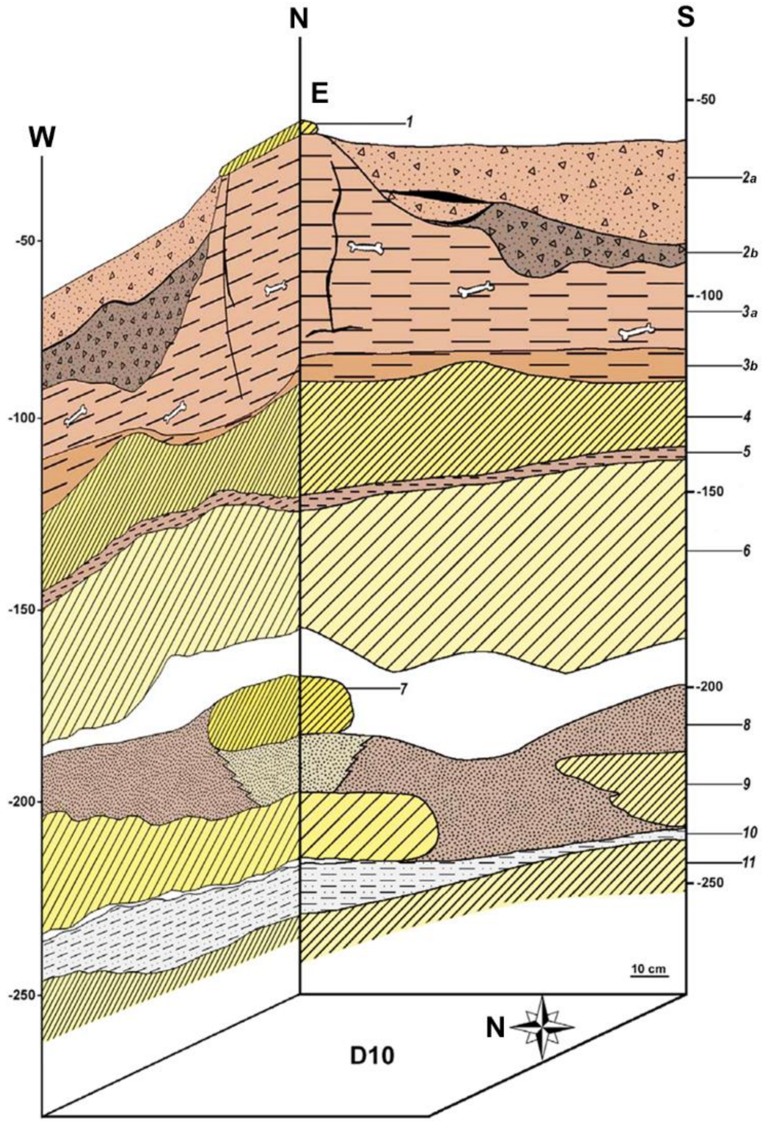

Figure 2.9 LAC II (D10 square) stratigraphic column. **1.** Calcite crust, **2.** Disordered material, **3.** Fossiliferous clay/silt stratum, **4.** Calcite crust, **5.** Silt stratum, **6.** Calcite crust, **7.** Calcite inclusion, **8.** Sandy stratum, **9.** Calcite crust, **10.** Clay/Silt stratum, **11.** Calcite crust. Modified after Chatzopoulou (2014).

In chamber LAC III (Figure 2.10) the excavation of squares R1 and R2 reached a depth of approximately 170 cm and revealed six strata. In both squares, the fossiliferous stratum – a brownish sandy clay with white calcareous pebbles and gravels – is very thick (70-120 cm). All strata are wedging out towards the walls of the cave and, consequently, they are inclined (SW inclination with dip angle 30°) (Tsoukala et al. 2006). The calcite crust underlying the fossiliferous stratum should have been the paleo-floor of Loutra Almopias Cave A for some time as it is indicated by the in situ stalagmite that was revealed (Tsoukala et al. 2006, Chatzopoulou 2014). The sediments underlying the fossiliferous stratum are sterile and not similar to those of other chambers, whereas the sedimentation ends on the cave's bedrock (Tsoukala et al. 2006).

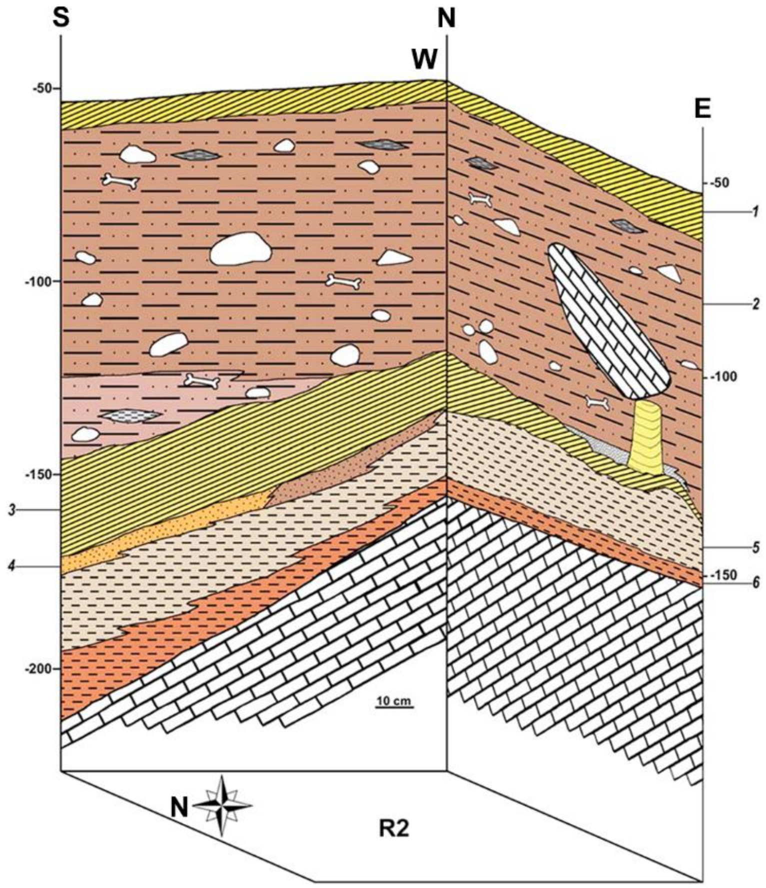

Figure 2.10 LAC III (R2 square) stratigraphic column. **1.** Calcite crust, **2.** Fossiliferous clay stratum, **3.** Calcite crust, **4.** Sand inclusions, **5.** Clay stratum, **6.** Clay stratum. Modified after Chatzopoulou (2014).

In chamber LAC Ia (Figure 2.11) the excavation reached a depth of approximately 30 cm and revealed three strata. During the excavation of 1996, a short excavation at the chamber on a surface area less than 1 m^2 resulted in the discovery of numerous large and small mammals as well as other groups (mainly birds) (Chatzopoulou 2014).

To sum up, despite the variation in lithology and thickness, it is evident that the brown fine grained fossiliferous stratum is placed at the same depth (-130 cm from datum point) in all chambers of the cave (apart from LAC Ia) (Tsoukala et al. 2006, Chatzopoulou 2014). The presence of *Ursus ingressus* is common in all chambers (Tsoukala and Rabeder 2005). Moreover, the sedimentation of the cave indicates cyclicity, between warm and humid intervals as it is indicated by the calcite crusts and colder intervals as it is indicated by the clastic sediments (Tsoukala et al. 2006, Chatzopoulou 2014). The calcite crusts are of significant thickness in chamber LAC II, the clastic sediments are dominant in chambers LAC Ib and LAC Ic, whereas chambers LAC I and LAC III are of an intermediate stage (Tsoukala et al. 2006, Chatzopoulou 2014).

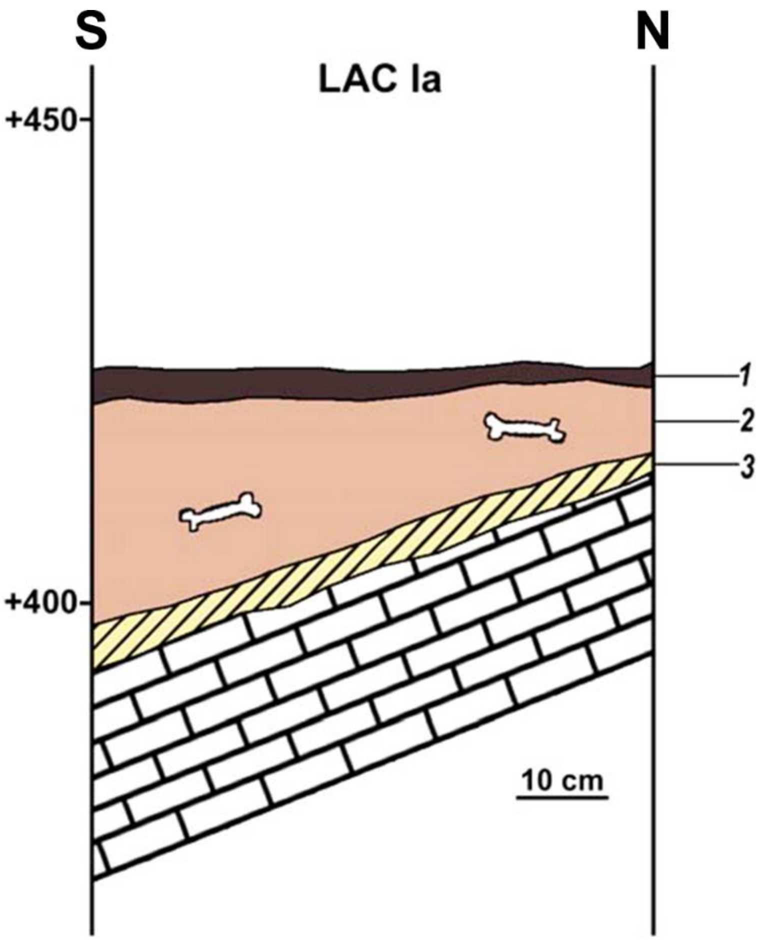

Figure 2.11 LAC Ia stratigraphic column. **1.** Calcite crust, **2.** Fossiliferous stratum, **3.** Calcareous formation. Modified after Chatzopoulou (2014).

All clastic sediments (fine-and coarse-grained) were brought into Loutra Almopias Cave A by flood events of the Thermopotamos River as it is indicated by their granulometry and the bench deposition outside the cave (Chatzopoulou 2014). Their composition is identical to the rocks of the surrounding area (limestones, dolomites, marbles, schists, phyllites, ophiolites), indicating that they are the result of erosional processes (Tsoukala et al. 2006, Chatzopoulou 2014).

Correlation of the lithostratigraphic columns was proven a hard task due to their differences in lithology (Chatzopoulou 2014). Although, its thickness varies, the fossiliferous stratum is common in all chambers and it is placed at the same depth (-130 cm from datum point). It seems that it was deposited during a flood event and it covered the older deposits and thus, its thickness is greater close to the point of supply of the clastic material, chamber LAC Ic (Chatzopoulou 2014).

Correlating the rest strata can be accomplished only within neighbouring chambers and not for the entire cave (Chatzopoulou 2014). The correlations can be seen in Figure 2.12. More specifically, the upper strata (compact deposits of the floor, red-brown clay, grey mica sand, fossiliferous sediment with cobbles) between chambers LAC Ib and LAC Ic can be correlated, as the deposition of grey mica sand and red-brown clay is the result of a later small scale flooding event, other than that of the fossiliferous stratum, which is recorded only in chambers LAC Ib and LAC Ic (Chatzopoulou 2014). Moreover, chambers LAC I and LAC II can be correlated (fossiliferous stratum, underlying crust, brown clay, underlying crust) (Chatzopoulou 2014). LAC III is possibly correlated with LAC I and LAC II (fossiliferous clay stratum and underlying calcite crust).

LAC Ia cannot be correlated with the cave's floor sediments, as not only it is located significantly higher, but it also differs in granularity and fauna composition, indicating a different depositional environment (Chatzopoulou 2014).

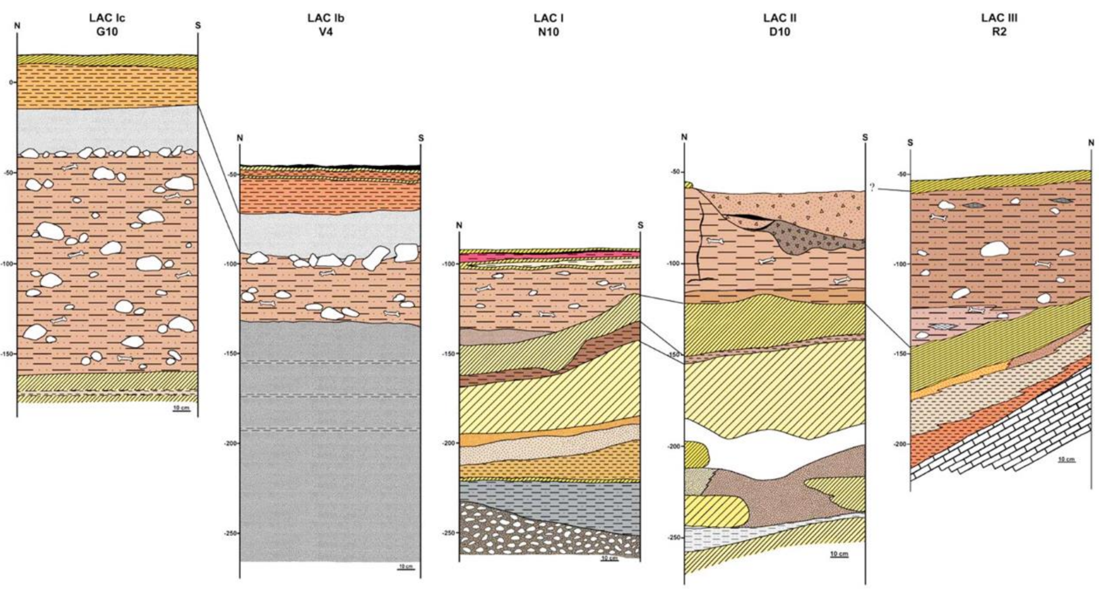

Figure 2.12 Stratigraphic correlation of the trench squares G10, V4, N10, D10 and R2 (LAC Ic, LAC Ib, LAC I, LAC II and LAC III respectively). Modified after Chatzopoulou (2014).

CHAPTER 3. MATERIAL AND METHODS

3.1 THE EXCAVATION

For the purpose of the palaeontological excavations at Loutra Almopias Cave A, a 1-meter square grid with N-S orientation was constructed in chambers LAC I, LAC Ib, LAC Ic, LAC II and LAC III. Every square of the grid was later given an alphanumeric register (one letter of the Latin alphabet for the N-S sides of the squares and an Arabian number for the W-E sides of the squares). One square at each chamber was selected to be the trench (guidance) square, where the excavation was accomplished at a quicker pace aiming to reveal the stratigraphy of each chamber and thus the position of the fossiliferous layers. On the remaining squares, the excavation was conducted by revealing layers approximately 5 cm thick and by the careful collection of the extracted sediments with precision tools. Once a 5 cm layer was cleared, the square was drawn in the excavation diary in scale and photographed. The co-ordinates of each fossil were also recorded as well as the azimuth for the elongated ones. Additionally, the depth of each layer was also recorded from the datum point, which was fixed in chamber LAC II just south of A10 square (Figure 3.1).

The extracted sediments were all collected in plastic bags with the extraction date, square code and depth that the sediment belongs to, noted on a label. These sediments were later washed at superimposed sieves. Two sieves were used, one with 3.0 mm diameter (top) and one with 0.8 mm (bottom). When the sediment was very coarse grained an additional sieve with 5.0 mm diameter was also used. More specifically, the sediment of each bag was put into a bucket with water and hydrogen peroxide (H_2O_2) for twelve hours, which aids on the easier detachment of the clay material from the fossils. Thereafter the material was emptied in the top sieve, where it was solely washed under constant water supply and occasionally with the use of a soft brush (only when mud lumps would not break). The water removed the mud and the finer materials with diameter less than 3.0 mm, whereas materials with diameter between 3.0 mm and 0.8 mm were placed on top of the bottom sieve[5]. The remained material on the top sieve has diameter greater than 3.0 mm[6]. The remained material on both sieves was left to dry in carton boxes and afterwards, it was stored for further processing and study. The process was repeated for each level separately. In between, the sieves were carefully cleaned from possible useless materials stuck on the openings in order to avoid cross contamination of the samples (Figure 3.1).

The material was subsequently transferred to the Laboratory of Palaeontology of the AUTh for further study. First of all, the material was screened under a JENA stereomicroscope with x10 eyepieces. The collected fossils that could reach to a certain identification level (maxillary/mandibular fragments, teeth, humeri) were placed on Rodico Cleaning Compound strips in 52 plastic transparent boxes (Figure A.1-52) and a registration number was marked next to each specimen (e.g. LAC23496), whereas the rest (mostly bone fragments) were stored for future study. All identified specimens (9004) have been registered in a database management system and they resulted from a total of 112 layers from 20 excavated squares.

3.2 NOMENCLATURE

Once all specimens were mounted, the identification of the fossils started based on the morphological characteristics of each specimen. For this purpose, the nomenclature established by Sevilla (1988) was followed for the maxillary/mandibular fragments and the teeth (Figure 3.2a-c) and the nomenclature established by Felten et al. (1973) was followed for the humeri (Figure 3.2d). Measurements of all the specimens were taken under a WILD Photomakroskop M400 as established by Sevilla (1988) (Figure 3.3-4).

The identifications of the fossils were based on the comparison of material with the descriptions and figures/photos available in publications dealing with Quaternary bats and with comparative material from the Natural History Museum of Crete (NHMC), the National Museum of Natural History in Sofia (NMNHS) and from the private collection of Assoc. Prof. Paloma Sevilla (qualitative only).

---

[5] Mostly micromammalian, avian, reptilian and amphibian remains with diameter larger than 0.8 mm.

[6] Mostly *Ursus ingressus* remains.

Figure 3.1 The palaeontological excavations at Loutra Almopias Cave A. The entrance of the cave from **a.** the outside and from **b.** the inside. **c.** View of chamber LAC I and the elevated chamber LAC Ia. **d.** Excavation of the cave's floor sediments, **e.** Close-up of a square during the excavation process and the collection of sediments in bags. **f.** The set of sieves used for the washing of the sediments. **g.** Fine grained material on the bottom sieve (0.8 mm diameter). **h.** Coarse (left) and fine (right) grained material left to dry. Photographs by LAC team.

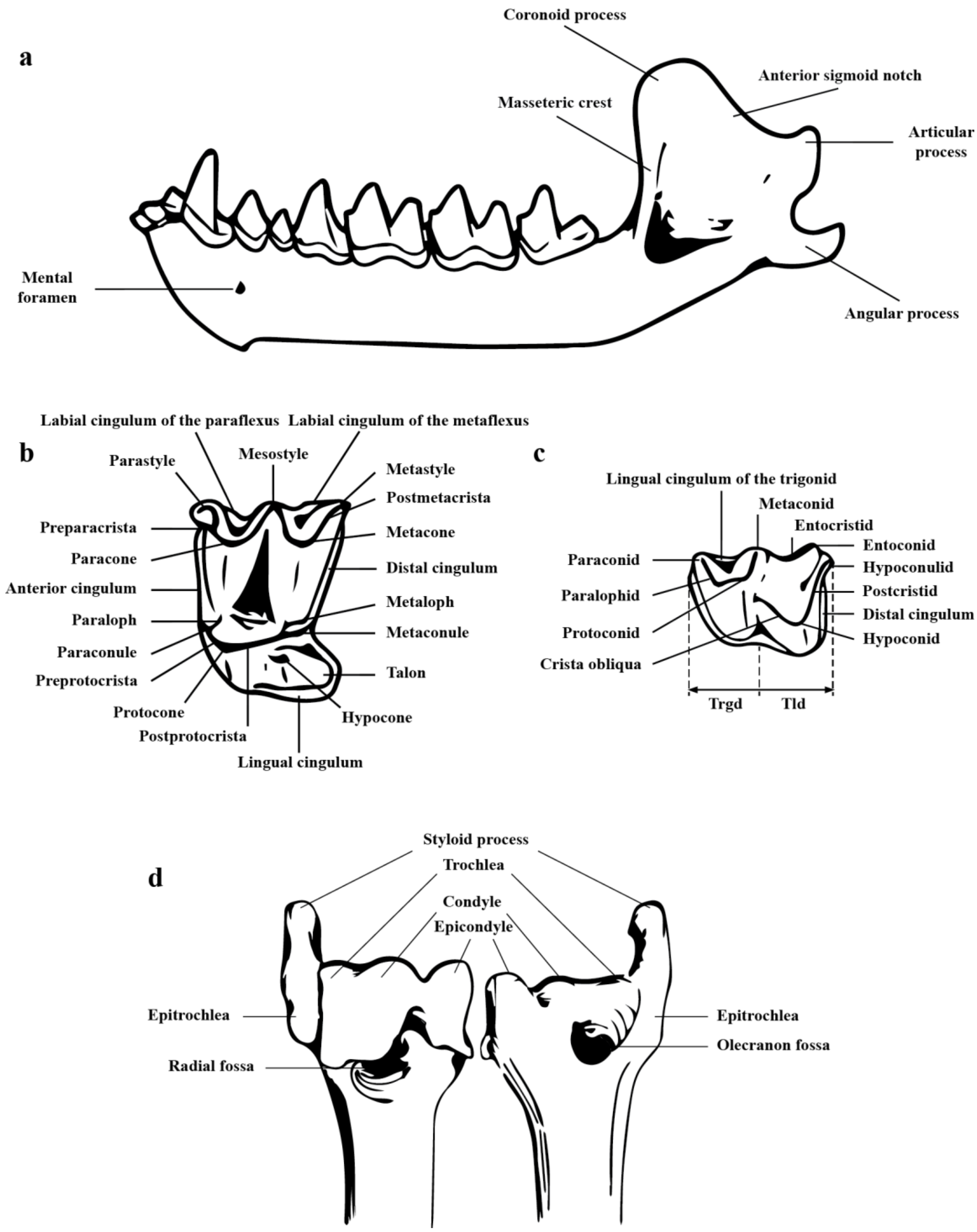

Figure 3.2 Nomenclature of **a.** the mandible (left mandible; labial view), **b.** the upper molars (left upper molar; occlusal view), **c.** the lower molars (left lower molar; occlusal view), **d.** the distal epiphysis of the humerus (distal epiphysis of right humerus; left – anterior view, right – posterior view). Modified after Sevilla (1988) (**a-c**) and Felten et al. (1973) (**d**).

The morphological characters (Figure 3.5) used for the identifications of the fossils were later quantified according to Sevilla and Lopez-Martinez (1986) and with the implementation of some extra characters from Sevilla (1988) they were also used for the description of the identified taxa and for phenetic analysis.

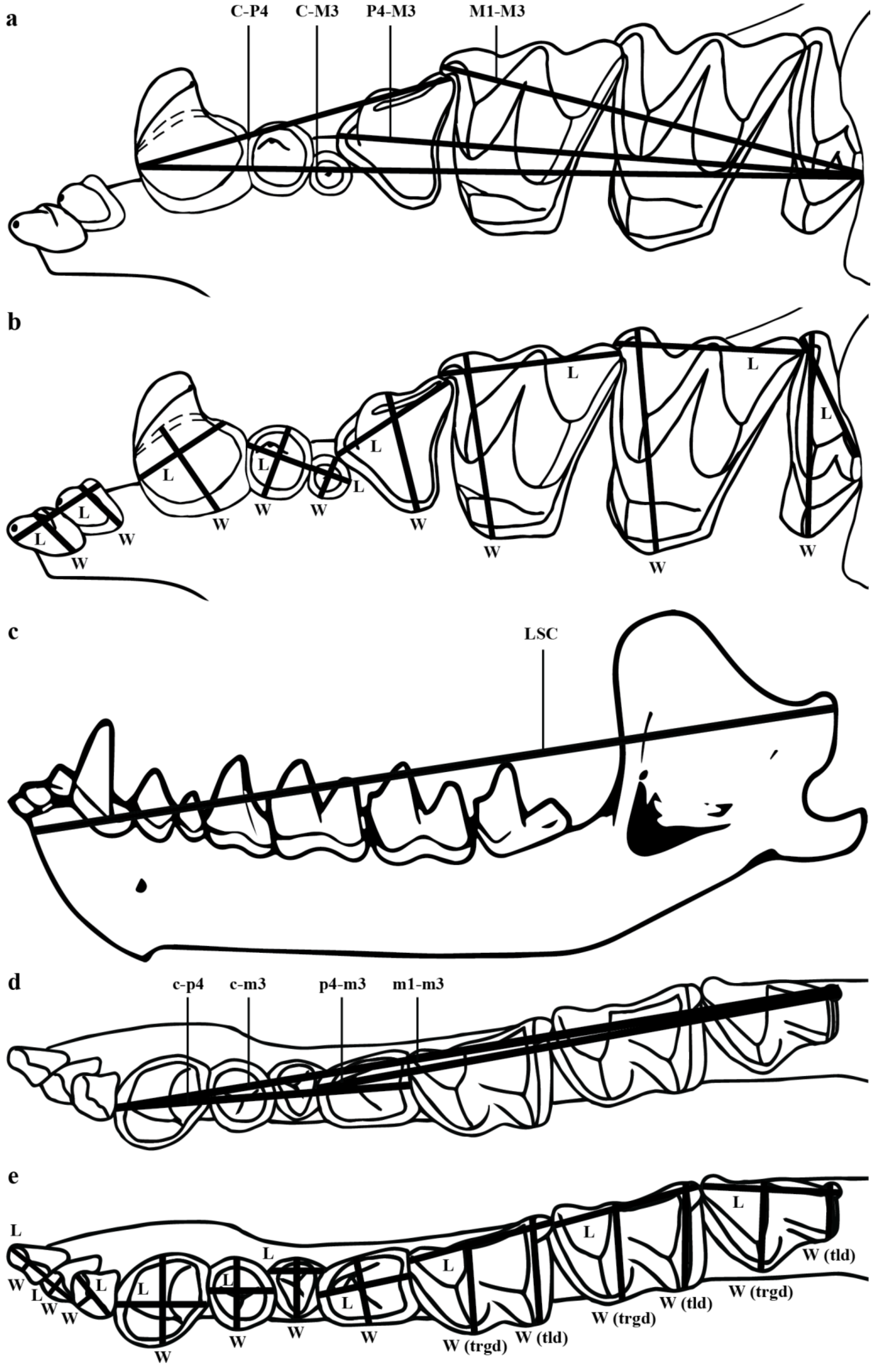

Figure 3.3 Measurements of the upper **a.** toothrows and **b.** teeth, **c.** the mandible, lower **d.** toothrows and **e.** teeth. L: length; W: width; LSC: symphysis-articular process length; trgd: trigonid; tld: talonid. Modified after Sevilla (1988).

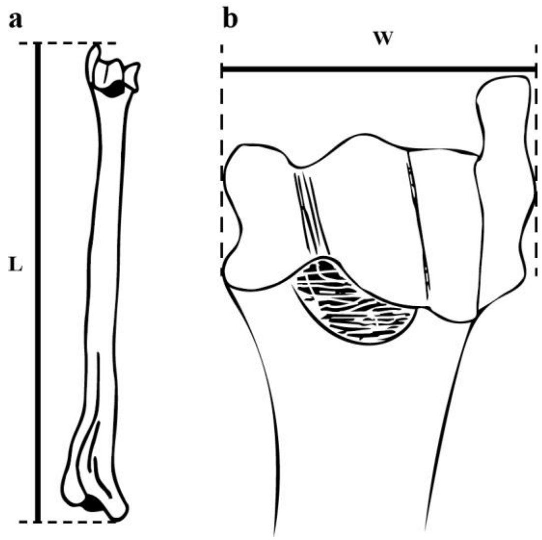

Figure 3.4 Measurements of **a.** the humerus length and **b.** its distal epiphysis width. L: length; W: width. Modified after Sevilla (1988).

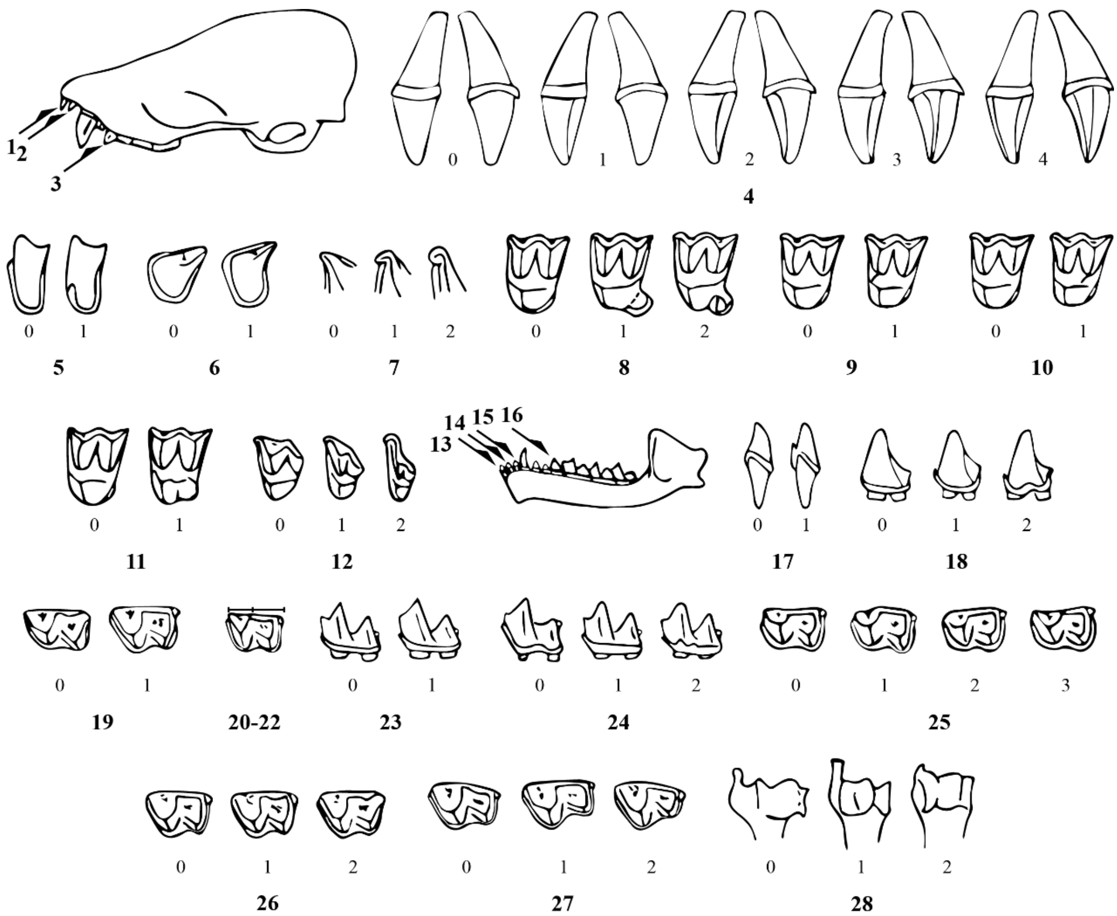

Figure 3.5 Morphological characters used for species identification and phylogenetic analysis. **1.** Number of cusps in I1: Tooth is absent (0), One (1), Two (2), Three (3); **2.** Number of cusps in I2: One and very small (0), One and well-developed (1), Two (2), Three (3); **3.** Number of upper premolars: One (P4) (0), Two (1), Three (2), Three – P3 with three roots (3); **4.** Number of grooves in C: None (0), One labial (1), One labial and one lingual (2), One labial and two lingual (3), Two labial and two lingual (4); **5.** Cingular cusplet at mesiolingual part of P4: Absent (0), Present (1); **6.**

Talon of P4: Not well-developed (0), Well-developed (1); **7.** Upper molars parastyle styles: Straight (0), Right angle (1), Curved (2); **8.** Two first upper molars: Without heel (0), With heel, but without hypocone (1), With heel and hypocone (2); **9.** Upper molars: Without paraloph (0), With paraloph (1); **10.** Two first upper molars: Without metaloph (0), With metaloph (1); **11.** Two first upper molars: Without metaconule (0), With metaconule (1); **12.** Distal reduction of M3: Minimal – affecting almost exclusively the postmetacrista (0), Intermediate – postparacrista and premetacrista somewhat reduced (1), Very strong – postparacrista and premetacrista strongly reduced (2); **13.** Number of cusps in i1: Tooth is absent (0), Two (1), Three (2), Four (3); **14.** Number of cusps in i2: Two (0), Three (1), Four (2); **15.** Number of cusps in i3: Two (0), Three (1), Four (2); **16.** Number of lower premolars: Two (0), Three (1), Three – p3 with two roots (2); **17.** Cingular cusplet at mesiolingual part of c: Absent (0), Present (1); **18.** Cingulum of p4 in labial view: Straight and very oblique (0), Concave towards the roots (1), With two concavities – each towards a root (2); **19.** Pattern of lower molars: Nyctalodont (0), Myotodont (1); **20.** Trigonid of m1: Open – length trigonid > length talonid (0), Regular – length trigonid ≃ length talonid (1), Closed – length trigonid < length talonid (2); **21.** Trigonid of m2: Open – length trigonid > length talonid (0), Regular – length trigonid ≃ length talonid (1), Closed – length trigonid < length talonid (2); **22.** Trigonid of m3: Open – length trigonid > length talonid (0), Regular – length trigonid ≃ length talonid (1), Closed – length trigonid < length talonid (2); **23.** Paralophid of lower molars: Angular (0), Concave (1); **24.** Thickness of labial cingulum in lower molars: Thin and uniform (0), Thick and uniform (1), Thick and irregular (2); **25.** Alignment of lingual cusps in lower molars: In line (0), Metaconid lingual (1), Hypoconulid labial (2), Hypoconulid lingual (3); **26.** Entocristid of lower molars: Straight (0), Concave (1), Concave/Convex (2); **27.** Reduction of the m3 talonid by displacement of: Entoconid (0), Hypoconid (1), Both (2); **28.** Styloid process of humerus: Long and sharp (0), Long and flat (1), Short and blunt (2). Modified after Sevilla and Lopez-Martinez (1986) and Sevilla (1988).

The drawings of the specimens were initially accomplished with pencil on paper with the use of a camera lucida on the JENA stereomicroscope, afterwards they were scanned and digitally processed with a photo editing software.

A length/width graph was generated for each measurable element of each species for LAC and LAC Ia (see CHAPTER 4). Additionally, the wear stage and consequently the age group of each dental element was recorded according to Sevilla (1986), with the implementation of one extra age group (4) for the severely worn teeth, with practically flat cusps (Figure 3.6).

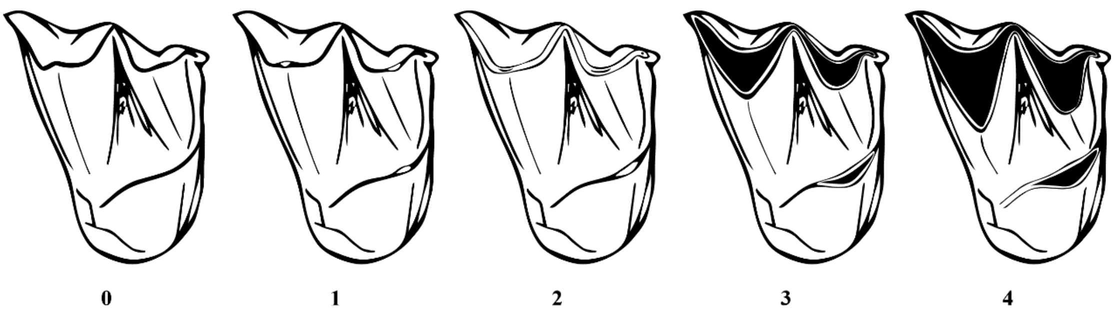

Figure 3.6 Age groups established according to the degree of wear of the chiropteran teeth. 0: Unworn (very young adults); 1: Slightly worn (young adults); 2: Worn (middle-aged adults); 3: Very worn (old adults); 4: Severely worn (very old adults). Modified after Sevilla (1986).

The statistical and the phenetic analysis were carried out in “PAST” (Hammer et al. 2001). For that purpose, the relative abundances of the identified taxa were quantified based on the number of the identified specimens (NISP) and the minimum number of individuals (MNI). Two – one for NISP and one for MNI – rarefaction curves were generated in order to investigate if the species richness corresponds well to the size of the assemblages. Additionally, a Kruskal-Wallis test was run in order to test the differences between the two chronologically different chiropteran faunas from Loutra Almopias Cave A. As the Kruskal-Wallis test does not assume normal distribution of the data, a Shapiro-Wilk test for normal distribution was also performed and visualised by normal probability plots. Moreover, the correlation of NISP and MNI was tested with a linear regression analysis. The interpretation of the results of the statistical analysis was based on Hammer and Harper (2006).

The chiropteran assemblages from Loutra Almopias Cave A were compared with other Late Pleistocene chiropteran assemblages from the Balkan Peninsula based on “Simpson’s Similarity Index” and “Pickford’s Index of Distance”.

CHAPTER 4. SYSTEMATIC PALAEONTOLOGY

CHIROPTERA Blumenbach, 1779

Chiroptera is the most diverse mammalian order after Rodentia, which currently includes at least 1100 extant species that occupy almost every corner of the Earth apart from the poles and some isolated islands (Simmons 2005a, 2005b).

4.1 FAMILY RHINOLOPHIDAE

Rhinolophidae Gray, 1825

Rhinolophidae, the Horseshoe Bats, comprise a single extant genus, *Rhinolophus*, which currently includes at least 77 extant species that span throughout most parts of Eurasia, Africa and Australia (Simmons 2005a). There is also a sole fossil genus, *Palaeonycteris*, with its earliest occurrence being *Palaeonycteris robustus* from the Early Miocene (or possibly late Oligocene) locality of Saint-Gérand-le-Puy, France (Amson 2021).

***Rhinolophus* Lacépède, 1799**

Type species *Vespertilio ferrum-equinum* Schreber, 1774

The earliest occurrence of *Rhinolophus* in the global fossil record is *Rhinolophus priscus* from the Late Eocene locality of Ste-Néboule, France (Sigé 1978), whereas the earliest occurrence of *Rhinolophus* in the fossil record of Greece is *Rhinolophus* gr. *delphinensis* from the Late Miocene locality of Elaiochoria 2, Chalkidiki (Hulva et al. 2007). There are currently five species occurring in Greece: *Rhinolophus ferrumequinum*, *Rhinolophus mehelyi*, *Rhinolophus blasii*, *Rhinolophus euryale* and *Rhinolophus hipposideros* (Hanák et al. 2001, Simmons 2005a, Sfougaris 2009). All of these species are also present in the fossil record of Greece (Piskoulis and Chatzopoulou in press), with the exception of *Rhinolophus euryale*, which is described for the first time from Loutra Almopias Cave A.

The dental formula of *Rhinolophus* is 1.1.2.3/2.1.3.3. There are several morphological characteristics that distinguish Rhinolophidae – and consequently *Rhinolophus* – from other chiropteran taxa, such as the attachment of premaxilla, which carries the upper incisors, only to the posterior part of the maxillary, whereas the presence of heel on the upper molars, the nyctalodont lower molars, the minute (and frequently displaced) third upper and lower premolar and the long and sharp styloid process of the humerus are common characteristics within European species. However, species discrimination within the genus is more complex, as all species share similar characteristics and thus, identification of fossils at species level is based almost exclusively on size.

Rhinolophus ferrumequinum **Schreber, 1774**

(Greater Horseshoe Bat)

Figure 4.2-3 and Figure A.53

Fossiliferous locality LAC I, LAC Ib, LAC Ic, LAC II, LAC III

Age Late Pleistocene

Material 787 identified specimens

LAC I: 1 right maxillary fragment with M1 (17285), 2 right C (17289, 17290), 3 left C (19934, 19983, 27498), 1 right P4 (19964), 1 left P4 (27501), 1 right M1 (17207), 2 left M1 (17208, 27463), 1 left M1-2 (17332), 2 left M2 (19959, 17206), 3 right M3 (19961, 27473, 27500), 1 left M3 (19980), 3 right c (19950, 19967, 17321), 3 left c (17336, 17223, 17319), 2 right p4 (17245, 19952), 1 left p4 (19978), 2 right m1-2 (27469, 27499), 3 right m2 (17210, 27487, 27507), 1 left m2 (19938), 2 right m3 (17287, 27474), 1 left m3 (16635), LAC Ib: 3 left C (17185, 16559, 19874), 1 right P4 (16507), 2 right M1 (17151, 19873), 2 left M1 (17180, 16563), 1 right M1-2 (19887), 2 right M2 (17152, 17181), 2 left M3 (17168, 19880), 1 right c (17159), 6 left c (17191, 16535, 16556, 19882, 19892, 27517), 1 left p2 (19870), 1 right m1 (17133), 1 left m1 (19875), 1 right m1-2 (17135), 1 left m1-2 (19872), 1 right m2 (16573), 1 left m2 (17170), 1 right m3 (16547), 1 left m3 (16435), LAC Ic: 2 right C (17956, 18049), 3 left C (17985, 17986, 18031), 7 right P4 (17895, 17896, 17982, 18046, 16417, 16418, 21456), 1 right M1 (21444), 1 left M2 (21445), 3 right c (17900, 18009, 21504), 1 left c (18050), 2 left p2 (17939, 18036), 3 right p4 (17880, 21495, 21498), 2 left p4 (17984, 21499), 1 left m1 (21474), 2 right m2 (18066, 21471), 1 left m2 (17878), 2 right m3 (17912, 16421), LAC II: 1 left maxillary fragment with P4-M3 (16679), 1 right maxillary fragment with P4-M1 (16380), 23 right C (21760, 21775, 21971, 22013, 22015, 22026, 22082, 22083, 22095, 22096, 22097, 22108, 22167, 22172, 22173, 22387, 27617, 27618, 27662, 27705, 27706, 27901, 27935), 18 left C (16074, 21763, 21774, 21782, 21791, 21796, 21801, 21963, 21970, 22014, 22084, 22171, 27708, 27721, 27724, 27816, 27904, 27910), 8 right P4 (21746, 21933, 22047, 22315, 27560, 27562, 27792, 27840), 6 left P4 (21838, 21755, 22001, 22043, 27573, 27698), 18 right

M1 (21712, 21728, 21960, 22006, 22142, 22145, 22263, 22275, 22277, 22278, 22287, 27650, 27651, 27652, 27691, 27717, 27867, 27868), 9 left M1 (16042, 21675, 21888, 22143, 22271, 22276, 22279, 27572, 27655), 1 right M1-2 (21934), 2 left M1-2 (27608, 27609), 14 right M2 (21896, 21899, 21900, 21959, 22073, 22140, 22144, 22262, 22265, 22266, 22282, 22284, 27733, 27734), 8 left M2 (21840, 21704, 21692, 22072, 22363, 22368, 22369, 27654), 6 right M3 (21733, 22042, 22079, 16384, 16385, 22302), 11 left M3 (16049, 21841, 21706, 22290, 22296, 27603, 27627, 27657, 27697, 27823, 27876), 1 right mandibular fragment (27782), 3 left mandibular fragments (27640, 27679, 27741), 1 left mandibular fragment with c, p2 and p4 (16673), 2 right mandibular fragments with m2-m3 (16144, 27582), 1 left mandibular fragment with m1-m3 (16169), 1 right mandibular fragment with m1-m2 (27713), 1 left i3 (27952), 19 right c (16069, 21783, 21879, 21951, 21953, 21966, 21989, 22020, 22050, 22090, 22187, 27587, 27613, 27629, 27660, 27809, 27912, 27916, 27946), 25 left c (16068, 21779, 21781, 21808, 21861, 21870, 21873, 21875, 21983, 21988, 22019, 22027, 22185, 22188, 22322, 22323, 27534, 27569, 27611, 27612, 27661, 27807, 27808, 27832, 27922), 2 left p2 (27621, 27667), 16 right p4 (21537, 21580, 21666, 21668, 21857, 16692, 22071, 22133, 16413, 27552, 27583, 27593, 27648, 27649, 27756, 27943), 16 left p4 (16067, 21563, 21591, 21956, 16354, 22003, 22057, 22135, 22385, 27524, 27531, 27672, 27732, 27780, 27895, 27898), 12 right m1 (21561, 21609, 21618, 21998, 22062, 22200, 16171, 27543, 27577, 27668, 27680, 27796), 14 left m1 (16033, 21649, 21853, 21856, 16349, 22068, 22122, 22125, 16400, 27527, 27528, 27547, 27755, 27765), 1 right m1-2 (27565), 2 left m1-2 (16403, 27595), 8 right m2 (21611, 21625, 21849, 22114, 16386, 16404, 27644, 27851), 7 left m2 (21585, 21648, 21968, 21997, 22036, 22224, 27594), 14 right m3 (21627, 21632, 21945, 21975, 16359, 16372, 22031, 22115, 22116, 22212, 16172, 27590, 27636, 27932), 17 left m3 (21535, 21636, 21851, 21996, 16145, 16152, 22235, 22240, 22350, 27550, 27682, 27683, 27684, 27685, 27764, 27803, 27850), <u>LAC III:</u> 25 right C (20191, 20194, 20195, 20205, 20280, 20281, 20283, 17488, 20850, 21357, 20916, 17860, 21013, 21017, 21196, 19149, 19341, 20063, 20569, 20570, 20572, 20684, 20685, 20686, 20688), 28 left C (20089, 20185, 20186, 20190, 20193, 20282, 20697, 21360, 21364, 21368, 17706a, 20932, 21026, 21097, 21099, 21104, 21197, 21205, 19342, 20076, 20084, 20085, 20311, 20376, 20475, 20477, 20568, 20687), 10 right P4 (20761, 17717, 20922, 21058, 19312, 20469, 20472, 20564, 20565, 20683), 12 left P4 (20835, 17485, 17487, 21342, 21344, 21351, 21356, 20872, 16448, 20923, 19313, 20052), 14 right M1 (20798, 21301, 21306, 20888, 20989, 21086, 21180, 19321, 20037, 20368, 20371, 20555, 20655, 20663), 8 left M1 (20842, 17691, 20892, 20030, 20031, 20459, 20666, 20671), 1 left M1-2 (20364), 7 right M2 (20276, 20747, 20796, 21307, 21314, 21334, 20987), 12 left M2 (20271, 20752, 20834, 17470, 21326, 17692, 20995, 21093, 21182, 19319, 20033, 20038), 11 right M3 (20170, 20171, 20802, 20804, 20805, 21315, 21316, 19327, 20465, 20676, 20677), 19 left M3 (20175, 20176, 20179, 20273, 20808, 17473, 20847, 20848, 21336, 21338, 17693, 20992, 19328, 20365, 20374, 20454, 20464, 20552, 20661), 7 right mandibular fragments (21238, 16437, 16446, 21063, 21147, 20326, 20330), 4 left mandibular fragments (20770, 21253, 21254, 20333), 1 right mandibular fragment with p4-m3 (17705), 1 left mandibular fragment with m1-m3 (21053), 1 right mandibular fragment with m1-m2 (21049), 2 right mandibular fragments with m2-m3 (21230, 20600), 2 left mandibular fragments with m2-m3 (21235, 20968), 1 left i2 (21441a), 38 right c (20095, 20126, 20188, 20196, 20197, 20203, 20207, 20284, 20285, 20694, 20698, 20762, 17489, 20853, 21367, 21377, 21382, 21386, 21398, 21403, 17709, 17710, 21019, 21023, 21100, 21101, 21103, 21106, 21125, 21192, 19297, 20072, 20377, 20379, 20480, 20577, 20578, 20691), 33 left c (20093, 20122, 20124, 20128, 20187, 20189, 20200, 20206, 20287, 20695, 20735, 20819, 20836, 20852, 20854, 20855, 21358, 17711, 21035, 21037, 21102, 21109, 19164, 19166, 19299, 21143, 20070, 20075, 20078, 20476, 20481, 20573, 20690), 12 right p2 (21418, 21423a, 20223, 21221, 20880, 20881, 17719, 20058, 20404, 20497, 20501, 20502), 16 left p2 (19137c, 21416, 21426a, 20219, 20222, 20225, 21411, 20882, 21139, 20008, 20054, 20314, 20315, 20403, 20405, 20596), 1 right/left p2 (21417), 16 right p4 (20163, 21287, 21289, 20866, 20961, 21002, 21052, 21075, 21081, 19132, 19133, 19134, 20045, 20348, 20541, 20643), 26 left p4 (20111, 20259, 20260, 20262, 20814, 20815, 17483, 17484, 21291, 21292, 21295, 21297, 20870, 21082, 21177, 21178, 19310, 20050, 20353, 20356, 20358, 20359, 20361, 20445, 20446, 20521), 17 right m1 (20146, 20149, 20231, 20775, 17477, 21227, 17697, 20907, 21067, 21141, 21155, 20015, 20335, 20421, 20422, 20423, 20623), 15 left m1 (20253, 20255, 20256, 20778, 20779, 17476, 17497, 21279, 17696, 21071, 21171, 19155, 20341, 20433, 20633), 5 right m1-2 (17701, 21159, 20043, 20619, 20621), 14 right m2 (20144, 20147, 20148, 20858, 21257, 21260, 21264, 17698, 17699, 21048, 21156, 19150, 20323, 20618), 7 left m2 (20143, 19153, 20020, 20022, 20325, 20334, 20535), 22 right m3 (20230, 20232, 20252, 17480, 17482, 21271, 20908, 20963, 21066, 21160, 21161, 19151, 19330, 20012, 20016, 20322, 20338, 20429, 20431, 20511, 20527, 20528), 12 left m3 (20742, 20782, 17481, 21236, 16462, 16451, 21167, 21169, 21172, 19332, 20007, 20023), 2 left humeri (20728, 20598)

Fossiliferous locality LAC Ia

Age latest Pleistocene

Material 741 identified specimens

1 right maxillary fragment with C and P4 (26527), 1 left maxillary fragment with C and P4 (19729), 1 left maxillary fragment with P4 (19731), 3 right maxillary fragments with P4-M1 (23130, 26515, 26516), 1 left maxillary fragment with P4-M1 (19754), 1 left maxillary fragment with P4-M2 (19740), 1 right maxillary fragment with M1 (23218), 1 left maxillary fragment with M2-M3 (23114), 2 right maxillary fragments with M3 (23173, 23178), 3 left maxillary fragments with M3 (23188, 23189, 23195), 48 right C (25444, 25463, 25493, 25509, 25514, 25529, 25537, 25541, 25550, 25569, 25578, 25583, 25590, 25591, 25594, 25595, 25647, 25686, 25710, 25715, 25742, 25777, 25791, 25812, 25835, 25852, 25862, 25863, 25875, 25885, 25887, 25888, 25897, 25908, 25912, 25919, 25953, 25978, 25989, 26033, 26206, 26238, 26264, 27060, 27064, 27066, 27074, 27082), 72 left C (25430, 25431, 25454, 25455, 25465, 25467, 25470, 25475, 25479, 25481, 25492, 25494, 25495, 25498, 25501, 25517, 25522, 25534, 25535, 25551, 25567, 25572, 25573, 25574, 25587, 25596, 25599, 25614, 25619, 25680, 25711, 25729, 25738, 25749, 25751, 25752, 25755, 25768, 25776, 25784, 25792, 25797, 25802, 25824, 25828, 25851, 25860, 25886, 25891, 25907, 25913, 25917, 25927, 25932, 25956, 26006, 26010, 26160, 26182, 26212, 26220, 26237, 26240, 26249, 27091, 27093, 27096, 27097, 27098, 27112, 27114, 27420), 18 right P4 (23269, 23270, 23273, 23274, 23276, 23280, 23281, 25226, 25240, 25251, 25265, 25285, 25313, 25338, 25341, 25346, 26519, 26520), 21 left P4 (23242, 23246, 23262, 25253, 25343, 25345, 25348, 25353, 25367, 25373, 25374, 25377, 25389, 25391, 25398, 25401, 25404, 25407, 25415, 26703, 26707), 1 right M1-2 (24665), 2 left M1-2 (24787, 24791), 22 right M1 (24381, 24388, 24396, 24400, 24401, 24416, 24418, 24432, 24433, 24435, 24436, 24469, 24477, 24481, 24500, 24502, 24509, 24522, 24556, 24557, 26557, 26560), 31 left M1 (23232, 24761, 24762, 24766, 24779, 24780, 24785, 24788, 24795, 24797, 24806, 24818, 24827, 24832, 24836, 24838, 24839, 24856, 24860, 24861, 24876, 24904, 24917, 24928, 24937, 24940, 24949, 24961, 24964, 26629, 27333), 17 right M2 (24377, 24385, 24426, 24445, 24452, 24460, 24462, 24479, 24504, 24512, 24523, 24527, 24531, 24538, 26575, 26597, 27240), 27 left M2 (23231, 24679, 24727, 24781, 24786, 24792, 24801, 24820, 24831, 24833, 24837, 24867, 24868, 24871, 24873, 24880, 24889, 24895, 24901, 24914, 24922, 24924, 24939, 24947, 26640, 26650, 27334), 23 right M3 (24986, 24988, 24993, 25127, 25129, 25140, 25141, 25142, 25143, 25148, 25152, 25153, 25154, 25159, 25161, 25162, 25165, 25169, 25172, 25196, 25205, 26611, 26613), 33 left M3 (24995, 24999, 25006, 25014, 25015, 25022, 25024, 25033, 25034, 25035, 25037, 25038, 25045, 25050, 25056, 25057b, 25058, 25059, 25064, 25065, 25069, 25081, 25086, 25087, 25095, 25096, 25106, 25109, 26538, 26540, 26671, 26672, 26680), 5 right mandibular fragments (22948, 22978, 22980, 22985, 26828), 7 left mandibular fragments (23026, 23028, 23039, 23044, 23050, 23066, 27294), 1 right mandibular fragment with i1 (22671), 1 left mandibular fragment with i2 and c-p2 (26818), 1 right mandibular fragment with c and p4-m1 (26725), 1 left mandibular fragment with c and p4-m1 (26788), 1 left mandibular fragment with c-p2 and p4-m2 (19658), 1 right mandibular fragment with p2-p4 (22661), 1 left mandibular fragment with p2 and p4-m2 (26782), 1 right mandibular fragment with p2 and p4-m3 (19634), 2 right mandibular fragments with p4 (19644, 19689), 5 left mandibular fragments with p4 (22627, 22776, 22781, 22795, 22802), 1 left mandibular fragment with p4 and m2 (19629), 3 left mandibular fragments with p4-m1 (22749, 22751, 22757), 3 left mandibular fragments with p4-m2 (19682, 19685, 22740), 4 right mandibular fragments with p4-m3 (19484, 19612, 22516, 22559), 2 left mandibular fragments with p4-m3 (19494, 19501), 3 right mandibular fragments with m1 (22534, 22542, 22677), 4 left mandibular fragments with m1 (22760, 22825, 22826, 22882), 3 left mandibular fragments with m1-m2 (19496,

22724, 22824), 3 right mandibular fragments with m1-m3 (22518, 22489, 22674), 2 left mandibular fragments with m1-m3 (22700, 22703), 4 right mandibular fragments with m2 (19693, 22578, 22488, 22680), 4 left mandibular fragments with m2 (19624, 22765, 22775, 22844), 4 right mandibular fragments with m2-m3 (22522, 22541, 22602, 26727), 3 left mandibular fragments with m2-m3 (22928, 22929, 22931), 7 right mandibular fragments with m3 (22462, 22577, 22599, 22479, 22633, 22642, 22686), 4 left mandibular fragments with m3 (22861, 22866, 22878, 22880), 2 right i3 (26365, 26375), 2 left i3 (26364, 26381), 50 right c (22668, 25456, 25510, 25548, 25592, 25630, 25631, 25633, 25645, 25651, 25671, 25682, 25688, 25703, 25728, 25731, 25762, 25766, 25767, 25808, 25810, 25813, 25832, 25838, 25855, 25895, 25954, 25958, 25979, 25991, 26011, 26032, 26069, 26126, 26130, 26155, 26162, 26191, 26203, 26216, 27131, 27138, 27139, 27146, 27147, 27155, 27157, 27162, 27432, 27433), 39 left c (25447, 25482, 25488, 25576, 25577, 25654, 25663, 25668, 25721, 25758, 25760, 25765, 25788, 25789, 25872, 25910, 25924, 25936, 25942, 25988, 26008, 26019, 26066, 26102, 26112, 26153, 26171, 26174, 26180, 26188, 26198, 26231, 26266, 27167, 27168, 27172, 27180, 27188, 27189), 2 right p2 (26325, 26329), 4 left p2 (26289, 26291, 26294, 26299), 21 right p4 (24181, 24187, 24190, 24198, 24202, 24210, 24212, 24226, 24232, 24234, 24237, 24242, 24243, 24258, 24263, 24265, 27031, 27033, 27038, 27249, 27402), 23 left p4 (24269, 24272, 24273, 24279, 24284, 24300, 24301, 24304, 24305, 24317, 24322, 24325, 24330, 24332, 24333, 24338, 24343, 24346, 24360, 24362, 26794, 27046, 27048), 2 right m1-2 (23431, 26915), 2 left m1-2 (23833, 26791), 40 right m1 (23331, 23333, 23339, 23356, 23370, 23376, 23399, 23309, 23315, 23318, 23415, 23420, 23425, 23436, 23476, 23477, 23483, 23489, 23491, 23501, 23503, 23504, 23537, 23544, 23550, 23551, 23553, 23556, 23560, 23583, 23584, 23599, 23607, 23620, 23669, 23673, 26908, 26912, 26920, 26927), 43 left m1 (23730, 23736, 23740, 23746, 23761, 23773, 23781, 23788, 23810, 23812, 23815, 23834, 23843, 23864, 23873, 23885, 23889, 23893, 23912, 23921, 23922, 23931, 23934, 23936, 23945, 23947, 23951, 23959, 23960, 23963, 23965, 23967, 23980, 23992, 24026, 24033, 24034, 24039, 24040, 24046, 26953, 26957, 26975), 21 right m2 (23348, 23360, 23396, 23400, 23401, 23403, 23311, 23411, 23422, 23432, 23456, 23463, 23466, 23502, 23547, 23549, 23590, 26868, 26873, 26905, 26926), 22 left m2 (23744, 23756, 23794, 23805, 23808, 23827, 23828, 23841, 23844, 23856, 23871, 23887, 23900, 23903, 23904, 23948, 23949, 23956, 24002, 26969, 26987, 27374), 21 right m3 (23338, 23352, 23355, 23310, 23414, 23423, 23430, 23505, 23605, 23626, 23645, 23682, 23710, 23716, 23718, 26736, 26743, 26932, 26933, 27367, 27368), 34 left m3 (23846, 23848, 23851, 23868, 23995, 24010, 24065, 24080, 24081, 24083, 24096, 24108, 24119, 24120, 24121, 24122, 24125, 24133, 24136, 24137, 24139, 24141, 24145, 24152, 24161, 24166, 24168, 24169, 24170, 26995, 27009, 27016, 27395, 27397), 1 right humerus (27450), 1 left humerus (26459)

Measurements Table 4.1 and Figure 4.1

Description *Rhinolophus ferrumequinum* is the largest member of the five Horseshoe Bat species that currently occur in Greece.

C: Very robust tooth with the cusp curved distally. It is trapezoidal in occlusal view. The crown forms an obtuse angle with the root. A heel is present at the lingual part of the tooth. The crown is relatively sharp lingually. A longitudinal groove occurs at the labial side of the tooth. The cingulum is thick and concave at its mesiolabial, distolabial and distolingual parts and convex at its mesial, labial, distal and lingual parts, with its maximum thickness at its mesiolingual part.

P4: Very robust tooth, with the cusp being connected with a crista to an accessory distolabial cusplet, which is imperceptibly curved. It is trapezoidal in occlusal view. A well-developed heel is present at the lingual part of the tooth. The crown, which is mildly constricted at its middle part, is relatively sharp lingually. The cingulum is thick and concave at its mesial, labial (strongly marked) and distal (strongly marked) parts and convex at its mesiolabial, distolabial and mesiolingual parts, with its maximum thickness at the mesial part of the heel.

Table 4.1 *Rhinolophus ferrumequinum*, Loutra Almopias Cave A. Measurements (in mm) from both LAC and LAC Ia. LAC: Late Pleistocene; LAC Ia: latest Pleistocene; n: number of measurable specimens; L: length; W: width; trgd: trigonid; tld: talonid; MEAN: average; MIN: minimum; MAX: maximum; SD: standard deviation; CV: coefficient of variation.

			n	**MEAN**	**MIN**	**MAX**	**SD**	**CV**
C	LAC	L	106	2.17	1.73	2.45	0.138	6.365
		W	106	1.63	1.11	1.93	0.136	8.331
	LAC Ia	L	119	1.97	1.76	2.23	0.084	4.256
		W	119	1.44	1.17	1.68	0.086	5.988
P4	LAC	L	47	1.47	1.30	1.66	0.070	4.746
		W	14	2.17	2.00	2.39	0.107	4.925
	LAC Ia	L	44	1.39	1.23	1.54	0.072	5.177
		W	37	1.84	1.66	2.07	0.107	5.800
M1	LAC	L	43	2.16	1.94	2.47	0.117	5.415
		W	45	2.22	1.91	2.67	0.167	7.523
	LAC Ia	L	60	1.99	1.79	2.17	0.091	4.600
		W	60	1.99	1.67	2.36	0.109	5.461
M2	LAC	L	39	2.04	1.68	2.20	0.128	6.289
		W	41	2.18	1.81	2.49	0.162	7.419
	LAC Ia	L	44	1.90	1.73	2.05	0.077	4.085
		W	43	2.01	1.76	2.26	0.120	5.936
M3	LAC	L	49	1.66	1.38	1.92	0.097	5.839
		W	49	2.15	1.85	2.35	0.108	5.025
	LAC Ia	L	61	1.58	1.38	1.75	0.069	4.370
		W	62	1.98	1.77	2.17	0.086	4.321
i2	LAC	L	1	0.64	-	-	-	-
		W	1	0.45	-	-	-	-
	LAC Ia	L	1	0.66	-	-	-	-
		W	1	0.50	-	-	-	-
i3	LAC	L	1	0.65	-	-	-	-
		W	1	0.42	-	-	-	-
	LAC Ia	L	5	0.66	0.61	0.69	0.032	4.892
		W	5	0.48	0.39	0.59	0.077	15.963
c	LAC	L	127	1.12	0.84	1.32	0.097	8.649
		W	129	1.51	1.09	1.77	0.110	7.264
	LAC Ia	L	93	1.03	0.90	1.20	0.071	6.897
		W	93	1.35	1.20	1.57	0.073	5.419
p2	LAC	L	35	0.95	0.81	1.07	0.059	6.215
		W	33	1.14	0.84	1.27	0.086	7.517
	LAC Ia	L	10	0.82	0.51	0.95	0.123	15.056
		W	9	0.94	0.56	1.06	0.149	15.925

p3	LAC Ia	L	1	0.30	-	-	-	-
		W	1	0.27	-	-	-	-
p4	LAC	L	81	1.30	1.12	1.43	0.063	4.897
		W	80	1.24	0.95	1.39	0.080	6.470
	LAC Ia	L	65	1.19	0.94	1.35	0.061	5.123
		W	66	1.09	0.83	1.26	0.080	7.357
m1	LAC	L	67	2.25	1.90	2.50	0.106	4.730
		W (trgd)	70	1.26	1.00	1.48	0.096	7.655
		W (tld)	76	1.35	1.09	1.55	0.090	6.667
	LAC Ia	L	116	2.09	1.87	2.27	0.075	3.586
		W (trgd)	117	1.13	0.92	1.35	0.085	7.524
		W (tld)	115	1.25	1.06	1.42	0.073	5.841
m2	LAC	L	49	2.19	2.01	2.35	0.074	3.389
		W (trgd)	51	1.31	1.08	1.48	0.095	7.229
		W (tld)	53	1.36	1.11	1.55	0.097	7.099
	LAC Ia	L	77	2.04	1.86	2.18	0.064	3.122
		W (trgd)	78	1.20	1.01	1.51	0.085	7.131
		W (tld)	76	1.28	1.11	1.49	0.077	6.010
m3	LAC	L	78	2.01	1.75	2.15	0.091	4.504
		W (trgd)	80	1.24	0.95	1.42	0.092	7.413
		W (tld)	79	1.06	0.77	1.35	0.098	9.186
	LAC Ia	L	85	1.88	1.72	2.09	0.075	3.992
		W (trgd)	85	1.15	0.95	1.38	0.082	7.180
		W (tld)	85	0.98	0.78	1.38	0.094	9.559
M1-M3	LAC	L	1	5.74	-	-	-	-
P4-M3	LAC	L	1	7.15	-	-	-	-
m1-m3	LAC	L	1	6.45	-	-	-	-
	LAC Ia	L	9	5.97	5.75	6.23	0.141	2.362
p4-m3	LAC	L	1	7.87	-	-	-	-
	LAC Ia	L	4	7.13	6.81	7.32	0.230	3.230
c-p4	LAC	L	1	3.19	-	-	-	-
	LAC Ia	L	2	2.98	2.96	2.99	0.021	0.713
Humerus	LAC	W	2	5.35	5.32	5.38	0.042	0.793
	LAC Ia	W	2	4.95	4.87	5.02	0.106	2.145

M1: Very robust tooth. It is subrectangular in occlusal view. Well-developed semicircular heel at the distolingual part of the tooth, without a hypocone. Parastyle, mesostyle, metastyle, paracone and metacone are well-developed. The metacone is slightly taller than the paracone. The parastyle forms an angle with the preparacrista. The mesial part of the ectoloph is narrower than the distal part. Additionally, the paracone and the cristae on both sides form a more obtuse angle than the metacone and the respective cristae. Paraloph, metaloph, paraconule and metaconule are absent. The distal and lingual cingulum, which are of average thickness, are absent beneath the metastyle and the anterior part of the triangular protocone. The anterior cingulum is only present at the mesiolingual part of the tooth.

M2: Not well-developed heel at the distolingual part of the tooth. The paracone and the cristae on both sides form a wider angle than the metacone and the respective cristae. The rest of the characters as M1.

M3: Very robust tooth. It is triangular in occlusal view. The heel is absent. Parastyle, mesostyle, paracone and metacone are well-developed, whereas the metastyle is absent. The postmetacrista that connects the mesostyle with the metacone is very short (practically absent). The metacone is slightly taller than the paracone. The parastyle forms an angle with the preparacrista. Paraloph, metaloph, paraconule and metaconule are absent. Both the anterior and distal cingulum are very thin and only present beneath the protocone, which is less triangular than in M1 and M2.

i2: Oval in occlusal view. Three cusps are present at the labial part of the tooth and a fourth accessory cusplet at the lingual. The posterior cusp is smaller than the middle cusp and the anterior is the smallest of the three.

i3: A fourth accessory cusplet is present at the distolingual part of the tooth. The posterior and the middle cusps are of approximately equal size and larger than the anterior cusp. The rest of the characters as for i2.

c: Very robust tooth with the cusp slightly curved distally. It is semicircular in occlusal view. It is convex mesially and concave distally. The distal part of the tooth is developed at the base of the crown, whereas the mesial part is developed in height. Respectively, the crown is in a more superior position towards the anterior part of the tooth. The distolabial part of the tooth is situated lower than the distolingual, which is higher than the former. The cingulum is of average thickness throughout the whole tooth. It reaches its maximum thickness at the labial/distolabial part of the tooth and its minimum at the mesial part, where it comes in contact with i3.

p2: Unicuspid. It is oval in occlusal view. It is convex at its mesial, labial, distal and lingual parts with the mesial and distal being relatively sharp. The labial part is elongated and narrow, whereas the lingual is short and wide. The cingulum is thin and uniform throughout the whole tooth.

p3: Unicuspid. It is circular in occlusal view. It is very slender and minute. It is placed on the labial side of the toothrow, compressed between the p2 and p4. Most frequently, it is lost in fossil mandibles that retain other teeth.

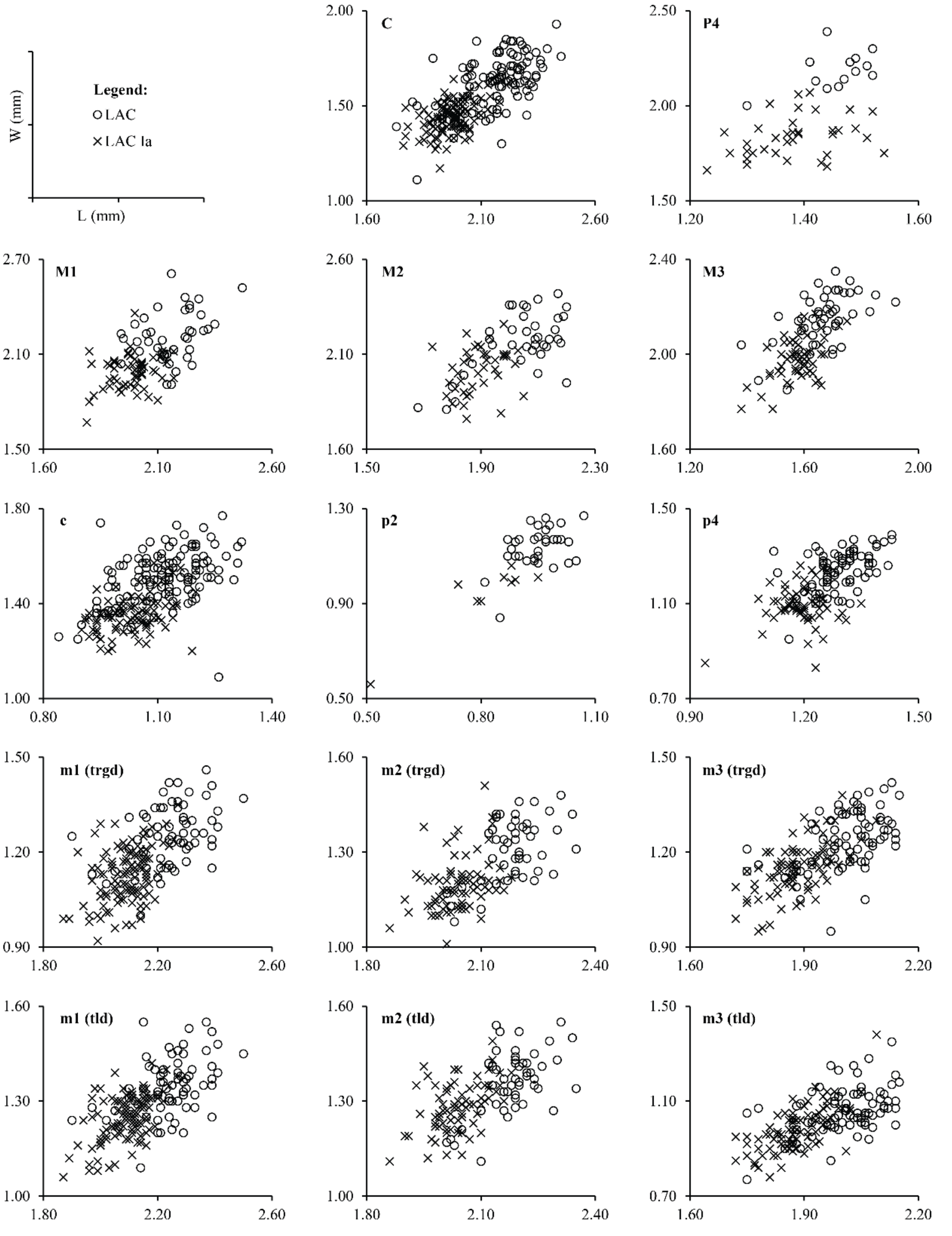

Figure 4.1 *Rhinolophus ferrumequinum*, Loutra Almopias Cave A. XY graphs with the measured (in mm) dental elements (C, P4, M1, M2, M3, c, p2, p4, m1, m2, m3). L: length, W: width, trgd: trigonid; tld: talonid.

p4: Robust tooth. It is trapezoidal in occlusal view. The mesiolingual part of the tooth is more elongated and higher than the mesiolabial part. The distolingual part of the tooth is higher than the distolabial. The cingulum is thin and uniform throughout the whole tooth and it bends down slightly at the level of each root, with the posterior convexity being placed slightly lower than the anterior.

m1: Nyctalodont. The trigonid is longer than the talonid. Paraconid, metaconid, entoconid, protoconid and hypoconid are well-developed. The protoconid is taller than the hypoconid. The paralophid is angular. The entocristid is curved. The hypoconulid is not as well-developed as the other cusps and it is positioned towards the labial part of the tooth. The labial cingulum is thin and uniform throughout the whole tooth. Lingual cingulum of the trigonid is also present.

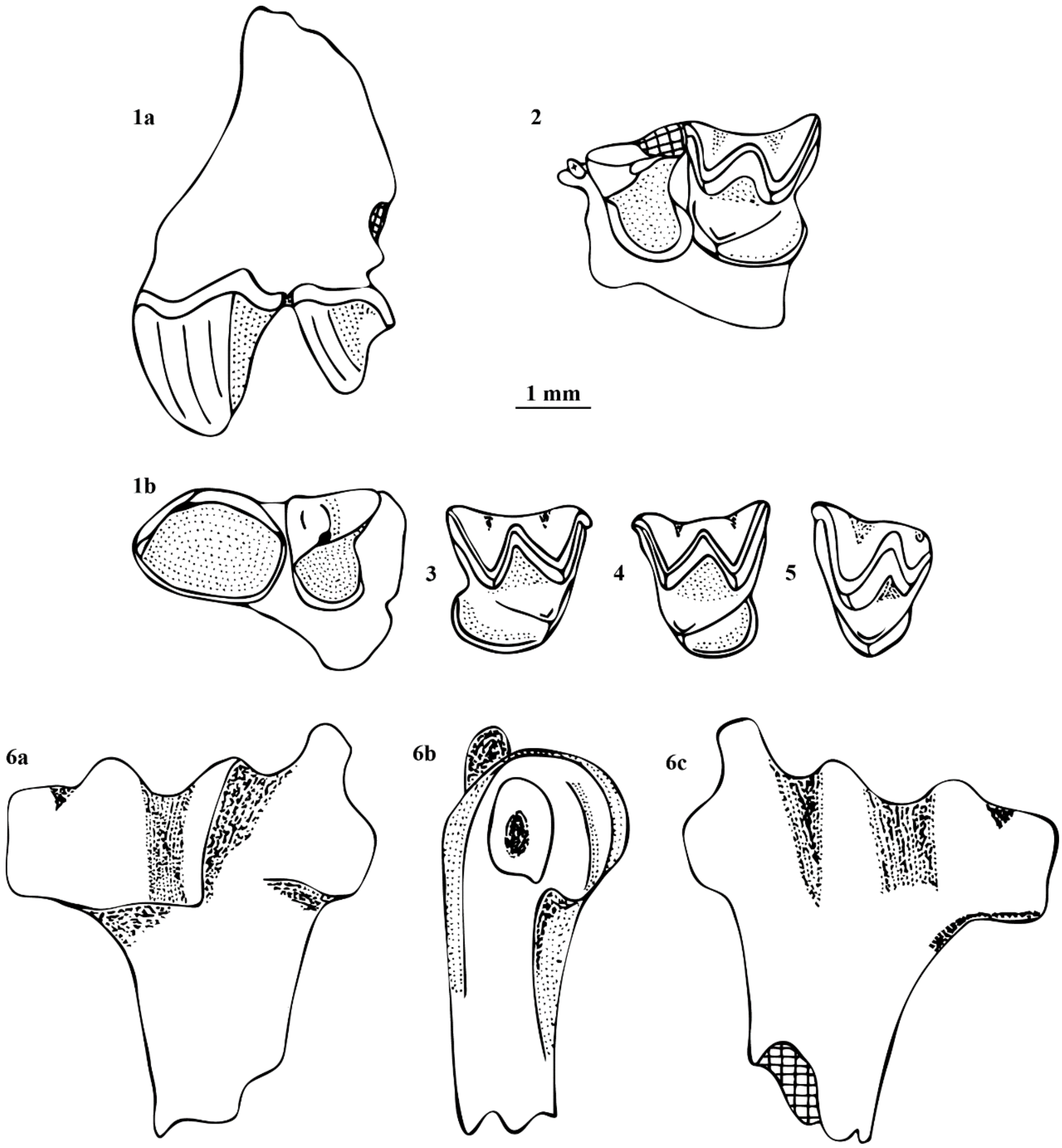

Figure 4.2 *Rhinolophus ferrumequinum*, Loutra Almopias Cave A. **1.** LAC19729 – Left maxillary fragment with C and P4 (**a.** labial, **b.** occlusal), **2.** LAC19754 – Left maxillary fragment with P3-M1, **3.** LAC17207 – Right M1, **4.** LAC17206 – Left M2, **5.** LAC17168 – Left M3, **6.** LAC26459 – Distal epiphysis of left humerus (**a.** anterior, **b.** lateral, **c.** posterior).

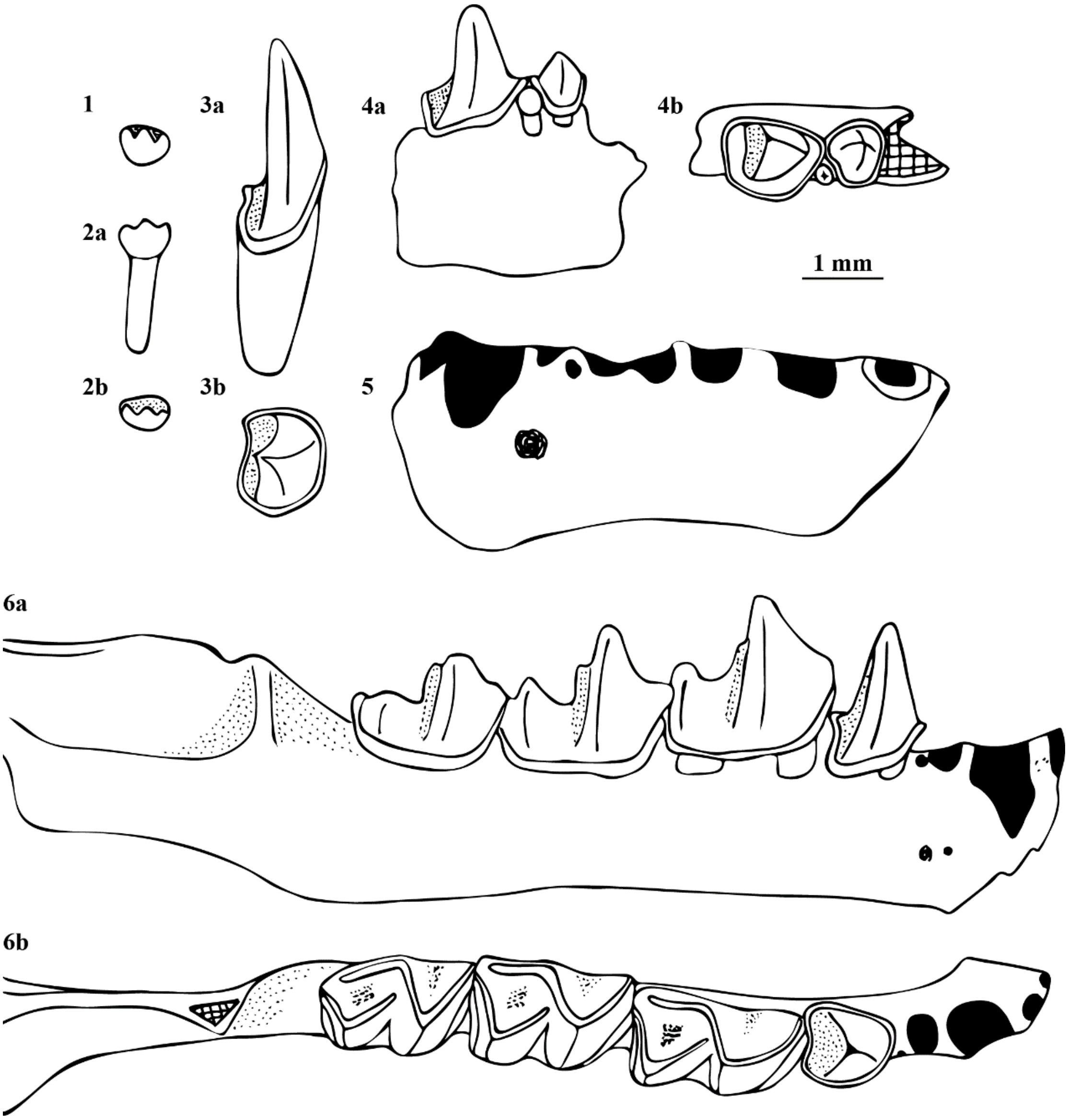

Figure 4.3 *Rhinolophus ferrumequinum*, Loutra Almopias Cave A. **1.** LAC27952 – Left i3, **2.** LAC21441a – Left i2 (**a.** labial, **b.** occlusal), **3.** LAC20694 – Right c (**a.** labial, **b.** occlusal), **4.** LAC22661 – Right mandibular fragment with p2-p4 (**a.** labial, **b.** occlusal), **5.** LAC20770 – Left mandibular fragment, **6.** LAC19484 – Right mandibular fragment with p4-m3 (**a.** labial, **b.** occlusal).

m2: The trigonid is not as long as in m1. The angle at the paralophid is more pronounced than in m1. The rest of the characters as m1.

m3: Nyctalodont. The trigonid is longer than the talonid. Paraconid, metaconid, entoconid, protoconid and hypoconid are well-developed. The protoconid is taller than the hypoconid. The paralophid is angular and more similar to m2. The entocristid is curved. The entoconid is on a more labial position than in the m1 or m2, so that the talonid is slightly narrower (the length remains more or less proportionate). The hypoconulid is slightly reduced. The labial cingulum is thin and uniform throughout the whole tooth. Lingual cingulum of the trigonid is absent.

Mandible: The coronoid process is relatively rounded and located higher, but not significantly, than the condyloid process. The anterior part of the masseter crest, which is thick, is relatively steep. The mandibular notch is relatively steep close to the coronoid process and flattens towards the condyloid process. The masseter crest is thin. The mental foramen is beneath the anterior part of p2. The lowest part of the symphysis is relatively rounded and projects downwards.

Humerus: The styloid process is long and sharp. The epitrochlea is very wide. A deep U-shaped valley is present between the trochlea and the condyle. A shallow valley is present between the condyle and the epicondyle. The condyle and the epicondyle are projecting laterally. The radial fossa and the olecranon fossa are very shallow (practically flat).

Discussion The morphological features described in addition to the measurements allow a definite attribution of the material to *Rhinolophus ferrumequinum*. It is the largest member of the five Horseshoe Bat species that currently occur in Greece and it is clearly distinguished from the rest of the species. Size differentiation between LAC and LAC Ia specimens is explained in detail in SECTION 5.6.

Occurrence Fossils of the Greater Horseshoe Bat are known only from Sarakenos Cave, Boeotia and Petralona Cave, Chalkidiki (viz. *Rhinolophus ferrumequinum topali*). Its modern distribution includes practically all mainland Greece and many islands (Hanák et al. 2001, GFDC 2021). On a global scale it is distributed from Northwestern Africa and the Iberian Peninsula up to Southeastern China, the Korean Peninsula and Japan (Simmons 2005a).

Ecology *Rhinolophus ferrumequinum* is a typical cave dweller and its habitat preferences include a diverse variety of (relatively) warm patches such as forests, pastures, meadows, etc. (Dietz et al. 2009).

Rhinolophus mehelyi Matschie, 1901

(Mehely's Horseshoe Bat)

Figure 4.6 and Figure A.54

Fossiliferous locality LAC I, LAC Ib, LAC Ic, LAC II, LAC III

Age Late Pleistocene

Material 191 identified specimens

<u>LAC I:</u> 1 left C (17226), 1 right M1 (17311), 1 left M1 (17331), 2 right M3 (19962, 17314), 2 right c (17243, 17222), 2 left c (17224, 17227), 2 right p4 (19958, 19977), 1 left p4 (19957), 1 right m1 (16641), 1 right m2 (19955), 2 left m2 (17257, 17211), 1 left m3 (19976), <u>LAC Ib:</u> 1 right P4 (16560), 1 left c (16533), 1 left m2 (19889), <u>LAC Ic:</u> 1 right M2 (21462), 1 left M3 (21465), 1 left c (21506), 1 left p4 (21501), 1 left humerus (21515), <u>LAC II:</u> 1 right maxillary fragment with C (21842), 1 right maxillary fragment with P4-M1 (27559), 3 left maxillary fragments with P4-M1 (16666, 16667, 27841), 2 right maxillary fragments with M2-M3 (16024, 16669), 3 right P4 (21749, 21750, 21752), 4 left P4 (16083, 21740, 22166, 27793), 3 right M1 (22358, 22367, 27866), 4 left M1 (16055, 21690, 22273, 27790), 1 right M2 (21898), 4 left M2 (21698, 21699, 27735, 27775), 4 right M3 (21730, 21942, 22297, 27874), 9 left M3 (21707, 21708, 21710, 22157, 22293, 22294, 22298, 22301, 27776), 1 right mandibular fragment with c and p4-m1 (21567), 1 left mandibular fragment with p4 (21583), 5 left mandibular fragments with p4-m1 (21584, 21589, 21837, 16661, 27847), 1 right mandibular fragment with p4-m3 (16192), 2 left mandibular fragments with p4-m3 (16715, 27843), 2 right mandibular fragments with m1-m2 (21826, 16136), 2 left mandibular fragments with m1-m2 (21582, 16678), 4 right mandibular fragments with m2-m3 (16394, 16396, 27633, 27777), 3 left mandibular fragments with m2-m3 (16357, 16398, 27845), 8 right c (16064, 16073, 16075, 21799, 21812, 21954, 21984, 22091), 11 left c (16080, 21548, 21549, 21772, 21950, 22099, 22182, 22186, 22326, 27554, 27703), 11 right p4 (21581, 21834, 21667, 21669, 21670, 21671, 21672, 22054, 22384, 27687, 27688), 7 left p4 (16134, 22138, 22386, 27553, 27781, 27894, 27933), 6 right m1 (16034, 21614, 21616, 21850, 22059, 22202), 4 left m1 (21644, 21647, 22035, 16141), 4 right m2 (16388, 21521, 16401, 27714), 3 left m2 (16031, 21562, 27883), 4 right m3 (16123, 16126, 16395, 27631), 5 left m3 (21642, 21835, 22069, 27670, 27849), 1 left humerus (27722), <u>LAC III:</u> 2 right maxillary fragments with M2-M3 (19326, 20009), 1 right C (21366), 1 right P4 (21340), 2 left P4 (21010, 20558), 1 right M1 (20793), 1 right M2 (20668), 1 left M2 (20548), 3 right M3 (20749, 17694, 20453), 1 left M3 (20035), 1 right mandibular fragment with p4-m1 (20960), 1 right mandibular fragment with p4-m2 (20764), 2 right mandibular fragments with m2-m3 (21228, 21050), 2 left mandibular fragments with m2-m3 (20966, 20324), 2 right c (21397, 21114), 3 left c (20826, 20080, 20486), 2 right p4 (20349, 20352), 2 left p4 (20227, 20416), 3 right m1 (21267, 20937, 20337), 1 left m1 (20634), 3 right m2 (17700, 17861, 20964), 3 left m2 (20027, 20637, 20639), 2 right m3 (21268, 20630), 2 left m3 (20745, 21170)

<u>Fossiliferous locality</u> LAC Ia

<u>Age</u> latest Pleistocene

<u>Material</u> 449 identified specimens

2 right maxillary fragments with C and P4 (23292, 23293), 1 left maxillary fragment with C-P4 (23299), 2 right maxillary fragments with P4 (19717, 27236), 1 left maxillary fragment with P4 (19728), 15 right maxillary fragments with P4-M1 (19751, 23122, 23123, 23125, 23126, 23128, 23129, 23132, 23160, 23161, 23163, 23164, 26513, 26514, 27231), 17 left maxillary fragments with P4-M1 (19713, 19716, 19723, 19724, 19727, 23137, 23139, 23140, 23141, 23149, 23152, 23153, 23154, 23155, 23157, 23158, 26542), 4 right maxillary fragments with P4-M2 (19739, 19769, 23121, 26512), 5 left maxillary fragments with P4-M2 (19759, 19762, 23133, 23135, 23136), 5 right maxillary fragments with P4-M3 (19753, 19756, 23073, 23074, 23075), 2 left maxillary fragments with P4-M3 (19770, 19772), 4 right maxillary fragments with M1 (23207, 23210, 23215, 23216), 4 left maxillary fragments with M1 (23208, 23212, 23214, 23219), 3 right maxillary fragments with M1-M2 (19749, 23087, 23088), 2 left maxillary fragments with M1-M2 (19742, 23085), 1 right maxillary fragment with M1-M3 (19768), 1 right maxillary fragment with M2 (23221), 3 left maxillary fragments with M2 (23204, 23205, 23211), 9 right maxillary fragments with M2-M3 (23090, 23091, 23092, 23093, 23098, 23099, 23100, 23101, 23102), 10 left maxillary fragments with M2-M3 (23103, 23104, 23105, 23106, 23107, 23108, 23112, 23117, 23118, 24983), 13 right maxillary fragments with M3 (23169, 23170, 23171, 23174, 23175, 23176, 23177, 23179, 23180, 23181, 23182, 23183, 23184), 6 left maxillary fragments with M3 (23187, 23191, 23192, 23193, 23194, 23196), 4 right C (25714, 25898, 27059, 27065), 1 left C (25922), 12 right P4 (23268, 23278, 25230, 25238, 25264, 25268, 25271, 25272, 25298, 25304, 25308, 26698), 10 left P4

(23244, 23245, 23259, 25380, 25387, 25388, 25396, 25427, 26711, 26717), 22 right M1 (24375, 24390, 24398, 24431, 24450, 24451, 24455, 24456, 24457, 24467, 24490, 24520, 24542, 24564, 24567, 24578, 24581, 24588, 24592, 24635, 24646, 24661), 16 left M1 (24681, 24742, 24746, 24751, 24755, 24769, 24809, 24875, 24930, 24933, 24942, 24962, 24963, 26622, 26652, 27336), 6 left M2 (24688, 24708, 24715, 24721, 24848, 24932), 4 left M3 (25013, 25026, 25053, 25107), 1 right mandibular fragment (19506), 1 left mandibular fragment (19533), 2 left mandibular fragments with i1 and c (22854, 22855), 1 left mandibular fragment with c (22858), 1 right mandibular fragment with c-p2 (22665), 1 right mandibular fragment with c and p4-m2 (22498), 1 left mandibular fragment with c-p2 and p4-m3 (27274), 2 left mandibular fragments with p2 (22696, 22853), 1 right mandibular fragment with p2 and p4-m1 (27252), 1 left mandibular fragment with p3-m3 (22720), 5 right mandibular fragments with p4 (22656, 22657, 22659, 22673, 22685), 3 left mandibular fragments with p4 (22786, 22787, 22788), 6 right mandibular fragments with p4-m1 (19664, 22538, 22586, 22593, 22672, 26762), 16 left mandibular fragments with p4-m1 (22744, 22746, 22759, 22768, 22769, 22770, 22779, 22783, 22790, 22791, 22794, 22798, 22799, 22805, 26778, 26787), 12 right mandibular fragments with p4-m2 (19490, 22456, 22457, 22461, 22517, 22551, 22564, 22600, 22487, 22683, 26737, 26747), 6 left mandibular fragments with p4-m2 (19500, 19650, 19652, 22736, 22742, 22806), 3 right mandibular fragments with p4-m3 (19620, 22455, 22504), 5 left mandibular fragments with p4-m3 (19503, 19505, 19678, 22699, 22714), 9 right mandibular fragments with m1 (22548, 22573, 22582, 22587, 22605, 22620, 22622, 22646, 22695), 7 left mandibular fragments with m1 (22763, 22764, 22817, 22819, 22831, 22845, 22850), 14 right mandibular fragments with m1-m2 (19692, 22460, 22465, 22536, 22537, 22546, 22557, 22572, 22583, 22471, 22481, 22495, 22623, 26729), 13 left mandibular fragments with m1-m2 (19623, 22731, 22732, 22734, 22735, 22737, 22726, 22727, 22808, 22818, 22829, 22830, 26771), 3 right mandibular fragments with m1-m3 (22464, 22485, 27260), 6 left mandibular fragments with m1-m3 (19504, 19631, 19711, 22698, 22705, 26801), 17 right mandibular fragments with m2 (19698, 22530, 22531, 22569, 22570, 22571, 22580, 22590, 22594, 22483, 22645, 22647, 22650, 22651, 22652, 22653, 22678), 13 left mandibular fragments with m2 (22747, 22766, 22811, 22820, 22823, 22832, 22833, 22838, 22840, 22885, 22891, 22937, 22942), 9 right mandibular fragments with m2-m3 (22467, 22501, 22547, 22592, 22596, 22612, 22478, 22482, 22644), 22 left mandibular fragments with m2-m3 (22897, 22898, 22899, 22905, 22910, 22911, 22913, 22914, 22916, 22925, 22926, 22927, 22933, 22935, 26784, 26785, 27277, 27287, 22886, 22887, 22888, 22890), 10 right mandibular fragments with m3 (22514, 22543, 22563, 22567, 22629, 22630, 22632, 22637, 22640, 22641), 16 left mandibular fragments with m3 (22862, 22865, 22870, 22872, 22873, 22875, 22879, 22881, 22892, 22893, 22894, 22901, 22904, 22918, 22922, 22924), 12 right c (25473, 25634, 25659, 25787, 25911, 26048, 26149, 26173, 26219, 27133, 27149, 27152), 12 left c (25439, 25640, 25858, 25859, 26023, 26132, 26139, 26177, 26259, 27170, 27182, 27434), 8 right p4 (24214, 24217, 24227, 24228, 24239, 24250, 24253, 24256), 5 left p4 (24319, 24364, 26799, 27052, 27272), 1 right m1 (26758), 1 left m1 (26947), 2 left m2 (23897, 23950), 2 right m3 (26930, 26936), 3 left m3 (24146, 26786, 26972), 7 right humeri (26479, 26480, 26482, 26488, 26494, 26497, 27449), 4 left humeri (26455, 26464, 26475, 27457)

Table of measurements Table 4.2 and Figure 4.4-5

Description *Rhinolophus mehelyi* is the largest member of the three medium-sized Horseshoe Bat species that currently occur in Greece.

C: Robust tooth with the cusp curved distally. It is trapezoidal in occlusal view. The crown forms an obtuse angle with the root. A heel is present at the lingual part of the tooth. The crown is relatively sharp lingually. The cingulum is thick and concave at its mesiolabial, distolabial and distolingual parts and convex at its mesial, labial, distal and lingual parts, with its maximum thickness at its labial part.

Table 4.2 *Rhinolophus mehelyi*, Loutra Almopias Cave A. Measurements (in mm) from both LAC and LAC Ia. LAC: Late Pleistocene; LAC Ia: latest Pleistocene; n: number of measurable specimens; L: length; W: width; trgd: trigonid; tld: talonid; MEAN: average; MIN: minimum; MAX: maximum; SD: standard deviation; CV: coefficient of variation.

			n	MEAN	MIN	MAX	SD	CV
C	LAC	L	2	1.60	1.55	1.65	0.071	4.419
		W	2	1.13	1.07	1.18	0.078	6.914
	LAC Ia	L	7	1.63	1.37	1.76	0.131	8.006
		W	7	1.22	1.10	1.31	0.081	6.636
P3	LAC Ia	L	1	0.37	-	-	-	-
		W	1	0.41	-	-	-	-
P4	LAC	L	15	1.06	0.88	1.32	0.100	9.431
		W	15	1.43	1.08	1.65	0.154	10.801
	LAC Ia	L	74	1.04	0.89	1.22	0.071	6.798
		W	73	1.32	1.06	1.74	0.134	10.129
M1	LAC	L	12	1.67	1.55	1.78	0.072	4.325
		W	12	1.58	1.32	1.82	0.148	9.363
	LAC Ia	L	95	1.58	1.32	1.79	0.071	4.510
		W	93	1.45	1.21	1.85	0.112	7.731
M2	LAC	L	12	1.59	1.34	1.67	0.093	5.841
		W	12	1.65	1.43	1.79	0.100	6.067
	LAC Ia	L	51	1.48	1.34	1.72	0.087	5.834
		W	50	1.51	1.32	1.74	0.100	6.585
M3	LAC	L	24	1.29	1.07	1.38	0.064	4.974
		W	24	1.62	1.42	1.75	0.081	4.977
	LAC Ia	L	50	1.17	1.03	1.29	0.069	5.899
		W	50	1.48	1.30	1.70	0.092	6.221
i2	LAC Ia	L	2	0.49	0.43	0.55	0.085	17.317
		W	2	0.27	0.24	0.29	0.035	13.342
i3	LAC Ia	L	2	0.46	0.41	0.51	0.071	15.372
		W	2	0.52	0.36	0.67	0.219	42.564
c	LAC	L	29	0.88	0.75	1.04	0.065	7.392
		W	29	1.14	1.09	1.24	0.042	3.649
	LAC Ia	L	30	0.87	0.73	0.97	0.053	6.138
		W	30	1.12	0.90	1.24	0.067	5.951
p2	LAC Ia	L	5	0.73	0.56	0.86	0.125	17.164
		W	5	0.72	0.59	0.80	0.080	11.076
p3	LAC Ia	L	1	0.35	-	-	-	-
		W	1	0.33	-	-	-	-
p4	LAC	L	39	1.01	0.88	1.14	0.055	5.493
		W	39	0.88	0.71	1.11	0.077	8.797
	LAC Ia	L	73	0.96	0.80	1.14	0.076	7.900
		W	73	0.83	0.55	1.00	0.114	13.821
m1	LAC	L	29	1.84	1.67	1.93	0.078	4.253
		W (trgd)	30	0.96	0.86	1.11	0.064	6.746
		W (tld)	29	1.02	0.86	1.11	0.065	6.379

	LAC Ia	L	101	1.73	1.37	1.90	0.091	5.257
		W (trgd)	103	0.92	0.67	1.13	0.078	8.476
		W (tld)	104	0.99	0.70	1.22	0.086	8.677
m2	LAC	L	31	1.68	1.53	1.81	0.074	4.414
		W (trgd)	34	0.96	0.81	1.13	0.069	7.161
		W (tld)	34	1.04	0.92	1.14	0.061	5.820
	LAC Ia	L	114	1.60	1.43	1.81	0.073	4.565
		W (trgd)	121	0.93	0.67	1.16	0.079	8.526
		W (tld)	119	1.00	0.82	1.19	0.071	7.128
m3	LAC	L	27	1.57	1.40	1.71	0.084	5.320
		W (trgd)	27	0.92	0.73	1.04	0.072	7.754
		W (tld)	26	0.83	0.63	0.93	0.064	7.673
	LAC Ia	L	80	1.47	1.32	1.67	0.075	5.123
		W (trgd)	80	0.89	0.70	1.10	0.074	8.367
		W (tld)	77	0.79	0.62	1.04	0.062	7.857
M1-M3	LAC Ia	L	8	4.09	3.97	4.25	0.104	2.555
P4-M3	LAC Ia	L	7	5.03	4.92	5.22	0.127	2.515
m1-m3	LAC	L	3	4.85	4.78	4.95	0.091	1.872
	LAC Ia	L	19	4.84	4.68	4.97	0.076	1.571
p4-m3	LAC	L	3	5.83	5.76	5.93	0.091	1.557
	LAC Ia	L	10	5.82	5.59	5.92	0.112	1.916
c-m3	LAC Ia	L	1	7.42	-	-	-	-
c-p4	LAC Ia	L	1	2.57	-	-	-	-
LSC	LAC	L	2	12.17	12.00	12.34	0.240	1.976
	LAC Ia	L	2	12.02	11.93	12.10	0.120	1.000
Humerus	LAC	W	2	4.52	4.49	4.55	0.042	0.939
	LAC Ia	W	11	4.47	4.02	4.71	0.212	4.752

P3: Unicuspid. It is circular in occlusal view. It is very slender and minute. It is in line with the main axis of the toothrow and frequently lost in fossil material.

P4: Robust tooth with the cusp being connected with a crista to an accessory distolabial cusplet, which is imperceptibly curved. It is subrectangular in occlusal view. A well-developed heel is present at the lingual part of the tooth. The crown, which is mildly constricted at its middle part, is relatively sharp lingually. The cingulum is of average thickness and concave at its mesial, labial and distal (strongly marked) parts and convex at its mesiolabial, distolabial and mesiolingual parts, with its maximum thickness at the mesial part of the heel. An accessory cusplet-like structure is present at the mesiolabial part of the tooth, where it comes into contact with P3.

M1: Robust tooth. It is subrectangular in occlusal view. Semicircular to subtriangular heel at the distolingual part of the tooth, which is not as well-developed as in *Rhinolophus ferrumequinum*, without hypocone. Parastyle, mesostyle, metastyle, paracone and metacone are well-developed. The metacone is slightly taller than the paracone. The parastyle forms an angle with the preparacrista. The mesial part of the ectoloph is narrower than the distal part. Additionally, the paracone and the cristae on both sides form a wider angle than the metacone and the respective cristae. Paraloph, metaloph, paraconule and metaconule are absent. The distal and lingual cingulum, which are of average thickness, are absent beneath the metastyle and the triangular protocone. The anterior cingulum is only present at the mesiolingual part of the tooth. The maximum thickness of the cingulum is at the lowest part of the heel.

M2: It is subtriangular in occlusal view. The heel is reduced to a point that only the cingulum is visible. The metacone and the cristae on both sides form an acuter angle than in M1. The rest of the characters as M1.

M3: Robust tooth. It is triangular in occlusal view. Parastyle, mesostyle, paracone and metacone are well-developed, whereas the metastyle is absent. The postmetacrista that connects the mesostyle with the metacone is very short (practically absent). The metacone and the paracone are approximately of the same height with the former slightly taller than the latter. The parastyle forms an angle with the preparacrista. Paraloph, metaloph, paraconule and metaconule are absent. Both the anterior and distal cingulum are very thin and only present beneath the protocone, which is less triangular than in M1 and M2.

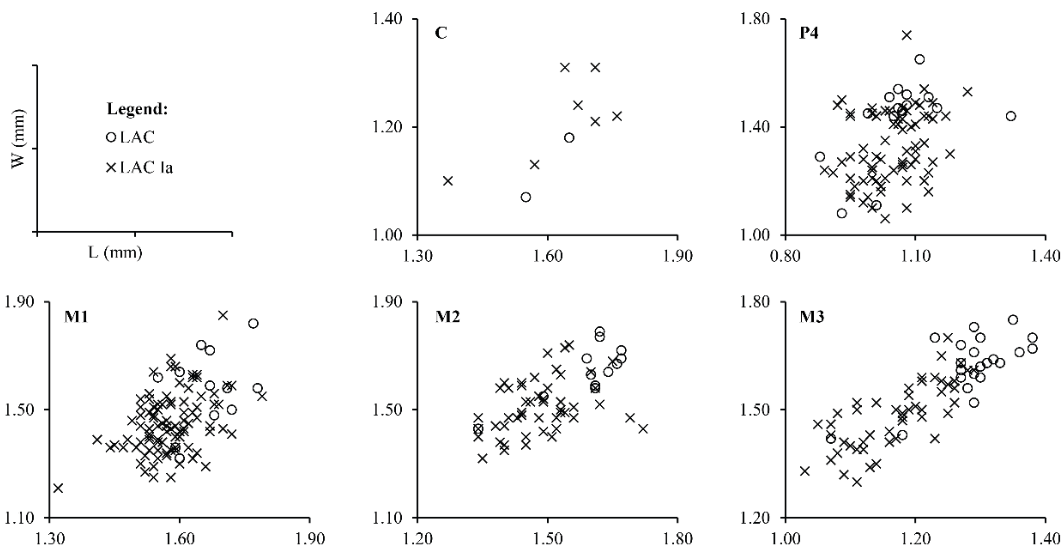

Figure 4.4 *Rhinolophus mehelyi*, Loutra Almopias Cave A. XY graphs with the measured (in mm) dental elements (C, P4, M1, M2, M3). L: length, W: width.

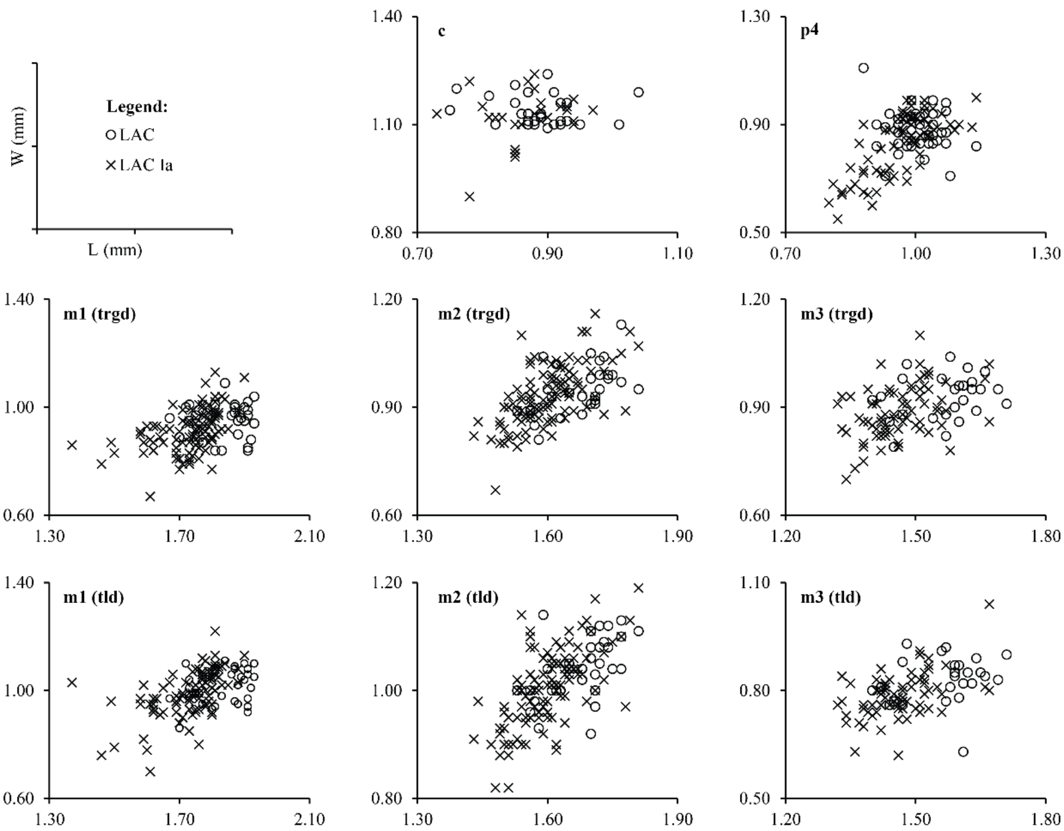

Figure 4.5 *Rhinolophus mehelyi*, Loutra Almopias Cave A. XY graphs with the measured (in mm) dental elements (c, p4, m1, m2, m3). L: length, W: width, trgd: trigonid; tld: talonid.

i2: Oval in occlusal view. Three cusps are present at the labial part of the tooth. The posterior cusp is somewhat sharper than the rest.

i3: Oval in occlusal view. Three cusps are present at the labial part of the tooth and a fourth accessory cusplet at its distolingual part. The middle cusp is the largest.

c: Robust tooth with the cusp slightly curved lingually. It is semicircular in occlusal view. It is convex mesially and concave distally. The distal part of the tooth is present at the base of the crown, whereas the mesial part is developed in height. Respectively, the crown is in a more superior position towards the anterior part of the tooth. The distolabial part of the tooth is situated lower than the distolingual, which is higher than the former. The cingulum is thin throughout the whole tooth and it reaches its maximum thickness at the labial/distolabial part of the tooth and its minimum at the mesial part, where it comes in contact with i3.

p2: Unicuspid. It is oval in occlusal view. The cusp is convex at its mesial, labial, distal and lingual parts with the mesial and distal edges being relatively sharp. The labial part is elongated and narrow, whereas the lingual short and wide. The cingulum is thin and uniform throughout the whole tooth.

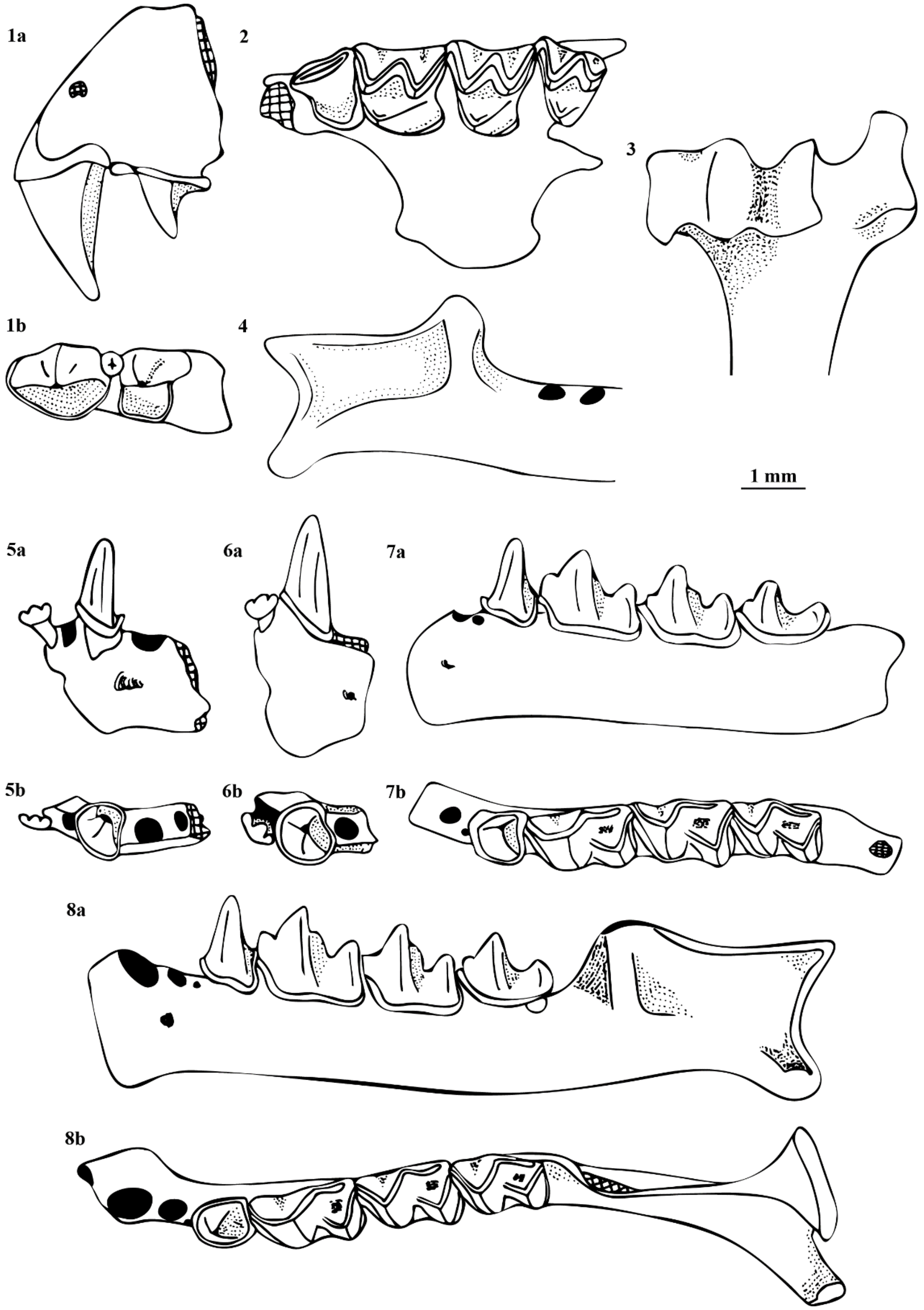

Figure 4.6 *Rhinolophus mehelyi*, Loutra Almopias Cave A. **1.** LAC23299 – Left maxillary fragment with C-P4 (**a.** labial, **b.** occlusal), **2.** LAC19722 – Left maxillary fragment with P4-M3, **3.** LAC21515 – Distal epiphysis of left humerus, **4.** LAC19506 – Left mandibular fragment, **5.** LAC22854 – Left mandibular fragment with i2 and c (**a.** labial, **b.** occlusal), **6.** LAC22855 – Left mandibular fragment with i3-c (**a.** labial, **b.** occlusal), **7.** LAC16715 – Left mandibular fragment with p4-m3 (**a.** labial, **b.** occlusal) **8.** LAC27843 – Left mandibular fragment with p4-m3 (**a.** labial, **b.** occlusal).

p3: Unicuspid. It is circular in occlusal view. It is very slender and minute. It is placed on the labial side of the toothrow, compressed between the p2 and p4. Most frequently, it is lost in fossil mandibles that retain other teeth.

p4: Robust tooth. It is trapezoidal in occlusal view. The mesiolingual part of the tooth is more elongated and higher than the mesiolabial part. The distolingual part of the tooth is higher than the distolabial. The cingulum is thin and uniform throughout the whole tooth and it bends down slightly at the level of each root, with the posterior convexity being placed slightly lower than the anterior.

m1: Nyctalodont. The trigonid is longer than the talonid. Paraconid, metaconid, entoconid, protoconid and hypoconid are well-developed. The protoconid is taller than the hypoconid. The paralophid is angular. The entocristid is curved. The hypoconulid is not as well-developed as the other cusps and it is positioned towards the labial part of the tooth. The labial cingulum is thin and uniform throughout the whole tooth. Lingual cingulum of the trigonid is also present, but hard to observe.

m2: The trigonid is not as long as in m1. The lingual cingulum of the trigonid is harder to observe than in m1. The rest of the characters as m1.

m3: Nyctalodont. The trigonid is longer than the talonid. Paraconid, metaconid, entoconid, protoconid and hypoconid are well-developed. The protoconid is taller than the hypoconid. The paralophid is angular and more similar to m2. The entocristid is curved. The entoconid is more towards the labial side of the tooth and thus, the talonid is reduced. The hypoconulid is reduced. The labial cingulum is thin and uniform throughout the whole tooth. Lingual cingulum of the trigonid is also present, but hard to observe.

Mandible: The coronoid process is relatively rounded and located higher, but not significantly, than the condyloid process. The anterior part of the masseter crest, which is relatively thick, is relatively steep. The mandibular notch is relatively steep to smooth close to the coronoid process and flattens towards the condyloid process. The angular process is elongated. The masseter crest is relatively thick. The mental foramen is beneath the anterior part of p2. The lowest part of the symphysis is relatively rounded and projects downwards.

Humerus: The styloid process is long and sharp. The epitrochlea is very wide. A deep U-shaped valley is present between the trochlea and the condyle. A shallow valley is present between the condyle and the epicondyle. The condyle and the epicondyle are projecting laterally. The radial fossa and the olecranon fossa are very shallow (practically flat).

Discussion The morphological features described in addition to the measurements allow a definite attribution of the material to *Rhinolophus mehelyi*. It is the largest member of the three medium-sized Horseshoe Bat species that currently occur in Greece and as its size range overlaps both *Rhinolophus blasii* and *Rhinolophus euryale*, only the largest specimens can be clearly distinguished.

Occurrence Fossils of the Mehely's Horseshoe Bat are known only from Petralona Cave, Chalkidiki. Its modern distribution includes Northeastern and Central Greece, Peloponnese and Lesvos Island (Hanák et al. 2001, GFDC 2021). On a global scale it is distributed in Northern Africa, the Iberian Peninsula and France, the Balkan Peninsula and several Mediterranean Islands, Transcaucasia, Turkey, Israel and Jordan, Iran, Iraq and Afghanistan (Simmons 2005a).

Ecology *Rhinolophus mehelyi* is a typical cave dweller and its habitat preferences include a diverse variety of low vegetation areas such as (semi-)steppes, meadows, etc. and in some cases more forested areas (Dietz et al. 2009).

Rhinolophus blasii Peters, 1866

(Blasius's Horseshoe Bat)

Figure 4.8 and Figure A.55

Fossiliferous locality LAC I, LAC Ib, LAC II, LAC III

Age Late Pleistocene

Material 16 identified specimens

LAC I: 1 right humerus (27954), LAC Ib: 1 left humerus (16590), LAC II: 1 right mandibular fragment with c-p2 (21560), 3 right p4 (21662, 22243, 27626), 1 left p4 (22055), 1 left humerus (27818), LAC III: 1 right mandibular fragment with p4-m1 (20959), 3 right p4 (21078, 21175, 20442), 3 left p4 (20263, 20942, 21006), 1 left humerus (20599)

Fossiliferous locality LAC Ia

Age latest Pleistocene

Material 43 identified specimens

1 right mandibular fragment with m2 (19492), 1 left mandibular fragment with m2-m3 (19708), 5 right p4 (24208, 24219, 24222, 24223, 24260), 6 left p4 (24275, 24276, 24278, 24348, 24356, 24361), 14 right humeri (26481, 26483, 26485, 26486, 26487, 26490, 26491, 26492, 26493, 26495, 26496, 26498, 26499, 26502), 16 left humeri (26454, 26456, 26457, 26458, 26460, 26461, 26465, 26466, 26469, 26470, 26472, 26474, 26477, 27220, 27226, 27229)

Measurements Table 4.3 and Figure 4.7

Description *Rhinolophus blasii* is the intermediate member of the three medium-sized Horseshoe Bat species that currently occur in Greece.

c: A cingular platform is present at the mesiolingual part of the tooth. The rest of the characters as for *Rhinolophus mehelyi*.

p2: As for *Rhinolophus mehelyi*.

p4: The mesiolingual part of the tooth is less developed than *Rhinolophus mehelyi*. The lingual part of the tooth is practically straight in occlusal view. The rest of the characters as for *Rhinolophus mehelyi*.

Table 4.3 *Rhinolophus blasii*, Loutra Almopias Cave A. Measurements (in mm) from both LAC and LAC Ia. LAC: Late Pleistocene; LAC Ia: latest Pleistocene; n: number of measurable specimens; L: length; W: width; trgd: trigonid; tld: talonid; MEAN: average; MIN: minimum; MAX: maximum; SD: standard deviation; CV: coefficient of variation.

			n	**MEAN**	**MIN**	**MAX**	**SD**	**CV**
c	LAC	L	1	0.81	-	-	-	-
		W	1	0.87	-	-	-	-
p2	LAC	L	1	0.85	-	-	-	-
		W	1	0.76	-	-	-	-
p4	LAC	L	11	0.89	0.78	0.99	0.058	6.574
		W	11	0.74	0.69	0.83	0.040	5.344
	LAC Ia	L	11	0.91	0.85	0.99	0.035	3.807
		W	11	0.71	0.57	0.80	0.063	8.859
m1	LAC	L	1	1.67	-	-	-	-
		W (trgd)	1	0.95	-	-	-	-
		W (tld)	1	0.94	-	-	-	-
m2	LAC Ia	L	2	1.52	1.49	1.54	0.035	2.334
		W (trgd)	2	0.89	0.88	0.90	0.014	1.589
		W (tld)	2	0.98	0.98	0.98	0.000	0.000
m3	LAC Ia	L	1	1.38	-	-	-	-
		W (trgd)	1	0.84	-	-	-	-
		W (tld)	1	0.76	-	-	-	-
Humerus	LAC	L	-	-	-	-	-	-
		W	3	4.06	4.00	4.09	0.052	1.280
	LAC Ia	L	2	26.39	26.30	26.48	0.127	0.482
		W	30	3.94	3.73	4.13	0.103	2.616

m1: The entocristid is less curved than in *Rhinolophus mehelyi*. The labial cingulum is slightly concave at its middle part. The rest of the characters as for *Rhinolophus mehelyi*.

m2: As for *Rhinolophus mehelyi*.

m3: The trigonid and the talonid are of almost equal length. The entoconid is more towards the labial side of the tooth and thus, the talonid is reduced, but less than in *Rhinolophus mehelyi*. The lingual cingulum of the trigonid is absent. The rest of the characters as for *Rhinolophus mehelyi*.

Mandible: The coronoid process is sharper than in *Rhinolophus mehelyi*. A minute convexity is present at the distal part of the mandibular notch. The mental foramen is beneath the middle part of p2. The rest of the characters as for *Rhinolophus mehelyi*.

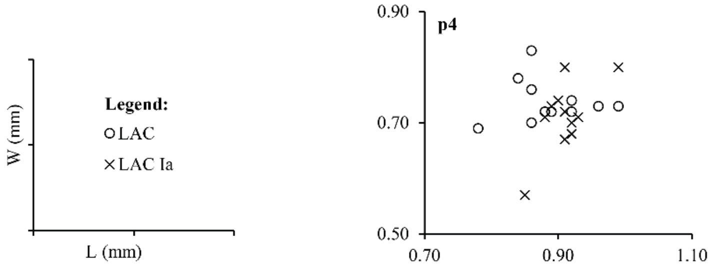

Figure 4.7 *Rhinolophus blasii*, Loutra Almopias Cave A. XY graphs with the measured (in mm) dental elements (p4). L: length, W: width.

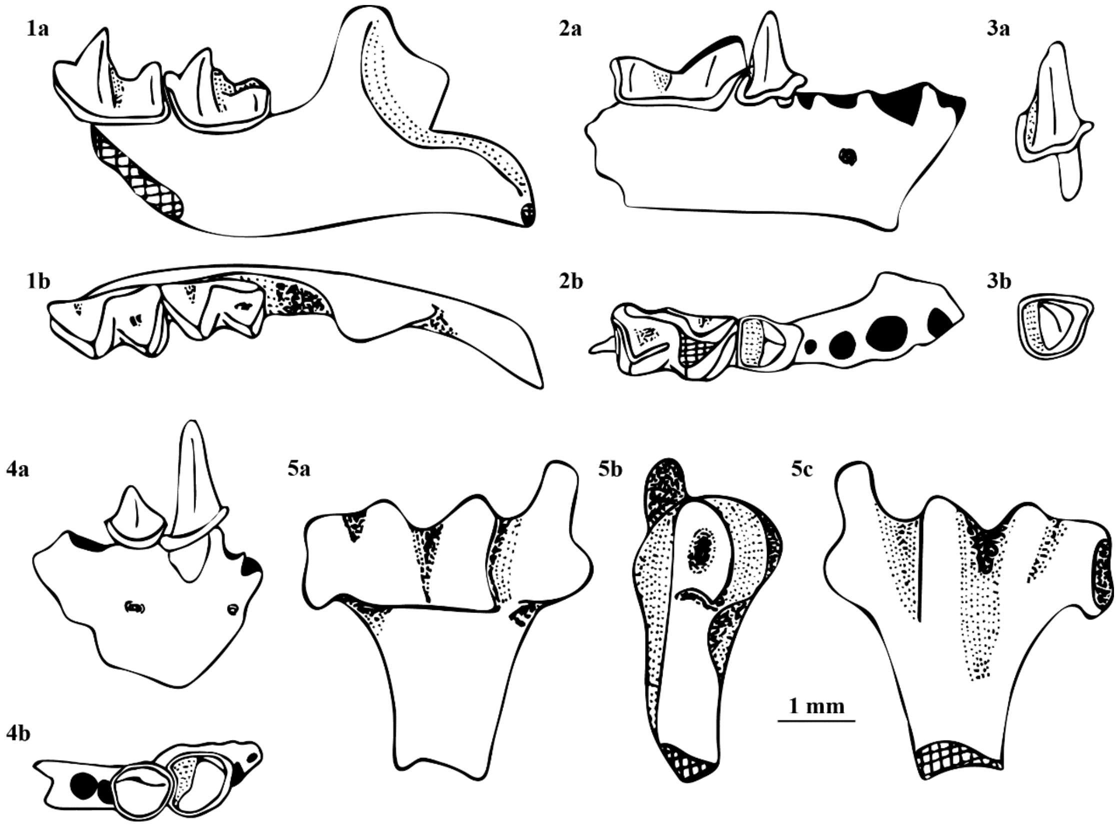

Figure 4.8 *Rhinolophus blasii*, Loutra Almopias Cave A. **1.** LAC19708 – Left mandibular fragment with m2-m3 (**a.** labial, **b.** occlusal), **2.** LAC20959 – Right mandibular fragment with p4-m1 (**a.** labial, **b.** occlusal), **3.** LAC20442 – Right p4 (**a.** labial, **b.** occlusal), **4.** LAC21560 – Right mandibular fragment with c-p2 (**a.** labial, **b.** occlusal), **5.** LAC26454 – Distal epiphysis of left humerus (**a.** anterior, **b.** lateral, **c.** posterior).

Humerus: The epitrochlea is narrower than in *Rhinolophus mehelyi*. A valley shallower than in *Rhinolophus mehelyi* is present between the condyle and the epicondyle. The rest of the characters as for *Rhinolophus mehelyi*.

Discussion The morphological features described in addition to the measurements allow a definite attribution of the material to *Rhinolophus blasii*. It is the intermediate member of the three medium-sized Horseshoe Bat species that currently occur in Greece and as its size range overlaps both *Rhinolophus mehelyi* and *Rhinolophus euryale*, only the specimens with distinct morphological features can be clearly distinguished.

Occurrence Fossils of the Blasius's Horseshoe Bat are known only from Charkadio Cave, Tilos. Its modern distribution includes most of mainland Greece and several islands, including Crete (Hanák et al. 2001, GFDC 2021). On a global scale it is distributed in Italy, most of the Balkan Peninsula, Asia Minor and Cyprus, most of the Levant region, Iran, Afghanistan, Pakistan and Yemen, Transcaucasia and Turkmenistan, Northwestern Africa, parts of the Horn of Africa and northeastern parts of Southern Africa (Simmons 2005a).

Ecology *Rhinolophus blasii* is a typical cave dweller and its habitat preferences include open areas in the close vicinity with scrublands and/or forested areas (Dietz et al. 2009).

Rhinolophus euryale Blasius, 1853

(Mediterranean Horseshoe Bat)

Figure 4.11-12 and Figure A.56

Fossiliferous locality LAC I, LAC Ib, LAC II, LAC III

Age Late Pleistocene

Material 58 identified specimens

LAC I: 1 right mandibular fragment (16680), 1 left mandibular fragment (17308), 1 left mandibular fragment with p4-m3 (17216), 1 left c (27465), 1 right m3 (19921), LAC Ib: 1 right C (16543), 1 left C (16477), LAC II: 8 right C (16689, 21766, 21874, 22412, 22413, 22414, 27619, 27620), 4 left C (21863, 21864, 21969, 22192), 1 left M1 (27869), 3 right M2 (21722, 22365, 27787), 2 left M2 (27540, 27791), 4 right M3 (21732, 21734, 21735, 22155), 1 right c (27914), 2 left c (21784, 22418), 2 right m3 (21833, 22213), 1 left m3 (22239), LAC III: 5 right C (21369, 20935, 21016, 21024, 20298), 2 left C (20734, 20296), 1 right P4 (20955), 1 right M1 (20656), 1 right M2 (20957), 2 left M2 (20272, 20997), 2 right M3 (20278, 21092), 1 right mandibular fragment with m2-m3 (16456), 2 left c (21031, 20398), 2 left p4 (21003, 21005), 1 left m1 (20985), 1 left m2 (20345), 1 right m3 (20980), 1 left m3 (20984)

Fossiliferous locality LAC Ia

Age latest Pleistocene

Material 220 identified specimens

1 left maxillary fragment with C-M1 (19746), 3 right maxillary fragments with P4-M1 (19725, 19732, 23119), 1 left maxillary fragment with P4-M1 (19735), 1 right maxillary fragment with P4-M3 (19743), 3 left maxillary fragments with P4-M3 (19758, 19760, 23069), 2 right maxillary fragments with M1-M3 (19736, 19763), 1 left maxillary fragment with M1-M3 (19755), 28 right C (25468, 25472, 25483, 25575, 25588, 25609, 25625, 25627, 25638, 25676, 25679, 25695, 25756, 25772, 25773, 25774, 25799, 25806, 25831, 25879, 25939, 25985, 25986, 26050, 26054, 26143, 26144, 26267), 42 left C (25464, 25485, 25503, 25511, 25521, 25563, 25607, 25608, 25611, 25648, 25664, 25667, 25670, 25689, 25696, 25709, 25733, 25793, 25815, 25878, 25882, 25903, 25926, 25963, 26038, 26053, 26056, 26058, 26060, 26068, 26091, 26109, 26128, 26135, 26146, 26147, 26186, 26189, 26257, 27117, 27419, 27421), 3 right P4 (23267, 23272, 23283), 8 left P4 (23243, 23252, 23261, 25334, 25357, 25381, 25428, 27347), 6 right M1 (24367, 24443, 24539, 24620, 24659, 26598), 10 left M1 (24677, 24748, 24757, 24804, 24847, 24850, 24864, 24870, 24879, 26656), 8 right M2 (23227, 24409, 24411, 24547, 24571, 24623, 24630, 24637), 4 left M2 (24730, 24758, 24894, 26644), 4 right M3 (25126, 25146, 25147, 25167), 4 left M3 (24996, 25004, 25055, 25084), 2 right mandibular fragments (19507, 19513), 1 left mandibular fragment with p2 and p4 (22851), 2 left mandibular fragments with p4 (22777, 22780), 1 right mandibular fragment with m1 (19668), 3 left mandibular fragments with m1 (19681, 22807, 22816), 5 right mandibular fragments with m2-m3 (19695, 19699, 22524, 22585, 22497), 2 left mandibular fragments with m1-m3 (19707, 22733), 3 right mandibular fragments with m2 (22459, 22507, 22655), 2 left mandibular fragments with m2 (22761, 22815), 2 right mandibular fragments with m1-m2 (22505, 22525), 1 left mandibular fragment with m1-m2 (22725), 6 right mandibular fragments with m3 (22532, 22565, 22566, 22568, 22609, 22636), 2 left mandibular fragments with m3 (22876, 22877), 1 right mandibular fragment with p4 and m2 (22493), 1 left mandibular fragment with p4-m3 (22721), 4 right c (25761, 25929, 25940, 27142), 7 left c (25850, 25921, 26123, 26228, 26229, 27178, 27436), 7 right p4 (24206, 24218, 24220, 24221, 24247, 24248, 24251), 5 left p4 (24277, 24293, 24349, 24350, 24351), 9 right m1 (23308, 23574, 23575, 23593, 23598, 23601, 23604, 23610, 23705), 6 left m1 (23890, 23901, 23946, 24051, 24057, 26948), 4 right m2 (23317, 23509, 23521, 23557), 5 left m2 (23792, 23906, 23957, 23996, 26946), 3 right m3 (23663, 23712, 26750), 4 left m3 (23822, 23836, 24076, 24078), 1 right humerus (27208), 2 left humeri (26453, 26476)

Measurements Table 4.4 and Figure 4.9-10

Description *Rhinolophus euryale* is the smallest member of the three medium-sized Horseshoe Bat species that currently occur in Greece.

C: Oval in occlusal view. A heel, smaller than in *Rhinolophus mehelyi*, is present at the lingual part of the tooth. The crown is relatively blunt lingually. The cingulum is thick and slightly concave at its mesiolabial, distolingual and mesiolingual parts and convex at its mesial, labial, distolabial, distal and lingual parts, with its maximum thickness at its mesiolabial part. The rest of the characters as for *Rhinolophus mehelyi*.

P4: The accessory cusplet-like structure is weakly developed. The rest of the characters as for *Rhinolophus mehelyi*.

M1: It is not robust. The heel is subtriangular. The parastyle forms a less marked angle with the preparacrista. The cingulum is thin. The rest of the characters as for *Rhinolophus mehelyi*.

M2: The heel is almost absent (slightly less reduced than in *Rhinolophus mehelyi*). The rest of the characters as for *Rhinolophus mehelyi*.

M3: The parastyle forms a less marked angle with the preparacrista. The rest of the characters as for *Rhinolophus mehelyi*.

Table 4.4 *Rhinolophus euryale*, Loutra Almopias Cave A. Measurements (in mm) from both LAC and LAC Ia. LAC: Late Pleistocene; LAC Ia: latest Pleistocene; n: number of measurable specimens; L: length; W: width; trgd: trigonid; tld: talonid; MEAN: average; MIN: minimum; MAX: maximum; SD: standard deviation; CV: coefficient of variation.

			n	**MEAN**	**MIN**	**MAX**	**SD**	**CV**
C	LAC	L	20	1.32	1.24	1.37	0.040	3.045
		W	20	0.97	0.85	1.14	0.074	7.585
	LAC Ia	L	71	1.31	1.19	1.62	0.062	4.745
		W	71	0.96	0.83	1.11	0.061	6.321
P3	LAC Ia	L	1	0.38	-	-	-	-
		W	1	0.33	-	-	-	-
P4	LAC	L	1	0.95	-	-	-	-
		W	1	1.20	-	-	-	-
	LAC Ia	L	20	0.98	0.81	1.07	0.071	7.256
		W	20	1.22	1.05	1.47	0.134	10.991
M1	LAC	L	2	1.72	1.69	1.74	0.035	2.062
		W	2	1.58	1.50	1.66	0.113	7.161
	LAC Ia	L	27	1.53	1.36	1.67	0.085	5.569
		W	27	1.46	1.31	1.61	0.087	5.970
M2	LAC	L	8	1.37	1.32	1.43	0.039	2.876
		W	7	1.50	1.37	1.61	0.084	5.578
	LAC Ia	L	19	1.38	1.30	1.50	0.059	4.249
		W	19	1.46	1.34	1.57	0.072	4.913
M3	LAC	L	6	1.18	1.13	1.20	0.026	2.240
		W	6	1.35	1.31	1.40	0.040	2.995
	LAC Ia	L	15	1.10	1.00	1.17	0.043	3.936
		W	15	1.36	1.19	1.45	0.074	5.439
c	LAC	L	6	0.69	0.67	0.70	0.011	1.588
		W	6	0.88	0.77	0.96	0.068	7.702
	LAC Ia	L	11	0.71	0.65	0.74	0.031	4.367
		W	11	0.85	0.73	0.96	0.062	7.307
p2	LAC Ia	L	1	0.82	-	-	-	-
		W	1	0.82	-	-	-	-
p3	LAC Ia	L	1	0.28	-	-	-	-
		W	1	0.22	-	-	-	-
p4	LAC	L	3	0.88	0.81	0.99	0.096	10.959
		W	3	0.69	0.65	0.76	0.061	8.816
	LAC Ia	L	17	0.86	0.78	0.99	0.062	7.085
		W	17	0.67	0.57	0.86	0.085	12.767

m1	LAC	L	3	1.51	1.46	1.58	0.061	4.038
		W (trgd)	3	0.83	0.73	0.92	0.096	11.531
		W (tld)	3	0.92	0.79	1.05	0.130	14.093
	LAC Ia	L	25	1.61	1.35	1.86	0.110	6.798
		W (trgd)	25	0.77	0.59	0.99	0.090	11.634
		W (tld)	25	0.86	0.72	1.02	0.074	8.679
m2	LAC	L	2	1.52	1.46	1.58	0.085	5.582
		W (trgd)	2	0.83	0.73	0.92	0.134	16.285
		W (tld)	2	0.92	0.79	1.05	0.184	19.984
	LAC Ia	L	25	1.49	1.22	1.76	0.098	6.553
		W (trgd)	26	0.82	0.69	0.99	0.074	8.987
		W (tld)	25	0.90	0.74	1.00	0.069	7.611
m3	LAC	L	8	1.35	1.30	1.45	0.049	3.596
		W (trgd)	8	0.82	0.75	0.99	0.079	9.580
		W (tld)	7	0.73	0.67	0.85	0.069	9.419
	LAC Ia	L	21	1.38	1.17	1.47	0.073	5.280
		W (trgd)	23	0.81	0.63	0.95	0.090	11.137
		W (tld)	22	0.72	0.55	0.86	0.077	10.722
M1-M3	LAC Ia	L	7	4.01	3.92	4.09	0.064	1.590
P4-M3	LAC Ia	L	4	4.91	4.82	5.00	0.074	1.497
m1-m3	LAC	L	1	4.65	-	-	-	-
	LAC Ia	L	2	4.29	4.28	4.29	0.007	1.165
p4-m3	LAC	L	1	5.60	-	-	-	-
	LAC Ia	L	1	5.32	-	-	-	-
LSC	LAC Ia	L	2	11.90	11.46	12.33	0.615	5.172
Humerus	LAC Ia	W	3	4.30	4.16	4.42	0.131	3.050

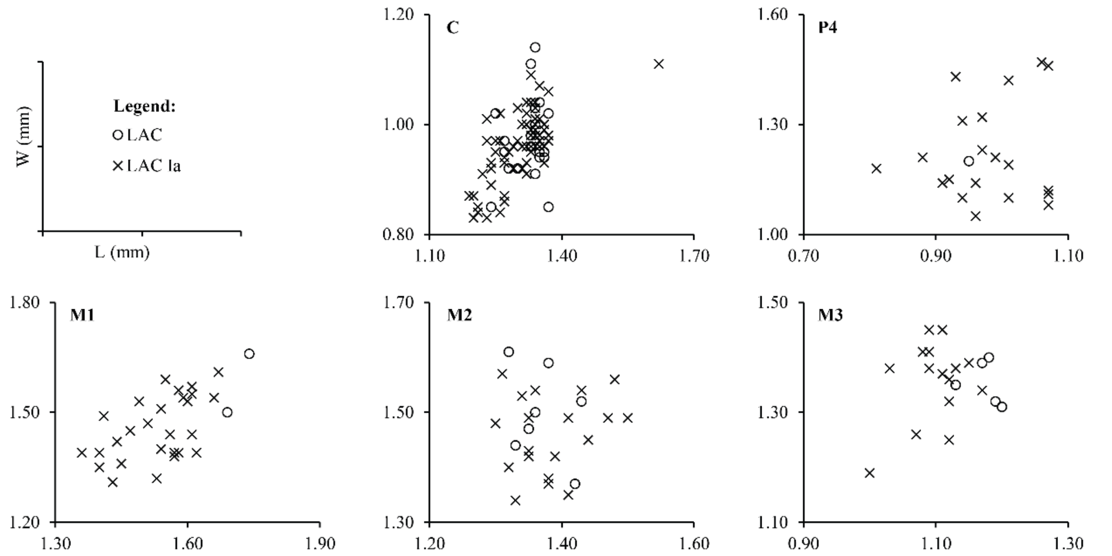

Figure 4.9. *Rhinolophus euryale*, Loutra Almopias Cave A. XY graphs with the measured (in mm) dental elements (C, P4, M1, M2, M3). L: length, W: width.

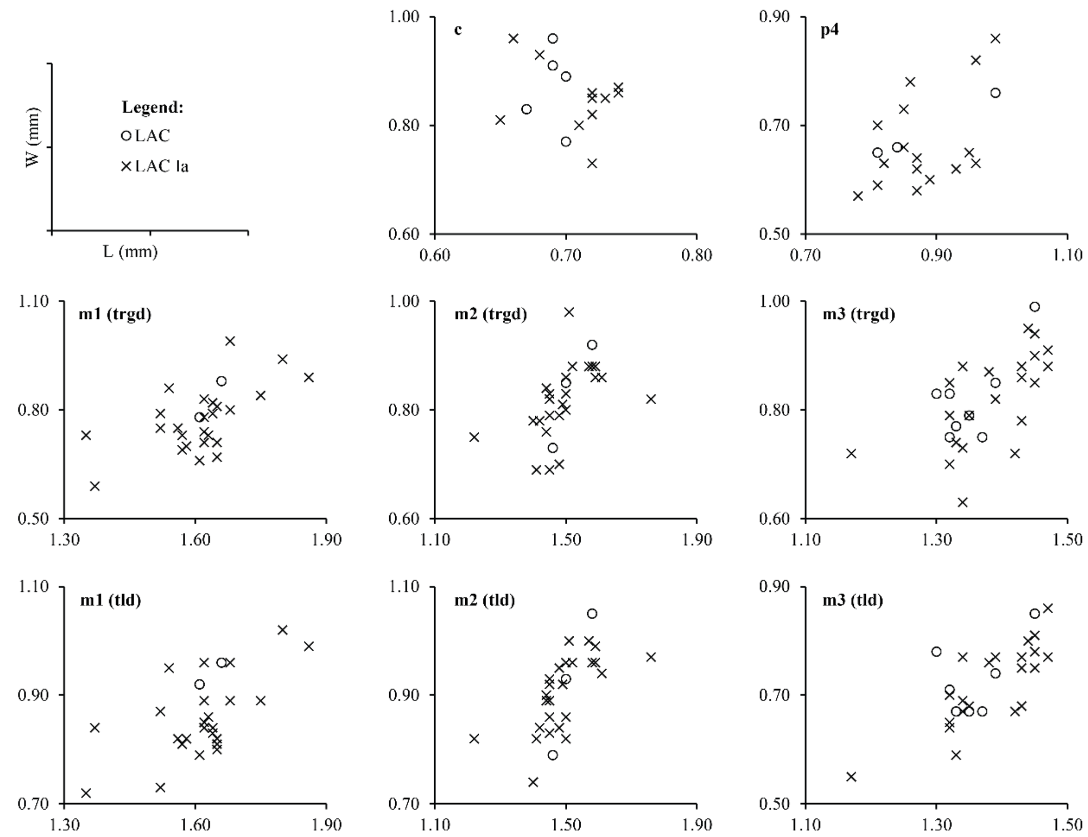

Figure 4.10 *Rhinolophus euryale*, Loutra Almopias Cave A. XY graphs with the measured (in mm) dental elements (c, p4, m1, m2, m3). L: length, W: width, trgd: trigonid; tld: talonid.

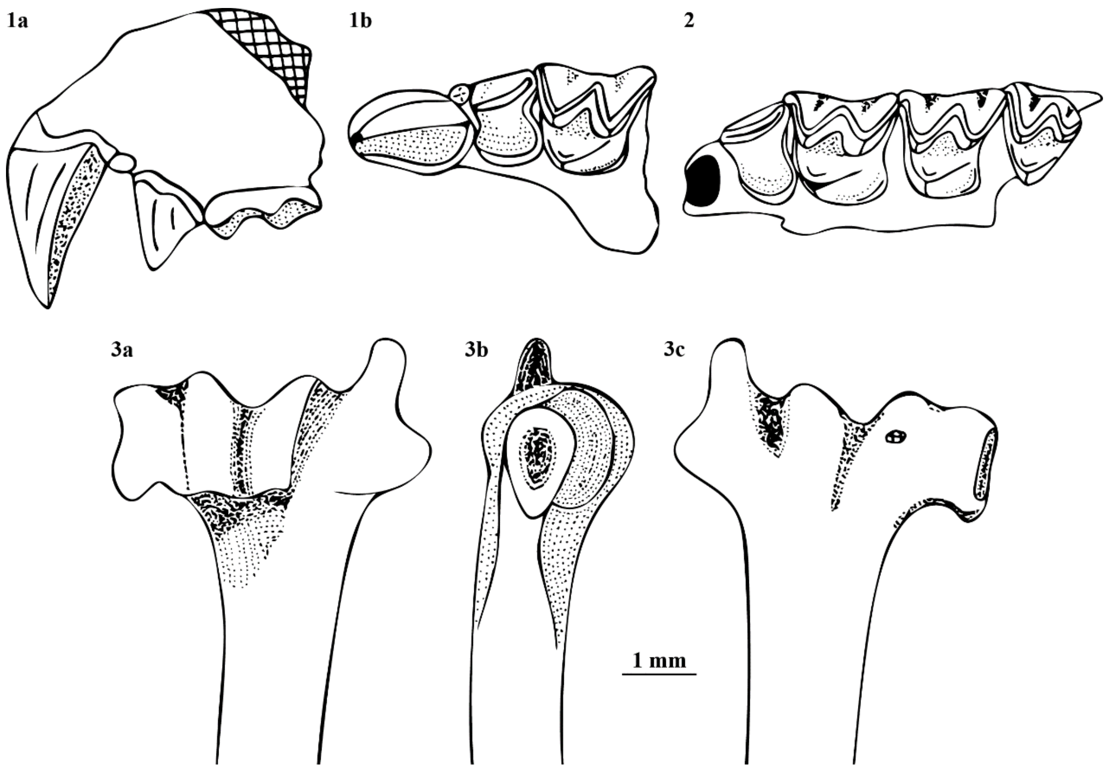

Figure 4.11 *Rhinolophus euryale*, Loutra Almopias Cave A. **1.** LAC19746 – Left maxillary fragment with C-M1 (**a.** labial, **b.** occlusal), **2.** LAC23069 – Left maxillary fragment with P4-M3, **3.** LAC26476 – Distal epiphysis of left humerus (**a.** anterior, **b.** lateral, **c.** posterior).

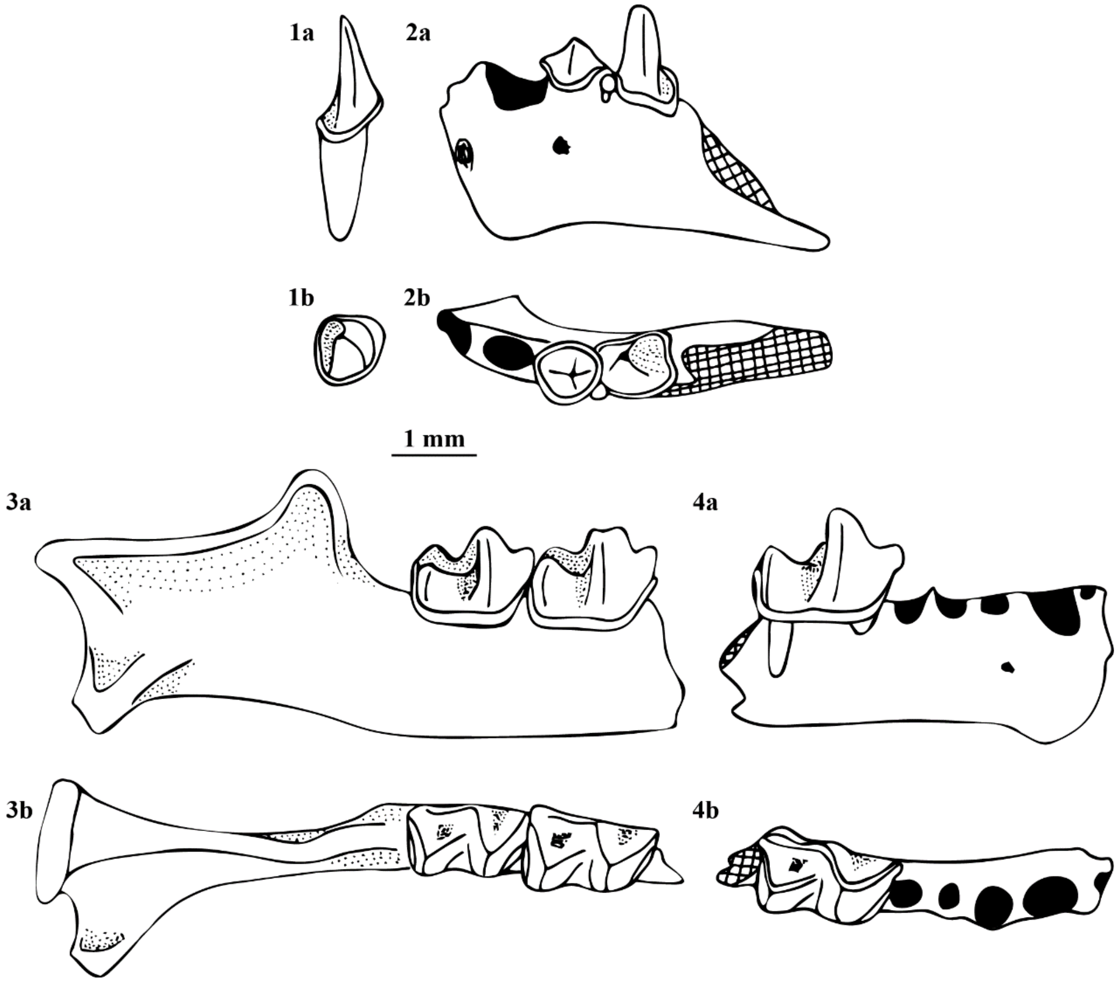

Figure 4.12 *Rhinolophus euryale*, Loutra Almopias Cave A. **1.** LAC27142 – Right c (**a.** labial, **b.** occlusal, **2.** LAC22851 – Left mandible fragment with p2-p4 (**a.** labial, **b.** occlusal), **3.** LAC19699 – Right mandibular fragment with m2-m3 (**a.** labial, **b.** occlusal), **4.** LAC19668 – Right mandibular fragment with m1 (**a.** labial, **b.** occlusal).

c: The distal part of the tooth is not as concave as it is in *Rhinolophus mehelyi*. The rest of the characters as for *Rhinolophus mehelyi* and *Rhinolophus blasii*.

p2: Circular in occlusal view. The labial part is almost equal in size and shape to the lingual. The rest of the characters as for *Rhinolophus mehelyi* and *Rhinolophus blasii*.

p3: As for *Rhinolophus mehelyi*.

p4: Slenderer than *Rhinolophus mehelyi*. The mesiolingual part of the tooth is less developed than *Rhinolophus mehelyi*, but more developed than *Rhinolophus blasii*. The concavity present at the middle part of the labial cingulum tends to be blunter than in *Rhinolophus mehelyi*. The rest of the characters as for *Rhinolophus mehelyi* and *Rhinolophus blasii*.

m1: The talonid is longer than in *Rhinolophus mehelyi* and the entocristid is slightly curved as in *Rhinolophus blasii*. The rest of the characters as for *Rhinolophus mehelyi* and *Rhinolophus blasii*.

m2: The lingual cingulum of the trigonid is absent. The rest of the characters as for *Rhinolophus mehelyi* and *Rhinolophus blasii*.

m3: As for *Rhinolophus blasii*.

Mandible: The coronoid process is slightly sharper than in *Rhinolophus mehelyi* and less sharp than in *Rhinolophus blasii*. The anterior part of the masseter crest is smoother than in *Rhinolophus mehelyi*. A minute convexity is present at the distal part of the mandibular notch. The rest of the characters as for *Rhinolophus mehelyi* and *Rhinolophus blasii*.

Humerus: The styloid process is to a more lateral position in respect to *Rhinolophus mehelyi*. The epitrochlea is narrower than in *Rhinolophus mehelyi* and *Rhinolophus blasii*. The rest of the characters as for *Rhinolophus mehelyi* and *Rhinolophus blasii*.

Discussion The morphological features described in addition to the measurements allow a definite attribution of the material to *Rhinolophus euryale*. It is the smallest member of the three medium-sized Horseshoe Bat species that currently occur in Greece and as its size range overlaps both *Rhinolophus mehelyi* and *Rhinolophus blasii*, only the smallest specimens can be clearly distinguished.

Occurrence The fossils of the Mediterranean Horseshoe Bat described from Loutra Almopias Cave A are the first known records of this species in Greece. Its modern distribution includes most of mainland Greece and the islands of Sporades, Lesvos and Rhodes (Hanák et al. 2001, GFDC 2021). On a global scale it is distributed from Northwestern Africa and the Iberian Peninsula all the way to the Balkan Peninsula and several Mediterranean Islands, Turkey, Transcaucasia and Turkmenistan, parts of the Levant and Iran and possibly Egypt (Simmons 2005a).

Ecology *Rhinolophus euryale* is a typical cave dweller and its habitat preferences include (riparian) forested areas and (riparian) scrublands (Dietz et al. 2009).

Rhinolophus mehelyi/blasii/euryale

Figure 4.14

Fossiliferous locality LAC I, LAC Ib, LAC Ic, LAC II, LAC III

Age Late Pleistocene

Material 459 identified specimens

LAC I: 6 right C (19925, 19933, 19943, 17220, 17221, 17318), 6 left C (17240, 19931, 19965, 19971, 27464, 27509), 1 right M2 (19922), 1 left M2 (17312), 1 left M3 (17313), 3 right c (17294, 17322, 27492), 4 left c (19924, 19951, 19966, 17291), 4 right m1 (17258, 17262, 17334, 16638), 2 left m1 (17259, 17212), 1 right m2 (19920), 2 left m2 (17214, 17215), 1 right m3 (19988), 4 left m3 (17256, 17260, 17263, 17317), LAC Ib: 4 left C (17190, 16482, 16557, 19898), 1 right P4 (16432), 1 right M1 (16510), 1 left M1 (16540), 1 right mandibular fragment with c and p4 (27953), 1 right mandibular fragment with m2-m3 (16430), 3 left c (17172, 16580, 19895), 1 right p4 (16476), 1 left m1 (16575), 2 right m3 (16433, 16546), LAC Ic: 3 right C (17867, 17958, 21509), 2 left C (17915, 18032), 1 right P4 (21457), 2 right c (18033, 21424), 2 left c (17937, 18012), 1 right p4 (17894), 1 right m1-2 (18007), 2 left m1 (21480, 21484), 1 right m2 (21478), 1 left m2 (17890), 1 right m3 (17892), 1 left m3 (17893), LAC II: 35 right C (16072, 16041, 16043, 16044, 21559, 21762, 21768, 21794, 21810, 21928, 16801, 16688, 21946, 21947, 21948, 21949, 21981, 22016, 22085, 22086, 22098, 22193, 22410, 22411, 27720, 27725, 27748, 27761, 27810, 27811, 27812, 27834, 27902, 27934, 27950), 29 left C (16066, 16071, 16078, 21551, 21553, 21566, 21764, 21770, 21868, 21872, 21964, 22174, 22420, 22421, 22422, 27557, 27566, 27568, 27574, 27665, 27813, 27814, 27835, 27836, 27905, 27907, 27908, 27936, 27951), 12 right P4 (21546, 21607, 21756, 16180, 16181, 16182, 21977, 16377, 16155, 16672, 27878, 27945), 7 left P4 (16086, 21547, 21839, 22044, 16153, 27794, 27842), 2 right M1-2 (21540, 21940), 1 left M1-2 (22038), 4 right M1 (21713, 21714, 22269, 27865), 2 left M1 (21687, 21890), 9 right M2 (16045, 16047, 21558, 21716, 21723, 21939, 22154, 22371, 27819), 22 left M2 (21677, 21678, 21680, 21681, 21684, 21685, 21691, 21695, 21922, 21980, 22077, 22150, 22267, 22280, 22283, 22356, 22361, 22366, 27602, 27716, 27789, 27870), 9 right M3 (21541, 21542, 21731, 21736, 21739, 22291, 22299, 27605, 27606), 3 left M3 (21893, 16347, 22156), 1 left mandibular fragment with i2, c-p2 and p4 (16744), 1 left mandibular fragment with p4 and m2-m3 (27570), 1 right mandibular fragment with m1-m2 (16622), 18 right c (16076, 21577, 21765, 21792, 21813, 21878, 16802, 21955, 22092, 22094, 22330, 27701, 27769, 27855, 27911, 27913, 27915, 27940), 28 left c (16070, 21578, 21780, 21785, 21787, 21790, 21800, 21806, 21807, 21876, 21881, 21973, 22025, 22051, 22088, 22191, 22324, 22325, 22389, 27535, 27779, 27805, 27806, 27833, 27920, 27921, 27923, 27948), 7 right p4 (21665, 22128, 22132, 16408, 22244, 22250, 27686), 2 left p4 (21590, 16025), 14 right m1 (16061, 21615, 21621, 21624, 21827, 21848, 21976, 21991, 16121, 16407, 22206, 22211, 27580, 27881), 13 left m1 (16060, 21524, 21586, 21646, 21943, 21974, 21992, 22070, 16118, 22348, 27671, 27802, 27846), 7 right m2 (21531, 21573, 21574, 22010, 16119, 22112, 22210,), 7 left m2 (21645, 21852, 21659, 16691, 21944, 16369, 27827), 15 right m3 (16029, 16030, 21517, 21530, 21626, 21633, 16146, 16124, 16391, 22214, 27591, 27592, 27730, 27797, 27798), 12 left m3 (16038, 21637, 21638, 21641, 16352, 22233, 22234, 22242, 27778, 27804, 27889, 27891), LAC III: 17 right C (20703, 20824, 20851, 21370, 21372, 21379, 21384, 20915, 20933, 21015, 21018, 21025, 21108, 21198, 20064, 20479, 20692), 12 left C (20286, 20714, 20837, 21374, 20914, 21028, 21124, 21200, 20086, 20378, 20484, 20571), 3 right P4 (20816, 19318, 20681), 4 right M1 (20800, 21304, 19324, 20449), 2 left M1 (20549, 20550), 3 right M2 (21311, 20028, 20370), 6 left M2 (21327, 21330, 21332, 20927, 20996, 20667), 7 right M3 (20172, 20849, 21317, 21318, 19145, 19344, 19345), 6 left M3 (20177, 21337, 20895, 20991, 21186, 19144), 1 left mandibular fragment with c and p4 (20965), 1 right mandibular fragment with p4-m2 (20140), 14 right c (20096, 20198, 21383, 20945, 20947, 21127, 21199, 19162, 20065, 20293, 20297, 20576, 20579, 20580), 18 left c (20192, 20212, 20699, 20707, 20719, 20823, 21405, 21029, 21030, 21034, 21038, 21098, 21119, 19160, 20299, 20304, 20388, 20390), 1 right p2 (20318), 1 left p2 (21428a), 1 right p4 (19136), 4 left p4 (21293, 21298, 16460, 21004), 1 right m1-2 (21275), 8 right m1 (20860, 21262, 16452, 20976, 20978, 21157, 21158, 20627), 2 left m1 (21283, 20983), 6 right m2 (20250, 20859, 20864, 19331, 20426, 20529), 3 left m2 (20346, 20607, 20640), 2 right m3 (20248, 20251), 5 left m3 (20258, 20784, 21278, 20912, 20347)

Fossiliferous locality LAC Ia

Age latest Pleistocene

Material 885 identified specimens

1 right maxillary fragment with C and P4-M1 (27235), 1 right maxillary fragment with P4-M3 (19766), 1 left maxillary fragment with P4-M3 (19767), 1 left maxillary fragment with M1-M3 (23072), 88 right C (23294, 23297, 25434, 25436, 25437, 25440, 25451, 25459, 25474, 25486, 25496, 25507, 25512, 25528, 25533, 25547, 25557, 25559, 25606, 25620, 25623, 25635, 25636, 25637, 25643, 25675, 25678, 25681, 25684, 25690, 25692, 25704, 25705, 25730, 25736, 25743, 25748, 25753, 25769, 25785, 25786, 25790, 25804, 25817, 25818, 25820, 25825, 25841, 25846, 25849, 25856, 25861, 25867, 25889, 25948, 25960, 25962, 25987, 26005, 26009, 26037, 26055, 26067, 26077, 26081, 26140, 26148, 26151, 26164, 26169, 26178, 26183, 26196, 26202, 26227, 26235, 26239, 26254, 26258, 26262, 27067, 27080, 27083, 27084, 27234, 27414, 27416, 27418), 99 left C (25438, 25457, 25458, 25462, 25497, 25502, 25513, 25539, 25554, 25555, 25556, 25558, 25562, 25564, 25568, 25589, 25602, 25639, 25646, 25649, 25652, 25660, 25666, 25674, 25687, 25698, 25726, 25732, 25737, 25741, 25746, 25750, 25757, 25759, 25770, 25778, 25780, 25803, 25819, 25830, 25837, 25842, 25854, 25869, 25874, 25880, 25892, 25909, 25928, 25931, 25941, 25943, 25944, 25947, 25971, 25974, 25975, 25980, 25990, 25995, 25996, 26002, 26003, 26007, 26020, 26031, 26034, 26039, 26057, 26065, 26073, 26076, 26078, 26107, 26158, 26184, 26190, 26194, 26201, 26205, 26224, 26242, 26245, 26256, 26260, 26261, 26263, 27092, 27099, 27108, 27118, 27121, 27122, 27123, 27124, 27129, 27422, 27424, 27425), 27 right P4 (23271, 23275, 23277, 23279, 23282, 25232, 25234, 25242, 25252, 25254, 25255, 25263, 25284, 25286, 25289, 25302, 25312, 25317, 25318, 25319, 26518, 26521, 26522, 26523, 26691, 27232, 27233), 23 left P4 (23247, 23248, 23249, 23250, 23251, 23260, 23257, 23258, 25323, 25328, 25330, 25332, 25347, 25350, 25383, 25390, 25393, 25400, 25403, 25411, 25418, 26712, 27243), 1 right M1-2 (26590), 1 left M1-2 (24714), 21 right M1 (23240, 24425, 24439, 24488, 24532, 24533, 24558, 24568, 24570, 24574, 24596, 24616, 24627, 24633, 24669, 26268, 26569, 26596, 26604, 27303, 27310), 22 left M1 (24710, 24718, 24725, 24731, 24753, 24783, 24793, 24798, 24810, 24816, 24822, 24829, 24835, 24854, 24877, 24878, 24925, 24941, 24951, 24953, 24966, 27338), 47 right M2 (24371, 24372, 24383, 24393, 24395, 24397, 24423, 24442, 24459, 24510, 24517, 24535, 24540, 24543, 24546, 24550, 24565, 24572, 24575, 24579, 24597, 24604, 24606, 24609, 24611, 24614, 24626, 24632, 24634, 24640, 24645, 24647, 24650, 24652, 24655, 24656, 24662, 24663, 24670, 26572, 26574, 26579, 26593, 26600, 26605, 27299, 27311), 47 left M2 (23239, 24643, 24673, 24674, 24680, 24683, 24686, 24687, 24691, 24694, 24696, 24706, 24707, 24719, 24720, 24722, 24723, 24729, 24732, 24733, 24734, 24743, 24747, 24754, 24763, 24768, 24812, 24853, 24858, 24863, 24866, 24874, 24883, 24886, 24905, 24916, 24920, 24945, 24946, 24954, 25094, 26623, 26637, 26655, 27332, 27335, 27337), 30 right M3 (24989, 24990, 24992, 25128, 25130, 25132, 25133, 25134, 25135, 25136, 25149, 25156, 25164, 25173, 25174, 25183, 25184, 25185, 25186, 25187, 25188, 25192, 25198, 26269, 26510, 26609, 26610, 26615, 27316, 27317), 45 left M3 (24507, 24994, 24998, 25007, 25008, 25009, 25010, 25016, 25017, 25019, 25020, 25021, 25025, 25027, 25028, 25036, 25043, 25047, 25054, 25066, 25089, 25092, 25097, 25098, 25099, 25101, 25102, 25103, 25104, 25105, 25108, 25110, 25111, 25112, 25113, 25114, 26673, 26675, 26676, 26677, 26678, 26679, 26681, 27339, 27341), 1 right mandibular fragment with c-p2 and p4 (26751), 1 right mandibular fragment with c-p2 and p4-m1 (22615), 1 left mandibular fragment with c-p2, p4 and m1-m2 (22743), 2 left mandibular fragments with c and p4 (22785, 27271), 1 right mandibular fragment with c and p4-m2 (19670), 1 right mandibular fragment with c and m1 (22616), 1 right mandibular fragment with p2 and p4-m3 (19622), 2 right mandibular fragments with p4 (19672, 19690), 2 right mandibular fragments with p4-m1 (26732, 27254), 2 left mandibular fragments with p4-m1 (19684, 22754), 3 right mandibular fragments with p4-m2 (19491, 19621, 19660), 3 left mandibular fragments with p4-m2 (19655, 19683, 22753), 5 right mandibular fragments with p4-m3 (19483, 22510, 22511, 22558, 22560), 4 left mandibular fragments with p4-m3 (19498, 22715, 22717, 22723), 3 right mandibular fragments with m1 (19614, 19688, 22452), 2 left mandibular fragments with m1 (19686, 22745), 2 left mandibular fragments with m1-m2 (19656, 22738), 7 right mandibular fragments with m1-m3 (19486, 22469, 22527, 22584, 22611, 22499, 22675), 9 left mandibular fragments with m1-m3 (19648, 19687, 22701, 22704, 22707, 22708, 22709, 22711, 22712), 2 right mandibular fragments with m2 (19493, 22480), 1 left mandibular fragment with m2 (22750), 1 right mandibular fragment with m2-m3 (19613), 1 left mandibular fragment with m2-m3 (26768), 2 right mandibular fragments with m3 (19662, 19697), 38 right c (25452, 25613, 25712, 25801, 25873, 25905, 25918, 25930, 25945, 25952, 25970, 25982, 26004, 26042, 26045, 26059, 26090, 26096,

26106, 26113, 26117, 26129, 26175, 26176, 26181, 26195, 26217, 26223, 26244, 26253, 27137, 27145, 27158, 27160, 27164, 27165, 27248, 27429), 27 left c (25433, 25435, 25545, 25546, 25584, 25617, 25747, 25964, 25969, 26022, 26029, 26035, 26047, 26074, 26075, 26101, 26118, 26154, 26156, 26165, 26233, 27169, 27181, 27184, 27185, 27186, 27439), 2 right p2 (26308, 26320), 6 left p2 (26287, 26290, 26296, 26316, 26319, 26349), 8 right p4 (24184, 24188, 24211, 24240, 24241, 24246, 24257, 24261), 9 left p4 (24310, 24311, 24313, 24314, 24315, 24331, 24354, 24359, 27051), 1 right m1-2 (23522), 2 left m1-2 (23837, 24061), 47 right m1 (23321, 23322, 23334, 23367, 23368, 23384, 23391, 23405, 23408, 23303, 23429, 23438, 23445, 23493, 23499, 23500, 23507, 23508, 23528, 23563, 23568, 23572, 23582, 23587, 23596, 23609, 23611, 23612, 23615, 23621, 23648, 23667, 23670, 23684, 23685, 23694, 23700, 23702, 26734, 26761, 26869, 26883, 26896, 26903, 27354, 27360, 27370), 61 left m1 (23745, 23750, 23757, 23778, 23795, 23807, 23809, 23813, 23819, 23821, 23832, 23835, 23838, 23855, 23863, 23866, 23891, 23902, 23911, 23915, 23917, 23924, 23925, 23927, 23928, 23935, 23938, 23953, 23955, 23972, 23975, 23991, 23997, 23998, 24008, 24012, 24013, 24016, 24019, 24020, 24025, 24037, 24041, 24044, 24048, 24054, 24062, 24074, 26943, 26944, 26950, 26952, 26973, 26978, 26981, 26983, 26986, 27006, 27377, 27378, 27383), 34 right m2 (23359, 23382, 23387, 23390, 23393, 23305, 23492, 23496, 23498, 23506, 23511, 23516, 23518, 23519, 23523, 23524, 23525, 23527, 23529, 23534, 23567, 23579, 23594, 23595, 23622, 23675, 23677, 23679, 23704, 26752, 26766, 26922, 27364, 27369), 37 left m2 (23755, 23777, 23780, 23793, 23797, 23806, 23816, 23823, 23831, 23860, 23905, 23910, 23918, 23920, 23926, 23933, 23939, 23962, 23966, 23982, 23985, 23993, 24000, 24007, 24011, 24023, 24031, 24043, 24060, 24066, 26805, 26945, 27276, 27283, 27288, 27384, 27390), 42 right m3 (23320, 23329, 23341, 23366, 23380, 23388, 23397, 23427, 23444, 23515, 23564, 23578, 23586, 23602, 23606, 23616, 23617, 23618, 23625, 23629, 23632, 23640, 23646, 23657, 23674, 23687, 23688, 23689, 23691, 23693, 23696, 23703, 23706, 23707, 23709, 23711, 23713, 23715, 26909, 26928, 26939, 26940), 49 left m3 (23743, 23820, 23829, 23849, 23850, 23869, 24024, 24027, 24028, 24035, 24042, 24073, 24075, 24077, 24082, 24085, 24087, 24089, 24095, 24098, 24099, 24100, 24111, 24113, 24123, 24127, 24130, 24147, 24150, 24157, 24164, 24165, 24175, 24178, 24179, 26792, 26795, 26963, 27005, 27008, 27010, 27021, 27025, 27026, 27291, 27388, 27394, 27396, 27398), 2 right humeri (27210, 27213), 6 left humeri (26471, 26473, 26478, 27217, 27224, 27228)

<u>Measurements</u> Table 4.5 and Figure 4.13

<u>Description</u> As species discrimination between the three medium-sized Horseshoe Bats that currently occur in Greece is nearly impossible, because they overlap in size and they share many similar morphological characteristics, the specimens that do not fulfil the needed criteria for species attribution are all grouped as *Rhinolophus mehelyi*/*blasii*/*euryale*. Consequently, no further descriptions are provided, as all specimens share characteristics that fall within the spectrum of the already described taxa.

Table 4.5 *Rhinolophus mehelyi*/*blasii*/*euryale*, Loutra Almopias Cave A. Measurements (in mm) from both LAC and LAC Ia. LAC: Late Pleistocene; LAC Ia: latest Pleistocene; n: number of measurable specimens; L: length; W: width; trgd: trigonid; tld: talonid; MEAN: average; MIN: minimum; MAX: maximum; SD: standard deviation; CV: coefficient of variation.

			n	**MEAN**	**MIN**	**MAX**	**SD**	**CV**
C	LAC	L	110	1.50	1.28	1.76	0.086	5.759
		W	110	1.08	0.80	1.23	0.080	7.372
	LAC Ia	L	187	1.46	1.34	1.73	0.075	5.122
		W	186	1.08	0.92	1.29	0.072	6.671
P4	LAC	L	23	1.05	0.92	1.14	0.049	4.641
		W	20	1.35	1.17	1.62	0.093	6.872

	LAC Ia	L	53	1.04	0.81	1.20	0.074	7.076
		W	50	1.31	1.11	1.41	0.067	5.117
M1	LAC	L	13	1.64	1.56	1.77	0.053	3.214
		W	13	1.57	1.37	1.76	0.129	8.194
	LAC Ia	L	41	1.57	1.40	1.73	0.082	5.193
		W	40	1.50	1.21	1.70	0.125	8.334
M2	LAC	L	38	1.53	1.41	1.63	0.063	4.102
		W	40	1.60	1.41	1.83	0.103	6.411
	LAC Ia	L	91	1.47	1.23	1.58	0.050	3.407
		W	92	1.57	1.37	1.73	0.078	5.003
M3	LAC	L	23	1.22	1.14	1.35	0.055	4.490
		W	25	1.49	1.31	1.67	0.088	5.946
	LAC Ia	L	74	1.19	1.06	1.27	0.046	3.896
		W	73	1.51	1.39	1.65	0.059	3.907
i2	LAC	L	1	0.55	-	-	-	-
		W	1	0.26	-	-	-	-
c	LAC	L	94	0.84	0.69	0.98	0.062	7.429
		W	94	0.98	0.76	1.11	0.080	8.078
	LAC Ia	L	71	0.81	0.70	0.90	0.044	5.407
		W	71	0.95	0.72	1.12	0.090	9.469
p2	LAC	L	3	0.79	0.74	0.89	0.084	10.571
		W	3	0.77	0.75	0.81	0.032	4.157
	LAC Ia	L	12	0.77	0.68	0.85	0.056	7.280
		W	12	0.68	0.55	0.77	0.064	9.374
p4	LAC	L	22	0.95	0.87	1.03	0.055	5.765
		W	22	0.83	0.59	0.97	0.092	11.102
	LAC Ia	L	45	0.91	0.78	1.11	0.071	7.859
		W	45	0.74	0.51	1.00	0.112	15.148
m1	LAC	L	44	1.77	1.55	1.89	0.070	3.944
		W (trgd)	50	0.85	0.72	1.09	0.087	10.153
		W (tld)	50	0.96	0.79	1.14	0.071	7.413
	LAC Ia	L	155	1.71	1.46	1.84	0.063	3.695
		W (trgd)	155	0.84	0.63	1.15	0.080	9.587
		W (tld)	157	0.93	0.69	1.17	0.077	8.288
m2	LAC	L	32	1.63	1.48	1.75	0.066	4.039
		W (trgd)	32	0.91	0.80	1.07	0.069	7.593
		W (tld)	32	0.99	0.81	1.12	0.071	7.169
	LAC Ia	L	111	1.56	1.36	1.68	0.054	3.474
		W (trgd)	112	0.89	0.77	1.05	0.061	6.900
		W (tld)	109	0.96	0.81	1.06	0.050	5.244
m3	LAC	L	42	1.47	1.34	1.58	0.066	4.479
		W (trgd)	45	0.87	0.74	1.03	0.064	7.404
		W (tld)	45	0.78	0.64	0.98	0.062	7.960
	LAC Ia	L	117	1.43	1.30	1.59	0.056	3.883
		W (trgd)	118	0.85	0.72	0.99	0.059	6.967
		W (tld)	117	0.75	0.57	0.89	0.057	7.535
M1-M3	LAC Ia	L	3	3.99	3.95	4.01	0.032	0.806
P4-M3	LAC Ia	L	2	4.88	4.85	4.90	0.035	0.725
C-P4	LAC Ia	L	1	3.04	-	-	-	-

m1-m3	LAC Ia	L	24	4.60	4.43	4.73	0.094	2.041
p4-m3	LAC Ia	L	10	5.49	5.32	5.72	0.115	2.095
c-p4	LAC	L	3	2.45	2.32	2.55	0.119	4.863
	LAC Ia	L	6	2.43	2.22	2.61	0.150	6.165
LSC	LAC Ia	L	5	11.84	11.57	11.99	0.172	1.452
Humerus	LAC Ia	L	1	26.87	-	-	-	-
		W	5	4.11	4.01	4.33	0.126	3.068

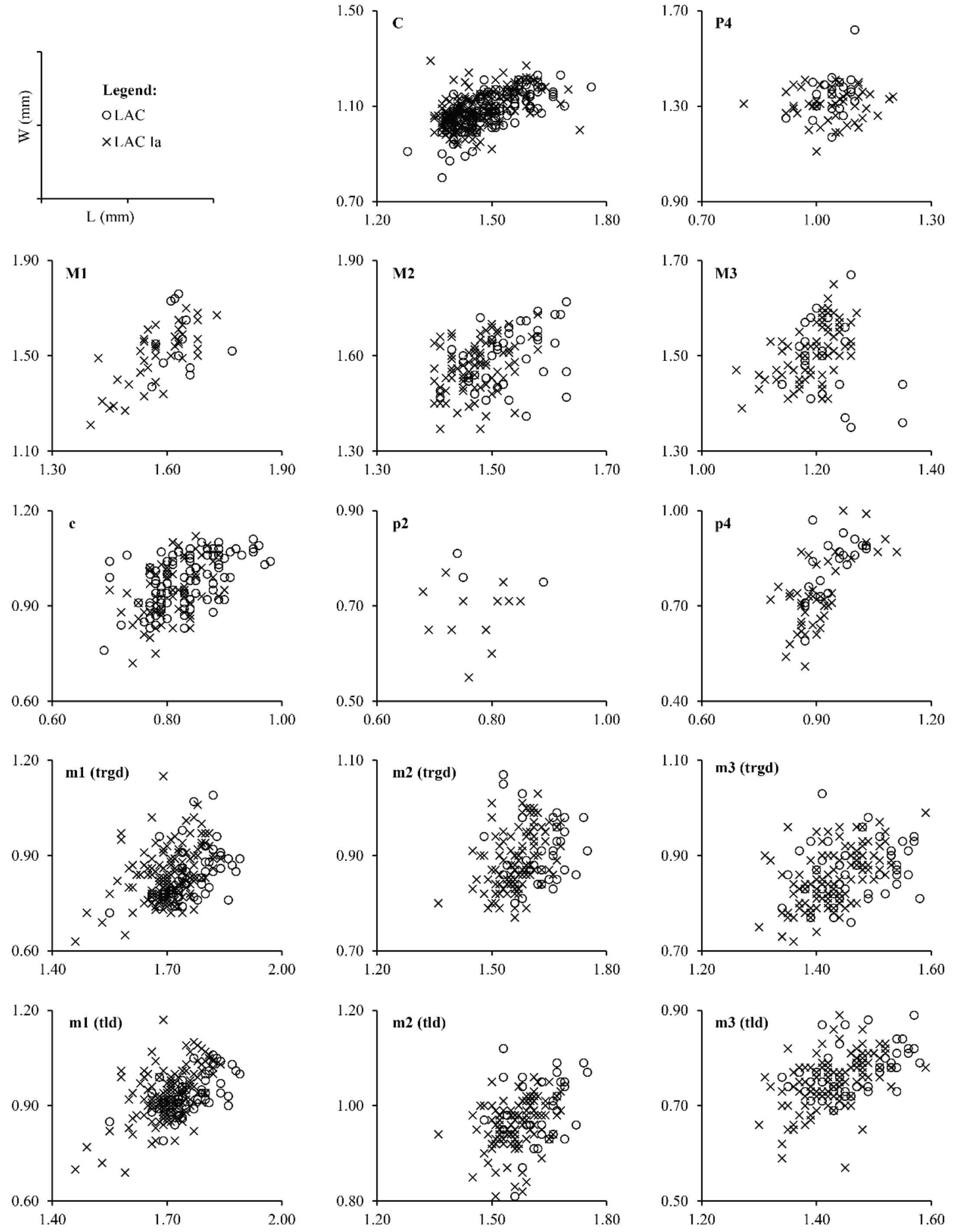

Figure 4.13 *Rhinolophus mehelyi*/*blasii*/*euryale*, Loutra Almopias Cave A. XY graphs with the measured (in mm) dental elements (C, P4, M1, M2, M3, c, p2, p4, m1, m2, m3). L: length, W: width, trgd: trigonid; tld: talonid.

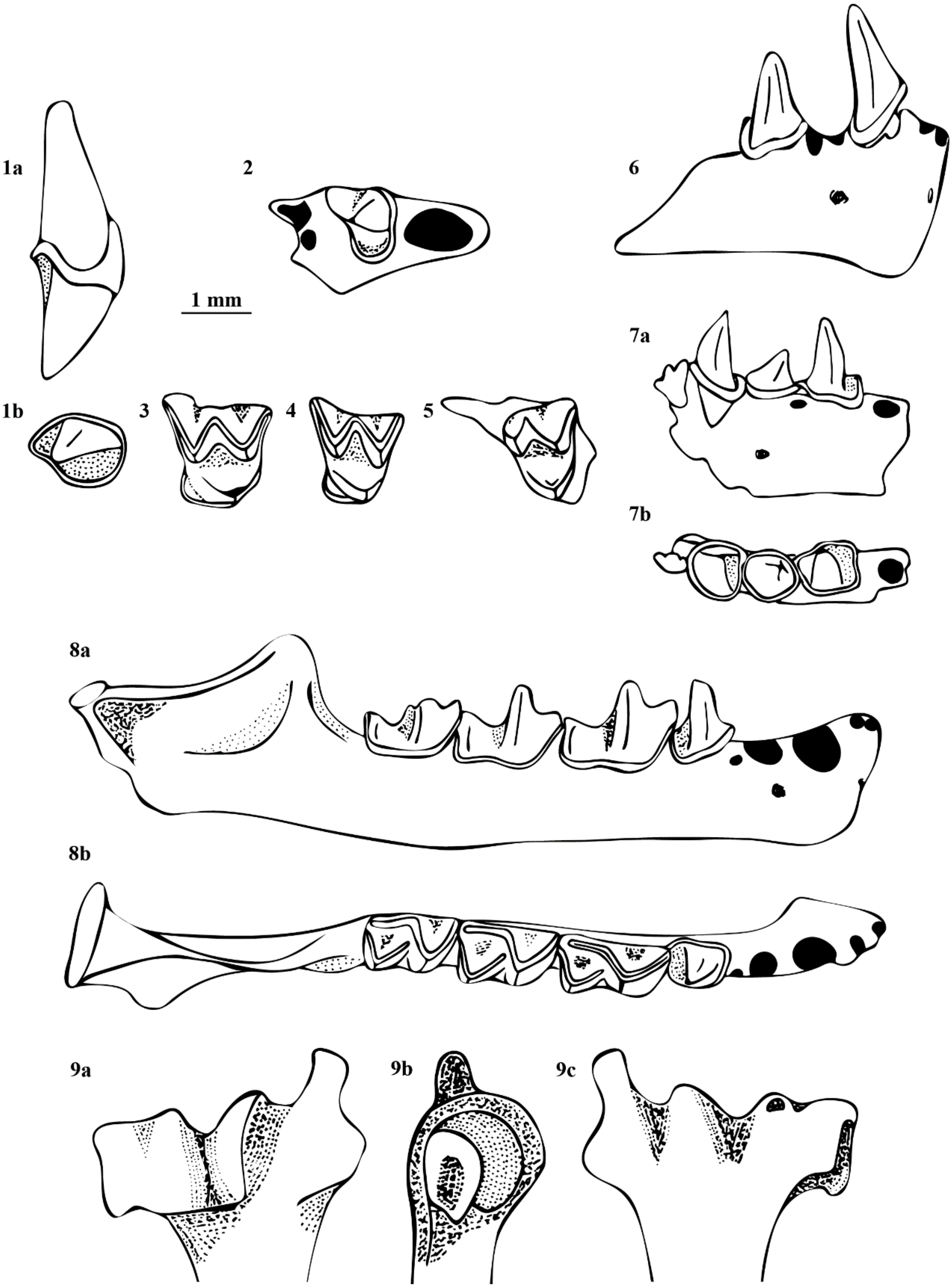

Figure 4.14 *Rhinolophus mehelyi*/*blasii*/*euryale*, Loutra Almopias Cave A. **1.** LAC20915 – Right C (**a.** labial, **b.** occlusal, **2.** LAC16432 – Right maxillary fragment with P4, **3.** LAC26569 – Right M1, **4.** LAC21723 – Right M2, **5.** LAC26510 – Right maxillary fragment with M3, **6.** LAC27953 – Right mandibular fragment with c and p4, **7.** LAC16744 – Left mandibular fragment with i3-p2 and p4 (**a.** labial, **b.** occlusal), **8.** LAC19483 – Right mandibular fragment with p4-m3 (**a.** labial, **b.** occlusal), **9.** LAC26478 – Distal epiphysis of left humerus (**a.** anterior, **b.** lateral, **c.** posterior).

Rhinolophus hipposideros **Bechstein, 1800**

(Lesser Horseshoe Bat)

Figure 4.17 and Figure A.57

Fossiliferous locality LAC I, LAC Ib, LAC Ic, LAC II, LAC III

Age Late Pleistocene

Material 35 identified specimens

LAC I: 1 right mandibular fragment (19936), LAC Ib: 1 right C (16525), 1 right m1 (17109), LAC Ic: 2 right C (17993, 21423), 1 left C (17957), 1 left M2 (18003), 1 left m3 (18048), LAC II: 1 left P4 (22376), 1 right M1 (27944), 1 left M1 (21886), 2 right M2 (21935, 27767), 1 right mandibular fragment with m1 and m3 (16660), 1 right c (21767), 1 right p4 (27856), 3 left m1 (21993, 16143, 22230), 1 right m2 (21613), 1 left m3 (22241), LAC III: 1 right C (21122), 2 left C (21212, 21400), 1 right P4 (19139), 2 left P4 (17486, 20559), 2 right M1 (20990, 20994), 3 left M2 (20118, 20547, 20999), 1 left c (21039), 1 right m3 (20017), 1 left m3 (20787)

Fossiliferous locality LAC Ia

Age latest Pleistocene

Material 118 identified specimens

1 right maxillary fragment with C and P4-M1 (19747), 1 left maxillary fragment with P4-M1 (23142), 1 right maxillary fragment with P4-M2 (23120), 1 right maxillary fragment with M1-M2 (23166), 1 right maxillary fragment with M1-M3 (23083), 1 left maxillary fragment with M1-M3 (27244), 1 right maxillary fragment with M2-M3 (23096), 1 left maxillary fragment with M2-M3 (23115), 1 left maxillary fragment with M3 (23201), 2 right C (26120, 26121), 7 left C (25896, 25949, 25999, 26027, 26043, 26093, 27423), 5 right P4 (25228, 25245, 25266, 25267, 25287), 3 left P4 (25333, 25352, 25386), 1 right M1-2 (25190), 4 right M1 (24366, 24582, 24622, 26592), 6 left M1 (24770, 24841, 24843, 24892, 24931, 24957), 5 right M2 (24368, 24498, 24657, 24660, 26583), 10 left M2 (24698, 24739, 24749, 24765, 24775, 24808, 24814, 24935, 26633, 26646), 4 right M3 (24991, 25168, 25170, 25171), 6 left M3 (24724, 25046, 25073, 25082, 25093, 25116), 1 right mandibular fragment (19508), 2 left mandibular fragments (23054, 23060), 1 right mandibular fragment with c-p2 and p4-m2 (26738), 1 left mandibular fragment p4 (22801), 1 left mandibular fragment p4-m1 (22755), 2 right mandibular fragments with p4-m2 (22466, 22475), 2 right mandibular fragments p4-m3 (22476, 27259), 1 right mandibular fragment with m1 (19669), 3 right mandibular fragments with m1-m3 (22603, 22606, 22474), 2 right mandibular fragments with m2-m3 (22521, 26760), 2 left mandibular fragments with m2-m3 (22903, 26804), 1 right mandibular fragment with m3 (22689), 1 left mandibular fragment with m3 (22864), 3 right c (26049, 26061, 27163), 5 left c (25998, 26085, 26122, 26170, 26353), 4 right m1 (23344, 23379, 26745, 26894), 2 left m1 (23984, 24038), 3 right m2 (23337, 23614, 26884), 5 left m2 (23874, 23907, 23909, 23941, 24153), 3 right m3 (23440, 23577, 23589), 3 left m3 (23973, 24112, 26797), 5 right humeri (26484, 26489, 26500, 26501, 27214), 3 left humeri (26462, 26463, 26467)

Measurements Table 4.6 and Figure 4.15-16

Description *Rhinolophus hipposideros* is the smallest member of the five Horseshoe Bat species that currently occur in Greece.

C: Small-sized tooth with the cusp curved distally. It is oval in occlusal view. The crown, which is short, forms an obtuse angle with the root. A small heel is present at the lingual part of the tooth. The crown is relatively sharp mesially and lingually. The cingulum is thick and convex at its labial and lingual parts with its maximum thickness at its mesiolabial part.

P4: Small-sized tooth with the cusp being connected with a crista to an accessory distolabial cusplet. It is subrectangular in occlusal view. A well-developed heel is present at the lingual part of the tooth. The crown, which is mildly constricted at its middle part, is relatively sharp lingually. The cingulum is thick and concave at its mesial, labial and distal (strongly marked) parts and convex at its mesiolabial, distolabial and mesiolingual parts, with its maximum thickness at the mesial part of the heel. An accessory cusplet-like structure is present at the mesiolabial part of the tooth, where it comes into contact with P3.

Table 4.6 *Rhinolophus hipposideros*, Loutra Almopias Cave A. Measurements (in mm) from both LAC and LAC Ia. LAC: Late Pleistocene; LAC Ia: latest Pleistocene; n: number of measurable specimens; L: length; W: width; trgd: trigonid; tld: talonid; MEAN: average; MIN: minimum; MAX: maximum; SD: standard deviation; CV: coefficient of variation.

			n	**MEAN**	**MIN**	**MAX**	**SD**	**CV**
C	LAC	L	7	0.96	0.88	1.02	0.055	5.742
		W	7	0.73	0.65	0.79	0.048	6.630
	LAC Ia	L	10	0.93	0.77	1.01	0.069	7.467
		W	10	0.71	0.55	0.81	0.079	11.177
P4	LAC	L	4	0.87	0.83	0.90	0.033	3.809
		W	2	1.17	1.08	1.25	0.120	10.318
	LAC Ia	L	11	0.80	0.71	0.91	0.061	7.541
		W	10	1.45	1.02	1.23	0.065	5.628
M1	LAC	L	3	1.45	1.39	1.54	0.079	5.474
		W	3	1.36	1.35	1.39	0.023	1.694
	LAC Ia	L	17	1.33	1.13	1.41	0.068	5.134
		W	17	1.26	1.12	1.44	0.087	6.904
M2	LAC	L	6	1.18	1.08	1.24	0.069	5.890
		W	6	1.17	0.98	1.30	0.110	9.363
	LAC Ia	L	20	1.24	1.12	1.36	0.061	4.939
		W	20	1.24	1.13	1.41	0.071	5.729
M3	LAC Ia	L	15	1.04	0.92	1.13	0.064	6.163
		W	15	1.25	1.13	1.36	0.064	5.111
c	LAC	L	2	0.58	0.56	0.60	0.028	4.877
		W	2	0.77	0.73	0.81	0.057	7.347
	LAC Ia	L	9	0.63	0.56	0.71	0.041	6.460
		W	9	0.67	0.53	0.77	0.076	11.325
p2	LAC Ia	L	1	0.60	-	-	-	-
		W	1	0.47	-	-	-	-
p4	LAC	L	1	0.65	-	-	-	-
		W	1	0.56	-	-	-	-

	LAC Ia	L	7	0.63	0.52	0.74	0.075	11.815
		W	7	0.60	0.49	0.65	0.056	9.389
m1	LAC	L	5	1.40	1.32	1.48	0.057	4.090
		W (trgd)	5	0.73	0.71	0.77	0.023	3.115
		W (tld)	5	0.83	0.79	0.86	0.027	3.188
	LAC Ia	L	15	1.36	1.30	1.44	0.038	2.770
		W (trgd)	15	0.73	0.56	0.85	0.075	10.231
		W (tld)	16	0.82	0.67	0.90	0.052	6.352
m2	LAC	L	1	1.33	-	-	-	-
		W (trgd)	1	0.81	-	-	-	-
		W (tld)	1	0.85	-	-	-	-
	LAC Ia	L	20	1.30	1.20	1.37	0.035	2.730
		W (trgd)	20	0.79	0.65	0.90	0.062	7.913
		W (tld)	20	0.84	0.76	0.97	0.055	6.630
m3	LAC	L	5	1.18	1.15	1.21	0.025	2.076
		W (trgd)	5	0.72	0.67	0.75	0.033	4.606
		W (tld)	4	0.69	0.66	0.72	0.026	3.742
	LAC Ia	L	17	1.19	1.10	1.33	0.052	4.382
		W (trgd)	17	0.74	0.58	0.87	0.071	9.674
		W (tld)	15	0.68	0.51	0.77	0.078	11.548
M1-M3	LAC Ia	L	2	3.58	3.51	3.65	0.099	2.765
m1-m3	LAC	L	1	3.93	-	-	-	-
	LAC Ia	L	4	3.81	3.78	3.84	0.028	0.723
p4-m3	LAC Ia	L	2	4.42	4.41	4.42	0.007	0.160
c-p4	LAC Ia	L	1	1.78	-	-	-	-
Humerus	LAC Ia	L	1	23.04	-	-	-	-
		W	8	3.23	3.02	3.49	0.153	4.748

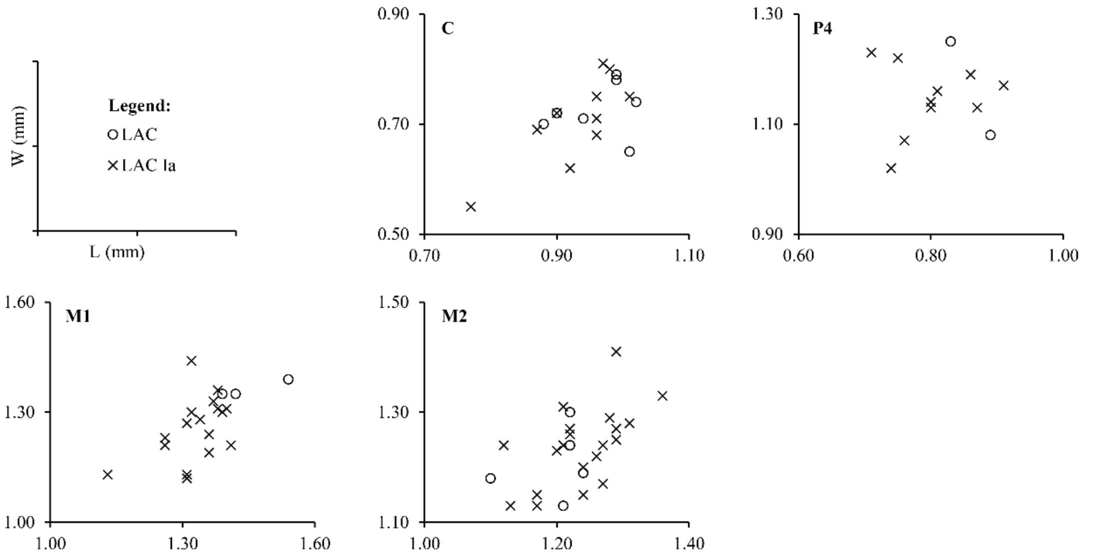

Figure 4.15 *Rhinolophus hipposideros*, Loutra Almopias Cave A. XY graphs with the measured (in mm) dental elements (C, P4, M1, M2). L: length, W: width.

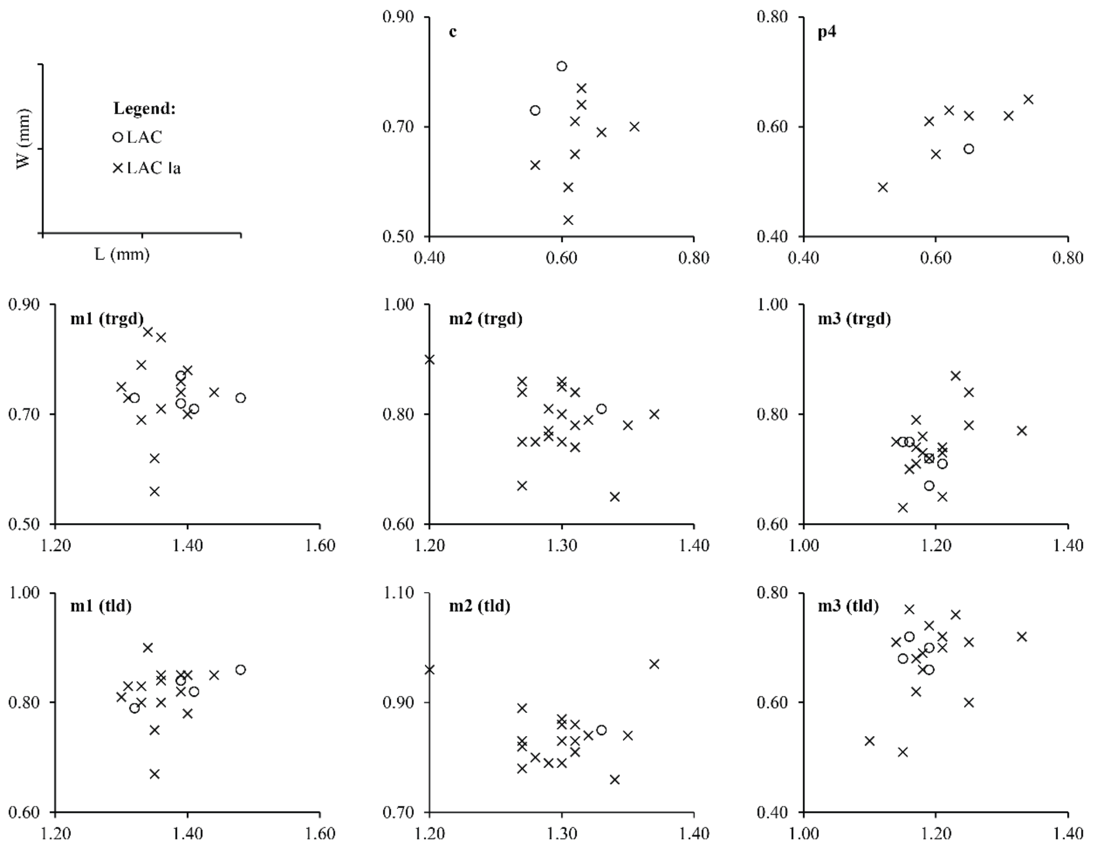

Figure 4.16 *Rhinolophus hipposideros*, Loutra Almopias Cave A. XY graphs with the measured (in mm) dental elements (c, p4, m1, m2, m3). L: length, W: width, trgd: trigonid; tld: talonid.

M1: It is subrectangular in occlusal view. Relatively well-developed semicircular to subtriangular heel at the distolingual part of the tooth, without hypocone. Parastyle, mesostyle, metastyle, paracone and metacone are slender. The metacone and the paracone are approximately of the same height with the former slightly taller than the latter. The parastyle forms an angle with the preparacrista. The ectoloph is symmetrical, with the mesial part somewhat wider than the distal part. Additionally, the paracone and the cristae on both sides form a wider angle than the metacone and the respective cristae. Paraloph, metaloph, paraconule and metaconule are absent. The anterior and the distal cingulum, which are thin, are absent beneath the parastyle, the triangular protocone and the metastyle. The lingual cingulum is only present around the heel.

M2: Not well-developed heel. The mesial part of the ectoloph is narrower than the distal part, but less than in M1. The rest of the characters as M1.

M3: It is triangular in occlusal view. The heel is absent. Parastyle, mesostyle, paracone and metacone are well-developed, whereas the metastyle is absent. The postmetacrista that connects the mesostyle with the metacone is absent. The metacone and the paracone are approximately of the same height, with the former slightly taller than the latter. The parastyle forms an angle with the preparacrista. Paraloph, metaloph, paraconule and metaconule are absent. Both the anterior and distal cingulum are very thin and only present beneath the protocone, which is less triangular than in M1 and M2.

c: Small-sized tooth with the cusp slightly curved lingually. It is subtriangular to semicircular in occlusal view. It is convex at its mesial and distolingual part and concave at its distolabial part. The distal part of the tooth is developed at the base of the crown, whereas the mesial part is developed in height. Respectively, the crown is in a more superior position towards the anterior part of the tooth. The distolabial part of the tooth is situated lower than the distolingual, which is higher than the former. The cingulum is thin throughout the whole tooth and it reaches its maximum thickness at the mesiolingual part of the tooth and its minimum at the mesial part, where it comes in contact with i3.

p2: Unicuspid. It is oval in occlusal view. The crown is convex at its mesial, labial, distal and lingual parts with the mesial and distal being relatively sharp. The labial part is elongated and narrow, whereas the lingual is short and wide. The cingulum is thin and uniform throughout the whole tooth, apart from its mesial and distal parts where it thickens.

p4: Small-sized tooth with the cusp slightly curved mesially. It is triangular in occlusal view. The mesiolingual part of the tooth is more elongated and higher than the mesiolabial part. The distolingual part of the tooth is higher than the distolabial. The mesial, distolabial and lingual parts of the tooth are convex and the mesiolabial and distal are concave. The cingulum is thin and uniform throughout the whole tooth and it bends down slightly at the level of each root, with the posterior convexity being placed slightly lower than the anterior. The cingulum appears to be flatter, when the tooth is worn and/or corroded (i.e. LAC26738 and LAC22476).

m1: Nyctalodont. The trigonid is longer than the talonid. Paraconid, metaconid, entoconid, protoconid and hypoconid are well-developed. The protoconid is taller than the hypoconid. The paralophid is angular. The entocristid is curved. The hypoconulid is relatively well-developed and it is positioned towards the labial part of the tooth. The labial cingulum is thin and uniform throughout the whole tooth, with a slight concavity at its mesial part.

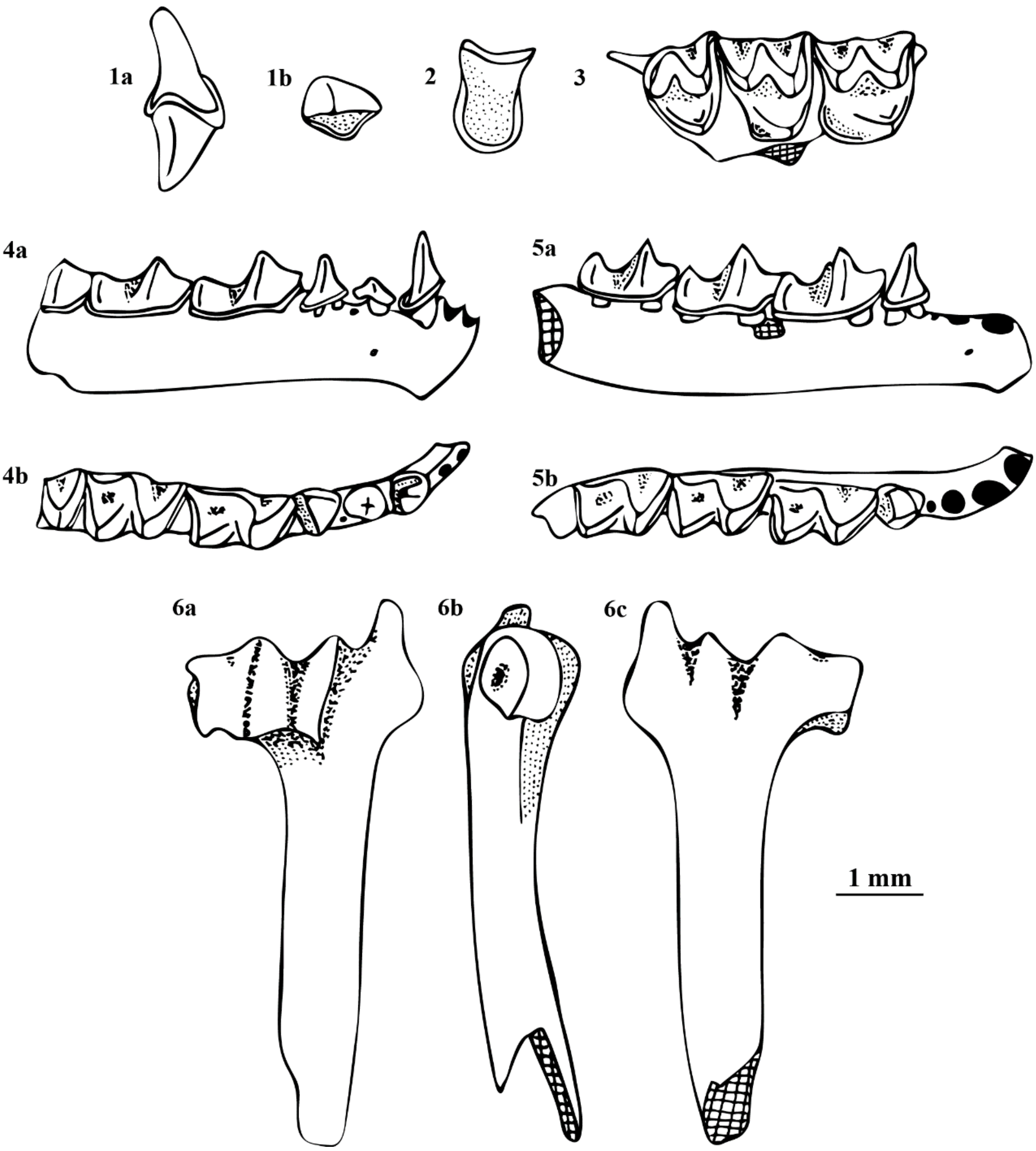

Figure 4.17 *Rhinolophus hipposideros*, Loutra Almopias Cave A. **1.** LAC16525 – Right C (**a.** labial, **b.** occlusal), 2. LAC22376 – Left P4, 3. LAC23083 – Right maxillary fragment with M1-M3, 4. LAC26738 – Right mandibular fragment with c-p2 and p4-m3 (**a.** labial, **b.** occlusal), 5. LAC22476 – Right mandibular fragment with p4-m3 (**a.** labial, **b.** occlusal), 6. LAC26462 – Distal epiphysis of left humerus (**a.** anterior, **b.** lateral, **c.** posterior).

m2: The trigonid and the talonid are of almost equal length. The entocristid is more curved. The labial cingulum is flat. The rest of the characters as m1.

m3: Nyctalodont. The trigonid and the talonid are of almost equal length. Paraconid, metaconid, entoconid, protoconid and hypoconid are well-developed. The protoconid is taller than the hypoconid. The paralophid is angular and more similar to m2. The entoconid is more towards the labial side of the tooth and thus, the talonid is reduced.

The hypoconulid is relatively reduced. The labial cingulum is thin and it becomes thinner towards the distal part.

Mandible: The masseter crest is thin. The mental foramen is minute and located beneath the middle part of p2. The lowest part of the symphysis is relatively pointed and projects downwards.

Humerus: The styloid process is long and sharp. The epitrochlea is relatively narrow. A deep U-shaped valley is present between the trochlea and the condyle. A shallow valley is present between the condyle and the epicondyle. The condyle and the epicondyle are projecting laterally. The radial fossa and the olecranon fossa are very shallow (practically flat).

Discussion The morphological features described in addition to the measurements allow a definite attribution of the material to *Rhinolophus hipposideros*. It is the smallest member of the five Horseshoe Bat species that currently occur in Greece and it is clearly distinguished from the rest of the species.

Occurrence Fossils of the Lesser Horseshoe Bat are known from Sarakenos Cave, Boeotia, Charkadio Cave, Tilos and Petralona Cave, Chalkidiki. Its modern distribution includes most of mainland Greece and several islands of the Aegean and the Ionian Sea, including Crete (Hanák et al. 2001, GFDC 2021). On a global scale it is distributed from Northwestern Africa, the Iberian Peninsula and Northern Europe (including Ireland) all the way to Kyrgyzstan and Kashmir, parts of the Levant and the Arabian Peninsula, Sudan and parts of the Horn of Africa (Simmons 2005a).

Ecology *Rhinolophus hipposideros* is a typical cave dweller and its habitat preferences are very diverse including forests and open areas, with the presence of water bodies being the only "limitation" (Dietz et al. 2009).

***Rhinolophus* sp.**

Figure 4.18

Fossiliferous locality LAC I, LAC Ib, LAC Ic, LAC II, LAC III

Age Late Pleistocene

Material 104 identified specimens

LAC I: 1 right C (19970), 1 left C (19935), 1 right M1-2 (19989), 1 left M3 (17249), 2 right mandibular fragments (16637, 16646), 3 left mandibular fragments (17328, 16632, 16633), 1 left p4 (19948), 1 right m1-3 (19930), LAC Ib: 1 right P4 (19899), 1 left P4 (19869), 1 left M1-2 (19902), 2 left mandibular fragments (16434, 19890), 1 left mandibular fragment with m2 (18844), 1 left m1-2 (17183), LAC Ic: 1

right mandibular fragment (17898), LAC II: 1 right C (27558), 2 right P4 (21743, 21745), 2 left P4 (21982, 27736), 1 left M1-2 (27695), 1 right M2 (21902), 1 right M3 (22295), 15 right mandibular fragments (21555, 21595, 21598, 21602, 21910, 16668, 16353, 16362, 16410, 16165, 22397, 22400, 27576, 27783, 27860), 9 left mandibular fragments (21604, 16619, 16016, 16020, 16023, 16411, 27784, 27785, 27786), 1 left mandibular fragment with c (16360), 1 left mandibular fragment with p4-m1 (16117), 1 left mandibular fragment with p4-m2 (21594), 1 left mandibular fragment with m1 (16370), 1 right mandibular fragment with m2-m3 (16393), 1 right c (22101), 1 left p2 (27666), 2 right m3 (22217, 27930), 1 left m3 (21588), 2 left humeri (27537, 27712), LAC III: 1 right maxillary fragment with P4-M1 (17496), 3 right P4 (20871, 21011, 21133), 8 left P4 (21341, 21385, 20920, 20951, 21032, 20300, 20308, 20393), 2 right/left P4 (21214, 21123), 1 left M1 (20117), 1 right M3 (20279), 1 left M3 (20557), 7 right mandibular fragments (20110, 20136, 20235, 16463, 16467, 16438, 20605), 12 left mandibular fragments (20237, 20240, 20241, 20242, 20243, 20244, 20970, 20971, 20972, 20974, 20975, 20610), 1 right mandibular fragment with m1 (21059), 1 right mandibular fragment with m2-m3 (20617), 1 right c (20098), 1 right m1-2 (19334), 1 left m3 (20524)

Fossiliferous locality LAC Ia

Age latest Pleistocene

Material 96 identified specimens

1 left maxillary fragment with P4-M1 (23138), 1 right C (26100), 1 left C (26265), 2 right P4 (25227, 25262), 1 left M1-2 (24773), 2 right M2 (24577, 24631), 3 left M2 (24642, 24849, 26670), 1 right M3 (25220), 1 left M3 (26539), 37 right mandibular fragments (19512, 22949, 22950, 22953, 22958, 22959, 22960, 22963, 22964, 22969, 22972, 22973, 22975, 22984, 22986, 22989, 22990, 22991, 22993, 22998, 22999, 23000, 23001, 23004, 23009, 23010, 23011, 23012, 26830, 26840, 26842, 26844, 26845, 27264, 27265, 27266, 27267), 32 left mandibular fragments (19520, 19522, 19525, 19527, 19532, 23015, 23018, 23023, 23024, 23027, 23029, 23030, 23031, 23033, 23035, 23036, 23042, 23043, 23046, 23048, 23055, 23056, 23058, 23061, 23064, 23067, 23068, 26850, 26853, 26854, 26859, 26860), 1 right mandibular fragment with i2 and c (22625), 1 left mandibular fragment with i3 (22945), 1 left mandibular fragment with c (23062), 1 right mandibular fragment with m1-m2 (22595), 1 left mandibular fragment with m1-m2 (22847), 1 right mandibular fragment with m2-m3 (22624), 1 left mandibular fragment with m2-m3 (26810), 2 right c (27148, 27166), 1 left c (26230), 1 right m1-2 (23535), 1 right m1-3 (23642), 1 right humerus (27448), 1 left humerus (26468)

Measurements Table 4.7

Description Here are grouped specimens that could not be identified beyond genus level, mostly because they are severely damaged (worn/digested/corroded/broken/etc.). Consequently, no further descriptions are provided.

Table 4.7 *Rhinolophus* sp., Loutra Almopias Cave A. Measurements (in mm) from both LAC and LAC Ia. LAC: Late Pleistocene; LAC Ia: latest Pleistocene; n: number of measurable specimens; L: length; W: width; trgd: trigonid; tld: talonid; MEAN: average; MIN: minimum; MAX: maximum; SD: standard deviation; CV: coefficient of variation.

			n	MEAN	MIN	MAX	SD	CV
C	LAC	L	3	1.46	1.36	1.64	0.159	10.905
		W	2	1.11	0.95	1.27	0.226	20.385
	LAC Ia	L	1	1.16	-	-	-	-
		W	1	1.87	-	-	-	-
P4	LAC	L	10	1.09	0.81	1.27	0.153	14.001
		W	2	1.08	1.05	1.10	0.035	3.289

	LAC Ia	L	2	1.07	0.96	1.17	0.149	13.943
		W	2	1.61	1.41	1.81	0.283	17.568
M1	LAC	L	2	1.65	1.57	1.72	0.106	6.448
		W	1	1.32	-	-	-	-
	LAC Ia	L	2	1.50	1.31	1.69	0.269	17.913
		W	2	1.61	1.59	1.63	0.028	1.757
M2	LAC Ia	L	2	1.32	1.30	1.34	0.028	2.143
		W	2	1.41	1.27	1.55	0.198	14.042
M3	LAC	L	1	1.41	-	-	-	-
		W	1	1.60	-	-	-	-
	LAC Ia	L	1	1.47	-	-	-	-
		W	1	1.68	-	-	-	-
i2	LAC Ia	L	1	0.74	-	-	-	-
		W	1	0.60	-	-	-	-
i3	LAC Ia	L	1	0.60	-	-	-	-
		W	1	0.30	-	-	-	-
c	LAC	L	2	0.78	0.75	0.80	0.035	4.562
		W	2	1.11	1.05	1.17	0.085	7.644
	LAC Ia	L	5	0.77	0.58	0.92	0.125	16.221
		W	5	0.95	0.69	1.26	0.248	26.179
p2	LAC	L	1	0.79	-	-	-	-
		W	1	0.89	-	-	-	-
p4	LAC	L	1	0.69	-	-	-	-
		W	1	0.98	-	-	-	-
m1	LAC	L	3	1.68	1.61	1.73	0.061	3.644
		W (trgd)	3	0.83	0.65	1.01	0.180	21.687
		W (tld)	4	0.86	0.72	1.02	0.146	16.990
	LAC Ia	L	2	1.55	1.38	1.71	0.233	15.103
		W (trgd)	3	0.76	0.64	0.84	0.109	14.130
		W (tld)	3	0.93	0.77	1.07	0.150	16.235
m2	LAC	L	3	1.66	1.35	1.84	0.267	16.133
		W (trgd)	3	0.92	0.74	1.05	0.163	17.608
		W (tld)	4	0.97	0.82	1.10	0.135	13.831
	LAC Ia	L	3	1.56	1.47	1.61	0.081	5.170
		W (trgd)	4	0.87	0.74	0.99	0.103	11.884
		W (tld)	3	0.98	0.83	1.11	0.141	14.383
m3	LAC	L	3	1.45	1.39	1.56	0.093	6.393
		W (trgd)	6	0.80	0.69	1.04	0.129	16.147
		W (tld)	5	0.71	0.50	1.08	0.229	32.054
	LAC Ia	L	2	1.60	1.58	1.61	0.021	1.330
		W (trgd)	2	0.95	0.88	1.01	0.092	9.727
		W (tld)	2	0.92	0.76	1.07	0.219	23.957
Humerus	LAC Ia	W	2	3.66	3.48	3.84	0.255	6.955

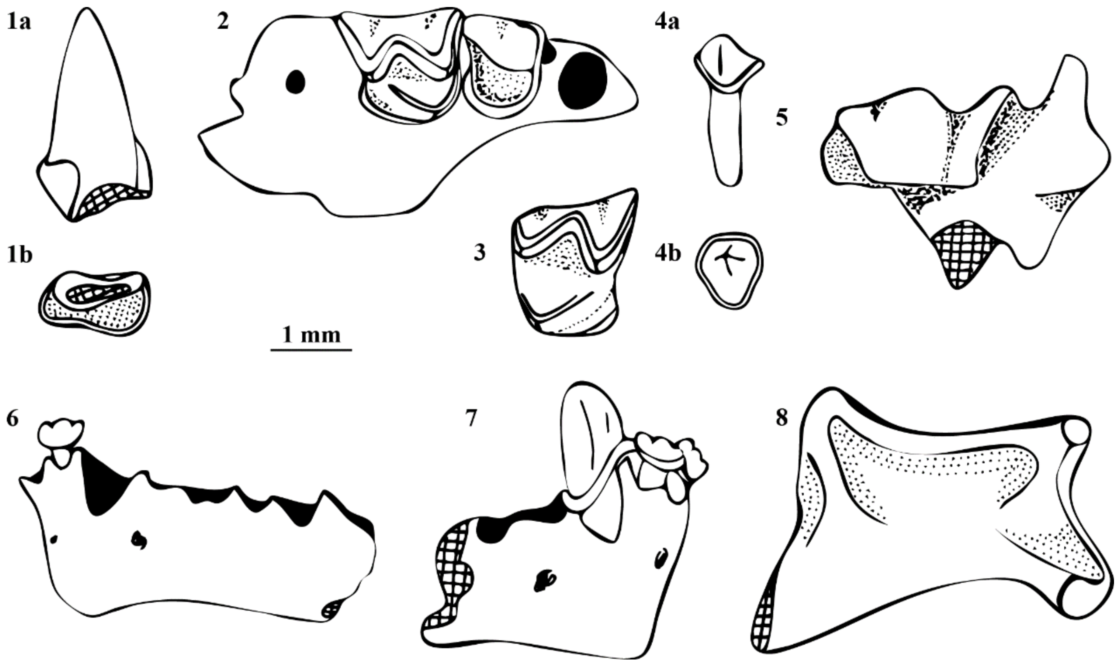

Figure 4.18 *Rhinolophus* sp., Loutra Almopias Cave A. **1.** LAC27558 – Right C (**a.** labial, **b.** occlusal), **2.** LAC17496 – Right maxillary fragment with P4-M1, **3.** LAC26670 – Left M2, **4.** LAC27666 – Left p2 (**a.** labial, **b.** occlusal), **5.** LAC26468 – Distal epiphysis of left humerus, **6.** LAC22945 – Left mandibular fragment with i3, **7.** LAC22625 – Right mandibular fragment with i2-c, **8.** LAC23068 – Left mandibular fragment.

4.2 FAMILY VESPERTILIONIDAE

Vespertilionidae Gray, 1821

Vespertilionidae, also known as the Vesper/Evening Bats or the Plain-nosed Bats, is the largest extant chiropteran family, which includes 46 genera and at least 389 species that are distributed globally except Antarctica (Simmons 2005a).

The earliest occurrence of Vespertilionidae in the global fossil record, is *Premonycteris vesper* from the Early Eocene (MP10) locality of Prémontré, France (Hand et al. 2016). The earliest occurrence of Vespertilionidae in the fossil record of Greece is cf. *Myotis* (small-sized) from the Late Miocene locality of Elaiochoria 2, Chalkidiki (Hulva et al. 2007).

Myotis Kaup, 1829

Type species *Vespertilio myotis* Borkhausen, 1797

The earliest occurrence of *Myotis* in the global fossil record is *Myotis belgicus* from the Early Oligocene locality of Boutersem and Hoogbutsel, Belgium (Gunnell et al. 2017). The earliest occurrence of Vespertilionidae in the fossil record of Greece is cf. *Myotis* (small-sized) from the Late Miocene fauna of Elaiochoria 2, Chalkidiki (Hulva et al. 2007). There are currently eleven species occurring in Greece: *Myotis myotis*, *Myotis blythii*, *Myotis bechsteinii*, *Myotis emarginatus*, *Myotis capaccinii*, *Myotis nattereri*, *Myotis aurascens*, *Myotis alcathoe*, *Myotis brandtii*, *Myotis daubentonii* and *Myotis mystacinus* (Hanák et al. 2001, Simmons 2005a, Sfougaris 2009). *Myotis myotis*, *Myotis blythii*, *Myotis blythii oxygnathus*, *Myotis bechsteinii*, *Myotis emarginatus*, *Myotis capaccinii*, *Myotis* cf. *daubentonii*, *Myotis* cf. *mystacinus*, *Myotis myotis*/*blythii*, *Myotis* sp., *Myotis* sp. I, *Myotis* sp. II, cf. *Myotis* (small-sized) are present in the fossil record of Greece (Piskoulis and Chatzopoulou in press), with *Myotis bechsteinii*, *Myotis capaccinii* and *Myotis* cf. *mystacinus* described for the first time from Loutra Almopias Cave A.

The dental formula of *Myotis* is: 2.1.3.3/3.1.3.3 and there are several morphological characteristics that distinguish *Myotis* from other chiropteran taxa, such as the absence of heel and/or talon on the upper molars, myotodont lower molars, thick cingulum on nearly all dental elements, short and blunt styloid process of the humerus and no lateral projection of the condyle and the epicondyle. Even though many species share very similar characteristics, identification of fossils at species level is not as complex as with other genera (e.g. *Rhinolophus*).

***Myotis myotis* Borkhausen, 1797**

(Greater Mouse-eared Bat)

Figure 4.21 and Figure A.58

Fossiliferous locality LAC I, LAC Ib, LAC Ic, LAC II, LAC III

Age Late Pleistocene

Material 183 identified specimens

LAC I: 1 right I1 (27467), 1 right C (27461), 1 right c (19949), 1 left c (27472), 2 left p2 (19972, 27505), 1 left p3 (19986), 1 right p4 (27478), 1 right m1 (17333), 2 right m3 (17264, 27475), 1 left m3 (27502), LAC Ib: 2 right I2 (17161, 27520), 1 left P2 (27519), 1 right c (16475), 1 left p3 (16549), 1 right m2 (17182), 1 left m3 (16683), 1 left humerus (27515), LAC Ic: 2 left I1 (21439, 21442), 1 right I2 (17943), 1 left C (18068), 1 left M1 (18063), 1 right M2 (21447), 1 left M2 (21446), 1 left mandibular fragment with i1-c (16424), 2 right c (17916, 21513), 1 right p2 (21428), 1 left p2 (21425), 1 right p3 (17940), 1 left p4 (21497), 3 right m1 (17877, 21473, 21477), 1 right m2 (16419), 2 right m3 (21485, 21488), 1 left m3 (21489), LAC II: 1 right I2 (22444), 1 left I2 (27837), 2 right C (22049, 22388), 1 left C (27614), 2 right P4 (21978, 22310), 2 left P4 (27610, 27795), 4 right M1 (21721, 21726, 21920, 22139), 1 left M1 (21885), 1 right M2 (22362), 2 left M2 (21539, 22005), 1 left M3 (16367), 8 right c (21793, 21952, 22189, 22332, 27536, 27589, 27700, 27759), 3 left c (21924, 27702, 27949), 2 right p2 (21824, 27622), 2 left p2 (27532, 27817), 1 right p3 (27710), 8 right p4 (21661, 21985, 22131, 22246, 22253, 22382, 27829, 27893), 3 left p4 (21673, 21917, 27584), 2 right m1 (21612, 21628), 5 left m1 (21855, 22067, 22218, 27801, 27826), 2 right m2 (21622, 22204), 2 left m2 (21911, 27646), 2 right m3 (22346, 27854), 4 left m3 (21657, 21915, 22236, 27637), LAC III: 1 right I1 (21436a), 1 left I2 (20131), 2 right C (20090, 20068), 4 left C (21378, 21027, 21126, 19340), 1 left P2 (20060), 1 left P3 (20948), 1 right P4 (17844), 1 left P4 (20183), 3 right M1 (20167, 20887, 20367), 4 left M1 (20268, 20924, 20362, 20458), 2 right M2 (21309, 20988), 2 left M2 (20165, 20791), 2 right M3 (21320, 21091), 1 left M3 (21335), 8 right c (20123, 20142, 20711, 21014, 21047, 21111, 20067, 20292), 6 left c (20712, 17490, 20934, 21113, 19296, 20474), 1 right p2 (20400), 6 left p2 (21218, 21223, 17722, 20953, 20320, 20591), 2 right p3 (20952, 20059), 1 left p3 (17723), 6 right p4 (20164, 20943, 21001, 21076, 21173, 20441), 3 left p4 (20261, 20360, 20544), 5 right m1 (20112, 20774, 20857, 20010, 20019), 6 left m1 (20155, 21163, 20021, 20026, 20340, 20536), 3 right m2 (20145, 20514, 20856), 1 left m2 (21164), 3 right m3 (21274, 20902, 20512), 3 left m3 (20780, 20941, 19157)

Fossiliferous locality LAC Ia

Age latest Pleistocene

Material 138 identified specimens

2 left maxillary fragments with M2 (23220, 23223), 1 right maxillary fragment with M2-M3 (27241), 1 left maxillary fragment with M3 (23198), 1 right P2 (26351), 2 right P3 (26341, 26350), 3 left P3 (26280, 26293, 26338), 8 right C (25561, 25601, 25724, 25725, 25800, 25959, 26159, 27072), 5 left C (25543, 25706, 25783, 27104, 27120), 1 right P4 (26695), 3 left P4 (23256, 25356, 25392), 11 right M1 (23230, 23238, 24406, 24413, 24465, 24485, 24503, 24524, 26558, 26578, 26586), 18 left M1 (24678, 24689, 24764, 24767, 24826, 24869, 24899, 24903, 24906, 24923, 24944, 24948, 26634, 26651, 26666, 27322, 27323, 27326), 4 right M2 (24530,24590, 26511, 26563), 3 left M2 (24897, 24907, 26654), 3 right M3 (25176, 26620, 27242), 1 left M3 (25044), 1 left mandibular fragment with i1-c (22859), 1 right mandibular fragment with m1-m2 (22502), 1 left mandibular fragment with m1-m2 (22728), 2 right mandibular fragments with m1-m3 (22450, 22506), 2 right mandibular fragments with m2-m3 (22453, 22454), 1 left mandibular fragment with m3 (22884), 13 right c (25487, 25571, 25701, 25833, 25839, 25857, 25871, 25951, 27140, 27144, 27151, 27156, 27161), 12 left c (25450, 25491, 25722, 25745, 25981, 26017, 26021, 26172, 26185, 27177, 27183, 27187), 2 right p4 (24192, 24229), 2 right m1-2 (23542, 26881), 9 right m1 (23451, 23469, 23538, 23540, 26882, 26913, 27348, 27349, 27353), 7 left m1 (23726, 23729, 23737, 23754, 23791, 23804, 27382), 6 right m2 (23377, 23378, 23435, 23465, 23484, 26871), 1 left m2 (23799), 10 left m3 (24118, 24124, 24154, 24156, 24159, 24173, 24174, 26775, 26796, 27017), 1 right humerus (27206)

Measurements Table 4.8 and Figure 4.19-20

Description *Myotis myotis* is the largest member of the eleven Vesper Bat species that currently occur in Greece.

I1: Tricuspid. It is oval in occlusal view. The mesial cusp is the largest and it covers approximately 1/3 of the tooth’s area, the labial is the smallest one and the lingual is slightly larger than the latter. The small cusps are both located distally.

I2: Unicuspid with the main cusp at its mesiolabial part and a small accessory cusplet present at its mesiolingual part. It is oval in occlusal view. A cingulum of average thickness is also present at the mesial part of the tooth.

C: Very robust tooth with the cusp curved distally. It is oval in occlusal view. The crown forms an obtuse angle with the root, which is however, not as marked as in *Rhinolophus ferrumequinum*. A thick ridge connects the distal base of the crown with the cusp. The crown is convex mesially, labially, distally and lingually and concave distolabially and distolingually and narrow lingually. The cusp is slightly concave distolabially and lingually. Two longitudinal grooves occur, one labially and one lingually. The cingulum is very thick, with its maximum thickness at the labial part of the tooth.

Table 4.8 *Myotis myotis*, Loutra Almopias Cave A. Measurements (in mm) from both LAC and LAC Ia. LAC: Late Pleistocene; LAC Ia: latest Pleistocene; n: number of measurable specimens; L: length; W: width; trgd: trigonid; tld: talonid; MEAN: average; MIN: minimum; MAX: maximum; SD: standard deviation; CV: coefficient of variation.

			n	**MEAN**	**MIN**	**MAX**	**SD**	**CV**
I1	LAC	L	4	0.82	0.76	0.90	0.060	7.365
		W	4	0.56	0.51	0.62	0.048	8.641
I2	LAC	L	6	0.69	0.57	0.86	0.116	16.852
		W	6	0.89	0.83	0.99	0.060	6.667
C	LAC	L	11	1.72	1.62	1.86	0.080	4.623
		W	11	1.39	1.32	1.46	0.049	3.495
	LAC Ia	L	13	1.74	1.62	1.87	0.076	4.394
		W	13	1.33	1.19	1.53	0.085	6.388
P2	LAC	L	2	0.83	0.81	0.84	0.021	2.571
		W	2	0.90	0.80	1.00	0.141	15.714
	LAC Ia	L	1	0.94	-	-	-	-
		W	1	0.95	-	-	-	-
P3	LAC	L	1	0.83	-	-	-	-
		W	1	0.76	-	-	-	-
	LAC Ia	L	5	0.80	0.73	0.85	0.048	6.000
		W	5	0.70	0.64	0.75	0.040	5.734
P4	LAC	L	6	1.83	1.65	1.99	0.138	7.545
		W	5	1.60	1.53	1.72	0.076	4.762
	LAC Ia	L	4	1.70	1.46	1.86	0.173	10.166
		W	4	1.47	1.31	1.70	0.188	12.801
M1	LAC	L	13	2.28	1.85	2.42	0.148	6.507
		W	13	2.29	2.02	2.57	0.176	7.687
	LAC Ia	L	27	2.33	2.13	2.62	0.098	4.195
		W	27	2.26	1.98	2.47	0.117	5.183
M2	LAC	L	8	2.46	2.33	2.68	0.109	4.428
		W	9	2.69	2.39	2.81	0.129	4.817
	LAC Ia	L	9	2.34	2.26	2.44	0.063	2.677
		W	9	2.71	2.58	2.82	0.089	3.265
M3	LAC	L	4	2.20	2.13	2.26	0.057	2.598
		W	3	2.81	2.73	2.85	0.069	2.466
	LAC Ia	L	6	2.09	1.89	2.18	0.104	4.954
		W	6	2.61	2.50	2.67	0.078	3.001
i1	LAC	L	1	0.73	-	-	-	-
		W	1	0.33	-	-	-	-

	LAC Ia	L	1	0.80	-	-	-	-
		W	1	0.36	-	-	-	-
i2	LAC	L	1	0.80	-	-	-	-
		W	1	0.41	-	-	-	-
	LAC Ia	L	1	0.65	-	-	-	-
		W	1	0.39	-	-	-	-
i3	LAC	L	1	0.97	-	-	-	-
		W	1	0.68	-	-	-	-
	LAC Ia	L	1	0.72	-	-	-	-
		W	1	0.42	-	-	-	-
c	LAC	L	31	1.20	0.99	1.39	0.095	7.874
		W	31	1.39	1.16	1.75	0.124	8.921
	LAC Ia	L	25	1.16	0.92	1.58	0.143	12.398
		W	25	1.40	0.73	1.64	0.195	13.953
p2	LAC	L	15	1.08	0.94	1.12	0.048	4.486
		W	15	1.10	1.04	1.17	0.036	3.298
p3	LAC	L	7	0.86	0.83	0.90	0.032	3.672
		W	7	1.04	0.99	1.09	0.037	3.368
p4	LAC	L	22	1.42	1.32	1.51	0.052	3.649
		W	22	1.12	1.00	1.22	0.066	5.839
	LAC Ia	L	2	1.44	1.38	1.49	0.078	5.420
		W	2	1.01	0.92	1.10	0.127	12.602
m1	LAC	L	20	2.22	1.94	2.35	0.103	4.656
		W (trgd)	21	1.34	1.06	1.52	0.115	8.590
		W (tld)	21	1.57	1.25	1.71	0.114	7.247
	LAC Ia	L	22	2.13	1.93	2.30	0.096	4.525
		W (trgd)	22	1.35	1.16	1.65	0.099	7.359
		W (tld)	21	1.57	1.39	1.74	0.074	4.727
m2	LAC	L	9	2.37	2.17	2.57	0.145	6.107
		W (trgd)	9	1.53	1.45	1.66	0.075	4.902
		W (tld)	10	1.65	1.56	1.81	0.078	4.720
	LAC Ia	L	13	2.18	1.99	2.44	0.123	5.662
		W (trgd)	13	1.43	1.25	1.60	0.096	6.726
		W (tld)	13	1.55	1.41	1.73	0.102	6.611
m3	LAC	L	17	2.00	1.71	2.35	0.166	8.303
		W (trgd)	18	1.36	1.14	1.56	0.132	9.753
		W (tld)	19	0.84	0.73	1.07	0.090	10.655
	LAC Ia	L	15	1.83	1.57	2.07	1.116	6.315
		W (trgd)	15	1.21	1.09	1.27	0.053	4.355
		W (tld)	15	0.80	0.67	0.93	0.067	8.433
m1-m3	LAC Ia	L	2	6.22	6.17	6.27	0.071	1.137
Humerus	LAC Ia	W	1	4.54	-	-	-	-

P2: Unicuspid. It is oval in occlusal view. A thin ridge connects the distal base of the crown with the cusp. A thick cingulum is also present, with its maximum thickness at its labial and lingual parts.

P3: Unicuspid. It is subcircular-subrectangular in occlusal view. A thin ridge connects the distal base of the crown with the cusp. A thick cingulum is also present, with its maximum thickness at its labial and lingual parts. The crown is convex mesially, labially, distally and lingually and concave distolabially and distolingually and narrow lingually.

P4: Robust tooth with the cusp being connected with a crista to an accessory distolabial cusplet. It is subtriangular in occlusal view. A not-well developed heel is present at the mesiolingual part of the tooth. The crown is relatively sharp lingually. The cingulum is thick and concave at its distolabial and distolingual parts and convex at its mesiolabial, distal and mesiolingual parts, with its maximum thickness at the distolabial part of the tooth. A small cingular platform is present at the mesiolabial part of the tooth.

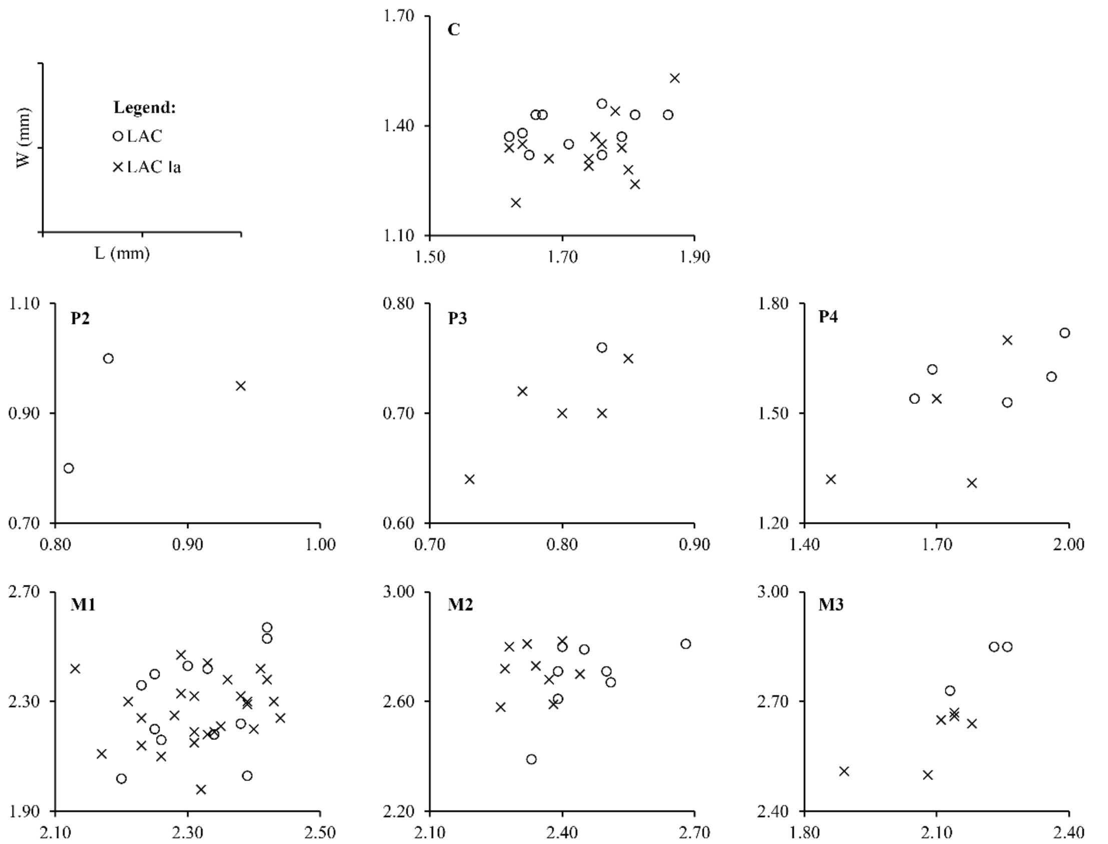

Figure 4.19 *Myotis myotis*, Loutra Almopias Cave A. XY graphs with the measured (in mm) dental elements (C, P2, P3, P4, M1, M2, M3). L: length, W: width.

M1: Very robust tooth. It is subrectangular in occlusal view. Parastyle, mesostyle, metastyle, paracone and metacone are well-developed. The metacone is taller than the paracone. The parastyle is curved and the metastyle slightly curves lingually. The mesial part of the ectoloph is narrower than the distal part. Additionally, the paracone, the metacone and the cristae on both sides form equal angles. Paraloph, metaloph, paraconule and metaconule are absent. The distal and lingual cingulum, which are thick, are absent beneath the metastyle and the triangular protocone. The mesiolabial part of the anterior cingulum is connected to the preprotocrista and its mesiolingual part, which starts from the mesial side of the protocone, runs towards the lingual side of the tooth.

M2: The mesial part of the ectoloph is wider than in M1. The rest of the characters as M1.

M3: Very robust tooth. It is triangular in occlusal view. The parastyle and the paracone are more developed than the mesostyle and the metacone, whereas the metastyle is absent. The postprotocrista that connects the metacone with the metastyle is also absent. The paracone is taller than the metacone. The parastyle is curved. The cingulum is of average thickness and disappears only beneath the mesial part of the triangular protocone.

i1: Oval in occlusal view. Four cusps are present at the labial part of the tooth. The middle cusps are well-developed and of equal size, whereas the distal cusp is the smallest.

i2: Oval in occlusal view. Three cusps are present at the labial part of the tooth and a fourth one at its distolingual part. The middle and the distal cusps are well-developed, whereas the distolingual cusp is the smallest.

i3: Subrectangular in occlusal view. Two cusps are present at the labial part of the tooth and two at its lingual part. The distolabial cusp is very well-developed, the mesiolabial is less developed than the latter, whereas the lingual cusps are equally developed and they are the smallest. Labial cingulum of average thickness is also present.

c: Very robust tooth with the cusp slightly curved lingually. It is semicircular in occlusal view. It is convex mesially and concave distally. The distal part of the tooth is developed at the base of the crown, whereas the mesial part is developed in height. Respectively, the crown is in a more superior position towards the anterior part of the tooth. The distolabial part of the tooth is situated lower than the distolingual, which is higher than the former. The cingulum is very thick throughout the whole tooth. It reaches its maximum thickness at the labial part of the tooth and it is absent at the mesial part, where it comes in contact with i3.

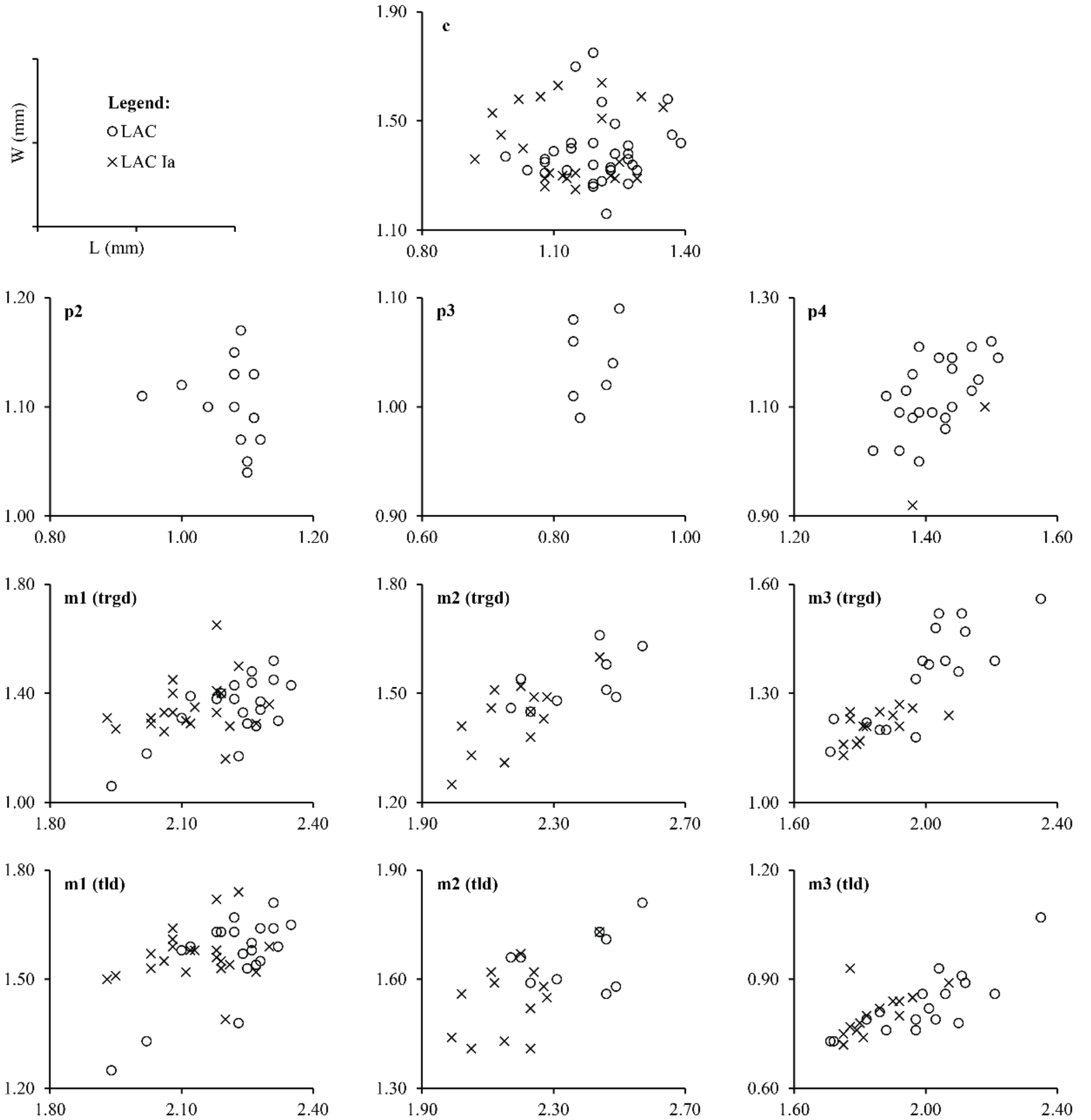

Figure 4.20 *Myotis myotis*, Loutra Almopias Cave A. XY graphs with the measured (in mm) dental elements (c, p2, p3, p4, m1, m2, m3). L: length, W: width, trgd: trigonid; tld: talonid.

p2: Unicuspid tooth. It is subcircular in occlusal view. The labial side is more convex than the lingual. The cingulum is very thick. It reaches its maximum thickness at its mesiolingual and distolingual parts, where one cusp-like form is present on each part.

p3: It is oval in occlusal view. It is convex mesially, labially and lingually. It is slightly concave distally. The labial side is more convex than the lingual. The rest of the characters as p2.

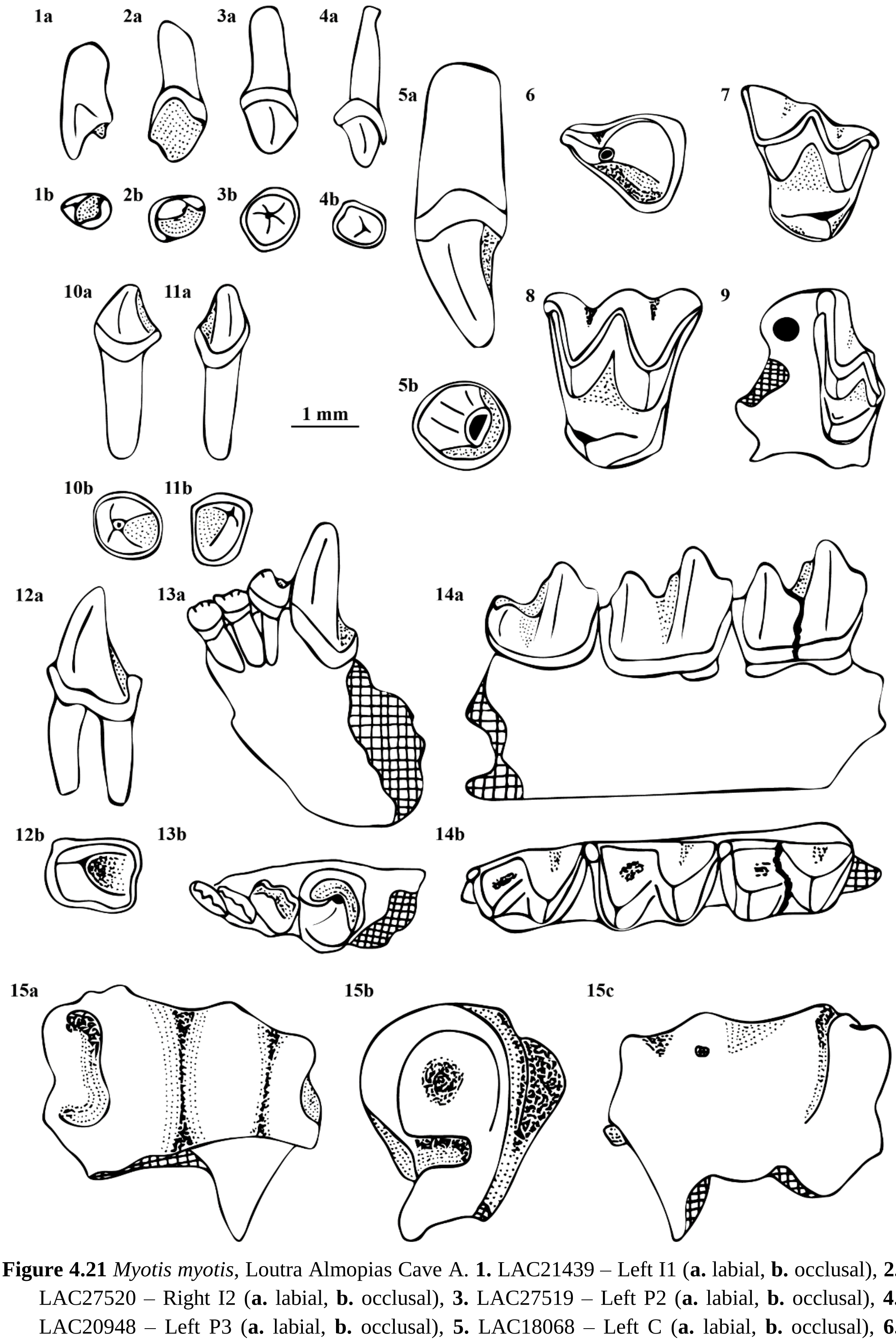

Figure 4.21 *Myotis myotis*, Loutra Almopias Cave A. **1.** LAC21439 – Left I1 (**a.** labial, **b.** occlusal), **2.** LAC27520 – Right I2 (**a.** labial, **b.** occlusal), **3.** LAC27519 – Left P2 (**a.** labial, **b.** occlusal), **4.** LAC20948 – Left P3 (**a.** labial, **b.** occlusal), **5.** LAC18068 – Left C (**a.** labial, **b.** occlusal), **6.** LAC21978 – Right P4, **7.** LAC21920 – Right M1, **8.** LAC21446 – Left M2, **9.** LAC16367 – Left maxillary fragment with M3, **10.** LAC21091 – Left p2 (**a.** labial, **b.** occlusal), **11.** LAC27710 – Right p3 (**a.** labial, **b.** occlusal), **12.** LAC21917 – Left p4 (**a.** labial, **b.** occlusal), **13.** LAC16424 – Left mandibular fragment with i1-c (**a.** labial, **b.** occlusal), **14.** LAC22450 – Right mandibular fragment with m1-m3 (**a.** labial, **b.** occlusal), **15.** LAC27206 – Distal epiphysis of right humerus (**a.** anterior, **b.** lateral, **c.** posterior).

p4: Very robust tooth. It is subrectangular in occlusal view. The mesiolingual part of the tooth is more elongated and developed higher than the mesiolabial part. The disto-lingual part of the tooth is developed higher than the distolabial. The cingulum is very thick and uniform throughout the whole tooth and it bends down slightly at the level of each root, with the posterior convexity being placed slightly lower than the anterior. Two cusp-like forms are also present, one mesiolingually and one distolingually.

m1: Myotodont. The trigonid and the talonid are of almost equal length. Paraconid, metaconid, entoconid, protoconid and hypoconid are well-developed. The protoconid is taller than the hypoconid. The paralophid is angular. The entocristid is straight. The hypoconulid is well-developed and it is placed in line with the lingual cusps. The labial cingulum is very thick throughout the whole tooth and it bends down slightly at the level of each root, with the posterior convexity being placed slightly lower than the anterior. Lingual cingulum of the trigonid is also present.

m2: The trigonid is wider than in m1. The labial cingulum is flatter than in m1, with the anterior convexity being more marked. The rest of the characters as m1.

m3: Myotodont. The trigonid is longer than the talonid. Paraconid, metaconid, entoconid, protoconid and hypoconid are well-developed. The protoconid is taller than the hypoconid, which displays an important reduction in height. The paralophid is angular (more marked than in m1 and m2). The entocristid is straight. The entoconid is more towards the labial side of the tooth and the hypoconid towards the lingual and thus, the talonid is significantly reduced. The hypoconulid is also significantly reduced. The labial cingulum is thinner than in m1 and m2 and uniform throughout the whole tooth. The lingual cingulum of the trigonid is absent.

Mandible: The mental foramen is beneath the gap between c and p2. The lowest part of the symphysis is relatively rounded and it slightly projects downwards.

Humerus: The styloid process is short and blunt. The epitrochlea is also short and wide. The valley between the trochlea and the condyle tends to be flat. A shallow valley is present between the condyle and the epicondyle. The condyle and the epicondyle are not projecting laterally. The radial fossa is relatively deep, whereas the olecranon fossa is very shallow (practically flat).

Remarks *Myotis myotis* and *Myotis blythii* not only share very similar characteristics, but they also overlap in size, with the former being only slightly larger than the latter and thus, species discrimination between the aforementioned is nearly impossible. The only element that clearly differs is the talonid of the m3, which is significantly reduced in *Myotis myotis* (Topal and Tusnady 1963). Mein (1975) established the criterion of the "Talonid Reduction Index"[7], for which values lower than 45% are attributed to *Myotis myotis* and values greater than 45% to *Myotis blythii*.

Discussion The morphological features described in addition to the measurements allow a definite attribution of the material to *Myotis myotis*. It is the largest member of the eleven Vesper Bat species that currently occur in Greece and as its size range overlaps *Myotis blythii*, only the largest specimens can be clearly distinguished (in addition to the m3 specimens with "Talonid Reduction Index" values lower than 45%).

Occurrence Fossils of the Greater Mouse-eared Bat are known from Petralona Cave, Chalkidiki. Its modern distribution includes most of mainland Greece and the islands of Corfu, Lesvos and Kos (Hanák et al. 2001, GFDC 2021). On a global scale it is distributed in South and Central Europe up to Ukraine, Southern England and most Mediterranean Islands, Azores, Asia Minor and parts of the Levant (Simmons 2005a).

Ecology *Myotis myotis* is a typical cave dweller and its habitat preferences include a variety of forested areas (Dietz et al. 2009).

Myotis blythii Tomes, 1857

(Lesser Mouse-eared Bat)

Figure 4.24-25 and Figure A.59

Fossiliferous locality LAC I, LAC Ib, LAC Ic, LAC II, LAC III

Age Late Pleistocene

Material 408 identified specimens

LAC I: 1 right maxillary fragment with I1 and C (27506), 2 right C (17293, 27462), 1 left C (19923), 1 right M1 (17330), 2 left M3 (19963, 27481), 1 right c (27471), 2 left c (19984, 19985), 1 left p4 (27479), 1 right m1 (17286), 2 left m1 (19953, 27489), 1 right m3 (19956), 2 left m3 (19939, 27490), LAC Ib: 1 right C (19912), 2 left C (19911, 27513), 2 left P4 (16694, 17134), 1 right M1 (16696), 3 right M2 (16697, 17706, 19908), 1 right M3 (27511), 1 left M3 (16511), 1 right c (16474), 2 left c (16470, 16534), 1 right p2 (19900), 1 right p3 (19886), 1 left p4 (16512), 1 left m2 (17157), LAC Ic: 1 right C (21505), 2 left C (21507, 21508), 3 right P4 (21455, 21458, 21459), 1 left P4 (17983), 4 right M1 (21448, 21449, 21451, 21452), 1 left M1 (18064), 1 right M3 (21466), 2 left M3 (21467, 21468), 1 right mandibular fragment (16425), 1 right mandibular fragment with m2-m3 (16422), 2 right c (21422, 21511), 3 left c (21420, 21512, 21514), 1 left p2 (18034), 3 right p3 (18017, 21427, 21429), 1 left p3 (21430), 2 right p4 (21500, 21503), 1 left p4 (21502), 1 left m1 (21476), 3 right m3 (17913, 21487, 21491), 2 left m3 (21486, 21492), LAC II: 6 right C (21814, 21927, 22087, 27663, 27774, 27900), 10 left C (21769, 21789, 21804, 21869, 22024, 22390, 22423, 27616, 27737, 27938), 2 left P2 (21820, 22430), 12 right P4 (21545, 21565,

[7] Talonid Reduction Index $= \frac{\text{Talonid Width} * 100}{\text{Length of m3}}$

21748, 21754, 21909, 22159, 22162, 22164, 22314, 22316, 22321, 27877), 12 left P4 (21606, 21747, 21907, 22000, 22161, 22163, 22317, 22379, 27542, 27563, 27768, 27879), 3 right M1 (21919, 22261, 22274), 3 left M1 (22334, 22335, 27838), 4 right M2 (21564, 22076, 22364, 27745), 3 left M2 (21538, 21674, 21701), 1 right M3 (22374), 6 left M3 (21961, 22303, 22304, 22305, 22306, 27658), 1 left mandibular fragment with m1-m3 (27844), 2 left mandibular fragments with m2-m3 (16127, 27928), 13 right c (21550, 21795, 21798, 21802, 21805, 21815, 21882, 21926, 22184, 22331, 27588, 27917, 27918), 9 left c (21773, 21776, 21797, 21871, 21925, 22021, 22190, 27630, 27919), 12 right p2 (21554, 21817, 21818, 21823, 22431, 22432, 22435, 22436, 22438, 22439, 22440, 22441), 7 left p2 (21819, 21883, 22030, 22194, 22434, 27771, 27925), 11 right p4 (21660, 21664, 21858, 21986, 22004, 22245, 22247, 22248, 22249, 22383, 27892), 14 left p4 (16077, 16687, 21860, 21918, 21987, 22002, 22056, 22255, 22258, 27830, 27831, 27896, 27897, 27899), 4 right m1 (21529, 21619, 16402, 22201), 13 left m1 (21635, 21652, 21836, 16368, 22066, 22121, 16389, 22219, 22221, 22225, 22347, 27544, 27549), 2 right m2 (21520, 22198), 1 left m2 (22229), 6 right m3 (21634, 21828, 21962, 16390, 22345, 27799), 6 left m3 (21523, 21536, 21655, 21656, 22232, 22237), LAC III: 1 right maxillary fragment with P4-M1 (19140), 2 left I1 (20737, 21140), 9 right C (20820, 21362, 17707, 20917, 21115, 21201, 20380, 20589, 20693), 8 left C (21110, 21210, 21376, 17708, 20918, 20071, 20077, 20478), 1 right P2 (20886), 3 left P2 (21431a, 21434a, 20317), 10 right P4 (20120, 21343, 21349, 20874, 21083, 21084, 21085, 20468, 20470, 20563), 7 left P4 (21009, 21345, 21346, 21352, 21353, 21354, 20873), 1 right M1-2 (21313), 1 left M1-2 (20267), 7 right M1 (20275, 20799, 20840, 21302, 20889, 20891, 20925), 6 left M1 (20269, 20751, 20807, 17471, 21324, 20998), 3 right M2 (21089, 19320, 20553), 5 left M2 (20270, 17469, 20890, 20551, 20654), 3 right M3 (17474, 19142, 19346), 1 left M3 (20929), 1 right mandibular fragment with m1-m3 (21046), 8 right c (21365, 21373, 21381, 20936, 20383, 20387, 20483, 20575), 10 left c (20199, 20202, 20204, 20716, 21387, 21116, 21118, 20382, 20482, 20574), 11 right p2 (19308b, 21430a, 21041, 21079, 19307, 19308a, 20056, 20402, 20496, 20498, 20592), 15 left p2 (21419, 21425a, 20130, 20221, 20722, 20724, 20763, 20830, 17493, 21220, 21412, 17720, 20057, 20500, 20594), 3 right p3 (21429a, 21042, 20499), 4 left p3 (21424a, 20218, 20723, 20595), 16 right p4 (20758, 20810, 20812, 20813, 21286, 21288, 21074, 21174, 19311, 20443, 20542, 20543, 20645, 20647, 20648, 20649), 13 left p4 (20162, 21294, 21296, 21299, 21300, 20869, 20967, 20354, 20355, 20357, 20444, 20447, 20650), 6 right m1 (20246, 21258, 21261, 21266, 20898, 20901), 6 left m1 (20154, 20254, 20783, 20899, 20903, 20432), 1 left m2 (20938), 5 right m3 (20962, 20409, 20428, 20534, 20629), 7 left m3 (20160, 20768, 21284, 20905, 21073, 20522, 20642)

Fossiliferous locality LAC Ia

Age latest Pleistocene

Material 588 identified specimens

1 right maxillary fragment with I1-C (23295), 1 right maxillary fragment with P4 (19718), 1 right maxillary fragment with P4-M1 (23225), 1 left maxillary fragment with P4-M1 (23156), 1 right maxillary fragment with P4-M3 (19765), 2 left maxillary fragments with P4-M3 (19764, 26529), 1 left maxillary fragment with M1 (23226), 5 right maxillary fragments with M2 (19734, 19745, 23202, 23209, 23222), 1 right maxillary fragment with M2-M3 (19737), 4 left maxillary fragments with M2-M3 (26530, 26531, 26532, 27246), 2 left maxillary fragments with M3 (23197, 23199), 1 right I1 (26409), 2 left I1 (26393, 26411), 49 right C (23296, 23298, 25469, 25506, 25526, 25552, 25570, 25580, 25610, 25629, 25662, 25677, 25694, 25700, 25702, 25718, 25754, 25779, 25798, 25809, 25823, 25826, 25836, 25864, 25877, 25914, 25915, 25967, 25976, 25993, 26041, 26064, 26116, 26152, 26193, 26246, 26255, 27063, 27068, 27069, 27071, 27073, 27075, 27077, 27081, 27086, 27087, 27088, 27413), 39 left C (23300, 25453, 25461, 25478, 25518, 25538, 25553, 25603, 25605, 25626, 25628, 25661, 25665, 25669, 25672, 25723, 25727, 25744, 25775, 25821, 25865, 25901, 25968, 25977, 26087, 26187, 26192, 26211, 26213, 26225, 26241, 27094, 27101, 27105, 27107, 27110, 27116, 27119, 27125), 2 right P2 (26301, 26302), 3 left P2 (26282, 26305, 26339), 1 left P3 (26288), 21 right P4 (23285, 25231, 25239, 25247, 25248, 25249, 25256, 25269, 25292, 25293, 25294, 25300, 25303, 25305, 25316, 25321, 25406, 26694, 26697, 26701, 27343), 29 left P4 (23254, 25299, 25331, 25342, 25349, 25354, 25355, 25375, 25378, 25382, 25384,

25397, 25399, 25402, 25413, 25414, 25416, 25417, 25420, 25421, 25423, 26544, 26545, 26708, 26710, 26714, 26715, 26718, 27346), 18 right M1 (23237, 23241, 24386, 24387, 24403, 24412, 24415, 24419, 24427, 24470, 24474, 24480, 24544, 24549, 24559, 26555, 26580, 27314), 9 left M1 (24711, 24778, 24782, 24784, 24885, 24926, 26649, 26664, 27325), 30 right M2 (23229, 23233, 24379, 24391, 24392, 24394, 24399, 24417, 24420, 24421, 24428, 24438, 24447, 24458, 24461, 24487, 24492, 24499, 24515, 24521, 24569, 24621, 26549, 26552, 26567, 26577, 27301, 27306, 27307, 27315), 16 left M2 (24771, 24789, 24821, 24824, 24840, 24857, 24891, 24900, 24909, 26535, 26630, 26645, 26660, 26665, 26669, 27321), 21 right M3 (25137, 25138, 25139, 25151, 25160, 25175, 25177, 25178, 25179, 25180, 25201, 25206, 25213, 25217, 25223, 25224, 26509, 26617, 26618, 26619, 27320), 18 left M3 (19720, 25030, 25031, 25032, 25039, 25041, 25051, 25063, 25071, 25074, 25076, 25077, 26541, 26684, 26685, 26686, 26687, 26688), 1 right mandibular fragment with i1, p2 and p4-m1 (19617), 1 right mandibular fragment with c (22666), 2 left mandibular fragments with c (22856, 22857), 1 left mandibular fragment with c-p3 (26803), 1 left mandibular fragment with c and p4 (22784), 1 left mandibular fragment with c-p4 (26780), 1 right mandibular fragment with c-m3 (19615), 2 right mandibular fragments with p3-p4 (22660, 27250), 1 right mandibular fragment with p3-m3 (19487), 2 left mandibular fragments with p3-m3 (19628, 26779), 2 right mandibular fragments with p4 and m2 (19667, 26739), 3 right mandibular fragments with p4-m2 (19619, 22484, 22496), 1 left mandibular fragment with p4-m2 (19674), 2 right mandibular fragments with p4-m3 (19616, 26723), 3 right mandibular fragments with m1 (19645, 22492, 22691), 4 left mandibular fragments with m1 (22842, 22843, 22848, 22849), 2 left mandibular fragments with m1-m2 (26790, 27278), 2 right mandibular fragments with m1-m3 (19618, 19640), 4 left mandibular fragments with m1-m3 (19654, 19712, 22697, 27275), 1 right mandibular fragment with m2 (19635), 2 left mandibular fragments with m2 (19709, 22814), 8 right mandibular fragments with m2-m3 (22470, 22508, 22519, 22529, 22554, 22588, 22490, 26726), 5 left mandibular fragments with m2-m3 (19495, 19710, 22915, 26769, 26817), 5 right mandibular fragments with m3 (22503, 22533, 22631, 22634, 22946), 7 left mandibular fragments with m3 (19705, 19706, 22868, 22902, 22908, 22917, 22923), 1 left i2 (26370), 1 left i3 (26377), 20 right c (25540, 25544, 25582, 25616, 25713, 25781, 25840, 25853, 25883, 25900, 25946, 26040, 26088, 26137, 26179, 27132, 27134, 27136, 27141, 27153), 26 left c (25445, 25524, 25597, 25604, 25615, 25618, 25650, 25656, 25717, 25834, 25893, 25894, 26012, 26028, 26071, 26072, 26124, 26200, 26252, 27171, 27175, 27179, 27191, 27437, 27438, 27441), 14 right p2 (26283, 26284, 26285, 26292, 26295, 26306, 26309, 26313, 26318, 26326, 26328, 26337, 26345, 26346), 10 left p2 (26281, 26286, 26298, 26324, 27192, 27193, 27194, 27195, 27196, 27400), 7 right p3 (26300, 26304, 26307, 26314, 26335, 26340, 26348), 4 left p3 (26279, 26317, 26322, 27197), 21 right p4 (24182, 24183, 24191, 24193, 24194, 24196, 24199, 24200, 24203, 24204, 24205, 24207, 24213, 24215, 24230, 24233, 24236, 24238, 24255, 27041, 27401), 23 left p4 (24270, 24280, 24287, 24288, 24306, 24307, 24308, 24316, 24318, 24323, 24326, 24329, 24334, 24335, 24336, 24339, 24340, 24344, 26816, 27044, 27047, 27055, 27056), 19 right m1 (23340, 23357, 23362, 23365, 23407, 23418, 23419, 23433, 23459, 23475, 23479, 23526, 23530, 23624, 23664, 23681, 26864, 26878, 26924), 30 left m1 (23742, 23747, 23759, 23765, 23766, 23779, 23782, 23785, 23789, 23798, 23853, 23862, 23878, 23880, 23882, 23883, 23886, 23894, 23913, 23923, 23986, 23988, 23999, 24006, 24029, 26777, 26942, 26954, 27001, 27012), 8 right m2 (23343, 23363, 23372, 23375, 23460, 23467, 26748, 26865), 13 left m2 (23727, 23734, 23738, 23749, 23751, 23752, 23776, 23783, 23872, 23879, 23881, 26772, 27003), 29 right m3 (23330, 23336, 23349, 23350, 23353, 23371, 23394, 23313, 23437, 23627, 23631, 23633, 23637, 23639, 23641, 23644, 23655, 23659, 26730, 26744, 26764, 26925, 26929, 26931, 26935, 26937, 26938, 27258, 27373), 19 left m3 (24097, 24101, 24102, 24104, 24129, 24148, 24149, 24155, 24160, 24162, 24163, 24167, 24172, 26776, 27014, 27015, 27018, 27020, 27289)

Measurements Table 4.9 and Figure 4.22-23

Description *Myotis blythii* is the second largest member of the eleven Vesper Bat species that currently occur in Greece.

I1: As for *Myotis myotis*.

I2: As for *Myotis myotis*.

C: The ridge that connects the distal base of the crown with the cusp is not as thick as in *Myotis myotis*. The rest of the characters as for *Myotis myotis*.

P2: As for *Myotis myotis*.

Table 4.9 *Myotis blythii*, Loutra Almopias Cave A. Measurements (in mm) from both LAC and LAC Ia. LAC: Late Pleistocene; LAC Ia: latest Pleistocene; n: number of measurable specimens; L: length; W: width; trgd: trigonid; tld: talonid; MEAN: average; MIN: minimum; MAX: maximum; SD: standard deviation; CV: coefficient of variation.

			n	**MEAN**	**MIN**	**MAX**	**SD**	**CV**
I1	LAC	L	3	0.71	0.66	0.77	0.056	7.842
		W	3	0.52	0.47	0.58	0.057	11.006
	LAC Ia	L	4	0.70	0.67	0.72	0.022	3.179
		W	4	0.51	0.48	0.56	0.036	7.013
I2	LAC Ia	L	1	0.63	-	-	-	-
		W	1	0.82	-	-	-	-
C	LAC	L	43	1.52	1.37	1.70	0.070	4.600
		W	43	1.17	1.07	1.31	0.063	5.410
	LAC Ia	L	87	1.54	1.39	1.66	0.061	3.937
		W	88	1.17	1.03	1.27	0.049	4.202
P2	LAC	L	5	0.67	0.65	0.70	0.019	2.862
		W	5	0.83	0.79	0.88	0.034	4.031
	LAC Ia	L	5	0.72	0.70	0.74	0.018	2.537
		W	5	0.83	0.76	0.88	0.049	5.902
P3	LAC Ia	L	1	0.65	-	-	-	-
		W	1	0.60	-	-	-	-
P4	LAC	L	48	1.48	1.30	1.63	0.073	4.945
		W	24	1.31	1.06	1.57	0.100	7.639
	LAC Ia	L	56	1.48	1.29	1.66	0.088	5.907
		W	51	1.32	1.10	1.50	0.096	7.305
M1	LAC	L	26	2.17	1.98	2.46	0.115	5.317
		W	26	2.11	1.66	2.55	0.182	8.626
	LAC Ia	L	32	2.12	1.93	2.46	0.136	6.413
		W	32	2.08	1.28	2.45	0.136	6.537
M2	LAC	L	16	2.20	2.04	2.43	0.100	4.554
		W	15	2.55	2.37	2.84	0.127	4.969
	LAC Ia	L	49	2.21	1.94	2.38	0.087	3.913
		W	53	2.56	2.16	2.91	0.148	5.763
M3	LAC	L	17	1.95	1.88	2.05	0.063	3.247
		W	17	2.39	2.15	2.52	0.106	4.430
	LAC Ia	L	46	1.92	1.58	2.08	0.111	5.785
		W	46	2.36	2.02	2.55	0.124	5.249
i1	LAC Ia	L	1	0.68	-	-	-	-
		W	1	0.24	-	-	-	-
i2	LAC Ia	L	1	0.68	-	-	-	-
		W	1	0.43	-	-	-	-

i3	LAC Ia	L	1	0.74	-	-	-	-
		W	1	0.64	-	-	-	-
c	LAC	L	50	1.00	0.86	1.25	0.083	8.286
		W	51	1.16	0.99	1.29	0.075	6.466
	LAC Ia	L	52	1.00	0.73	1.13	0.079	7.918
		W	53	1.16	1.01	1.32	0.064	5.534
p2	LAC	L	49	0.87	0.65	0.97	0.060	6.892
		W	49	0.93	0.75	1.09	0.066	7.033
	LAC Ia	L	28	0.89	0.74	1.07	0.059	6.603
		W	28	0.92	0.81	0.99	0.050	5.502
p3	LAC	L	11	0.68	0.57	0.83	0.067	9.844
		W	11	0.86	0.77	1.04	0.069	8.032
	LAC Ia	L	19	0.71	0.62	0.79	0.049	6.934
		W	19	0.85	0.69	0.94	0.057	6.694
p4	LAC	L	57	1.15	1.05	1.29	0.051	4.464
		W	58	0.88	0.73	1.05	0.052	5.900
	LAC Ia	L	61	1.15	1.04	1.31	0.050	4.284
		W	60	0.88	0.73	1.10	0.071	8.102
m1	LAC	L	33	2.00	1.78	2.22	0.099	4.937
		W (trgd)	33	1.13	0.92	1.29	0.089	7.835
		W (tld)	34	1.35	1.14	1.50	0.074	5.463
	LAC Ia	L	75	1.96	1.78	2.17	0.085	4.319
		W (trgd)	75	1.13	0.91	1.36	0.091	8.063
		W (tld)	75	1.33	1.13	1.54	0.089	6.658
m2	LAC	L	6	2.04	1.96	2.11	0.052	2.538
		W (trgd)	8	1.37	1.24	1.51	0.091	6.669
		W (tld)	8	1.46	1.35	1.56	0.077	5.273
	LAC Ia	L	57	2.06	1.83	2.24	0.091	4.424
		W (trgd)	57	1.31	1.14	1.46	0.078	5.989
		W (tld)	57	1.42	1.22	1.59	0.078	5.499
m3	LAC	L	37	1.81	1.57	1.98	0.097	5.346
		W (trgd)	37	1.23	1.04	1.36	0.081	6.594
		W (tld)	37	0.89	0.73	1.00	0.075	8.424
	LAC Ia	L	85	1.80	1.58	1.99	0.088	4.917
		W (trgd)	85	1.23	0.96	1.41	0.092	7.442
		W (tld)	85	0.88	0.54	1.05	0.088	10.018
M1-M3	LAC Ia	L	3	5.36	5.22	5.57	0.185	3.455
P4-M3	LAC Ia	L	3	6.54	6.37	6.82	0.247	3.773
m1-m3	LAC	L	1	5.88	-	-	-	-
	LAC Ia	L	12	5.94	5.62	6.28	0.216	3.634
p4-m3	LAC Ia	L	7	7.25	6.88	7.52	0.216	2.982
c-m3	LAC Ia	L	2	9.71	9.41	10.01	0.424	4.369
c-p4	LAC Ia	L	6	3.67	3.41	3.85	0.196	5.357
LSC	LAC Ia	L	1	14.93	-	-	-	-

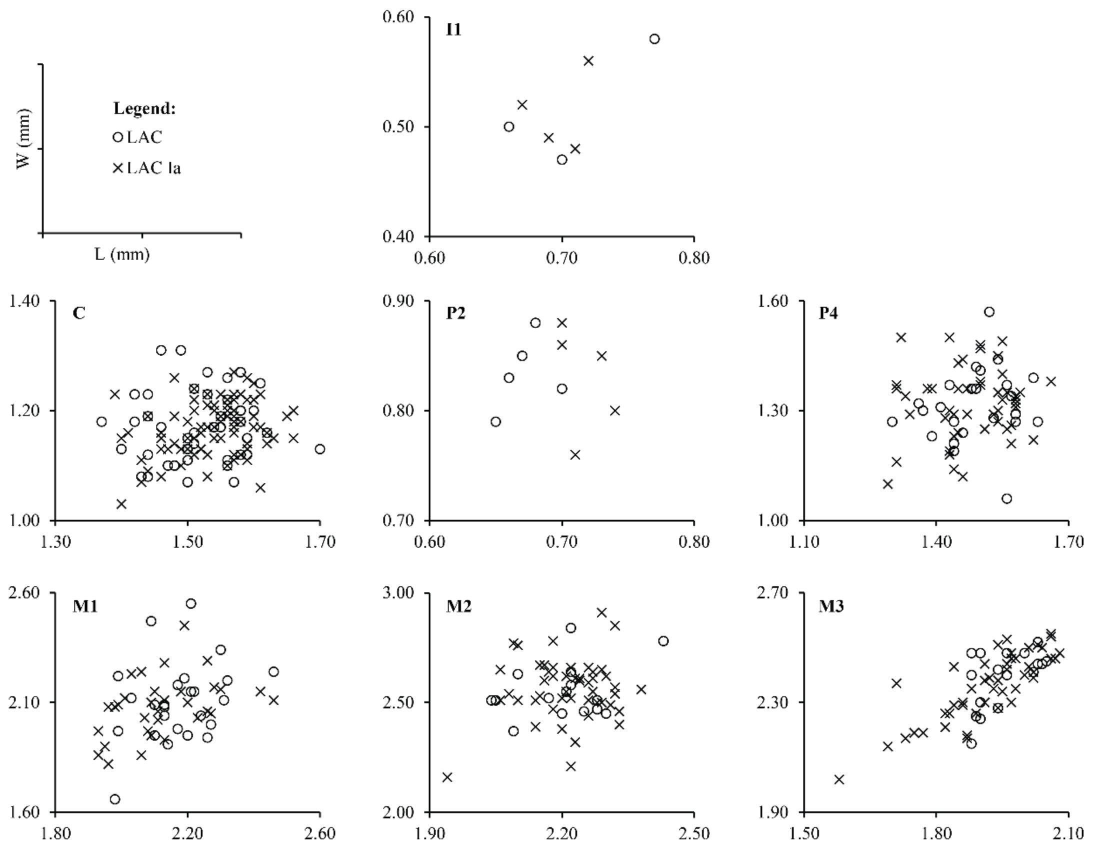

Figure 4.22 *Myotis blythii*, Loutra Almopias Cave A. XY graphs with the measured (in mm) dental elements (I1, C, P2, P4, M1, M2, M3). L: length, W: width.

P3: As for *Myotis myotis*.

P4: As for *Myotis myotis*.

M1: As for *Myotis myotis*.

M2: As for *Myotis myotis*.

M3: As for *Myotis myotis*.

i1: As for *Myotis myotis*.

i2: As for *Myotis myotis*.

i3: As for *Myotis myotis*.

c: As for *Myotis myotis*.

p2: As for *Myotis myotis*.

p3: It is slightly concave mesially and distally. The rest of the characters as for *Myotis myotis*.

m1: As for *Myotis myotis*.

m2: As for *Myotis myotis*.

m3: The trigonid and the talonid are of almost equal length. The rest of the characters as for *Myotis myotis*.

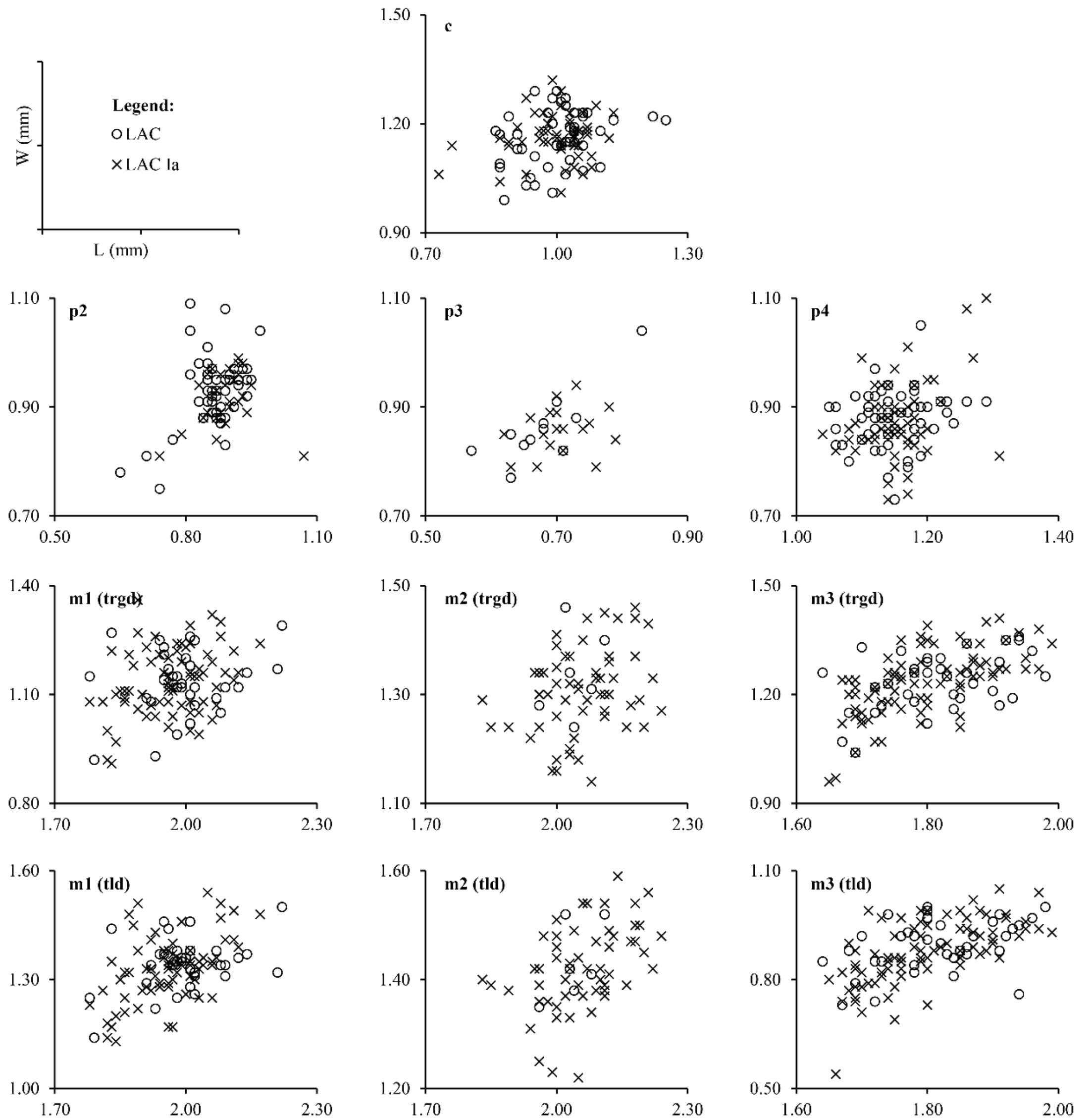

Figure 4.23 *Myotis blythii*, Loutra Almopias Cave A. XY graphs with the measured (in mm) dental elements (c, p2, p3, p4, m1, m2, m3). L: length, W: width, trgd: trigonid; tld: talonid.

Mandible: The coronoid process is relatively rounded and located higher than the condyloid process. The masseter crest is thick and steep. The mandibular notch is relatively steep all the way towards the condyloid process (relatively convex at its anterior part and relatively concave at its posterior part). The mental foramen is beneath the anterior part of p2. The rest of the characters as for *Myotis myotis*.

<u>Remarks</u> As for *Myotis myotis*.

Discussion The morphological features described in addition to the measurements allow a definite attribution of the material to *Myotis blythii*. It is the second largest member of the eleven Vesper Bat species that currently occur in Greece and as its size range overlaps *Myotis myotis*, only the smallest specimens can be clearly distinguished (in addition to the m3 specimens with “Talonid Reduction Index” values greater than 45%).

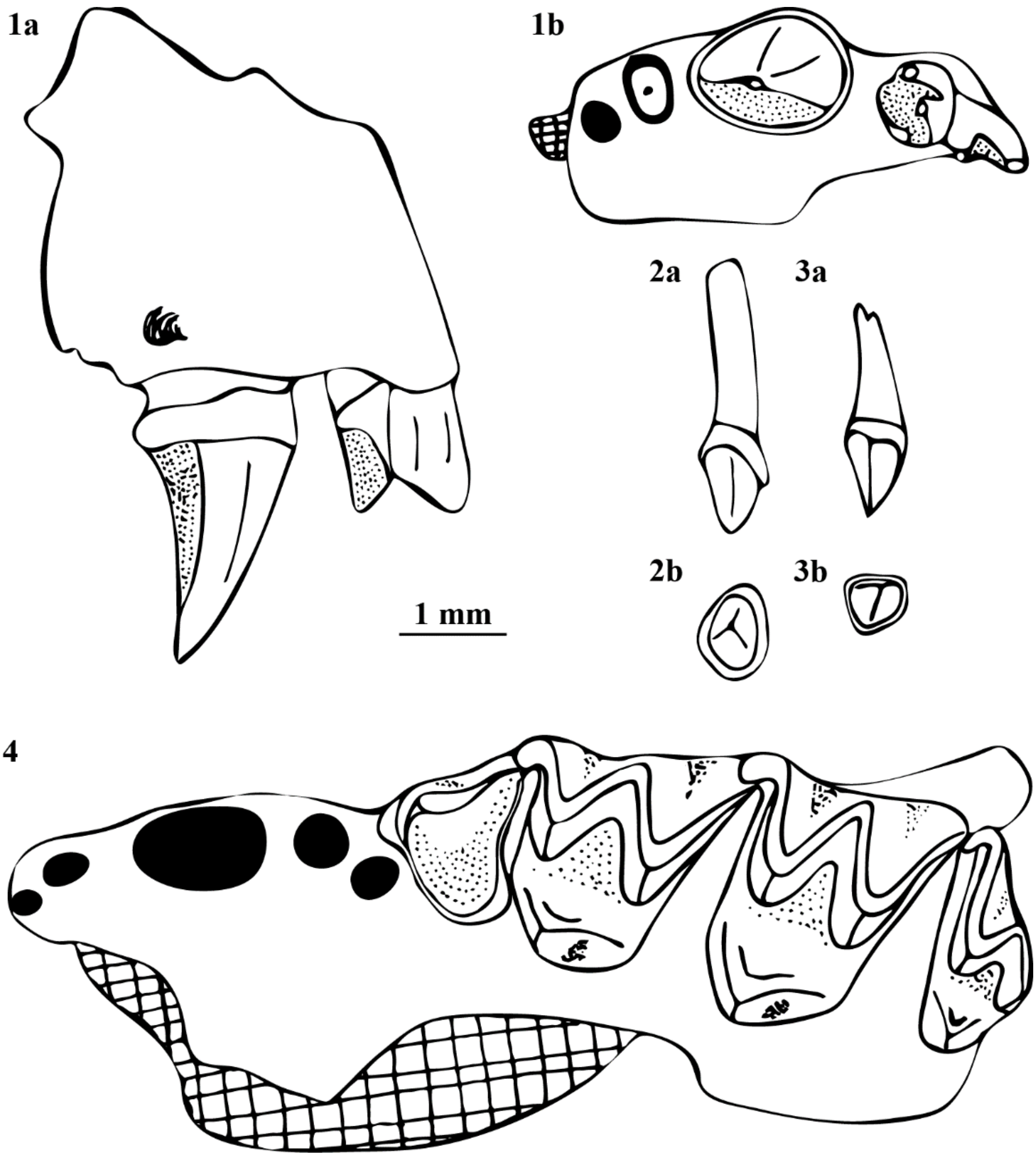

Figure 4.24 *Myotis blythii*, Loutra Almopias Cave A. **1.** LAC23925 – Right maxillary fragment with I1-C (**a.** labial, **b.** occlusal), **2.** LAC20317 – Left P2 (**a.** labial, **b.** occlusal), **3.** LAC26288 – Left P3 (**a.** labial, **b.** occlusal), **4.** LAC19764 – Left maxillary fragment with P4-M3.

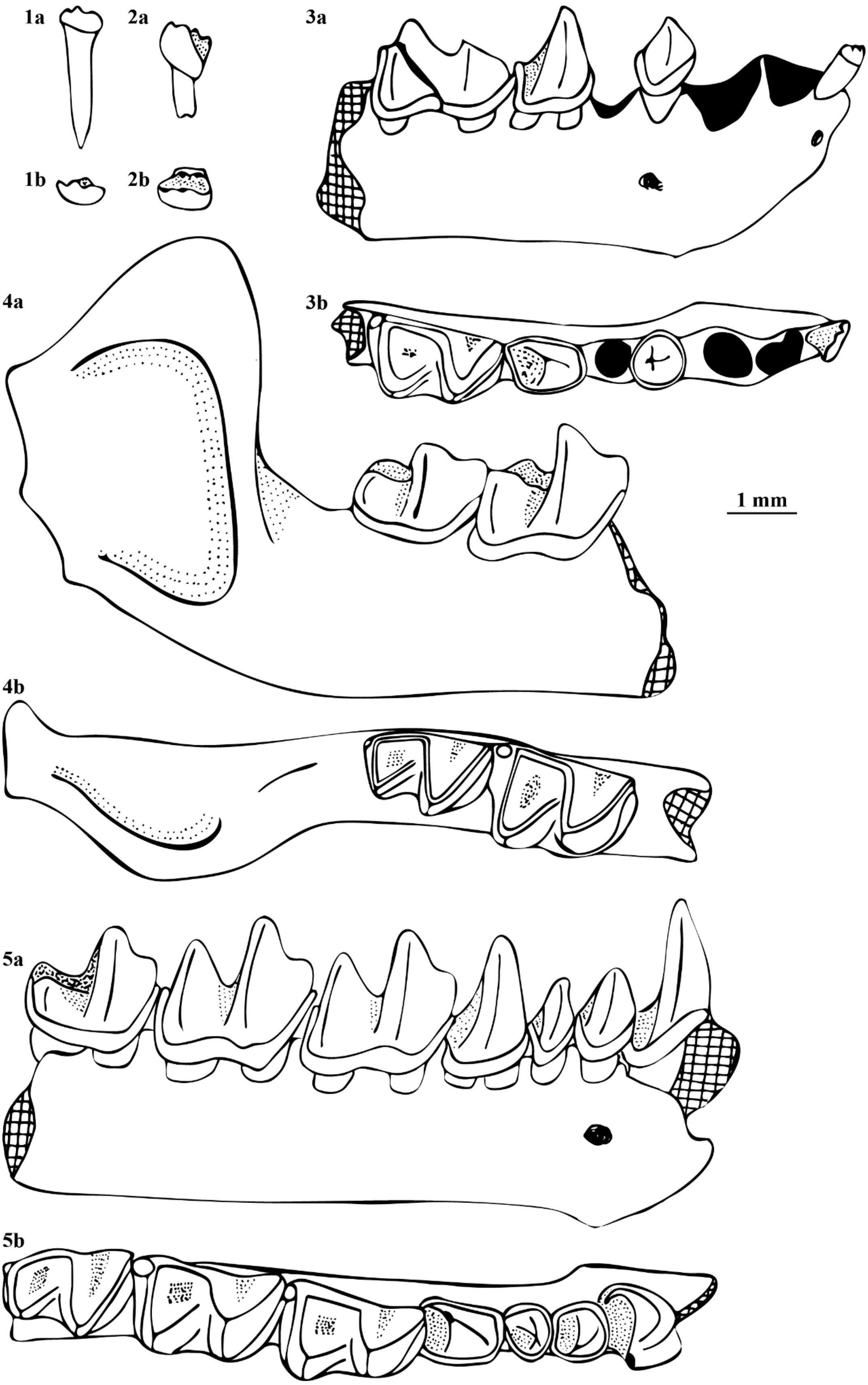

Figure 4.25 *Myotis blythii*, Loutra Almopias Cave A. **1.** LAC26370 – Left i2 (**a.** labial, **b.** occlusal), **2.** LAC26377 – Left i3 (**a.** labial, **b.** occlusal), **3.** LAC19617 – Right mandibular fragment with i1, p3, and p4-m1 (**a.** labial, **b.** occlusal), **4.** LAC22470 – Right mandibular fragment with m2-m3 (**a.** labial, **b.** occlusal), **5.** LAC19615 – Right mandibular fragment with c-m3 (**a.** labial, **b.** occlusal).

Occurrence Fossils of the Lesser Mouse-eared Bat are known from Sarakenos Cave, Boeotia, Charkadio Cave, Tilos, Kalamakia Cave, Lakonia and Petralona Cave, Chalkidiki. Its modern distribution includes most of mainland Greece and some Ionian and Aegean islands including Crete (Hanák et al. 2001, GFDC 2021). On a global scale it is distributed in the Mediterranean region of Spain all the way to Bulgaria, Turkmenistan, Kyrgyzstan, and Afghanistan (Simmons 2005a).

Ecology *Myotis blythii* is a typical cave dweller and its habitat preferences include a variety of open areas such as meadows, pastures, etc. (Dietz et al. 2009).

Myotis myotis/blythii

Figure 4.28-29

Fossiliferous locality LAC I, LAC Ib, LAC Ic, LAC II, LAC III

Age Late Pleistocene

Material 302 identified specimens

LAC I: 1 right I1 (27466), 2 right/left C (17337, 17338), 1 left C (19968), 1 left P4 (17247), 1 left M1-2 (27486), 1 left M1 (17316), 1 right M2 (17315), 2 left M3 (17251, 17209), 1 right i1 (17339), 1 left i1 (19987), 2 right p4 (19942, 27497), 1 right m1-2 (17217), 1 left m1-2 (19941), 1 left m1 (27476), 2 right m2 (19954, 27488), LAC Ib: 1 right P2 (16469), 1 left M1-2 (17105), 1 left M1 (16509), 1 right M2 (16517), 1 right M3 (19910), 1 left M3 (19909), 2 right c (16550, 19861), 1 right p2 (16468), 1 right p3 (16524), 1 right m1-2 (17108), 1 left m1 (16681), 1 left m2 (16682), 1 right m3 (19871), 1 left humerus (16581), LAC Ic: 1 right I1 (17994), 2 left I1 (21436, 21437), 1 right I2 (21435), 1 left I2 (21438), 1 right C (21421), 1 left M1-2 (21454), 1 left M1 (21450), 1 right M2 (21453), 2 right M3 (21464, 21469), 1 right mandibular fragment (17996), 1 right i1 (21443), 1 left i2 (21441), 2 right c (18051, 21510), 3 right p2 (18018, 18069, 18071), 3 left p2 (18035, 18070, 18072), 1 right p3 (17938), 1 left p4 (21496), 2 right m1 (18065, 21470), 1 right m2 (21472), LAC II: 1 right I1 (27926), 1 right I2 (21884), 1 left I2 (22394), 4 right P4 (21759, 21908, 21923, 21931), 9 left P4 (21753, 21757, 21758, 21904, 21905, 21906, 21932, 22380, 27719), 2 left M1-2 (27718, 27739), 3 left M1 (21892, 27539, 27873), 3 right M2 (21936, 21937, 27607), 1 left M2 (16056), 8 right M3 (16040, 16051, 21737, 21738, 21941, 22307, 22308, 27696), 4 left M3 (21543, 21895, 22081, 27521), 1 right i1 (22447), 9 right c (21761, 21778, 21862, 21866, 16415, 22333, 22393, 27555, 27760), 6 left c (21771, 22018, 22089, 22183, 22327, 27924), 3 right p2 (22058, 22195, 27941), 7 left p2 (21821, 21929, 21930, 22429, 22433, 22437, 27623), 1 left p3 (22029), 6 right p4 (21663, 22130, 22251, 27529, 27551, 27600), 7 left p4 (21859, 22134, 22136, 22254, 22256, 22257, 27690), 1 right m1-2 (27643), 1 left m1-2 (22352), 10 right m1 (21630, 22061, 16120, 22109, 22110, 22199, 22339, 22340, 22343, 27548), 15 left m1 (21533, 21640, 21653, 21654, 21913, 21914, 22127, 16387, 22220, 22222, 22223, 22228, 22337, 27887, 27890), 4 right m2 (21631, 21995, 22113, 27942), 4 left m2 (16037, 21912, 22034, 27523), 2 right m3 (21629, 27800), 2 left m3 (16036, 27931), 1 left humerus (27726), LAC III: 5 right I1 (21437a, 20101, 20132, 21225, 20406), 5 left I1 (20102, 20726, 21137, 21138, 20504), 4 right I2 (21422a, 21432a, 21438a, 20949), 6 left I2 (21421a, 20885, 20950, 21128, 19137a, 19295), 2 right C (21363, 21204), 3 left C (21361, 21107, 20689), 2 left P2 (21415, 20319), 1 left P3 (19137b), 1 right P4 (19314), 5 left P4 (20119, 21355, 20921, 21012, 19138), 2 left M1-2 (20180, 20930), 1 right M1 (20801), 2 left M1 (20753, 20460), 2 right M2 (20993, 21088), 2 left M2 (20843, 19141), 7 right M3 (20731, 20732, 17475, 17695, 20894, 17863, 20466), 4 left M3 (21339, 20931, 17862, 21185), 1 right mandibular fragment (16461), 2 left i1 (21442a, 20597), 1 right i2 (20062), 2 left i2 (21043, 21044), 1 right i3 (20061), 3 left i3 (21439a, 21045, 19294), 5 right c (20696, 17491, 21390, 21391, 19165), 5 left c (21371, 20875, 21207, 20288, 20290), 7 right p2 (21433a, 20720, 21219, 21222, 17721, 20316, 20593), 5 left p2 (21414, 21427a, 20220, 20721, 21040), 1 right p3 (21413), 4 left p3 (21420a, 20224, 20055, 20401), 7 right p4 (20811, 20867, 20868, 20044, 20047, 20644, 20646), 5 left p4 (20727, 20919, 20944, 21080, 19135), 1 right m1-2 (20771), 7 right m1 (20939, 20940, 19329, 20336, 20411, 20420, 20620), 4 left m1 (21280, 21281, 20904, 20434), 3 right m2 (20741, 20900, 20011), 2 left m2 (20115, 20632), 2 right m3 (21272, 20906), 2 left m3 (20744, 20523)

Fossiliferous locality LAC Ia

Age latest Pleistocene

Material 459 identified specimens

1 right/left milk tooth (26379), 1 right maxillary fragment with P3-P4 (19722), 1 left maxillary fragment with P4 (19715), 4 right maxillary fragments with P4-M1 (19726, 19744, 23124, 26517), 2 right maxillary fragments with M1 (23203, 23224), 1 right maxillary fragment with M1-M2 (19748), 1 right maxillary fragment with M2-M3 (19721), 1 right maxillary fragment with M3 (23185), 1 left maxillary fragment with M3 (23200), 6 right I1 (26372, 26400, 27201, 27202, 27442, 27443), 4 left I1 (26368, 26384, 26394, 27198), 4 right I2 (26332, 26389, 26399, 27199), 3 left I2 (26360, 26361, 26382), 20 right C (25460, 25471, 25477, 25480, 25549, 25691, 25933, 25965, 25966, 26015, 26089, 26167, 26221, 27058, 27070, 27078, 27089, 27409, 27412, 27417), 18 left C (25520, 25532, 25598, 25600, 25612, 25624, 25699, 25816, 25957, 25997, 26127, 26134, 26168, 26243, 27095, 27102, 27111, 27126), 2 right P2 (26310, 26331), 1 left P2 (26342), 1 left P3 (26321), 11 right P4 (23284, 25250, 25274, 25296, 25306, 25307, 25309, 25310, 25311, 25315, 26702), 10 left P4 (23255, 25336, 25340, 25351, 25372, 25425, 26709, 26720, 27344, 27345), 7 right M1-2 (24471, 24483, 24489, 24514, 24599, 24607, 24671), 4 left M1-2 (24955, 24956, 24965, 24972), 22 right M1 (23234, 24437, 24444, 24454, 24463, 24464, 24493, 24494, 24497, 24526, 24613, 26546, 26551, 26556, 26559, 26562, 26564, 26584, 26589, 27298, 27308, 27309), 21 left M1 (24790, 24799, 24800, 24817, 24823, 24825, 24887, 24888, 24890, 24908, 24910, 24981, 26536, 26537, 26625, 26627, 26636, 26648, 26657, 26663, 27324), 7 right M2 (24376, 24405, 24506, 24525, 24528, 24545, 25048), 9 left M2 (24713, 24834, 24862, 24882, 24936, 24950, 24973, 24975, 27245), 8 right M3 (25181, 25200, 25214, 25221, 25222, 25225, 26525, 26526), 5 left M3 (25012, 25029, 25042, 25052, 25078), 4 right mandibular fragments (19509, 19510, 22966, 22976), 1 right mandibular fragment with c and p3-p4 (19673), 1 left mandibular fragment with p2 (22940), 1 left mandibular fragment with p2-p3 (22860), 1 left mandibular fragment with p3-m1 (27273), 1 right mandibular fragment with p4 (22669), 1 right mandibular fragment with p4-m1 (19663), 1 left mandibular fragment with p4-m1 (26789), 1 left mandibular fragment with p4-m3 (26767), 2 right mandibular fragments with m1 (22520, 22581), 1 left mandibular fragment with m1 (22821), 5 right mandibular fragments with m1-m2 (22528, 22589, 22619, 26721, 27261), 4 left mandibular fragments with m1-m2 (19651, 22813, 22828, 26774), 4 right mandibular fragments with m2 (22545, 22556, 22574, 22681), 3 left mandibular fragments with m2 (22773, 22841, 22938), 1 right mandibular fragment with m2-m3 (22550), 1 left mandibular fragment with m2-m3 (22936), 2 right mandibular fragments with m3 (22608, 22687), 1 left i1 (26380), 4 right i2 (26369, 26371, 26373, 26378), 2 left i2 (26366, 26385), 1 left i3 (26363), 23 right c (25525, 25531, 25579, 25622, 25632, 25642, 25683, 25739, 25764, 25844, 25845, 25876, 25923, 25992, 25994, 26079, 26207, 26218, 27135, 27150, 27154, 27159, 27431), 18 left c (25446, 25505, 25719, 25795, 25811, 25822, 25870, 25937, 25938, 25955, 25961, 26016, 26157, 26163, 27173, 27176, 27435, 27440), 2 right p2 (26312, 26336), 1 left p3 (26333), 23 right p4 (24185, 24186, 24189, 24195, 24197, 24224, 24235, 24244, 24245, 24252, 24254, 24259, 24264, 24266, 27028, 27030, 27032, 27034, 27035, 27036, 27039, 27042, 27043), 33 left p4 (24271, 24281, 24283, 24285, 24286, 24289, 24290, 24294, 24295, 24296, 24297, 24298, 24299, 24302, 24303, 24309, 24312, 24320, 24327, 24328, 24337, 24341, 24347, 24352, 24357, 26812, 27045, 27050, 27053, 27054, 27057, 27404, 27406), 2 right m1-2 (23473, 23541), 38 right m1 (23326, 23328, 23351, 23361, 23312, 23410, 23412, 23424, 23428, 23442, 23449, 23450, 23453, 23455, 23481, 23482, 23486, 23490, 23536, 23539, 23545,

23558, 23569, 23671, 26735, 26757, 26759, 26866, 26870, 26874, 26885, 26889, 26892, 26902, 26907, 27350, 27351, 27352), 39 left m1 (23728, 23731, 23733, 23741, 23748, 23771, 23775, 23784, 23786, 23811, 23826, 23839, 23857, 23861, 23884, 23892, 23895, 23896, 23929, 23930, 23958, 23978, 23983, 24032, 24072, 26941, 26961, 26965, 26966, 26974, 26977, 26980, 26988, 26992, 26994, 26997, 27286, 27387, 27391), 28 right m2 (23358, 23364, 23369, 23392, 23417, 23421, 23434, 23448, 23454, 23457, 23461, 23464, 23470, 23474, 23543, 23555, 23662, 23672, 26742, 26753, 26754, 26872, 26875, 26876, 26877, 26906, 26921, 27255), 21 left m2 (23768, 23769, 23787, 23814, 23825, 23852, 23854, 23858, 23865, 23876, 23898, 23974, 26773, 26964, 26991, 26998, 27002, 27281, 27282, 27375, 27376), 4 right m3 (23630, 23719, 26728, 26934), 6 left m3 (24116, 24142, 24144, 24151, 26770, 26783), 2 right humeri (26441, 26449)

Measurements Table 4.10, Figure 4.26-27 and Figure 4.30

Description As species discrimination between the two large-sized Vesper Bats that currently occur in Greece is nearly impossible, the specimens that do not fulfil the needed criteria for species attribution are all grouped as *Myotis myotis*/*blythii*. No further descriptions are provided, as all specimens share characteristics that fall within the spectrum of the already described taxa.

Table 4.10 *Myotis myotis*/*blythii*, Loutra Almopias Cave A. Measurements (in mm) from both LAC and LAC Ia. LAC: Late Pleistocene; LAC Ia: latest Pleistocene; n: number of measurable specimens; L: length; W: width; trgd: trigonid; tld: talonid; MEAN: average; MIN: minimum; MAX: maximum; SD: standard deviation; CV: coefficient of variation.

			n	**MEAN**	**MIN**	**MAX**	**SD**	**CV**
I1	LAC	L	16	0.76	0.59	0.92	0.080	10.443
		W	16	0.57	0.44	0.75	0.076	13.277
	LAC Ia	L	11	0.75	0.72	0.85	0.039	5.114
		W	11	0.56	0.51	0.64	0.045	8.057
I2	LAC	L	13	0.64	0.56	0.70	0.048	7.492
		W	13	0.76	0.60	0.87	0.078	10.296
	LAC Ia	L	6	0.67	0.55	0.87	0.120	17.916
		W	6	0.77	0.41	0.86	0.177	23.020
C	LAC	L	7	1.64	1.60	1.72	0.044	2.647
		W	7	1.29	1.23	1.34	0.037	2.878
	LAC Ia	L	38	1.63	1.34	1.80	0.073	4.467
		W	37	1.24	1.01	1.32	0.063	5.098
P2	LAC	L	3	0.82	0.70	0.90	0.106	12.906
		W	3	0.89	0.87	0.92	0.027	2.973
	LAC Ia	L	3	0.84	0.81	0.85	0.023	2.760
		W	3	0.79	0.77	0.80	0.017	2.193
P3	LAC	L	1	0.78	-	-	-	-
		W	1	0.63	-	-	-	-
	LAC Ia	L	2	0.69	0.59	0.78	0.134	19.613
		W	2	0.71	0.60	0.82	0.156	21.911
P4	LAC	L	20	1.61	1.46	1.82	0.078	4.841
		W	3	1.45	1.43	1.46	0.015	1.056
	LAC Ia	L	27	1.63	1.53	1.72	0.048	2.961
		W	25	1.37	1.24	1.48	0.057	4.199

M1	LAC	L	8	2.21	2.08	2.35	0.096	4.332
		W	8	2.22	1.93	2.64	0.218	9.841
	LAC Ia	L	49	2.20	1.87	2.44	0.118	5.366
		W	50	2.19	1.96	2.46	0.119	5.425
M2	LAC	L	2	2.28	2.20	2.35	0.106	4.662
		W	4	2.64	2.52	2.78	0.130	4.943
	LAC Ia	L	10	2.26	1.95	2.33	0.115	5.098
		W	10	2.59	2.16	2.82	0.188	7.261
M3	LAC	L	20	2.08	1.97	2.14	0.046	2.233
		W	14	2.53	2.41	2.63	0.058	2.288
	LAC Ia	L	10	2.06	1.95	2.13	0.048	2.343
		W	9	2.51	2.40	2.56	0.049	1.942
i1	LAC	L	6	0.71	0.65	0.78	0.044	6.121
		W	6	0.43	0.39	0.49	0.039	7.814
	LAC Ia	L	2	0.59	0.45	0.73	0.198	33.558
		W	2	0.36	0.26	0.45	0.134	37.845
i2	LAC	L	5	0.73	0.66	0.80	0.050	6.858
		W	5	0.57	0.47	0.76	0.114	19.872
	LAC Ia	L	6	0.74	0.69	0.78	0.031	4.145
		W	6	0.53	0.50	0.56	0.020	3.734
i3	LAC	L	3	0.76	0.69	0.82	0.065	8.599
		W	3	0.72	0.66	0.78	0.060	8.333
	LAC Ia	L	1	0.65	-	-	-	-
		W	1	0.55	-	-	-	-
c	LAC	L	28	1.13	1.00	1.30	0.066	5.866
		W	29	1.22	1.08	1.39	0.073	5.943
	LAC Ia	L	42	1.15	0.94	1.47	0.079	6.930
		W	41	1.19	1.08	1.31	0.056	4.675
p2	LAC	L	29	0.96	0.87	1.06	0.063	6.565
		W	29	1.02	0.85	1.16	0.059	5.773
	LAC Ia	L	3	0.94	0.88	1.00	0.035	6.383
		W	3	1.01	1.00	1.02	0.010	0.990
p3	LAC	L	7	0.73	0.65	0.77	0.045	6.189
		W	7	0.91	0.80	0.99	0.062	6.744
	LAC Ia	L	5	0.76	0.61	0.98	0.140	18.292
		W	5	0.80	0.69	0.94	0.101	12.606
p4	LAC	L	28	1.22	1.11	1.30	0.043	3.508
		W	28	0.93	0.73	1.12	0.082	8.813
	LAC Ia	L	62	1.22	1.11	1.32	0.046	3.755
		W	62	0.92	0.72	1.06	0.057	6.199
m1	LAC	L	38	2.11	1.87	2.26	0.082	3.876
		W (trgd)	42	1.25	1.05	1.44	0.089	7.100
		W (tld)	43	1.45	1.23	1.63	0.074	5.143
	LAC Ia	L	94	2.05	1.86	2.22	0.069	3.343
		W (trgd)	95	1.24	1.08	1.47	0.067	5.452
		W (tld)	95	1.43	1.25	1.59	0.053	3.677
m2	LAC	L	16	2.15	2.07	2.26	0.064	2.950
		W (trgd)	18	1.33	1.23	1.47	0.058	4.371
		W (tld)	17	1.47	1.36	1.58	0.061	4.162

	LAC Ia	L	68	2.11	1.85	2.15	0.006	3.553
		W (trgd)	68	1.36	1.18	1.50	0.062	4.535
		W (tld)	68	1.48	1.33	1.59	0.054	3.647
m3	LAC	L	7	1.81	1.56	2.00	0.133	7.357
		W (trgd)	9	1.20	1.09	1.35	0.089	7.375
		W (tld)	8	0.85	0.70	1.09	0.111	13.012
	LAC Ia	L	12	1.82	1.67	1.97	0.098	5.389
		W (trgd)	14	1.22	1.07	1.39	0.077	6.327
		W (tld)	11	0.82	0.71	0.88	0.056	6.873
m1-m3	LAC Ia	L	1	5.90	-	-	-	-
p4-m3	LAC Ia	L	1	7.13	-	-	-	-
c-p4	LAC Ia	L	1	3.75	-	-	-	-
Humerus	LAC	W	2	4.08	4.05	4.10	0.035	0.868
	LAC Ia	W	2	4.14	4.08	4.20	0.085	2.050

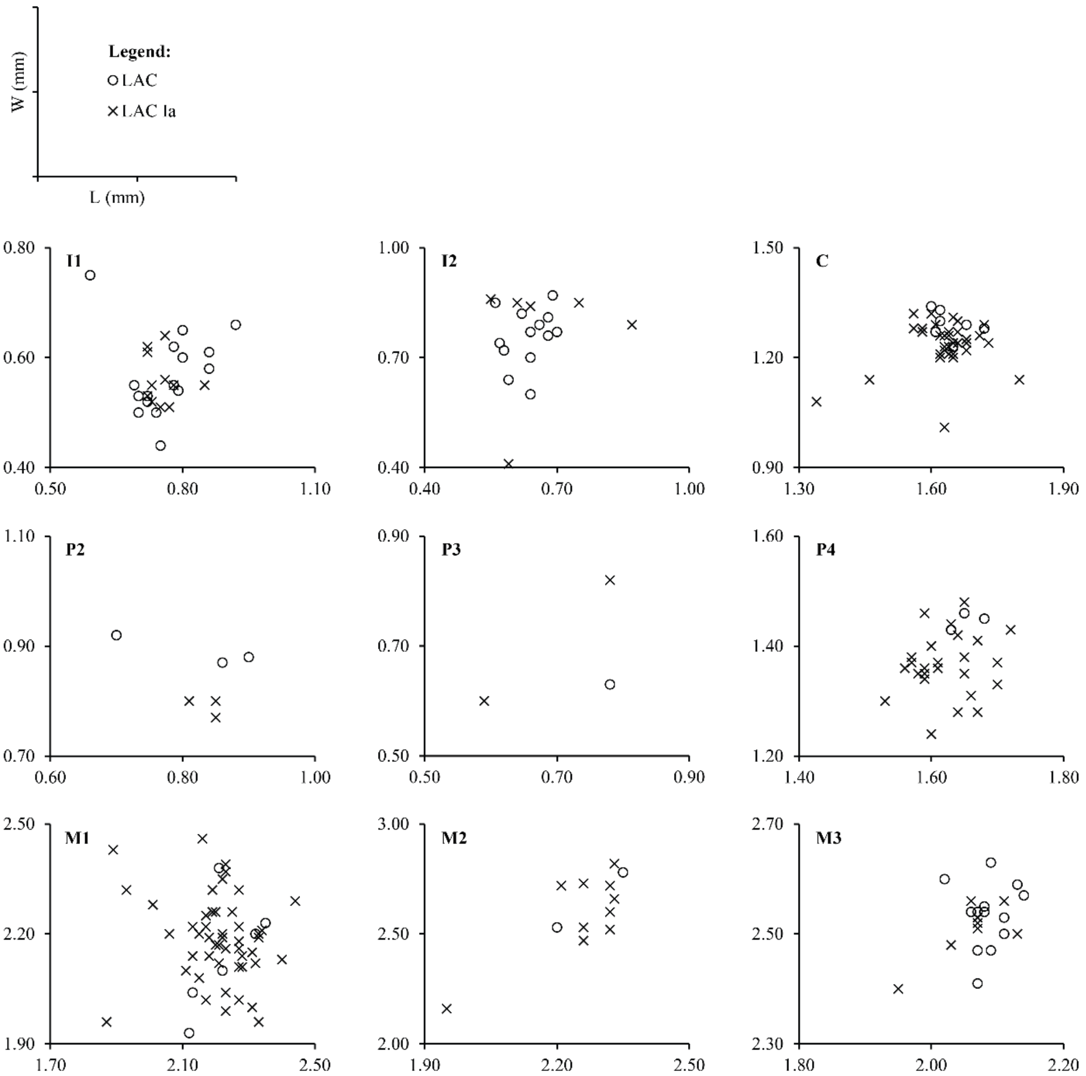

Figure 4.26 *Myotis myotis/blythii*, Loutra Almopias Cave A. XY graphs with the measured (in mm) dental elements (I1, I2, C, P2, P3, P4, M1, M2, M3). L: length, W: width.

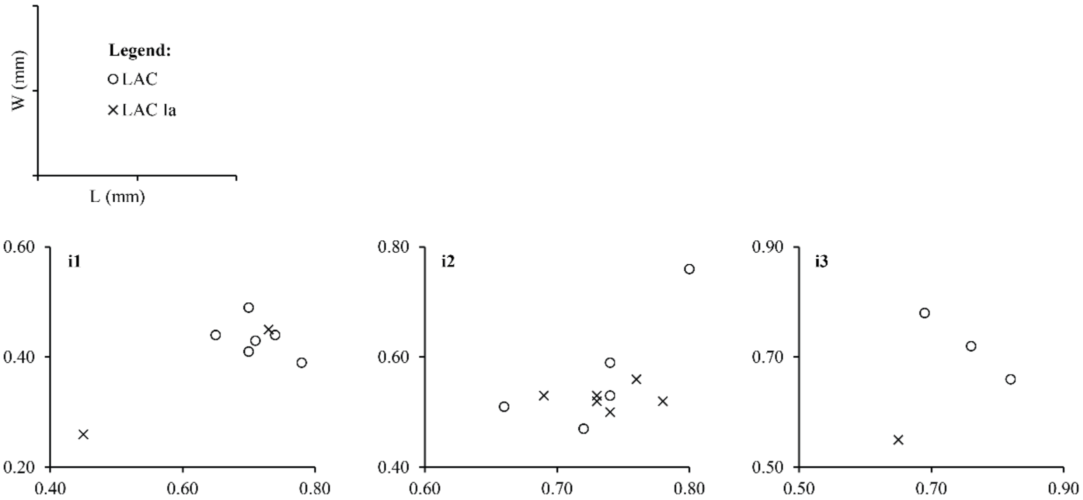

Figure 4.27 *Myotis myotis/blythii*, Loutra Almopias Cave A. XY graphs with the measured (in mm) dental elements (i1, i2, i3). L: length, W: width.

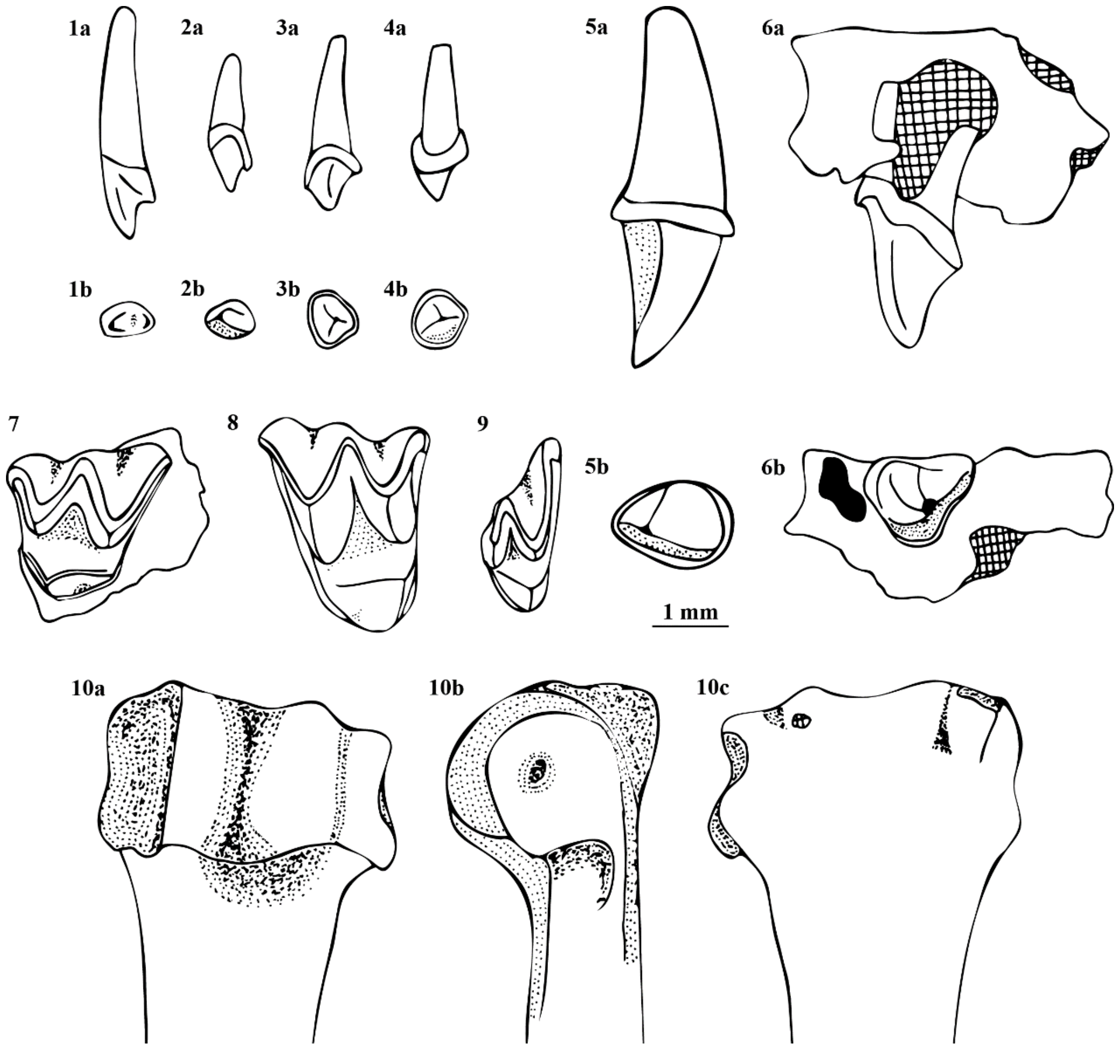

Figure 4.28 *Myotis myotis/blythii*, Loutra Almopias Cave A. **1.** LAC20726 – Left I1 (**a.** labial, **b.** occlusal), **2.** LAC21421a – Left I2 (**a.** labial, **b.** occlusal), **3.** LAC26331 – Right P2 (**a.** labial, **b.**

occlusal), **4.** LAC26321 – Left P3 (**a.** labial, **b.** occlusal), **5.** LAC27409 – Right C (**a.** labial, **b.** occlusal), **6.** LAC19715 –Left maxillary fragment with P4 (**a.** labial, **b.** occlusal), **7.** LAC26556 – Left M1, **8.** LAC16517 – Right M2, **9.** LAC19910 – Right M3, **10.** LAC26449 – Distal epiphysis of right humerus (**a.** anterior, **b.** lateral, **c.** posterior).

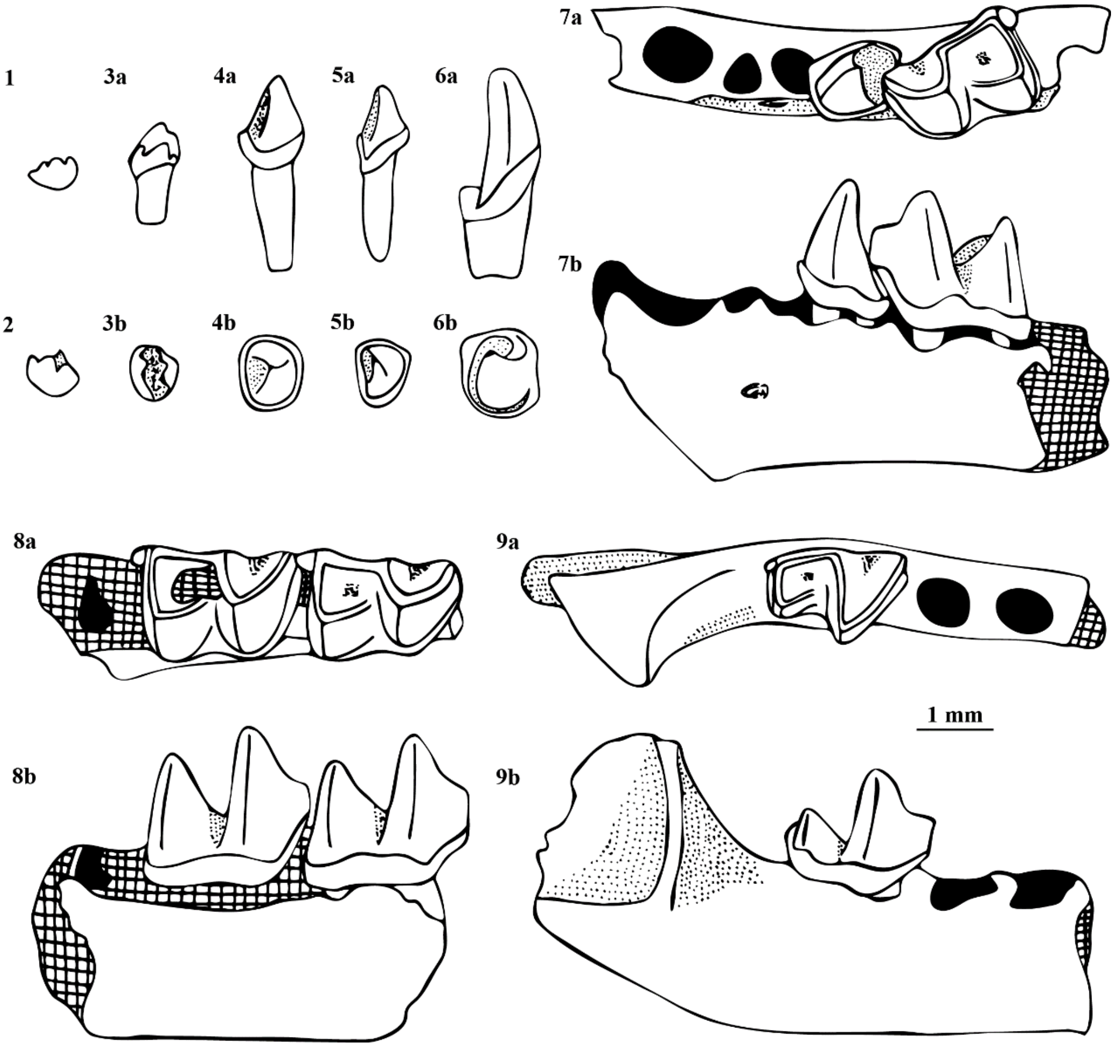

Figure 4.29 *Myotis myotis/blythii*, Loutra Almopias Cave A. **1.** LAC22447 – Right i1, **2.** LAC21044 – Left i2, **3.** LAC21439a – Left i3 (**a.** labial, **b.** occlusal), **4.** LAC16468 – Right p2 (**a.** labial, **b.** occlusal), **5.** LAC21413 – Right p3 (**a.** labial, **b.** occlusal), **6.** LAC21862 – Right c (**a.** labial, **b.** occlusal), **7.** LAC26789 – Left mandibular fragment with p4-m1 (**a.** labial, **b.** occlusal), **8.** LAC26721 – Right mandibular fragment with m1-m2 (**a.** labial, **b.** occlusal), **9.** LAC26728 – Right mandibular fragment with m3 (**a.** labial, **b.** occlusal).

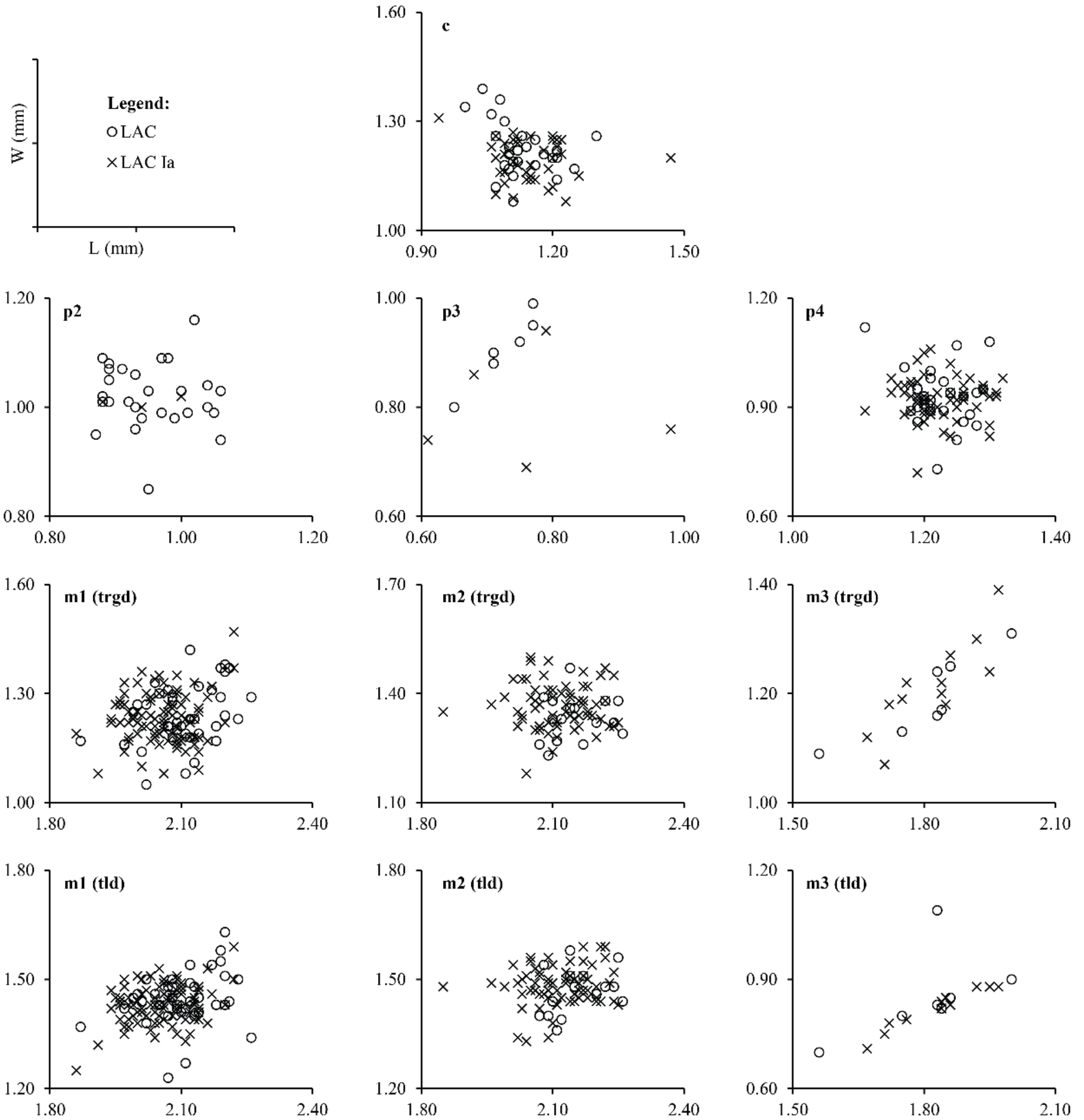

Figure 4.30 *Myotis myotis/blythii*, Loutra Almopias Cave A. XY graphs with the measured (in mm) dental elements (c, p2, p3, p4, m1, m2, m3). L: length, W: width, trgd: trigonid; tld: talonid.

Myotis bechsteinii Kuhl, 1817

(Bechstein's Bat)

Figure 4.32 and Figure A.60

Fossiliferous locality LAC I, LAC Ic, LAC II, LAC III

Age Late Pleistocene

Material 13 identified specimens

LAC I: 1 right p4 (19926), 1 left humerus (27482), LAC Ic: 1 right m3 (21483), LAC II: 1 right p4 (22252), 1 right m1 (22341), 2 left m3 (22012, 27828), LAC III: 1 right I1 (20505), 1 left C (21195), 1 right M3 (20928), 1 right p2 (20503), 1 right m1 (20150), 1 left m1 (21276)

Fossiliferous locality LAC Ia

Age latest Pleistocene

Material 58 identified specimens

1 left P3 (26323), 1 right C (25920), 1 left P4 (25394), 3 right M1 (24414, 24484, 24587), 4 left M1 (24745, 24912, 24976, 27328), 2 right M2 (24589, 24610), 1 left M2 (24802), 1 left M3 (25001), 1 left mandibular fragment with c and p4-m2 (26808), 1 right mandibular fragment with p4-m2 (19659), 1 left mandibular fragment with m2 (22752), 1 left mandibular fragment with m2-m3 (22472), 2 left mandibular fragments with m3 (22889, 22921), 8 right m1 (23327, 23319, 23416, 23571, 23680, 26904, 27357, 27361), 6 left m1 (23802, 23888, 23916, 24005, 26960, 26989), 4 right m2 (23494, 23546, 23559, 27359), 6 left m2 (23762, 23803, 23824, 23914, 26985, 27000), 6 right m3 (23325, 23647, 23650, 23654, 23717, 26900), 4 left m3 (24106, 26955, 27023, 27024), 2 right humerus (27445, 27446), 2 left humeri (27452, 27456)

Measurements Table 4.11 and Figure 4.31

Description *Myotis bechsteinii* is the largest of the medium-sized Vesper Bat species that currently occur in Greece.

I1: Tricuspid. It is oval in occlusal view. The mesial cusp is the largest and it covers approximately 1/3 of the tooth's area, the lingual is the smallest and the labial is slightly larger than the latter. The small cusps are both located distally. A cingulum of average thickness is also present throughout the whole tooth.

C: Very robust tooth with the cusp curved distally. It is oval in occlusal view. The crown, practically, forms no angle with the root. A thick ridge connects the distal base of the crown with the cusp. The crown is convex mesially, concave distolabially and distolingually and narrow lingually. Two longitudinal grooves occur, one labially and one lingually. The cingulum, which is of average thickness, is slightly convex labially and lingually (strongly marked).

P3: Unicuspid. It is subtriangular in occlusal view. A thin ridge connects the distal base of the crown with the cusp. A thick cingulum is also present, with its maximum thickness at its labial and lingual parts. The crown is flat mesially, convex labially, distally and lingually and concave distolabially and distolingually.

P4: Robust tooth with the cusp being connected with a crista to an accessory distolabial cusplet. It is subtriangular in occlusal view. A not well-developed heel is present in the mesiolingual part of the tooth. The crown is convex mesially and lingually and concave distally. The cingulum, which is of average thickness, is continuous throughout the whole tooth apart from its distal part.

M1: Robust tooth. It is subrectangular in occlusal view. Parastyle, mesostyle, paracone and metacone are well-developed, whereas the metastyle is somewhat less developed. The metacone is taller than the paracone. The parastyle forms an angle with the preparacrista and the metastyle slightly curves lingually. The mesial part of the ectoloph is narrower than the distal part. Additionally, the paracone, the metacone and the cristae on both sides form equal angles. Paraloph, metaloph and metaconule are absent. The paraconule is minute. The distal and lingual cingulum, which are of average thickness, are absent beneath the metastyle and the triangular protocone. The mesiolabial part of the anterior cingulum is connected to the preprotocrista and its mesiolingual part, which starts from the mesial side of the protocone, runs towards the lingual side of the tooth.

M2: The mesial part of the ectoloph is wider than in M1. The rest of the characters as M1.

M3: Very robust tooth. It is triangular in occlusal view. The parastyle and the paracone are more developed than the mesostyle and the metacone, whereas the metastyle is absent. The postprotocrista that connects the metacone with the metastyle is also absent. The paracone is taller than the metacone. The parastyle forms an angle with the preparacrista. The paraconule is well-developed. The cingulum is of average thickness and disappears only beneath the mesial part of the protocone, which is triangular.

c: Very robust tooth with the cusp slightly curved lingually. It is semicircular in occlusal view. It is convex mesially and concave distally. The distal part of the tooth is developed at the base of the crown, whereas the mesial part is developed in height. Respectively, the crown is in a more superior position towards the anterior part of the tooth. The distolabial part of the tooth is situated lower than the distolingual, which is higher than the former. The cingulum is thick throughout the whole tooth. It reaches its maximum thickness at the labial part of the tooth and it is absent at the mesial part, where it comes in contact with i3.

Table 4.11 *Myotis bechsteinii*, Loutra Almopias Cave A. Measurements (in mm) from both LAC and LAC Ia. LAC: Late Pleistocene; LAC Ia: latest Pleistocene; n: number of measurable specimens; L: length; W: width; trgd: trigonid; tld: talonid; MEAN: average; MIN: minimum; MAX: maximum; SD: standard deviation; CV: coefficient of variation.

			n	**MEAN**	**MIN**	**MAX**	**SD**	**CV**
I1	LAC	L	1	0.53	-	-	-	-
		W	1	0.51	-	-	-	-
C	LAC	L	1	1.15	-	-	-	-
		W	1	0.93	-	-	-	-
	LAC Ia	L	1	1.10	-	-	-	-
		W	1	0.87	-	-	-	-
P3	LAC Ia	L	1	0.68	-	-	-	-
		W	1	0.59	-	-	-	-
P4	LAC Ia	L	1	1.26	-	-	-	-
		W	1	1.19	-	-	-	-

M1	LAC Ia	L	7	1.60	1.52	1.74	0.075	4.651
		W	7	1.72	1.57	1.87	0.101	5.862
M2	LAC Ia	L	1	1.59	1.59	1.59	0.000	0.000
		W	1	1.90	1.83	1.96	0.092	4.851
M3	LAC	L	1	1.72	-	-	-	-
		W	1	1.96	-	-	-	-
	LAC Ia	L	1	1.42	-	-	-	-
		W	1	1.84	-	-	-	-
c	LAC Ia	L	1	0.90	-	-	-	-
		W	1	0.83	-	-	-	-
p2	LAC	L	1	0.64	-	-	-	-
		W	1	0.80	-	-	-	-
p4	LAC	L	3	1.01	0.93	1.06	0.072	7.139
		W	3	0.81	0.73	0.91	0.092	11.315
	LAC Ia	L	1	0.85	-	-	-	-
		W	1	0.68	-	-	-	-
m1	LAC	L	4	1.50	1.43	1.56	0.056	3.713
		W (trgd)	4	0.98	0.94	1.00	0.027	2.714
		W (tld)	4	1.05	0.98	1.13	0.064	6.107
	LAC Ia	L	15	1.48	1.38	1.55	0.047	3.211
		W (trgd)	15	0.95	0.83	1.02	0.053	5.602
		W (tld)	15	1.05	0.97	1.13	0.042	4.040
m2	LAC	L	1	-	-	-	-	-
		W (trgd)	1	-	-	-	-	-
		W (tld)	1	-	-	-	-	-
	LAC Ia	L	13	1.51	1.43	1.57	0.038	2.533
		W (trgd)	13	0.98	0.86	1.07	0.064	6.482
		W (tld)	13	1.04	0.93	1.10	0.048	4.603
m3	LAC	L	3	1.47	1.41	1.56	0.082	5.553
		W (trgd)	3	0.93	0.86	1.07	0.121	13.037
		W (tld)	3	0.77	0.69	0.86	0.086	11.246
	LAC Ia	L	13	1.46	1.32	1.66	0.108	7.393
		W (trgd)	13	0.96	0.80	1.10	0.106	11.073
		W (tld)	13	0.70	0.62	0.77	0.046	6.554
c-p4	LAC Ia	L	1	2.77	-	-	-	-
Humerus	LAC	W	1	2.85	-	-	-	-
	LAC Ia	W	4	2.87	2.85	2.90	0.022	0.753

p2: Unicuspid with the cusp slightly curved distally. It is subcircular in occlusal view. The labial side is more convex than the lingual. The cingulum is of average thickness and continuous throughout the whole tooth.

p4: Robust tooth. It is subrectangular to pentagonal in occlusal view. The mesiolingual part of the tooth is more elongated and developed higher than the mesiolabial part. The distolingual part of the tooth is developed higher than the distolabial. The crown is convex labially and lingually and concave distally. The cingulum is thick and uniform throughout the whole tooth and it bends down slightly at the level of each root, with the posterior convexity being placed slightly lower than the anterior. A cingular platform is present at the mesiolingual part of the tooth.

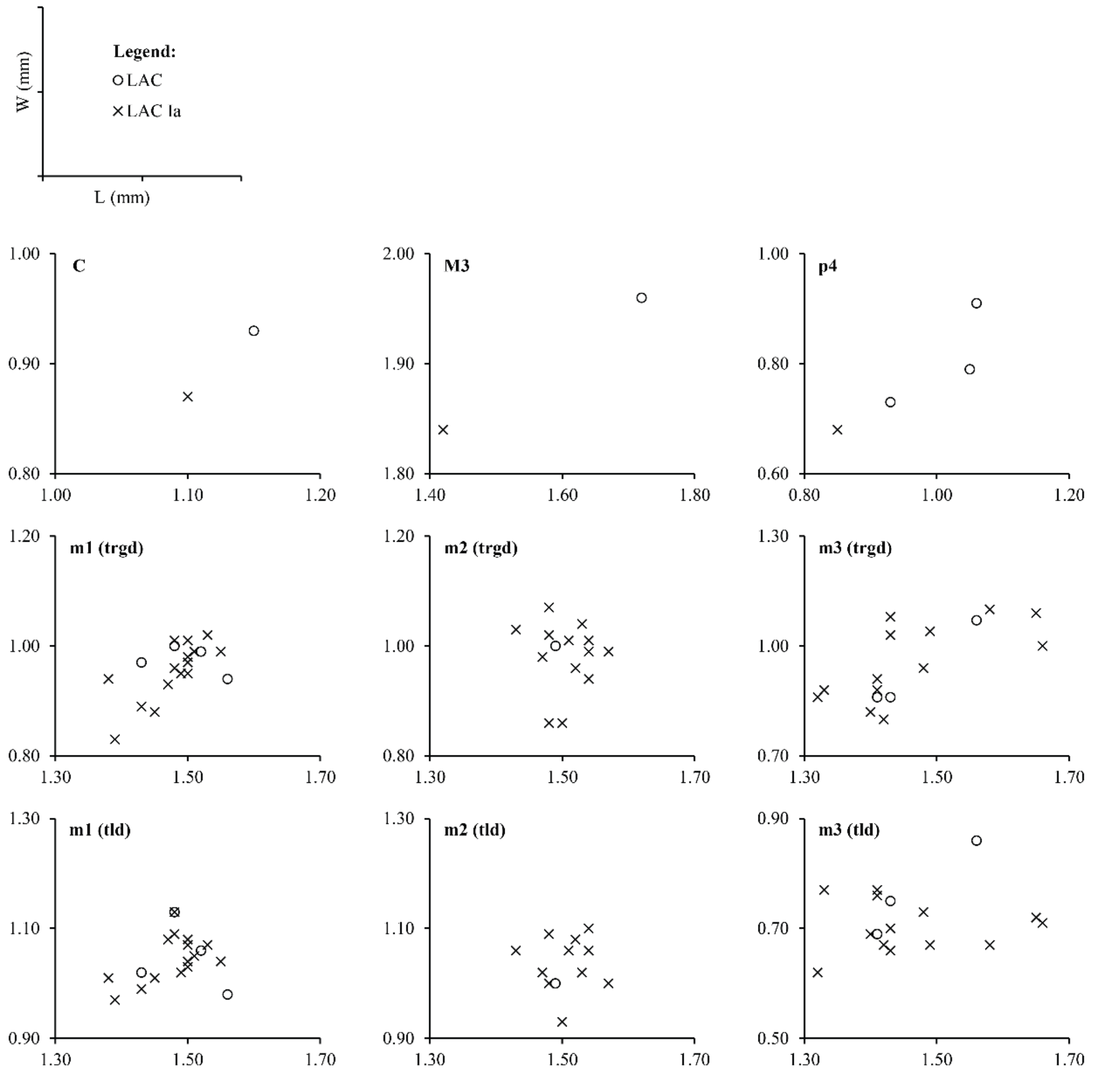

Figure 4.31 *Myotis bechsteinii*, Loutra Almopias Cave A. XY graphs with the measured (in mm) dental elements (C, M3, p4, m1, m2, m3). L: length, W: width, trgd: trigonid; tld: talonid.

m1: Myotodont. The talonid is longer than the trigonid. Paraconid, metaconid, entoconid, protoconid and hypoconid are well-developed. The protoconid is taller than the hypoconid. The paralophid is angular. The entocristid is straight. The hypoconulid is well-developed and slightly developed lingually, together with the entoconid. The labial cingulum is thick throughout the whole tooth and it bends down slightly at the level of each root, with the posterior convexity being placed slightly lower than the anterior. Lingual cingulum of the trigonid is also present.

m2: The trigonid is wider than in m1. The labial cingulum is flatter than in m1. The rest of the characters as m1.

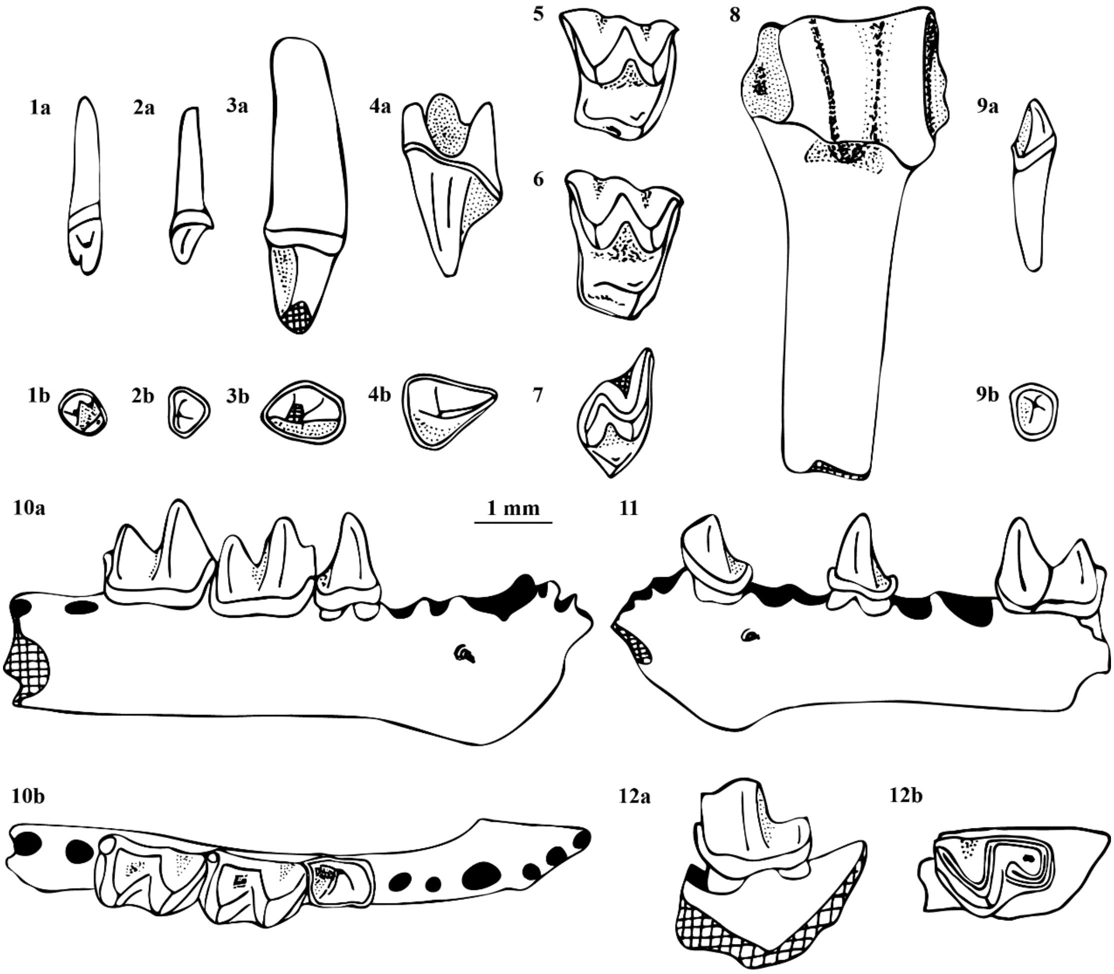

Figure 4.32 *Myotis bechsteinii*, Loutra Almopias Cave A. **1.** LAC20505 – Right I1 (**a.** labial, **b.** occlusal), **2.** LAC26323 – Right P3 (**a.** labial, **b.** occlusal), **3.** LAC25920 – Right C (**a.** labial, **b.** occlusal), **4.** LAC25394 – Left P4 (**a.** labial, **b.** occlusal), **5.** LAC24587 – Right M1, **6.** LAC24589 – Right M2, **7.** LAC20928 – Right M3, **8.** LAC27482 – Distal epiphysis of left humerus, **9.** LAC20503 – Right p2 (**a.** labial, **b.** occlusal), **10.** LAC19659 – Right mandibular fragment with p4-m2 (**a.** labial, **b.** occlusal), **11.** LAC26808 – Left mandibular fragment with c, p4 and m2, **12.** LAC22889 – Left m3 (**a.** labial, **b.** occlusal).

m3: Myotodont. The talonid is longer than the trigonid. Paraconid, metaconid, entoconid, protoconid and hypoconid are well-developed. The protoconid is taller than the hypoconid. The paralophid is angular (more obtuse angle than in m1 and m2). The entocristid is straight. The entoconid is more towards the labial side of the tooth and the hypoconid towards the lingual and thus, the talonid is reduced. The hypoconulid is not well-developed. The labial cingulum is thick and uniform throughout the whole tooth. Lingual cingulum of the trigonid is absent.

Mandible: The mental foramen is beneath the gap between c and p2. The lowest part of the symphysis is relatively pointed.

Humerus: The styloid process is short and blunt. The epitrochlea is also short and wide. The valley between the trochlea and the condyle tends to be flat. A shallow valley is present between the condyle and the epicondyle. The condyle and the epicondyle are not projecting laterally. The radial fossa is relatively deep, whereas the olecranon fossa is very shallow (practically flat).

Discussion The morphological features described in addition to the measurements allow a definite attribution of the material to *Myotis bechsteinii*. It is the largest of the medium-sized Vesper Bat species that currently occur in Greece and it is clearly distinguished from the rest of the species.

Occurrence The fossils of the Bechstein's Bat described from Loutra Almopias Cave A are the first known records of this species in Greece. Its modern distribution includes a few sparse records from most of mainland Greece (Hanák et al. 2001, GFDC 2021). On a global scale it is distributed in Europe, including England and Southern Sweden all the way to Caucasus and Iran (Simmons 2005a).

Ecology *Myotis bechsteinii* hibernates mostly in hollow trees, however, caves are used as well and its habitat preferences include a variety of forested areas (Dietz et al. 2009).

Myotis emarginatus Geoffroy, 1806

(Geoffroy's Bat)

Figure 4.35 and Figure A.61

Fossiliferous locality LAC I, LAC Ib, LAC Ic, LAC II, LAC III

Age Late Pleistocene

Material 45 identified specimens

LAC I: 1 right m2 (17213), LAC Ib: 1 right m1 (16690), 1 left m1 (16513), LAC Ic: 1 right p3 (17963), LAC II: 1 left C (22427), 1 right P4 (22046), 1 left P4 (21744), 2 right M1 (21901, 22354), left M1 (21694), 1 right M2 (21725), 2 left m1 (22349, 27884), 2 right m2 (21518, 27880), 1 right m3 (22063), 1 left m3 (22037), LAC III: 1 right C (21217), 2 left C (20215, 20384), 1 right P4 (20567), 2 left P4 (21191, 20473), 2 right M1 (19147, 20369), 3 left M1 (20274, 21329, 20373), 1 right M2 (20166), 2 left M2 (20168, 20266), 3 right c (21392, 21407, 21193), left c (20092), 3 left p4 (20161, 21290, 20049), 1 left m1 (20863), 1 right m2 (20979), 1 left m2 (20538), 1 right m3 (20153), 3 left m3 (20257, 20910, 20540)

<u>Fossiliferous locality</u> LAC Ia

<u>Age</u> latest Pleistocene

<u>Material</u> 76 identified specimens

16 right M1 (24380, 24389, 24410, 24422, 24446, 24473, 24491, 24562, 24573, 26568, 26571, 26591, 26594, 26599, 26601, 26606), 2 left M1 (24736, 26668), 2 right M2 (24408, 27300), 5 left M2 (24702, 24918, 24969, 26631, 27331), 1 left M3 (25003), 1 left mandibular fragment with p4-m2 (22767), 1 right mandibular fragment with m2-m3 (22604), 1 right mandibular fragment with m3 (22635), 2 left mandibular fragments with m3 (22863, 22920), 1 left p2 (26297), 6 right m1 (23512, 23665, 23686, 26888, 26890, 27365), 7 left m1 (23753, 23796, 23990, 24036, 24047, 24049, 26809), 7 right m2 (23520, 23561, 23562, 23566, 23678, 26886, 26897), 8 left m2 (23842, 23867, 23954, 23969, 24001, 24004, 26982, 26999), 9 right m3 (23413, 23576, 23600, 23623, 23643, 23695, 23701, 27371, 27372), 7 left m3 (23735, 24086, 24094, 24134, 24143, 24171, 27292)

<u>Measurements</u> Table 4.12 and Figure 4.33-34

<u>Description</u> *Myotis emarginatus* is one of the medium-sized members of the eleven Vesper Bat species that currently occur in Greece.

C: Robust tooth with the cusp curved distally. It is oval in occlusal view. The crown, practically, forms no angle with the root. A thin ridge connects the distal base of the crown with the cusp. The crown is convex mesially and slightly concave distolabially and distolingually and it becomes narrow distally. Two longitudinal grooves occur, one labially and one lingually. The cingulum, which is of average thickness, is thicker labially than lingually.

Table 4.12 *Myotis emarginatus*, Loutra Almopias Cave A. Measurements (in mm) from both LAC and LAC Ia. LAC: Late Pleistocene; LAC Ia: latest Pleistocene; n: number of measurable specimens; L: length; W: width; trgd: trigonid; tld: talonid; MEAN: average; MIN: minimum; MAX: maximum; SD: standard deviation; CV: coefficient of variation.

			n	**MEAN**	**MIN**	**MAX**	**SD**	**CV**
C	LAC	L	4	0.97	0.84	1.08	0.103	10.719
		W	4	0.77	0.65	0.82	0.079	10.265
P4	LAC	L	5	1.18	1.09	1.28	0.076	6.426
		W	5	0.96	0.76	1.03	0.112	11.662
M1	LAC	L	7	1.42	1.31	1.47	0.057	4.025
		W	7	1.47	1.41	1.51	0.033	2.269
	LAC Ia	L	17	1.46	1.36	1.56	0.050	3.452
		W	17	1.53	1.41	1.64	0.062	4.072
M2	LAC	L	4	1.34	1.31	1.39	0.037	2.769
		W	4	1.63	1.58	1.70	0.051	3.138
	LAC Ia	L	8	1.50	1.44	1.56	0.039	2.586
		W	8	1.76	1.63	1.86	0.090	5.098
M3	LAC Ia	L	1	1.45	-	-	-	-
		W	1	1.53	-	-	-	-
c	LAC	L	4	0.84	0.76	0.87	0.053	6.271
		W	4	0.78	0.72	0.84	0.050	6.452

p2	LAC Ia	L	1	0.58	-	-	-	-
		W	1	0.59	-	-	-	-
p3	LAC	L	1	0.55	-	-	-	-
		W	1	0.61	-	-	-	-
p4	LAC	L	3	0.91	0.88	0.95	0.036	3.962
		W	3	0.57	0.51	0.65	0.072	12.651
	LAC Ia	L	1	0.92	-	-	-	-
		W	1	0.62	-	-	-	-
m1	LAC	L	5	1.40	1.28	1.47	0.072	5.180
		W (trgd)	5	0.78	0.69	0.91	0.096	12.188
		W (tld)	5	0.88	0.81	0.98	0.079	9.010
	LAC Ia	L	14	1.35	1.23	1.44	0.069	5.096
		W (trgd)	14	0.80	0.71	0.99	0.078	9.733
		W (tld)	14	0.88	0.76	0.99	0.072	8.194
m2	LAC	L	5	1.32	1.21	1.43	0.090	6.816
		W (trgd)	5	0.79	0.73	0.82	0.035	4.475
		W (tld)	5	0.85	0.83	0.87	0.018	2.127
	LAC Ia	L	17	1.39	1.24	1.48	0.069	4.950
		W (trgd)	17	0.87	0.76	0.97	0.052	6.016
		W (tld)	17	0.92	0.79	1.00	0.051	5.547
m3	LAC	L	6	1.26	1.22	1.30	0.035	2.749
		W (trgd)	6	0.80	0.75	0.89	0.055	6.860
		W (tld)	6	0.67	0.62	0.79	0.064	9.518
	LAC Ia	L	20	1.29	1.14	1.42	0.075	5.769
		W (trgd)	20	0.83	0.69	0.91	0.059	7.112
		W (tld)	20	0.68	0.61	0.76	0.046	6.687

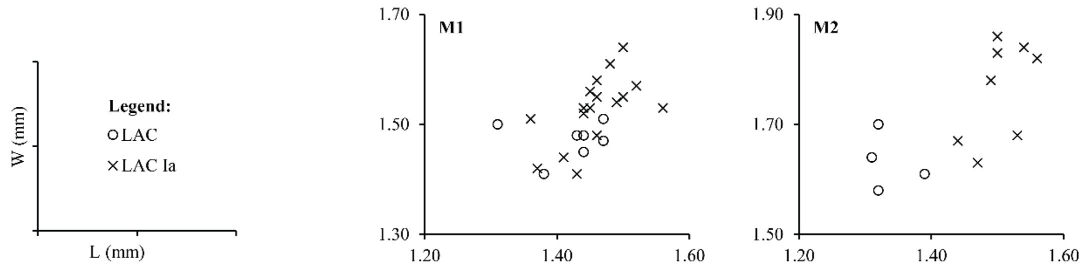

Figure 4.33 *Myotis emarginatus*, Loutra Almopias Cave A. XY graphs with the measured (in mm) dental elements (M1, M2). L: length, W: width.

P4: Medium-sized tooth with the cusp being connected with a crista to an accessory distolabial cusplet. It is subtriangular in occlusal view. A not well-developed heel is present at the mesiolingual part of the tooth. The crown is convex mesially and lingually and concave distally. The cingulum, which is of average thickness, is continuous throughout the whole tooth apart from its distal part. A cingular platform is present at the mesiolabial part of the tooth.

M1: Medium-sized tooth. It is subrectangular in occlusal view. Parastyle, mesostyle, metastyle, paracone and metacone are well-developed. The metacone is taller than the paracone. The parastyle forms an angle with the preparacrista and the metastyle slightly curves lingually. The mesial part of the ectoloph is narrower than the distal part. Additionally, the paracone, the metacone and the cristae on both sides form equal angles. Paraloph, metaloph and metaconule are present, but not well-developed. The paraconule is well-developed. The distal and lingual cingulum, which are of average thickness, are absent beneath the metastyle and the triangular protocone. The mesiolabial part of the anterior cingulum is connected to the preprotocrista and its mesiolingual part, which starts from the mesial side of the protocone, runs towards the lingual side of the tooth.

M2: The mesial part of the ectoloph is wider than in M1. The rest of the characters as M1.

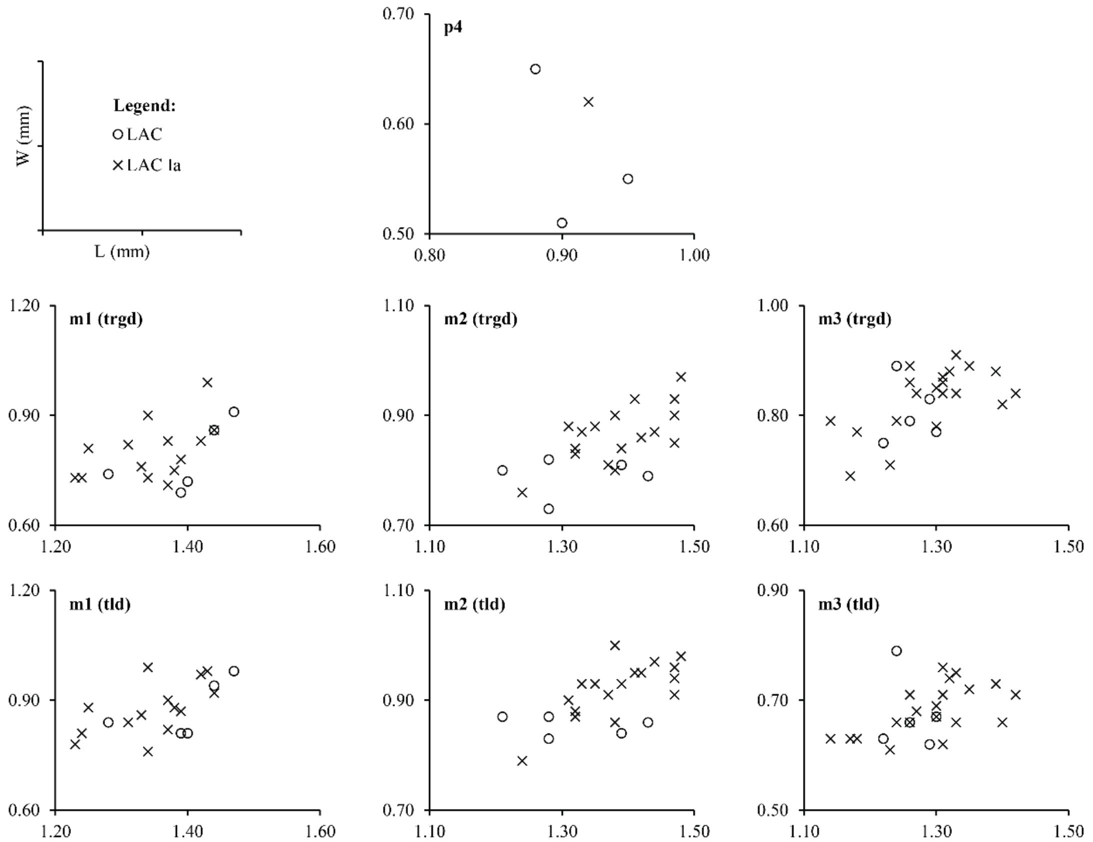

Figure 4.34 *Myotis emarginatus*, Loutra Almopias Cave A. XY graphs with the measured (in mm) dental elements (p4, m1, m2, m3). L: length, W: width, trgd: trigonid; tld: talonid.

M3: Robust tooth. It is triangular in occlusal view. The parastyle and the paracone are more developed than the mesostyle and the metacone, whereas the metastyle is absent. The postmetacrista that connects the metacone with the metastyle is also absent. The paracone is taller than the metacone. The parastyle forms practically no angle with the preparacrista. The paraloph and the paraconule are well-developed. The lingual cingulum is thin and it disappears beneath the lingual part of the triangular protocone.

c: Robust tooth with the cusp slightly curved lingually. It is semicircular in occlusal view. It is convex mesially and concave distally. The distal part of the tooth is developed at the base of the crown, whereas the mesial part is developed in height. Respectively, the crown is moved to a more superior position towards the anterior part of the tooth. The distolabial part of the tooth is situated lower than the distolingual, which is higher than the former. The cingulum is thick throughout the whole tooth. It reaches its maximum thickness at the labial part of the tooth and its minimum at the mesial part, where it comes in contact with i3. A cingular cusplet is also present at the mesiolingual part of the tooth.

p2: Unicuspid tooth with the cusp slightly curved distally. It is subcircular in occlusal view. The labial side is more convex than the lingual. The cingulum is of average thickness and continuous throughout the whole tooth. An accessory cusplet is present at the mesiolingual part of the tooth.

p3: It is convex mesially, labially and lingually. It is slightly concave distally. The lingual side is more convex than the labial. The rest of the characters as p2.

p4: Robust tooth. It is subrectangular to pentagonal in occlusal view. The mesiolingual part of the tooth is more elongated and developed higher than the mesiolabial part. The distolingual part of the tooth is developed higher than the distolabial. The crown is convex labially and lingually and concave distally. The cingulum is thick and uniform throughout the whole tooth and it bends down slightly at the level of each root, with the posterior convexity being placed slightly lower than the anterior. A cingular platform is present at the mesiolingual part of the tooth and an accessory cusplet at the distolingual.

m1: Myotodont. The talonid is longer than the trigonid. Paraconid, metaconid, entoconid, protoconid and hypoconid are well-developed. The protoconid is taller than the hypoconid. The paralophid is angular. The entocristid is straight. The hypoconulid is well-developed and slightly developed lingually, together with the entoconid. The labial cingulum is thick throughout the whole tooth and it bends down slightly at the level of each root, with the posterior convexity being placed slightly lower than the anterior. Lingual cingulum of the trigonid is also present.

m2: The trigonid is wider than in m1. The labial cingulum is flatter than in m1. The rest of the characters as m1.

m3: Myotodont. The talonid is longer than the trigonid. Paraconid, metaconid, entoconid, protoconid and hypoconid are well-developed. The protoconid is taller than the hypoconid. The paralophid is angular (more obtuse angle than in m1 and m2). The entocristid is straight. The entoconid is more towards the labial side of the tooth and the hypoconid towards the lingual and thus, the talonid is reduced. The hypoconulid is well-developed. The labial cingulum is thick and uniform throughout the whole tooth. Lingual cingulum of the trigonid is absent.

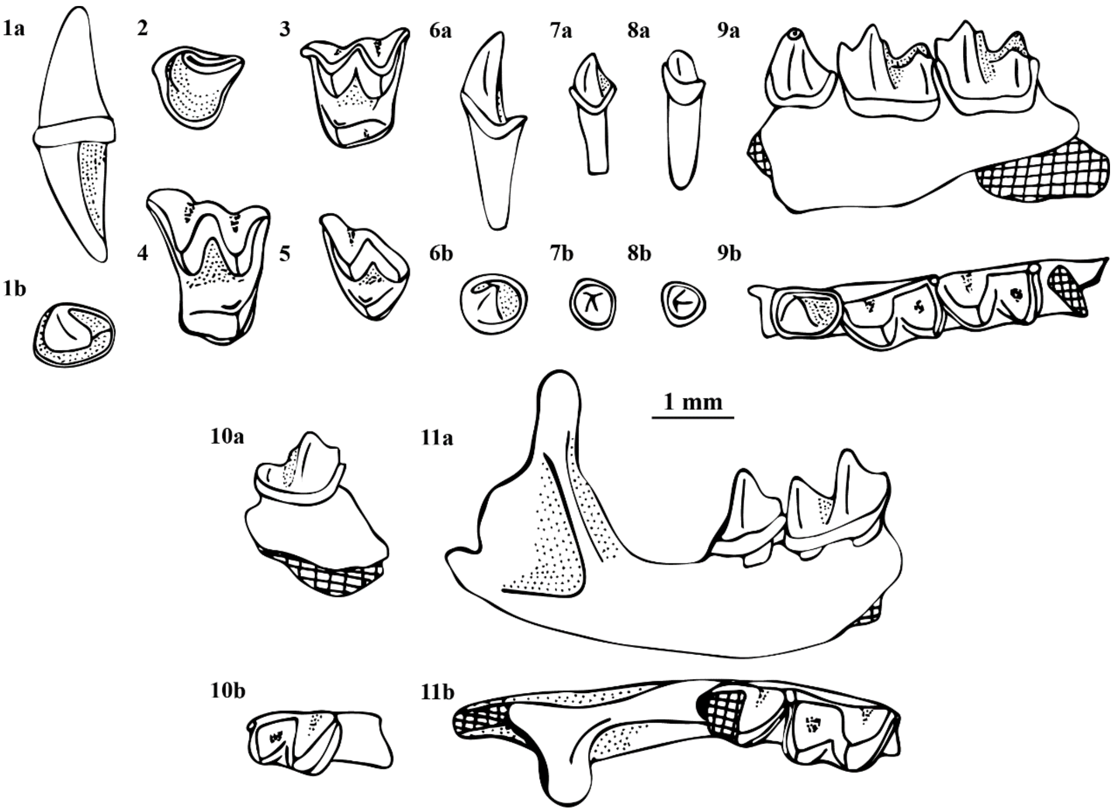

Figure 4.35 *Myotis emarginatus*, Loutra Almopias Cave A. **1.** LAC20384 – Left C (**a.** labial, **b.** occlusal), **2.** LAC20473 – Left P4, **3.** LAC21694 – Left M1, **4.** LAC24408 – Right M2, **5.** LAC25003 – Left M3, **6.** LAC20092 – Left c (**a.** labial, **b.** occlusal), **7.** LAC26297 – Left p2 (**a.** labial, **b.** occlusal), **8.** LAC17963 – Left p3 (**a.** labial, **b.** occlusal), **9.** LAC22767 – Left mandibular fragment with p4-m2 (**a.** labial, **b.** occlusal), **10.** LAC22635 – Right m3 (**a.** labial, **b.** occlusal), **11.** LAC22604 – Right mandibular fragment with m2-m3 (**a.** labial, **b.** occlusal).

Discussion The morphological features described in addition to the measurements allow a definite attribution of the material to *Myotis emarginatus*. It is an intermediate member of the medium-sized Vesper Bat species that currently occur in Greece and it is clearly distinguished from the rest of the species.

Occurrence Fossils of the Geoffroy's Bat are known from Petralona Cave, Chalkidiki. Its modern distribution includes most of mainland Greece and several islands including Crete and Corfu (Hanák et al. 2001, GFDC 2021). On a global scale it is distributed from Northwestern Africa to the Iberian Peninsula, South Europe (up to the Netherlands) and Southern Poland, Crimea Peninsula, Caucasus, Kyrgyzstan, Tajikistan, Uzbekistan, most parts of the Levant and parts of Middle East (Saudi Arabia, Oman, Iran, Afghanistan) (Simmons 2005a).

Ecology *Myotis emarginatus* is a typical cave dweller and its habitat preferences include a variety of forested areas, except from coniferous forests (Dietz et al. 2009).

Myotis capaccinii Bonaparte, 1837

(Long-fingered Myotis)

Figure 4.36 and Figure A.62

Fossiliferous locality LAC Ia

Age latest Pleistocene

Material 19 identified specimens

1 right maxillary fragment with P4-M1 (23162), 1 left maxillary fragment with P4-M1 (23150), 1 right M1 (27313), 1 left M1 (24929), 1 right M2 (24629), 1 right mandibular fragment with m1-m3 (22477), 1 left mandibular fragment with m2-m3 (22934), 1 left mandibular fragment with m3 (22871), 1 right p3 (26367), 5 left m1 (23830, 23943, 23944, 24059, 24068), 3 right m3 (23649, 23720, 27366), 2 left m3 (24131, 26824)

Measurements Table 4.13

Description *Myotis capaccinii* is the smallest of the medium-sized members of the eleven Vesper Bat species that currently occur in Greece.

P4: Small-sized tooth, with the cusp being connected with a crista to an accessory distolabial cusplet. It is subtriangular in occlusal view. A not well-developed heel is present at the mesiolingual part of the tooth. The crown is convex mesially and lingually, concave distally and relatively sharp lingually. The cingulum, which is thick, is continuous throughout the whole tooth, with its maximum thickness at its distolabial part. A small cingular platform is present at the mesiolabial part of the tooth and an accessory cingular cusplet is present at the mesiolingual part of the tooth.

Table 4.13 *Myotis capaccinii*, Loutra Almopias Cave A. Measurements (in mm) from LAC Ia. LAC Ia: latest Pleistocene; n: number of measurable specimens; L: length; W: width; trgd: trigonid; tld: talonid; MEAN: average; MIN: minimum; MAX: maximum; SD: standard deviation; CV: coefficient of variation.

			n	**MEAN**	**MIN**	**MAX**	**SD**	**CV**
P4	LAC Ia	L	2	0.94	0.92	0.95	0.021	2.269
		W	2	0.93	0.87	0.99	0.085	9.124
M1	LAC Ia	L	4	1.30	1.25	1.38	0.057	4.397
		W	4	1.27	1.20	1.30	0.045	3.565
M2	LAC Ia	L	1	1.28	-	-	-	-
		W	1	1.64	-	-	-	-
p3	LAC Ia	L	1	0.42	-	-	-	-
		W	1	0.56	-	-	-	-
m1	LAC Ia	L	6	1.25	1.21	1.30	0.036	2.907
		W (trgd)	6	0.74	0.70	0.80	0.038	5.128
		W (tld)	6	0.82	0.76	0.86	0.038	4.628
m2	LAC Ia	L	2	1.25	1.23	1.26	0.021	1.704
		W (trgd)	2	0.78	0.74	0.81	0.050	6.387
		W (tld)	2	0.83	0.82	0.84	0.014	1.704
m3	LAC Ia	L	8	1.17	1.10	1.23	0.042	3.569
		W (trgd)	8	0.72	0.67	0.77	0.038	5.271
		W (tld)	8	0.63	0.55	0.68	0.041	6.517
m1-m3	LAC Ia	L	1	3.93	-	-	-	-

M1: Small-sized tooth. It is subrectangular in occlusal view. Parastyle, mesostyle, metastyle, paracone and metacone are well-developed. The metacone is taller than the paracone. The parastyle forms an angle with the preparacrista and the metastyle slightly curves lingually. The mesial part of the ectoloph is narrower than the distal part. Additionally, the paracone, the metacone and the cristae on both sides form equal angles. Paraloph, metaloph, paraconule and metaconule are well-developed. The distal and lingual cingulum, which are of average thickness, are absent beneath the metastyle and the triangular protocone. The mesiolabial part of the anterior cingulum is connected to the preprotocrista and its mesiolingual part, which starts from the mesial side of the protocone, runs towards the lingual side of the tooth.

M2: The parastyle is more pronounced than the metastyle. The mesial part of the ectoloph is wider than in M1. The rest of the characters as M1.

p3: Unicuspid tooth with the cusp slightly curved distally. It is oval in occlusal view. The lingual side is more convex than the labial. The cingulum is of average thickness and continuous throughout the whole tooth. Two accessory cusplets are present, one at the mesiolingual part of the tooth and one at the distolingual.

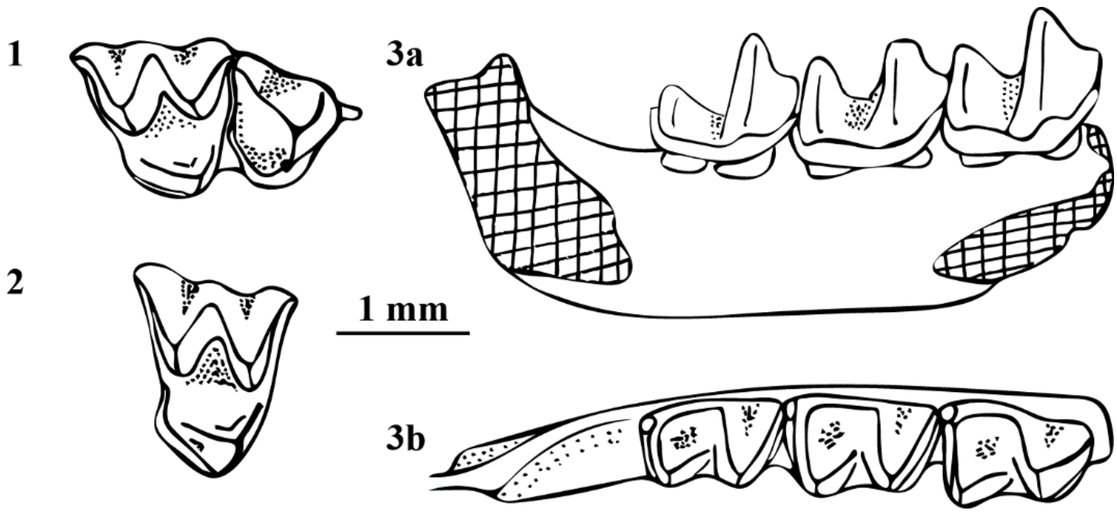

Figure 4.36 *Myotis capaccinii*, Loutra Almopias Cave A. **1.** LAC23162 – Right maxillary fragment with P4-M1, **2.** LAC24629 – Right M2, 3. LAC22477 – Right mandibular fragment with m1-m3 (**a.** labial, **b.** occlusal).

m1: Myotodont. The talonid is longer than the trigonid. Paraconid, metaconid, entoconid, protoconid and hypoconid are well-developed. The protoconid is taller than the hypoconid. The paralophid is angular. The entocristid is straight. The hypoconulid is well-developed and it is placed to a more labial position in respect to the lingual cusps. The labial cingulum is thick beneath the protoconid and slightly thinner beneath the hypoconid. Lingual cingulum of the trigonid is also present.

m2: The trigonid is wider and shorter than in m1. The thickening of the labial cingulum is less pronounced than in m1. The rest of the characters as m1.

m3: Myotodont. The talonid is longer than the trigonid. Paraconid, metaconid, entoconid, protoconid and hypoconid are well-developed. The protoconid is taller than the hypoconid. The paralophid is angular (more obtuse angle than in m1 and m2). The entocristid is straight. The entoconid is more towards the labial side of the tooth and the hypoconid towards the lingual and thus, the talonid is reduced. The hypoconulid is well-developed. The labial cingulum is thick beneath the protoconid and slightly thinner beneath the hypoconid. Lingual cingulum of the trigonid is also present.

Mandible: The anterior part of the masseter crest, which is of average thickness, is relatively steep.

<u>Discussion</u> The morphological features described in addition to the measurements allow a definite attribution of the material to *Myotis capaccinii*. It is the smallest of the medium-sized members of the eleven Vesper Bat species that currently occur in Greece and it is clearly distinguished from the rest of the species.

Occurrence The fossils of the Long-fingered Myotis described from Loutra Almopias Cave A are the first known records of this species in Greece. Its modern distribution includes most of mainland Greece, a few islands of the Eastern Aegean and the Ionian Sea and Crete (Hanák et al. 2001, GFDC 2021). On a global scale it is distributed from Northwest Africa to several areas of the Mediterranean zone (including several European islands), Bulgaria, Turkey, a big part of the Levant and parts of Middle East and Uzbekistan (Simmons 2005a).

Ecology *Myotis capaccinii* is a typical cave dweller and its habitat preferences are mostly limited to karst limestone areas with the presence of water (Dietz et al. 2009).

Myotis mystacinus Kuhl, 1817

(Whiskered Myotis)

Figure 4.37 and Figure A.63

Fossiliferous locality LAC Ia

Age latest Pleistocene

Material 4 identified specimens

1 left M1 (24805), 1 left M2 (24692), 1 left mandibular fragment (26855), 1 left humerus (27455)

Measurements Table 4.14

Description *Myotis mystacinus* is the smallest of the eleven Vesper Bat species that currently occur in Greece.

M1: Small-sized tooth. It is subrectangular in occlusal view. Parastyle, mesostyle, metastyle, paracone and metacone are well-developed. The metacone is taller than the paracone. The parastyle forms an angle with the preparacrista and the metastyle curves lingually. The mesial part of the ectoloph is narrower than the distal part. Additionally, the paracone, the metacone and the cristae on both sides form equal angles. Paraloph, and metaloph are absent. The paraconule and the metaconule are well-developed. The distal and lingual cingulum, which are of average thickness, are absent beneath the metastyle and the triangular protocone. The mesiolabial part of the anterior cingulum is connected to the preprotocrista and its mesiolingual part, which starts from the mesial side of the protocone, runs towards the lingual side of the tooth.

M2: Metaconule is not as well-developed as in M1. The distolingual part of the tooth is slightly concave at the base of the crown. The rest of the characters as M1.

Mandible: The coronoid process is angular and located to a slightly more inferior position than the articular process. The anterior part of the masseter crest, which is thin, is steep. The anterior sigmoid notch is positioned slightly lower than the articular process and on the same level with the coronoid process.

Humerus: The styloid process is short and blunt. The epitrochlea is significantly reduced. The valley between the trochlea and the condyle tends to be flat. A shallow valley is present between the condyle and the epicondyle. The condyle and the epicondyle are not projecting laterally. The radial fossa and the olecranon fossa are relatively deep, with the latter extending from the middle part of the epiphysis to the styloid process.

Table 4.14 *Myotis mystacinus*, Loutra Almopias Cave A. Measurements (in mm) from LAC Ia. LAC Ia: latest Pleistocene; n: number of measurable specimens; L: length; W: width; MEAN: average; MIN: minimum; MAX: maximum; SD: standard deviation; CV: coefficient of variation.

			n	**MEAN**	**MIN**	**MAX**	**SD**	**CV**
M1	LAC Ia	L	1	1.27	-	-	-	-
		W	1	1.22	-	-	-	-
Humerus	LAC Ia	W	1	2.24	-	-	-	-

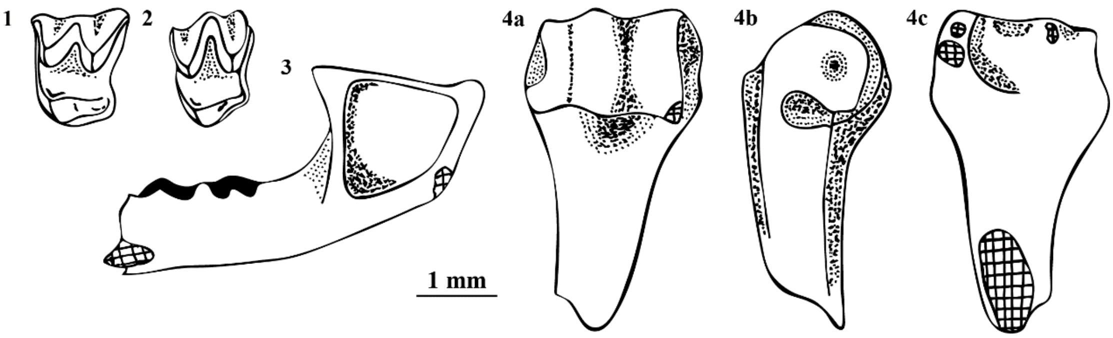

Figure 4.37 *Myotis mystacinus*, Loutra Almopias Cave A. **1.** LAC24805 – Left M1, **2.** LAC24692 – Left M2, **3.** LAC20855 – Left mandibular fragment, **4.** LAC27455 - Distal epiphysis of left humerus (**a.** anterior, **b.** lateral, **c.** posterior).

Discussion The morphological features described in addition to the measurements allow a definite attribution of the material to *Myotis mystacinus*. It is the smallest of the eleven Vesper Bat species that currently occur in Greece and it is clearly distinguished from the rest of the species.

Occurrence The fossils of the Whiskered Myotis described from Loutra Almopias Cave A are the first known records of this species in Greece. Its modern distribution includes most of northern mainland Greece, Corfu, Crete and possibly Peloponnese (Hanák et al. 2001, GFDC 2021). On a global scale it is distributed from Northwest

Africa to the Iberian Peninsula, Northern Europe (up to the southern parts of the British Isles) and the southern parts of Scandinavia, Central Russia and the Ural Mountains, Kazakhstan and parts of the Levant (Simmons 2005a).

Ecology *Myotis mystacinus* is a typical cave dweller and its habitat preferences include a variety of (semi-)open areas, as well as forested areas with the presence of water bodies (Dietz et al. 2009).

***Myotis* sp.**

Figure 4.38

Fossiliferous locality LAC I, LAC Ib, LAC Ic, LAC II, LAC III

Age Late Pleistocene

Material 39 identified specimens

LAC I: 1 left M1 (27459), 1 left m1-2 (27470), LAC Ib: 1 right humerus (27514), LAC Ic: 1 right p2 (21426), 1 right m3 (17879), LAC II: 1 right maxillary fragment with M2 (21608), 2 right P4 (22107, 22381), 1 left P4 (27659), 3 right M3 (21903, 22080, 22336), 1 left M3 (22300), 1 right mandibular fragment (16021), 5 left mandibular fragments (27864, 16623, 16624, 16163, 22403), 1 left c (22103), 3 right m1-2 (21847, 22060, 22208), 1 left humerus (27624), LAC III: 1 milk tooth (21440a), 1 left C (21105), 1 left P4 (21190), 1 right M1 (20372), 2 left M3 (20664, 20665), 4 right mandibular fragments (20234, 21240, 16439, 21146), 1 left mandibular fragment (17494), 1 left c (20588), 1 left p2 (20313), 2 left m3 (20159, 20909)

Fossiliferous locality LAC Ia

Age latest Pleistocene

Material 47 identified specimens

2 right P4 (25233, 25273), 1 right M1-2 (24641), left M1-2 (24970, 24974, 26658), 3 right M1 (24566, 24591, 24593), 4 left M1 (24705, 24977, 24980, 26659), 1 right M3 (25212), 7 right mandibular fragments (19514, 22974, 26836, 26837, 26843, 27263, 27269), 6 left mandibular fragments (19523, 19526, 19530, 23032, 26856, 27295), 1 right mandibular fragment with i1-i2 (22947), 1 left mandibular fragment with m1-m2 (22941), 1 right mandibular fragment with m2 (22649),1 right mandibular fragment with m3 (22628), 1 right p3 (26344), 4 right m1-2 (23346, 23676, 26867, 26917), 3 left m1-2 (24103, 26996, 27392), 1 right m1 (27355), 5 left m1 (24003, 24053, 24067, 24071, 26949), 1 right m3 (23660), 1 left humerus (27451)

Measurements Table 4.15

Description Here are grouped specimens that could not be identified beyond genus level, mostly because they are severely damaged (worn/digested/corroded/broken/etc.). Consequently, no further descriptions are provided.

Table 4.15 *Myotis* sp., Loutra Almopias Cave A. Measurements (in mm) from both LAC and LAC Ia. LAC: Late Pleistocene; LAC Ia: latest Pleistocene; n: number of measurable specimens; L: length; W: width; trgd: trigonid; tld: talonid; MEAN: average; MIN: minimum; MAX: maximum; SD: standard deviation; CV: coefficient of variation.

			n	MEAN	MIN	MAX	SD	CV
C	LAC	L	1	1.31	-	-	-	-
		W	1	0.86	-	-	-	-
P4	LAC	L	4	1.33	1.26	1.43	0.073	5.529
		W	-	-	-	-	-	-
	LAC Ia	L	1	1.12	-	-	-	-
		W	1	1.69	-	-	-	-
M1	LAC	L	1	1.65	-	-	-	-
		W	1	1.37	-	-	-	-
	LAC Ia	L	7	1.52	1.21	1.89	0.077	18.333
		W	7	1.55	1.28	1.83	0.211	13.630
M3	LAC	L	1	1.82	-	-	-	-
		W	1	2.32	-	-	-	-
	LAC Ia	L	1	1.36	-	-	-	-
		W	1	1.53	-	-	-	-
i1	LAC	L	1	0.52	-	-	-	-
		W	1	0.34	-	-	-	-
	LAC Ia	L	1	0.52	-	-	-	-
		W	1	0.72	-	-	-	-
i2	LAC Ia	L	1	0.49	-	-	-	-
		W	1	0.30	-	-	-	-
p2	LAC	L	2	0.81	0.68	0.93	0.177	21.960
		W	2	0.90	0.80	0.99	0.134	15.011
p3	LAC Ia	L	1	0.81	-	-	-	-
		W	1	0.90	-	-	-	-
m1	LAC	L	2	1.58	1.41	1.74	0.233	14.816
		W (trgd)	4	0.98	0.84	1.12	0.143	14.546
		W (tld)	3	0.92	0.79	1.08	0.148	16.193
	LAC Ia	L	14	1.33	1.05	1.62	0.152	11.498
		W (trgd)	14	0.81	0.60	1.01	0.123	15.117
		W (tld)	14	0.84	0.64	1.04	0.119	14.236
m2	LAC Ia	L	2	1.28	1.13	1.43	0.212	16.573
		W (trgd)	1	0.72	-	-	-	-
		W (tld)	1	0.77	-	-	-	-
m3	LAC	L	1	1.28	-	-	-	-
		W (trgd)	2	0.88	0.87	0.88	0.007	0.808
		W (tld)	2	0.75	0.74	0.76	0.014	1.886
	LAC Ia	L	2	1.30	1.20	1.40	0.141	10.879
		W (trgd)	2	0.85	0.83	0.86	0.021	2.510
		W (tld)	2	0.68	0.65	0.70	0.035	5.238
Humerus	LAC	W	2	2.72	2.65	2.79	0.099	3.640

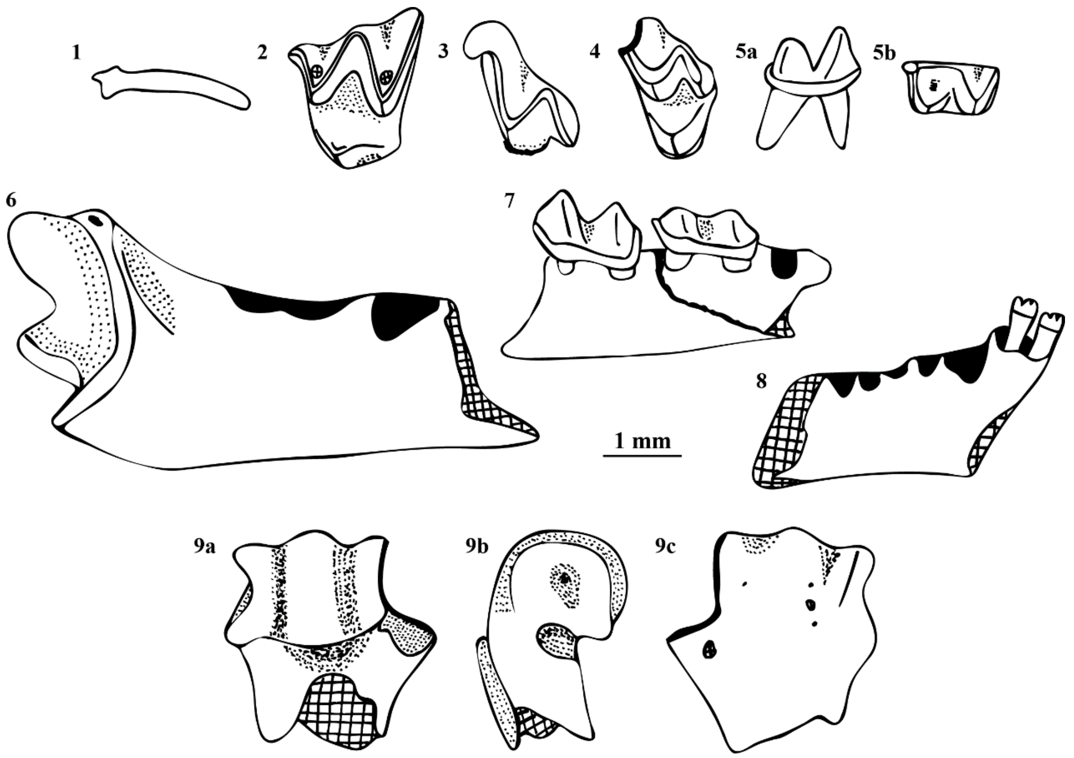

Figure 4.38 *Myotis* sp., Loutra Almopias Cave A. **1.** LAC21440a – Left milk tooth, **2.** LAC26659 – Left M1, **3.** LAC20664 – Left M3, **4.** LAC20665 – Left M3, **5.** LAC23346 – Right m1-2 (a. labial, b. occlusal), **6.** LAC22974 – Right mandibular fragment, **7.** LAC22941 – Left mandibular fragment with m1-m2, **8.** LAC22947 – Right mandibular fragment with i1-i2, **9.** LAC27451 – Distal epiphysis of left humerus (**a.** anterior, b. lateral, **c.** posterior).

Nyctalus Bowdich, 1825

Type species *Nyctalus verrucosus* Bowdich, 1825 (= *Vespertilio leisleri* Kuhl, 1817)

The earliest occurrence of *Nyctalus* in the global fossil record is *Nyctalus storchi* from the Late Oligocene of Ronheim 1A, Germany (Horáček 2001). The earliest occurrence of *Nyctalus* in the fossil record of Greece is *Nyctalus* cf. *noctula* from the Middle Pleistocene locality of Petralona Cave, Chalkidiki (Horacek and Poulianos 1988). There are currently three species occurring in Greece (*Nyctalus lasiopterus*, *Nyctalus noctula* and *Nyctalus leisleri*) (Hanák et al. 2001, Simmons 2005a, Sfougaris 2009). *Nyctalus lasiopterus* and *Nyctalus leisleri* are described in Greece for the first time from Loutra Almopias Cave A.

The dental formula of *Nyctalus* is: 2.1.2.3/3.1.2.3 and there are several morphological characteristics that distinguish *Nyctalus* from other chiropteran taxa, such as the absence of heel and/or talon on the upper molars, nyctalodont lower molars with thick and irregular cingulum, short and blunt styloid process of the humerus and deep diagonal valley between the trochlea and the condyle. Species discrimination within the genus is based almost exclusively on size.

Nyctalus lasiopterus Schreber, 1780

(Giant Noctule)

Figure 4.39 and Figure A.64

Fossiliferous locality LAC Ia

Age latest Pleistocene

Material 2 identified specimens

1 left M1 (24726), 1 right humerus (26448)

Measurements Table 4.16

Description *Nyctalus lasiopterus* is the largest member of the three Noctule Bat species that currently occur in Greece.

M1: Very robust tooth. It is subrectangular in occlusal view. Parastyle, mesostyle, metastyle, paracone and metacone are well-developed. The metacone is slightly taller than the paracone. The parastyle forms an angle with the preparacrista and the metastyle slightly curves lingually. The mesial part of the ectoloph is narrower than the distal part. Additionally, the paracone and the cristae on both sides form a wider angle than the metacone and the respective cristae. Paraloph, metaloph, paraconule and metaconule are well-developed. The cingulum is thick and it becomes thinner beneath the protocone, which is triangular. No lingual cingulum is present.

Humerus: The styloid process is short and blunt (triangular in lateral view). The epitrochlea is very small. The trochlea is very large and robust and set obliquely to the diaphysis. A deep diagonal valley is present between the trochlea and the condyle. The condyle is very narrow. A shallow valley is present between the condyle and the epicondyle. The condyle and the epicondyle are not projecting laterally. The radial fossa is deep, whereas the olecranon fossa is shallow and it extends over the entire width of the epiphysis.

Table 4.16 *Nyctalus lasiopterus*, Loutra Almopias Cave A. Measurements (in mm) from LAC Ia. LAC Ia: latest Pleistocene; n: number of measurable specimens; L: length; W: width; MEAN: average; MIN: minimum; MAX: maximum; SD: standard deviation; CV: coefficient of variation.

			n	MEAN	MIN	MAX	SD	CV
M1	LAC Ia	L	1	2.12	-	-	-	-
		W	1	2.63	-	-	-	-
Humerus	LAC Ia	W	1	3.60	-	-	-	-

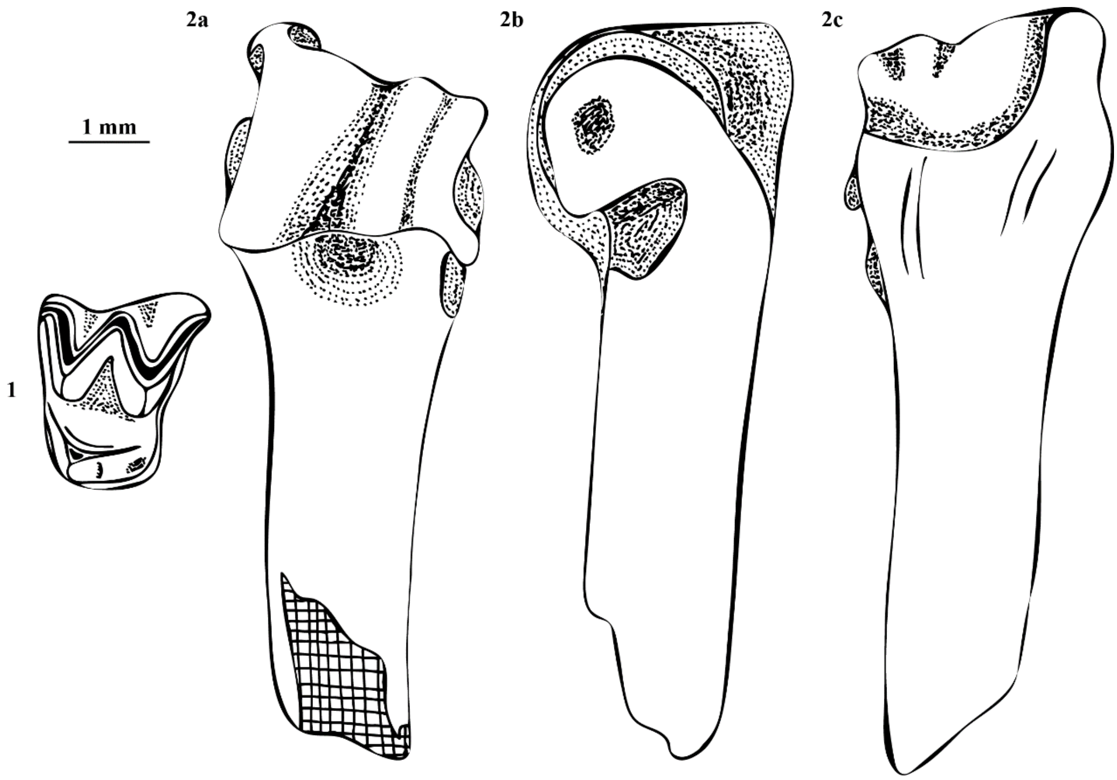

Figure 4.39 *Nyctalus lasiopterus*, Loutra Almopias Cave A. **1.** LAC24726 – Left M1, **2.** LAC26448 – Distal epiphysis of right humerus (**a.** anterior, **b.** lateral, **c.** posterior).

Discussion The morphological features described in addition to the measurements allow a definite attribution of the material to *Nyctalus lasiopterus*. It is the largest member of the three Noctule Bat species that currently occur in Greece and it is clearly distinguished from the rest of the species.

Occurrence The fossils of the Giant Noctule described from Loutra Almopias Cave A are the first known records of this species in Greece. Its modern distribution includes most possibly all mainland Greece (Hanák et al. 2001, GFDC 2021). On a global scale it is distributed from Northern Africa (Morocco, Libya and possibly Algeria) to Western Europe all the way to Caucasus (including the Balkans and Asia Minor), Kazakhstan and Iran (Simmons 2005a).

Ecology *Nyctalus lasiopterus* hibernates mostly in hollow trees and its habitat preferences include forested areas (Dietz et al. 2009).

Nyctalus noctula Schreber, 1774

(Noctule Bat)

Figure 4.43-44 and Figure A.65

<u>Fossiliferous locality</u> LAC I, LAC Ib, LAC Ic, LAC II, LAC III

<u>Age</u> Late Pleistocene

<u>Material</u> 104 identified specimens

<u>LAC I:</u> 1 right I2 (17246), 1 right C (17320), 1 left C (17239), 1 right/left C (19932), 1 left M1 (17248), 1 left M2 (27485), 1 right c (17242), 1 left c (17241), 1 right p3 (27510), 1 right m1 (17255), 2 left m1 (17252, 17253), 1 right m2 (17254), 1 right m3 (19940), 1 left m3 (19927), <u>LAC Ib:</u> 1 right I1 (16523), 1 left M1 (16564), 1 left M3 (16542), 1 left c (19866), <u>LAC Ic:</u> 1 right I1 (17961), 1 left I1 (17904), 1 right C (17868), 1 right M1 (18027), 1 right c (17987), 1 right p3 (17902), 1 left p3 (17903), 1 right/left p3 (17882), 1 right p4 (17917), 1 left m1-2 (18029), 1 right m3 (21490), <u>LAC II:</u> 5 right C (21811, 21867, 22017, 22329, 27747), 4 left C (27533, 27615, 27664, 27770), 2 right P4 (21979, 16378), 3 right M1 (21938, 22264, 27820), 2 left M1 (22074, 27585), 2 right M3 (27541, 27656), 2 left M3 (16039, 27604), 1 left mandibular fragment (16179), 1 right mandibular fragment with m2-m3 (16716), 1 right c (21865), 3 left c (21965, 22102, 27947), 1 left p3 (21822), 1 right p4 (27530), 1 right m1 (21570), 3 left m1 (16348, 27599, 27645), 1 left m2 (22120), 2 right m3 (16351, 22032), 2 left m3 (22238, 27752), <u>LAC III:</u> 1 right maxillary fragment with M2-M3 (19325), 1 right I2 (20725), 1 left I2 (20099), 1 right C (20121), 2 left C (21359, 20289), 3 right P4 (20182, 20264, 21187), 1 right M1 (20277), 2 left M1 (21094, 20363), 3 right M2 (21090, 19322, 20039), 1 left M2 (20032), 1 left mandibular fragment with m1-m2 (20608), 1 right mandibular fragment with m2-m3 (20141), 3 right c (19163, 19298, 20069), 2 left c (21112, 20294), 1 left p3 (20053), 1 left p4 (20827), 3 right m1 (17479, 21270, 20438), 5 left m1 (20781, 17478, 21282, 19154, 20526), 4 right m3 (20977, 21142, 20041, 20042)

<u>Fossiliferous locality</u> LAC Ia

<u>Age</u> latest Pleistocene

<u>Material</u> 322 identified specimens

1 right maxillary fragment with I1-I2 (23302), 1 right maxillary fragment with C and P4 (19752), 1 left maxillary fragment with C-M3 (19773), 1 right maxillary fragment with P3-M1 (27230), 1 right maxillary fragment with P4-M1 (23131), 1 left maxillary fragment with P4-M1 (23148), 1 left maxillary fragment with P4-M3 (26528), 1 left maxillary fragment with M1 (19738), 1 right maxillary fragment with M1-M3 (19741), 2 right maxillary fragments with M2 (19750, 23217), 4 right maxillary fragments with M2-M3 (19771, 23095, 26508, 27237), 1 left maxillary fragment with M2-M3 (23110), 2 right maxillary fragments with M3 (23172, 23186), 2 right I1 (26383, 26387), 4 left I1 (26390, 26392, 26401, 26402), 2 right I2 (26359, 26376), 19 right C (25476, 25489, 25508, 25516, 25542, 25581, 25585, 25657, 25707, 25734, 25814, 25843, 25899, 25935, 26092, 26136, 27061, 27085, 27415), 17 left C (25484, 25499, 25500, 25515, 25527, 25566, 25641, 25655, 26070, 26108, 26250, 27100, 27103, 27109, 27113, 27115, 27426), 7 right P4 (19719, 25229, 25236, 25243, 25270, 26692, 26696), 10 left P4 (25376, 25379, 25405, 25412, 25419, 25424, 25426, 26713, 26716, 26719), 16 right M1 (24402, 24449, 24466, 24505, 24513, 24537, 24548, 24560, 24598, 24649, 26554, 26582, 26587, 26595, 27297, 27302), 9 left M1 (24819, 24844, 24884, 24919, 24927, 24938, 26635, 26642, 26662), 1 right M1-2 (24585), 14 right M2 (24404, 24453, 24476, 24486, 24501, 24608, 24619, 24648, 26547, 26550, 26561, 26576, 26588, 27312), 11 left M2 (23236, 24690, 24712, 24756, 24830, 24846, 24865, 24881, 24943, 24978, 27327), 11 right M3 (25150, 25157, 25158, 25199, 25208, 25211, 25218, 25219, 26612, 26614, 27319), 13 left M3 (24997, 25023, 25040, 25049, 25057a, 25060, 25061, 25062, 25079, 25080, 25085, 25088, 27340), 6 right mandibular fragments (26841, 19518, 22961, 22981, 22996, 22997), 8 left mandibular fragments (26826, 26858, 26862, 19524, 19531, 19701, 23016, 23034), 1 right mandibular fragment with i1 and p4 (19641), 1 left mandibular fragment with c-p4 (27270), 1 right mandibular fragment with c and p4-m1 (19637), 1 right mandibular fragment with c-m1 (27251), 1 right mandibular fragment with c-m2 (26722), 2 left mandibular fragments with c-m3 (19626, 19627), 2 right mandibular fragments with p4 (19636, 19642), 1 left mandibular fragment with p4 (19676), 1 right mandibular fragment with p4 and m2 (22670), 1 left mandibular fragment with p4 and m2-m3 (19675), 1 left mandibular fragment with p4-m2 (19657), 1 right mandibular fragment with p4-m1 and m3 (19488), 2 right mandibular fragments

with m1 (22539, 22690), 2 left mandibular fragments with m1 (22812, 22835), 2 right mandibular fragments with m1-m2 (22544, 27257), 3 left mandibular fragments with m1-m2 (22739, 22762, 22827), 1 left mandibular fragment with m1-m3 (19703), 1 right mandibular fragment with m2 (22473), 1 left mandibular fragment with m2 (22912), 1 right mandibular fragment with m2-m3 (19694), 2 left mandibular fragments with m2-m3 (22909, 22932), 2 right mandibular fragments with m3 (19691, 19700), 3 left mandibular fragments with m3 (22874, 22896, 22907), 3 left i3 (26386, 26397, 26404), 16 right c (25490, 25685, 25716, 25720, 25740, 25763, 25902, 25906, 25925, 25950, 25984, 26018, 26030, 27143, 27428, 27430), 10 left c (25466, 25644, 25697, 25827, 25916, 26001, 26051, 26214, 27174, 27190), 4 right p3 (26315, 26327, 26334, 26347), 2 left p3 (26303, 26330), 7 right p4 (26234, 26271, 26272, 26273, 26274, 26275, 27403), 6 left p4 (24274, 24363, 26276, 26277, 26813, 27049), 14 right m1 (22597, 23342, 23373, 23395, 23452, 23458, 23472, 23485, 23488, 23585, 23668, 26741, 26911, 27256), 15 left m1 (22809, 23732, 23774, 23800, 23970, 24009, 24022, 24050, 24140, 26958, 26976, 26990, 26993, 27381, 27385), 12 right m2 (22575, 22576, 22679, 22693, 23383, 23386, 23462, 23468, 23478, 23552, 23554, 27356), 8 left m2 (23770, 23772, 23859, 23870, 23877, 23919, 23989, 27389), 14 right m3 (23323, 23406, 23304, 23306, 23314, 23446, 23487, 23548, 23628, 23635, 23636, 23638, 23651, 23652), 3 left m3 (24107, 27013, 27290), 3 right humeri (26438, 26439, 27207), 3 left humeri (26420, 26422, 27458)

Measurements Table 4.17 and Figure 4.40-42

Description *Nyctalus noctula* is the medium-sized member of the three Noctule Bat species that currently occur in Greece.

I1: Bicuspid. It is oval in occlusal view. The mesial cusp is the largest and it covers approximately 2/3 of the tooth’s area. The distal cusp is separated from the mesial by a deep valley. A thick cingulum is also present throughout the whole tooth.

I2: Bicuspid. It is oval in occlusal view. The mesial cusp is the largest and it covers approximately 1/3 of the tooth’s area. The mesial cusp is separated from the distal by a deep valley. The tooth has a depressed lingual surface. A third accessory cusplet is present at the lingual part of the tooth. A thin cingulum is present only mesially. A deep valley separates the distolingual from the mesiolingual part of the tooth, too.

C: Very robust tooth with the cusp curved distally. It is trapezoidal in occlusal view. The crown forms an obtuse angle with the root. A heel is present at the mesiolingual part of the tooth. The crown is convex mesiolabially and labially, slightly concave distolingually and flat lingually. A longitudinal groove occurs at the labial side of the tooth. The cingulum is very thick throughout the whole tooth and it reaches its maximum thickness mesiolingually, where an accessory cusplet is present. A mesiolabial and a distolingual concavity is observed when in occlusal view, with the latter being pronounced.

P3: Unicuspid. It is subtriangular in occlusal view. The cusp is present at the mesial part of the tooth. The tooth has a depressed lingual surface. A relatively thick cingulum is also present throughout the whole tooth and it reaches its maximum thickness distally, where an accessory cusplet is present.

Table 4.17 *Nyctalus noctula*, Loutra Almopias Cave A. Measurements (in mm) from both LAC and LAC Ia. LAC: Late Pleistocene; LAC Ia: latest Pleistocene; n: number of measurable specimens; L: length; W: width; trgd: trigonid; tld: talonid; MEAN: average; MIN: minimum; MAX: maximum; SD: standard deviation; CV: coefficient of variation.

			n	MEAN	MIN	MAX	SD	CV
I1	LAC	L	1	1.18	-	-	-	-
		W	1	0.89	-	-	-	-
	LAC Ia	L	7	0.93	0.69	1.13	0.141	15.138
		W	7	0.87	0.54	0.99	0.153	17.457
I2	LAC	L	5	0.96	0.86	1.09	0.085	8.839
		W	5	0.74	0.64	0.80	0.064	8.698
	LAC Ia	L	3	0.72	0.66	0.78	0.060	8.411
		W	3	0.91	0.80	0.97	0.098	10.746
C	LAC	L	15	1.96	1.75	2.25	0.127	6.469
		W	15	1.52	1.31	1.73	0.131	8.603
	LAC Ia	L	38	1.94	1.63	2.19	0.121	6.217
		W	38	1.57	1.32	1.83	0.101	6.410
P3	LAC Ia	L	2	0.50	0.46	0.53	0.003	1.000
		W	2	0.65	0.58	0.72	0.099	15.230
P4	LAC	L	5	1.25	1.09	1.46	0.160	12.824
		W	3	1.80	1.73	1.86	0.067	3.692
	LAC Ia	L	20	1.22	1.05	1.42	0.091	7.456
		W	18	1.86	1.71	1.97	0.088	4.705
M1	LAC	L	9	1.95	1.85	2.03	0.063	3.236
		W	9	2.16	2.03	2.40	0.114	5.243
	LAC Ia	L	32	1.95	1.66	2.18	0.110	5.606
		W	31	2.20	1.91	2.50	0.129	5.866
M2	LAC	L	5	1.93	1.85	2.00	0.064	3.323
		W	5	2.30	2.09	2.39	0.129	5.583
	LAC Ia	L	34	1.94	1.71	2.08	0.093	4.774
		W	33	2.32	1.87	2.61	0.153	6.574
M3	LAC	L	6	1.90	1.74	1.99	0.091	4.789
		W	6	2.17	1.78	2.34	0.203	9.347
	LAC Ia	L	33	1.94	1.69	2.18	0.105	5.425
		W	33	2.30	2.06	2.54	0.130	5.652
i1	LAC Ia	L	1	0.88	-	-	-	-
		W	1	0.43	-	-	-	-
i3	LAC Ia	L	3	0.73	0.72	0.74	0.010	1.370
		W	3	0.66	0.62	0.68	0.032	4.895
c	LAC	L	12	1.03	0.93	1.14	0.071	6.838
		W	13	1.46	1.30	1.56	0.068	4.664
	LAC Ia	L	32	0.99	0.86	1.20	0.085	8.526
		W	32	1.42	1.28	1.55	0.075	5.263

p3	LAC	L	5	0.83	0.78	0.89	0.047	5.623
		W	6	1.20	1.13	1.29	0.061	5.032
	LAC Ia	L	11	0.84	0.71	0.94	0.078	9.284
		W	11	1.13	0.97	1.30	0.119	10.499
p4	LAC	L	3	0.90	0.82	0.96	0.074	8.160
		W	3	1.24	1.15	1.31	0.083	6.697
	LAC Ia	L	27	0.89	0.77	1.10	0.063	7.077
		W	27	1.16	1.02	1.31	0.076	6.562
m1	LAC	L	15	1.92	1.75	2.08	0.099	5.179
		W (trgd)	16	1.28	1.17	1.40	0.080	6.209
		W (tld)	16	1.41	1.20	1.65	0.131	9.301
	LAC Ia	L	43	1.88	1.68	2.04	0.090	4.798
		W (trgd)	45	1.31	1.13	1.47	0.084	6.461
		W (tld)	45	1.44	1.32	1.60	0.078	5.435
m2	LAC	L	4	1.81	1.74	1.89	0.062	3.451
		W (trgd)	4	1.26	1.11	1.37	0.119	9.457
		W (tld)	5	1.40	1.32	1.50	0.080	5.670
	LAC Ia	L	31	1.85	1.65	2.02	0.080	4.332
		W (trgd)	33	1.27	1.05	1.42	0.078	6.167
		W (tld)	33	1.38	1.19	1.54	0.081	5.858
m3	LAC	L	10	1.74	1.60	1.93	0.102	5.874
		W (trgd)	12	1.16	1.06	1.30	0.072	6.224
		W (tld)	11	0.96	0.80	1.14	0.103	10.645
	LAC Ia	L	29	1.75	1.60	1.98	0.087	4.953
		W (trgd)	30	1.13	1.01	1.30	0.080	7.101
		W (tld)	28	0.97	0.74	1.14	0.078	8.096
M1-M3	LAC Ia	L	3	5.07	4.90	5.19	0.153	3.017
P4-M3	LAC Ia	L	2	6.17	6.04	6.30	0.184	2.980
C-M3	LAC Ia	L	1	8.01	-	-	-	-
C-P4	LAC Ia	L	1	3.00	-	-	-	-
m1-m3	LAC Ia	L	2	5.39	5.38	5.40	0.014	0.262
p4-m3	LAC Ia	L	2	6.11	6.07	6.15	0.057	0.926
c-m3	LAC Ia	L	2	7.85	7.80	7.89	0.064	0.811
c-p4	LAC Ia	L	6	2.68	2.56	2.85	0.099	3.695
Humerus	LAC Ia	W	6	3.20	2.97	3.35	0.146	4.571

P4: Very robust tooth, with the cusp being connected with a crista to an accessory distolabial cusplet, which is imperceptibly curved. It is trapezoidal in occlusal view. A well-developed heel is present in the lingual part of the tooth. The crown is convex mesiolabially and labially and flat lingually. The cingulum is thick, with its maximum thickness at the mesiolingual part of the tooth, where a robust cingular cusplet is present.

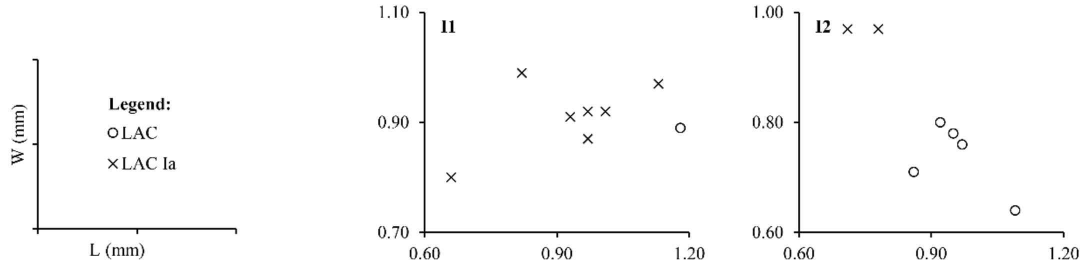

Figure 4.40 *Nyctalus noctula*, Loutra Almopias Cave A. XY graphs with the measured (in mm) dental elements (I1, I2). L: length, W: width.

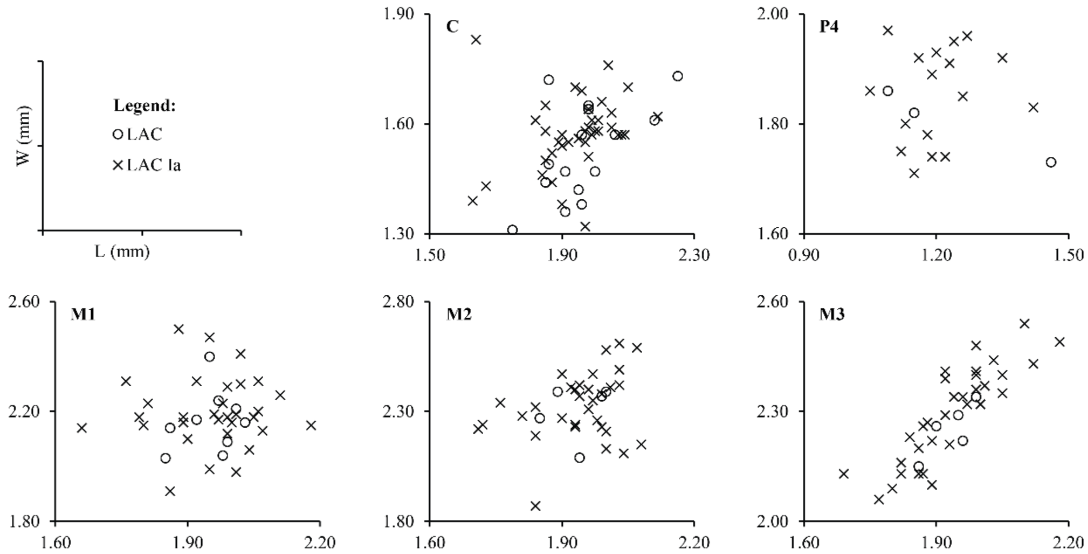

Figure 4.41 *Nyctalus noctula*, Loutra Almopias Cave A. XY graphs with the measured (in mm) dental elements (C, P4, M1, M2, M3). L: length, W: width.

M1: Very robust tooth. It is subrectangular in occlusal view. Parastyle, mesostyle, metastyle, paracone and metacone are well-developed. The metacone is slightly taller than the paracone. The parastyle forms an angle with the preparacrista and the metastyle slightly curves lingually. The mesial part of the ectoloph is narrower than the distal part. Additionally, the paracone and the cristae on both sides form a wider angle than the metacone and the respective cristae. Paraloph, metaloph, paraconule and metaconule are well-developed. The postprotocrista is angled close to the metaconule. The cingulum is thick throughout the whole tooth, apart from its anterior part, where it is thinner.
M2: The mesial part of the ectoloph is wider than in M1. The rest of the characters as M1.
M3: Very robust tooth. It is subtriangular in occlusal view. Parastyle, mesostyle, paracone and metacone are well-developed, whereas the metastyle and the postmetacrista that connects the metacone with the metastyle are absent. The paracone is slightly

taller than the metacone. The parastyle forms an angle with the preparacrista. A concavity is present at the distolingual base of the crown. The cingulum is absent only beneath the triangular protocone.

i1: Oval in occlusal view. Three cusps are present at the labial part of the tooth. All cusps, which are separated by shallow valleys, are in line and of approximately the same size. A small widening occurs at the distal part of the tooth. A thin cingulum is present only lingually.

i3: Subrectangular in occlusal view Two cusps are present at the labial part of the tooth and two at its lingual part. The labial cusps are of equal size and they are separated by a valley, as well as the lingual cusps. A deeper valley separates the labial from the lingual cusps. A thin cingulum is present beneath the mesiolingual cusp.

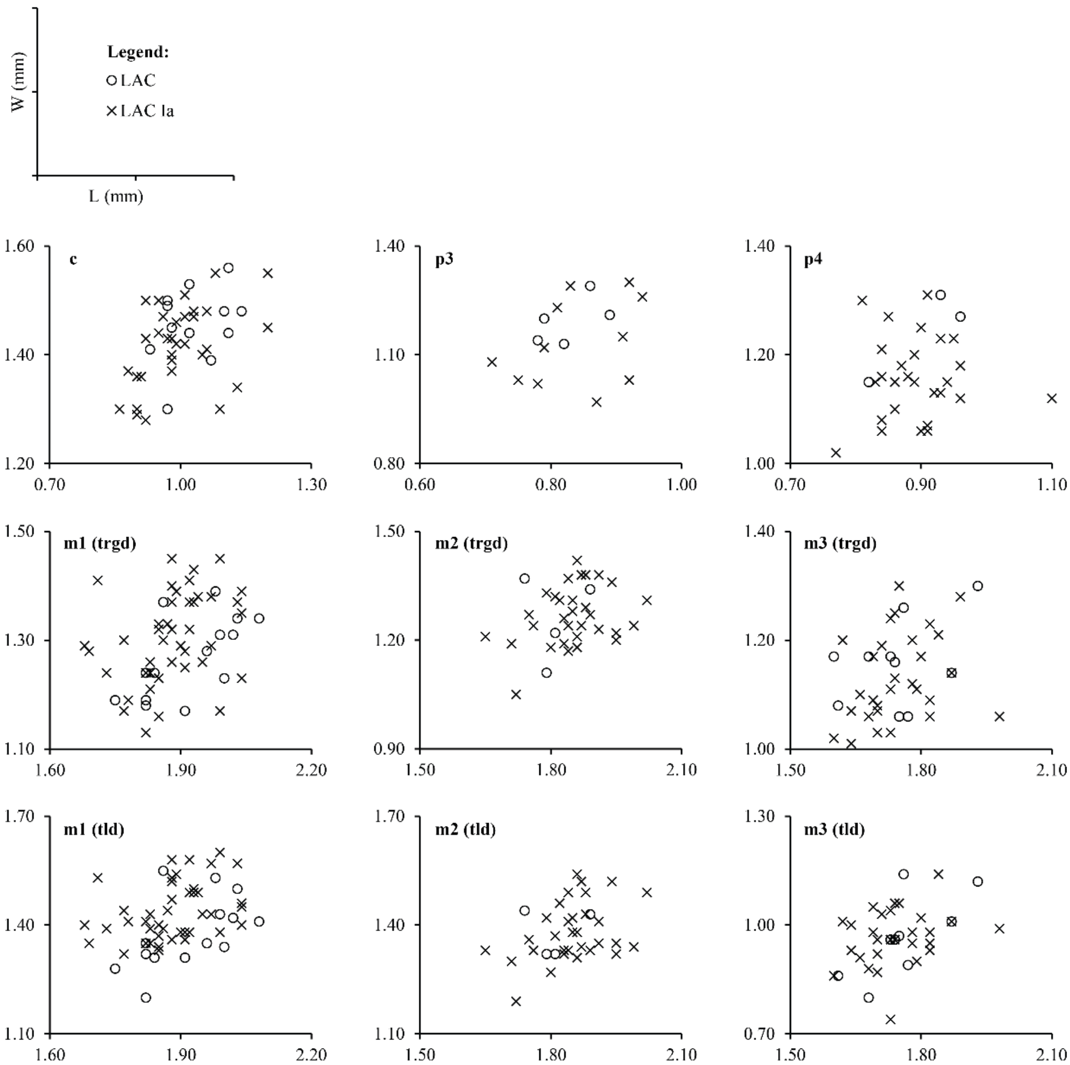

Figure 4.42 *Nyctalus noctula*, Loutra Almopias Cave A. XY graphs with the measured (in mm) dental elements (c, p3, p4, m1, m2, m3). L: length, W: width, trgd: trigonid; tld: talonid.

c: Very robust tooth with the cusp slightly curved lingually. It is semicircular in occlusal view. It is convex mesially and concave distally. The distal part of the tooth is developed at the base of the crown, whereas the mesial part is developed in height. Respectively, the crown is in a more superior position towards the anterior part of the tooth. The distolabial part of the tooth is situated lower than the distolingual, which is higher than the former. The cingulum is thick throughout the whole tooth. It reaches its maximum thickness at the mesiolingual and distolingual parts of the tooth, where two cingular cusplets are present.

p3: Unicuspid. It is subtriangular in occlusal view. It is convex at its mesial and labial parts, slightly concave lingually and relatively flat distally. The cingulum is very thick and it reaches its maximum thickness at the mesiolingual and distolingual parts of the tooth, where two cingular cusplets are present.

p4: It has two roots. It is convex at its mesial part and slightly concave distally. The crown is taller than in p3. The cingular cusplets are in a more lingual position. The rest of the characters as p3.

m1: Nyctalodont. The talonid is longer than the trigonid. Paraconid, metaconid, entoconid, protoconid and hypoconid are well-developed. The paraconid is in a more labial position. The protoconid is taller than the hypoconid. The paralophid is concave. The entocristid is concave. The hypoconulid is not as well-developed as the other cusps and positioned in line with the entoconid and the metaconid. The labial cingulum is thick beneath the protoconid and slightly thinner beneath the hypoconid. Lingual cingulum of the trigonid is also present.

m2: The paraconid is in a more lingual position than in m1 and it is in line with the metaconid, the entoconid and the hypoconulid. The entocristid is imperceptibly concave. The thickening of the labial cingulum is less pronounced than in m1. The rest of the characters as m1.

m3: Nyctalodont. The talonid is longer than the trigonid. The protoconid and the hypoconid are well-developed, whereas the paraconid, the metaconid and the entoconid are not as well-developed as in m1 and m2. The protoconid is taller than the hypoconid. The paralophid is concave. The entoconid is more towards the labial side of the tooth and thus, the talonid is reduced. The hypoconulid is significantly reduced. The labial cingulum is thick and uniform throughout the whole tooth. The lingual cingulum of the trigonid is absent.

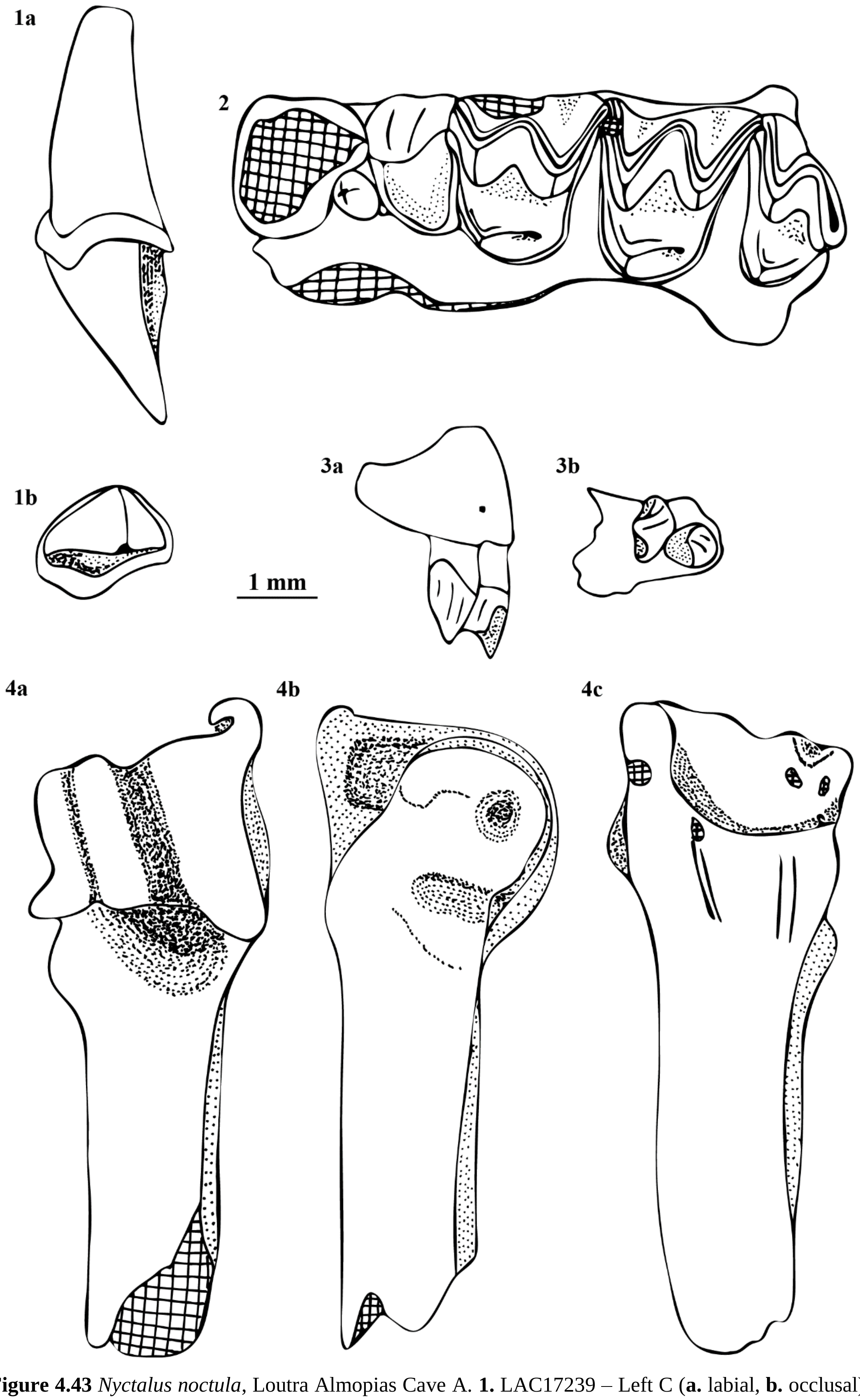

Figure 4.43 *Nyctalus noctula*, Loutra Almopias Cave A. **1.** LAC17239 – Left C (**a.** labial, **b.** occlusal), **2.** LAC19773 – Left maxillary fragment with C-M3, **3.** LAC23302 – Right maxillary fragment with I1-I2 (**a.** labial, **b.** occlusal), **4.** LAC26420 – Distal epiphysis of left humerus (**a.** anterior, **b.** lateral, **c.** posterior).

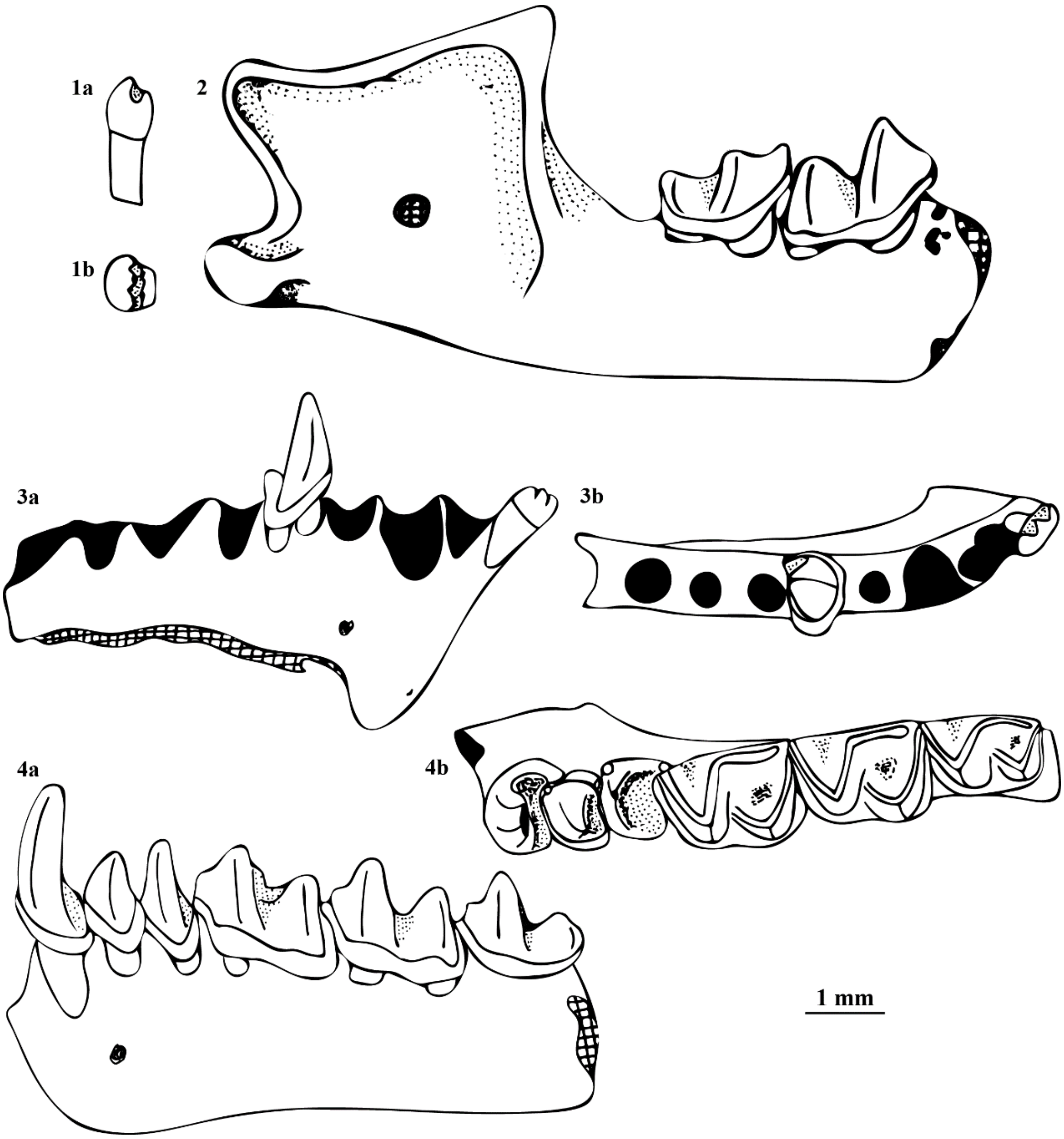

Figure 4.44 *Nyctalus noctula*, Loutra Almopias Cave A. **1.** LAC26386 – Left i3 (**a.** labial, **b.** occlusal), **2.** LAC19694 – Right mandibular fragment with m2-m3, **3.** LAC19641 – Right mandibular fragment with i1 and p4 (**a.** labial, **b.** occlusal), **4.** LAC19626 – Right mandibular fragment with c-m3 (**a.** labial, **b.** occlusal).

Mandible: The coronoid process is angular and located higher, but not significantly, than the articular process. The anterior part of the masseter crest, which is of average thickness, is relatively steep. The anterior sigmoid notch is convex close to the coronoid process and concave towards the condyloid process. The angular process is short and wide and it projects diagonally backwards and on the same level with the body of the mandible. The mental foramen is beneath the anterior part of p2. The lowest part of the symphysis is pointed and projects downwards.

Humerus: The styloid process is short and blunt (triangular in lateral view). The epitrochlea is very small. The trochlea is very large and robust and set obliquely to the diaphysis. A deep diagonal valley is present between the trochlea and the condyle. The condyle is very narrow. A shallow valley is present between the condyle and the epicondyle. The condyle and the epicondyle are not projecting laterally. The radial fossa is deep, whereas the olecranon fossa is shallow and it extends over the entire width of the epiphysis.

Discussion The morphological features described in addition to the measurements allow a definite attribution of the material to *Nyctalus noctula*. It is the medium-sized member of the three Noctule Bat species that currently occur in Greece and it is clearly distinguished from the rest of the species.

Occurrence Fossils of the Noctule Bat are known from Sarakenos Cave, Boeotia and Petralona Cave, Chalkidiki. Its modern distribution includes practically all mainland Greece north of Peloponnese including the islands of Thasos and Euboea (Hanák et al. 2001, GFDC 2021). On a global scale it is distributed from Europe to the Urals and the Caucasus (including Southern Scandinavia), Turkey, Israel and Oman, Turkmenistan, Kazakhstan, Uzbekistan, Kyrgyzstan, Tajikistan and Southwestern Siberia, Himalayas, Myanmar, Vietnam and Malaysia and possibly in Algeria (Simmons 2005a).

Ecology *Nyctalus noctula* hibernates in hollow trees and its habitat preferences include forested areas (Dietz et al. 2009).

Nyctalus leisleri Kuhl, 1817

(Leisler's Bat)

Figure 4.46 and Figure A.66

Fossiliferous locality LAC Ib, LAC Ic, LAC II, LAC III

Age Late Pleistocene

Material 9 identified specimens

LAC Ib: 1 left c (19884), LAC Ic: 1 left I2 (17920), 1 right c (21431), 1 left m2 (17929), LAC II: 1 right p4 (22409), LAC III: 2 right M3 (20169, 20173), 1 right c (20381), 1 left c (20301)

Fossiliferous locality LAC Ia

Age latest Pleistocene

Material 40 identified specimens

1 right maxillary fragment with P4-M1 (23165), 1 left maxillary fragment with P4- M1 (23159), 1 right C (27410), 2 left C (25693, 27128), 4 right P4 (25258, 25301, 25314, 25327), 1 left P4 (26705), 2 left

M3 (25002, 25068), 2 right mandibular fragments with p4 (22663, 22667), 5 left mandibular fragments with p4 (22778, 22792, 22793, 22796, 22944), 4 right c (25441, 26026, 26114, 26356), 3 left c (26046, 26084, 26150), 1 right p3 (26311), 5 right p4 (24209, 24225, , 26270, 27029, 27253), 3 left p4 (24321, 24345, 24358), 1 left m1 (23767), 2 right m2 (23613, 26914), 2 left m2 (23932, 23942)

Measurements Table 4.18 and Figure 4.45

Description *Nyctalus leisleri* is the smallest member of the three Noctule Bat species that currently occur in Greece.

I2: Bicuspid. It is oval in occlusal view. The mesial cusp is the largest and it covers approximately 1/3 of the tooth's area. The mesial cusp is separated from the distal by a deep valley. The tooth has a depressed lingual surface. A cingulum of average thickness is present mesially and lingually. A deep valley separates the distolingual from the mesiolingual part of the tooth, too.

Table 4.18 *Nyctalus leisleri*, Loutra Almopias Cave A. Measurements (in mm) from both LAC and LAC Ia. LAC: Late Pleistocene; LAC Ia: latest Pleistocene; n: number of measurable specimens; L: length; W: width; trgd: trigonid; tld: talonid; MEAN: average; MIN: minimum; MAX: maximum; SD: standard deviation; CV: coefficient of variation.

			n	MEAN	MIN	MAX	SD	CV
I2	LAC	L	1	0.96	-	-	-	-
		W	1	0.66	-	-	-	-
C	LAC Ia	L	3	1.23	1.17	1.32	0.082	6.640
		W	3	1.07	0.95	1.24	0.151	14.143
P4	LAC Ia	L	7	0.98	0.81	1.12	0.091	9.299
		W	7	1.22	1.04	1.30	0.085	6.986
M1	LAC Ia	L	2	1.38	1.30	1.45	0.106	7.714
		W	2	1.47	1.39	1.54	0.106	7.240
M3	LAC	L	2	1.44	1.38	1.49	0.078	5.420
		W	1	1.58	-	-	-	-
	LAC Ia	L	2	1.46	1.45	1.46	0.104	4.954
		W	2	1.67	1.59	1.74	0.106	6.370
c	LAC	L	4	0.72	0.66	0.79	0.062	8.635
		W	4	0.93	0.84	1.04	0.094	10.036
	LAC Ia	L	7	0.65	0.60	0.70	0.142	6.354
		W	7	0.88	0.79	0.98	0.061	6.926
p3	LAC Ia	L	1	0.64	-	-	-	-
		W	1	0.90	-	-	-	-
p4	LAC	L	1	0.57	-	-	-	-
		W	1	0.80	-	-	-	-
	LAC Ia	L	14	0.68	0.57	0.88	0.077	11.298
		W	14	0.81	0.70	0.92	0.064	7.924
m1	LAC Ia	L	1	1.59	-	-	-	-
		W (trgd)	1	1.12	-	-	-	-
		W (tld)	1	1.22	-	-	-	-

m2	LAC	L	-	-	-	-	-	-
		W (trgd)	1	0.81	-	-	-	-
		W (tld)	-	-	-	-	-	-
	LAC Ia	L	4	1.45	1.39	1.51	0.152	3.561
		W (trgd)	4	0.90	0.77	0.95	0.084	9.415
		W (tld)	4	0.98	0.85	1.06	0.091	9.316

C: Robust tooth with the cusp curved distally. It is subtriangular in occlusal view. The crown forms practically no angle with the root. A small heel is present in the mesiolingual part of the tooth. The crown is convex mesially and labially and flat (to slightly concave) distolingually. The cingulum is of average thickness throughout the whole tooth. A mesiolabial and a distolingual concavity are observed when in occlusal view, with the latter being pronounced.

P4: Robust tooth, with the cusp being connected with a crista to an accessory distolabial cusplet, which is imperceptibly curved. It is trapezoidal in occlusal view. A well-developed heel is present in the lingual part of the tooth. The crown is convex mesiolabially and labially and flat lingually. The crown is convex mesially, labially and distally. The cingulum is thick, with its maximum thickness at the mesiolingual part of the tooth, where a robust cingular cusplet is present.

M1: Robust tooth. It is subrectangular in occlusal view. Parastyle, mesostyle, metastyle, paracone and metacone are well-developed. The metacone is on the same height with the paracone. The parastyle forms an angle with the preparacrista. The mesial part of the ectoloph is narrower than the distal part. Additionally, the paracone and the cristae on both sides form a wider angle than the metacone and the respective cristae. Paraloph, metaloph, paraconule and metaconule are well-developed. The cingulum is of average thickness and absent only beneath the triangular protocone. The postprotocrista is angled close to the metaconule.

M3: Robust tooth. It is subtriangular in occlusal view. Parastyle, mesostyle, paracone and metacone are well-developed, whereas the metastyle and the postmetacrista that connects the metacone with the metastyle are absent. The paracone is slightly taller than the metacone. The parastyle forms an angle with the preparacrista. A concavity is present at the distolingual base of the crown. The cingulum is absent only beneath the triangular protocone.

c: Robust tooth with the cusp slightly curved lingually. It is semicircular in occlusal view. It is convex mesially and concave distally. The distal part of the tooth is developed at the base of the crown, whereas the mesial part is developed in height. Respectively, the crown is in a more superior position towards the anterior part of the tooth. The distolabial part of the tooth is situated lower than the distolingual, which is higher than the former. The cingulum is thin throughout the whole tooth. It reaches its maximum thickness at the mesiolingual and distolingual parts of the tooth, where two cingular cusplets are present.

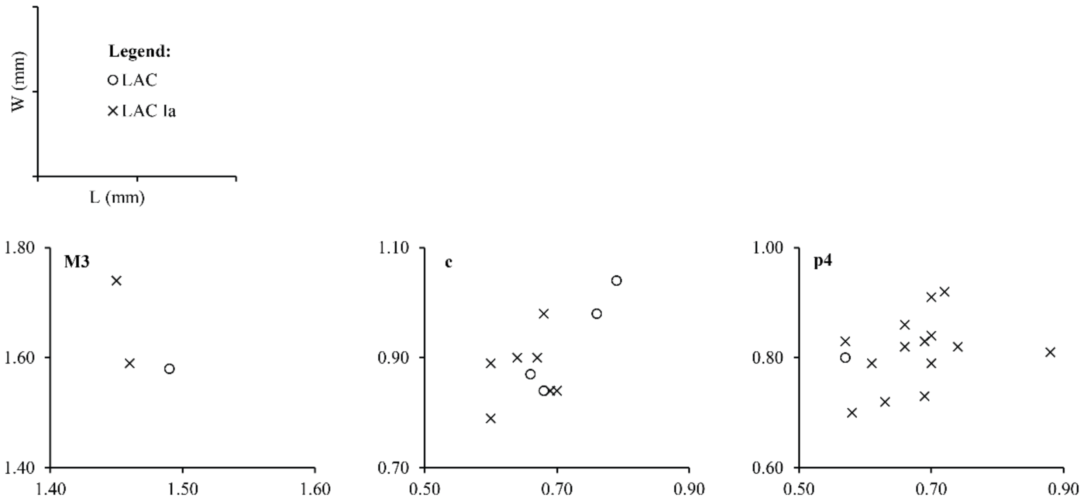

Figure 4.45 *Nyctalus leisleri*, Loutra Almopias Cave A. XY graphs with the measured (in mm) dental elements (M3, c, p4). L: length, W: width.

p3: Unicuspid. It is subtriangular in occlusal view. It is convex at its mesial and labial parts, slightly concave lingually and relatively flat distally. The cingulum is thin and it reaches its maximum thickness at the mesiolingual and distolingual parts of the tooth, where two cingular cusplets are present.

p4: It has two roots. It is subrectangular in occlusal view. It is convex at its mesial part and slightly concave distally. The crown is taller than in p3. The cingular cusplets are in a more lingual position. The rest of the characters as p3.

m1: Nyctalodont. The talonid is longer than the trigonid. Paraconid, metaconid, entoconid, protoconid and hypoconid are well-developed. The paraconid is in a more labial position. The protoconid is taller than the hypoconid. The paralophid is concave. The entocristid is concave. The hypoconulid is not well-developed and positioned in line with the entoconid and the metaconid. The labial cingulum is thick beneath the protoconid and slightly thinner beneath the hypoconid. Lingual cingulum of the trigonid is also present.

m2: The paraconid is in a more lingual position than in m1 and it is in line with the metaconid, the entoconid and the hypoconulid. The entocristid is imperceptibly concave. The hypoconulid is well-developed and positioned in line with the entoconid and the metaconid. The thickening of the labial cingulum is less pronounced than in m1. The rest of the characters as m1.

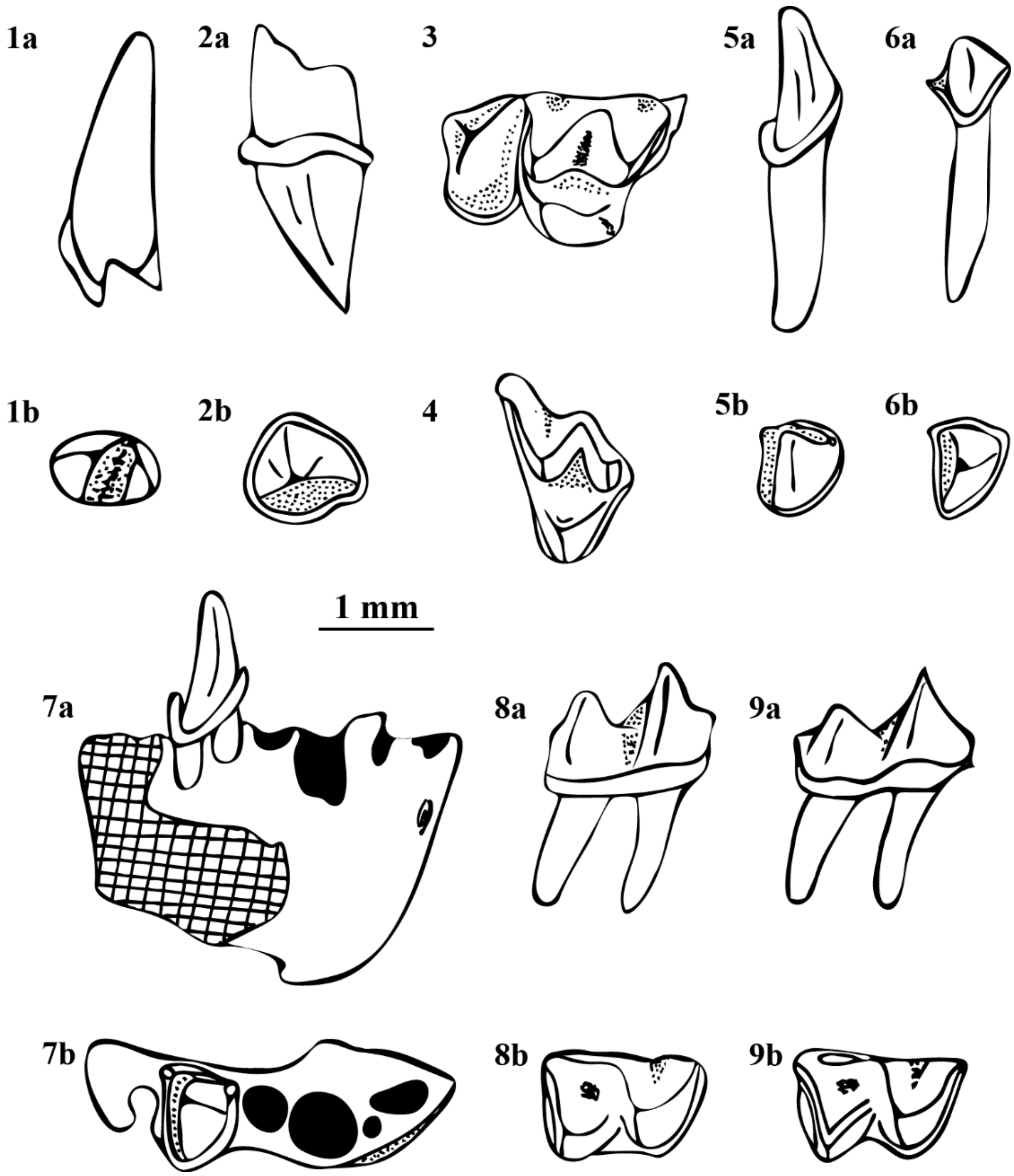

Figure 4.46 *Nyctalus leisleri*, Loutra Almopias Cave A. **1.** LAC17920 – Left I2 (**a.** labial, **b.** occlusal), **2.** LAC25693 – Left C (**a.** labial, **b.** occlusal), **3.** LAC23159 – Left maxillary fragment with C-P4, **4.** LAC25003 – Left M3, **5.** LAC25441 – Right c (**a.** labial, **b.** occlusal), **6.** LAC26311 – Right p3 (**a.** labial, **b.** occlusal), **7.** LAC22663 – Right mandibular fragment with p4 (**a.** labial, **b.** occlusal), **8.** LAC23613 – Right m2 (**a.** labial, **b.** occlusal), **9.** LAC26914 – Right m2 (**a.** labial, **b.** occlusal).

<u>Discussion</u> The morphological features described in addition to the measurements allow a definite attribution of the material to *Nyctalus leisleri*. It is the smallest member of the three Noctule Bat species that currently occur in Greece and it is clearly distinguished from the rest of the species.

<u>Occurrence</u> The fossils of the Leisler's Bat described from Loutra Almopias Cave A are the first known records of this species in Greece. Its modern distribution includes practically all mainland Greece and the islands of Thasos, Rhodes and Crete (Hanák et al. 2001, GFDC 2021). On a global scale it is distributed from Northwestern Africa to Western Europe and all the way the Urals and the Caucasus (including Madeira Islands, Britain and Ireland, Sweden, Southern Finland and the Baltic states), Turkey, Pakistan, Afghanistan and Western Himalayas (Simmons 2005a).

<u>Ecology</u> *Nyctalus leisleri* hibernates in hollow trees and its habitat preferences include forested areas (Dietz et al. 2009).

***Pipistrellus* Kaup, 1829**

Type species *Vespertilio pipistrellus* Schreber, 1774

The earliest occurrence of *Pipistrellus* in the global fossil record is *Pipistrellus* sp. from the Tortonian locality of Lufeng, China (Qiu et al. 1985). The earliest occurrence of *Pipistrellus* in the fossil record of Greece is *Pipistrellus*? sp. from the Middle Pleistocene locality of Petralona Cave, Chalkidiki (Horacek and Poulianos 1988). There are currently five species occurring in Greece (*Pipistrellus pipistrellus*, *Pipistrellus pygmaeus*, *Pipistrellus kuhlii*, *Pipistrellus nathusii* and *Pipistrellus hanaki*) (Hanák et al. 2001, Simmons 2005a, Sfougaris 2009). *Pipistrellus pipistrellus* is described for the first time in Greece from Loutra Almopias Cave A.

The dental formula of *Pipistrellus* is: 2.1.2.3/3.1.2.3 and there are several morphological characteristics that distinguish *Pipistrellus* from other chiropteran taxa, such as the absence of heel/talon on the upper molars, nyctalodont lower molars, very small size, short and blunt styloid process of the humerus and no lateral projection of the condyle and the epicondyle. However, species discrimination within the genus is more complex, as all species share very similar characteristics and thus, identification of fossils at species level is based almost exclusively on size.

Pipistrellus pipistrellus Schreber, 1774

(Common Pipistrelle Bat)

Figure 4.48 and Figure A.67

Fossiliferous locality LAC I, LAC Ib, LAC Ic, LAC II, LAC III

Age Late Pleistocene

Material 30 identified specimens

LAC I: 1 right C (19969), LAC Ib: 1 right C (17137), LAC Ic: 2 left C (17991, 18052), 1 right M1 (17910), 1 right M3 (17871), 1 right m1 (17891), 1 left m3 (18030), LAC II: 1 left C (22426), 1 left M1 (27788), 1 right M2 (21729), 1 right m3 (21620), LAC III: 6 right C (20087, 21389, 21022, 19304, 20306, 20307), 5 left C (17716, 21135, 20083, 20303, 20493), 1 right P4 (20265), 1 right M1 (21312), 2 left M2 (21000, 21096), 1 right mandibular fragment (20766), 1 left c (20211), 1 left m1 (20790)

Fossiliferous locality LAC Ia

Age latest Pleistocene

Material 34 identified specimens

1 right maxillary fragment with P4-M3 (23084), 1 right maxillary fragment with M1-M3 (23081), 1 right P4 (25288), 2 left P4 (23265, 25358), 4 right M1 (24602, 24617, 24618, 25018), 1 left M1 (24772), 2 right M2 (24516, 26548), 1 left M3 (25118), 1 right mandibular fragments with p4 and m2 (22552), 1 left mandibular fragments with p4 and m2 (22771), 1 right mandibular fragment with p4-m3 (22549), 2 right mandibular fragments with m2-m3 (22535, 26763), 1 right mandibular fragment with m3 (22618), 3 right c (25829, 26013, 26086), 2 right m1 (23580, 26923), 1 left m1 (24015), 2 right m2 (23374, 23441), 2 left m2 (24063, 27284), 1 right m3 (23699), 2 left m3 (24114, 24128), 1 right humerus (26452), 1 left humerus (26451)

Measurements Table 4.19 and Figure 4.47

Description *Pipistrellus pipistrellus* is (together with *Pipistrellus pygmaeus*) the smallest member of the five Pipistrelle Bat species that currently occur in Greece.

Table 4.19 *Pipistrellus pipistrellus*, Loutra Almopias Cave A. Measurements (in mm) from both LAC and LAC Ia. LAC: Late Pleistocene; LAC Ia: latest Pleistocene; n: number of measurable specimens; L: length; W: width; trgd: trigonid; tld: talonid; MEAN: average; MIN: minimum; MAX: maximum; SD: standard deviation; CV: coefficient of variation.

			n	MEAN	MIN	MAX	SD	CV
C	LAC	L	15	0.89	0.79	1.06	0.066	7.365
		W	15	0.67	0.60	0.74	0.045	6.701
P4	LAC	L	1	0.88	-	-	-	-
		W	1	0.89	-	-	-	-
	LAC Ia	L	4	0.81	0.78	0.89	0.053	6.464
		W	4	0.89	0.82	0.95	0.055	6.154
M1	LAC	L	2	1.12	1.06	1.17	0.078	6.976
		W	2	1.11	1.05	1.16	0.078	7.039
	LAC Ia	L	6	1.11	1.07	1.18	0.039	3.480
		W	5	1.06	0.99	1.12	0.064	6.030

M2	LAC	L	2	1.14	1.13	1.14	0.007	0.623
		W	2	1.41	1.37	1.45	0.057	4.012
	LAC Ia	L	4	1.08	1.00	1.15	0.061	5.709
		W	4	1.28	1.14	1.39	0.124	9.723
M3	LAC	L	1	0.97	-	-	-	-
		W	1	1.00	-	-	-	-
	LAC Ia	L	3	1.06	0.91	1.16	0.131	12.351
		W	3	1.27	1.11	1.36	0.139	10.939
c	LAC	L	1	0.56	-	-	-	-
		W	1	0.60	-	-	-	-
	LAC Ia	L	3	0.60	0.56	0.64	0.040	6.667
		W	3	0.62	0.57	0.67	0.050	8.075
p4	LAC Ia	L	3	0.54	0.51	0.60	0.052	9.623
		W	3	0.50	0.48	0.51	0.015	3.076
m1	LAC	L	2	1.09	1.07	1.10	0.021	1.955
		W (trgd)	2	0.74	0.66	0.82	0.113	15.289
		W (tld)	2	0.87	0.80	0.94	0.099	11.379
	LAC Ia	L	4	1.03	1.00	1.06	0.025	2.421
		W (trgd)	4	0.63	0.54	0.73	0.084	13.314
		W (tld)	4	0.73	0.70	0.75	0.026	3.615
m2	LAC Ia	L	9	1.03	0.87	1.14	0.078	7.505
		W (trgd)	9	0.61	0.47	0.72	0.074	12.080
		W (tld)	9	0.70	0.60	0.77	0.056	7.992
m3	LAC	L	2	0.99	0.98	1.00	0.014	1.429
		W (trgd)	2	0.57	0.53	0.61	0.057	9.924
		W (tld)	2	0.53	0.50	0.56	0.042	8.005
	LAC Ia	L	7	0.97	0.90	1.04	0.046	4.765
		W (trgd)	7	0.59	0.54	0.64	0.036	6.065
		W (tld)	7	0.50	0.41	0.64	0.073	14.680
M1-M3	LAC Ia	L	1	2.69	-	-	-	-
P4-M3	LAC Ia	L	1	3.54	-	-	-	-
m1-m3	LAC Ia	L	1	2.99	-	-	-	-
p4-m3	LAC Ia	L	1	3.51	-	-	-	-
LSC	LAC Ia	L	1	8.01	-	-	-	-
Humerus	LAC Ia	W	2	1.95	1.91	1.99	0.057	2.901

C: Very small tooth with the cusp slightly curved distally. It is subtriangular in occlusal view. The crown forms practically no angle with the root. A small heel is present at the lingual part of the tooth. The crown is convex at its labial part and flat at its lingual part. A longitudinal groove occurs at the labial side of the tooth. The cingulum is of average thickness throughout the whole tooth. The crown becomes narrower abruptly at the middle part of the tooth (in height), which is visible in labial and lingual view.

P4: Small-sized tooth, with the cusp being connected with a crista to an accessory distolabial cusplet. A relatively well-developed, but depressed, heel is present at the lingual part of the tooth. The crown is convex labially and mesially and concave lingually. The base of the crown is concave at its distal part. The cingulum is thin, with its maximum thickness at the mesiolingual part of the tooth, where a robust cingular cusplet is present.

M1: Small-sized tooth. It is subrectangular in occlusal view. Parastyle, mesostyle, metastyle, paracone and metacone are well-developed. The metacone is on the same height with the paracone. The parastyle forms an angle with the preparacrista. The mesial part of the ectoloph is narrower than the distal part. Additionally, the angles formed by the paracone, the metacone and the cristae on both sides are equal. Metaloph is absent. Paraloph, paraconule and metaconule are well-developed. The cingulum is of average thickness throughout the whole tooth, apart from the base of the protocone, where it is thinner.

M2: Wider than M1. The mesial part of the ectoloph is almost equally wide to the distal part. The rest of the characters as M1.

M3: Small-sized tooth. It is triangular in occlusal view. Parastyle, mesostyle, paracone and metacone are well-developed, whereas the metastyle and the postmetacrista that connects the metacone with the metastyle are absent. The metacone is slightly taller than the paracone. The parastyle forms an angle with the preparacrista. A concavity is present at the distolingual base of the crown. The cingulum, which is thin, is absent only beneath the triangular protocone.

c: Small-sized tooth with the cusp slightly curved distally. It is semicircular in occlusal view. It is convex mesially and labially and concave distally and lingually. The distal part of the tooth is developed at the base of the crown, whereas the mesial part is developed in height. Respectively, the crown is in a more superior position towards the anterior part of the tooth. The cingulum is of average thickness throughout the whole tooth. It reaches its maximum thickness at the mesiolingual and distolingual parts of the tooth, where two cingular cusplets are present and connected with a widened lingual crista.

p4: Small-sized tooth with the cusp slightly curved lingually. It is subtriangular in occlusal view. The crown is convex labially and concave lingually and distally. The cingulum is of average thickness and uniform throughout the whole tooth. Two cingular cusplets are also present, one at the mesiolingual part of the tooth and one at the distolingual.

m1: Nyctalodont. The talonid is longer than the trigonid. Paraconid, metaconid, entoconid, protoconid and hypoconid are well-developed. The protoconid is taller than the hypoconid. The paralophid is concave. The entocristid is straight. The hypoconulid is small and slightly developed lingually, together with the entoconid. The labial cingulum is thick beneath the protoconid and slightly thinner beneath the hypoconid.

m2: Trigonid is wider than in m1. The entoconid is slightly moved labially. The labial cingulum is thick beneath the hypoconid. The rest of the characters as m1.

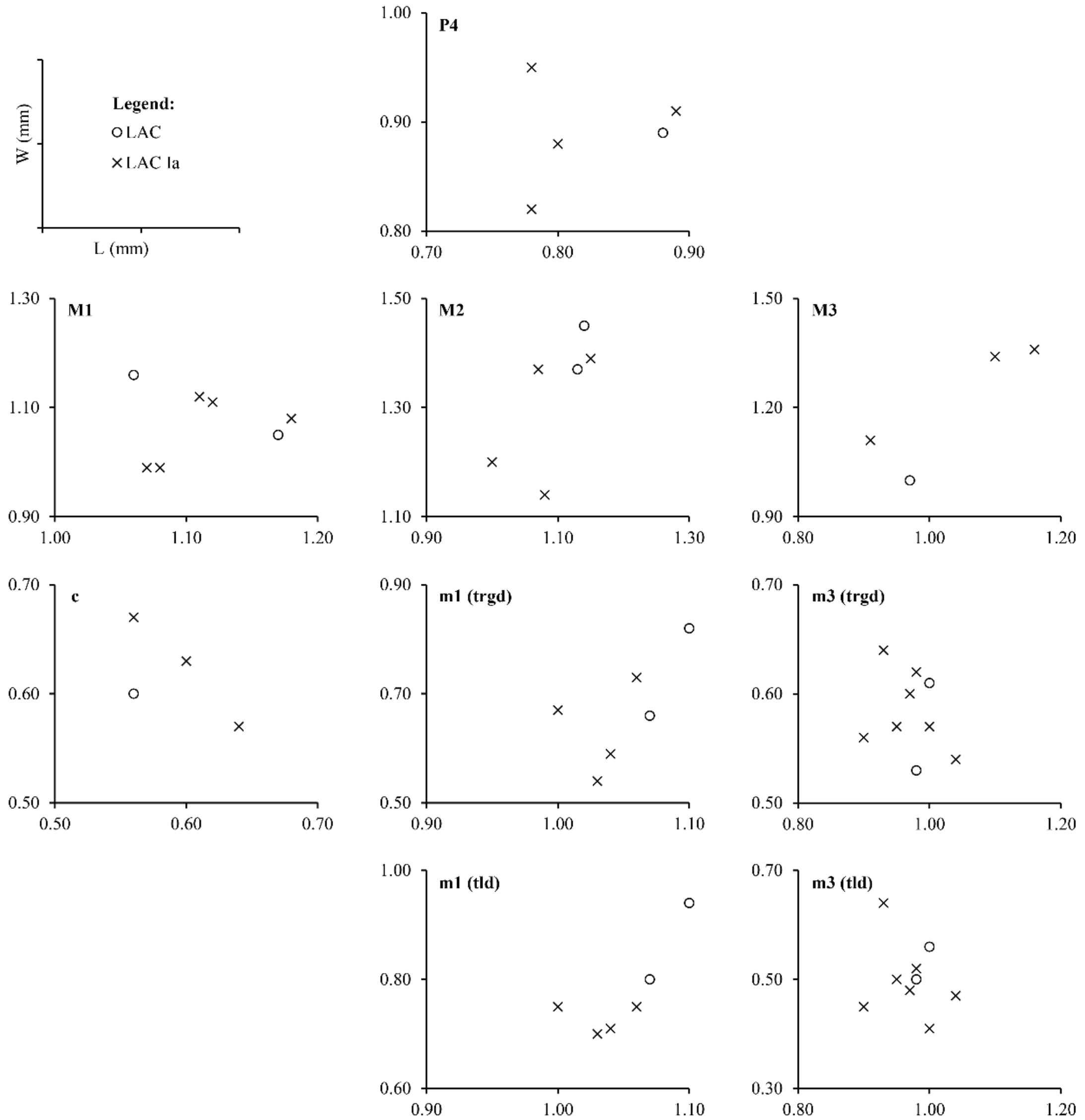

Figure 4.47 *Pipistrellus pipistrellus*, Loutra Almopias Cave A. XY graphs with the measured (in mm) dental elements (P4, M1, M2, M3, c, m1, m3). L: length, W: width, trgd: trigonid; tld: talonid.

m3: Nyctalodont. The talonid is longer than the trigonid. Paraconid, metaconid, entoconid, protoconid and hypoconid are well-developed. The protoconid is taller than the hypoconid. The paralophid is concave. The entocristid is imperceptibly curved. The entoconid is more towards the labial side of the tooth and thus, the talonid is reduced. The hypoconulid is well-developed and positioned slightly lingually. The labial cingulum is thick beneath the protoconid (not as pronounced as in m1) and slightly thinner beneath the hypoconid.

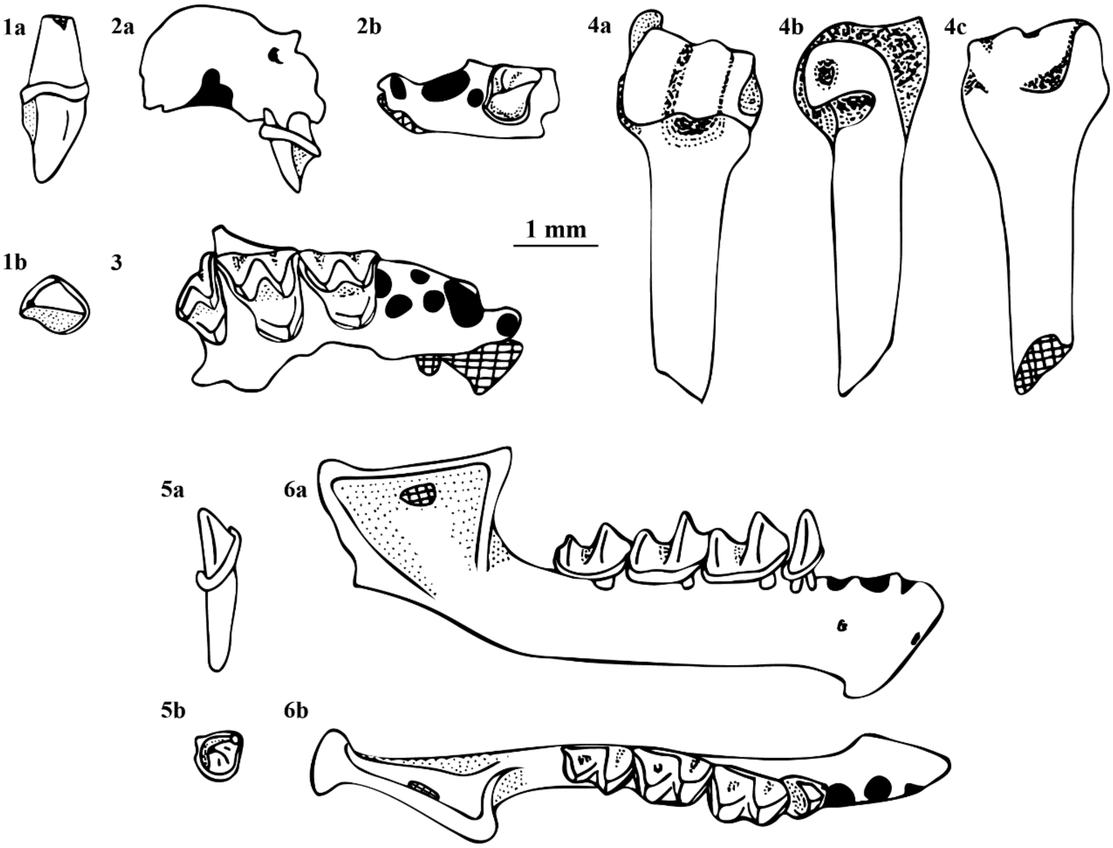

Figure 4.48 *Pipistrellus pipistrellus*, Loutra Almopias Cave A. **1.** LAC21389 – Right C (**a.** labial, **b.** occlusal), **2.** LAC23265 – Left maxillary fragment with P4 (**a.** labial, **b.** occlusal), **3.** LAC23081 – Right maxillary fragment with M1-M3, **4.** LAC26452 – Distal epiphysis of right humerus (**a.** anterior, **b.** lateral, **c.** posterior), **5.** LAC26013 – Right c (**a.** labial, **b.** occlusal), **6.** LAC22549 – Right mandibular fragment with p4-m3 (**a.** labial, **b.** occlusal).

Mandible: The coronoid process is angular and located higher, but not significantly than the articular process. The anterior part of the masseter crest, which is of average thickness, is slightly concave. The anterior sigmoid notch is straight and slightly concave at the anterior part of the articular process, which is well-developed. The mental foramen is relatively large and beneath the anterior part of p3. The anterior part of the symphysis strongly projects downwards.

Humerus: The styloid process is short and blunt (triangular in lateral view). The epitrochlea is very small. A relatively deep diagonal valley is present between the trochlea and the condyle. A shallow valley is present between the condyle and the epicondyle. The condyle and the epicondyle are not projecting laterally. The radial fossa and the olecranon fossa are deep, with the latter extending from the middle part of the epiphysis to the styloid process.

Remarks *Pipistrellus pipistrellus* is very similar to *Pipistrellus pygmaeus*. The latter was recognized as a separate species during the 1990s, based on the terminal frequencies of their echolocation calls and their DNA sequences (Hanák et al. 2001, Dietz et al. 2009). Both species overlap greatly in size and in accordance with their identical morphological features, species discrimination is practically impossible (up to date), when working with skeletal and dental material. However, the described fossils are assigned to *Pipistrellus pipistrellus*, as extant populations of *Pipistrellus pygmaeus* are rather uncommon in Greece (Hanák et al. 2001, Dietz et al. 2009, GFDC 2021).

Discussion The morphological features described in addition to the measurements allow a definite attribution of the material to *Pipistrellus pipistrellus*. It is the smallest member of the five Pipistrelle Bat species that currently occur in Greece and it is clearly distinguished from the rest of the species.

Occurrence The fossils of the Common Pipistrelle Bat described from Loutra Almopias Cave A are the first known records of this species in Greece. Its modern distribution includes practically all mainland Greece, several Aegean Islands and Crete (Hanák et al. 2001, GFDC 2021). On a global scale it is distributed from Northwestern Africa to Western Europe (including the British Isles and Southern Denmark) and all the way to the Volga, the Caucasus and Kazakhstan, Turkey, parts of the Levant, Afghanistan, Pakistan, Kashmir, Myanmar and Northwestern China and possibly Korea, Japan and Taiwan (Simmons 2005a).

Ecology *Pipistrellus pipistrellus* hibernates in both hollow trees and caves and its habitat preferences include forested areas with the presence of water bodies (Dietz et al. 2009).

Vespertilio Linnaeus, 1758

Type species *Vespertilio murinus* Linnaeus, 1758

The earliest occurrence of *Vespertilio* in the global fossil record is cf. *Vespertilio* (sp. nov.) from the Early Miocene (MN4) locality of Rembach, Germany (Rosina and

Rummel 2017). The earliest occurrence of *Vespertilio* in the fossil record of Greece is *Vespertilio murinus* from the Middle Pleistocene locality of Petralona Cave, Chalkidiki (Horacek and Poulianos 1988). There is currently one species occurring in Greece (*Vespertilio murinus*) (Hanák et al. 2001, Simmons 2005a).

The dental formula of *Vespertilio* is: 2.1.1.3/3.1.2.3 and there are several morphological characteristics that distinguish *Vespertilio* from other chiropteran taxa, such as the absence of heel/talon on the upper molars, myotodont lower molars, thick cingulum on nearly all dental elements, short and blunt styloid process of the humerus and no lateral projection of the condyle and the epicondyle.

Vespertilio murinus **Linnaeus, 1758**

(Parti-coloured Bat)

Figure 4.50-51 and Figure A.68

Fossiliferous locality LAC I, LAC Ib, LAC II, LAC III

Age Late Pleistocene

Material 19 identified specimens

LAC I: 1 right C (27491), 1 right M2 (19960), LAC Ib: 1 right C (19893), 1 left C (19867), 1 left M1 (16508), LAC II: 1 right maxillary fragment with C-P4 (16379), 2 left C (22391, 27937), 1 left P4 (22378), 1 left M1 (21688), 1 left M2 (21689), 2 left M3 (22292, 27822), 1 left m1 (27888), LAC III: 1 right C (21021), 1 right M1 (20748), 1 right M2 (20450), 1 right m1 (20530), 1 left m2 (20342)

Fossiliferous locality LAC Ia

Age latest Pleistocene

Material 154 identified specimens

1 left maxillary fragment with M3 (23190), 13 right C (25448, 25504, 25519, 25523, 25530, 25560, 25653, 25794, 25848, 26141, 27076, 27079, 27090), 7 left C (25708, 25881, 26080, 26082, 26099, 26105, 26232), 11 right P4 (23289, 25235, 25241, 25244, 25260, 25275, 25278, 25324, 26690, 26693, 26700), 7 left P4 (25365, 25370, 25395, 25409, 25410, 25422, 26704), 13 right M1 (24378, 24382, 24434, 24529, 24534, 24561, 24586, 24595, 24612, 26565, 26566, 26581, 26585), 10 left M1 (24695, 24796, 24803, 24828, 24855, 24915, 24921, 24952, 24979, 26626), 7 right M2 (24424, 24475, 24518, 24519, 26553, 26603, 27305), 10 left M2 (24685, 24774, 24794, 24813, 24845, 24852, 26639, 26643, 26653, 26667), 11 right M3 (25145, 25166, 25191, 25193, 25194, 25195, 25202, 25203, 25204, 26616, 27318), 8 left M3 (25005, 25067, 25072, 25083, 25100, 25121, 25124, 26674), 1 right mandibular fragment (19511), 1 right mandibular fragment with c-m1 (19671), 1 left mandibular fragment with p3-p4 (26814), 1 right mandibular fragment with p4 and m2-m3 (19485), 1 right mandibular fragment with p4-m3 (26724), 1 left mandibular fragment with m1-m3 (22702), 1 right mandibular fragment with m1-m2 (22515), 1 right mandibular fragment with m2 (22523), 10 right m1 (23354, 23381, 23398, 23573, 23588, 23608, 26887, 26910, 26916, 27362), 9 left m1 (23758, 23760, 23763, 23875, 23908, 24017, 24058, 26970, 27004), 8 right m2 (23324, 23335, 23495, 23497, 23532, 26731, 26740, 26879), 9 left m2 (23801, 23961, 23987, 24055, 26962, 26967, 26971, 26979, 27380), 1 right m3 (23656), 4 left m3

(23840, 24126, 26781, 27022), 3 right humeri (26429, 26436, 27212), 3 left humeri (26427, 27223, 27453, 27454)

Measurements Table 4.20 and Figure 4.49

Description *Vespertilio murinus* is the sole member of the Parti-coloured Bats that currently occur in Greece.

C: Robust tooth with the cusp curved distally. It is subtriangular in occlusal view. The crown forms practically no angle with the root. The crown is convex labially and flat lingually. A heel is present at the mesiolingual part of the tooth. A longitudinal groove occurs at the labial side of the tooth. The cingulum is thick and it reaches its maximum thickness mesiolingually, where a cingular platform is present. The base of the crown is concave distolingually.

Table 4.20 *Vespertilio murinus*, Loutra Almopias Cave A. Measurements (in mm) from both LAC and LAC Ia. LAC: Late Pleistocene; LAC Ia: latest Pleistocene; n: number of measurable specimens; L: length; W: width; trgd: trigonid; tld: talonid; MEAN: average; MIN: minimum; MAX: maximum; SD: standard deviation; CV: coefficient of variation.

			n	MEAN	MIN	MAX	SD	CV
C	LAC	L	7	1.11	1.03	1.15	0.041	3.658
		W	7	1.15	0.98	1.23	0.095	8.324
	LAC Ia	L	20	1.14	0.98	1.39	0.116	10.133
		W	20	1.13	1.04	1.24	0.060	5.289
P4	LAC	L	2	1.04	1.02	1.05	0.021	2.050
		W	2	1.27	1.27	1.27	0.000	0.000
	LAC Ia	L	17	0.97	0.85	1.11	0.079	8.116
		W	16	1.29	1.08	1.41	0.103	8.042
M1	LAC	L	4	1.49	1.44	1.55	0.051	3.412
		W	4	1.60	1.56	1.65	0.040	2.534
	LAC Ia	L	23	1.45	1.32	1.59	0.064	4.394
		W	23	1.55	1.34	1.87	0.114	7.333
M2	LAC	L	1	1.63	-	-	-	-
		W	1	1.89	-	-	-	-
	LAC Ia	L	16	1.48	1.31	1.58	0.073	4.932
		W	16	1.75	1.50	1.87	0.109	6.249
M3	LAC	L	2	1.50	1.47	1.52	0.035	2.365
		W	2	1.64	1.56	1.71	0.106	6.487
	LAC Ia	L	17	1.49	1.34	1.61	0.073	4.928
		W	17	1.65	1.49	1.79	0.084	5.094
c	LAC Ia	L	1	0.78	-	-	-	-
		W	1	0.98	-	-	-	-
p3	LAC Ia	L	2	0.45	0.44	0.46	0.014	3.143
		W	2	0.53	0.44	0.61	0.120	22.897
p4	LAC Ia	L	4	0.70	0.68	0.73	0.024	3.388
		W	4	0.80	0.74	0.87	0.056	7.003

m1	LAC	L	2	1.45	1.39	1.51	0.085	5.852
		W (trgd)	2	0.87	0.80	0.94	0.099	11.379
		W (tld)	2	0.93	0.87	0.99	0.085	9.124
	LAC Ia	L	22	1.44	1.35	1.51	0.053	3.704
		W (trgd)	22	0.91	0.78	1.05	0.069	7.580
		W (tld)	23	0.99	0.80	1.12	0.081	8.183
m2	LAC	L	1	1.42	-	-	-	-
		W (trgd)	1	0.92	-	-	-	-
		W (tld)	1	0.96	-	-	-	-
	LAC Ia	L	22	1.42	1.31	1.57	0.068	4.783
		W (trgd)	22	0.95	0.87	1.06	0.056	5.870
		W (tld)	22	1.00	0.92	1.08	0.052	5.215
m3	LAC Ia	L	8	1.29	1.21	1.39	0.063	4.888
		W (trgd)	8	0.84	0.75	0.95	0.061	7.283
		W (tld)	8	0.70	0.63	0.79	0.055	7.818
C-P4	LAC	L	1	2.18	-	-	-	-
m1-m3	LAC Ia	L	2	4.24	4.10	4.37	0.191	4.508
p4-m3	LAC Ia	L	2	4.90	4.78	5.02	0.170	3.463
c-p4	LAC Ia	L	1	1.76	-	-	-	-
LSC	LAC Ia	L	1	10.96	-	-	-	-
Humerus	LAC Ia	W	7	2.84	2.76	2.92	0.061	2.147

P4: Robust tooth with the cusp being connected with a crista to an accessory distolabial cusplet. It is subrectangular in occlusal view. A heel is present at the lingual part of the tooth. The crown is convex labially and mesiolabially and flat lingually. The base of the crown is concave mesially, labially and distally. The cingulum is thick and it reaches its maximum thickness mesiolingually, where a cingular cusplet is present. A small cingular platform is also present at the mesiolabial part of the tooth.

M1: Robust tooth. It is subrectangular in occlusal view. Parastyle, mesostyle, metastyle, paracone and metacone are well-developed. The metacone is taller than the paracone. The parastyle forms an angle with the preparacrista and the metastyle slightly curves lingually. The mesial part of the ectoloph is narrower than the distal part. Additionally, the paracone, the metacone and the cristae on both sides form equal angles. Paraloph, metaloph and metaconule are absent. The paraconule is well-developed. The postprotocrista is slightly curved. The cingulum, which is thick, is continuous throughout the whole tooth.

M2: The mesial part of the ectoloph is wider than in M1. The rest of the characters as M1.

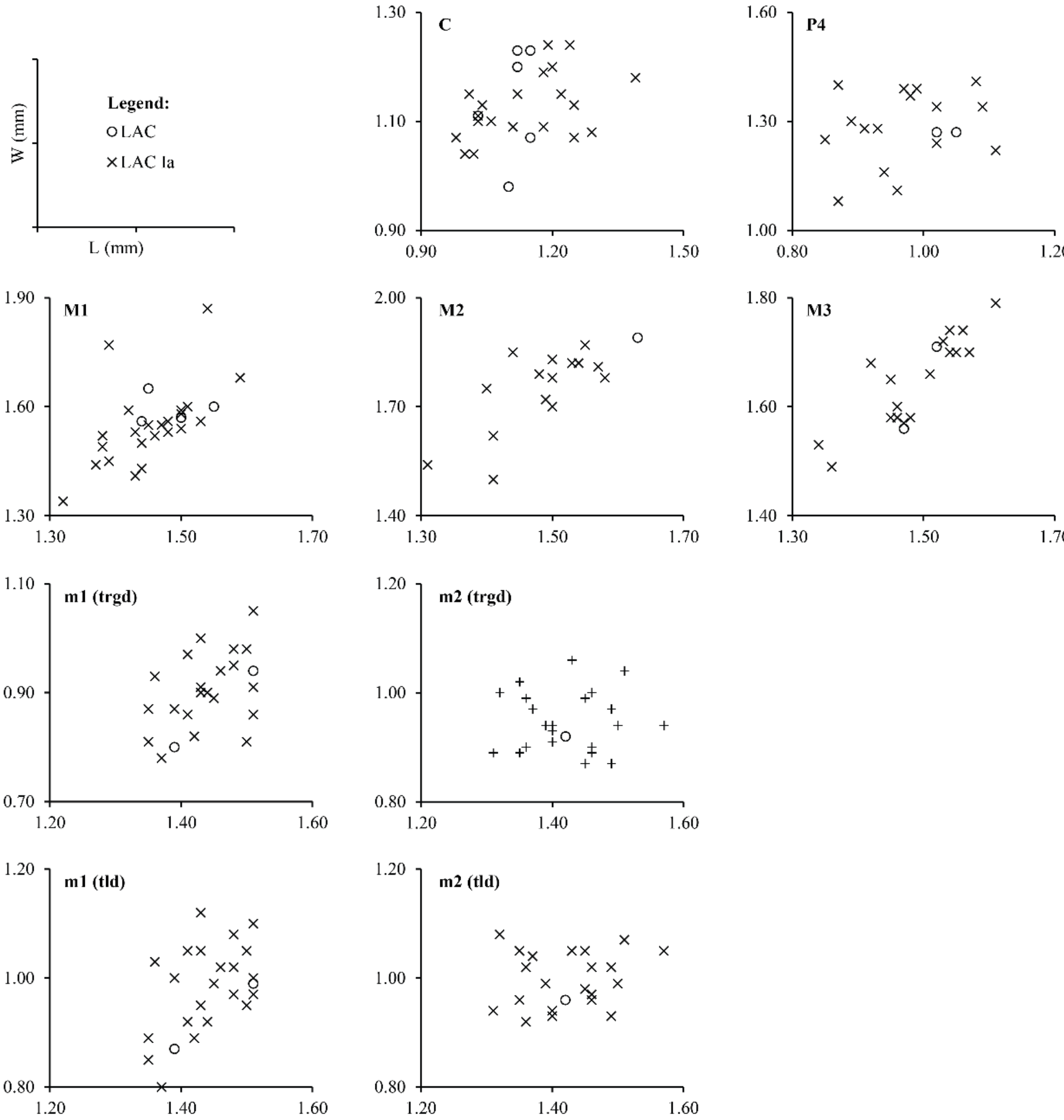

Figure 4.49 *Vespertilio murinus*, Loutra Almopias Cave A. XY graphs with the measured (in mm) dental elements (C, P4, M1, M2, M3, m1, m2). L: length, W: width, trgd: trigonid; tld: talonid.

M3: Robust tooth. It is triangular in occlusal view. The parastyle, the paracone and the metacone are more developed than the mesostyle, whereas the metastyle is absent. The postmetacrista that connects the metacone with the metastyle is also absent. The paracone is taller than the metacone. The parastyle forms an angle with the preparacrista. The paraconule is not well-developed. The cingulum is of average thickness throughout the whole tooth. The base of the crown in concave distally.

c: Robust tooth with the cusp slightly curved lingually. It is semicircular in occlusal view. It is convex mesially and flat distally. The distal part of the tooth is developed at the base of the crown, whereas the mesial part is developed in height. Respectively, the crown is in a more superior position towards the anterior part of the tooth. The distolabial part of the tooth is situated lower than the distolingual, which is higher than the former. The cingulum is thick throughout the whole tooth. It reaches its maximum thickness at the mesiolingual and distolingual parts of the tooth, where two cingular cusplets are present and connected with a widened lingual crista.

p3: Small-sized unicuspid tooth. It is oval in occlusal view. The crown is convex mesially and slightly concave distally. The cingulum is relatively thick throughout the whole tooth.

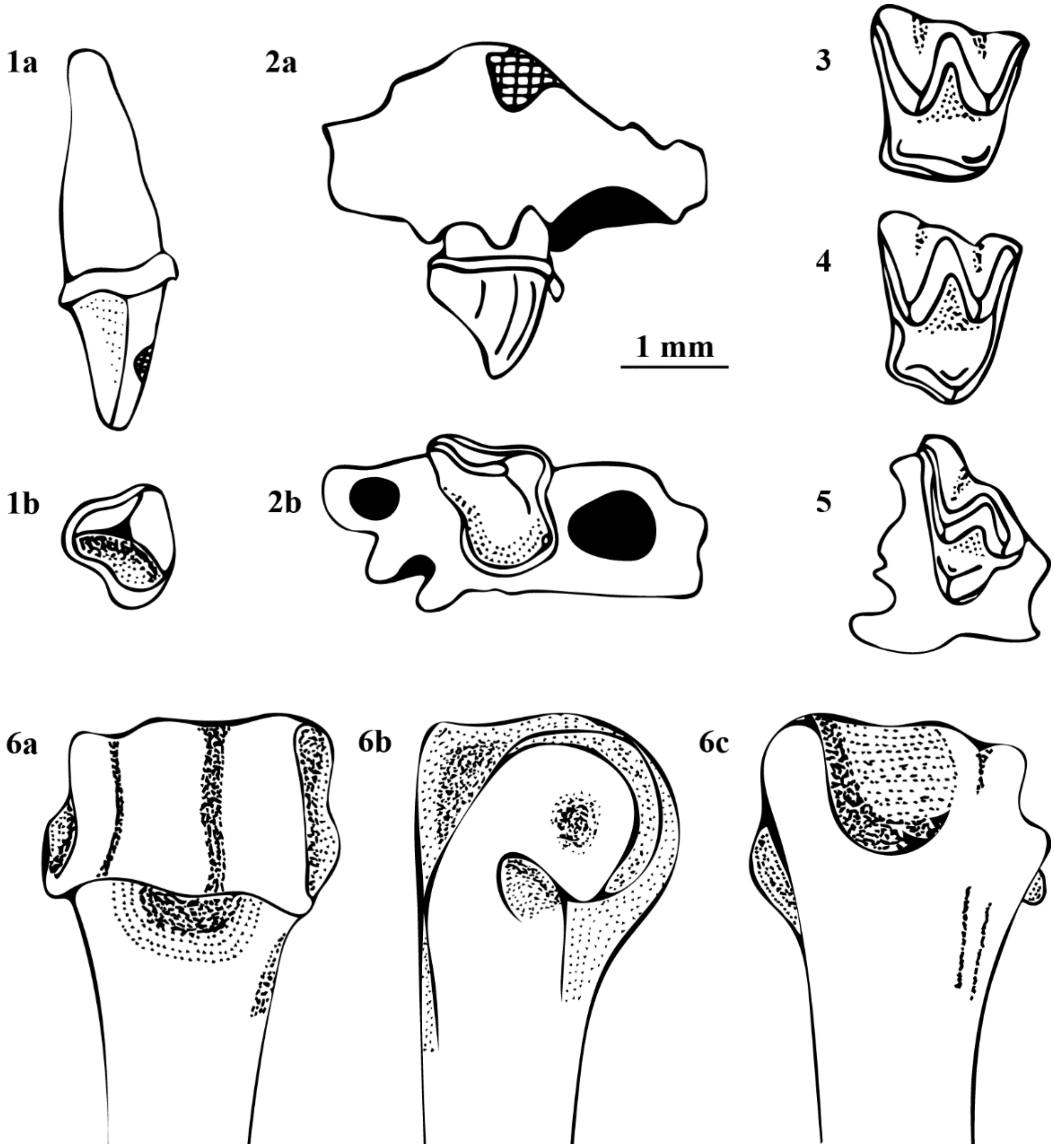

Figure 4.50 *Vespertilio murinus*, Loutra Almopias Cave A. **1.** LAC19867 – Right C (**a.** labial, **b.** occlusal), **2.** LAC23289 – Right maxillary fragment with P4 (**a.** labial, **b.** occlusal), **3.** LAC24382 – Right M1, **4.** LAC24424 – Right M2, **5.** LAC23190 – Left M3, **6.** LAC26427 – Distal epiphysis of left humerus (**a.** anterior, **b.** lateral, **c.** posterior).

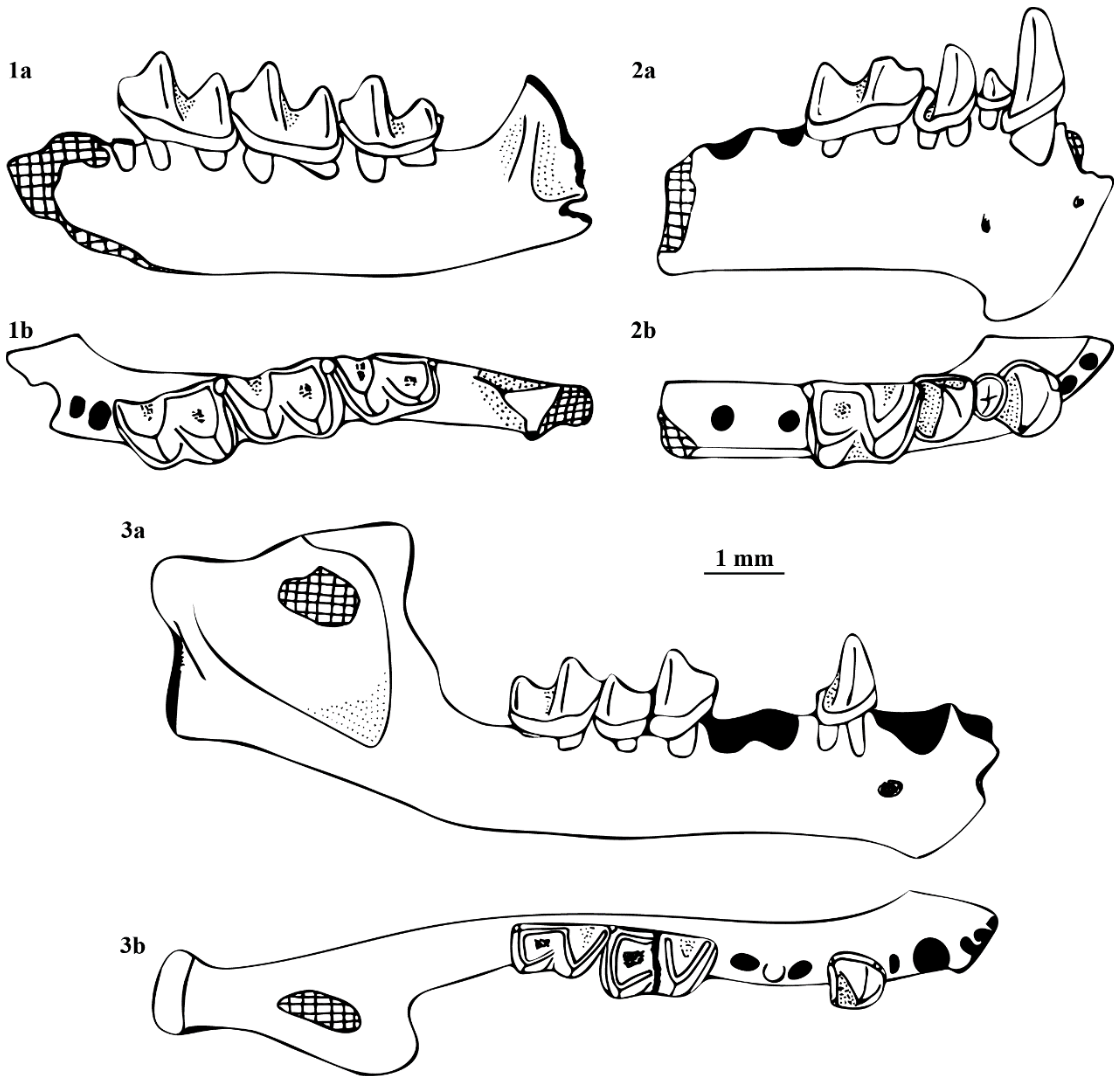

Figure 4.51 *Vespertilio murinus*, Loutra Almopias Cave A. **1.** LAC22702 – Left mandibular fragment with m1-m3 (**a.** labial, **b.** occlusal), **2.** LAC19671 – Right mandibular fragment with c-m1 (**a.** labial, **b.** occlusal), **3.** LAC19485 – Right mandibular fragment with p4 and m2-m3 (**a.** labial, **b.** occlusal).

p4: Robust tooth with the cusp slightly curved distally. It is subtriangular in occlusal view. The mesiolingual part of the tooth is more elongated and higher than the mesiolabial part. The distolingual part of the tooth is higher than the distolabial. The crown is convex mesiolabially, concave lingually and relatively flat distally. The cingulum is thick throughout the whole tooth and it reaches its maximum thickness mesiolingually and distolingually, where two cingular cusplets are present.

m1: Myotodont. The trigonid and the talonid are of almost equal length. Paraconid, metaconid, entoconid, protoconid and hypoconid are well-developed. The protoconid is taller than the hypoconid. The paralophid is concave. The entocristid is curved. The hypoconulid is well-developed and in line with the lingual cusps. The labial cingulum is thick throughout the whole tooth and it bends down slightly at the level of each root, with the posterior convexity being placed slightly lower than the anterior.

m2: The trigonid is wider than in m1. The labial cingulum is flatter, with the anterior convexity being more marked. The rest of the characters as m1.

m3: Myotodont. The talonid is longer than the trigonid. Paraconid, metaconid, entoconid, protoconid and hypoconid are well-developed. The protoconid is taller than the hypoconid. The paralophid is concave. The entocristid is curved. The entoconid is more towards the labial side of the tooth and thus, the talonid is reduced. The hypoconulid is also significantly reduced. The labial cingulum is thick throughout the whole tooth.

Mandible: The coronoid process is angular and located higher, but not significantly, than the articular process. The anterior part of the masseter crest, which is of average thickness, is slightly concave. The anterior sigmoid notch is straight close to the coronoid process and concave towards the articular process. The angular process is short and projects anteriorly. The mental foramen is beneath the anterior part of p4. The anterior part of the symphysis strongly projects downwards.

Humerus: The styloid process is short and blunt (subtriangular in lateral view). The epitrochlea is small. A shallow diagonal valley separates the trochlea from the condyle. A shallow valley is present between the condyle and the epicondyle. The condyle and the epicondyle are not projecting laterally. The radial fossa and the olecranon fossa are deep, with the latter extending from the middle part of the epiphysis to the styloid process.

<u>**Discussion**</u> The morphological features described in addition to the measurements allow a definite attribution of the material to *Vespertilio murinus*. It is the sole member of the Parti-coloured Bats that currently occur in Greece.

<u>**Occurrence**</u> Fossils of the Parti-coloured Bat are known only from Petralona Cave, Chalkidiki. Its modern distribution includes Central and Northeastern mainland Greece (Hanák et al. 2001, GFDC 2021). On a global scale it is distributed from Eastern France all the way to Northeastern China and Korea and from Norway and Central Russia to Iran (Simmons 2005a).

<u>**Ecology**</u> *Vespertilio murinus* hibernates in both hollow trees and caves and its habitat preferences include open areas with the presence of water bodies (Dietz et al. 2009).

Eptesicus **Rafinesque, 1820**

Type species *Eptesicus melanops* Rafinesque, 1820 (= *Vespertilio fuscus* Beauvois, 1796)

The earliest occurrence of *Eptesicus* in the global fossil record is *Eptesicus aurelianensis* from the Early Miocene (MN3) locality of Wintershof-West, Germany (Ziegler 1993). The earliest occurrence of *Eptesicus* in the fossil record of Greece is *Eptesicus* sp. from the Middle Pleistocene locality of Petralona Cave, Chalkidiki (Horacek and Poulianos 1988). There are currently two species occurring in Greece (*Eptesicus serotinus* and *Eptesicus bottae*) (Hanák et al. 2001, Simmons 2005a, Sfougaris 2009).

The dental formula of *Eptesicus* is: 2.1.1.3/3.1.2.3 and there are several morphological characteristics that distinguish *Eptesicus* from other chiropteran taxa, such as the absence of heel/talon on the upper molars, myotodont lower molars, very thick cingulum on nearly all dental elements, short and blunt styloid process of the humerus and no lateral projection of the condyle and the epicondyle. However, species discrimination within the genus is more complex, as all species share very similar characteristics and thus, identification of fossils at species level is based almost exclusively on size.

Eptesicus serotinus **Schreber, 1774**

(Serotine Bat)

Figure 4.53 and Figure A.69

<u>Fossiliferous locality</u> LAC I, LAC Ib, LAC Ic, LAC II, LAC III

<u>Age</u> Late Pleistocene

<u>Material</u> 18 identified specimens

<u>LAC I:</u> 1 right maxillary fragment with C-P4 (27483), 1 right M1 (27496), <u>LAC Ib:</u> 1 right P4 (17186), <u>LAC Ic:</u>1 left M1 (21460), 1 right c (17914), <u>LAC II:</u> 1 left C (22175), 1 right P4 (22309), 1 left P4 (21999), 3 left M1 (22259, 27694, 27758), 1 left p4 (27689), <u>LAC III:</u> 1 right P4 (20184), 1 right M1 (20841), 1 right M2 (20116), 1 right p4 (21077), 1 left p4 (20051), 1 right m1 (17864)

<u>Fossiliferous locality</u> LAC Ia

<u>Age</u> latest Pleistocene

<u>Material</u> 45 identified specimens

1 left maxillary fragment with C-M2 (27247), 1 left I1 (26391), 5 right C (25847, 25890, 25934, 26204, 26215), 2 left C (25621, 25796), 3 right P4 (23291, 25246, 26699), 4 left P4 (23253, 25335, 25344, 25363), 4 right M1 (24478, 24496, 24636, 24638), 3 left M1 (24759, 24815, 24851), 1 right M2 (24430),

2 left M2 (24760, 24902), 1 left mandibular fragment (19497), 1 left mandibular fragment with c-m1 (26802), 4 right p4 (24201, 24231, 27027, 27040), 6 left p4 (24291, 24292, 24324, 24342, 26819, 27407), 2 right m1 (23480, 26880), 3 left m1 (23899, 23968, 27386), 1 left m2 (26968), 1 left m3 (27019)

Measurements Table 4.21 and Figure 4.52

Description *Eptesicus serotinus* is the largest member of the two Serotine Bat species that currently occur in Greece.

I1: Unicuspid. It is trapezoidal in occlusal view. The cusp is at the middle part of the tooth and a small accessory cusplet is present distolingually, right beneath the main cusp. A thick cingulum is also present throughout the whole tooth.

C: Very robust tooth with the cusp slightly curved distally. It is trapezoidal in occlusal view. The crown forms practically no angle with the root. A thick ridge connects the distal base of the crown with the cusp. The crown is convex mesiolabially and concave distolabially, distolingually and mesiolingually. A longitudinal groove occurs in the labial side of the tooth. The cingulum is very thick, with its maximum thickness at the labial part of the tooth.

P4: Very robust tooth with the cusp being connected with a crista to an accessory distolabial cusplet. It is subrectangular in occlusal view. A well-developed heel is present at the mesiolingual part of the tooth. The base of the crown is concave at its mesial, labial and distal parts and convex at its mesiolabial, mesiolingual and lingual parts. The cingulum is thick and it reaches its maximum thickness mesiolingually, where a cingular cusplet is present. A small cingular platform is also present at the mesiolabial part of the tooth.

M1: Very robust tooth. It is subrectangular in occlusal view. Parastyle, mesostyle, metastyle, paracone and metacone are well-developed. The metacone is taller than the paracone. The parastyle forms an angle with the preparacrista and the metastyle slightly curves lingually. The mesial part of the ectoloph is narrower than the distal part. Additionally, the paracone, the metacone and the cristae on both sides form equal angles. Paraloph and metaloph are absent. Metaconule and paraconule are present. The cingulum is very thick and continuous throughout the whole tooth. Thin labial cingulum of the metaflexus and paraflexus is also present.

M2: The mesial part of the ectoloph is narrower than the distal part, but less than in M1. The crown is mildly constricted at its middle part. The rest of the characters as M1.

Table 4.21 *Eptesicus serotinus*, Loutra Almopias Cave A. Measurements (in mm) from both LAC and LAC Ia. LAC: Late Pleistocene; LAC Ia: latest Pleistocene; n: number of measurable specimens; L: length; W: width; trgd: trigonid; tld: talonid; MEAN: average; MIN: minimum; MAX: maximum; SD: standard deviation; CV: coefficient of variation.

			n	**MEAN**	**MIN**	**MAX**	**SD**	**CV**
I1	LAC Ia	L	1	0.83	-	-	-	-
		W	1	0.57	-	-	-	-
C	LAC	L	2	2.17	2.05	2.29	0.170	7.821
		W	2	1.64	1.61	1.66	0.035	2.162
	LAC Ia	L	8	2.01	1.89	2.10	0.068	3.357
		W	8	1.54	1.42	1.68	0.098	6.346
P4	LAC	L	5	1.52	1.41	1.56	0.061	4.029
		W	4	1.71	1.60	1.85	0.112	6.546
	LAC Ia	L	8	1.45	1.33	1.58	0.084	5.758
		W	7	1.69	1.59	1.91	0.108	6.383
M1	LAC	L	5	2.19	1.85	2.38	0.221	10.075
		W	5	2.22	1.72	2.38	0.279	12.581
	LAC Ia	L	8	2.04	1.89	2.24	0.104	5.071
		W	8	2.18	2.01	2.40	0.136	6.252
M2	LAC	L	1	1.79	-	-	-	-
		W	1	2.18	-	-	-	-
	LAC Ia	L	3	1.96	1.93	2.03	0.058	2.941
		W	4	2.32	2.23	2.41	0.086	3.710
c	LAC	L	1	1.31	-	-	-	-
		W	1	1.62	-	-	-	-
	LAC Ia	L	1	1.29	-	-	-	-
		W	1	1.52	-	-	-	-
p3	LAC Ia	L	1	0.80	-	-	-	-
		W	1	0.86	-	-	-	-
p4	LAC	L	3	1.16	1.12	1.20	0.040	3.474
		W	3	1.07	1.02	1.13	0.057	5.331
	LAC Ia	L	11	1.14	1.04	1.23	0.055	4.800
		W	11	1.03	0.94	1.13	0.060	5.844
m1	LAC	L	1	1.93	-	-	-	-
		W (trgd)	1	1.10	-	-	-	-
		W (tld)	1	1.31	-	-	-	-
	LAC Ia	L	6	1.98	1.84	2.11	0.111	5.587
		W (trgd)	6	1.23	1.15	1.33	0.074	5.992
		W (tld)	6	1.38	1.31	1.49	0.064	4.632
m2	LAC Ia	L	1	1.94	-	-	-	-
		W (trgd)	1	1.19	-	-	-	-
		W (tld)	1	1.28	-	-	-	-
m3	LAC Ia	L	1	1.73	-	-	-	-
		W (trgd)	1	1.29	-	-	-	-
		W (tld)	1	0.84	-	-	-	-
C-P4	LAC	L	1	3.43	-	-	-	-
	LAC Ia	L	1	3.30	-	-	-	-
c-p4	LAC Ia	L	1	2.96	-	-	-	-

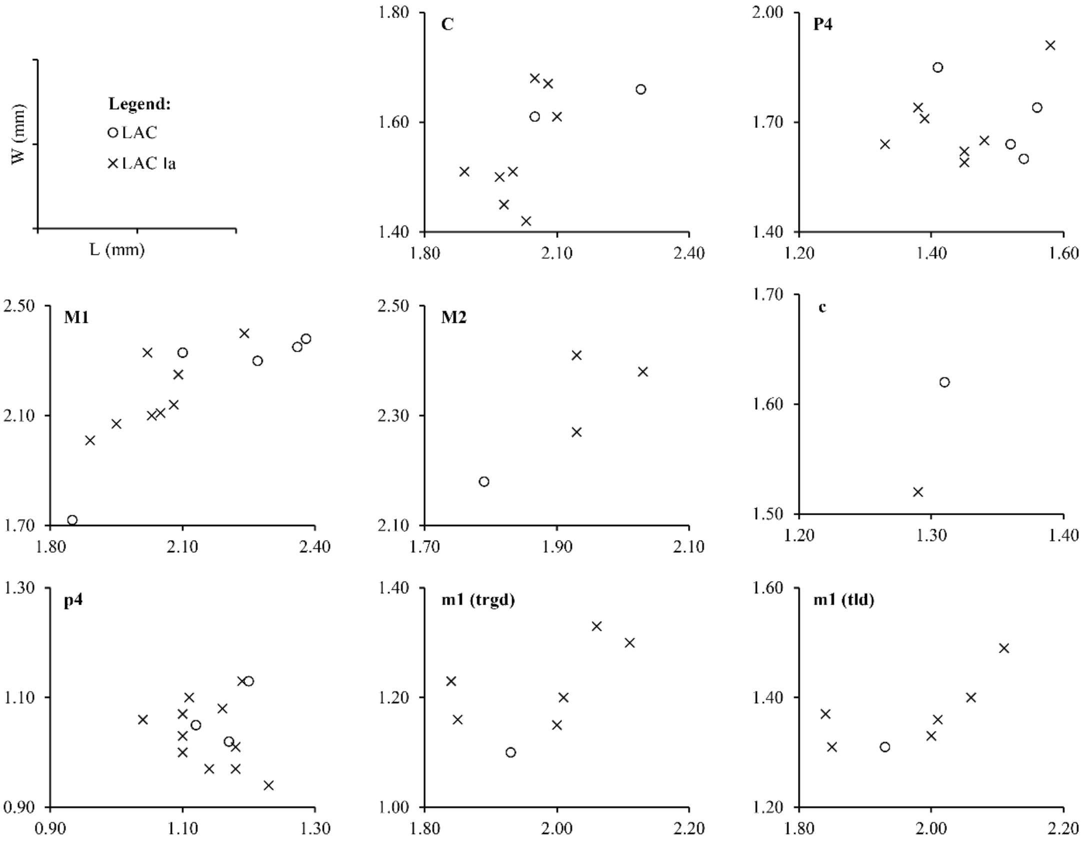

Figure 4.52 *Eptesicus serotinus*, Loutra Almopias Cave A. XY graphs with the measured (in mm) dental elements (C, P4, M1, M2, c, p4, m1). L: length, W: width, trgd: trigonid; tld: talonid.

c: Very robust tooth with the cusp slightly curved lingually. It is trapezoidal in occlusal view. It is convex mesiolabially and concave distally and mesiolingually. The distal part of the tooth is developed at the base of the crown, whereas the mesial part is developed in height. Respectively, the crown is in a more superior position towards the anterior part of the tooth. The distolabial part of the tooth is situated lower than the distolingual, which is higher than the former. The cingulum is very thick throughout the whole tooth. It reaches its maximum thickness at the mesiolingual part of the tooth, where a cingular cusplet is present, and it is absent at the mesial part where it comes in contact with i3. An additional cingular cusplet is present at the distolingual part of the tooth.

p3: Unicuspid. It is subcircular in occlusal view. The labial side is more convex than the lingual. The cingulum is very thick. It reaches its maximum thickness at its mesiolingual and distolingual parts, where one cusp-like form is present on each part.

p4: Very robust tooth. It is subrectangular in occlusal view. The lingual part of the tooth is higher than the labial part. The crown is concave mesiolabially, slightly concave mesiolingually and convex distally. The cingulum is very thick and uniform throughout the whole tooth and it bends down slightly at the level of each root, with the posterior convexity being placed slightly lower than the anterior. Two cusp-like forms are also present, one mesiolingually and one distolingually.

m1: Myotodont. The trigonid is longer than the talonid. Paraconid, metaconid, entoconid, protoconid and hypoconid are well-developed. The protoconid is taller than the hypoconid. The paralophid is concave. The entocristid is straight. The hypoconulid is well-developed and it is placed in line with the lingual cusps. The labial cingulum is very thick throughout the whole tooth and it bends down slightly at the level of each root, with the posterior convexity being placed slightly lower than the anterior. Lingual cingulum of the trigonid is also present.

m2: The trigonid and the talonid are of almost equal length. Trigonid is also wider than in m1. The paraconid, which is more developed than in m1 and/or the other cusps, is in a more lingual position and thus, it is not in line with the other lingual cusps. The rest of the characters as m1.

m3: Myotodont. The trigonid and the talonid are of almost equal length. Paraconid, metaconid, entoconid, protoconid and hypoconid are moderately developed. The protoconid is taller than the hypoconid. The paralophid is concave. The entocristid is straight. The entoconid is more towards the labial side of the tooth and thus, the talonid is reduced. The hypoconulid is also significantly reduced. The labial cingulum is very thick throughout the whole tooth.

Mandible: The masseter crest is thick and steep. The mental foramen is beneath p3. The lowest part of the symphysis is relatively rounded and it slightly projects downwards.

Discussion The morphological features described in addition to the measurements allow a definite attribution of the material to *Eptesicus serotinus*. It is the largest member of the two Serotine Bat species that currently occur in Greece and it is clearly distinguished from the rest of the species.

Occurrence Fossils of the Serotine Bat are known only from Sarakenos Cave. Its modern distribution includes practically all mainland Greece, several Aegean and Ionian Islands and Crete (Hanák et al. 2001, GFDC 2021). On a global scale it is distributed from Northern Africa to Western Europe and all the way to China and the Korean Peninsula and Taiwan (Simmons 2005a).

Ecology *Eptesicus serotinus* is a cave dweller and its habitat preferences include both open and forested areas with or without the presence of water bodies (Dietz et al. 2009).

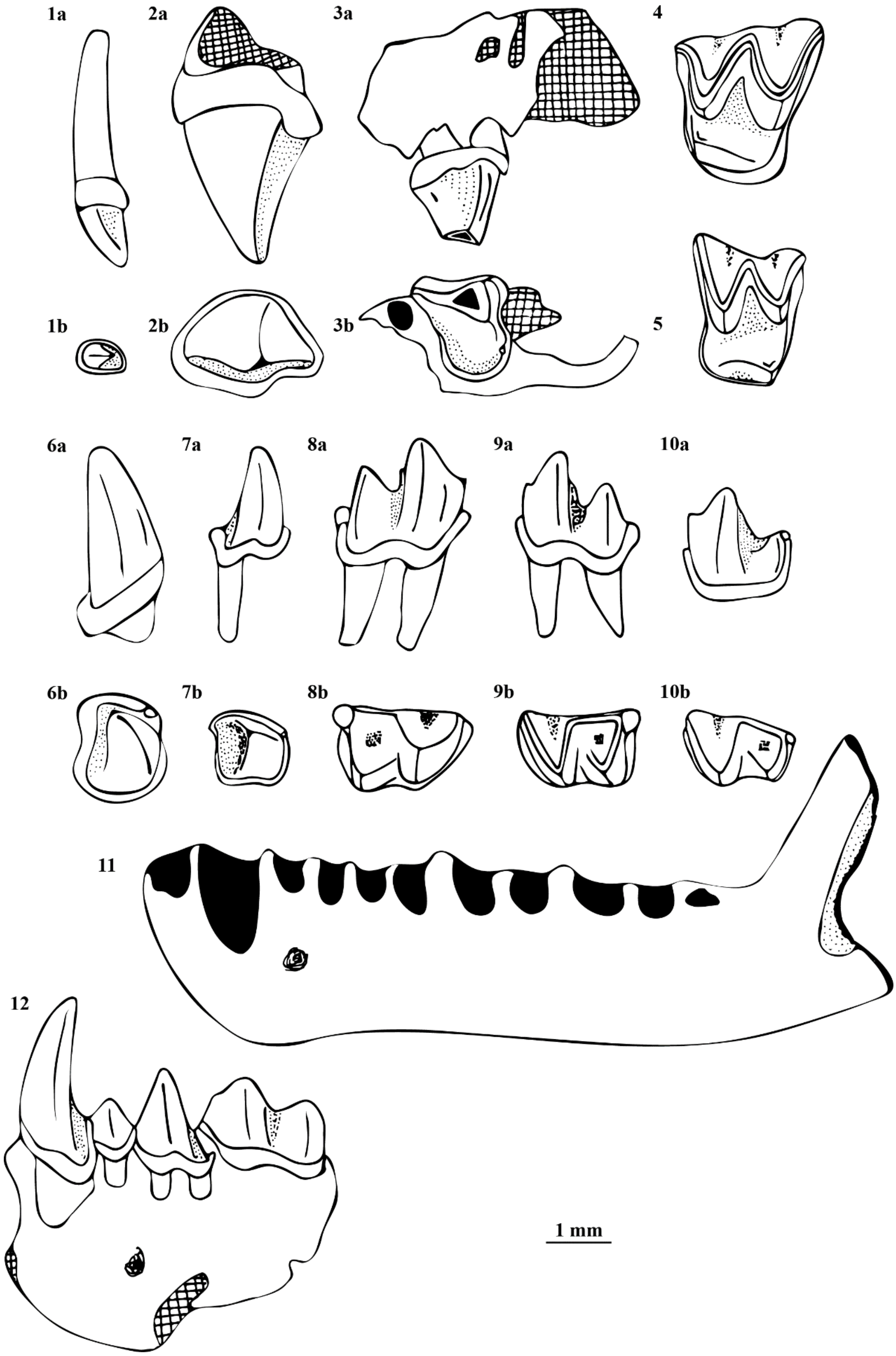

Figure 4.53 *Eptesicus serotinus*, Loutra Almopias Cave A. **1.** LAC26391 – Left I1 (**a.** labial, **b.** occlusal), **2.** LAC22175 – Left C (**a.** labial, **b.** occlusal), **3.** LAC23291 – Right maxillary fragment with P4 (**a.** labial, **b.** occlusal), **4.** LAC27694 – Left M1, **5.** LAC20116 – Right M2, **6.** LAC17914 – Right c (**a.** labial, **b.** occlusal), **7.** LAC21077 – Right p4 (**a.** labial, **b.** occlusal), **8.** LAC23480 – Right m1 (**a.** labial, **b.** occlusal), **9.** LAC26968 – Left m2 (**a.** labial, **b.** occlusal), **10.** LAC27019 – Left m3 (**a.** labial, **b.** occlusal), **11.** LAC19497 – Left mandibular fragment, **12.** LAC26802 – Left mandibular fragment with c-m1.

***Plecotus* Geoffroy Saint-Hilaire, 1818**

Type species *Vespertilio auritus* Linnaeus, 1758

The earliest occurrence of *Plecotus* in the global fossil record is *Plecotus schoepfelii* from the Early Miocene (MN3) localities of Petersbuch 28 and 62, Germany (Rosina and Rummel 2012). The earliest (prior to this research) occurrence of *Plecotus* in the fossil record of Greece is *Plecotus austriacus* from the Holocene layers of Charkadio Cave, Tilos (Piskoulis and Chatzopoulou in press). There are currently four species occurring in Greece (*Plecotus auritus*, *Plecotus austriacus*, *Plecotus kolombatovici* and *Plecotus macrobullaris*) (Hanák et al. 2001, Simmons 2005a, Sfougaris 2009).

The dental formula of *Plecotus* is: 2.1.2.3/3.1.3.3 and there are several morphological characteristics that distinguish *Plecotus* from other chiropteran taxa, such as the absence of heel/talon on the upper molars, myotodont lower molars, very short and blunt styloid process of the humerus and no lateral projection of the condyle and the epicondyle. However, species discrimination within the genus is more complex, as all species share very similar characteristics and thus, identification of fossils at species level is based almost exclusively on size.

***Plecotus auritus* Linnaeus, 1758 *vel Plecotus austriacus* Fischer, 1829**

(Brown Long-eared Bat *vel* Gray Long-eared Bat)

Figure 4.55 and Figure A.70-71

Fossiliferous locality LAC III

Age Late Pleistocene

Material 1 identified specimen

LAC III: 1 left maxillary fragment with M2-M3 (19143)

Fossiliferous locality LAC Ia

Age latest Pleistocene

Material 3 identified specimens

2 left M2 (24644, 24716), 1 right mandibular fragment with m1-m2 (22526)

Measurements Table 4.22 and Figure 4.54

Description The scanty specimens that have been attributed to the genus *Plecotus* are not enough for species discrimination and thus they are all grouped as *Plecotus auritus/austriacus*.

Table 4.22 *Plecotus auritus*//*austriacus*, Loutra Almopias Cave A. Measurements (in mm) from both LAC and LAC Ia. LAC: Late Pleistocene; LAC Ia: latest Pleistocene; n: number of measurable specimens; L: length; W: width; trgd: trigonid; tld: talonid; MEAN: average; MIN: minimum; MAX: maximum; SD: standard deviation; CV: coefficient of variation.

			n	**MEAN**	**MIN**	**MAX**	**SD**	**CV**
M2	LAC	L	1	1.30	-	-	-	-
		W	1	1.60	-	-	-	-
	LAC Ia	L	2	1.45	1.40	1.49	0.064	4.404
		W	2	1.62	1.59	1.64	0.035	2.189
M3	LAC	L	1	1.22	-	-	-	-
		W	1	1.55	-	-	-	-
m1	LAC Ia	L	1	1.41	-	-	-	-
		W (trgd)	1	0.77	-	-	-	-
		W (tld)	1	0.91	-	-	-	-
m2	LAC Ia	L	1	1.40	-	-	-	-
		W (trgd)	1	0.79	-	-	-	-
		W (tld)	1	0.91	-	-	-	-

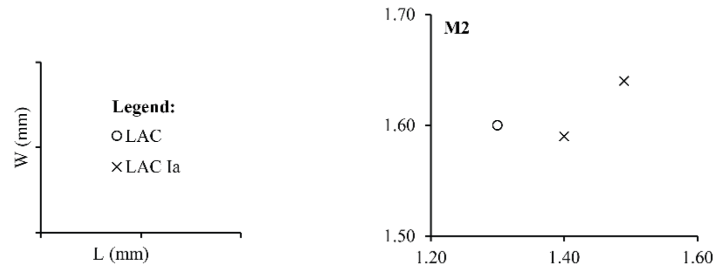

Figure 4.54 *Plecotus auritus*/*austriacus*, Loutra Almopias Cave A. XY graphs with the measured (in mm) dental elements (M2). L: length, W: width

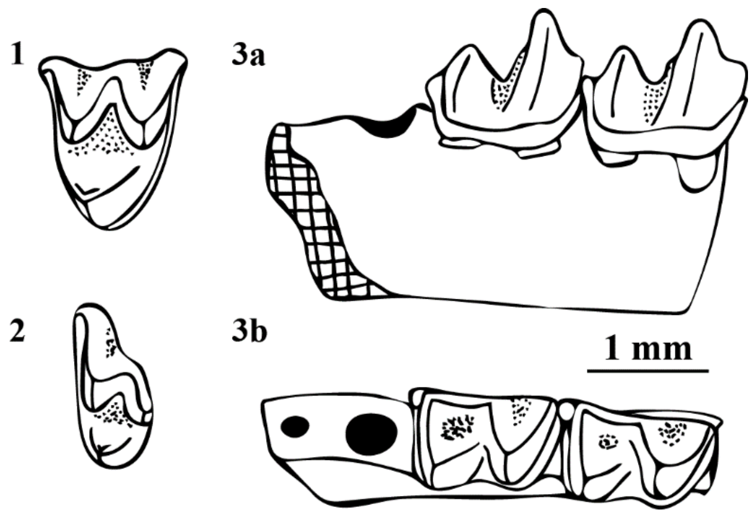

Figure 4.55 *Plecotus auritus/austriacus*, Loutra Almopias Cave A. **1.** LAC24644 – Left M2, **2.** LAC19143 – Left M3, **3.** LAC22526 – Right mandibular fragment with m1-m2 (**a.** labial, **b.** occlusal).

M2: Medium-sized tooth. It is subrectangular in occlusal view. Parastyle, mesostyle, metastyle, paracone and metacone are well-developed. The metacone is taller than the paracone. The parastyle forms an angle with the preparacrista and the metastyle slightly curves lingually. The mesial part of the ectoloph is narrower than the distal part. Additionally, the paracone, the metacone and the cristae on both sides form equal angles. Paraloph, metaloph and metaconule are absent. The paraconule is not well-developed. The cingulum, which is of average thickness, is continuous throughout the whole tooth.

M3: Medium-sized tooth. It is triangular in occlusal view. The parastyle, the paracone, the mesostyle and the metacone are well-developed, whereas the metastyle is absent, as well as the postmetacrista that connects the metastyle with the metacone. The paracone is taller than the metacone. The parastyle forms an angle with the preparacrista. The crista that connects the paracone with the mesostyle is shorter than the crista that connects the mesostyle with the metacone. The paraconule is not well-developed. The cingulum, which is of average thickness, is continuous throughout the whole tooth.

m1: Myotodont. The trigonid is longer than the talonid. Paraconid, metaconid, entoconid, protoconid and hypoconid are well-developed. The protoconid is taller than the hypoconid. The paralophid is angular. The entocristid is concave. The hypoconulid is located at a more lingual position than the entoconid, as well as the paraconid and thus, the lingual cusps are not aligned. The labial cingulum is thick and uniform throughout the whole tooth. Lingual cingulum of the trigonid is also present.

m2: The trigonid and the talonid are of almost equal length. The labial cingulum develops a notch between the trigonid and the talonid. The rest of the characters as m1.

Discussion *Plecotus auritus* and *Plecotus austriacus* not only share very similar characteristics, but they also overlap in size, with the former being only slightly smaller than the latter and thus, species discrimination between the aforementioned is nearly impossible. The scanty specimens, the morphological features described in addition to the measurements allow attribution of the material to *Plecotus auritus/austriacus*.

Occurrence Fossils of the Brown/Gray Long-eared Bat are known only from Charkadio Cave, Tilos (viz. *Plecotus austriacus*). The modern distribution of *Plecotus auritus* includes Northwestern Greece and some mountainous areas of Northern and Central Greece and Peloponnese, whereas the modern distribution of *Plecotus austriacus* includes Northeastern Greece and some mountainous areas of Northern and Central Greece (Hanák et al. 2001, GFDC 2021). On a global scale it is distributed from

North Africa to the Iberian Peninsula, the British Isles, Norway and all the way to India, Nepal, China, the Korean Peninsula and Japan (Simmons 2005a).

Ecology Both *Plecotus auritus* and *Plecotus austriacus* hibernate in hollow trees and caves, while the habitat preferences of the former include temperate forests (and similar areas), whereas the habitat preferences of the latter include open landscapes with warmer climate (Dietz et al. 2009).

***Barbastella* Gray, 1821**

Type species *Vespertilio barbastellus* Schreber, 1774

The earliest occurrence of *Barbastella* in the global fossil record is *Barbastella maxima* from the Late Miocene locality of Gritsev, Ukraine (Rosina et al. 2019). There is currently one species occurring in Greece (*Barbastella barbastellus*) (Hanák et al. 2001, Simmons 2005a). Fossils of *Barbastella* are described in Greece for the first time from Loutra Almopias Cave A.

The dental formula of *Barbastella* is: 2.1.2.3/3.1.2.3 and there are several morphological characteristics that distinguish *Barbastella* from other chiropteran taxa, such as the absence of heel/talon on the upper molars, nyctalodont lower molars, very small size, very short and blunt styloid process of the humerus and no lateral projection of the condyle and the epicondyle.

***Barbastella barbastellus* Schreber, 1774**

(Western Barbastelle Bat)

Figure 4.57 and Figure A.72

Fossiliferous locality LAC I, LAC Ib, LAC Ic, LAC II, LAC III

Age Late Pleistocene

Material 225 identified specimens

LAC I: 1 left maxillary fragment with M1-M2 (27484), 1 right C (27480), 1 right P4 (19982), 1 left M2 (19990), 1 right m2 (17261), 1 left m2 (19928), LAC Ib: 2 right C (17137, 16528), 1 left C (19885), 1 left P4 (16536), 4 right M1 (16695, 19901, 17167, 16538), 1 left mandibular fragment (16606), 1 right m1 (17155), 1 left m2 (16514), 2 right m3 (17156, 16516), 1 left m3 (16548), LAC Ic: 3 left I1 (17870, 17921, 17965), 5 right C (17919, 17962, 18010, 18011, 18073), 2 left C (17869, 17990), 1 right P4 (18006), 1 left M1 (17925), 2 right M2 (17887, 17950), 1 left M2 (17949), 1 right M3 (17911), 1 left M3 (17888), 2 right c (17960, 18054), 1 left c (17941), 1 right p4 (17918), 1 left p4 (17933), 3 right m1 (17889, 17954, 16420), 2 left m1 (17952, 17976), 3 right m2 (17928, 21479, 21482), 2 left m2 (17927, 17977), 5 right m3 (17872, 17930, 17955, 17979, 17980), 4 left m3 (17931, 17932, 18008, 21493), LAC II: 3 right C (21552, 22428, 27556), 7 left C (21809, 21880, 21967, 22023, 27575, 27709, 27939), 1 right

P4 (21751), 1 right M1-2 (27693), 13 right M1 (16046, 16057, 21715, 21727, 21897, 22007, 22041, 22260, 22285, 22286, 22372, 27653, 27692), 6 left M1 (16048, 21891, 22075, 22151, 22359, 27757), 1 right M2 (22360), 4 left M2 (21697, 22008, 22289, 27871), 1 right mandibular fragment with c-p4 (21579), 1 left mandibular fragment with p4 (16676), 1 left mandibular fragment with m1-m2 (16371), 1 right mandibular fragment with m2-m3 (27727), 2 right m1 (22209, 27729), 6 left m1 (21525, 21639, 21643, 21650, 22226, 27564), 3 right m2 (16062, 22205, 27642), 4 left m2 (22126, 22351, 27766, 27772), 3 right m3 (21522, 27578, 27723), 2 left m3 (16358, 27638), 2 right humeri (27749, 27750), LAC III: 13 right C (20125, 20127, 20129, 20214, 20216, 20217, 21216, 21396, 21404, 20074, 20302, 20489, 20492), 16 left C (20091, 20213, 20717, 21208, 21395, 17713, 21121, 21136, 21213, 19305, 20079, 20291, 20385, 20396, 20487, 20488), 2 right P4 (20375, 20471), 2 left P4 (21188, 21189), 5 right M1 (20844, 21310, 20036, 20662, 20669), 8 left M1 (20756, 20757, 20846, 21321, 20893, 21183, 20034, 20546), 5 right M2 (20803, 17472, 21305, 19146, 20670), 3 left M2 (21331, 20462, 20467), 1 left M3 (20178), 1 right mandibular fragment with m2-m3 (21051), 1 right c (20309), 4 left c (21409, 21410, 21206, 19159), 3 right p4 (21176, 20048, 20350), 2 left p4 (21179, 20652), 5 right m1 (20151, 21269, 20013, 20014, 20439), 8 left m1 (20786, 20865, 17703, 21165, 19335, 20435, 20437, 20539), 15 right m2 (20152, 20247, 20861, 21263, 21265, 21069, 21162, 20018, 20339, 20430, 20532, 20533, 20602, 20624, 20625), 3 left m2 (20158, 20788, 20025), 2 right m3 (17704, 21070), 2 left m3 (21168, 19158), 1 left humerus (20507)

Fossiliferous locality LAC Ia

Age Late Pleistocene

Material 124 identified specimens

1 left maxillary fragment with P4-M2 (23134), 1 left maxillary fragment with M1 (23213), 1 right maxillary fragment with M2-M3 (26506), 2 left maxillary fragments with M2-M3 (23111, 26533), 5 right C (25442, 25735, 26119, 26248, 27062), 5 left C (25536, 25586, 25904, 26210, 26543), 1 right P4 (25237), 9 right M1 (24369, 24580, 24583, 24601, 24639, 24651, 24666, 26570, 26608), 12 left M1 (24675, 24676, 24693, 24717, 24842, 24958, 24971, 25131, 25155, 26624, 26638, 26661), 4 right M2 (24594, 24624, 24625, 26607), 3 left M2 (24728, 24859, 24893), 1 right M3 (25144), 4 left M3 (25000, 25070, 25091, 25122), 2 left mandibular fragments (26857, 26863), 1 left mandibular fragment with c-p3 (22852), 1 right mandibular fragment with c-p4 (22617), 1 left mandibular fragment with p3-p4 (26821), 1 left mandibular fragment with p4 (22943), 1 left mandibular fragment with p4 and m2 (19704),1 left mandibular fragment with m1-m2 (22836), 1 left mandibular fragment with m1-m3 (22710), 1 right mandibular fragment with m2 (22579), 1 left mandibular fragment with m2-m3 (26811), 3 right mandibular fragments with m3 (22638, 22643, 22688), 1 right c (26355), 3 left c (26222, 26357, 26358), 2 right p4 (24249, 26827), 1 left p4 (24355), 4 right m1 (23389, 23597, 26895, 27363), 10 left m1 (23764, 23847, 23937, 23977, 24014, 24030, 24052, 26822, 26959, 27393), 10 right m2 (23316, 23443, 23513, 23533, 23570, 23591, 23603, 23619, 23690, 26901), 8 left m2 (22846, 23952, 23976, 23979, 24064, 24069, 24132, 27285), 7 right m3 (23385, 23634, 23653, 23683, 23721, 26765, 26919), 3 left m3 (24105, 24176, 27399), 6 right humeri (26443, 26446, 27203, 27204, 27209, 27447), 6 left humeri (26415, 26424, 277216, 27218, 27222, 27227)

Measurements Table 4.23 and Figure 4.56

Description *Barbastella barbastellus* is the sole member of the Barbastelles that currently occur in Greece.

I1: Bicuspid. It is oval in occlusal view. The mesial cusp is the largest and it covers more than half of the tooth's area. Both cusps curve lingually. A thin cingulum is also present throughout the whole tooth.

C: Small-sized tooth with the cusp curved distally. It is oval in occlusal view. The crown forms practically no angle with the root. A small heel is present at the mesiolingual part of the tooth. The crown is convex mesially, slightly concave distolabially and concave distolingually. Two longitudinal grooves occur, one labially and one lingually. The cingulum is of average thickness throughout the whole tooth. A small cingular platform is present at the mesiolingual part of the tooth.

Table 4.23 *Barbastella barbastellus*, Loutra Almopias Cave A. Measurements (in mm) from both LAC and LAC Ia. LAC: Late Pleistocene; LAC Ia: latest Pleistocene; n: number of measurable specimens; L: length; W: width; trgd: trigonid; tld: talonid; MEAN: average; MIN: minimum; MAX: maximum; SD: standard deviation; CV: coefficient of variation.

			n	MEAN	MIN	MAX	SD	CV
I1	LAC	L	3	0.64	0.62	0.67	0.025	3.912
		W	3	0.42	0.39	0.45	0.031	7.217
C	LAC	L	50	1.03	0.88	1.21	0.068	6.586
		W	49	0.74	0.62	0.88	0.060	8.094
	LAC Ia	L	10	1.03	0.96	1.08	0.045	4.333
		W	10	0.74	0.70	0.79	0.029	3.906
P4	LAC	L	8	0.96	0.91	1.01	0.034	3.577
		W	1	1.10	-	-	-	-
	LAC Ia	L	2	0.88	0.79	0.97	0.127	14.464
		W	2	1.30	1.25	1.35	0.071	5.439
M1	LAC	L	33	1.26	1.04	1.42	0.092	7.259
		W	33	1.32	1.02	1.48	0.086	6.561
	LAC Ia	L	23	1.24	1.03	1.38	0.093	7.469
		W	23	1.29	1.13	1.49	0.096	7.390
M2	LAC	L	13	1.27	1.13	1.35	0.061	4.781
		W	15	1.41	1.23	1.59	0.104	7.352
	LAC Ia	L	11	1.26	1.15	1.42	0.075	6.001
		W	10	1.40	1.30	1.49	0.050	3.600
M3	LAC	L	3	1.14	1.05	1.21	0.082	7.180
		W	3	1.38	1.37	1.39	0.012	0.835
	LAC Ia	L	8	1.13	1.09	1.21	0.046	4.104
		W	8	1.35	1.29	1.49	0.062	4.612
c	LAC	L	9	0.58	0.47	0.69	0.065	11.125
		W	9	0.65	0.57	0.75	0.055	8.492
	LAC Ia	L	6	0.58	0.50	0.64	0.050	8.583
		W	6	0.66	0.62	0.72	0.038	5.750
p3	LAC	L	1	0.33	-	-	-	-
		W	1	0.36	-	-	-	-
	LAC Ia	L	3	0.42	0.40	0.45	0.025	5.945
		W	3	0.45	0.41	0.48	0.035	7.862
p4	LAC	L	8	0.72	0.66	0.77	0.042	5.856
		W	8	0.56	0.47	0.67	0.065	11.733
	LAC Ia	L	7	0.74	0.64	0.80	0.053	7.061
		W	7	0.54	0.51	0.60	0.032	5.797

m1	LAC	L	26	1.36	1.20	1.46	0.073	5.367
		W (trgd)	28	0.66	0.48	0.81	0.078	11.712
		W (tld)	28	0.72	0.60	0.89	0.067	9.223
	LAC Ia	L	16	1.34	1.23	1.40	0.053	3.983
		W (trgd)	16	0.60	0.50	0.77	0.071	11.783
		W (tld)	16	0.68	0.59	0.77	0.046	6.756
m2	LAC	L	34	1.24	1.11	1.35	0.049	3.954
		W (trgd)	36	0.68	0.61	0.79	0.045	6.553
		W (tld)	36	0.71	0.64	0.82	0.038	5.410
	LAC Ia	L	23	1.22	1.11	1.31	0.057	4.678
		W (trgd)	23	0.66	0.59	0.78	0.049	7.350
		W (tld)	23	0.70	0.63	0.77	0.043	6.178
m3	LAC	L	22	1.11	1.03	1.21	0.050	4.483
		W (trgd)	23	0.63	0.54	0.74	0.058	9.109
		W (tld)	23	0.51	0.43	0.63	0.054	10.509
	LAC Ia	L	15	1.09	0.93	1.23	0.087	7.980
		W (trgd)	15	0.63	0.49	0.76	0.073	11.612
		W (tld)	15	0.49	0.36	0.55	0.057	11.672
m1-m3	LAC Ia	L	1	3.53	-	-	-	-
c-p4	LAC	L	1	1.59	-	-	-	-
	LAC Ia	L	1	1.68	-	-	-	-
Humerus	LAC	W	3	2.85	2.79	2.92	0.067	2.339
	LAC Ia	W	11	2.81	2.57	3.06	0.140	4.986

P4: Small-sized tooth, with the cusp being connected with a crista to an accessory distolabial cusplet. It is subrectangular in occlusal view. A well-developed heel is present at the mesiolingual part of the tooth. The crown is convex mesiolabially, relatively concave labially and mesially and concave lingually. The base of the crown is concave mesially labially and distally. The cingulum is thin and it reaches its maximum thickness at its mesiolingual part. A cingular widening occurs at the mesiolabial part of the tooth.

M1: Small-sized tooth. It is subrectangular in occlusal view. Parastyle, mesostyle, metastyle, paracone and metacone are well-developed. The metacone is slightly taller than the paracone. The parastyle forms an angle with the preparacrista and the metastyle slightly curves lingually. The mesial part of the ectoloph is narrower than the distal part. Additionally, the paracone, the metacone and the cristae on both sides form equal angles. Paraloph, metaloph and metaconule are absent. The paraconule is not well-developed. The crown is mildly constricted distally. The cingulum is thin and continuous throughout the whole tooth.

M2: The mesial part of the ectoloph is wider than in M1. The rest of the characters as M1.

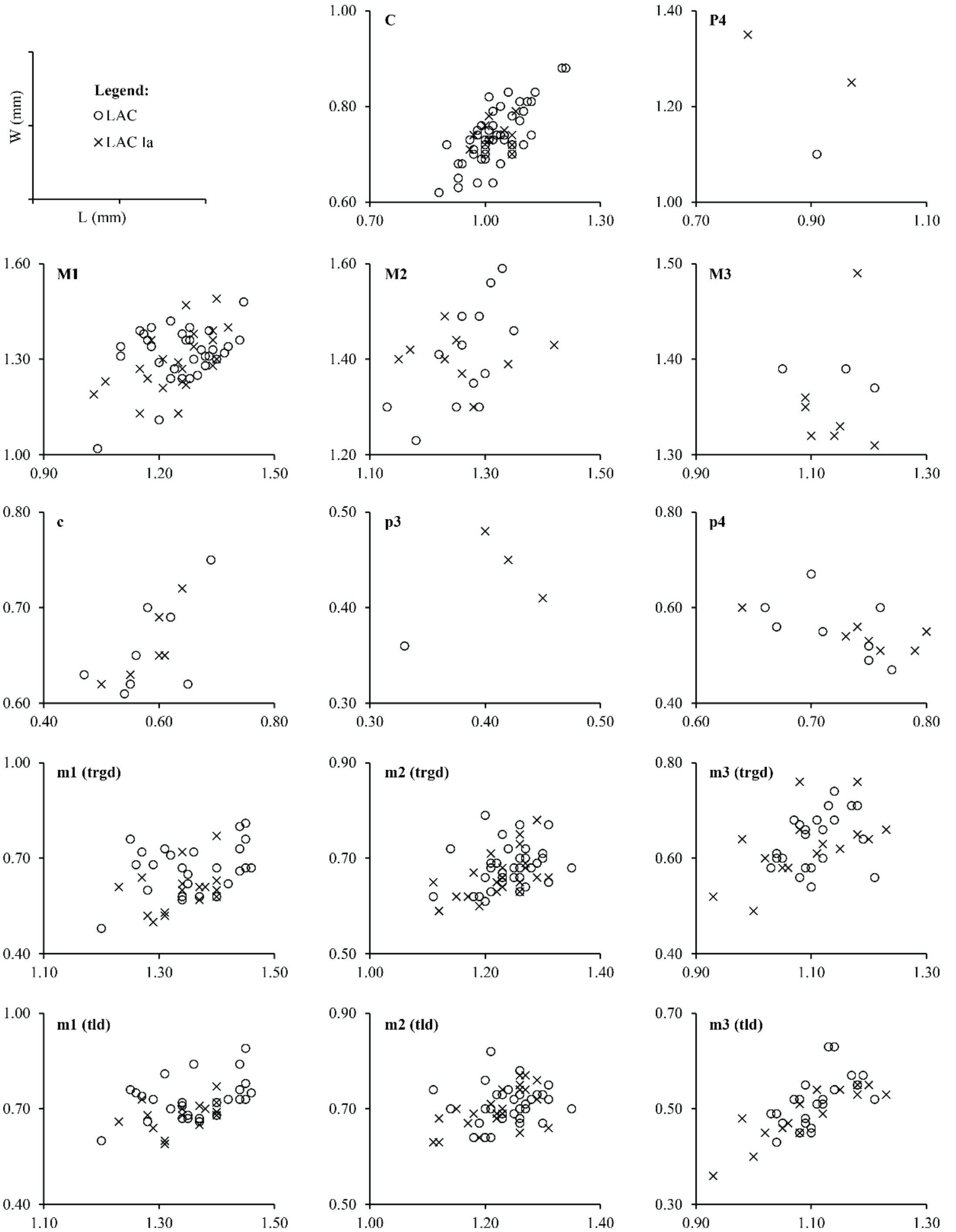

Figure 4.56 *Barbastella barbastellus*, Loutra Almopias Cave A. XY graphs with the measured (in mm) dental elements (C, P4, M1, M2, M3, c, p3, p4, m1, m2, m3). L: length, W: width, trgd: trigonid; tld: talonid.

M3: Small-sized tooth. It is triangular in occlusal view. The parastyle and the paracone are more developed than the mesostyle and the metacone, with the latter being minute, whereas the metastyle is absent, as well as the postmetacrista that connects the metacone with the metastyle. The paracone is taller than the metacone. The parastyle forms an angle with the preparacrista. Paraloph, metaloph and metaconule are absent. The paraconule is not well-developed. The cingulum is thin and continuous throughout the whole tooth.

c: Small-sized tooth with the cusp slightly curved lingually. It is subtriangular in occlusal view. It is convex mesially and concave distally. The distal part of the tooth is developed at the base of the crown, whereas the mesial part is developed in height. Respectively, the crown is in a more superior position towards the anterior part of the tooth. The cingulum is thick throughout the whole tooth and it reaches its maximum thickness at the mesiolingual and distolingual parts of the tooth, where two cingular cusplets are present and connected with a widened lingual crista.

p3: Very small unicuspid tooth. It is subcircular in occlusal view. The cingulum is thick and it reaches its maximum thickness labially.

p4: Small-sized tooth with the cusp slightly curved mesially. It is trapezoidal in occlusal view. The crown is convex mesiolabially, slightly concave distally and flat lingually. The cingulum is thick and concave towards the roots and it reaches its maximum thickness at the mesiolingual and distolingual parts of the tooth, where two cingular cusplets are present and connected with a widened lingual crista.

m1: Nyctalodont. The trigonid is longer than the talonid. Paraconid, metaconid, entoconid, protoconid and hypoconid are well-developed. The protoconid is taller than the hypoconid. The paralophid is angular. The entocristid is concave. The hypoconulid is well-developed and it is positioned to a more labial position than the entoconid and thus, the lingual cusps are not aligned. The labial cingulum, which is of average thickness throughout the whole tooth, develops an imperceptible thickening beneath the protoconid, whereas it bends down slightly at the level of each root, with the posterior convexity being placed slightly lower than the anterior.

m2: The paraconid is in a more lingual position. The trigonid is wider than in m1. The labial cingulum is flat and uniform. Lingual cingulum of the trigonid is also present. The rest of the characters as m1.

m3: Nyctalodont. The trigonid is longer than the talonid. Paraconid, metaconid and protoconid are better developed than the entoconid and the hypoconid, which are reduced. The protoconid is taller than the hypoconid. The paralophid is angular. The entocristid is concave. The entoconid is more towards the labial side of the tooth and the hypoconid towards the lingual and thus, the talonid is reduced. The hypoconulid is reduced. The labial cingulum is slightly thinner than in m1 and m2 and uniform throughout the whole tooth. Lingual cingulum of the trigonid is absent.

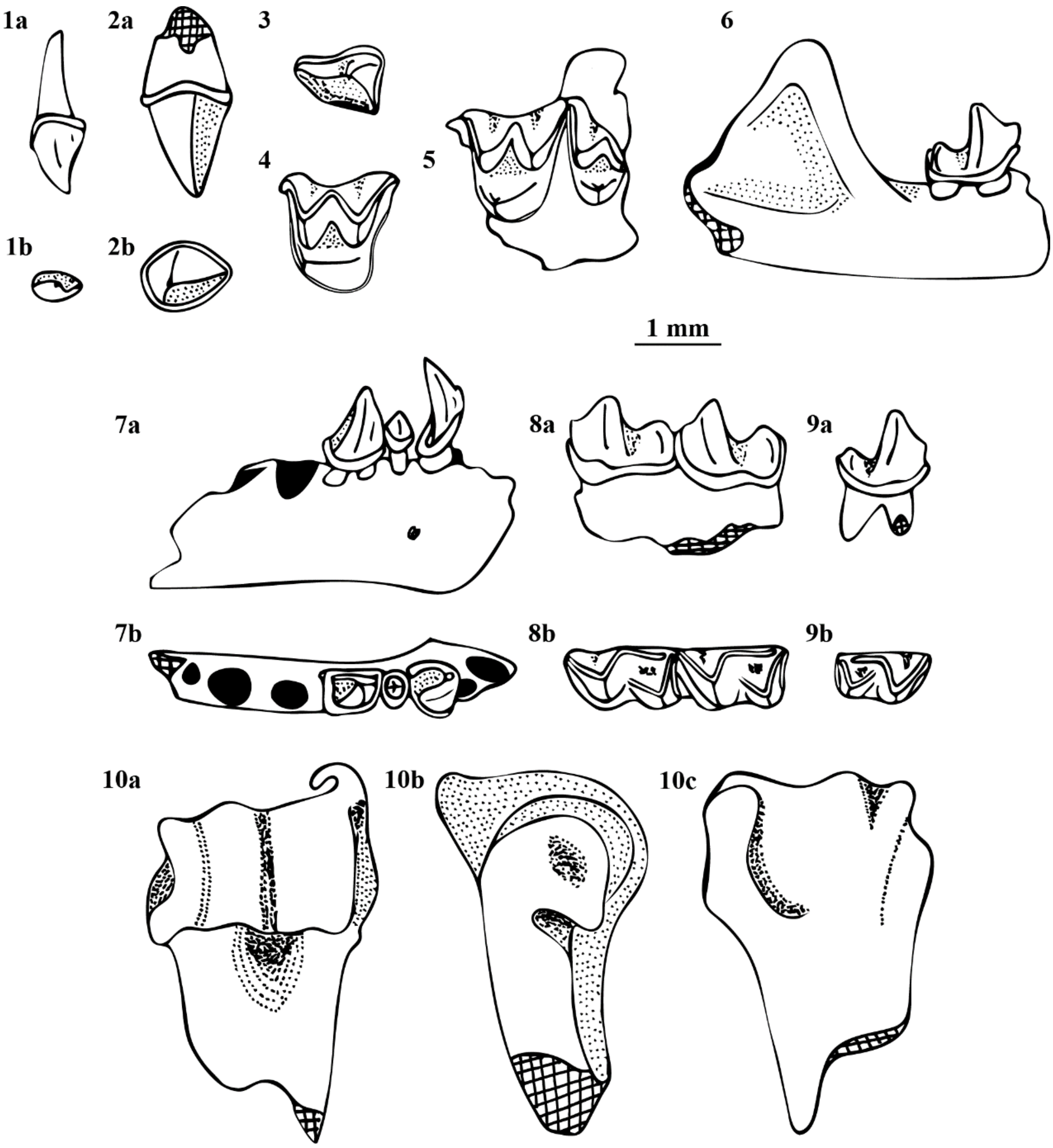

Figure 4.57 *Barbastella barbastellus*, Loutra Almopias Cave A. **1.** LAC17870 – Left I1 (**a.** labial, **b.** occlusal), **2.** LAC27575 – Left C (**a.** labial, **b.** occlusal), **3.** LAC20471 – Right P4, **4.** LAC22359 – Left M1, **5.** LAC23111 – Left maxillary fragment with M2-M3, **6.** LAC22688 – Right mandibular fragment with m3, **7.** LAC22617 – Right mandibular fragment with c-p4 (**a.** labial, **b.** occlusal), **8.** LAC16371 – Left mandibular fragment with m1-m2 (**a.** labial, **b.** occlusal), **9**. LAC17156 – Right m3 (**a.** labial, **b.** occlusal), **10.** LAC26415 – Distal epiphysis of left humerus (**a.** anterior, **b.** lateral, **c.** posterior).

Mandible: The coronoid process is angular. The masseter crest is thick and relatively steep. The anterior sigmoid notch is almost flat and relatively steep. The articular process is situated on approximately the same level as the superior part of the mandibular body. The angular process projects diagonally downwards. The mental foramen is beneath the gap between c and p3. The lowest part of the symphysis is relatively rounded and it slightly projects downwards.

Humerus: The styloid process is short and blunt (triangular in lateral view). The epitrochlea is short and wide. The valley between the trochlea and the condyle is shallow. A shallow valley is also present between the condyle and the epicondyle. The condyle and the epicondyle are not projecting laterally. The radial fossa is deep, whereas the olecranon fossa is relatively shallow and it extends from the middle part of the epiphysis to the styloid process.

Discussion The morphological features described in addition to the measurements allow a definite attribution of the material to *Barbastella barbastellus*. It is the sole member of the Barbastelles that currently occur in Greece.

Occurrence The fossils of the Western Barbastelle Bat described from Loutra Almopias Cave A are the first known records of this species in Greece. Its modern distribution includes Northeastern, Northern and Central mainland Greece (Hanák et al. 2001, GFDC 2021). On a global scale it is distributed from Northwestern Africa to Western Europe and England all the way to Caucasus (including Bulgaria, Turkey, Crimea Peninsula, the Canary Islands and several other Mediterranean Islands) and possibly Senegal (Simmons 2005a).

Ecology *Barbastella barbastellus* is a cave dweller and its habitat preferences include mostly forested areas (Dietz et al. 2009).

4.3 FAMILY MINIOPTERIDAE

Miniopteridae Mein and Tupinier, 1977

Miniopteridae, the Long-fingered Bats, comprise a single genus, *Miniopterus*, which currently includes at least 19 extant species that span throughout most parts of Eurasia, Africa and Australia (Simmons 2005a).

Miniopterus Bonaparte, 1837

Type species *Vespertilio ursinii* Bonaparte, 1837 (= *Vespertilio schreibersii* Kuhl, 1817)

The earliest occurrence of *Miniopterus* in the global fossil record is *Miniopterus fossilis* from the Middle Miocene (MN6a) locality of Zapfe’s fissures, Slovakia (Sabol and Holec 2002)[8]. The earliest occurrence of *Miniopterus* in the fossil record of Greece is *Miniopterus schreibersii* from the Early Pleistocene locality of Vathy, Kalymnos (Kuss 1973). There is currently one species occurring in Greece (*Miniopterus schreibersii*) (Hanák et al. 2001, Simmons 2005a). The latter is also present in the fossil record of Greece (Piskoulis and Chatzopoulou in press).

The dental formula of *Miniopterus* is: 2.1.3.3/3.1.3.3 and there are several morphological characteristics that distinguish Miniopteridae – and consequently *Miniopterus* – from other chiropteran taxa, such as the presence of heel on the upper molars, nyctalodont lower molars, third upper and third lower premolars with three and two roots respectively, long and flat styloid process of the humerus and no lateral projection of the condyle and the epicondyle.

***Miniopterus schreibersii* Kuhl, 1817**

(Schreibers' Bent-winged Bat)

Figure 4.60 and Figure A.73

Fossiliferous locality LAC I, LAC Ib, LAC Ic, LAC II, LAC III

Age Late Pleistocene

Material 556 identified specimens

LAC I: 3 right C (17244, 19946, 19991), 4 left C (19944, 19945, 19947, 17225), 1 left M1 (19979), 1 left M2 (17250), 1 right M3 (19981), 1 left mandibular fragment (17265), 1 right m1 (16644), 1 left m1 (19929), 1 right m2 (27508), 1 left m3 (16636), LAC Ib: 3 right C (16527, 18687, 19868), 6 left C (17160, 16526, 16529, 19862, 19883, 19897), 1 right M3 (19881), 1 left mandibular fragment with c-p3 (16428), 1 right mandibular fragment with m1-m2 (16429), 1 right c (19864), 1 right p4 (17188), 3 right m1 (17154, 19876, 19888), 2 right m2 (17169, 17139), 1 right humerus (16578), 1 left humerus (19904), LAC Ic: 2 right C (17881, 17989), 4 left C (17936, 17988, 21432, 21433), 2 right M1 (21461, 21463), 3 left M3 (17981, 18004, 18005), 2 right mandibular fragments (17873, 17935), 1 left mandibular fragment (17997), 3 right c (17992, 18014, 21440), 3 left c (18015, 18016, 21434), 1 right p3 (18053), 1 left p4 (18047), 4 right m1 (17953, 17975, 18067, 21475), 2 left m1 (17978, 21481), 2 right m3 (16423, 16142), LAC II: 1 left maxillary fragment with P3-P4 (16663), 1 left maxillary fragment with P4-M1 (16670), 4 right maxillary fragments M2-M3 (16382, 16383, 16156, 16157), 13 right C (16079, 21777, 21788, 21972, 22022, 22179, 22180, 22392, 22415, 22416, 22425, 27707, 27903), 20 left C (16065, 21877, 21957, 21958, 22052, 22053, 22093, 22100, 22170, 22176, 22177, 22178, 22419, 22424, 27567, 27581, 27762, 27815, 27906, 27909), 1 right P3 (16376), 1 left P3 (22197), 8 right P4 (21544, 22106, 22160, 22311, 22318, 22319, 22320, 22377), 10 left P4 (21741, 21742, 22045, 22048, 22104, 22105, 22165, 22312, 22313, 27699), 10 right M1 (16053, 16058, 22078, 22147, 22149, 22152, 22153, 16381, 22272, 22355), 17 left M1 (16694a, 21676, 21682, 21686, 21703, 21696, 21700, 21887, 21921, 22039, 22040, 22146, 22281, 22288, 22357, 22370, 27746), 1 left M1-2 (27872), 8 right M2 (16054, 21717, 21718,

[8] This is preferred here because *Miniopterus* sp. from the Early Miocene of Europe mentioned by McKenna and Bell (1997), lacks sufficient information.

21719, 21720, 21724, 22268, 27821), 11 left M2 (21679, 21683, 21702, 21705, 21711, 21693, 21889, 22141, 22148, 22270, 27601), 6 right M3 (21605, 22158, 22373, 22375, 27586, 27839), 1 left M3 (21894), 6 right mandibular fragments (16698, 16017, 16374, 22396, 22399, 27579), 6 left mandibular fragments (16022, 16412, 16414, 22405, 22406, 27596), 1 right mandibular fragment with i3-p4 (16662), 1 right mandibular fragment with p2-p4 (16011), 2 right mandibular fragments with p4-m1 (21516, 21576), 1 left mandibular fragment with p4-m2 (16168), 4 right mandibular fragments with m1-m2 (21568, 16026, 16027, 16399), 1 left mandibular fragment with m1-m3 (16116), 7 right mandibular fragments with m2-m3 (21571, 21572, 16397, 27634, 27635, 27852, 27853), 1 left mandibular fragment with m2-m3 (27824), 2 right c (21786, 22417), 6 left c (16013, 21803, 22169, 22181, 22328, 27704), 1 right p3 (22407), 1 left p3 (16375), 1 right p4 (22129), 2 left p4 (22137, 22408), 12 right m1 (21532, 21623, 21831, 22033, 16135, 22111, 22117, 22119, 22203, 22207, 16167, 22344), 16 left m1 (21534, 21587, 21854, 21916, 16356, 21990, 22011, 22065, 22123, 22124, 16405, 16406, 22227, 27681, 27885, 27886), 2 right m1-2 (22064, 27744), 10 right m2 (21569, 21610, 21829, 21830, 21832, 16665, 16355, 22118, 22342, 27754), 6 left m2 (21651, 16122, 22231, 27647, 27848, 27929), 10 right m3 (21519, 21617, 16125, 16392, 22215, 22216, 16170, 27669, 27740, 27882), 3 left m3 (21526, 21592, 21658), 2 right humeri (27738, 27763), 3 left humeri (27711, 27751, 27927), LAC III: 1 left maxillary fragment with M2-M3 (20958), 29 right C (20201, 20210, 20700, 20701, 20704, 20709, 20710, 20821, 20829, 20838, 21211, 21375, 21388, 21393, 20877, 17712, 20946, 21020, 21134, 21202, 21203, 19301, 20305, 20395, 20485, 20581, 20583, 20584, 20585), 28 left C (20088, 20209, 20706, 20715, 17492, 21209, 21215, 21399, 20878, 20879, 20883, 20884, 17718, 17865, 21120, 21129, 19161, 19302, 19303, 20073, 20295, 20310, 20394, 20397, 20399, 20490, 20494, 20586), 1 left P3 (20560), 8 right P4 (20817, 17715, 19315, 19317, 20561, 20562, 20566, 20680), 10 left P4 (20733, 20760, 20818, 21347, 21348, 21350, 17714, 16449, 19316, 20682), 9 right M1 (20730, 20794, 20795, 21087, 21095, 21181, 20452, 20554, 20660), 6 left M1 (20792, 21325, 21328, 20896, 20926, 20673), 9 right M2 (20797, 21308, 20897, 20956, 20029, 20448, 20556, 20658, 20659), 11 left M2 (20754, 20755, 20806, 21323, 21333, 21184, 20461, 20657, 20672, 20674, 20675), 4 right M3 (20750, 21322, 20678, 20679), 7 left M3 (20174, 20809, 21237, 20366, 20455, 20456, 20457), 16 right mandibular fragments (20832, 21241, 21242, 16458, 21062, 21148, 20327, 20329, 20413, 20414, 20515, 20516, 20518, 20603, 20604, 20606), 13 left mandibular fragments (20005, 21244, 21246, 21247, 21251, 16465, 20973, 21064, 20332, 20611, 20612, 20613, 20614), 1 right mandibular fragment with p2-p3 (21231), 1 right mandibular fragment with p4-m1 (20831), 6 right mandibular fragments with m1-m2 (20765, 21226, 21144, 20410, 20513, 20601), 2 left mandibular fragments with m1-m2 (20233, 20769), 1 right mandibular fragment with m2-m3 (20408), 1 left mandibular fragment with m2-m3 (20519), 16 right c (19159b, 20100, 20702, 20718, 21402, 21408, 20876, 20954, 21117, 21130, 19300, 20082, 20312, 20386, 20391, 20582), 27 left c (20491, 20094, 20208, 20705, 20708, 20713, 20736, 20822, 20825, 20828, 21394, 21401, 21406, 21033, 21036, 21131, 21132, 21194, 19306a, 19306b, 20081, 20389, 20392, 20495, 20506, 20587, 20590), 2 right p3 (20226, 21234), 3 right p4 (20759, 21007, 20351), 5 left p4 (16436, 20520, 20545, 20651, 20653), 12 right m1 (20249, 20738, 20772, 20773, 20776, 20777, 20833, 20862, 21229, 20531, 20626, 20628), 12 left m1 (20156, 20157, 20743, 20767, 20789, 21277, 21072, 21166, 19333, 20609, 20635, 20636), 7 right m2 (17702, 16457, 20006, 20407, 20425, 20427, 20510), 10 left m2 (20729, 20746, 20785, 20911, 21285, 16453, 16454, 16455, 20537, 20638), 6 right m3 (20739, 21273, 16450, 20981, 19156, 20631), 4 left m3 (21057, 19336, 20344, 20641), 1 right humerus (20508), 1 left humerus (20228)

Fossiliferous locality LAC Ia

Age latest Pleistocene

Material 399 identified specimens

4 right maxillary fragments with P3-P4 (23286, 23287, 23288, 23290), 2 left maxillary fragments with P3-P4 (19714, 23264), 2 left maxillary fragments with P3-M1 (19730, 23147), 1 right maxillary fragment with P3-M3 (27239), 1 right maxillary fragment with P4-M1 (23127), 4 left maxillary fragments with P4-M1 (23143, 23144, 23145, 23146), 1 left maxillary fragment with P4-M2 (23151), 3 right maxillary fragments with P4-M3 (19761, 23076, 23077), 1 left maxillary fragment with P4-M3 (19757), 2 right

maxillary fragments with M1-M2 (23086, 24984), 6 right maxillary fragments with M1-M3 (19733, 23078, 23079, 23080, 23082, 26503), 2 left maxillary fragments with M1-M3 (23070, 23071), 8 right maxillary fragments with M2-M3 (23089, 23094, 23097, 23167, 23168, 24985, 26504, 26505), 4 left maxillary fragments with M2-M3 (23109, 23113, 23116, 26534), 18 right C (25443, 25673, 25782, 25973, 26052, 26083, 26097, 26098, 26104, 26115, 26133, 26145, 26166, 26197, 26209, 26226, 26247, 27411), 22 left C (25449, 25658, 25771, 25805, 25807, 25866, 25868, 25884, 25983, 26025, 26044, 26063, 26094, 26103, 26110, 26131, 26138, 26142, 26161, 27127, 27130, 27427), 3 right P3 (25429, 26352, 26524), 1 left P3 (23263), 18 right P4 (25257, 25259, 25261, 25276, 25277, 25279, 25280, 25281, 25282, 25283, 25295, 25297, 25322, 25325, 25326, 26689, 27238, 27342), 12 left P4 (23266, 25329, 25359, 25360, 25361, 25362, 25364, 25366, 25368, 25369, 25408, 26706), 14 right M1 (23228, 24370, 24373, 24440, 24448, 24472, 24482, 24600, 24615, 24628, 24653, 24654, 24658, 26573), 23 left M1 (23206, 23235, 24697, 24699, 24701, 24703, 24709, 24735, 24737, 24740, 24741, 24750, 24776, 24911, 24959, 24960, 24967, 24982, 26621, 26628, 26647, 27329, 27330), 17 right M2 (24365, 24374, 24384, 24407, 24429, 24441, 24468, 24495, 24511, 24536, 24541, 24576, 24584, 24603, 26507, 26602, 27304), 14 left M2 (24682, 24700, 24704, 24738, 24744, 24752, 24777, 24811, 24872, 24896, 24913, 24968, 26632, 26641), 6 right M3 (24987, 25182, 25207, 25210, 25215, 25216), 8 left M3 (25011, 25075, 25117, 25119, 25120, 25123, 26682, 26683), 6 right mandibular fragments (22968, 22971, 22979, 22987, 23725, 26839), 5 left mandibular fragments (23025, 23051, 23052, 23059, 23065), 1 right mandibular fragment with i2-m2 (19638), 1 left mandibular fragment with i3-p3 (22939), 1 right mandibular fragment with i3-p4 (22626), 1 left mandibular fragment with i3-p4 and m2 (22772), 1 left mandibular fragment with c, p4 and m1 (22804), 1 left mandibular fragment with p2-p4 (22789), 1 right mandibular fragment with p2-m2 (19666), 1 left mandibular fragment with p2-m2 (26806), 1 right mandibular fragment with p2-m3 (27262), 1 left mandibular fragment with p2-m3 (19499), 3 right mandibular fragments with p3-p4 (22658, 22662, 22664), 2 left mandibular fragments with p3-p4 (22782, 22803), 1 right mandibular fragment with p3 and m1 (22614), 2 right mandibular fragments with p3-m1 (19489, 22684), 1 left mandibular fragment with p3-m1 (22758), 1 right mandibular fragment with p3 and m2 (22463), 1 right mandibular fragment with p3-m2 (22601), 1 right mandibular fragment with p3-m3 (22513), 7 left mandibular fragments with p3-m3 (19632, 19633, 19647, 22716, 22718, 22722, 26793), 4 right mandibular fragments with p4-m1 (19665, 22512, 22540, 22555), 2 left mandibular fragments with p4-m1 (19679, 22800), 1 right mandibular fragment with p4-m2 (22509), 3 left mandibular fragments with p4-m2 (19646, 22741, 22834), 1 left mandibular fragment with p4 and m3 (26800), 3 right mandibular fragments with p4-m3 (22458, 22553, 22486), 2 left mandibular fragments with p4-m3 (19630, 22719), 4 right mandibular fragments with m1-m2 (19639, 19643, 22561, 22648), 7 left mandibular fragments with m1-m2 (19502, 19677, 22729, 22730, 26798, 26823, 27279), 4 right mandibular fragments with m1-m3 (19611, 22562, 22598, 22613), 3 left mandibular fragments with m1-m3 (19653, 22706, 22713), 8 right mandibular fragments with m2-m3 (19661, 22451, 22468, 22607, 22610, 22494, 22682, 26733), 6 left mandibular fragments with m2-m3 (22867, 22900, 22906, 22919, 22930, 26815), 6 right c (26000, 26014, 26024, 26062, 26208, 26354), 3 left c (25432, 26111, 26125), 1 right p2 (26343), 1 left p3 (27405), 4 right p4 (24216, 24262, 24267, 24268), 5 left p4 (22797, 24282, 24353, 26278, 27408), 12 right m1 (22621, 22676, 22692, 23332, 23426, 23447, 23510, 23514, 23565, 23581, 26746, 26749), 14 left m1 (19649, 19680, 22810, 22839, 23940, 23964, 23981, 24021, 24045, 24056, 24135, 26825, 26984, 27280), 1 left m1-2 (24018), 6 right m2 (22491, 23517, 23592, 26755, 26756, 26891), 7 left m2 (19625, 22748, 22756, 22837, 22895, 24070, 26956), 9 right m3 (19696, 22500, 22639, 23402, 23307, 23658, 23697, 23698, 23714), 14 left m3 (22869, 22883, 24079, 24084, 24088, 24090, 24091, 24092, 24109, 24110, 24158, 26820, 27007, 26807), 16 right humeri (26428, 26430, 26431, 26432, 26433, 26434, 26435, 26437, 26440, 26442, 26444, 26445, 26447, 26450, 27205, 27211), 15 left humeri (26412, 26413, 26414, 26416, 26417, 26418, 26419, 26421, 26423, 26425, 26426, 27215, 27219, 27221, 27225)

Measurements Table 4.24 and Figure 4.58-59

<u>Description</u> *Miniopterus schreibersii* is the sole member of the Bent-winged Bats that currently occurs in Greece.

C: Medium-sized tooth with the cusp slightly curved distally. It is oval in occlusal view. The crown is in line with the root and it is convex labially, slightly concave mesially and distally and flat lingually. Four longitudinal grooves occur, two labially and two lingually. The cingulum is of average thickness throughout the whole tooth.

Table 4.24 *Miniopterus schreibersii*, Loutra Almopias Cave A. Measurements (in mm) from both LAC and LAC Ia. LAC: Late Pleistocene; LAC Ia: latest Pleistocene; n: number of measurable specimens; L: length; W: width; trgd: trigonid; tld: talonid; MEAN: average; MIN: minimum; MAX: maximum; SD: standard deviation; CV: coefficient of variation.

			n	**MEAN**	**MIN**	**MAX**	**SD**	**CV**
C	LAC	L	111	1.05	0.85	1.16	0.046	4.361
		W	111	0.81	0.66	0.91	0.045	5.555
	LAC Ia	L	40	1.01	0.85	1.09	0.454	4.483
		W	40	0.82	0.71	0.89	0.043	5.225
P3	LAC	L	4	0.92	0.83	0.99	0.077	8.442
		W	4	0.95	0.85	1.02	0.074	7.830
	LAC Ia	L	13	0.97	0.88	1.09	0.059	6.085
		W	13	0.91	0.77	1.02	0.064	6.992
P4	LAC	L	36	1.11	0.95	1.27	0.075	6.724
		W	31	1.35	1.23	1.50	0.050	3.729
	LAC Ia	L	49	1.12	0.95	1.27	0.073	6.547
		W	47	1.32	1.12	1.48	0.079	6.005
M1	LAC	L	43	1.41	1.13	1.59	0.096	6.800
		W	42	1.53	1.37	1.71	0.088	5.729
	LAC Ia	L	55	1.41	1.24	1.52	0.052	3.676
		W	56	1.43	1.23	1.64	0.094	6.547
M2	LAC	L	38	1.40	1.16	1.51	0.062	4.463
		W	39	1.63	1.35	1.84	0.117	7.137
	LAC Ia	L	56	1.41	1.27	1.56	0.063	4.470
		W	57	1.60	1.29	1.76	0.100	6.240
M3	LAC	L	25	1.38	1.20	1.47	0.078	5.663
		W	25	1.62	1.31	1.76	0.111	6.809
	LAC Ia	L	39	1.32	1.01	1.46	0.079	5.945
		W	39	1.58	1.27	1.72	0.090	5.711
i2	LAC Ia	L	2	0.52	0.43	0.60	0.120	23.341
		W	2	0.40	0.36	0.43	0.050	12.531
i3	LAC	L	1	0.53	-	-	-	-
		W	1	0.50	-	-	-	-
	LAC Ia	L	4	0.55	0.50	0.59	0.045	8.145
		W	4	0.50	0.46	0.54	0.037	7.468
c	LAC	L	59	0.67	0.55	0.79	0.053	7.873
		W	59	0.79	0.60	0.94	0.054	6.888

	LAC Ia	L	14	0.63	0.59	0.68	0.027	4.313
		W	14	0.78	0.73	0.83	0.035	4.441
p2	LAC	L	3	0.53	0.50	0.57	0.036	6.803
		W	3	0.56	0.47	0.61	0.076	13.602
	LAC Ia	L	8	0.53	0.45	0.62	0.048	8.898
		W	8	0.60	0.52	0.69	0.054	8.901
p3	LAC	L	7	0.64	0.62	0.66	0.014	2.210
		W	7	0.60	0.46	0.69	0.089	14.970
	LAC Ia	L	28	0.59	0.45	0.67	0.044	7.599
		W	28	0.60	0.52	0.65	0.033	5.587
p4	LAC	L	17	0.71	0.66	0.82	0.042	5.817
		W	17	0.72	0.59	0.81	0.059	8.151
	LAC Ia	L	51	0.71	0.54	0.81	0.049	6.871
		W	51	0.70	0.58	0.81	0.049	6.914
m1	LAC	L	67	1.46	1.33	1.58	0.057	3.888
		W (trgd)	74	0.83	0.63	1.00	0.074	8.927
		W (tld)	72	0.91	0.71	1.05	0.056	6.083
	LAC Ia	L	76	1.43	1.29	1.58	0.051	3.538
		W (trgd)	78	0.81	0.67	0.93	0.057	7.130
		W (tld)	79	0.91	0.72	1.00	0.048	5.252
m2	LAC	L	53	1.39	1.27	1.51	0.058	4.180
		W (trgd)	59	0.82	0.69	0.95	0.062	7.580
		W (tld)	55	0.87	0.78	0.99	0.041	4.731
	LAC Ia	L	68	1.35	1.06	1.56	0.070	5.197
		W (trgd)	70	0.79	0.65	0.93	0.060	7.504
		W (tld)	67	0.85	0.70	0.94	0.050	5.899
m3	LAC	L	38	1.20	1.11	1.38	0.067	5.584
		W (trgd)	38	0.70	0.57	0.96	0.062	8.900
		W (tld)	38	0.63	0.51	0.80	0.050	7.922
	LAC Ia	L	56	1.20	0.99	1.31	0.052	4.314
		W (trgd)	59	0.70	0.55	0.80	0.045	6.467
		W (tld)	56	0.62	0.36	0.70	0.056	9.046
M1-M3	LAC Ia	L	13	3.49	3.29	3.64	0.112	3.219
P4-M3	LAC Ia	L	5	4.30	4.14	4.50	0.132	3.078
m1-m3	LAC	L	1	3.96	-	-	-	-
	LAC Ia	L	18	3.95	3.82	4.03	0.059	1.499
p4-m3	LAC Ia	L	13	4.57	4.44	4.67	0.065	1.424
c-p4	LAC Ia	L	4	2.40	2.34	2.47	0.059	2.465
LSC	LAC Ia	L	4	10.45	9.75	11.00	0.579	5.546
Humerus	LAC	L	-	-	-	-	-	-
		W	9	2.73	2.54	2.87	0.104	3.798
	LAC Ia	L	1	25.83	-	-	-	-
		W	31	2.85	2.60	3.06	0.136	4.794

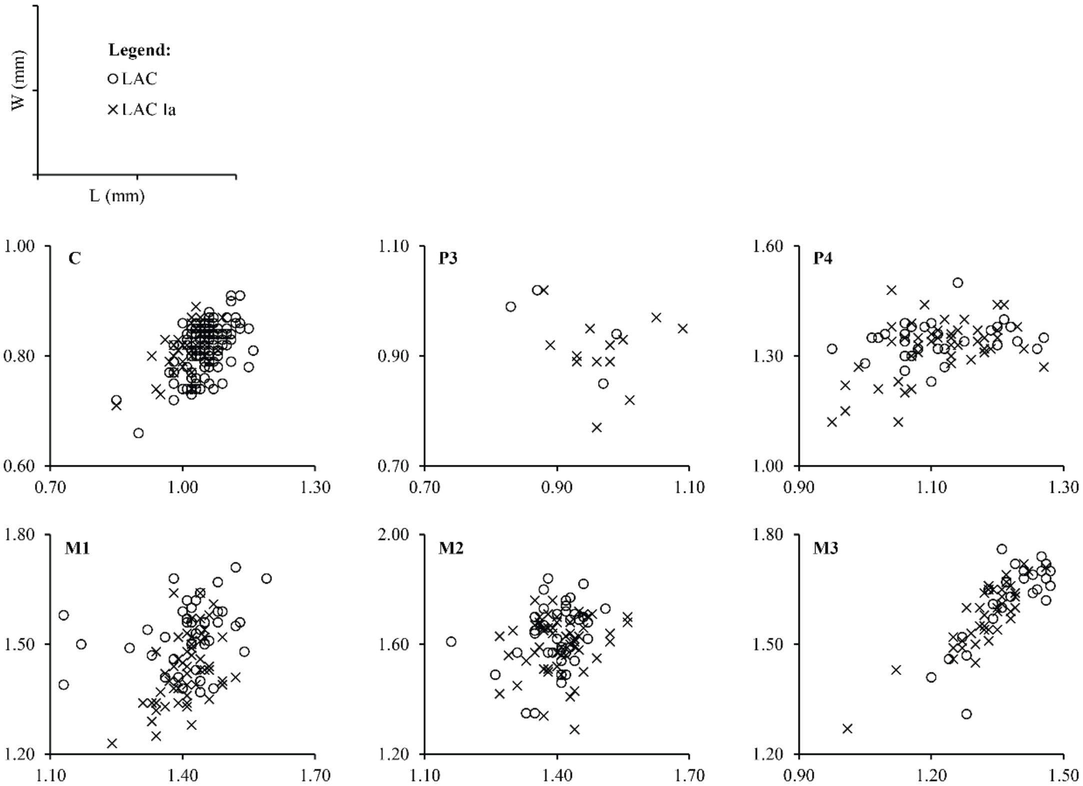

Figure 4.58 *Miniopterus schreibersii*, Loutra Almopias Cave A. XY graphs with the measured (in mm) dental elements (C, P3, P4, M1, M2, M3). L: length, W: width.

P3: Unicuspid tooth with three roots. It is subtriangular in occlusal view. The cusp is developed towards the mesiolabial part of the tooth. Two cingular platforms are present mesiolingually and labially and a small heel is present lingually. The cingulum is relatively thin throughout the whole tooth.

P4: Medium-sized tooth with the cusp being connected with a crista to an accessory distolabial cusplet. It is trapezoidal in occlusal view. A well-developed heel is present at the lingual part of the tooth. The crown is convex labially and concave mesially and lingually. The cingulum is relatively thin throughout the whole tooth. A cingular cusplet is present at the mesiolingual part of the tooth and a cingular platform is present at the mesiolabial part.

M1: Medium-sized tooth. It is subrectangular in occlusal view. A well-developed rounded heel is present at the distolingual part of the tooth without hypocone. Parastyle, mesostyle, metastyle, paracone and metacone are well-developed. The metacone and the paracone are approximately of the same height. The parastyle is curved. The mesial part of the ectoloph is narrower than the distal part. Additionally, the paracone and the cristae on both sides form a wider angle than the metacone and the respective cristae. Paraloph, metaloph, paraconule and metaconule are well-developed. The cingulum, which is relatively thin, is continuous throughout the whole tooth, with its maximum thickness being around the heel.

M2: The heel is shorter, but wider than in M1. The mesial part of the ectoloph is wider than in M1. The rest of the characters as M1.

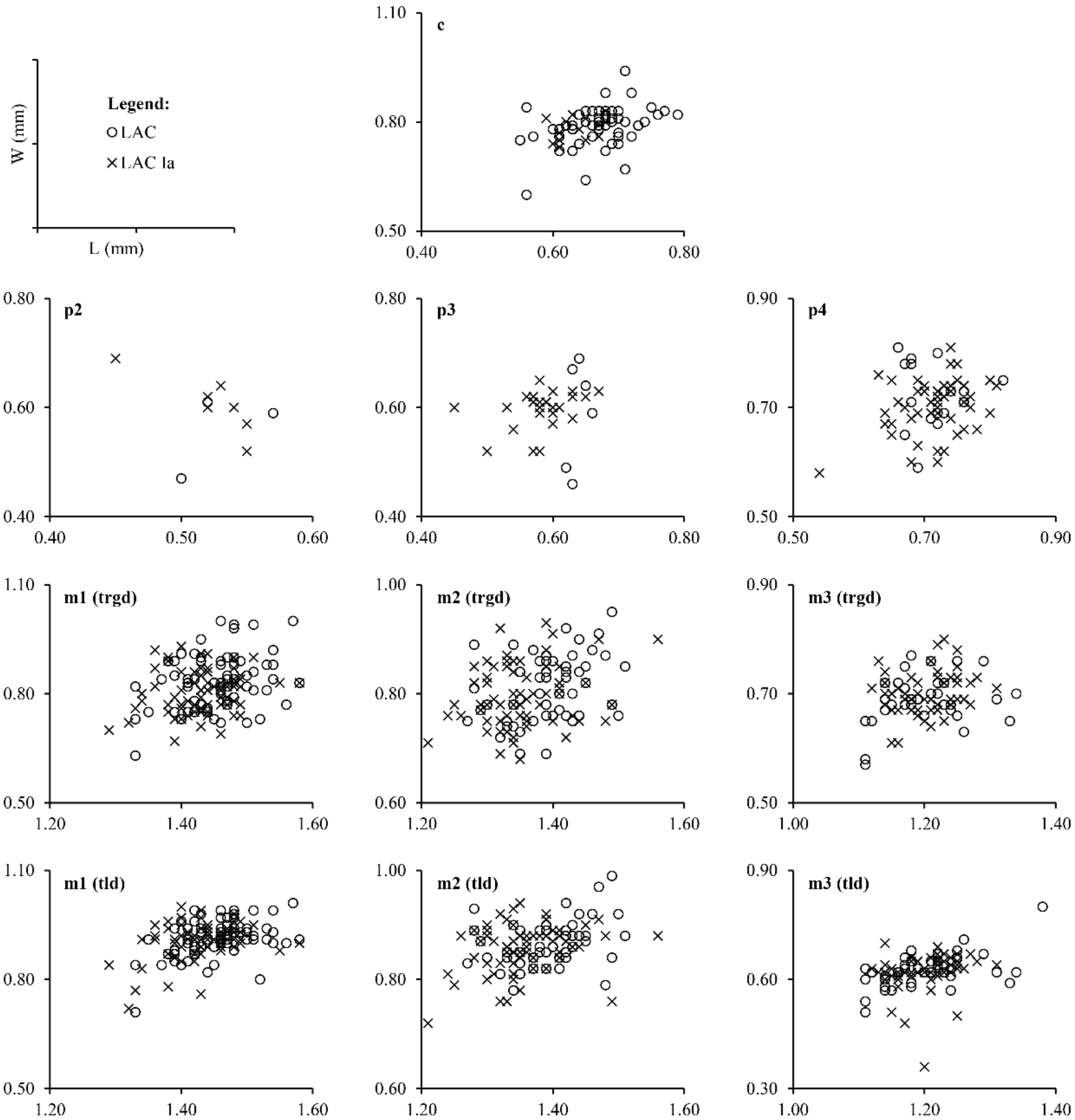

Figure 4.59 *Miniopterus schreibersii*, Loutra Almopias Cave A. XY graphs with the measured (in mm) dental elements (c, p2, p3, p4, m1, m2, m3). L: length, W: width, trgd: trigonid; tld: talonid.

M3: Medium-sized tooth. It is triangular in occlusal view. Parastyle, mesostyle, paracone and metacone are well-developed, whereas the metastyle and the postmetacrista are absent. The paracone is slightly taller than the metacone. The parastyle is curved. Paraloph is present. The cingulum, which is thin, is continuous throughout the whole tooth, apart from the distal end (beneath the metacone).

i2: Oval in occlusal view. Three cusps are present at the labial part of the tooth. The middle cusp is the largest of the three with the mesial and the distal cusps being of equal size.

i3: Oval in occlusal view. Two cusps are present at the labial part of the tooth and one at its lingual part. The mesial cusp is the smallest and the middle one is the largest. A deep valley separates the two mesial cusps from the distal cusp.

c: Medium-sized tooth with the cusp slightly curved lingually. It is trapezoidal in occlusal view. It is convex labially and concave distally and lingually. The distal part of the tooth is developed at the base of the crown, whereas the mesial part is developed in height. Respectively, the crown is in a more superior position towards the mesial part of the tooth. The distolabial part of the tooth is situated lower than the distolingual, which is higher than the former. The cingulum is thin throughout the whole tooth and it is absent at the mesial part where it comes in contact with i3. It reaches its maximum thickness at the mesiolingual and distolingual parts of the tooth, where two cingular cusplets are present and connected with a widened lingual crista.

p2: Unicuspid tooth, with a single root and with the cusp slightly curved distally. It is subcircular in occlusal view. The crown is convex mesiolabially and slightly concave distally and lingually. The cingulum, which is thin throughout the whole tooth is absent mesially, where it comes into contact with c. A cingular cusplet is present mesiolingually.

p3: Unicuspid tooth with two roots and with the cusp slightly curved mesially. It is subrectangular in occlusal view. The crown is convex mesiolabially and slightly concave distally and lingually. The cingulum is thin. Two cingular cusplets are present, one mesiolingually and one distolingually.

p4: The cingular cusplets are well-developed. It is overall larger and more robust than p3. The rest of the characters as p3.

m1: Nyctalodont. The trigonid and the talonid are of almost equal length. Paraconid, metaconid, entoconid, protoconid and hypoconid are well-developed. The protoconid is taller than the hypoconid. The paralophid is concave. The entocristid is slightly curved. The hypoconulid is well-developed and it is positioned to a more labial position than the entoconid and thus, the lingual cusps are not aligned. The labial cingulum is thick beneath the protoconid and slightly thinner beneath the hypoconid. Lingual cingulum of the trigonid is also present.

m2: The talonid is longer than the trigonid. The thickening of the labial cingulum is less pronounced than in m1. The rest of the characters as m1.

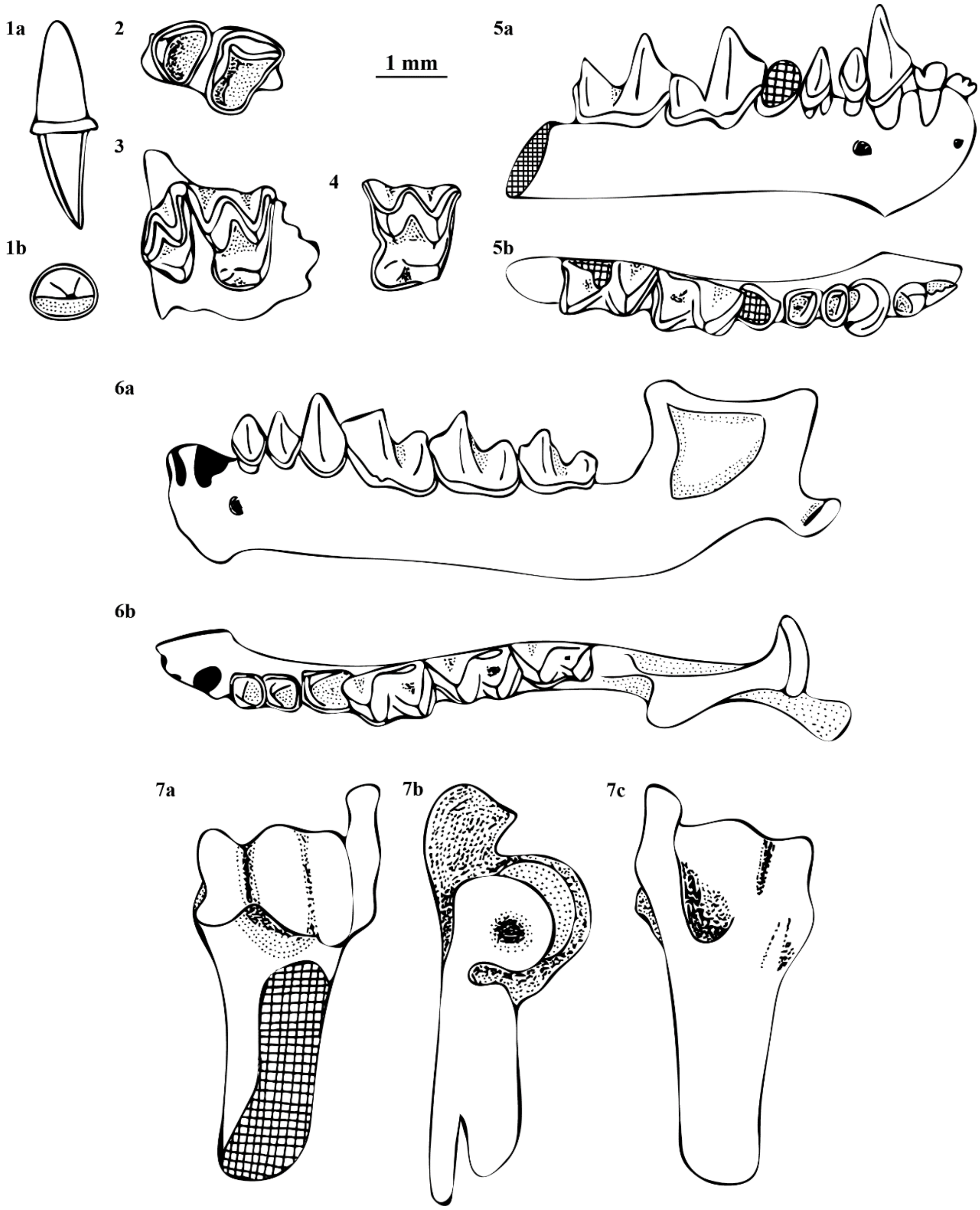

Figure 4.60 *Miniopterus schreibersii*, Loutra Almopias Cave A. **1.** LAC27127 – Left C (**a.** labial, **b.** occlusal), **2.** LAC16663 – Left maxillary fragment with P3-P4, **3.** LAC16383 – Right maxillary fragment with M2-M3, **4.** LAC22147 – Right M1, **5.** LAC19638 – Right mandibular fragment with i2-m2 (**a.** labial, **b.** occlusal), **6.** LAC19499 – Left mandibular fragment with p2-m3 (**a.** labial, **b.** occlusal), **7.** LAC26414 – Distal epiphysis of left humerus (**a.** anterior, **b.** lateral, **c.** posterior).

m3: Nyctalodont. The talonid is longer than the trigonid. Paraconid, metaconid, entoconid, protoconid and hypoconid are well-developed. The protoconid is taller than the hypoconid. The paralophid is concave. The entocristid is slightly curved. The entoconid is more towards the labial side of the tooth and thus, the talonid is reduced. The hypoconulid is slightly reduced. The labial cingulum is thick beneath the protoconid and slightly thinner beneath the hypoconid, but less pronounced than in m1 and m2. Lingual cingulum of the trigonid is also present.

Mandible: The coronoid process is angular and located at the same height with the articular process. The anterior part of the masseter crest, which is thick, is steep. The anterior sigmoid notch is positioned to a more inferior position than the coronoid and the articular process and it is flat. The angular process projects diagonally downwards. The mental foramen is beneath the anterior part of p2. The lowest part of the symphysis is relatively pointed and projects downwards.

Humerus: The styloid process is long and flat. The epitrochlea is wide. An almost flat diagonal valley is present between the trochlea and the condyle. A deep diagonal valley is present between the condyle and the epicondyle. The condyle and the epicondyle are not projecting laterally. The radial fossa and the olecranon fossa are deep, with the latter extending from the middle part of the epiphysis to the styloid process.

Discussion The morphological features described in addition to the measurements allow a definite attribution of the material to *Miniopterus schreibersii*. It is the sole member of the Bent-winged Bats that currently occurs in Greece.

Occurrence Fossils of the Schreibers' Bent-winged Bat are known from Petralona Cave, Chalkidiki and Vathy, Kalymnos. Its modern distribution includes practically all mainland Greece, several islands and Crete (Hanák et al. 2001, GFDC 2021). On a global scale it is distributed from Northwestern and sub-Saharan Africa to Southern Europe all the way to Caucasus, Iran, China, Japan, Southeastern Asia, Philippines to New Guinea and Australia and Solomon Islands (Simmons 2005a).

Ecology *Miniopterus schreibersii* is a cave dweller and its habitat preferences include mostly forested areas (Dietz et al. 2009).

Chiroptera indet.

Figure 4.61

Fossiliferous locality LAC I, LAC Ib, LAC Ic, LAC II, LAC III

<u>Age</u> Late Pleistocene

<u>Material</u> 209 identified specimens

<u>LAC I:</u> 1 left I1-2 (19973), 1 left I1 (27493), 1 left C (17292), 1 right M1-2 (27468), 3 right mandibular fragments (19937, 17219, 16643), 3 left mandibular fragments (17266, 17329, 27503), 1 right mandibular fragment with m1 (17335), 1 left p2 (17295), 2 right m1-2 (27460, 27477), left m1-2 (17218), right m1-3 (27504), <u>LAC Ib:</u> 1 right/left C (19894), 1 right M1-2 (19903), right M1-3 (17158, 17136), 1 left M3 (17153), 1 right/left mandibular fragment (27518), 10 right mandibular fragments (16594, 16595, 16596, 16597, 16604, 17174, 17175, 16579, 19877, 27512), 7 left mandibular fragments (16607, 16608, 16609, 16431, 19860, 19878, 19879), 2 right c (17189, 19896), 1 left c (17173), 1 right m1-2 (19907), 3 left m1-2 (19865, 19905, 19906), 2 right m1-3 (17171, 17184), 1 right m3 (16574), 1 right humerus (27516), <u>LAC Ic:</u> 1 right I1 (17901), 1 left M1-2 (18028), 1 left M3 (17926), 5 right mandibular fragments (17897, 17966, 18019, 18020, 16426), 2 left mandibular fragments (17934, 16427), 1 right c (17964), <u>LAC II:</u> 1 right/left milk tooth (21825), 1 right maxillary fragment with P4 (21603), 1 right I1 (16695a), 2 left I1 (22442, 22443), 3 left P4 (27522, 27561, 27632), 1 left M1-2 (21709), 1 left M2 (27773), right M3 (16059, 27875), 2 right/left mandibular fragments (21593, 27546), 31 right mandibular fragments (16084, 21528, 21556, 21596, 21597, 21599, 21600, 21601, 21843, 21845, 16616, 16618, 16621, 16686, 16699, 16361, 16366, 16128, 16132, 16014, 16416, 22395, 22398, 27571, 27639, 27674, 27675, 27857, 27858, 27859, 27861), 34 left mandibular fragments (21527, 21557, 21846, 16617, 16363, 16364, 16365, 16373, 16129, 16130, 16131, 16409, 22401, 22402, 22404, 27525, 27526, 27545, 27597, 27598, 27625, 27641, 27673, 27676, 27677, 27678, 27715, 27731, 27742, 27743, 27753, 27825, 27862, 27863), 1 right mandibular fragment with m2-m3 (27728), 1 left mandibular fragment with m2-m3 (16620), 1 left m3 (16664), 1 left humerus (27538), 3 undefined teeth fragments (16133, 22196, 22445), <u>LAC III:</u> 1 right I2 (20097), 1 left C (21380), 3 right M1-2 (20181, 19323, 20040), 1 left M1-2 (20845), 1 right M1-3 (19343), 1 right M3 (21319), 1 left M3 (19148), 20 right mandibular fragments (20133, 20134, 20135, 20137, 20740, 21239, 21256, 16464, 17724, 17725, 17726, 16447, 21060, 21061, 21149, 21150, 20000, 20001, 20328, 20517), 28 left mandibular fragments (20138, 20139, 20236, 20238, 20239, 20245, 21245, 21248, 21249, 21250, 21252, 21255, 16466, 21065, 21151, 21152, 21153, 21154, 20002, 20003, 20004, 20331, 20415, 20418, 20419, 20525, 20615, 20616), 1 right mandibular fragment with m1-2 (21232), 1 right/left p4 (20046), 1 right m1-3 (19337), 1 right m2 (20982), 1 right m3 (21233)

<u>Fossiliferous locality</u> LAC Ia

<u>Age</u> latest Pleistocene

<u>Material</u> 129 identified specimens

1 right I1-2 (26395), 5 right I1 (23301, 26362, 26388, 26403, 27200), 9 left I1 (26374, 26396, 26398, 26405, 26406, 26407, 26408, 26410, 27444), 1 left C (25972), 2 right P4 (25290, 25291), 4 left P4 (25320, 25339, 25371, 25385), 2 right M1-2 (24605, 24664), 2 left M1-2 (24684, 24807), 4 right M3 (25163, 25189, 25197, 25209), 1 left M3 (25090), 36 right mandibular fragments (19515, 19516, 19517, 19519, 22951, 22952, 22954, 22955, 22956, 22957, 22962, 22965, 22967, 22970, 22977, 22982, 22983, 22988, 22992, 22994, 22995, 23002, 23003, 23005, 23006, 23007, 23008, 23661, 26829, 26831, 26832, 26833, 26834, 26835, 26838, 27268), 31 left mandibular fragments (19521, 19528, 19529, 19702, 23013, 23014, 23017, 23019, 23020, 23021, 23022, 23037, 23038, 23040, 23041, 23045, 23047, 23049, 23053, 23057, 23063, 24177, 26846, 26847, 26848, 26849, 26851, 26852, 26861, 27293, 27296), 3 right c (25565, 25593, 26199), 1 left c (26095), 5 right m1-2 (23404, 23409, 23439, 26898, 26918), 4 left m1-2 (23817, 23971, 24138, 26951), 2 right m1-3 (23347, 23692), left m1-3 (23818), 3 right m1 (23708, 26899, 27358), 2 left m1 (23790, 27379), 1 right m2 (23345), 1 left m2 (23739), 4 right m3 (23722, 23723, 23724, 24180), 4 left m3 (23845, 24093, 24115, 27011)

<u>Comments</u> Here are grouped specimens that could not be identified beyond order level, mostly because they are severely damaged (worn/digested/corroded/broken/etc.). Consequently, no further descriptions are provided.

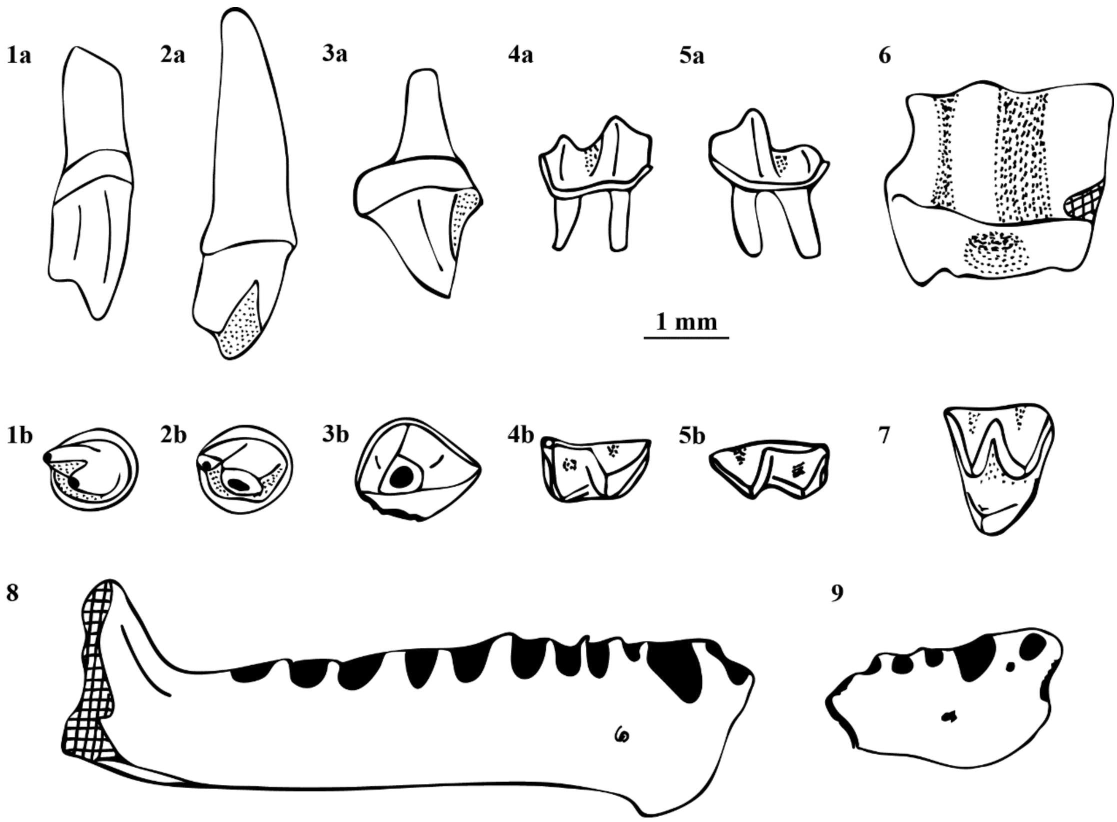

Figure 4.61 Chiroptera indet, Loutra Almopias Cave A. **1.** LAC16695a – Right I1 (**a.** labial, **b.** occlusal), **2.** LAC20097 – Right I2 (**a.** labial, **b.** occlusal), **3.** LAC27522 – Left P4 (**a.** labial, **b.** occlusal), **4.** LAC 26898 – Right m1-2 (**a.** labial, **b.** occlusal), **5.** LAC27011 – Left m3 (**a.** labial, **b.** occlusal), **6.** LAC27538 – Distal epiphysis of left humerus, **7.** LAC27773 – Left M2, **8.** LAC22951 – Right mandibular fragment, **9.** LAC20328 – Right mandibular fragment.

CHAPTER 5. RESULTS AND DISCUSSION

5.1 SYSTEMATIC RESULTS

The systematic palaeontology led to the identification of 17 species from the Late Pleistocene cave floor sediments (LAC) and 20 species from the latest Pleistocene elevated chamber LAC Ia from a total of 9004 specimens. Overall, three families have been identified in both chronological units: Rhinolophidae (the dominant representative for both LAC and LAC Ia), Vespertilionidae and Miniopteridae. More specifically, 5 species of Rhinolophidae, 11 species of Vespertilionidae (genera: 4 *Myotis*, 2 *Nyctalus*, 1 *Pipistrellus*, 1 *Vespertilio*, 1 *Eptesicus*, 1 *Plecotus*, 1 *Barbastella*) and 1 species of Miniopteridae have been identified from LAC, whereas from LAC Ia the respective species are 5 Rhinolophidae, 14 Vespertilionidae (genera: 6 *Myotis*, 3 *Nyctalus*, 1 *Pipistrellus*, 1 *Vespertilio*, 1 *Eptesicus*, 1 *Plecotus*, 1 *Barbastella*) and 1 Miniopteridae (Figure 5.1). The identification of 20 chiropteran species in the fossil record of Loutra Almopias Cave A adds up to the previously recognised mammalian orders of Carnivora, Artiodactyla, Rodentia, Lagomorpha, Erinaceomorpha and Soricomorpha, making it the most diverse (Tsoukala et al. 2006, Chatzopoulou 2014, Nagel et al. 2019)[9] and outnumbered only by the avian order of Passeriformes (Boev and Tsoukala 2019).

Both the number of the identified specimens (NISP) and the minimum number of individuals (MNI) are greater for LAC Ia than LAC (Table 5.1). More specifically, 3811 chiropteran specimens were identified from LAC and 5193 from LAC Ia.

---

[9] For the orders of Erinaceomorpha and Soricomorpha the classification suggested by Hutterer (2005a, 2005b) is followed here. As the status of what was formerly known as Insectivora and/or Eulipotyphla is still a matter of discussion and because the purpose of this chapter is not to provide an updated taxonomy of those orders, here is followed the last widely accepted valid work of this kind.

Respectively, the MNI from LAC is 398, whereas from LAC Ia the MNI is 597. The 995 individuals (out of 9004 identified specimens) are also indicating that during the Late Pleistocene Chiroptera was the most populous order that occupied the Loutra Almopias Cave A (Tsoukala et al. 2006, Chatzopoulou 2014, Nagel et al. 2019, Boev and Tsoukala 2019).

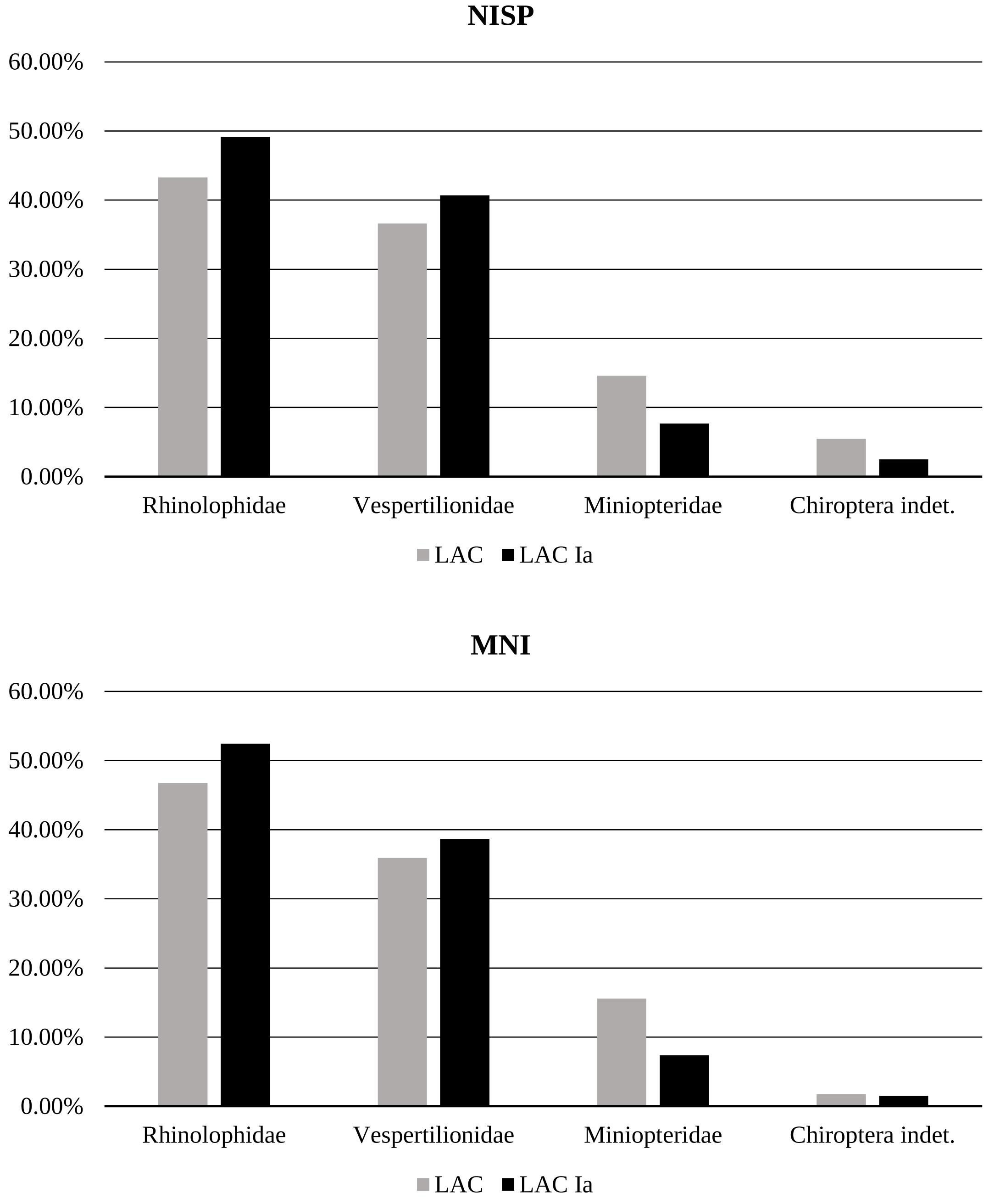

Figure 5.1 Proportion of the chiropteran families identified from LAC and LAC Ia based on their NISP (top) and MNI (bottom). LAC: Late Pleistocene; LAC Ia: latest Pleistocene; NISP: Number of Identified Specimens; MNI: Minimum Number of Individuals.

Table 5.1 The NISP and MNI for LAC and LAC Ia and their respective proportions (%). NISP: Number of Identified Specimens; MNI: Minimum Number of Individuals; LAC: Late Pleistocene; LAC Ia: latest Pleistocene.

Species		LAC	LAC (%)	LAC Ia	LAC Ia (%)	TOTAL	TOTAL (%)
Rhinolophus ferrumequinum	**NISP**	787	20.65	741	14.27	1528	16.97
	MNI	69	17.34	73	12.23	142	14.27
Rhinolophus mehelyi	**NISP**	191	5.01	449	8.65	640	7.11
	MNI	20	5.03	65	10.89	85	8.54
Rhinolophus blasii	**NISP**	16	0.42	43	0.83	59	0.66
	MNI	7	1.76	16	2.68	23	2.31
Rhinolophus euryale	**NISP**	58	1.52	220	4.24	278	3.09
	MNI	14	3.52	43	7.20	57	5.73
Rhinolophus mehelyi/blasii/euryale	**NISP**	459	12.04	885	17.04	1344	14.93
	MNI	61	15.33	99	16.58	160	16.08
Rhinolophus hipposideros	**NISP**	35	0.92	118	2.27	153	1.70
	MNI	4	1.01	14	2.35	18	1.81
Rhinolophus sp.	**NISP**	104	2.73	96	1.85	200	2.22
	MNI	11	2.76	3	0.50	14	1.41
Myotis myotis	**NISP**	183	4.80	138	2.66	321	3.57
	MNI	20	5.03	18	3.02	38	3.82
Myotis blythii	**NISP**	408	10.71	588	11.32	996	11.06
	MNI	30	7.54	50	8.38	80	8.04
Myotis myotis/blythii	**NISP**	302	7.92	459	8.84	761	8.45
	MNI	23	5.78	48	8.04	71	7.14
Myotis bechsteinii	**NISP**	13	0.34	58	1.12	71	0.79
	MNI	2	0.50	9	1.51	11	1.11
Myotis emarginatus	**NISP**	45	1.18	76	1.46	121	1.34
	MNI	4	1.01	15	2.51	19	1.91
Myotis capaccinii	**NISP**	0	0.00	19	0.37	19	0.21
	MNI	0	0.00	5	0.84	5	0.50

Myotis mystacinus	**NISP**	0	0.00	4	0.08	4	0.04
	MNI	0	0.00	1	0.17	1	0.10
Myotis sp.	**NISP**	39	1.02	47	0.91	86	0.96
	MNI	3	0.75	9	1.51	12	1.21
Nyctalus lasiopterus	**NISP**	0	0.00	2	0.04	2	0.02
	MNI	0	0.00	1	0.17	1	0.10
Nyctalus noctula	**NISP**	104	2.73	322	6.20	426	4.73
	MNI	12	3.02	27	4.52	39	3.92
Nyctalus leisleri	**NISP**	9	0.24	40	0.77	49	0.54
	MNI	2	0.50	8	1.34	10	1.01
Pipistrellus pipistrellus	**NISP**	30	0.79	34	0.65	64	0.71
	MNI	8	2.01	6	1.01	14	1.41
Vespertilio murinus	**NISP**	19	0.50	154	2.97	173	1.92
	MNI	4	1.01	14	2.35	18	1.81
Eptesicus serotinus	**NISP**	18	0.47	45	0.87	63	0.70
	MNI	7	1.76	4	0.67	11	1.11
Plecotus auritus/austriacus	**NISP**	1	0.03	3	0.06	4	0.04
	MNI	1	0.25	2	0.34	3	0.30
Barbastella barbastellus	**NISP**	225	5.90	124	2.39	349	3.88
	MNI	27	6.78	14	2.35	41	4.12
Miniopterus schreibersii	**NISP**	556	14.59	399	7.68	955	10.61
	MNI	62	15.58	44	7.37	106	10.65
Chiroptera indet.	**NISP**	209	5.48	129	2.48	338	3.75
	MNI	7	1.76	9	1.51	16	1.61
TOTAL	**NISP**	3811	100.00	5193	100.00	9004	100.00
	MNI	398	100.00	597	100.00	995	100.00

Out of the 20 species that were identified from LAC Ia, only three are not present in LAC: *Myotis capaccinii*, *Myotis mystacinus* and *Nyctalus lasiopterus*, whereas the rest are common in both assemblages. In terms of species representation and based on both their NISP and MNI (Table 5.1), *Rhinolophus ferrumequinum* is the dominant taxon in the sediments of LAC, followed by *Miniopterus schreibersii*, *Rhinolophus mehelyi*/*blasii*/*euryale* and *Myotis blythii*, whereas the most dominant taxon in the sediments of LAC Ia is *Rhinolophus mehelyi*/*blasii*/*euryale*, together with *Rhinolophus ferrumequinum*, *Rhinolophus mehelyi* and *Myotis blythii* (Figure 5.2-3). On the contrary, *Plecotus auritus*/*austriacus* is the least represented taxon in LAC, followed by *Nyctalus leisleri* and *Myotis bechsteinii*, whereas in LAC Ia the least represented taxa are *Nyctalus lasiopterus*, *Plecotus auritus*/*austriacus* and *Myotis mystacinus* (Figure 5.2-3).

Furthermore, the proportions of the relative abundance (Table 5.2) of *Barbastella barbastellus*, *Miniopterus schreibersii* and *Myotis myotis* significantly decreased from Late to latest Pleistocene, both in terms of their NISP and MNI. On the contrary, *Myotis bechsteinii*, *Nyctalus leisleri*, *Myotis emarginatus*, *Rhinolophus hipposideros*, *Vespertilio murinus*, *Rhinolophus mehelyi* and *Rhinolophus euryale* present the largest increases in the proportion of their relative abundance. It is worth noting that in the case of *Eptesicus serotinus*, although its relative abundance is increasing from Late to latest Pleistocene (+83.47%) when NISP is considered, the opposite trend occurs when MNI is taken into account, resulting in a decrease of -61.90%.

In respect to the Greek fossil record of Chiroptera, *Rhinolophus euryale*, *Myotis bechsteinii*, *Myotis capaccinii*, *Myotis mystacinus*, *Nyctalus lasiopterus*, *Nyctalus leisleri*, *Pipistrellus pipistrellus* and *Barbastella barbastellus* are described for the first time in Greece from Loutra Almopias Cave A (Piskoulis and Chatzopoulou in press).

Myotis capaccinii appears in the fossil record of an Upper Pleistocene locality from the Balkan Peninsula for the first time in Loutra Almopias Cave A (latest Pleistocene LAC Ia). Loutra Almopias Cave A represents also the southernmost appearance of *Rhinolophus ferrumequinum*, *Rhinolophus mehelyi*, *Rhinolophus blasii*, *Rhinolophus euryale*, *Rhinolophus hipposideros*, *Myotis myotis*, *Myotis bechsteinii*, *Myotis emarginatus*, *Myotis capaccinii*, *Myotis mystacinus*, *Nyctalus lasiopterus*, *Nyctalus noctula*, *Nyctalus leisleri*, *Pipistrellus pipistrellus*, *Vespertilio murinus*, *Eptesicus serotinus*, *Plecotus auritus*/*austriacus*, *Barbastella barbastellus* and *Miniopterus schreibersii* in the Balkan Peninsula, extending the fossil record of the these species further south.

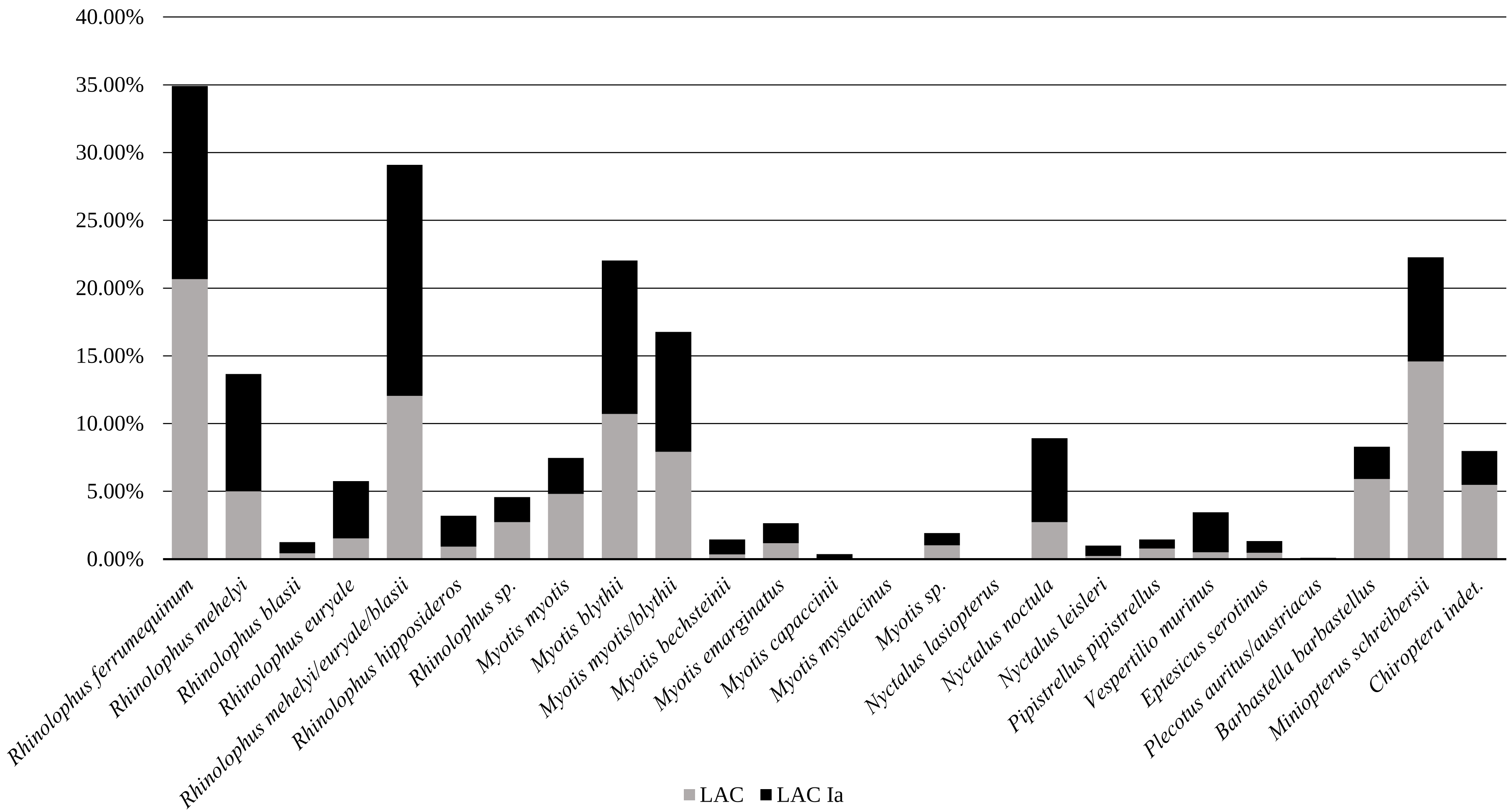

Figure 5.2 Variation of relative abundance of chiropteran species in LAC and LAC Ia, based on their NISP. LAC: Late Pleistocene; LAC Ia: latest Pleistocene; NISP: Number of Identified Specimens.

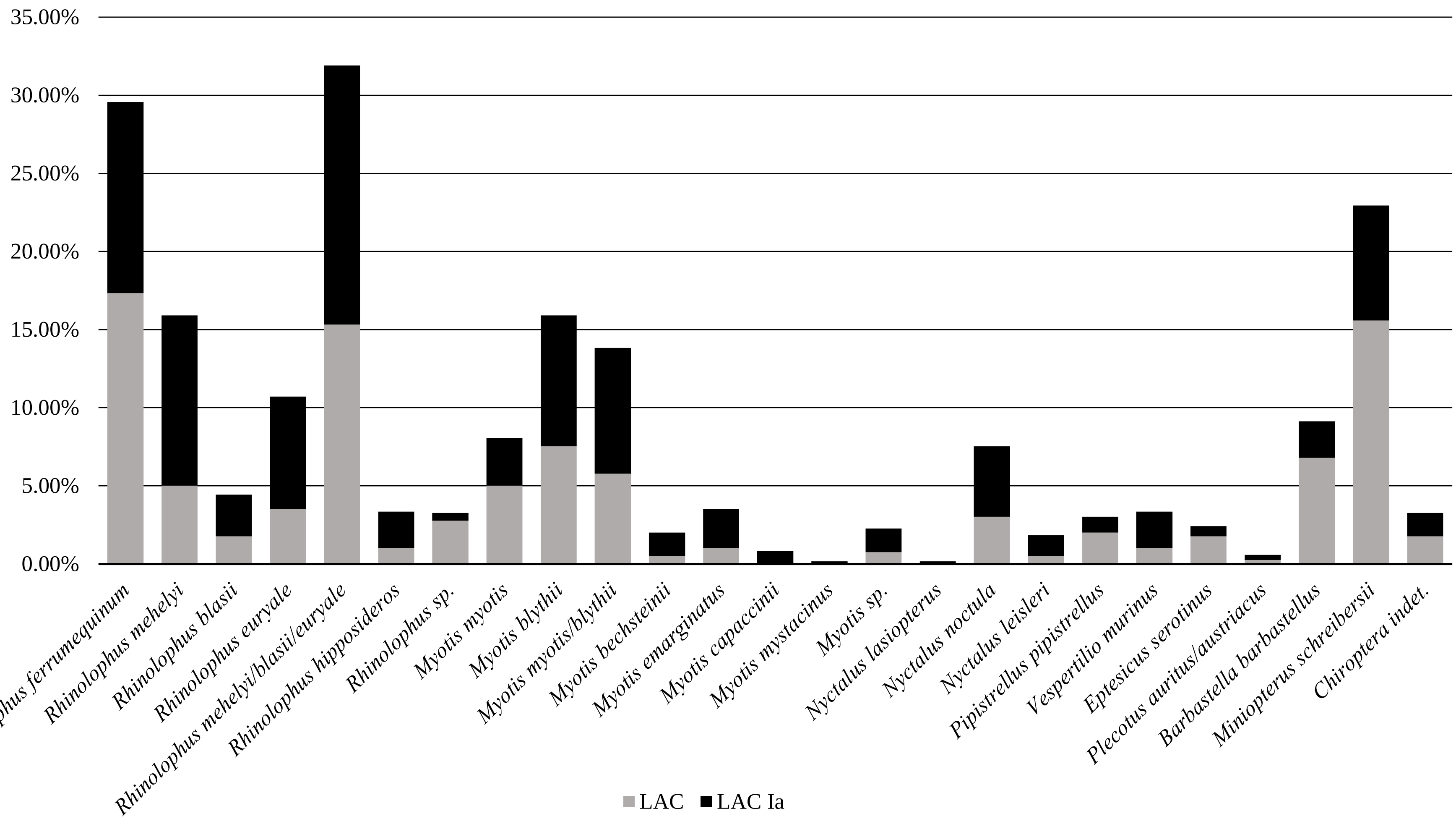

Figure 5.3 Variation of relative abundance of chiropteran species in LAC and LAC Ia, based on their MNI. LAC: Late Pleistocene; LAC Ia: latest Pleistocene; MNI: Minimum Number of Individuals.

Table 5.2 Difference between proportions of relative abundance of the chiropteran taxa retrieved from Loutra Almopias Cave A floor sediments (LAC) and from the elevated chamber LAC Ia. NISP: Number of Identified Specimens; MNI: Minimum Number of Individuals; LAC: Late Pleistocene; LAC Ia: latest Pleistocene.

Species		**LAC (%)**	**LAC Ia (%)**	**Difference (%)**
Rhinolophus ferrumequinum	**NISP**	20.65	14.27	-30.90
	MNI	17.34	12.23	-29.47
Rhinolophus mehelyi	**NISP**	5.01	8.65	+72.52
	MNI	5.03	10.89	+116.67
Rhinolophus blasii	**NISP**	0.42	0.83	+97.23
	MNI	1.76	2.68	+52.38
Rhinolophus euryale	**NISP**	1.52	4.24	+178.37
	MNI	3.52	7.20	+104.76
Rhinolophus mehelyi/blasii/euryale	**NISP**	12.04	17.04	+41.50
	MNI	15.33	16.58	+8.20
Rhinolophus hipposideros	**NISP**	0.92	2.27	+147.42
	MNI	1.01	2.35	+133.33
Rhinolophus sp.	**NISP**	2.73	1.85	-32.26
	MNI	2.76	0.50	-81.82
Myotis myotis	**NISP**	4.80	2.66	-44.66
	MNI	5.03	3.02	-40.00
Myotis blythii	**NISP**	10.71	11.32	+5.76
	MNI	7.54	8.38	+11.11
Myotis myotis/blythii	**NISP**	7.92	8.84	+11.54
	MNI	5.78	8.04	+39.13
Myotis bechsteinii	**NISP**	0.34	1.12	+227.42
	MNI	0.50	1.51	+200.00
Myotis emarginatus	**NISP**	1.18	1.46	+23.94
	MNI	1.01	2.51	+150.00
Myotis capaccinii	**NISP**	0.00	0.37	-
	MNI	0.00	0.84	-
Myotis mystacinus	**NISP**	0.00	0.08	-
	MNI	0.00	0.17	-
Myotis sp.	**NISP**	1.02	0.91	-11.56
	MNI	0.75	1.51	+100.00
Nyctalus lasiopterus	**NISP**	0.00	0.04	-
	MNI	0.00	0.17	-
Nyctalus noctula	**NISP**	2.73	6.20	+127.22
	MNI	3.02	4.52	+50.00
Nyctalus leisleri	**NISP**	0.24	0.77	+226.17
	MNI	0.50	1.34	+166.67
Pipistrellus pipistrellus	**NISP**	0.79	0.65	-16.83
	MNI	2.01	1.01	-50.00
Vespertilio murinus	**NISP**	0.50	2.97	+494.82
	MNI	1.01	2.35	+133.33
Eptesicus serotinus	**NISP**	0.47	0.87	+83.47
	MNI	1.76	0.67	-61.90
Plecotus auritus/austriacus	**NISP**	0.03	0.06	+120.16
	MNI	0.25	0.34	+33.33
Barbastella barbastellus	**NISP**	5.90	2.39	-59.56
	MNI	6.78	2.35	-65.43
Miniopterus schreibersii	**NISP**	14.59	7.68	-47.34
	MNI	15.58	7.37	-52.69
Chiroptera indet.	**NISP**	5.48	2.48	-54.70
	MNI	1.76	1.51	-14.29

Despite the fact that Loutra Almopias Cave A is an important Late Pleistocene site for the Balkans, it is also of great significance for the Greek region, as it is the richest and most diverse. It is worth mentioning that prior to Loutra Almopias Cave A, the Middle Pleistocene locality of Petralona Cave was the richest and most diverse, with 19 taxa present, amongst which the following bat species were recorded: *Rhinolophus ferrumequinum topali*, *Myotis* cf. *daubentonii* and *Hypsugo savii* (Sickenberg 1964, 1971, Kretzoi 1977, Kretzoi and Poulianos 1981, Horacek and Poulianos 1988, Tsoukala 1989). Those three are recorded only in Petralona Cave within the Greek region.

In order to continue the analysis of the data at the species level, it is important to investigate whether the taxa identified from LAC and LAC Ia are representative enough, in terms of size and species richness of these fossiliferous assemblages. This is accomplished with the generation of rarefaction curves (Figure 5.4), which show that as the curve flattens, further examination of material will not significantly increase species number. The same occurs if we take into account both the NISP and the MNI. More specifically, a sample size with about 1000 NISP and/or 250 MNI would, most possibly, yield the same number of taxa.

After that, a Kruskal-Wallis test was run in order to investigate if the chiropteran populations from LAC and LAC Ia have significant differences. The Kruskal-Wallis test does not assume normal distribution and thus two statistical tests were run for both NISP and MNI in order to check if the identified taxa are normally distributed. The Shapiro-Wilk test for normal distribution reported W values greater than p in all cases and consequently the identified chiropteran populations are – as expected – not normally distributed (Table 5.3). This is also evident from the normal probability plots (Figure 5.5), where the data significantly diverge from the fitted straight line both for NISP and MNI. Consequently, the Kruskal-Wallis test results obtained from the sample medians (Table 5.4) showed that there are no significant differences between LAC and LAC Ia, as $H_c > H$ for both NISP and MNI.

Additionally, it is considered essential to examine the correlation between NISP and MNI. This is accomplished with a linear regression analysis (Figure 5.6). The linear correlation coefficient (r) for LAC is $r = 0.9550$ and for LAC Ia, $r = 0.9630$. Therefore, a strong positive correlation for NISP and MNI is occurring, as $r > 0.90$ in both cases, meaning that both factors can be used for further analyses of the data (viz. at species level). To sum up, the results of the palaeoecological and palaeoenvironmental analyses will not diverge significantly if either NISP or MNI is used.

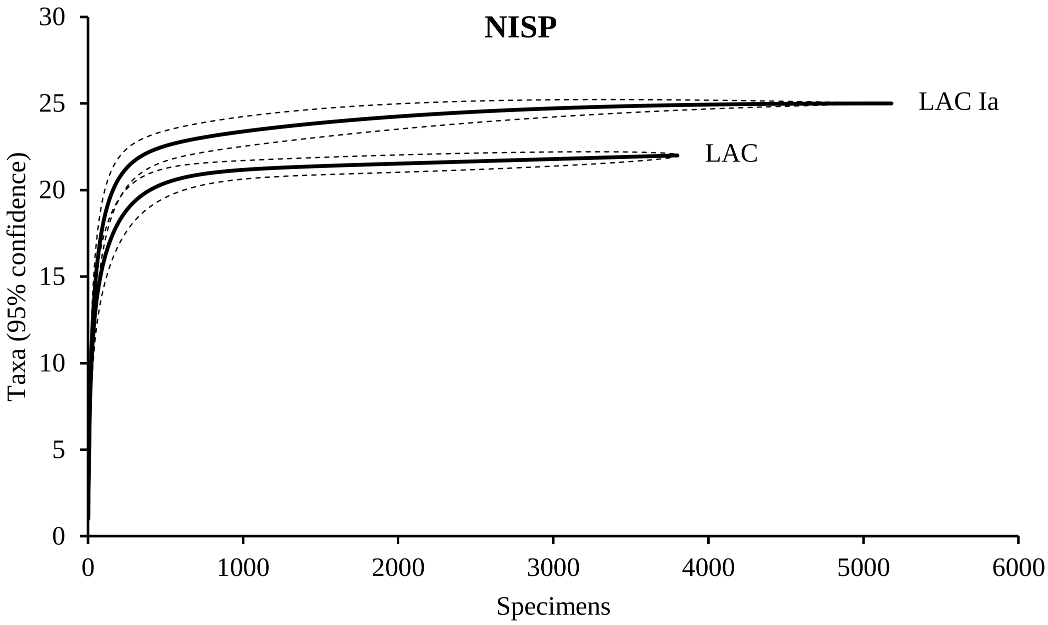

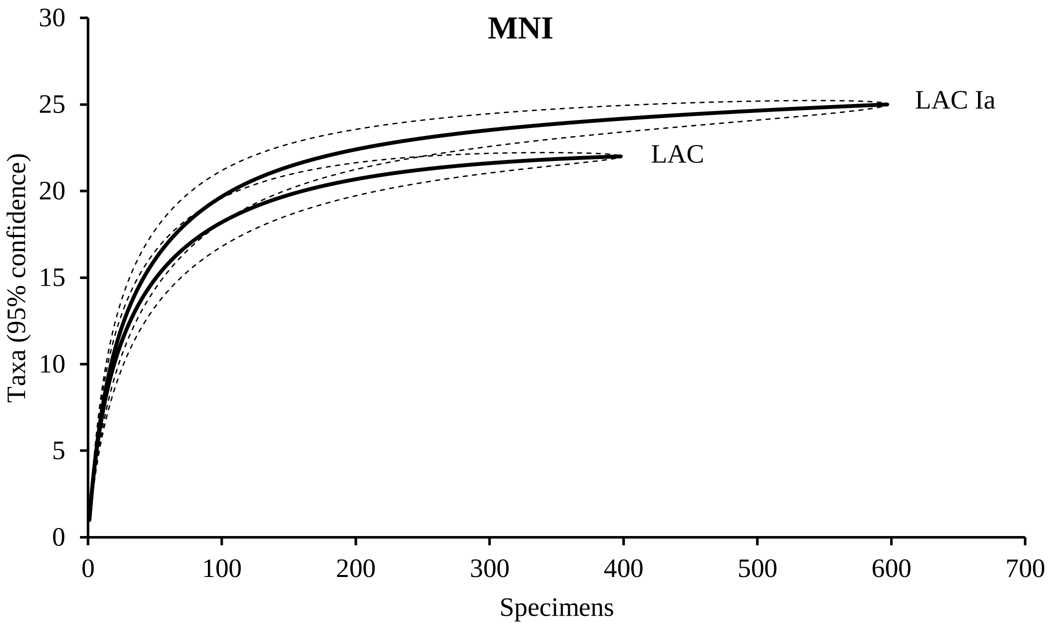

Figure 5.4 Rarefaction curves with 95% confidence intervals for LAC and LAC Ia based on their NISP (top) and MNI (bottom). LAC: Late Pleistocene; LAC Ia: latest Pleistocene; NISP: Number of Identified Specimens; MNI: Minimum Number of Individuals.

Table 5.3 Shapiro-Wilk test for normal distribution. N: number of taxa; Shapiro-Wilk *W*: Shapiro-Wilk test statistic; *p*(normal): probability; NISP: Number of Identified Specimens; MNI: Minimum Number of Individuals; LAC: Late Pleistocene; LAC Ia: latest Pleistocene..

	NISP		**MNI**	
	LAC	**LAC Ia**	**LAC**	**LAC Ia**
N	22	25	22	25
Shapiro-Wilk *W*	0.788000	0.7873000	0.7531000	0.8021000
***p*(normal)**	0.0003267	0.0001408	0.0001006	0.0002465

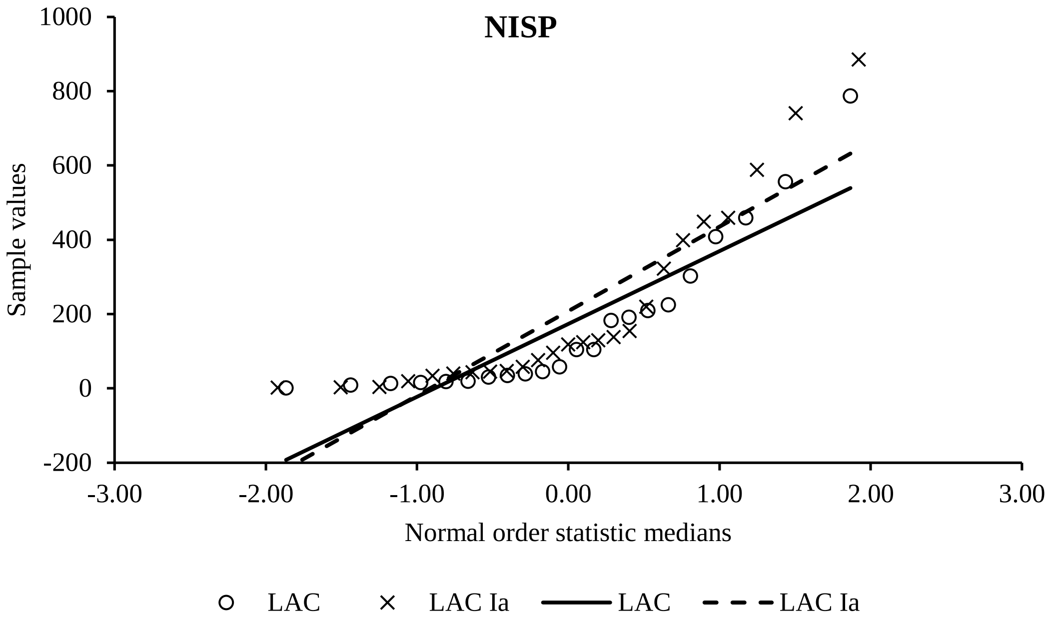

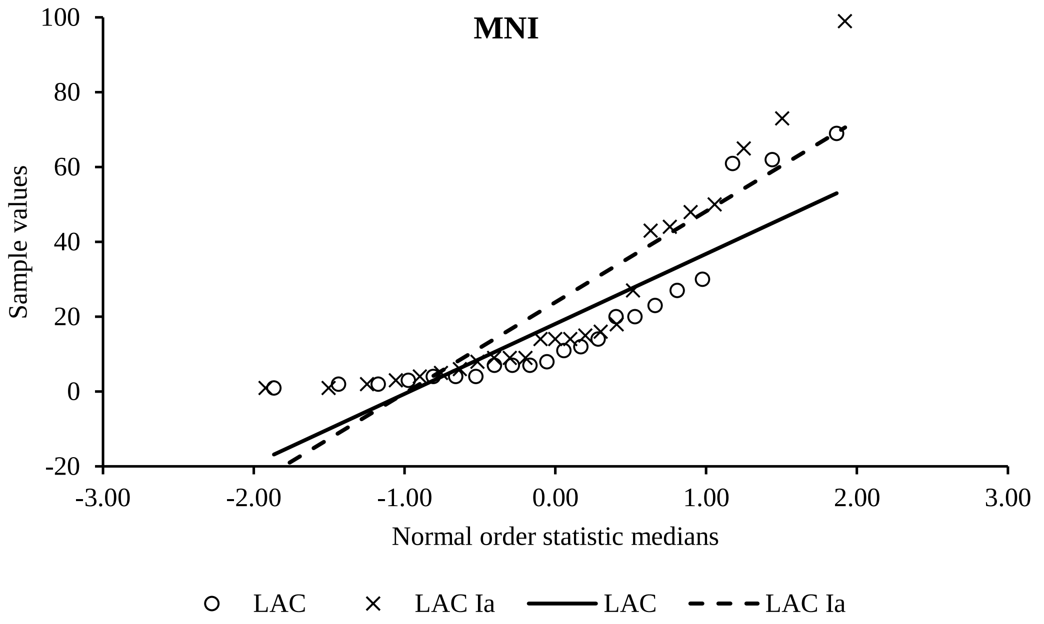

Figure 5.5 Normal probability plots for LAC and LAC Ia, based on their NISP (top) and MNI (bottom). NISP: r = 0.8863 (LAC), r = 0.8881 (LAC Ia); MNI: r = 0.8700 (LAC), r = 0.8952 (LAC Ia). LAC: Late Pleistocene; LAC Ia: latest Pleistocene; NISP: Number of Identified Specimens; MNI: Minimum Number of Individuals; r: Correlation coefficient.

Table 5.4 Kruskal-Wallis test for equal medians. H(chi^2): test statistic; H_c(tie corrected): critical value; p(same): probability; NISP: Number of Identified Specimens; MNI: Minimum Number of Individuals; LAC: Late Pleistocene; LAC Ia: latest Pleistocene.

	NISP	**MNI**
***H*(chi^2)**	0.4091	0.5728
H_c(tie corrected)	0.4092	0.5742
***p*(same)**	0.5224	0.4486

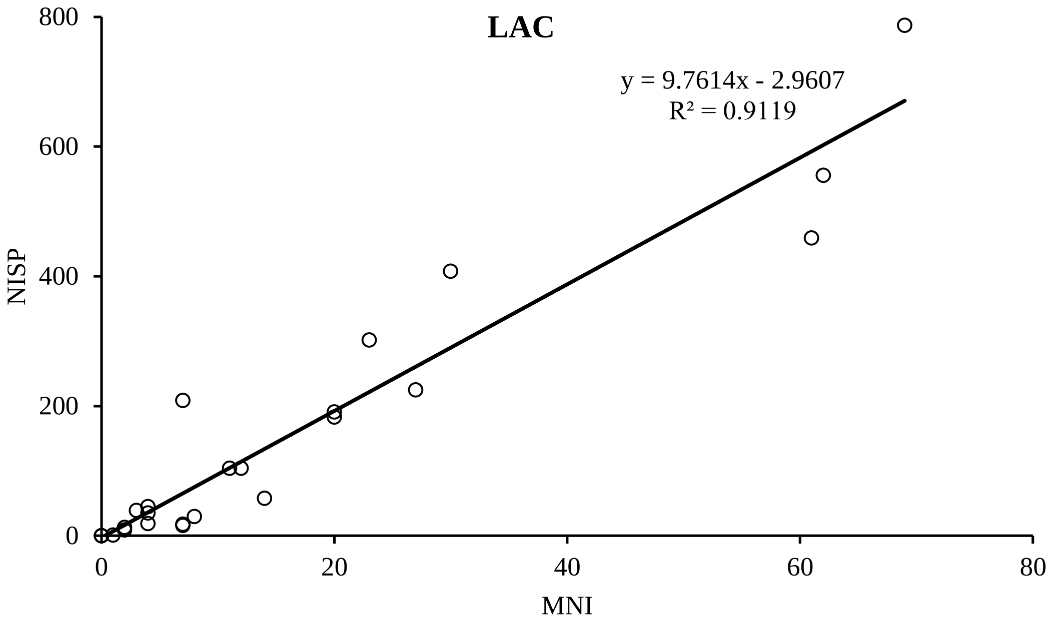

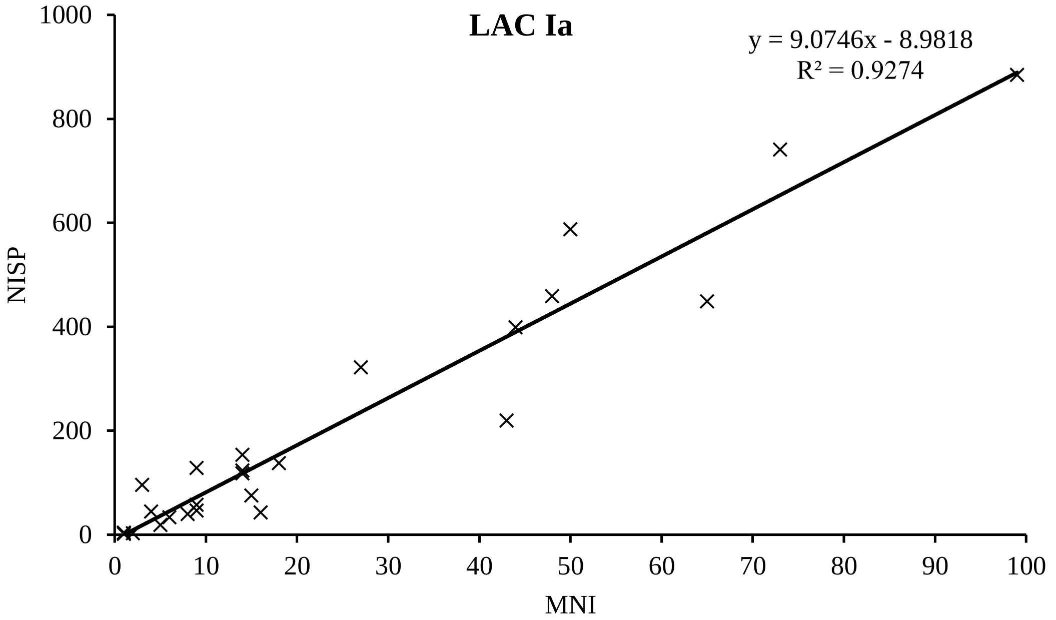

Figure 5.6 Relationship between NISP and MNI for LAC (top) and LAC Ia (bottom). LAC: $r = 0.9550$; LAC Ia: $r = 0.9630$. NISP: Number of Identified Specimens; MNI: Minimum Number of Individuals; LAC: Late Pleistocene; LAC Ia: latest Pleistocene; r: Linear correlation coefficient.

5.2 TAPHONOMIC ANALYSIS

From the Late Pleistocene LAC, 3575 (out of 3811) dental and postcranial elements were found to be corroded and/or worn, whereas the respective number from the latest Pleistocene LAC Ia was 4868 (out of 5193). 71.50% of the dental elements from LAC present some degree of wear and/or damage, whilst this number is almost 10% smaller (62.00%) for the dental elements from the latest Pleistocene LAC Ia (Figure 5.7).

Furthermore, there is a quite significant proportion (21.60%) of dental elements from LAC that are damaged to some degree, with the respective number for LAC Ia being substantially decreased to 12.79% (Figure 5.8). There is also a small proportion of dental elements that present some form of corrosion and/or wear, but could not be further specified (Figure 5.8).

The difference in the proportions of the damaged material is mainly due to the fact that the deposition of the cave's floor fossiliferous clay stratum occurred due a mass flooding event of the cave, which – apart from the fossils – transported a large amount of pebbles (see SECTION 2.3). Regardless of the fact that Chiroptera are not easily fossilised due to their small and delicate skeleton (Gunnel and Simmons 2005) it appears that the bat remains were damaged due to within-cave transportation, which should not have been extensive as it is indicated by the preservation of the fossils (Andrews 1990). In respect to LAC Ia, the water action should have been minimal, which is supported by the presence of various cranial and postcranial elements with different hydrodynamic properties such as mandibles, maxillary fragments, isolated teeth, long bones and cochleas (own observations) in the assemblage.

On the other hand 27.78% of the dental elements from LAC present some form of corrosion on their enamel (evidence of digestion), whilst this number is almost 5% larger (32.74%) for the dental elements from the latest Pleistocene LAC Ia (Figure 5.7).

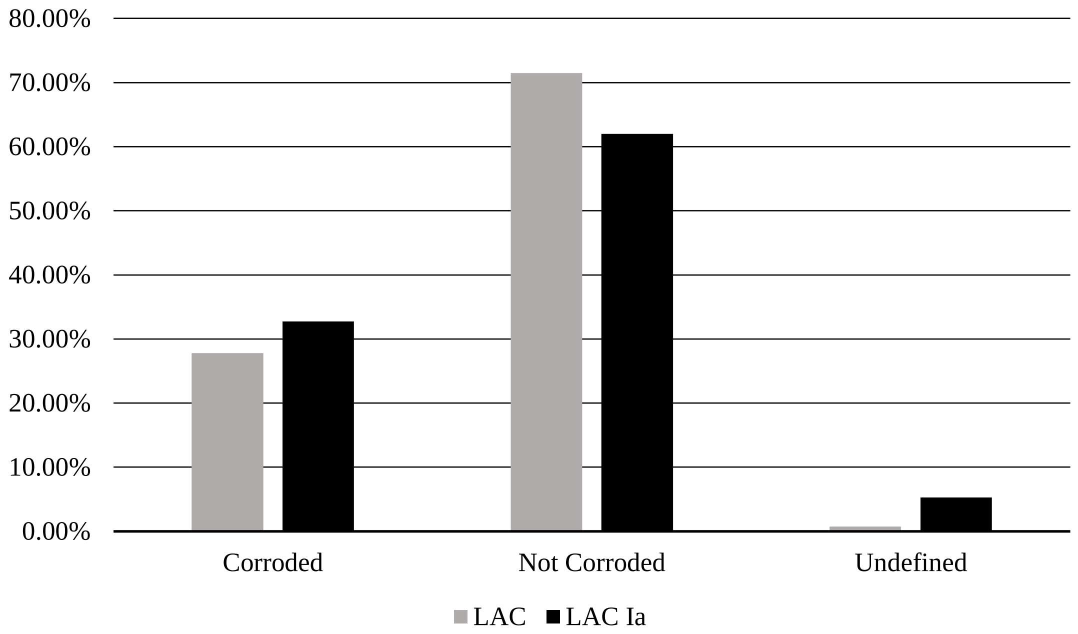

Figure 5.7 Variation in the proportion of corroded/not corroded dental elements. LAC: Late Pleistocene; LAC Ia: latest Pleistocene.

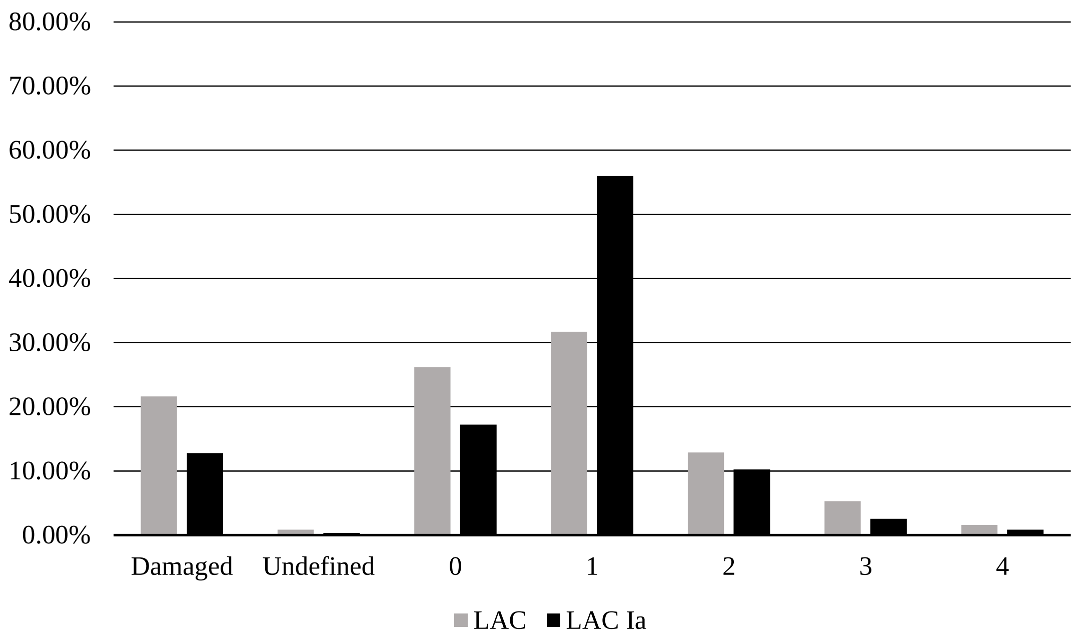

Figure 5.8 Variation in the proportion of the age groups of the dental elements. LAC: Late Pleistocene; LAC Ia: latest Pleistocene; 0: unworn (very young adults); 1: slightly worn (young adults); 2: worn (middle-aged adults); 3: very worn (old adults); 4: severely worn (very old adults).

Therefore, it is evident that a significant amount of bat fossils retrieved from Loutra Almopias Cave A is a result of predation as approximately 1/4 of bat fossils from LAC present some degree of corrosion, whereas the respective number from LAC Ia is 1/3. On the contrary, the material without corrosion belongs to animals that roosted in the cave and died there.

In respect to the dental elements that are not corroded, five age groups have been established according to their wear stage (Figure 3.6), with 0 corresponding to very young adults (unworn teeth) and 4 corresponding to very old adults (severely worn). The vast majority of the specimens from both LAC and LAC Ia correspond to (very) young adults, with the respective percentages being 57.82% and 73.19% (Figure 5.8).

In terms of the age groups established (Figure 5.8) it is evident that mortality was higher for very young and young adults in both LAC and LAC Ia assemblages (57.82% and 73.19% respectively). In combination with the fact that mortality in Chiroptera is higher for individuals that are in their early maturity or for older individuals during their hibernation (Hill and Smith 1984, Sevilla and Chaline 2004), it would be safe to assume that the Loutra Almopias Cave A acted as a nursery roost for a plethora of bats and sporadically, as a warm refuge during colder periods. A pattern that is already established for Southern Europe (Iberian, Italian and Balkan Peninsulas) during the

Pleistocene glaciation, which acted as a refugium for a many taxa that migrated from Northern and Central Europe (Hewitt 1999). Similarly, the large and small mammal faunas from Loutra Almopias Cave A are also following this trend (Tsoukala et al. 2006, Chatzopoulou 2014, Nagel et al. 2019).

In addition to that, more than 80% of the bat species from both faunal assemblages of the Loutra Almopias Cave A are typical cave dwellers, with a negligible increase in taxa that roost in trees and in taxa with mixed roosting preferences in LAC Ia (Figure 5.9). It is common though for tree dwelling species to seek shelter in caves during colder periods or in colder regions (Sevilla 1990).

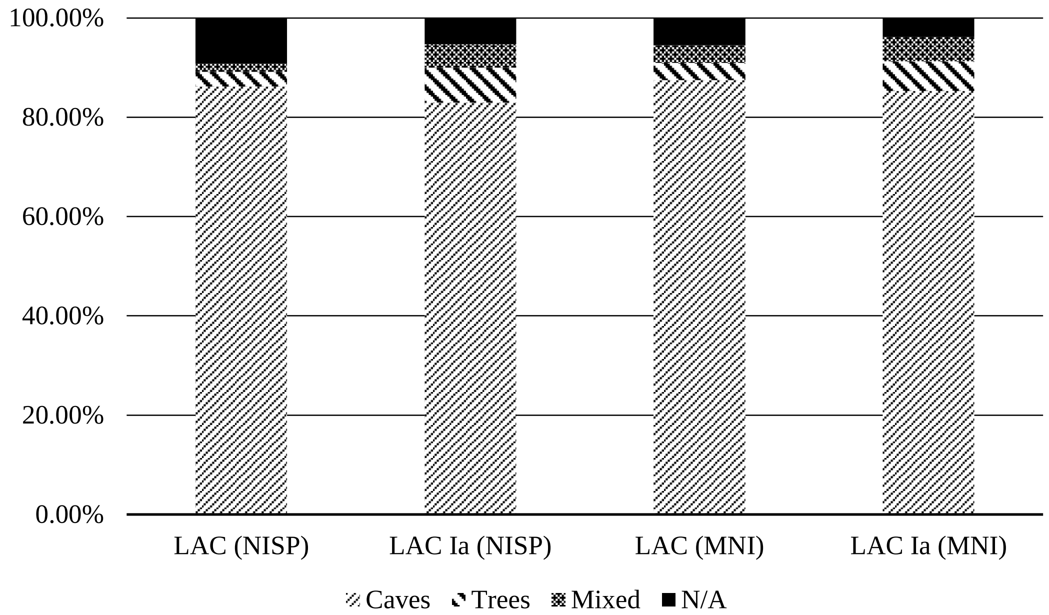

Figure 5.9 Variation in the proportion of bat species from Loutra Almopias Cave A grouped according to their roosting preference. LAC: Late Pleistocene; LAC Ia: latest Pleistocene; NISP: Number of Identified Specimens; MNI: Minimum Number of Individuals.

In respect to LAC Ia, the water action should have been minimal. A large avian predator (most possibly the European Eagle Owl, *Bubo bubo*) must have been using the cave or a rock shelter above LAC Ia (most probable scenario), and thus small mammals (including bats) were transported to the chamber. Approximately 1/4 of bat fossils from LAC present some degree of corrosion, whereas the respective number from LAC Ia is 1/3. The latter, in accordance with the increase in taxa that roost in trees and in taxa with mixed roosting preferences in LAC Ia, cannot exclude that bats comprised a significant amount of the European Eagle Owl’s diet, which has been documented to specialize on certain prey, including bats (Andrews 1990).

Consequently, the relatively good preservation of most of the chiropteran fossils in combination with the corrosion observed on many of them can exclude the probability of bats being the basic food of the predator (Sevilla 2015) and of very intense flooding events. Therefore, both LAC and LAC Ia were most probably mixed assemblages of nursery roosts, with chiropteran remains being accumulated due to death by natural causes and predation.

5.3 BIOSTRATIGRAPHY AND DATING

From an evolutionary perspective, bats are a good example of evolutionary stasis among vertebrates, as the oldest known fossils have already “modern” anatomical adaptations and they show a very low rate of morphological change through time (Gunnell and Simmons 2005). Taxa are long-lasting, ruling out the possibility of using chiropteran fossils as biostratigraphic indicators (Sevilla 2016). For instance, fossils of the genus *Rhinolophus* are known since the Early Oligocene, the genus *Myotis* has a record starting at the Late Oligocene and other genera such as *Miniopterus*, *Eptesicus*, *Plecotus* and *Pipistrellus* have Miocene fossils (see Gunnell and Simmons 2005). At species level, the duration of the taxa is also extended, especially when compared with other small mammals (i.e. rodents). Most of the species currently found in Europe are known from Late Pliocene/Early Pleistocene sites. Thus, it is not possible to try to establish the age of an assemblage from its fossil bats. Slight changes in size that might be used for dating purposes have been reported for some species – such as the larger size in *Myotis myotis* in the Early Pleistocene of Spain (Sevilla and Chaline 2004) or in *Eptesicus praeglacialis* from the latest Pliocene-Early Pleistocene of Hungary and Romania (Sevilla, P. pers. comm.) – however, these records are punctual occurrences and, consequently, they are of little use in biostratigraphy. Nevertheless, it is important to place the rich bat assemblages from LAC and LAC Ia in a chronological context.

The earliest occurrence of a chiropteran taxon that is present in the fossil record of Loutra Almopias Cave A is *Rhinolophus* ex gr. *euryale* from the Ruscinian (MN15b) locality of Muselievo (Bulgaria) (Popov 2004). However, most of the chiropteran taxa described from Loutra Almopias Cave A originated during the Early and the Middle Pleistocene (Figure 5.10) (Salari et al. 2019 and references therein, Tata and Kotsakis 2005 and references therein, Sevilla 1988 and references therein, Horacek and Poulianos 1988 and references therein). Thereafter, neither LAC nor LAC Ia are older than the Middle Pleistocene.

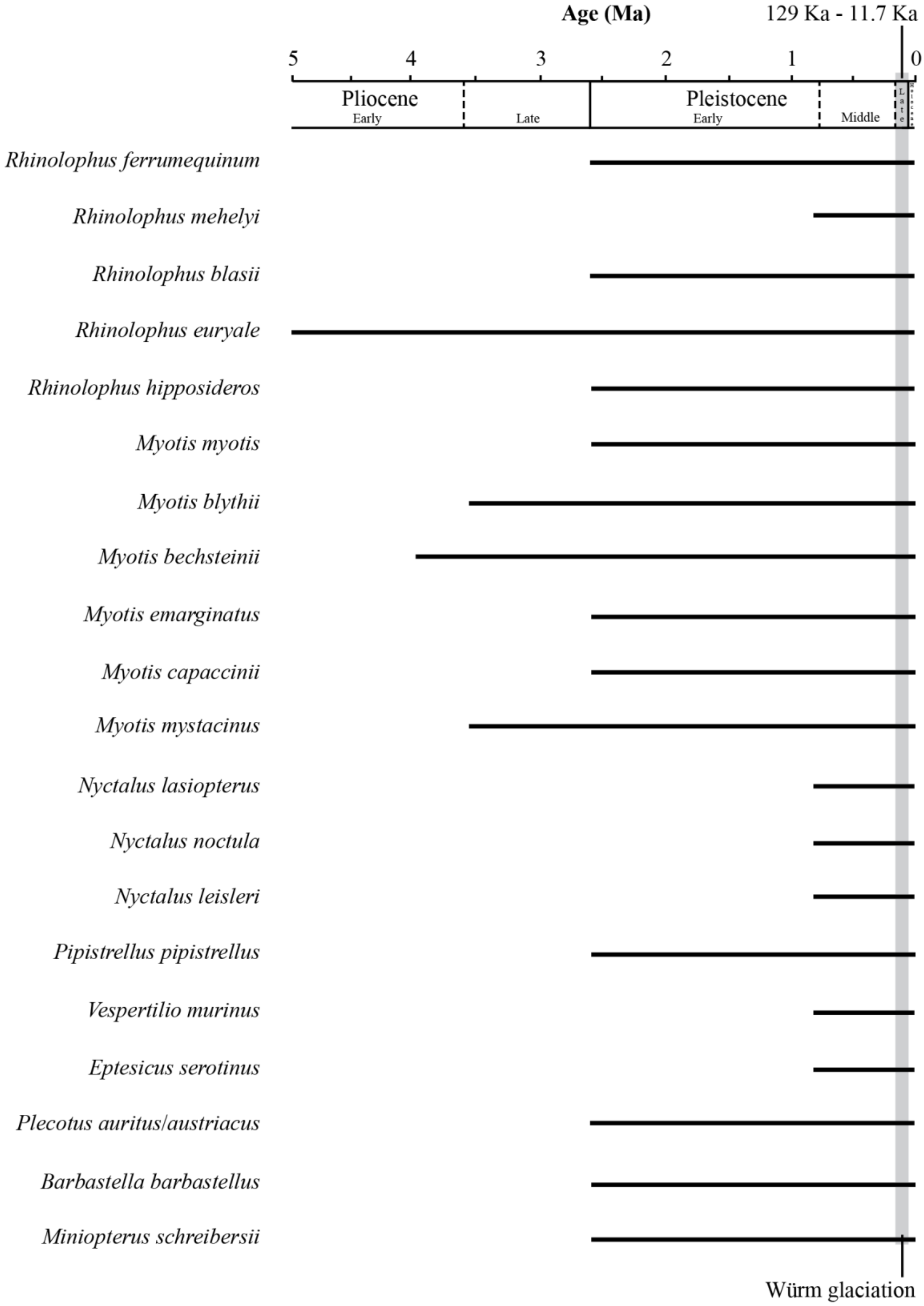

Figure 5.10 Biochronological overview of the chiropteran taxa retrieved from Loutra Almopias Cave A (Salari et al. 2019 and references therein: *Rhinolophus ferrumequinum*, *Rhinolophus mehelyi*, *Rhinolophus euryale*, *Myotis myotis*, *Myotis capaccinii*, *Myotis mystacinus*, *Plecotus auritus/austriacus*, *Miniopterus schreibersii*; Tata and Kotsakis 2005 and references therein: *Rhinolophus blasii*; Sevilla 1988 and references therein: *Rhinolophus hipposideros*, *Myotis bechsteinii*, *Myotis emarginatus*, *Nyctalus lasiopterus*, *Nyctalus leisleri*, *Pipistrellus pipistrellus*, *Eptesicus serotinus*, *Barbastella barbastellus*; Horacek and Poulianos 1988 and references therein: *Myotis blythii*, *Nyctalus noctula*, *Vespertilio murinus*).

The excavations that lasted more than 20 years, brought to light a plethora of small and large mammals (see CHAPTER 1), some of which are of high biostratigraphic importance. More specifically, the presence of *Crocidura suaveolens* and *Arvicola amphibius* (= *Arvicola terrestris*) in both LAC and LAC Ia fossiliferous assemblages, indicate an age younger than the Riss Glaciation (MIS 6-10) (Chatzopoulou 2014 and references therein). Moreover, *Erinaceus europaeus* (only in LAC), *Crocidura leucodon*, *Mus spicilegus* (only in LAC) and *Lepus timidus* (only in LAC Ia) indicate an age younger than the onset of the Würm Glaciation (MIS 2-6), whereas the presence of *Ochotona pusilla* in both LAC and LAC Ia fossiliferous assemblages, places both faunas before the Holocene epoch (Chatzopoulou 2014 and references therein). Similarly, certain large mammals (viz. *Ursus ingressus*, *Crocuta crocuta spelaea* and *Panthera pardus*) that were found in LAC, all disappear from the fossil record at the end of the Würm Glaciation (Tsoukala et al. 2006, Nagel et al. 2019).

Therefore, the biostratigraphy of Loutra Almopias Cave A large and small mammal fossiliferous assemblages indicates an age during the last glacial period, the Würm Glaciation – which roughly coincides with Late Pleistocene – for both faunas.

Apart from the biostratigraphic analysis, several absolute dating methods were applied on sediments, speleothems, charcoals and fossils. The Ephorate of Palaeoanthropology and Speleology (EPS), Ministry of Culture dated sediments from Loutra Almopias Cave A, as well as from the surrounding area with the method of Electron Spin Resonance (ESR)[10]. More specifically, Kabouroglou et al. (2006) collected calcareous material from the sediments of the bench deposits from rock shelter ZA and from the excavated square N10 (chamber LAC I). Dating of the bench deposits (sample LTR-1) resulted in an age of 35.000 Ka BP ±5.250 Ka. Dating of the calcitic crust that is overlaying the fossiliferous clay stratum (samples LTR-5 and LTR-6) resulted in an age of 5.500 Ka BP ±1.375 Ka and 4.500 Ka BP ±1.125 Ka respectively. Dating of the calcitic crust that is underlaying the fossiliferous clay stratum (sample LTR-4) resulted in an age of 20.000 Ka BP ±3.000 Ka for its upper part and 14.000 Ka BP ±2.100 Ka for its lower part. Dating of the fourth (from the top) calcitic crust

[10] Dating was conducted at the Laboratory of Archaeometry of the Institute of Materials Science – now merged with the Institute of Microelectronics and Physical Chemistry to the Institute of Nanoscience and Nanotechnology (INN) – of the National Centre for Scientific Research “Demokritos” (NCSR “Demokritos”).

(sample LTR-3) was not successful and dating of the fifth (from the top) calcitic crust (sample LTR-2) resulted in an age of 22.500 Ka BP ±3.375 Ka. Accordingly, Kabouroglou et al. (2006) concluded that the fossiliferous clay stratum should have been deposited between 14.000-12.000 Ka BP. In a later study, Kabouroglou et al. (2008) redated the bench deposits at 37.000 Ka BP.

Moreover, Zacharias et al. (2008) dated aluminosilicate minerals of the cave deposits with the method of Optically Stimulated Luminescence (OSL). More specifically, Kabouroglou et al. (2007) collected two samples (LUM12_06 and LUM13_06) from square X1 (chamber LAC Ic) and one sample (LUM14_06) from square I1 (chamber LAC I) – both squares excavated by EPS. Samples from square X1 were collected, from a depth of 62 cm and 179 cm from the datum point, from fluvio-torrential deposits (sands) that are underlying the fossiliferous clay stratum and resulted in an age of 21.910 Ka BP ±3.000 Ka and 26.700 Ka BP ±3.900 Ka respectively. Sample from square I1 was collected, from a depth of 294 cm from the datum point, from fluvio-torrential deposits that are underlying the fossiliferous clay stratum and resulted in an age of 24.100 Ka BP ±3.300 Ka. Kabouroglou et al. (2008) also collected samples from squares V4 and V5 (chamber LAC Ib), from a depth of 70 and 65 cm from the datum point respectively, from the black sandy stratum overlaying the fossiliferous clay stratum and resulted in an age of 11.500 Ka BP ±1.600 Ka and 13.400 Ka BP ±1.900 Ka respectively (Zacharias et al. 2008), concluding that the fossiliferous clay stratum should have been completely deposited before 11.500 Ka BP.

In addition, Kabouroglou et al. (2006) collected one charcoal from the inner parts of a stalagmite from the upper strata of square X1 (chamber LAC Ic), from a depth of 75 cm above the datum point. The collected sample (DEM-1787 and OxA-13995) was dated with the ^{14}C Accelerator Mass Spectrometry (AMS) method[7,11] and resulted in an age of 4.820 Ka BC ±0.100 Ka. Moreover, Kabouroglou et al. (2007) collected two more charcoals (samples DEM-1526 and DEM-1654), from the uppermost 13 cm of the cave's floor from squares J2 and W8 (adjacent to chamber LAC Ib) – both squares excavated by EPS. The dating resulted in an age of 4.820 Ka BC ±0.100 Ka and 5.135 Ka BC ±0.085 Ka respectively (Kabouroglou et al. 2008). However, several inconsistencies are observed in these dating results (Kabouroglou et al. 2006, 2007,

[11] Dating was conducted at the Research Laboratory for Archaeology and History of Art (University of Oxford).

2008), which are sometimes given in years BP and sometimes in years BC, sample DEM-1526 being from square Y8 in Kabouroglou et al. (2007) and from square J2 in Kabouroglou et al. (2008), etc. Consequently, they can only be treated with caution and thus the only safe outcome is that the aforementioned belong to the Holocene epoch.

Apart from EPS, the Department of Palaeontology (University of Vienna) and in cooperation with the Aristotle University of Thessaloniki (AUTh) dated the calcitic crust underlying the fossiliferous clay stratum and a stalagmite that was stuck on the first (from the top) calcitic crust from squares G10 and G11 (chamber LAC Ic) with the U/Th method[12]. The former resulted in an age of 29.900 Ka BP ±3.400 Ka and the latter in an age of 3.670 Ka BP ±0.003 Ka (Frischauf, C. pers. comm. to Tsoukala, E.).

Rabeder et al. (2006) dated the calcitic crusts overlaying (sample 22770) and underlaying (sample 22772) the fossiliferous clay stratum from the N10 square (chamber LAC I) with the ^{14}C method[13]. The former resulted in an age of 32.060 Ka BP ±0.520/0.490 Ka (36.494 cal Ka BP ±0.520 Ka) and the latter in an age of 33.910 Ka BP ±0.590/0.550 Ka (39.179 cal Ka BP ±1.269 Ka).

Except for the previously mentioned absolute dating methods that were applied on sediments, cave decorations and charcoals, it was also considered necessary to directly date the fossil material. For that reason, Rabeder et al. (2006) dated seven *Ursus ingressus* samples with the AMS method[10]. Dating was only possible in one sample (sample LAC7573), due to the lack of collagen from the rest of the samples. The sample – a Gamssulzen Cave Bear femur from square N10 (chamber LAC I) – was retrieved from a depth of 120 cm from the datum point and it resulted in an age of 37.880 Ka BP ±0.370/0.360 Ka (42.361 cal Ka BP ±0.378 Ka). Rabeder et al. (2006) concluded that the excavated large mammal fauna was not found in situ, but it was transferred to its current site, together with a large amount of pebbles, from various parts of Loutra Almopias Cave A. This was caused by flood events of the river Thermopotamos (see SECTION 5.2) that occurred between 34.000-32.000 Ka BP.

Apart from the large mammals, attempts were also made to date the micromammalian fauna that was retrieved from the cave's floor sediments with the AMS method, but this was not possible, due to lack of collagen in the fossils (Chatzopoulou 2014). In respect to the fossils from chamber LAC Ia, the AMS dating

[12] Dating was conducted at the Curt Engelhorn Zentrum Archäometrie (Mannheim).

[13] Dating was conducted at the Centre for Isotope Research (University of Groningen).

method[14] was applied on micromammals (sample 60) which resulted in an age of 11.230 Ka BP ±0.110 Ka (13.125 cal Ka BP ±0.144 Ka). A second sample, a *Lepus* tibia (sample 5631) was dated at an age of 12.350 Ka BP ±0.040 Ka (14.535 cal Ka BP ±0.331 Ka). Consequently, the fauna from LAC Ia is younger than the fauna retrieved from the cave floor sediments and it roughly coincides with the onset of Younger Dryas (Chatzopoulou 2014).

Recently, for the purpose of this study, it was considered essential to date chiropteran fossils with the AMS dating method[10] from both LAC and LAC Ia. Dating of one sample (LAC-Chir.) from square B10 (chamber LAC II), from a depth of 87-123 cm below the datum point and of one sample (LAC Ia-Chir.) from LAC Ia, from a depth of 400-414 cm above the datum point was not possible, due to the lack of collagen from the fossils.

5.4 PALAEOENVIRONMENTAL ANALYSIS AND HABITAT USE

Despite the fact that bats are not good biostratigraphic indicators, modern detailed studies on the ecology of extant Chiroptera, such as their habitat and roosting preferences, their foraging environment, etc., can be used as an extra source of information for more precise palaeoenvironmental reconstructions – when fossils of extant bats are unearthed (Sevilla and Chaline 2011).

In respect to the climatological preferences of each taxon, the vast majority (over 80%) of the chiropteran species found in the sediments of Loutra Almopias Cave A have a preference for warm/hot climatic conditions (Figure 5.11). Nevertheless, a small increase in the proportion of species that have a preference in cool/cold climatic conditions is observed during latest Pleistocene.

More specifically, *Rhinolophus mehelyi*, *Rhinolophus blasii*, *Rhinolophus euryale*, *Myotis capaccinii* and *Miniopterus schreibersii* are species with strict Mediterranean affinities and *Rhinolophus ferrumequinum*, *Rhinolophus hipposideros*, *Myotis myotis*, *Myotis blythii*, *Myotis emarginatus*, *Pipistrellus pipistrellus* and *Eptesicus serotinus* are species with broader affinities to Mediterranean climate (Dietz et al. 2009, Salari and Silvestri 2015, Barova and Streit 2018). On the contrary, *Myotis bechsteinii*, *Myotis mystacinus*, *Nyctalus lasiopterus*, *Nyctalus noctula*, *Nyctalus leisleri*, *Barbastella*

[14] Dating was conducted at the Vienna Environmental Research Accelerator (University of Vienna).

barbastellus and *Vespertilio murinus* are all species with affinities to Nemoral climate (Dietz et al. 2009, Salari and Silvestri 2015, Barova and Streit 2018).

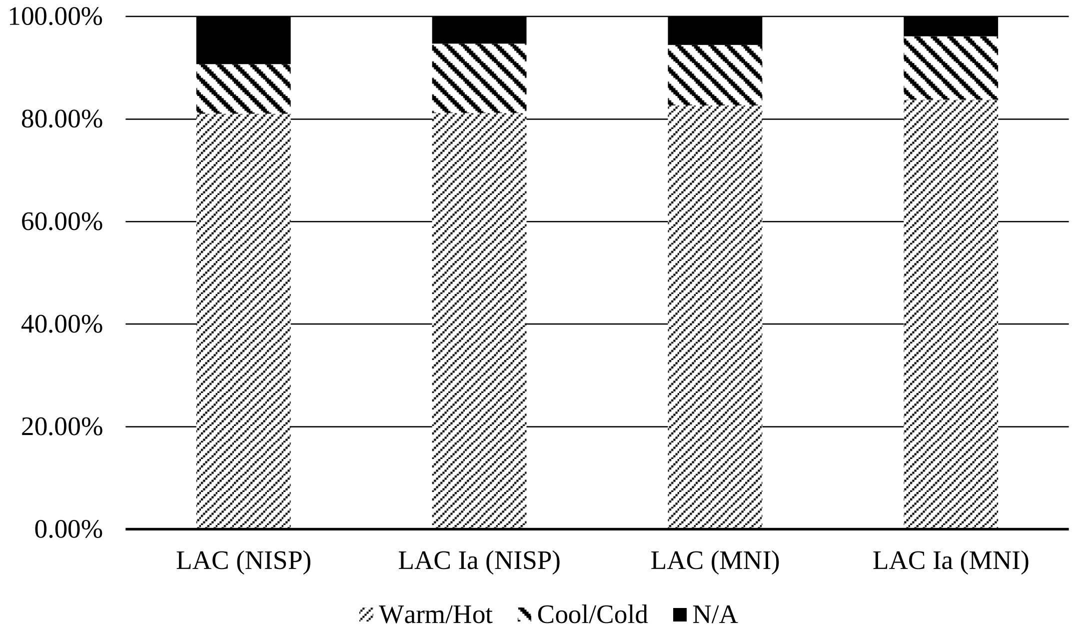

Figure 5.11 Variation in the proportion of bat species from Loutra Almopias Cave A grouped according to their climatic preference. LAC: Late Pleistocene; LAC Ia: latest Pleistocene; NISP: Number of Identified imperative Specimens; MNI: Minimum Number of Individuals.

Despite the fact that the fossil chiropteran assemblages from Loutra Almopias Cave A are indicative of a palaeoclimate similar to nowadays Mediterranean climate (viz. dry summers and mild, wet winters), a – minor, but still important – increase is observed in the proportion of species with a preference in a palaeoclimate similar to the current Nemoral climate (viz. moderate temperate climate with short frost periods), indicating a potential climate differentiation in the vicinity of Loutra Almopias Cave A between Late and latest Pleistocene, possibly related to the onset of Younger Dryas Chronozone (Piskoulis 2018, 2020).

Defining the chronology of the two chiropteran assemblages (see SECTION 5.3) was crucial, as it aided in the direct comparison of Loutra Almopias Cave A with high resolution pollen data from Lakes Ohrid (North Macedonia/Albania) (Francke et al. 2019, Wagner et al. 2019) and Prespa (Greece/North Macedonia/Albania) (Wagner et al. 2012, Panagiotopoulos et al. 2013, 2014, Francke et al. 2019) and other palaeoclimatic data from the vicinity of the cave, such as Lake Maliq (Albania) (Bordon et al. 2009) and Mount Smolikas (Greece) (Hughes 2004, Hughes et al. 2006). The climate proxies used from Lakes Ohrid and Prespa were total inorganic carbon (TIC), total organic carbon (TOC), Ca, $\delta^{13}C$ and the simulated precipitation and surface air temperature from Lake Ohrid (Figure 5.12).

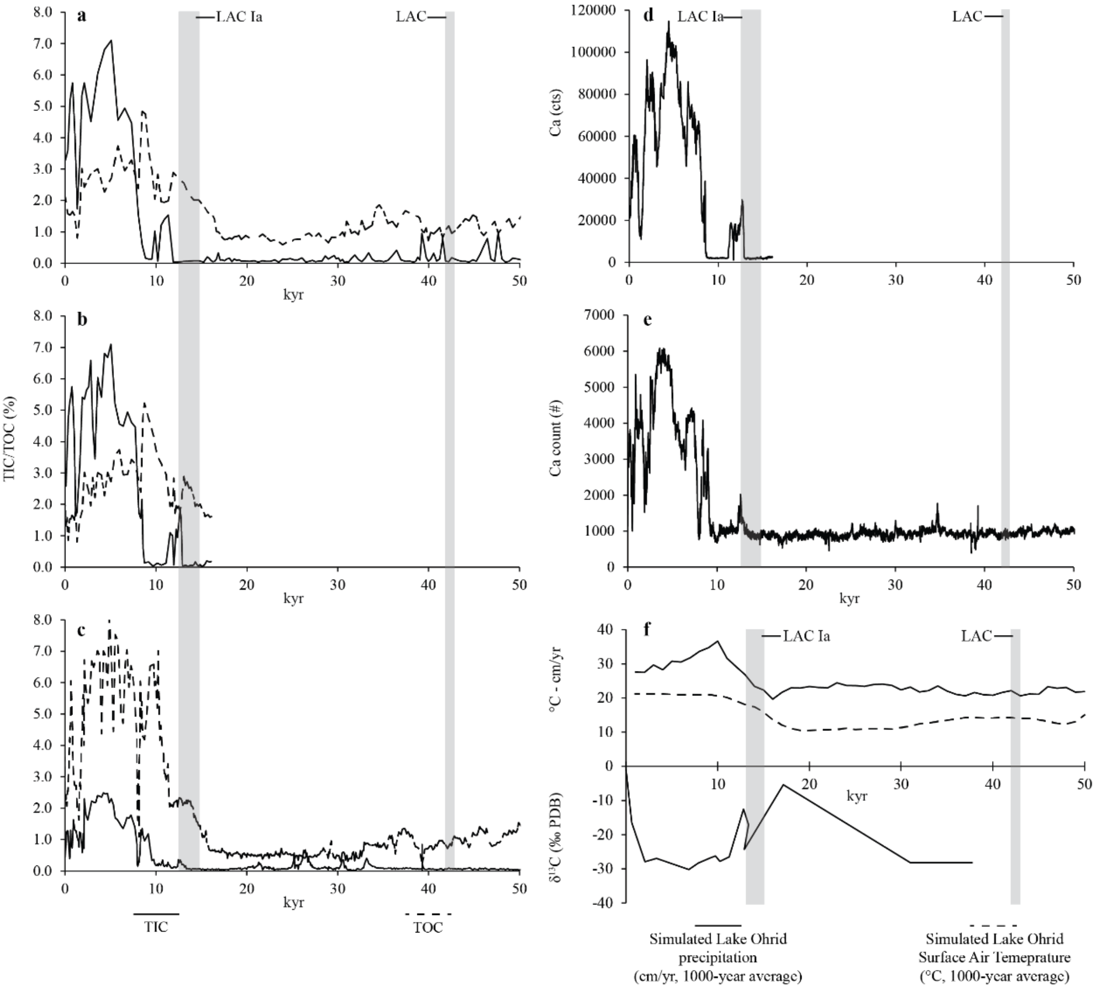

Figure 5.12 Climate proxies obtained from lake cores plotted against time. **a.** TIC and TOC from Lake Ohrid (data from Wagner et al. 2019), **b.** TIC and TOC from Lake Ohrid (data from Francke et al. 2019), **c.** TIC and TOC of Lake Prespa (data from Wagner et al. 2012), **d.** Ca from Lake Prespa (data from Francke et al. 2019), **e.** Ca from Lake Prespa (data from Wagner et al. 2012), **f.** Simulated precipitation and surface air temperature from Lake Ohrid and $\delta^{13}C$ from Lake Prespa (data from Wagner et al. 2012, 2019). TIC: Total Inorganic Carbon; TOC: Total Organic Carbon. Modified after Piskoulis (2020).

The proxies obtained from the pollen records of Lakes Ohrid, Prespa and Maliq (Bordon et al. 2009, Wagner et al. 2012, Panagiotopoulos et al. 2013, 2014, Francke et al. 2019, Wagner et al. 2019) indicate a (relatively) cold and dry climate, with low spring and summer temperatures for the time frame that corresponds to LAC and a (relatively) warm and wet climate, but with low spring and summer temperatures for the time frame that corresponds to LAC Ia (Piskoulis 2020)[15]. Additionally, the last glacial-periglacial activity in Greece occurred during Late Pleistocene on Mount Smolikas, where according to climate reconstructions a temperature drop of 6.24ºC and a simultaneous increase in precipitation occurred (Hughes 2004, Hughes et al. 2006). This drop in temperature might seem odd when compared to the overall warming of the lake basins, however, the diverse topography and the high altitude of Mount Smolikas (2637 m) indicate a local effect (Piskoulis 2020). Furthermore, the presence of *Lepus timidus*, *Lagopus lagopus* and *Plectrophenax nivalis* in the LAC Ia faunal assemblage, indicate cool/cold climatic conditions (Chatzopoulou 2014, Boev and Tsoukala 2019). However, these taxa show a response to the glacial-interglacial oscillations with a time lag (Piskoulis 2020). Consequently, this all indicates a correlation of the LAC Ia chiropteran faunal assemblage with the onset of the Younger Dryas Chronozone in the region of Northern Greece.

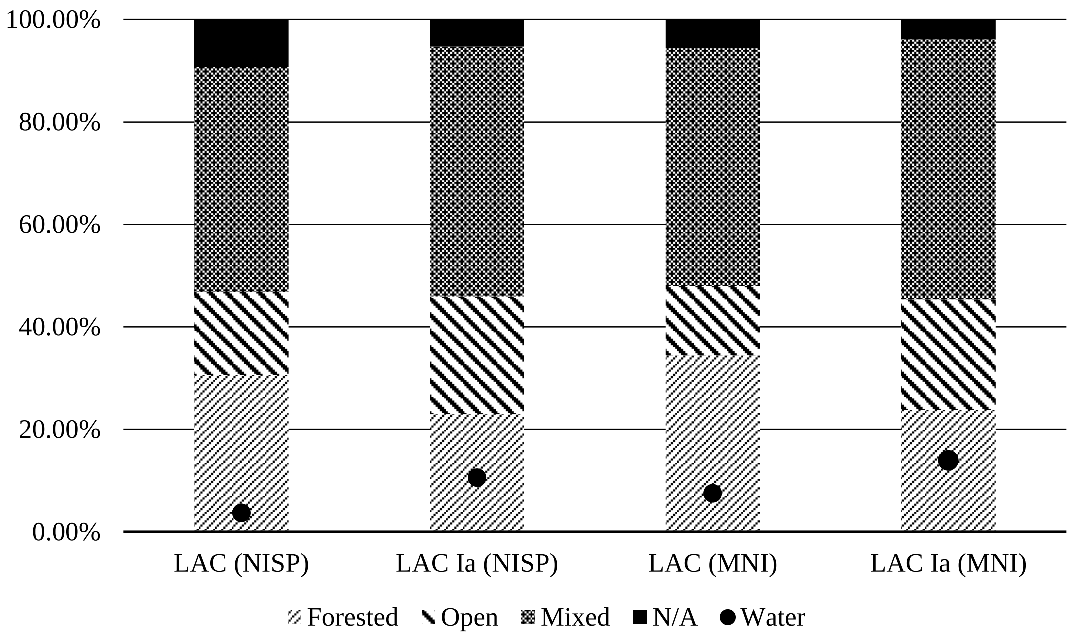

Figure 5.13 Variation in the proportion of bat species from Loutra Almopias Cave A grouped according to their habitat preference. LAC: Late Pleistocene; LAC Ia: latest Pleistocene; NISP: Number of Identified Specimens; MNI: Minimum Number of Individuals.

[15] Samples for pollen analysis were collected from squares Q11 (LAC I) and D10 (LAC II), however, the pollen sum was insufficient for statistical analysis. Nevertheless, 23 taxa have been identified which a indicate a rather temperate climate, under relatively dry conditions (Unpublished data, Tsoukala, E. pers. comm.).

A pattern similar to the palaeoclimatic preferences of the chiropteran taxa from Loutra Almopias Cave A is apparent in the case of cave-dwelling species and species that prefer trees for roosting (Figure 5.9). More specifically, the latter were slightly increased during the latest Pleistocene. Taxa with mixed roosting preferences were also, negligibly, increased in the sediments of the elevated chamber LAC Ia.

In respect to their habitat preferences the majority of the identified taxa prefer a mixed environment with both open and wooded areas (Figure 5.13). During the Late Pleistocene more species with a preference to forest habitats occur. On the contrary, the proportion of species with a preference for open areas increased during the latest Pleistocene. Additionally, the proportion of taxa whose only limitation is the presence of water doubled during latest Pleistocene (Figure 5.13).

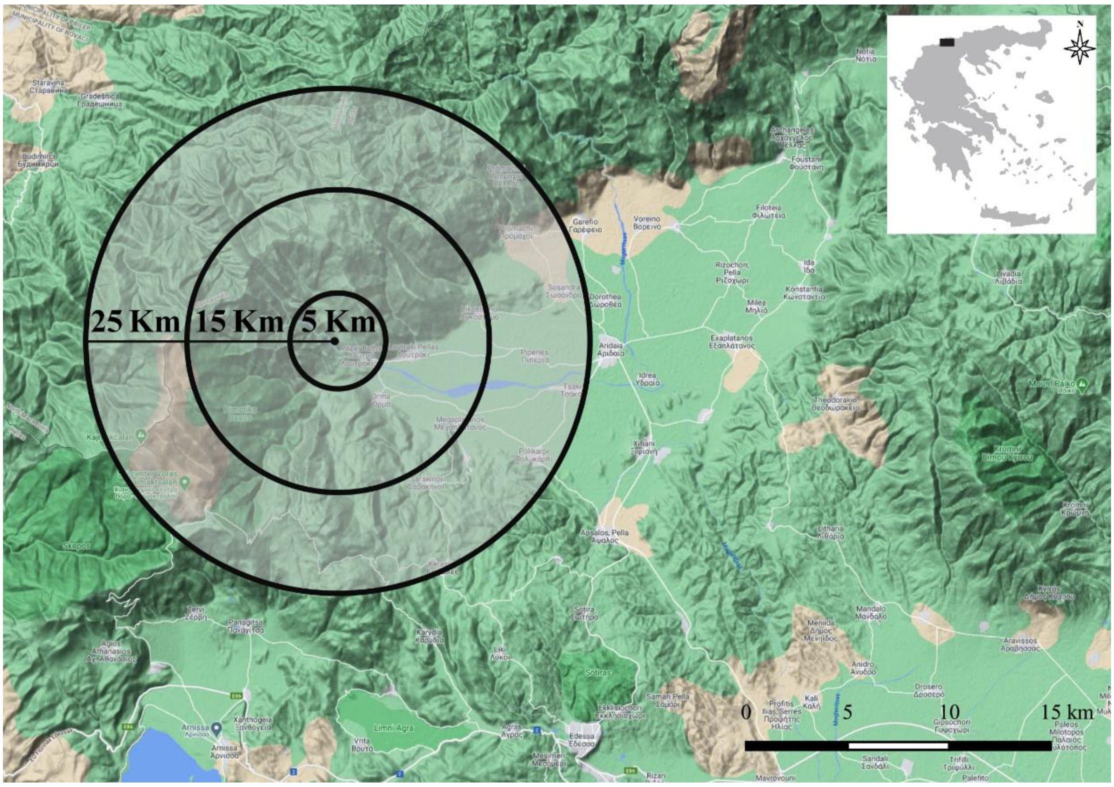

Figure 5.14 The maximum foraging radius of the chiropteran species retrieved from Loutra Almopias Cave A sediments centred on the entrance of the cave. Map generated using Google Maps (Google Terrain).

Although many European bat species are known to migrate over long distances, foraging usually takes place within 10 Km (for most of the species) from the roosting place; however, there are some species (*Myotis myotis*, *Myotis blythii*, *Myotis capaccinii*, *Nyctalus lasiopterus* and *Nyctalus noctula*) that can travel up to 26 Km to hunt (Dietz et al. 2009, Barova and Streit 2018). It is evident that the broader region of Loutra Almopias Cave A has a variety of landscapes, including plains, mountains, rivers, etc. (see CHAPTER 2) within the foraging radius of most of the taxa (Figure 5.14), which explains the great diversity in terms of chiropteran species.

It is noteworthy that species representation in both faunal assemblages corresponds well to the behaviour of each taxon (Dietz et al. 2009). Rhinolophidae dominate the fossil record (more than 40%) as all species form large colonies and mix well with other species. The same occurs with the large-sized *Myotis* (*Myotis myotis* and *Myotis blythii*) and *Miniopterus schreibersii*. In contrast, the rest of the taxa do not form large colonies and their coexistence with other species is not so extensive.

Although, it is quite interesting that even if *Myotis emarginatus* and *Myotis capaccinii* form large colonies and get along well with other species, they are underrepresented in the fossil record of Loutra Almopias Cave A, with the latter being present only in LAC Ia. Consequently, it is apparent that both LAC and LAC Ia faunal assemblages are dominated by large and/or medium-sized taxa. However, despite the fact that small-sized bats are usually not preserved in the fossil record as they are more prone to breakage (Sevilla 2015), oversampling has minimized a possible size-bias and reached to the best possible reconstruction of the bat faunas from Loutra Almopias Cave A and the adjacent region. Thus, underrepresentation of *Myotis emarginatus* and *Myotis capaccinii* must be due to other factors (i.e. climatic, food availability, etc.).

5.5 BIOGEOGRAPHY

The distribution of Chiroptera in the Balkan Peninsula during the Late Pleistocene (Figure 5.15) is relatively sparse with most localities being in the Istrian Peninsula and the adjacent region, Serbia, Bulgaria and Southern Greece. Apart from this, the identification of chiropteran specimens in most localities did not go further than Chiroptera indet. (Hijenska Cave, Ljubićeva Cave, Šandalja I + II, Vrtare Male, Mujina Cave, Vela Spila, Mališina Stijena, Petnička Cave, Smolućka Cave, Vasiljska Cave, Popšićka Cave, Vrelska Cave, Varkiza 1, 2, Anonymous Cave of Schisto at Keratsini, Franchthi Cave, Naxos, Liko Cave, Bate Cave, Kharoumes 5). The most complete records come from the Bulgarian localities Magura, Razishka Cave, Cave 16, Bacho Kiro, the Croatian locality Vindija Cave, the Slovenian locality Snezna Jama Cave and the Italian locality Caverna degli Orsi (Table 5.5). Nowadays, Croatia, Bulgaria and Greece are the richest countries in chiropteran species in Europe (Ulrich et al. 2007).

Loutra Almopias Cave A is an important Late Pleistocene site for Chiroptera as not only it fills the biogeographical gap between Southern Greece and Central Balkans, but it is also the richest and most diverse in the Balkan Peninsula (and subsequently Greece). However, the absence of Late Pleistocene (and not only) chiropteran records from other regions of the Balkan Peninsula is apparent and shows the need for more research on this specific topic.

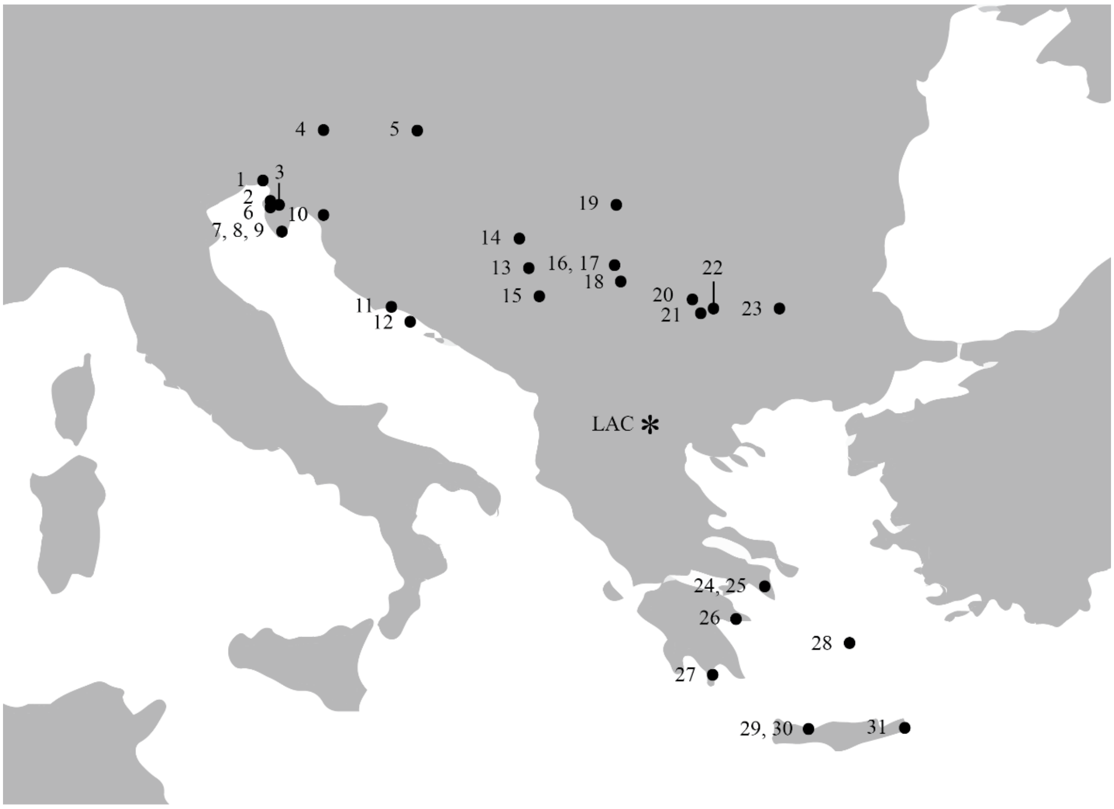

Figure 5.15 Biogeographical distribution of Chiroptera in the Balkan Peninsula during Late Pleistocene. LAC: Loutra Almopias Cave A; **Italy:** **1.** Grotta dell'Orso[1], **2.** Caverna degli Orsi[2], **Slovenia:** **3.** Črni Kal 3[3], **4.** Snežna Jama Cave[3, 4], **Croatia:** **5.** Vindija Cave[5], **6.** Hijenska Cave[6], **7.** Ljubićeva Cave[6], **8.** Šandalja I + II[6], **9.** Marlera I[6], **10.** Vrtare Male[6], **11.** Mujina Cave[6], **12.** Vela Spila[6], **Montenegro:** **13.** Mališina Stijena[7], **Serbia:** **14.** Petnička Cave[8], **15.** Smolućka Cave[8], **16.** Vasiljska Cave[8], **17.** Popšićka Cave[8], **18.** Vrelska Cave[8], **Romania:** **19.** Comarnic Cave[9], **Bulgaria:** **20.** Magura[10], **21.** Razishka Cave[10], **22.** Cave 16[10], **23.** Bacho Kiro[10], **Greece:** **24.** Varkiza 1, 2[11], **25.** Anonymous Cave of Schisto at Keratsini[11], **26.** Franchthi Cave[11], **27.** Kalamakia Cave[11], **28.** Naxos[11], **29.** Liko Cave[11], **30.** Bate Cave[11], **31**. Kharoumes 5[11]. [1]Bon et al. 1991, [2]Berto and Rubinato 2013, [3]Aguilar et al. 1998, [4]Sigé et al. 2003, [5]Mauch Lenardić 2009, [6]Mauch Lenardić et al. 2018, [7]Bogićević and Dimitrijević 2004, [8]Dimitrijević 1996, [9]Povară 2019, [10]Popov 2018, [11]Piskoulis and Chatzopoulou in press.

Nevertheless, it was considered essential to compare the chiropteran faunas from Loutra Almopias Cave A with the aforementioned Late Pleistocene faunas from the Balkan Peninsula. This was achieved with the calculation of “Simpson’s Similarity

Index"[16] (Raup and Crick 1979) and "Pickford's Index of Distance"[17] (Pickford 1981) (Table 5.6). In the first case (Simpson's Similarity Index: SSI), similarity between two faunas occurs when the resulted index is close to 1.00, but it is worth noting that this index should be considered with caution for faunas with few identified taxa. In the second case (Pickford's Index of Distance: PID), similarity between two faunas occurs when the resulted index is close to 0.00 and it is considered a reliable index as it takes into account both occurring and not-occurring taxa between the compared faunas.

From Table 5.6 it is evident that Late Pleistocene LAC and latest Pleistocene LAC Ia are very similar to each other with SSI being 1.00 and PID being 0.00. The similarity between LAC and LAC Ia with the extant bat fauna of Greece is relatively strong (SSI = 0.73 and 0.76 respectively, PID = 0.13 and 0.12 respectively). Moreover, LAC is very similar to Magura, Comarnic Cave, Marlera I, Grotta dell'Orso and Caverna degli Orsi (SSI = 1.00, PID = 0.00) and LAC Ia is very similar to Magura, Comarnic Cave, Marlera I, Črni Kal 3, Grotta dell'Orso and Caverna degli Orsi (SSI = 1.00, PID = 0.00). On the contrary, there is no similarity between the bat faunas of LAC, Kalamakia Cave and Bacho Kiro (SSI = 0.67 and 0.60 respectively, PID = 0.30 and 0.29 respectively) and between the bat faunas of LAC Ia, Kalamakia Cave and Bacho Kiro (SSI = 0.67 and 0.60 respectively, PID = 0.31 and 0.26 respectively).

The similarity between LAC and LAC Ia to Vindija Cave is also relatively strong (SSI = 0.71 and 0.71 respectively, PID = 0.11 and 0.12 respectively). However, LAC Ia is somewhat similar also to Razishka Cave (SSI = 0.67, PID = 0.20), Cave 16 (SSI = 0.69, PID = 0.18) and Snezna Jama Cave (SSI = 0.80, PID = 0.17).

All chiropteran species that have been identified form the sediments of Loutra Almopias Cave A are currently inhabiting the Greek region and the broader region of the cave, with the exception of *Rhinolophus mehelyi* and *Rousettus aegyptiacus* (Dietz et al. 2009, Strachinis et al. 2018, IUCN 2021). In addition to that, there are no recent records from the studied cave indicating permanent presence of Chiroptera in it (Paragamian 2021). There are, however, six species (*Rhinolophus ferrumequinum*, *Rhinolophus blasii*, *Rhinolophus euryale*, *Rhinolophus hipposideros*, *Myotis blythii* and *Miniopterus schreibersii*) documented in the nearby Varathron Cave (Life GRECABAT 2021).

---

[16] $\text{Simpson's Similarity Index} = \frac{\text{number of shared taxa}}{\text{number of taxa occurring in the smaller sample}}$

[17] $\text{Pickford's Index of Distance} = \frac{\text{number of taxa occuring only in fauna A} * \text{number of taxa occuring only in fauna B}}{\text{total number of taxa occuring in fauna A} * \text{total number of taxa occuring in fauna B}}$

Table 5.5 Chiropteran taxa recorded in Late Pleistocene localities from the Balkan Peninsula, including the current distribution of Chiroptera in Greece (Hanák et al. 2001, Simmons 2005a, Sfougaris 2009, Strachinis et al. 2018). Localities mentioned in the text, but not included here (Hijenska Cave, Ljubićeva Cave, Šandalja I + II, Vrtare Male, Mujina Cave, Vela Spila, Mališina Stijena, Petnička Cave, Smolućka Cave, Vasiljska Cave, Popšićka Cave, Vrelska Cave, Varkiza 1, 2, Anonymous Cave of Schisto at Keratsini, Franchthi Cave, Naxos, Liko Cave, Bate Cave, Kharoumes 5) have recorded only Chiroptera indet. * Originally *Myotis* ex gr. *mystacinus/brandtii* in Mauch Lenardić (2009), but the term aff. is preferred here. ** Originally *Barbastella darjeligensis* in Popov (2000, 2018), but *Barbastella leucomelas* is preferred here as the former is a subspecies of the latter (Simmons 2005a).

Species \ **Locality**	**Greece (Extant)**	**LAC**	**LAC Ia**	**Kalamakia Cave**	**Magura**	**Razishka Cave**	**Cave 16**	**Bacho Kiro**	**Comarnic Cave**	**Vindija Cave**	**Marlera I**	**Črni Kal 3**	**Snezna Jama Cave**	**Grotta dell'Orso**	**Caverna degli Orsi**
Rhinolophus ferrumequinum	+	+	+			+	+	+	+	+	+		aff.		+
Rhinolophus mehelyi	+	+	+												+
Rhinolophus blasii	+	+	+												
Rhinolophus euryale	+	+	+		+					+			aff.	+	
Rhinolophus mehelyi/euryale/blasii		+	+												
Rhinolophus hipposideros	+	+	+						+	+					
Rhinolophus sp.		+	+	+											+
Myotis myotis	+	+	+						+	+		cf.			+
Myotis blythii	+	+	+	cf.	+	+	+	+	+	+					
Myotis myotis/blythii		+	+												
Myotis bechsteinii	+	+	+			+	+	+		+		cf.	aff.		
Myotis dasycneme								+							
Myotis emarginatus	+	+	+			+				+					
Myotis nattereri	+					+	+	+		+					
Myotis capaccinii	+		+												
Myotis alcathoe	+														
Myotis aurascens	+														
Myotis daubentonii	+									+					

Myotis brandtii	+														
Myotis mystacinus	+		+			+	+					cf.	aff.		
Myotis daubentonii/brandtii							+								
*Myotis mystacinus/brandtii**										aff.					
Myotis sp.		+	+												+
Nyctalus lasiopterus	+		+				+								
Nyctalus noctula	+	+	+			+	+								+
Nyctalus leisleri	+	+	+			+	+								
Hypsugo savii	+					+									
Pipistrellus kuhlii	+														
Pipistrellus nathusii	+														
Pipistrellus pipistrellus	+	+	+			+	+			+					
Pipistrellus pygmaeus	+														
Pipistrellus hanaki	+														
Pipistrellus sp.				+											
Vespertilio murinus	+	+	+				+	+							
Eptesicus serotinus	+	+	+			+	+	+		+					
Eptesicus nilssonii						+	+			?					
Eptesicus bottae	+														
Plecotus auritus	+					cf.	cf.	cf.		+					
Plecotus austriacus	+														
Plecotus auritus/austriacus		+	+												
Plecotus kolombatovici	+														
Plecotus macrobullaris	+														
Barbastella barbastellus	+	+	+		+					+					
Barbastella leucomelas **						cf.	cf.	cf.							
Miniopterus schreibersii	+	+	+		+	+	+	+		+					+
Tadarida teniotis	+														
Rousettus aegyptiacus	+														
Vespertilioninae indet.													+		
Chiroptera indet.		+	+							+	+				

Table 5.6 Comparison of LAC and LAC Ia chiropteran assemblages with other Late Pleistocene chiropteran assemblages for the Balkan Peninsula based on “Simpson’s Similarity Index” (top right) and “Pickford’s Index of Distance” (bottom left). The current distribution of Chiroptera in Greece is also included (Hanák et al. 2001, Simmons 2005a, Sfougaris 2009, Strachinis et al. 2018).

Simpson’s similarity index / **Pickford’s index of distance**	**Greece (Extant)**	**LAC**	**LAC Ia**	**Kalamakia Cave**	**Magura**	**Razishka Cave**	**Cave 16**	**Bacho Kiro**	**Comarnic Cave**	**Vindija Cave**	**Marlera I**	**Črni Kal 3**	**Snezna Jama Cave**	**Grotta dell'Orso**	**Caverna degli Orsi**
Greece (Extant)		0.73	0.76	0.33	1.00	0.93	0.88	0.80	1.00	0.88	0.50	1.00	0.80	1.00	0.71
LAC	0.13		1.00	0.67	1.00	0.60	0.56	0.60	1.00	0.71	1.00	0.67	0.60	1.00	1.00
LAC Ia	0.12	0.00		0.67	1.00	0.67	0.69	0.60	1.00	0.71	1.00	1.00	0.80	1.00	1.00
Kalamakia Cave	0.65	0.30	0.31		0.33	0.33	0.33	0.33	0.33	0.33	0.00	0.00	0.00	0.00	0.33
Magura	0.00	0.00	0.00	0.50		0.50	0.50	0.50	0.25	1.00	0.00	0.00	0.25	1.00	0.25
Razishka Cave	0.04	0.24	0.20	0.62	0.43		0.87	0.80	0.50	0.67	0.50	0.67	0.60	0.00	0.43
Cave 16	0.08	0.26	0.18	0.62	0.44	0.03		0.90	0.50	0.56	0.50	0.67	0.60	0.00	0.43
Bacho Kiro	0.16	0.29	0.26	0.60	0.40	0.09	0.04		0.50	0.70	0.50	0.33	0.40	0.00	0.29
Comarnic Cave	0.00	0.00	0.00	0.50	0.56	0.43	0.44	0.40		1.00	0.50	0.33	0.25	0.00	0.50
Vindija Cave	0.07	0.11	0.12	0.63	0.00	0.14	0.02	0.18	0.00		1.00	0.67	0.60	1.00	0.43
Marlera I	0.50	0.00	0.00	1.00	1.00	0.47	0.47	0.45	0.38	0.00		0.00	0.50	0.00	0.50
Črni Kal 3	0.00	0.30	0.00	1.00	1.00	0.29	0.29	0.60	0.50	0.29	1.00		0.67	0.00	0.33
Snezna Jama Cave	0.18	0.35	0.17	1.00	0.60	0.32	0.33	0.48	0.60	0.33	0.40	0.20		1.00	0.20
Grotta dell'Orso	0.00	0.00	0.00	1.00	0.00	0.67	0.94	1.00	1.00	0.00	1.00	1.00	0.00		0.00
Caverna degli Orsi	0.25	0.00	0.00	0.57	0.64	0.46	0.54	0.57	0.36	0.47	0.43	0.57	0.69	1.00	

All species found in Loutra Almopias Cave A are also present in the records of the previously mentioned localities from the Balkan Peninsula (Table 5.5), with the exception of *Myotis capaccinii*, which is described for the first time from the fossil record of an Upper Pleistocene locality from the Balkan Peninsula (latest Pleistocene LAC Ia). Most common species are *Rhinolophus ferrumequinum* (Razishka Cave, Cave 16, Bacho Kiro, Comarnic Cave, Vindija Cave, Marlera I, Snezna Jama Cave, Caverna degli Orsi), *Myotis blythii* (Kalamakia Cave, Magura, Razishka Cave, Cave 16, Bacho Kiro, Comarnic Cave, Vindija Cave), *Myotis bechsteinii* (Razishka Cave, Cave 16, Bacho Kiro, Črni Kal 3, Snezna Jama Cave, Vindija Cave) and *Miniopterus schreibersii* (Magura, Razishka Cave, Cave 16, Bacho Kiro, Vindija Cave, Caverna degli Orsi).

The results of the similarity analysis between chiropteran faunas from the Balkan Peninsula indicate that during Late Pleistocene the distribution of bats followed a similar pattern for the whole region with the exceptions of Kalamakia Cave and Bacho Kiro, which can be due to regional differentiations of climate, geography, etc. Nevertheless, it has already been established that during the Pleistocene glacial oscillations Southern Europe (Iberian, Italian and Balkan Peninsulas) acted as a refugium for many taxa that migrated from Northern and Central Europe (Hewitt 1999). Similarly, the large and small mammal faunas (including Chiroptera) from Loutra Almopias Cave A are following this perspective (Tsoukala et al. 2006, Chatzopoulou 2014, Nagel et al. 2019).

5.6 *RHINOLOPHUS FERRUMEQUINUM* FROM LOUTRA ALMOPIAS CAVE A TOOTH SIZE DIFFERENTIATION

Research carried out by De Paz (1995) and Kryštufek (1993) indicated that the body size of the Greater Horseshoe Bat, *Rhinolophus ferrumequinum*, is associated with its geographic distribution. More specifically, it comes to antithesis with Bergmann's rule[18] as in the Western Palaearctic it appears to be smaller in the West and larger in the East. Moreover, Kryštufek (1993) found evidence that this body size variation is driven by precipitation. A subsequent study by Budinski et al. (2015) found that its cranial size is larger when the temperatures are higher. Last but not least, Jiang et al. (2019) found that *Rhinolophus ferrumequinum* populations from the Palearctic are associated with

[18] Bergmann's rule states that populations of a given species tend to be of larger size in colder regions, while the opposite occurs in warmer regions.

Allen's rule and consequently their forearm length is positively correlated with mean temperature.

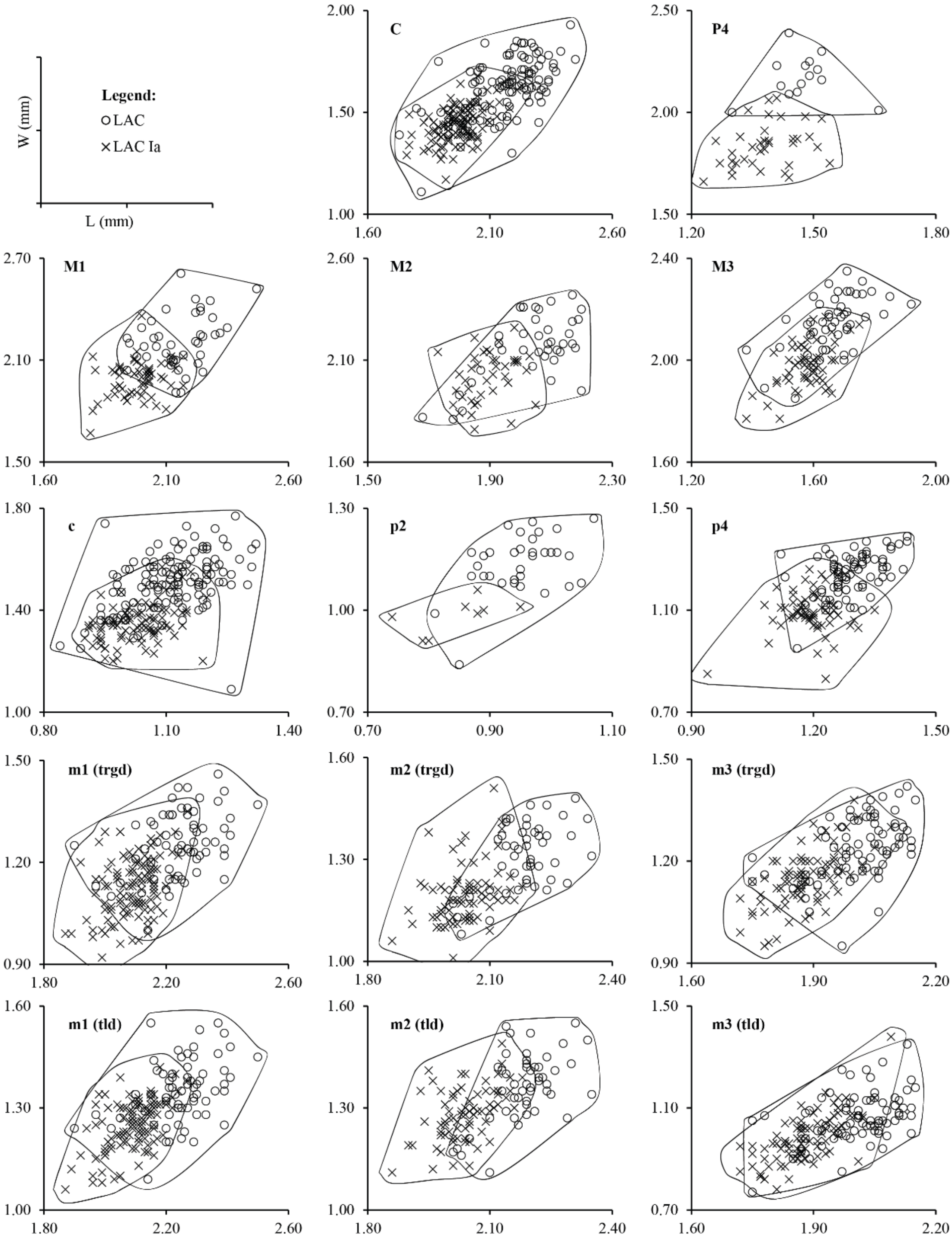

Figure 5.16 *Rhinolophus ferrumequinum*, Loutra Almopias Cave A. XY graphs with the measured (in mm) dental elements (C, P4, M1, M2, M3, c, p2, p4, m1, m2, m3) and the associated convex hulls. LAC: Late Pleistocene; LAC Ia: latest Pleistocene; L: length, W: width, trgd: trigonid; tld: talonid. Modified after Piskoulis (2020).

Given the aforementioned and taking into account the apparent tooth size differentiation of *Rhinolophus ferrumequinum* within the two chronologically different units (LAC and LAC Ia) of Loutra Almopias Cave A (Figure 5.16), a possible correlation of its body size with alterations in climate was examined, the first analysis based solely on fossil material (Piskoulis 2018, 2020).

The generated XY graphs (Figure 5.16) showed that the measured elements of *Rhinolophus ferrumequinum* from Late Pleistocene LAC and latest Pleistocene LAC Ia are in general well separated (see SECTION 4.1). Moreover, there is an overall size decrease of the dental elements of the taxon from LAC to LAC Ia[19]. To be more specific, the maximum values of the specimens from LAC are greater than the maximum values of the specimens from LAC Ia, and accordingly, the minimum values of the specimens from LAC are greater than the minimum values of the specimens from LAC Ia. Nonetheless, there are some cases where an overlap occurs between the minimum values of the specimens from LAC and those from LAC Ia (i.e. C, M2, etc.). As suggested by Jiang et al. (2019), body mass is the optimum solution to infer body size estimations, because it is a cubic measure. Consequently, body mass and body size are positively correlated. Thereafter, Piskoulis (2020) calculated the estimated body mass of each specimen (Table A.6-11) as described by Gunnell et al. (2009) and the results are consistent with the overall size reduction observed (Table 5.7).

Table 5.7 *Rhinolophus ferrumequinum*, Loutra Almopias Cave A. Reconstructed body mass based on the area of M1, p4 and m1 as described by Gunnell et al. (2009). LAC: Late Pleistocene; LAC Ia: latest Pleistocene; MEAN: average; MIN: minimum; MAX: maximum. The body mass is given in grams (g). Modified after Piskoulis (2020).

		MEAN	**MIN**	**MAX**
M1	LAC	21.89	17.98	28.91
	LAC Ia	17.95	13.40	21.63
p4	LAC	22.90	16.33	27.62
	LAC Ia	18.96	12.26	22.29
m1	LAC	22.97	17.45	28.05
	LAC Ia	19.68	14.72	23.75

Kryštufek's (1993) interpretation on the connection between precipitation and body size of *Rhinolophus ferrumequinum*, which is in accordance to the aforesaid, is based on the "resource restriction" hypothesis (Kryštufek 1993 and references therein), which – in short – states that dry days are preferred for foraging and consequently contribute

[19] This was validated by performing a Chi-square test. For more details see Piskoulis (2020).

in the increase of its body size (Piskoulis 2020). Furthermore, the data presented in Piskoulis (2020) indicate increased precipitation during the time frame of LAC Ia (Figure 5.12) and therefore a possible dependence of *Rhinolophus ferrumequinum*'s body size on precipitation as suggested by Kryštufek (1993) and not on temperature as suggested by De Paz (1995), Budinski et al. (2015) and Jiang et al. (2019). Hence, Piskoulis (2020) concluded that body size and precipitation are negatively correlated and thus, the former is climate-dependent.

As already mentioned, several taxa from Central and Northern Europe resorted to Southern Europe during Pleistocene glacial oscillations, which acted as a refugium (Hewitt 1999). Extant *Rhinolophus ferrumequinum* populations from Europe have their origins in those refugia, namely the Iberian, the Italian and the Balkan Peninsulas and Anatolia (Rossiter et al. 2007, Bilgin et al. 2009, Flanders et al. 2009). In addition, recent phylogeographic studies by Flanders et al. (2009) support the idea that *Rhinolophus ferrumequinum* colonized Europe once before and once after the Last Glacial Maximum. Piskoulis (2020) does not rule out that the size-differentiation that was analysed above can be a result of the marked genetic diversity that was described by Rossiter et al. (2007), Bilgin et al. (2009) and Flanders et al. (2009). Allometry (Budinski et al. 2015) cannot be excluded, too, despite the fact that the data presented in Piskoulis (2020) do not present a significant difference in their proportions. On the contrary, sexual dimorphism seems to be trivial (Budinski et al. 2015, Jiang et al. 2019). Nonetheless, "a combination of the aforementioned factors cannot be excluded" (Piskoulis 2020).

It was also examined whether there are more chiropteran taxa that show a similar pattern or not, however, the generated XY graphs and the associated tables of measurements (see CHAPTER 4) do not present a significant tooth size differentiation between the dental elements of any chiropteran taxon from LAC and LAC Ia.

5.7 PHENETIC ANALYSIS

Bat fossils prior to the Neogene are usually fragmentary and not particularly abundant; therefore, the establishment of their evolutionary traits is not an easy task (Gunnell and Simmons 2005). Taxonomists have to rely on the available features found in the most common skeletal parts to assign the remains to a particular taxon. Thus, classification of fossil material is based on morphology. Although Early Eocene bat fossils present remarkable similarities to their extant relatives, there are several morphological adaptations in their teeth and humeri that allowed them to colonise new environment, outpower their competitors and, eventually, rapidly diversify (Sadier et al. 2020). Some of the adaptations involve features that cannot be detected in the fossil record (i.e. the differences in their echolocation calls), but others such as differences in size or in tooth morphology are accessible in fossils. The validity of the features commonly used to identify bats from fossil material was tested by Sevilla and Lopez-Martinez (1986) who compared the standard features used to identify species in the field and skeletal features used for fossils, obtaining a high correlation between both classifications.

The characters used to identify the fossil material from Loutra Almopias Cave A consisted basically on the same as those described by Sevilla and Lopez-Martinez (1986) and they were refined with characters from Sevilla (1988). A few species that were not considered in these papers were added to the analysis (*Rhinolophus blasii*, *Myotis bechsteinii*, *Myotis capaccinii*, *Myotis mystacinus* and *Vespertilio murinus*) since they were present in the site. In order to check that the changes introduced were not interfering with the quality of the identifications, a phenetic analysis was conducted. This resulted in the production of a distribution matrix (Table 5.9) from a total of 28 characters, 27 of which are related to dental elements and one to the distal epiphysis of the humerus. The cluster analysis that followed resulted in the generation of one dendrogram with the implementation of a "Paired Group (UPGMA)" algorithm and "Euclidean" similarity index (Figure 5.17).

In the resulted dendrogram *Rhinolophus* forms a separate branch from the rest of the taxa and *Miniopterus schreibersii* is well-separated from *Rhinolophus*, but closely related to Vespertilionidae. *Myotis* forms a separate cluster within the Vespertilionidae and it is closely related to *Plecotus* and *Barbastella*. *Nyctalus* forms a separate cluster, too, which is closely related to *Pipistrellus*. *Vespertilio* and *Eptesicus* are closely related to the latter.

The clusters resulted from the analysis indicate that the dental and postcranial features that were used leave Rhinolophidae distinctly apart from Vespertilionidae and Miniopteridae. The latter agree with modern classifications based on non-morphological characters (Gunnell and Simmons 2005, Sadier et al 2020, etc.). Within the Vespertilionid cluster, *Miniopterus schreibersii* is the most distant due to the presence of what might be considered as more primitive features in bat dentition (viz. longer toothrows, nyctalodont lower molars, two-rooted p3, less reduced third molars and upper molars with talons) (Smith et al. 2012).

Table 5.8 Distribution matrix of the various dental and postcranial elements across the studied chiropteran species from Loutra Almopias Cave A as established in CHAPTER 3 (Figure 3.5).

Species	**1**	**2**	**3**	**4**	**5**	**6**	**7**	**8**	**9**	**10**	**11**	**12**	**13**	**14**	**15**	**16**	**17**	**18**	**19**	**20**	**21**	**22**	**23**	**24**	**25**	**26**	**27**	**28**
Rhinolophus ferrumequinum	0	-	1	1	0	1	1	1	0	0	0	0	0	1	1	1	0	2	0	0	0	0	0	0	2	2	0	0
Rhinolophus mehelyi	0	-	1	1	1	1	1	1	0	0	0	0	0	1	1	1	0	2	0	0	0	0	0	0	2	2	0	0
Rhinolophus blasii	0	-	1	-	-	-	-	-	-	-	-	-	0	-	-	1	0	2	0	0	0	1	0	0	2	2	0	0
Rhinolophus euryale	0	-	1	1	1	1	1	1	0	0	0	0	0	-	-	1	0	2	0	0	0	1	0	0	2	2	0	0
Rhinolophus hipposideros	0	-	1	1	1	1	1	1	0	0	0	0	0	-	-	1	0	2	0	0	1	1	0	0	2	2	0	0
Myotis myotis	3	3	2	2	0	0	2	0	0	0	0	2	3	2	2	1	0	2	1	1	1	0	0	1	0	0	2	2
Myotis blythii	3	3	2	2	0	0	2	0	0	0	0	2	3	2	2	1	0	2	1	1	1	1	0	1	0	0	2	-
Myotis bechsteinii	3	-	2	2	0	0	1	0	0	0	0	1	-	-	-	1	0	2	1	2	2	2	0	1	1	0	2	2
Myotis emarginatus	-	-	2	2	0	0	1	0	1	1	1	1	-	-	-	1	1	2	1	2	2	2	0	1	1	0	2	-
Myotis capaccinii	-	-	2	-	1	0	1	0	1	1	1	-	-	-	-	1	-	-	1	2	2	2	0	2	2	0	2	-
Myotis mystacinus	-	-	2	-	-	-	1	0	0	0	1	-	-	-	-	1	-	-	1	-	-	-	-	-	-	-	-	2
Nyctalus lasiopterus	-	-	1	-	-	-	1	0	1	1	1	-	-	-	-	0	-	-	0	-	-	-	-	-	-	-	-	2
Nyctalus noctula	2	2	1	1	1	1	1	0	1	1	1	1	2	-	2	0	1	0	0	2	2	2	1	2	0	1	0	2
Nyctalus leisleri	-	2	1	0	1	1	1	0	1	1	1	1	-	-	-	0	1	0	0	2	2	-	1	2	0	1	-	-
Pipistrellus pipistrellus	-	-	1	1	1	1	1	0	1	0	1	1	-	-	-	0	1	1	0	2	2	2	1	2	3	0	0	2
Vespertilio murinus	-	-	0	1	1	1	1	0	0	0	0	1	-	-	-	0	1	0	1	1	1	2	1	1	0	2	0	2
Eptesicus serotinus	1	-	0	1	1	1	1	0	0	0	1	-	-	-	-	0	1	2	1	0	1	1	1	1	0	0	0	-
Plecotus auritus/austriacus	-	-	1	-	-	-	1	0	0	0	0	2	-	-	-	1	-	-	1	0	1	-	0	1	3	1	-	-
Barbastella barbastellus	2	-	1	2	0	1	1	0	0	0	0	1	-	-	-	0	1	1	0	0	0	0	0	1	2	1	2	2
Miniopterus schreibersii	-	-	3	4	1	1	2	1	1	1	1	1	-	1	1	2	1	0	0	1	2	2	1	2	2	2	1	1

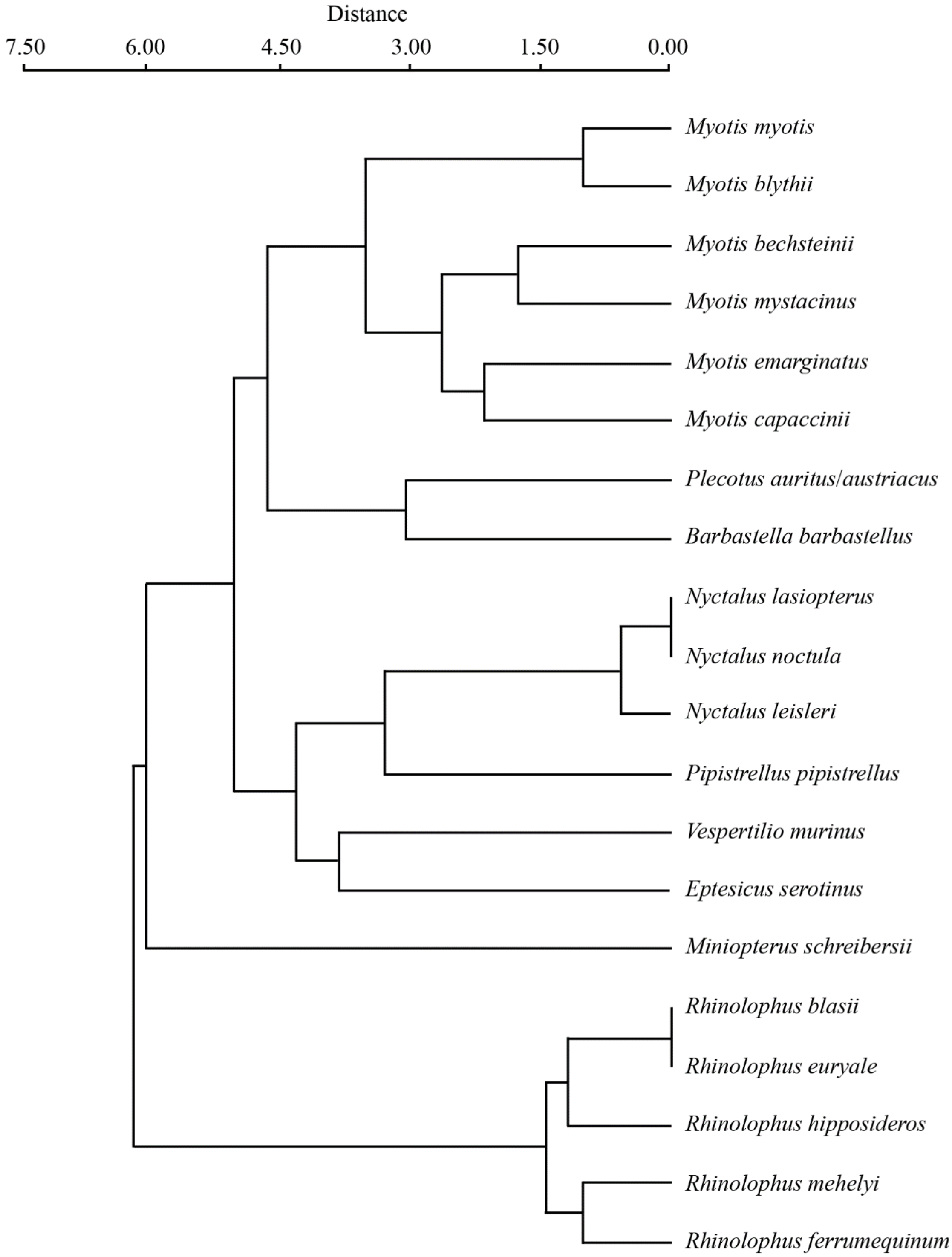

Figure 5.17 Dendrogram of cluster analysis of the various dental and postcranial elements across the studied chiropteran species from Loutra Almopias Cave A. Algorithm: Paired Group (UPGMA); Similarity Index: Euclidean.

The next cluster contains two different groups that can be interpreted in terms of the degree of shortening of the toothrow, which is higher in the *Nyctalus*/*Pipistrellus*/*Vespertilio*/*Eptesicus* cluster than in the *Myotis*/*Barbastella*/*Plecotus* group, which display relatively long toothrows (a primitive feature) (Smith et al. 2012).

Other characters that seem to influence the results of the dendrogram shown in Figure 5.17 have to do with the presence of certain features such as paraconule, metaconule, paraloph and metaloph in the upper molars, which although absent in the oldest bat fossils, they are already present in some Middle Eocene species (Smith et al. 2012).

As mentioned previously, establishing the polarity of morphological traits in bat teeth in order to conduct a phylogenetic analysis is not an easy task, due to the scarcity of fossils and to the fact that the earliest known specimens are already diversified and with derived features. However, there are sets of characteristics in the teeth that are shared in closely related taxa and enable to obtain good classifications without conducting a phylogenetic analysis. Thanks to these characteristics, the fragmentary material of bats that is typical of most palaeontological sites can be identified obtaining good systematic results.

CHAPTER 6. CONCLUSIONS

The thorough examination of the chiropteran specimens retrieved from the two chronologically different fossil assemblages of Loutra Almopias Cave A – the Upper Pleistocene cave's floor sediments (LAC) and the latest Pleistocene elevated chamber LAC Ia – resulted in the identification of 17 species from LAC and 20 from LAC Ia from three families:

- Rhinolophidae: *Rhinolophus ferrumequinum*, *Rhinolophus mehelyi*, *Rhinolophus blasii*, *Rhinolophus euryale*, *Rhinolophus mehelyi*/*blasii*/*euryale*, *Rhinolophus hipposideros*, *Rhinolophus* sp.;
- Vespertilionidae: *Myotis myotis*, *Myotis blythii*, *Myotis myotis*/*blythii*, *Myotis bechsteinii*, *Myotis emarginatus*, *Myotis capaccinii* (only in LAC Ia), *Myotis mystacinus* (only in LAC Ia), *Myotis* sp., *Nyctalus lasiopterus* (only in LAC Ia), *Nyctalus noctula*, *Nyctalus leisleri*, *Pipistrellus pipistrellus*, *Vespertilio murinus*, *Eptesicus serotinus*, *Plecotus auritus*/*austriacus*, *Barbastella barbastellus*;
- Miniopteridae: *Miniopterus schreibersii*;
- Chiroptera indet.

Both the number of identified specimens (NISP) and the minimum number of individuals (MNI) are higher for LAC Ia (NISP = 5193, MNI = 597) than LAC (NISP = 3811, MNI = 398). The 995 individuals (out of 9004 identified specimens) also show that during Late Pleistocene Chiroptera was the most densely populated order occupying Loutra Almopias Cave A.

Consequently, the Late Pleistocene chiropteran fauna from Loutra Almopias Cave A is, so far, the richest and most diverse in the Balkan Peninsula and therefore Greece.

Eight species: *Rhinolophus euryale*, *Myotis bechsteinii*, *Myotis capaccinii*, *Myotis mystacinus*, *Nyctalus lasiopterus*, *Nyctalus leisleri*, *Pipistrellus pipistrellus* and *Barbastella barbastellus* are described for the first time in the Greek fossil record.

One species: *Myotis capaccinii* is described for the first time in the fossil record of a Late Pleistocene locality from the Balkan Peninsula.

Nineteen species: *Rhinolophus ferrumequinum*, *Rhinolophus mehelyi*, *Rhinolophus blasii*, *Rhinolophus euryale*, *Rhinolophus hipposideros*, *Myotis myotis*, *Myotis bechsteinii*, *Myotis emarginatus*, *Myotis capaccinii*, *Myotis mystacinus*, *Nyctalus lasiopterus*, *Nyctalus noctula*, *Nyctalus leisleri*, *Pipistrellus pipistrellus*, *Vespertilio murinus*, *Eptesicus serotinus*, *Plecotus auritus*/*austriacus*, *Barbastella barbastellus* and *Miniopterus schreibersii* refer to the southernmost appearance of the Late Pleistocene of the Balkan Peninsula, extending the fossil record of those taxa, further south.

The corrosion observed on the specimens from Loutra Almopias Cave A does not indicate regular predation from the European Eagle Owl, *Bubo bubo* – as in the case of the rest of the small mammals – but opportunistic.

The Loutra Almopias Cave A served primarily as a nursery roost for a plethora of bats, as it is indicated by the wear degree of the dental elements and secondarily as a warm refuge during colder periods.

Two chiropteran samples were attempted to be dated by the Centre for Isotope Research (University of Groningen), one from square B10 (chamber LAC II) and one from LAC Ia, but both failed due to lack of collagen, as it happened with six out of seven previous attempts on *Ursus ingressus* material, indicating that the conditions for collagen preservation were not ideal.

An increase in cold-adapted species is observed in the latest Pleistocene LAC Ia, which roughly coincides with the onset of Younger Dryas. Nevertheless, the majority of the identified species are cave dwellers and have a preference for warm climatic conditions. In respect to their foraging environment, a variety of different landscapes are used with a preference in mixed and/or forested areas with the presence of water bodies, being a must for a significant proportion of the identified taxa. This explains the great diversity of chiropteran species.

All chiropteran species that have been identified from the sediments of Loutra Almopias Cave A are currently inhabiting the Greek region and the broader region of the cave, with the exception of *Rhinolophus mehelyi*. All species found in Loutra

Almopias Cave A are also present in the records of several localities from the Balkan Peninsula (with the most common species being *Rhinolophus ferrumequinum*, *Myotis blythii*, *Myotis bechsteinii* and *Miniopterus schreibersii*), with the exception of *Myotis capaccinii*.

The similarity analysis between chiropteran faunas from the Balkan Peninsula indicate that during Late Pleistocene the distribution of bats followed a similar pattern for the whole region (with a few exceptions).

The morphological characteristics of the chiropteran specimens from Loutra Almopias Cave A are similar to those of their extant representatives indicating only minor alterations to their body size.

The only exception to the latter is the body size of *Rhinolophus ferrumequinum*, which decreases from Late to latest Pleistocene, indicating that it is dependent on climate and more specifically on precipitation rather than temperature.

In addition to this, Loutra Almopias Cave A not only acted as a refugium during the Pleistocene glacial oscillations, but also as a starting point for the repopulation of Central and Northern Europe after the Last Glacial Maximum.

The phenetic analysis of the chiropteran features used to identify the species from Loutra Almopias Cave A is the first ever conducted for Chiroptera from the Greek region. The implementation of extra characters did not affect the expected results and therefore, the reliability of the added characters as criteria for species discrimination of fossil material of extant bats is confirmed.

In conclusion, this study is the first thorough examination of a Greek chiropteran fauna and its results prove its significance not only for the Greek region, but also for the broader area of the Balkan Peninsula. This study is expected to act as a solid background for further examination of different aspects of the fauna (i.e. genetic analysis, microwear analysis, etc.), which in addition to an improved taxonomy of the already known chiropteran assemblages from the Greek region and a direct comparison with other chiropteran faunas from European fossil sites, will allow us to improve our knowledge of the various ecomorphological aspects of chiropteran geographical distribution.

ABSTRACT

The aim of the present PhD Thesis is the thorough examination of the rich chiropteran collection that has been retrieved from the two chronologically different fossiliferous assemblages of Loutra Almopias Cave A (Pella, Macedonia, Greece), which will contribute to the knowledge of the Quaternary bats of the Greek region and the Balkan Peninsula. The aforesaid, will ultimately allow us to better understand the evolutionary trends of Quaternary Chiroptera and the mechanisms that led to their dispersal.

The specimens retrieved from the cave’s floor sediments (LAC) are of Late Pleistocene age, whereas the specimens retrieved from the elevated chamber LAC Ia are of latest Pleistocene age. Attempts to establish a more precise chronology for LAC and LAC Ia failed due to lack of collagen from the fossils.

The purpose was served by the first comprehensive systematic taxonomy and phenetic analysis of a fossil chiropteran fauna from the Greek region, correlation of the studied specimens with the two chronologically different faunal assemblages of the cave site and other modern and fossil faunal assemblages from the Greek region and the broader region of the Balkan Peninsula (biogeography), taphonomic analysis and a palaeoclimatological/palaeoecological approach, based on the bats’ biocoenosis.

All the aforementioned were based on the determination of the 9004 chiropteran specimens (3811 from LAC and 5193 from LAC Ia) according to their morphological and metrical characteristics, which resulted in the identification of 17 species from LAC and 20 species from LAC Ia from three families (Rhinolophidae, Vespertilionidae and Miniopteridae) and nine genera (*Rhinolophus*, *Myotis*, *Nyctalus*, *Pipistrellus*, *Vespertilio*, *Eptesicus*, *Plecotus*, *Barbastella* and *Miniopterus*).

Eight species described from Loutra Almopias Cave A are the first known records of their kind in Greece and one species is the first known record of a Late Pleistocene locality from the Balkan Peninsula. Nineteen species refer to the southernmost appearance of the Late Pleistocene of the Balkan Peninsula, extending the fossil record of those taxa further south.

Loutra Almopias Cave A served primarily as a nursery roost for a plethora of bats and secondarily as a warm refuge during colder periods. Moreover, predation from the European Eagle Owl, *Bubo bubo*, was opportunistic, indicating a mixed assemblage. In addition to this, Loutra Almopias Cave A not only acted as a refugium during the Pleistocene glacial oscillations, but also as a starting point for the repopulation of Central and Northern Europe after the Last Glacial Maximum.

An increase in cold-adapted species is observed during the latest Pleistocene LAC Ia, which roughly coincides with the onset of Younger Dryas. Nevertheless, the majority of the identified species are cave dwellers and have a preference for warm climatic conditions. In respect to their foraging environment, a variety of different landscapes are used with a preference in mixed and/or forested areas with the presence of water bodies, being a must for a significant proportion of the identified taxa.

The morphological characteristics of the chiropteran specimens from Loutra Almopias Cave A are similar to those of their extant representatives indicating only minor alterations to their body size. The only exception to this is the body size of the Greater Horseshoe Bat, *Rhinolophus ferrumequinum*, which decreases from Late to latest Pleistocene, indicating its dependency on climate.

The phenetic analysis of the chiropteran species from Loutra Almopias Cave A is the first ever conducted for Chiroptera from the Greek region and it confirms the reliability of the method for species discrimination of European Chiroptera.

In conclusion, the Late Pleistocene bat fauna from Loutra Almopias Cave A is, up to date, the richest and most diverse not only from the Greek region, but from the Balkan Peninsula, too.

ΠΕΡΙΛΗΨΗ

Ο σκοπός τις παρούσας Διδακτορικής Διατριβής είναι η σε βάθος μελέτη της πλούσιας πανίδας Χειρόπτερων που προέκυψαν από τις δυο διαφορετικές χρονολογικά πανίδες του Σπηλαίου Α των Λουτρών Αλμωπίας (Πέλλα, Μακεδονία), η οποία συμβάλλει στη γνώση των Τεταρτογενών νυχτερίδων του Ελληνικού χώρου και της Βαλκανικής Χερσονήσου. Τα παραπάνω, αναμένεται να συνεισφέρουν στη βελτίωση της γνώσης αναφορικά με τις εξελικτικές τάσεις των Τεταρτογενών Χειρόπτερων και τους μηχανισμούς που οδήγησαν στην εξάπλωσή τους.

Τα απολιθώματα που ανακτήθηκαν από τα ιζήματα του δαπέδου του σπηλαίου (LAC) είναι ηλικίας Άνω Πλειστόκαινου, ενώ τα απολιθώματα που ανακτήθηκαν από τον υπερυψωμένο θάλαμο LAC Ia είναι ηλικίας ανώτατου Πλειστόκαινου. Προσπάθειες για χρονολόγηση δειγμάτων από τον LAC και τον LAC Ia, απέτυχαν λόγω απουσίας κολλαγόνου από τα απολιθώματα.

Ο σκοπός εξυπηρετήθηκε από την πρώτη ενδελεχή συστηματική ταξινόμηση και φαινετική ανάλυση απολιθωμάτων Χειρόπτερων από τον Ελληνικό χώρο, συσχέτιση των μελετημένων απολιθωμάτων μεταξύ των δυο διαφορετικών χρονολογικά πανίδων του Σπηλαίου Α, αλλά και με άλλες σύγχρονες και απολιθωμένες πανίδες από τον Ελληνικό χώρο και τη Βαλκανική Χερσόνησο (βιογεωγραφία), ταφονομική ανάλυση και παλαιοκλιματική/παλαιοοικολογική προσέγγιση βασισμένη στις βιοκοινωνίες Χειρόπτερων.

Όλα τα παραπάνω βασίστηκαν στον προσδιορισμό 9004 απολιθωμάτων Χειρόπτερων (3811 από τον LAC και 5193 από τον LAC Ia) σύμφωνα με το μορφολογικά και μετρικά τους χαρακτηριστικά, με αποτέλεσμα τον προσδιορισμό 17 ειδών από τον LAC και 20 ειδών από τον LAC Ia από τρεις οικογένειες (Rhinolophidae, Vespertilionidae και Miniopteridae) και εννιά γένη (*Rhinolophus, Myotis, Nyctalus, Pipistrellus, Vespertilio, Eptesicus, Plecotus, Barbastella* και *Miniopterus*).

Οκτώ είδη περιγράφονται για πρώτη φορά σε απολιθωματοφόρο αρχείο από τον Ελληνικό χώρο από το Σπήλαιο Α των Λουτρών Αλμωπίας και ένα είδος περιγράφεται για πρώτη φορά σε απολιθωματοφόρο θέση ηλικίας Άνω Πλειστόκαινου από τη Βαλκανική Χερσόνησο. Δεκαεννιά είδη κάνουν τη νοτιότερη εμφάνισή τους από θέση ηλικίας Άνω Πλειστόκαινου της Βαλκανικής Χερσονήσου, επεκτείνοντας το απολιθωματοφόρο αρχείο αυτών των ειδών νοτιότερα.

Το Σπήλαιο Α των Λουτρών Αλμωπίας φαίνεται, με βάση τα απολιθώματα, ότι χρησιμοποιήθηκε πρωτευόντως ως χώρος γέννησης και δευτερευόντως ως θερμό καταφύγιο κατά τη διάρκεια ψυχρών περιόδων. Επίσης, παρατηρείται θήρευση από τον Ευρασιατικό Μπούφο, *Bubo bubo*, η οποία όμως ήταν καιροσκοπική. Αυτό οδηγεί στο συμπέρασμα ότι τα απολιθώματα νυχτερίδων του Σπηλαίου Α προέκυψαν τόσο λόγω θανάτου από φυσικά αίτια, όσο και λόγω θήρευσης. Παράλληλα, το Σπήλαιο Α των Λουτρών Αλμωπίας, όχι μόνο χρησιμοποιήθηκε ως καταφύγιο κατά τη διάρκεια των παγετωδών περιόδων του Πλειστόκαινου, αλλά και ως αφετηρία για την επανακατοίκηση της Κεντρικής και Βόρειας Ευρώπης μετά το τέλος του τελευταίου παγετώδους μέγιστου.

Κατά το Ανώτατο Πλειστόκαινο παρατηρείται αύξηση των ψυχρόφιλων ειδών, η οποία συμπίπτει περίπου με την έναρξη της Νεότερης Δρυάδος. Παρ' όλα αυτά, οι πλειοψηφία των αναγνωρισμένων ειδών είναι τρωγλόφιλα με προτίμηση στα θερμά κλίματα. Αναφορικά με το περιβάλλον κυνηγιού, προσδιορίζεται ως μικτού τύπου ή/και κλειστού με την παρουσία νερού να είναι απαραίτητη για ένα σημαντικό ποσοστό των αναγνωρισμένων ειδών.

Τα μορφολογικά χαρακτηριστικά των απολιθωμάτων Χειρόπτερων από το Σπήλαιο Α των Λουτρών Αλμωπίας είναι παρόμοια με αυτά των αρτίγονων, εμφανίζοντας μόνο μικρές διαφοροποιήσεις στο μέγεθός τους. Μόνη εξαίρεση αποτελεί ο Τρανορινόλοφος, *Rhinolophus ferrumequinum*, του οποίου το μέγεθος μειώνεται από το Άνω στο ανώτατο Πλειστόκαινο, καταδεικνύοντας την εξάρτησή σου από τις κλιματικές συνθήκες.

Η φαινετική ανάλυση των νυχτερίδων του Σπηλαίου Α των Λουτρών Αλμωπίας είναι η πρώτη που πραγματοποιείται σε Χειρόπτερα από τον Ελληνικό χώρο και επιβεβαιώνει τη χρησιμότητα της μεθόδου για αναγνώριση ειδών νυχτερίδων του Ευρωπαϊκού χώρου.

Συμπερασματικά, η πανίδα των Χειρόπτερων ηλικίας Άνω Πλειστόκαινου από το Σπήλαιο Α των Λουτρών Αλμωπίας, με τα μέχρι τώρα δεδομένα, αποδεικνύεται ως η πλουσιότερη και η πιο ποικίλη τόσο από τον Ελληνικό χώρο, όσο και από τη Βαλκανική Χερσόνησο.

REFERENCES

Adams, R. A. and Carter, R.T., 2017. Megachiropteran bats profoundly unique from microchiropterans in climbing and walking locomotion: Evolutionary implications. *PLoS ONE*, 12, e0185634.

Aguilar, J. P., Crochet, J. Y., Krivic, K., Marandat, B., Michaux, J., Mihevc, A., Sigé, B. and Šebela, S., 1998. Pleistocene small mammals from some karstic fillings of Slovenia-preliminary results. *Acta carsologica*, 27, 141-150.

Amson, E., 2021. Humeral diaphysis structure across mammals. *Evolution*, 75, 748-755.

Andrews, P., 1990. Owls, Caves and Fossils. The University of Chicago Press, Chicago.

Barova, S. and Streit, A., 2018. Action Plan for the Conservation of All Bat Species in the European Union 2018-2024. European Commission & UNEP/Eurobats, Brussels.

Berto, C. and Rubinato, G., 2013. The upper Pleistocene mammal record from Caverna degli Orsi (San Dorligo della Valle–Dolina, Trieste, Italy): A faunal complex between eastern and western Europe. *Quaternary International*, 284, 7-14.

Bilgin, R., Çoraman, E., Karataş, A. and Morales, J. C., 2009. Phylogeography of the greater horseshoe bat, *Rhinolophus ferrumequinum* (Chiroptera: Rhinolophidae), in southeastern Europe and Anatolia, with a specific focus on whether the Sea of Marmara is a barrier to gene flow. *Acta Chiropterologica*, 11, 53-60.

Boev, Z. and Tsoukala, E., 2019. Late Pleistocene and Earliest Holocene avifauna from the Loutra Almopias Cave (Macedonia, Greece). *Historia naturalis bulgarica*, 40, 1-31.

Bogićević, K. and Dimitrijević, V., 2004. Quaternary fauna from Mališina Stijena near Pljevlja (Montenegro). *Zbornik radova Odbora za kras i speleologiju*, 8, 119-133.

Bon, M., Piccoli, G. and Sala, B., 1991. I giacimenti quaternari di vertebrati fossili nell'Italia nord-orientale. *Memorie di Scienze Geologiche dell'Università di Padova*, 43, 185-231

Bordon, A., Peyron, O., Lézine, A. M., Brewer, S. and Fouache, E., 2009. Pollen-inferred late-glacial and Holocene climate in southern Balkans (Lake Maliq). *Quaternary International*, 200, 19-30.

Budinski, I., Jojic, V., Jovanovic, V. M., Bjelic-Cabrilo, O., Paunovic, M. and Vujosevica, M., 2015. Cranial variation of the greater horseshoe bat *Rhinolophus ferrumequinum* (Chiroptera: Rhinolophidae) from the central Balkans. *Zoologischer Anzeiger-A Journal of Comparative Zoology*, 254, 8-14.

Carter, R. T. and Adams, R. A., 2015. Postnatal ontogeny of the cochlea and flight ability in Jamaican fruit bats (Phyllostomidae) with implications for the evolution of echolocation. *Journal of anatomy*, 226, 301-308.

Carter, R. T. and Adams, R. A., 2016. Integrating ontogeny of echolocation and locomotion gives unique insights into the origin of bats. *Journal of Mammalian Evolution*, 23, 413-421.

Chatzopoulou, K., 2003. The Late Pleistocene small mammal fauna from Loutra Aridea Bear-cave (Pella, Macedonia, Greece). *Additional Data. Atti del museo civico di storia naturale di Trieste*, 49, 35-45.

Chatzopoulou, K., 2005a. The stratigraphy from the Loutra Aridéas Bear-Cave (Pella, Macedonia, Greece) with emphasis on two new chambers. *Proceedings of the 14th International Congress of Speleology, 21-28 August 2005, Kalamos/Athens*.

Chatzopoulou, K., 2005b. The small mammal fauna from the Loutra Aridea bear-Cave (Pella, Macedonia, Greece) with Emphasis on the Third chamber. *Abhandlungen der Naturhistorischen Gesellschaft zu Nürnberg*, 45, 57-64.

Chatzopoulou, K., 2014. The micromammals of the Quaternary deposits from cave A, Loutra Almopias (Pella, Northern Greece). Stratigraphy-Taphonomy-Paleoenvironment. *PhD Thesis, Scientific Annals, School of Geology, Aristotle University of Thessaloniki, No 166, 390 pp.* [in Greek: Μελέτη των μικροθηλαστικών των τεταρτογενών αποθέσεων του Σπηλαίου Α των Λουτρών Αλμωπίας (Πέλλα, Μακεδονία). Στρωματογραφία-Ταφονομία-Παλαιοπερι-βάλλον].

Chatzopoulou, K., Vasileiadou, A., Koliadimou, K., Tsoukala, E., Rabeder, G. and Nagel, D., 2001. Preliminary report on the Late Pleistocene small mammal fauna from the Loutraki Bear-cave (Pella, Macedonia, Greece). *Cuadernos do Laboratorio Xeolóxico de Laxe*, 26, 485-495.

Darlas, A. and Psathi, E., 2016. The Middle and Upper Paleolithic on the western coast of the Mani Peninsula (southern Greece). In: Harvati, K. and Roksandic, M. (eds) *Paleoanthropology of the Balkans and Anatolia: Human evolution and its context*. Springer, Dordrecht, 95-117.

De Paz, O., 1995. Geographic variation of the greater horseshoe bat (*Rhinolophus ferrumequinum*) in the west-half of the Palearctic region. *Myotis*, 32, 33-44.

Dermitzakis, M., 1977. The Quaternary fossil mammals in the caves and karstic-holes of Crete Island and their significance. *Bulletin de la Société Spéléologique de Gréce*, 14, 152-190 [in Greek: Τα ευρήματα θηλαστικών του τεταρτογενούς των σπηλαίων και καρστικών εγκοίλων της νήσου Κρήτης και η σημασία αυτών].

Dietz, C., von Helversen, O. and Nill, D., 2009. Bats of Britain, Europe and Northwest Africa. A&C Black Publishers, London.

Dimitrijević, V., 1996. Upper Pleistocene mammals from cave deposits of Serbia. *Geološki anali Balkanskog poluostrva*, 61, 179-370.

Doukas, C. S. and Papayianni, K., 2016. Small mammals in the Plio/Pleistocene sediments of Greece. In: Harvati, K. and Roksandic, M. (eds) *Paleoanthropology of the Balkans and Anatolia: Human evolution and its context*. Springer, Dordrecht, 291-302.

Eleftheriadis, G., 1977. Study of the volcanic rocks in South Almopia. *PhD Thesis, Scientific Annals, Faculty of Physics and Mathematics*, *Aristotle University of Thessaloniki, No 77, 173 pp.* [in Greek: Συμβολή εις την μελέτην των ηφαιστειογενών πετρωμάτων της Νοτίου Αλμωπίας].

Eleftheriadis, G., 2006. The geology of Almopia speleopark. *Scientific annals, School of Geology, Aristotle University of Thessaloniki*, special volume 98, 27-32.

Felten, H., Helfricht, A. and Storch, G., 1973. Die Bestimmung der europäischen Fledermäuse nach der distalen Epiphyse des Humerus. *Senckenbergiana biologica*, 54, 291-297.

Flanders, J. O. N., Jones, G., Benda, P., Dietz, C., Zhang, S., Li, G., Sharifi, M. and Rossiter, S.J., 2009. Phylogeography of the greater horseshoe bat, *Rhinolophus ferrumequinum*: contrasting results from mitochondrial and microsatellite data. *Molecular Ecology*, 18, 306-318.

Fracasso, M. P. A., de Oliveira Salles, L. and Perini, F. A., 2011. Upper molar morphology and relationships among higher taxa in bats. *Journal of mammalogy*, 92, 421-432.

Francke, A., Dosseto, A., Panagiotopoulos, K., Leicher, N., Lacey, J. H., Kyrikou, S., Wagner, B., Zanchetta, G., Kouli, K. and Leng, M. J., 2019. Sediment residence time reveals Holocene shift from climatic to vegetation control on catchment erosion in the Balkans. *Global and Planetary Change*, 177, 186-200.

Georgiadis, I., Chatzopoulou, K., Kantiranis, N., Ioakeimidis, I. and Tsirambides, A., 2019. Petrography and provenance of floor sediments from the Loutra Almopias Cave (Pella, Macedonia, Greece). *International Journal of Speleology*, 48, 237-248.

Granatosky, M. C., Amanat, S., Panyutina, A. A. and Youlatos, D., 2021. Gait mechanics of a blind echolocating rodent: Implications for the locomotion of small arboreal mammals and proto-bats. *Journal of Experimental Zoology*, 335, 436-453.

Gunnell, G. F. and Simmons, N. B., 2005. Fossil evidence and the origin of bats. *Journal of Mammalian Evolution*, 12, 209-246.

Gunnell, G. F., Smith, R. and Smith, T., 2017. 33 million year old Myotis (Chiroptera, Vespertilionidae) and the rapid global radiation of modern bats. *PLOS One*, 12, e0172621.

Gunnell, G. F., Worsham, S. R., Seiffert, E. R. and Simons, E. L., 2009. *Vampyravus orientalis* Schlosser (Chiroptera) from the Early Oligocene (Rupelian), Fayum, Egypt—body mass, humeral morphology and affinities. *Acta Chiropterologica*, 11, 271-278.

Hammer, Ø. and Harper, D. A. T., 2006. Paleontological Data Analysis. Blackwell Publishing, Oxford.

Hammer, Ø., Harper, D. A. T. and Ryan, P. D., 2001. PAST: Paleontological statistics software package for education and data analysis. *Palaeontologia Electronica*, 4, 1-9.

Hanák, V., Benda, P., Ruedi, M., Horáček, I. and Sofianidou, T. S., 2001. Bats (Mammalia: Chiroptera) of the Eastern Mediterranean. Part 2. New records and review of distribution of bats in Greece. *Acta Societatis Zoologicae Bohemicae*, 65, 279-346.

Hand, S., Novacek, M., Godthelp, H. and Archer, M., 1994. First Eocene bat from Australia. *Journal of Vertebrate Paleontology*, 14, 375-381.

Hand, S. J., Sigé, B., Archer, M. and Black, K. H., 2016. An evening bat (Chiroptera: Vespertilionidae) from the late Early Eocene of France, with comments on the antiquity of modern bats. *Palaeovertebrata*, 40, e2.

Harvati, K., Darlas, A., Bailey, S. E., Rein, T. R., El Zaatari, S., Fiorenza, L., Kullmer, O. and Psathi, E., 2013. New Neanderthal remains from Mani peninsula, southern Greece: the Kalamakia middle Paleolithic cave site. *Journal of Human Evolution*, 64, 486-499.

Hewitt, G. M., 1999. Post-glacial re-colonization of European biota. *Biological journal of the Linnean Society*, 68, 87-112.

Hill, J. and Smith, J., 1984. Bats: A Natural History. University of Texas Press, Austin.

Hoofer, S. R. and Van Den Bussche, R. A., 2003. Molecular phylogenetics of the chiropteran family Vespertilionidae. *Acta Chiropterologica*, 5, 1-63.

Horáček, I., 1991, Enigma of Otonycteris: ecology, relationship, classification. *Myotis*, 29, 17-30.

Horáček, I., 2001. On the early history of vespertilionid bats in Europe: the Lower Miocene record from the Bohemian Massif. *Lynx (Praha)*, 32, 123-154.

Horacek, I. and Poulianos, N., 1988. Further data on bats of the Early Pleistocene site, Petralona, Greece. *Abstracts of the 2nd Panellenic Congress of Anthropology, 27-29 May 1988, Athens*.

Hughes, P. D., 2004. Quaternary Glaciation in the Pindus Mountains. *PhD Thesis, Darwin College, University of Cambridge, 362 pp.*

Hughes, P. D., Woodward, J. C. and Gibbard, P. L., 2006. The last glaciers of Greece. *Zeitschrift für Geomorphologie*, 50, 37-61.

Hulva, P., Horáček, I. and Benda, P., 2007. Molecules, morphometrics and new fossils provide an integrated view of the evolutionary history of Rhinopomatidae (Mammalia: Chiroptera). *BMC Evolutionary Biology*, 7, 165.

Hutterer, R., 2005a. Order Erinaceomorpha. In: Wilson, D. E. and Reeder, D. M. (eds) *Mammal species of the world: a taxonomic and geographic reference (vol 1)*. Johns Hopkins University Press, Baltimore, 212-219.

Hutterer, R., 2005b. Order Soricomorpha. In: Wilson, D. E. and Reeder, D. M. (eds) *Mammal species of the world: a taxonomic and geographic reference (vol 1)*. Johns Hopkins University Press, Baltimore, 220-311.

Jiang, T., Wang, J., Wu, H., Csorba, G., Puechmaille, S. J., Benda, P., Boireau, J., Toffoli, R., Courtois, J.-Y., Nyssen, P., Colombo, R. and Feng, J., 2019. The patterns and possible causes of global geographical variation in the body size of the greater horseshoe bat (*Rhinolophus ferrumequinum*). *Journal of Biogeography*, 46, 2363-2377.

Kabouroglou, E. and Chatzitheodorou, T., 1999. Geomorphological changes and sedimentation of the A cave (Agiasma) of Loutraki (Pella, Macedonia, Greece). *Proceedings of the 5th Congress of the Greek Geographic Society*, Athens, 83-93 [in Greek: Γεωμορφολογικές μεταβολές και ιζηματογένεση σπηλαίου Α (Αγίασμα) Λουτρακίου Ν. Πέλλας (Μακεδονία)].

Kabouroglou, E., Bassiakos, I and Bouzas, D., 2006. The cave A' in the Aridaia-Loutraki area. *Archaeological Work in Macedonia and Thrace*, 18, 573-589 [in Greek: Παλαιοντολογική-ιζηματολογική ανασκαφική έρευνα 2004 και χρονολογικές μελέτες σπηλαίου Α' Λουτρακίου Αριδαίας].

Kabouroglou, E., Chatzitheodorou, T., Bouzas, D., Zacharias, N. and Mitsis, I., 2007. Palaeontological-sedimentological excavation research 2005 in cave A' at Aridaia-Loutraki area. *Archaeological Work in Macedonia and Thrace*, 19, 293-308 [in Greek: Παλαιοντολογική-ιζηματολογική ανασκαφική έρευνα 2005 σπηλαίου Α' Λουτρακίου Αριδαίας].

Kabouroglou, E., Bouzas, D. and Chatzitheodorou, T., 2008. Palaeontological-sedimentological excavational research of Cave A' Loutraki Aridaia. New evidence. *Archaeological Work in Macedonia and Thrace*, 20, 673-684 [in Greek: Παλαιοντολογικές-ιζηματολογικές ανασκαφικές έρευνες σπηλαίου Α' Λουτρακίου Αριδαίας. Νεότερα στοιχεία].

Kolendrianou, M., Ligkovanlis, S., Maniakas, I., Tzortzi, M. and Iliopoulos, G., 2020. The Palaeolithic cave of Kalamakia (Mani Peninsula), Greece: new insights on the palaeoenvironment using microvertebrates and mesowear analysis of ruminant teeth. *Heliyon*, 6, e03958.

Kotsakis, T., Melentis, J. and Sirna, G., 1976. Seconda spedizione paleontologica Lincea nell'isola di Creta (1975). *Rendiconti dell'Accademia Nazionale dei Lincei*, 223, 3-10.

Kotsakis, T., Petronio, C. and Sirna, G., 1979. The Quaternary vertebrates of the Aegean islands: palaeogeographical implications. *Annales Géologiques des Pays Hélléniques*, 30, 31-64.

Kretzoi, M., 1977. The fauna of small vertebrates of the Middle Pleistocene at Petralona. *Anthropos*. 4, 131-143.

Kretzoi, M. and Poulianos. N. A., 1981. Remarks on the Middle and Lower Pleistocene Vertebrate Fauna in the Petralona Cave. *Anthropos*, 8, 57-72.

Kryštufek, B., 1993. Geographic variation in the greater horseshoe bat *Rhinolophus ferrumequinum* in south-eastern Europe. *Acta Theriologica*, 38, 67-79.

Kurtén, B., 1976. The cave bear story: life and death of a vanished animal. Columbia University Press, New York.

Kuss, S. E., 1970. Abfolge und Alter der Pleistozänen Säugetierfaunen der Insel Kreta. *Berichte der Naturforschenden Gesellschaft Freiburg im Breisgau*, 60, 35-83.

Kuss, S. E., 1973. Die pleistozänen Säugetierfaunen der ostmediterranen Inseln. Ihr Alter und ihre Herkunft. *Berichte der Naturforschenden Gesellschaft Freiburg im Breisgau*, 63, 49-71.

Lack, J. B., Roehrs, Z. P., Stanley Jr, C. E., Ruedi, M. and Van Den Bussche, R. A., 2010. Molecular phylogenetics of *Myotis* indicate familial-level divergence for the genus *Cistugo* (Chiroptera). *Journal of Mammalogy*, 91, 976-992.

Lazaridis, G., 2006. Almopia Speleopark (Pella, Macedonia, Greece): Morphology-speleogenesis of the caves. *Scientific annals, School of Geology, Aristotle University of Thessaloniki*, special volume 98, 33-40.

Mauch Lenardić, J., 2009. Small mammals (Insectivora, Chiroptera and Rodentia) from the Middle Pleistocene to Holocene strata of Vindija cave (NW Croatia). In: Steguweit, L. (ed) *Abstract Book, Hugo Obermaier Gesellschaft, 51st Annual Meeting, 14-18 April 2009, Ljubljana*.

Mauch Lenardić, J., Sršen, A. O. and Radović, S., 2018. Quaternary fauna of the Eastern Adriatic (Croatia) with the special review on the Late Pleistocene sites. *Quaternary international*, 494, 130-151.

Mavridis, F., Kormazopoulou, L., Papadea, A., Apostolikas, O., Yamaguchi, D., Tankosic, Z., Kotzamani, G., Trantalidou, K., Karkanas, P., Maniatis, Y., Papagianni, K. and Lambropoulos, D., 2013. Anonymous Cave of Schisto at Keratsini, Attika: a preliminary report on a diachronic cave occupation from the Pleistocene/Holocene transition to the Byzantine times. In: Mavridis, F. and Jensen, J. T. (eds) *Stable places and changing perceptions: Cave archaeology in Greece*. Archaeopress, Oxford, BAR International Series 2558, 248-284.

Mayhew, D. F., 1977. The endemic Pleistocene murids of Crete I-II. *Proceedings of the Koninklijke Nederlandse Akademie van Wetenschappen. Series B: Palaeontology Geology Physics Chemistry Anthropology*, 80, 182-214.

McKenna, M. C. and Bell, S. K., 1997. Classification of Mammals: above the species level. Columbia University Press, New York.

Mein, P., 1975. Les Chiroptères (Mammalia) du gisement pléistocène moyen des Abimes de la Fage à Noailles (Corrèze). *Publications du musée des Confluences*, 13, 57-67.

Mein, P. and Tupinier, Y., 1977. Formule dentaire et position systématique du Minioptère (Mammalia, Chiroptera). *Mammalia*, 41, 207-212.

Mercier, J., 1966. Étude géologique des zones Internes des Hellénides en Macédoine centrale (Grèce). Contribution á l'étude du métamorphisme et de l'évolution magmatique des zones Internes des Hellénides. *PhD Thesis, Faculté des Sciences de l'Université de Paris, 792 pp.*

Mercier, J., 1968. Étude géologique des zones internes des Hellénides en Macédoine centrale (Gréce). *Annales Géologiques des Pays Hélléniques*, 20, 1-792.

Mercier, J., Vergely, P. and Bebien J., 1975. Les ophiolites helléniques "obductees" au Jurassique supérieur sont-elles les vestiges d' un ocean tethysien ou d' une mer marginale peri-europeene. *Bulletin de la Société géologique de France. Compte rendu sommaire des séances de la Société géologique de France*, 4, 108-112.

Miller-Butterworth, C. M., Murphy, W. J., O'Brien, S. J., Jacobs, D. S., Springer, M. S. and Teeling, E. C., 2007. A family matter: conclusive resolution of the taxonomic position of the long-fingered bats, *Miniopterus*. *Molecular Biology and Evolution*, 24, 1553-1561.

Mountrakis, D., 1976. Contribution in the knowledge of the geology of the north boundary of the Axios and Pelagonian zones in the K. Loutraki-Orma area (Almopia). *PhD Thesis, Scientific Annals, Faculty of Physics and Mathematics, Aristotle University of Thessaloniki, No 16, 164 pp.* [in Greek: Συμβολή εις την γνώσιν της γεωλογίας του Βορείου ορίου των ζωνών Αξιού και Πελαγονικής εις την Περιοχήν Κ. Λουτρακίου - Όρμας (Αλμωπίας)].

Mountrakis, D., 1986. The Pelagonian zone in Greece: a polyphase-deformed fragment of the Cimmerian continent and its role in the geotectonic evolution of the eastern Mediterranean. *The Journal of Geology*, 94, 335-347.

Mountrakis, D., 2010. Geology and geotectonic evolution of Greece. University Studio Press, Thessaloniki. [in Greek: Γεωλογία και γεωτεκτονική εξέλιξη της Ελλάδας].

Murphy, W. J., Eizirik, E., Johnson, W. E., Zhang, Y. P., Ryder, O. A. and O'Brien, S. J., 2001. Molecular phylogenetics and the origins of placental mammals. *Nature*, 409, 614-618.

Nagel, D., Pacher, M., and Tsoukala, E., 2019. Large mammals except cave-bears from the Loutra Almopias Cave, Late Pleistocene, Macedonia, Greece. In: Nagel, D. and Kavcik-Graumann, N. (eds) *Berichte der Geologischen Bundesanstalt, Festschrift zum 80. Geburtstag von emer. Univ.-Prof. Dr. Mag. Gernot Rabeder*, 132, 123-147.

Panagiotopoulos, K., Aufgebauer, A., Schäbitz, F. and Wagner, B., 2013. Vegetation and climate history of the Lake Prespa region since the Lateglacial. *Quaternary International*, 293, 157-169.

Panagiotopoulos, K., Böhm, A., Leng, M. J., Wagner, B. and Schäbitz, F., 2014. Climate variability over the last 92 ka in SW Balkans from analysis of sediments from Lake Prespa. *Climate of the Past*, 10, 643-660.

Paragamian, K., 2021. Fauna of the cave Spilaio Arkoudospilia, Loutra Loutrakiou, Almopia, Kentriki Makedonia. In: Paragamian, K., Poulinakis, M., Paragamian, S. and Nikoloudakis, I. (eds) *Cave fauna of Greece database - Hellenic Institute of Speleological Research*, https://database.inspee.gr/ (downloaded on 28-01-2021.

Patras, D., 1990. Hydrogeological and hydrochemical investigations in the area of the Loutraki - Aridaia thermal springs (Pozar thermal baths). *Proceedings of the 2nd Congress for Thermometallic Waters*, Thessaloniki, 167-185 [in Greek: Υδρογεωλογικές και υδροχημικές έρευνες στην περιοχή των θερμομεταλλικών πηγών Λουτρακίου Αριδαίας (Λουτρά Πόζαρ)].

Pereswiet-Soltan, A., 2016. First record of serotine bat *Eptesicus serotinus* (Chiroptera: Vespertilionidae) from Early-Mid Holocene in Southern Europe (Beotia-Greece). *Hystrix, the Italian Journal of Mammalogy*, 27, 209-211.

Pickford, M., 1981. Preliminary Miocene mammalian biostratigraphy for western Kenya. *Journal of Human Evolution*, 10, 73-97.

Piskoulis, P., 2018. *Rhinolophus ferrumequinum* (Chiroptera): Tooth size variation from Late to Latest Pleistocene of Loutra Almopias Cave (Macedonia, Greece).

In: Vaz, N. and Sá, A. A. (eds) *XXXIV Jornadas de Paleontologia & IV Congresso Ibérico de Paleontologia, 26-29 September 2018, Vila Real*.

Piskoulis, P., 2019. Late Pleistocene bats (Mammalia: Chiroptera) from Loutra Almopias Cave (Pella, Macedonia, Greece): preliminary results. In: Blanco, F., Carro Rodríguez, P. M., Domínguez García, A. C., Gamboa, S., Linares Ruiz, M., Mateos-Carralafuente, J. R., Menéndez, I., Martín Perea, D. M., Martínez Monleón, M., Martínez Nebreda, S., Navalón, G., Porras, L., Prieto, I., Püschel, T. A. and Ruiz-Galván, A. (eds) *4th International Meeting of Early-stage Researchers in Palaeontology, 11-14 June 2019, Cuenca*.

Piskoulis, P., 2020. Potential precipitation-driven body size differentiation of *Rhinolophus ferrumequinum* from the Late to latest Pleistocene of Loutra Almopias Cave A (Pella, Macedonia, Greece). *Neues Jahrbuch für Geologie und Paläontologie-Abhandlungen*, 297, 311-323.

Piskoulis, P. and Chatzopoulou, K., in press. The fossil record of bats (Mammalia: Chiroptera) in Greece. In: Vlachos, E. (ed) *The Fossil Vertebrates of Greece - A synopsis of the fossil record and taxonomy*. Springer International Publishing.

Popov, V. V., 2000. The small mammals (Mammalia: Insectivora, Chiroptera, Lagomorpha, Rodentia) from Cave 16 (North Bulgaria) and the paleoenvironmental changes during the Late Pleistocene. In: Ginter, B., Kozlowski, J. K. and Laville, K. (eds) *Temnata Cave. Excavations in Karlukovo Karst Area, Bulgaria*. Jagellonian University Press, Krakow, 2, 13-65.

Popov, V. V., 2004. Pliocene small mammals (Mammalia, Lipotyphla, Chiroptera, Lagomorpha, Rodentia) from Muselievo (North Bulgaria). *Geodiversitas*, 26, 403-491.

Popov, V. V., 2018. Bats in Bulgaria: Patterns of Species Distribution, Richness, Rarity, and Vulnerability Derived from Distribution Models. In: Mikkola, H. (ed) *Bats*, 39-62.

Povară, I., 2019. Domanului Mountains: Comarnic Cave (Pestera de la Cantonul Comarnic, Pestera din Ogasul Ponicovei). In: Ponta, G. M. L. and Onac, B. P. (eds) *Cave and Karst Systems of Romania*, 249-255.

Qiu, Z. D., Han, D. F., Qi, G. Q. and Lin, Y. F., 1985. A preliminary report on a micromammalian assemblage from the hominoid locality of Lufeng, Yunnan. *Acta Anthropologica Sinica*, 4, 13-32.

Rabeder, G., Tsoukala, E. and Kavcik, N., 2006. Chronological and systematic position of cave bears from Loutra Arideas (Pella, Macedonia, Greece). *Scientific annals, School of Geology, Aristotle University of Thessaloniki*, special volume 98, 69-74.

Raup, D. M. and Crick, R. E., 1979. Measurement of faunal similarity in paleontology. *Journal of Paleontology*, 53, 1213-1227.

Ravel, A., Marivaux, L., Tabuce, R., Adaci, M., Mahboubi, M., Mebrouk, F. and Bensalah, M., 2011. The oldest African bat from the early Eocene of El Kohol (Algeria). *Naturwissenschaften*, 98, 397-405.

Reumer, J. W. F. and Doukas, C. S., 1985. Early Pleistocene Insectivora (Mammalia) from Tourkobounia (Athens, Greece). *Proceedings of the Koninklijke Nederlandse Akademie van Wetenschappen. Series B: Palaeontology Geology Physics Chemistry Anthropology*, 88, 111-121.

Revilliod, P., 1922. Contribution a l'étude des chiroptères des terrains tertiaires. Troisième partie et fin. *Mémoires de la Société Paléontologique Suisse*, 45, 133-195.

Rosina, V. V. and Rummel, M., 2012. The bats (Chiroptera, Mammalia) from the Early Miocene of Petersbuch (Bavaria, Southern Germany). *Geobios*, 45, 463-478.

Rosina, V. V. and Rummel, M., 2017. The new Early Miocene bat records from the Molasse sites of South Germany. *Fossil Imprint*, 73, 227-235.

Rosina, V. V., Kruskop, S. and Semenov, Y., 2019. New Late Miocene plecotine bats (Chiroptera, Vespertilionidae: Plecotini) from Gritsev, Ukraine. *Palaeovertebrata*, 42, e2.

Rossiter, S. J., Benda, P., Dietz, C., Zhang, S. and Jones, G., 2007. Rangewide phylogeography in the greater horseshoe bat inferred from microsatellites: implications for population history, taxonomy and conservation. *Molecular Ecology*, 16, 4699-4714.

Sabol, M. and Holec, P., 2002. Temporal and spatial distribution of Miocene mammals in the Western Carpathians (Slovakia). *Geologica Carpathica*, 53, 269-279.

Sadier, A., Urban, D. J., Anthwal, N., Howenstine, A. O., Sinha, I. and Sears, K. E., 2020. Making a bat: The developmental basis of bat evolution. *Genetics and Molecular Biology*, 43, e20190146.

Salari, L. and Silvestri, L., 2015. Holocene bats (Mammalia, Chiroptera) from five caves of Central Apennines (Italy). *Barbastella*, 8, 27-41.

Salari, L., Agnelli, P., Calcagnile, L., Di Maita, J., Grasso, R., Quarta, G., Santoro, C. and Spena, M. T., 2019. The fossil bat assemblages from the Grotta dei Pipistrelli in Pantalica (southeastern Sicily, Italy): Chronological and palaeoecological implications. *Comptes Rendus Palevol*, 18, 417-441.

Schmidt-Kittler, N., de Bruijn, H. and Doukas, K., 1995. The vertebrate locality Maramena (Macedonia, Greece) at the Turolian-Ruscinian boundary (Neogene). 1. General Introduction. *Münchner Geowissenschaftliche Abhandlungen Reihe A: Geologie und Paläontologie*, 28, 9-18.

Sevilla, P., 1986. Identificación de los principales quirópteros ibéricos a partir de sus dientes aislados. Valor sistemático de los caracteres morfológicos y métricos dentarios. *Doñana. Acta Vertebrata*, 13, 111-130.

Sevilla, P., 1988. Estudio paleontológico de los Quirópteros del Cuaternario español. *Paleontologia i Evolució*, 22, 113-233.

Sevilla, P., 1990. The fauna of bats from the Upper Pleistocene locality of Santenay (Côte-d'Or, France). *Quaternaire*, 2, 101-110.

Sevilla, P., 2015. The early Pleistocene Bats from Cueva Victoria. *Mastia*, 11-13, 239-251.

Sevilla, P., 2016. Bats from Azokh Caves. In: Fernández-Jalvo, Y., King, T., Yepiskoposyan, L. and Andrews, P. (eds) *Azokh Cave and the Transcaucasian Corridor*. Springer Nature, Dordrecht, 177-189.

Sevilla, P. and Chaline, J., 2004. The fossil middle Pleistocene bats from the Cave of Aldène (Hérault, France). *Zona arqueológica (Miscelánea en homenaje a Emiliano Aguirre. Tomo 2: Paleontología)*, 4, 593-602.

Sevilla, P. and Chaline, J., 2011. New data on bat fossils from middle and upper Pleistocene localities of France. *Geobios*, 44, 289-297.

Sevilla, P. and López-Martínez, N., 1986. Comparative systematic value between dental and external: Skeletal features in western European Chiroptera. In: Russell, D. E., Santoro, J.-P. and Sigogneau-Russell, D. (eds) *Teeth Revisited: Proceedings of the VIIIth International Symposium on Dental Morphology*, Paris, Mémoires du Museum national d'histoire naturelle Série C Géologie, 53, 255-266.

Sfougaris, A., 2009. Mammals. In: Legakis, A. and Maragou, P. (eds) *The Red Book of the Threatened Animals of Greece*. Hellenic Zoological Society, Athens, 355-425. [in Greek: Το Κόκκινο Βιβλίο των Απειλούμενων Ζώων της Ελλάδας].

Sickenberg, O., 1964. Die Säugetierfauna der Höhle Petralona bei Thessaloniki (Vor. Mit.). *Geological and Geophysical Research*, 9, 1-16.

Sickenberg, O., 1971. Revision der Wirbeltierfauna der Höhle petralona (Griech. Mazedonien). *Annales Géologiques des Pays Hélléniques*, 23, 230-264.

Sige, B., 1978. Insectivores et Chiropteres. In: Gèze, B., Rage, J.-C., Vergnaud-Grazzini, C., de Broin, F., Buffetaud, E., Moure-Chauviré, C., Crochet, J.-Y., Sigé, B., Sudre, J., Remy, J.-A., Lange-Badré, B., de Bonis, L., Hartenberger, J.-L. and Vianey-Liaud, M. (eds) *La poche à phosphate de Sainte-Néboule (Lot) et sa faune de vertébrés du Ludien supérieur*. Palaeovertebrata, Montpellier, 8, 243-268.

Sigé, B., Mihevc, A. and Aguilar, J.-P., 2003. Les chiroptères actuels et fossiles (Pléistocène supérieur) d'une grotte d'altitude des Alpes de Slovénie, témoins d'une détérioration climatique. *Coloquios de Paleontología*, Vol. Ext. 1, 637-645.

Sigé, B., Mein, P., Jousse, H. and Aguilar, J. P., 2014. Un nouveau Rhinopomatidae (Chiroptera) du Paléokarst miocène de Baixas (Pyrénées-Orientales, France); apport zoogéographique. *Geodiversitas*, 36, 257-282.

Simmons, N. B., 1994. The Case for Chiropteran Monophyly. *American Museum Novitates*, 3103, 1-54.

Simmons, N. B., 2005a. Order Chiroptera. In: Wilson, D. E. and Reeder, D. M. (eds) *Mammal species of the world: a taxonomic and geographic reference (vol 1)*. Johns Hopkins University Press, Baltimore, 312-529.

Simmons, N. B., 2005b. An Eocene big bang for bats. *Science*, 307, 527-528.

Simmons, N. B., Seymour, K. L., Habersetzer, J. and Gunnell, G. F., 2008. Primitive Early Eocene bat from Wyoming and the evolution of flight and echolocation. *Nature*, 451, 818-821.

Simmons, N. B., Seymour, K. L., Habersetzer, J. and Gunnell, G. F., 2010. Inferring echolocation in ancient bats. *Nature*, 466, E8-E9.

Smith, T., Rana, R. S., Missiaen, P., Rose, K. D., Sahni, A., Singh, H. and Singh, L., 2007. High bat (Chiroptera) diversity in the Early Eocene of India. *Naturwissenschaften*, 94, 1003-1009.

Smith, T., Habersetzer, J., Simmons, N. B. and Gunnell, G. F., 2012. Systematics and paleobiogeography of early bats. In: Gunnell, G. F. and Simmons, N. B. (eds)

Evolutionary History of Bats–Fossils, Molecules and Morphology. Cambridge University Press, Cambridge, 23-66.

Springer, M. S., Teeling, E. C., Madsen, O., Stanhope, M. J. and de Jong, W. W., 2001. Integrated fossil and molecular data reconstruct bat echolocation. *Proceedings of the National Academy of Sciences of the United States of America*, 98, 6241-6246.

Stiner, M. C. and Munro, N. D., 2011. On the evolution of diet and landscape during the Upper Paleolithic through Mesolithic at Franchthi Cave (Peloponnese, Greece). *Journal of Human Evolution*, 60, 618-636.

Storch, G., 1975. Eine Mittelpleistozäne Nager-Fauna von der Insel Chios, Ägais (Mammalia, Rodentia). *Senckenbergiana biologica*, 56, 165-189.

Strachinis, I., Kalaentzis, K., Katsiyiannis, P. and Kazilas, C., 2018. First record of the Egyptian fruit bat, *Rousettus aegyptiacus* (Pteropodidae), from Kastellorizo island, Greece. *Mammalia*, 82, 611-613.

Symeonidis, N., Bachmayer, F. and Zapfe, H., 1973. Grabungen in der Zwergelefanten-Höhle „Charkadio" auf der Insel Tilos (Dodekanes, Griechenland). *Annalen des Naturhistorischen Museums in Wien*, 77, 133-139.

Symeonidis, N., Bachmayer, F. and Zapfe, H., 1980. Ergebnisseweiterer Grabungen in der Höhle von Vraona (Attika, Griechenland). *Annales Géologiques des Pays Hélléniques*, 30, 291-299.

Tabuce, R., Antunes, M. T. and Sigé, B., 2009. A new primitive bat from the earliest Eocene of Europe. *Journal of Vertebrate Paleontology*, 29, 627-630.

Tata, C. and Kotsakis, T., 2005. Italian fossil chiropteran assemblages: a preliminary report. *Geo.Alp*, 2, 53-60.

Teeling, E. C., Springer, M. S., Madsen, O., Bates, P., O'brien, S. J. and Murphy, W. J., 2005. A molecular phylogeny for bats illuminates biogeography and the fossil record. *Science*, 307, 580-584.

Tejedor, M. F., Czaplewski, N. J., Goin, F. J. and Aragón, E., 2005. The oldest record of South American bats. *Journal of Vertebrate Paleontology*, 25, 990-993.

Topal, G. and Tusnady, G., 1963. Data for the craniometric investigation of *Myotis myotis* BORK, and *Myotis oxygnathus* MONTIC. in Hungary (Mammalia). *Annales historico-naturales Musei nationalis hungarici*, 55, 543-549.

Tsirambides, A., 1998. Study of floor sediments from the Agiasma cave of Loutraki Pella (Macedonia). *Bulletin of the Geological Society of Greece*, 32, 339-349 [in Greek: Μελέτη ιζημάτων δαπέδου από το Σπήλαιο Αγιάσματος Λουτρακίου Πέλλας (Μακεδονία)].

Tsirambides, A. E., 2006. The sedimentology of the bear cave of Almopia speleopark (Pella, Macedonia, Greece). *Scientific annals, School of Geology, Aristotle University of Thessaloniki (AUTH),* special volume 98, 75-78.

Tsoukala, E., 1989. Contribution to the study of the Pleistocene fauna of large mammals (Carnivora, Perissodactyla, Artiodactyla) from Petralona Cave (Chalkidiki, N. Greece). *PhD Thesis, School of Geology, Aristotle University of Thessaloniki, No 8, 360 pp.* [in Greek: Συμβολή στη μελέτη της παλαιοπανίδας των μεγάλων σπονδυλωτών (Carnivora, Perissodactyla, Artiodactyla) του σπηλαίου των Πετραλώνων της Χαλκιδικής].

Tsoukala, E., 1994. Bärenreste aus Loutraki (Mazedonien, Griechenland) - "*Ursus spelaeus*". *2nd Höhlenbären Symposium, 15-18 September 1994, Corvara.*

Tsoukala, E. and Rabeder, G., 2005. Cave bears and Late Pleistocene associated faunal remains from Loutra Arideas (Pella, Macedonia, Greece). 15 years of research. *Naturhistorische Gesellschaft Nürnberg*, 45, 225-236.

Tsoukala, E., Chatzopoulou, K., Rabeder, G., Pappa, S., Nagel, D. and Withalm, G., 2006. Paleontological and stratigraphical research in Loutra Arideas Bear Cave (Almopia Speleopark, Pella, Macedonia, Greece). *Scientific annals, School of Geology, Aristotle University of Thessaloniki*, special volume 98, 41-67.

Tsoukala, E., Rabeder, G. and Verginis, S., 1998. *Ursus spelaeus* and associated faunal remains from Loutraki (Pella, Macedonia, Greece) - Excavations of 1996. Geological and geomorphological approach. *4th International Höhlenbären Symposium, 17-19 September 1998, Velenje.*

Tsoukala E., Rabeder, G. and Verginis, S., 2001. *Ursus spelaeus* and Late Pleistocene associated faunal remains from Loutraki (Pella, Macedonia, Greece) - Excavations of 1999. *Cuadernos do Laboratorio Xeolóxico de Laxe*, 26, 441-446.

Ulrich, W., Sachanowicz, K. and Michalak, M., 2007. Environmental correlates of species richness of European bats (Mammalia: Chiroptera). *Acta chiropterologica*, 9, 347-360.

van de Weerd, A., 1973. Rodentia from two Pleistocene fissure fillings near Athens. *Proceedings of the Koninklijke Nederlandse Akademie van Wetenschappen.*

Series B: Palaeontology Geology Physics Chemistry Anthropology, 76, 148-166.

van der Geer, A. A., Lyras, G. A., van den Hoek Ostende, L. W., de Vos, J. and Drinia, H., 2014. A dwarf elephant and a rock mouse on Naxos (Cyclades, Greece) with a revision of the palaeozoogeography of the Cycladic Islands (Greece) during the Pleistocene. *Palaeogeography, Palaeoclimatology, Palaeoecology*, 404, 133-144.

Vasileiadou, K. and Koufos, G. D., 2005. The micromammals from the Early/Middle Miocene locality of Antonios, Chalkidiki, Greece. *Annales de Paléontologie*, 91, 197-225.

Vasileiadou, K. and Zouros, N., 2012. Early Miocene micromammals from the Lesvos Petrified Forest (Greece): preliminary results. *Palaeobiodiversity and Palaeoenvironments*, 92, 249-264.

Vasileiadou, K. V., Koufos, G. D. and Syrides, G. E., 2003. Silata, a new locality with micromammals from the Miocene/Pliocene boundary of the Chalkidiki peninsula, Macedonia, Greece. *Deinsea*, 10, 549-562.

Vasileiadou, K., Böhme, M., Neubauer, T. A., Georgalis, G. L., Syrides, G. E., Papadopoulou, L. and Zouros, N., 2017. Early Miocene gastropod and ectothermic vertebrate remains from the Lesvos Petrified Forest (Greece). *PalZ*, 91, 541-564.

Vougioukalakis, G. E., 2002. Petrological, Geochemical and Volcanological study of the Pliocene Volcanic formations of Almopia and their Correlation with the Geothermal manifestations in the area. *PhD Thesis, School of Geology, Aristotle University of Thessaloniki, 303 pp.* [in Greek: Πετρολογική, Γεωχημική και Ηφαιστειολογική μελέτη των Πλειοκαινικών Ηφαιστειακών σχηματισμών της Αλμωπίας. Συσχετισμός τους με τις Γεωθερμικές εκδηλώσεις της περιοχής].

Wagner, B., Aufgebauer, A., Vogel, H., Zanchetta, G., Sulpizio, R. and Damaschke, M., 2012. Late Pleistocene and Holocene contourite drift in Lake Prespa (Albania/FYR of Macedonia/Greece). *Quaternary International*, 274, 112-121.

Wagner, B., Vogel, H., Francke, A., Friedrich, T., Donders, T., Lacey, J. H., Leng, M. J., Regattieri, E., Sadori, L., Wilke, T. and Zanchetta, G., 2019. Mediterranean winter rainfall in phase with African monsoons during the past 1.36 million years. *Nature*, 573, 256-260.

Youlatos, D., Panyutina, A. A., Tsinoglou, M. and Volodin, I. A., 2020. Locomotion and postures of the Vietnamese pygmy dormouse *Typhlomys chapensis* (Platacanthomyidae, Rodentia): climbing and leaping in the blind. *Mammalian Biology*, 100, 485-496.

Zacharias, N., Kabouroglou, E., Bassiakos, Y. and Michael, C. T., 2008. Dating and analysis of speleosediments from Aridaia at Macedonia, Greece. *Radiation measurements*, 43, 791-796.

Ziegler, R., 1993. Die Chiroptera (Mammalia) aus dem Untermiozän von Wintershof-West bei Eichstätt (Bayern). *Mitteilungen der Bayerischen Staatssamlung für Paläontologie und historische Geologie*, 33, 119-154.

Online Sources

Greek Fauna Documentation Center (GFDC), 2021, www.icgf.myspecies.info (downloaded on 15-05-2021)

The IUCN Red List of Threatened Species (IUCN), 2021, www.iucnredlist.org (downloaded on 26-04-2021)

Life GRECABAT (Life GRECABAT), 2021, www.lifegrecabat.eu (downloaded on 26-04-2021)

United Nations Environment Programme and EUROBATS (UNEP/EUROBATS), 2021, www.eurobats.org (downloaded on 14-04-2021)

APPENDIX

Table A.1 Mammalian species representation per chamber (Tsoukala et al. 2006, Chatzopoulou 2014, Nagel et al. 2019). Chiroptera is excluded (see Table A.5).

Species	**LAC**					**LAC Ia**
	LAC I	**LAC Ib**	**LAC Ic**	**LAC II**	**LAC III**	
Carnivora						
Ursus ingressus	+	+	+	+	+	
Mustela nivalis						+
Mustela (*Putorius*) *putorius*						+
Martes foina	+	+			+	+
Martes martes					+	+
Martes sp.			+			+
Meles meles				+	+	
Mustelidae indet.	+	+	+	+	+	+
Canis lupus	+		+			+
Vulpes vulpes	+			+	+	+
Felis silvestris aff. *catus*						+
Panthera pardus	+		+	+		
Crocuta crocuta spelaea	+	+	+			
Artiodactyla						
Capra ibex	+	+		+	+	+
Rupicapra rupicapra		+	+			
Cervus elaphus	+	+	+			
Dama dama	+	+	+			
Bos primigenius		+				+
Insectivora						
Erinaceus cf. *europaeus*				+		
Talpa europaea			+		+	+
Talpa sp. (*minor*)				+		
Sorex araneus	+	+			+	+
Sorex minutus			+	+	+	+
Neomys sp.				+	+	+
Crocidura leucodon	+	+	+	+	+	+
Crocidura suaveolens			+	+	+	+
Rodentia						
Spermophilus citellus		+	+	+		+
Apodemus mystacinus epimelas	+	+		+	+	+
Apodemus sylvaticus & *A. flavicollis*	+	+	+	+	+	+
Apodemus uralensis	+			+	+	+
Mus spicilegus	+	+	+	+	+	+
Cricetulus migratorius	+	+	+	+	+	+
Mesocricetus newtoni	+	+	+	+	+	+
Arvicola terrestris	+	+	+	+	+	+

Microtus arvalis & *M. agrestis*	+	+	+	+	+	+
Microtus (*Chionomys*) *nivalis*	+	+	+	+	+	+
Microtus (*Pitymys*) cf. *subterraneus*	+	+	+	+	+	+
Clethrionomys glareolus	+			+	+	+
Dryomys nitedula	+	+	+	+	+	+
Glis glis	+		+	+	+	+
Muscardinus avellanarius				+	+	+
Sicista subtilis					+	
Spalax leucodon	+	+	+	+	+	+
Lagomorpha						
Ochotona pusilla				+	+	+
Lepus timidus						+
Lepus europaeus				+		+

Table A.2 Avian species representation per chamber (Boev and Tsoukala 2019).

Species	**LAC**	**LAC Ia**
Galliformes		
Perdix perdix	+	+
Perdix sp.	+	+
Alectoris graeca	+	+
Alectoris sp.	+	+
Francolinus francolinus		+
Francolinus sp.		+
Alectoris/*Francolinus*		+
Perdix/*Francolinus*		+
Perdicinae gen.		+
Tetrao tetrix		+
Lagopus cf. *lagopus*	+	+
aff. *Lagopus* sp.		+
cf. *Bonasa bonasia*	+	
Bonasa bonasia/*Lagopus muta*		+
Columbiformes		
Columba livia	+	+
Columba palumbus	+	+
Caprimulgiformes		
? *Caprimulgus* sp.		+
Accipitriformes		
Buteo sp. cf. *B. lagopus*		+
Falconiformes		
Falco sp. cf. *F. peregrinus*	+	+
Falco sp. ex gr. *F. cherrug*		+
Falco sp. cf. *tinnunculus*		+
Falco sp. cf. *vespertinus*		+
Falco sp. ex gr. *tinnunculus*		+
Strigiformes		
Bubo bubo	+	+
Athene noctua		+

cf. *Otus scops*		+
Piciformes		
cf. *Dryocopus martius*		+
cf. Picidae		+
Passeriformes		
Galerida sp. cf. *G. cristata*		+
Melanocorhypha calandra	+	+
Melanocorhypha sp.		+
Alauda sp.		+
Lulula arborea		+
cf. *Hirundo* sp.		+
Riparia/Ptyonoprogne		+
Anthus sp.	+	+
Bombicylla garrulus		+
Cinclus cinclus		+
Turdus sp. cf. *T. vuscivorus*		+
Turdus sp.	+	+
Sylvia sp. cf. *S. borin*		+
Phoenicurus sp. cf. *P. ochruros*		+
Erithacus/Luscinia		+
Parus major		+
Sitta cf. *europaea*		+
Sitta sp.		+
Garrulus glandarius		+
Pica pica	+	+
Pica sp.		+
Pyrrhocorax graculus	+	+
Pyrrhocorax cf. *pyrrhocorax*		+
Pyrrhocorax sp. (*P. graculus/pyrrhocorax*)		+
Corvidae gen. - 1		+
Corvidae gen. - 2		+
cf. Corvidae gen.		+
Sturnus sp. cf. *S. vulgaris*		+
Fringilla sp. cf. *F. coelebs*		+
Carduelis sp. cf. *C. carduelis*		+
cf. *Chloris chloris*		+
Carduelis sp.		+
Loxia curvirostra	+	+
Coccothraustes coccothraustes	+	+
Pyrrhula pyrrhula	+	+
Fringillidae gen.	+	+
Emberiza calandra		+
cf. *Plectrophenax nivalis*		+
Emberiza sp. cf. *E. cirlus*		+
Emberizidae gen.		+
Oscines Non-Corvidae indet.		+
Non-Passeriformes indet.	+	+

Table A.3 Amphibian species representation per chamber (Rauscher, K. L. pers. comm. to Tsoukala, E.).

Species	LAC	LAC Ia
Anura		
Bufo bufo	+	+
Pseudepidalea viridis	+	+
Bombina variegata	+	
Pelobates syriacus		+
Hyla arborea		+
Rana temporaria		+

Table A.4 Reptilian species representation per chamber (Rauscher, K. L. pers. comm. to Tsoukala, E.).

Species	LAC	LAC Ia
Squamata		
Anguis fragilis	+	
Pseudopus apodus		+
Varanidae indet.	+	
Lacerta agilis	+	
Lacerta vivipara	+	
Lacerta trilineata		+
Lacerta viridis	+	+
Ophisops elegans	+	
Podarcis muralis	+	+
Coronella austriaca		+
Scincidae indet.	+	

Table A.5 Chiropteran species representation per chamber prior to this research as for (a) Piskoulis (2018), (b) Piskoulis (2019) and (c) Piskoulis and Chatzopoulou (in press).

Species	LAC	LAC Ia
Chiroptera		
Rhinolophus ferrumequinum	+[a, b, c]	+[a, c]
Rhinolophus mehelyi	cf.[a], +[b, c]	cf.[a], +[c]
Rhinolophus blasii	cf.[a], ?[b, c]	cf.[a], ?[c]
Rhinolophus euryale	cf.[a], +[b, c]	cf.[a], +[c]
Rhinolophus mehelyi/blasii/euryale	+[c]	+[c]
Rhinolophus hipposideros	+[a, b, c]	+[a, c]
Rhinolophus sp.	+[a, b, c]	+[a, c]
Myotis myotis	+[b, c]	+[c]
Myotis blythii	cf.[a], +[b, c]	+[a, c]
Myotis myotis/blythii	+[b, c]	+[c]
Myotis bechsteinii	+[b, c]	cf.[a], +[c]
Myotis emarginatus	+[b, c]	+[c]
Myotis nattereri	+[a]	
Myotis daubentonii	cf.[a]	
Myotis capaccinii	cf.[a], +[c]	+[c]
Myotis mystacinus	?[c]	?[c]
Myotis sp.	+[a, b, c]	+[a, c]

Nyctalus lasiopterus	?[c]	?[c]
Nyctalus noctula	+[a, b, c]	+[a, c]
Nyctalus leisleri	+[a, b, c]	+[a, c]
Pipistrellus pipistrellus	+[b, c]	+[c]
Pipistrellus kuhlii	+[b]	
Pipistrellus sp.		+[a]
Vespertilio murinus	+[a, c]	+[a, c]
Eptesicus serotinus	+[b, c]	cf.[a], +[c]
Plecotus auritus/austriacus	+[c]	+[c]
Barbastella barbastellus	+[b, c]	+[c]
Miniopterus schreibersii	+[a, b, c]	+[a, c]
Chiroptera indet.	+[a, b, c]	+[a, c]

Table A.6 *Rhinolophus ferrumequinum*, Loutra Almopias Cave A. Reconstructed body mass (in grams) from LAC based on the area of M1 (Piskoulis 2020). The equation used is: ln y = a ln x + ln b (Gunnell et al. 2009). LAC: Late Pleistocene; y: body mass; x: measurement parameter; a: slope of regression line; b: y-intercept of regression line.

L	**W**	**Area**	**Ln**	**Equation**	**Body Mass**
2.07	2.24	4.64	1.534	3.06	21.23
1.98	2.12	4.20	1.435	2.95	19.13
2.28	2.45	5.59	1.720	3.25	25.81
2.00	2.29	4.58	1.522	3.04	20.96
2.22	2.46	5.46	1.698	3.23	25.21
2.04	2.33	4.75	1.559	3.08	21.79
2.32	2.26	5.24	1.657	3.18	24.15
2.24	2.41	5.40	1.686	3.21	24.90
2.05	2.23	4.57	1.520	3.04	20.92
2.16	2.61	5.64	1.729	3.26	26.06
2.17	2.13	4.62	1.531	3.05	21.16
2.13	2.10	4.47	1.498	3.02	20.44
2.16	1.91	4.13	1.417	2.93	18.78
2.12	2.11	4.47	1.498	3.02	20.44
2.29	2.35	5.38	1.683	3.21	24.82
2.10	2.40	5.04	1.617	3.14	23.17
2.47	2.52	6.22	1.828	3.36	28.91
2.15	2.04	4.39	1.478	3.00	20.03
2.22	2.21	4.91	1.590	3.11	22.53
2.02	2.12	4.28	1.455	2.97	19.53
2.23	2.20	4.91	1.590	3.11	22.52
2.14	1.91	4.09	1.408	2.92	18.60
2.18	1.99	4.34	1.467	2.99	19.80
2.01	2.18	4.38	1.477	3.00	20.01
2.23	2.08	4.64	1.534	3.06	21.24
2.24	2.25	5.04	1.617	3.14	23.17
2.25	2.24	5.04	1.617	3.14	23.17
1.94	2.23	4.33	1.465	2.98	19.74
2.24	2.13	4.77	1.563	3.09	21.88
2.22	2.38	5.28	1.665	3.19	24.35

2.30	2.25	5.18	1.644	3.17	23.82
2.25	2.03	4.57	1.519	3.04	20.90
1.94	2.04	3.96	1.376	2.89	17.98
2.06	2.18	4.49	1.502	3.02	20.53
2.10	2.14	4.49	1.503	3.02	20.54
2.12	2.07	4.39	1.479	3.00	20.04
2.35	2.29	5.38	1.683	3.21	24.82
2.24	2.39	5.35	1.678	3.21	24.68
1.95	2.20	4.29	1.456	2.97	19.57
2.13	2.09	4.45	1.493	3.01	20.34
2.12	2.19	4.64	1.535	3.06	21.26
2.14	2.10	4.49	1.503	3.02	20.54

Table A.7 *Rhinolophus ferrumequinum*, Loutra Almopias Cave A. Reconstructed body mass (in grams) from LAC Ia based on the area of M1 (Piskoulis 2020). The equation used is: ln y = a ln x + ln b (Gunnell et al. 2009). LAC Ia: latest Pleistocene; y: body mass; x: measurement parameter; a: slope of regression line; b: y-intercept of regression line.

L	**W**	**Area**	**Ln**	**Equation**	**Body Mass**
2.04	1.88	3.84	1.344	2.86	17.40
1.89	2.03	3.84	1.345	2.86	17.40
1.91	1.95	3.72	1.315	2.83	16.87
2.10	1.81	3.80	1.335	2.85	17.23
2.02	2.03	4.10	1.411	2.93	18.66
2.03	2.04	4.14	1.421	2.94	18.86
1.88	2.04	3.84	1.344	2.86	17.40
1.89	1.90	3.59	1.278	2.79	16.24
2.03	1.97	4.00	1.386	2.90	18.18
2.08	2.08	4.33	1.465	2.98	19.74
2.03	1.98	4.02	1.391	2.91	18.27
2.00	1.96	3.92	1.366	2.88	17.80
1.95	1.90	3.71	1.310	2.82	16.78
1.99	2.03	4.04	1.396	2.91	18.37
2.01	1.84	3.70	1.308	2.82	16.75
1.82	1.84	3.35	1.209	2.71	15.09
2.01	1.92	3.86	1.350	2.86	17.51
1.80	2.12	3.82	1.339	2.85	17.31
1.98	2.15	4.26	1.449	2.97	19.41
1.80	1.80	3.24	1.176	2.68	14.58
1.81	2.04	3.69	1.306	2.82	16.72
1.99	2.03	4.04	1.396	2.91	18.37
1.91	2.01	3.84	1.345	2.86	17.42
1.93	2.04	3.94	1.370	2.88	17.88
1.92	1.93	3.71	1.310	2.82	16.78
2.00	1.89	3.78	1.330	2.84	17.13
1.97	2.11	4.16	1.425	2.94	18.93
2.00	2.00	4.00	1.386	2.90	18.18
1.98	1.91	3.78	1.330	2.84	17.14
2.08	2.00	4.16	1.426	2.94	18.95

1.79	1.67	2.99	1.095	2.59	13.40
2.09	1.99	4.16	1.425	2.94	18.94
2.06	1.83	3.77	1.327	2.84	17.09
2.12	2.12	4.49	1.503	3.02	20.55
1.97	2.02	3.98	1.381	2.90	18.08
1.94	1.86	3.61	1.283	2.79	16.32
1.97	2.02	3.98	1.381	2.90	18.08
2.03	2.03	4.12	1.416	2.93	18.76
2.00	2.07	4.14	1.421	2.94	18.85
2.03	2.05	4.16	1.426	2.94	18.95
2.17	1.95	4.23	1.443	2.96	19.29
1.93	1.88	3.63	1.289	2.80	16.41
2.14	2.05	4.39	1.479	3.00	20.03
1.91	2.05	3.92	1.365	2.88	17.78
2.12	1.95	4.13	1.419	2.93	18.82
2.00	2.36	4.72	1.552	3.07	21.63
2.03	2.01	4.08	1.406	2.92	18.56
1.96	1.91	3.74	1.320	2.83	16.96
1.86	1.88	3.50	1.252	2.76	15.79
1.94	1.86	3.61	1.283	2.79	16.32
1.97	2.10	4.14	1.420	2.94	18.84
2.04	2.02	4.12	1.416	2.93	18.76
1.89	1.94	3.67	1.299	2.81	16.60
2.17	2.12	4.60	1.526	3.05	21.05
2.01	1.96	3.94	1.371	2.88	17.89
2.12	2.12	4.49	1.503	3.02	20.55
2.02	2.01	4.06	1.401	2.92	18.47
2.11	2.08	4.39	1.479	3.00	20.04
1.91	2.06	3.93	1.370	2.88	17.87
1.98	2.09	4.14	1.420	2.94	18.84

Table A.8 *Rhinolophus ferrumequinum*, Loutra Almopias Cave A. Reconstructed body mass (in grams) from LAC based on the area of p4 (Piskoulis 2020). The equation used is: ln y = a ln x + ln b (Gunnell et al. 2009). LAC: Late Pleistocene; y: body mass; x: measurement parameter; a: slope of regression line; b: y-intercept of regression line.

L	**W**	**Area**	**Ln**	**Equation**	**Body Mass**
1.28	1.31	1.68	0.517	3.17	23.73
1.33	1.30	1.73	0.548	3.19	24.39
1.26	1.21	1.52	0.422	3.08	21.81
1.25	1.28	1.60	0.470	3.13	22.76
1.26	1.27	1.60	0.470	3.13	22.77
1.43	1.39	1.99	0.687	3.32	27.62
1.23	1.34	1.65	0.500	3.15	23.37
1.26	1.25	1.58	0.454	3.11	22.45
1.32	1.31	1.73	0.548	3.19	24.39
1.26	1.12	1.41	0.344	3.01	20.35
1.31	1.26	1.65	0.501	3.15	23.40
1.30	1.29	1.68	0.517	3.17	23.74

1.30	1.28	1.66	0.509	3.16	23.57
1.32	1.31	1.73	0.548	3.19	24.39
1.37	1.30	1.78	0.577	3.22	25.05
1.23	1.12	1.38	0.320	2.99	19.92
1.22	1.18	1.44	0.364	3.03	20.72
1.37	1.29	1.77	0.569	3.21	24.87
1.34	1.15	1.54	0.432	3.09	22.01
1.39	1.34	1.86	0.622	3.26	26.07
1.37	1.26	1.73	0.546	3.19	24.36
1.34	1.23	1.65	0.500	3.15	23.37
1.23	1.14	1.40	0.338	3.01	20.24
1.35	1.30	1.76	0.562	3.21	24.72
1.30	1.11	1.44	0.367	3.03	20.76
1.32	1.19	1.57	0.452	3.11	22.39
1.38	1.27	1.75	0.561	3.21	24.69
1.41	1.36	1.92	0.651	3.29	26.75
1.26	1.19	1.50	0.405	3.07	21.48
1.24	1.14	1.41	0.346	3.01	20.38
1.32	1.20	1.58	0.460	3.12	22.56
1.32	1.32	1.74	0.555	3.20	24.56
1.26	1.17	1.47	0.388	3.05	21.16
1.21	1.31	1.59	0.461	3.12	22.57
1.32	1.10	1.45	0.373	3.04	20.88
1.29	1.30	1.68	0.517	3.17	23.74
1.28	1.14	1.46	0.378	3.04	20.97
1.16	0.95	1.10	0.097	2.79	16.33
1.18	1.12	1.32	0.279	2.95	19.20
1.31	1.26	1.65	0.501	3.15	23.40
1.27	1.23	1.56	0.446	3.10	22.28
1.13	1.23	1.39	0.329	3.00	20.08
1.26	1.21	1.52	0.422	3.08	21.81
1.28	1.22	1.56	0.446	3.10	22.28
1.33	1.32	1.76	0.563	3.21	24.73
1.25	1.26	1.58	0.454	3.11	22.45
1.32	1.28	1.69	0.524	3.17	23.90
1.31	1.19	1.56	0.444	3.10	22.24
1.33	1.33	1.77	0.570	3.21	24.89
1.22	1.17	1.43	0.356	3.02	20.56
1.30	1.35	1.76	0.562	3.21	24.72
1.28	1.23	1.57	0.454	3.11	22.44
1.28	1.23	1.57	0.454	3.11	22.44
1.26	1.24	1.56	0.446	3.10	22.29
1.12	1.32	1.48	0.391	3.05	21.22
1.43	1.37	1.96	0.672	3.31	27.27
1.38	1.37	1.89	0.637	3.27	26.41
1.37	1.23	1.69	0.522	3.17	23.84
1.28	1.18	1.51	0.412	3.07	21.62
1.33	1.37	1.82	0.600	3.24	25.56
1.37	1.27	1.74	0.554	3.20	24.53

1.25	1.30	1.63	0.486	3.14	23.08
1.25	1.27	1.59	0.462	3.12	22.61
1.23	1.10	1.35	0.302	2.98	19.60
1.27	1.23	1.56	0.446	3.10	22.28
1.42	1.26	1.79	0.582	3.22	25.15
1.29	1.11	1.43	0.359	3.03	20.62
1.25	1.19	1.49	0.397	3.06	21.33
1.30	1.27	1.65	0.501	3.15	23.41
1.28	1.18	1.51	0.412	3.07	21.62
1.36	1.21	1.65	0.498	3.15	23.34
1.32	1.29	1.70	0.532	3.18	24.06
1.26	1.20	1.51	0.413	3.07	21.64
1.20	1.15	1.38	0.322	2.99	19.95
1.39	1.35	1.88	0.629	3.27	26.24
1.28	1.26	1.61	0.478	3.13	22.93
1.32	1.31	1.73	0.548	3.19	24.39
1.39	1.23	1.71	0.536	3.18	24.15
1.29	1.24	1.60	0.470	3.12	22.76
1.24	1.32	1.64	0.493	3.15	23.23

Table A.9 *Rhinolophus ferrumequinum*, Loutra Almopias Cave A. Reconstructed body mass (in grams) from LAC Ia based on the area of p4 (Piskoulis 2020). The equation used is: ln y = a ln x + ln b (Gunnell et al. 2009). LAC Ia: latest Pleistocene; y: body mass; x: measurement parameter; a: slope of regression line; b: y-intercept of regression line.

L	**W**	**Area**	**Ln**	**Equation**	**Body Mass**
1.08	1.12	1.21	0.190	2.88	17.74
1.24	1.13	1.40	0.337	3.01	20.23
1.20	1.04	1.25	0.222	2.90	18.24
1.09	0.97	1.06	0.056	2.76	15.74
0.94	0.85	0.80	-0.224	2.51	12.26
1.18	1.14	1.35	0.297	2.97	19.50
1.15	1.08	1.24	0.217	2.90	18.16
1.17	1.13	1.32	0.279	2.96	19.20
1.20	1.08	1.30	0.259	2.94	18.87
1.18	1.09	1.29	0.252	2.93	18.74
1.23	0.83	1.02	0.021	2.72	15.25
1.15	1.18	1.36	0.305	2.98	19.66
1.14	1.07	1.22	0.199	2.88	17.87
1.23	0.99	1.22	0.197	2.88	17.85
1.23	1.22	1.50	0.406	3.07	21.50
1.31	1.03	1.35	0.300	2.97	19.56
1.19	1.26	1.50	0.405	3.07	21.48
1.20	1.08	1.30	0.259	2.94	18.87
1.17	1.08	1.26	0.234	2.91	18.45
1.24	1.08	1.34	0.292	2.97	19.43
1.30	1.06	1.38	0.321	2.99	19.93
1.17	1.11	1.30	0.261	2.94	18.90
1.19	1.06	1.26	0.232	2.91	18.42

1.23	1.10	1.35	0.302	2.98	19.60
1.17	1.08	1.26	0.234	2.91	18.45
1.18	1.08	1.27	0.242	2.92	18.59
1.18	1.11	1.31	0.270	2.95	19.05
1.21	1.04	1.26	0.230	2.91	18.38
1.20	1.17	1.40	0.339	3.01	20.26
1.17	1.11	1.30	0.261	2.94	18.90
1.26	1.08	1.36	0.308	2.98	19.70
1.24	1.08	1.34	0.292	2.97	19.43
1.21	1.03	1.25	0.220	2.90	18.22
1.26	1.24	1.56	0.446	3.10	22.29
1.19	1.07	1.27	0.242	2.92	18.57
1.22	1.04	1.27	0.238	2.92	18.51
1.29	1.04	1.34	0.294	2.97	19.46
1.15	1.07	1.23	0.207	2.89	18.01
1.35	1.10	1.49	0.395	3.06	21.30
1.11	1.19	1.32	0.278	2.95	19.19
1.26	1.08	1.36	0.308	2.98	19.70
1.12	1.11	1.24	0.218	2.90	18.18
1.25	1.10	1.38	0.318	2.99	19.89
1.22	1.11	1.35	0.303	2.98	19.62
1.18	1.08	1.27	0.242	2.92	18.59
1.16	1.10	1.28	0.244	2.92	18.61
1.20	1.09	1.31	0.268	2.95	19.02
1.20	1.07	1.28	0.250	2.93	18.71
1.15	1.16	1.33	0.288	2.96	19.36
1.25	1.12	1.40	0.336	3.01	20.21
1.21	1.15	1.39	0.330	3.00	20.10
1.12	1.04	1.16	0.153	2.84	17.15
1.20	1.16	1.39	0.331	3.00	20.11
1.24	1.05	1.30	0.264	2.94	18.94
1.22	1.24	1.51	0.414	3.08	21.65
1.15	1.13	1.30	0.262	2.94	18.91
1.20	1.20	1.44	0.365	3.03	20.72
1.25	0.95	1.19	0.172	2.86	17.45
1.13	1.11	1.25	0.227	2.91	18.32
1.21	0.93	1.13	0.118	2.81	16.63
1.18	1.07	1.26	0.233	2.91	18.43
1.16	1.09	1.26	0.235	2.92	18.46
1.18	1.22	1.44	0.364	3.03	20.72
1.25	1.25	1.56	0.446	3.10	22.29
1.10	1.06	1.17	0.154	2.84	17.17

Table A.10 *Rhinolophus ferrumequinum*, Loutra Almopias Cave A. Reconstructed body mass (in grams) from LAC based on the area of m1 (Piskoulis 2020). The equation used is: ln y = a ln x + ln b (Gunnell et al. 2009). LAC: Late Pleistocene; tld: talonid; y: body mass; x: measurement parameter; a: slope of regression line; b: y-intercept of regression line.

L	W (tld)	Area	Ln	Equation	Body Mass
2.27	1.42	3.22	1.170	3.197	24.468
1.90	1.24	2.36	0.857	2.870	17.631
2.22	1.36	3.02	1.105	3.129	22.850
2.37	1.46	3.46	1.241	3.271	26.350
2.30	1.28	2.94	1.080	3.103	22.256
2.29	1.32	3.02	1.106	3.130	22.879
2.31	1.38	3.19	1.159	3.186	24.186
2.14	1.09	2.33	0.847	2.859	17.448
2.27	1.30	2.95	1.082	3.105	22.311
2.29	1.45	3.32	1.200	3.228	25.239
2.25	1.35	3.04	1.111	3.135	22.995
2.39	1.25	2.99	1.094	3.118	22.599
2.30	1.34	3.08	1.126	3.150	23.347
2.27	1.39	3.16	1.149	3.175	23.928
2.39	1.37	3.27	1.186	3.214	24.872
2.29	1.33	3.05	1.114	3.138	23.060
2.36	1.35	3.19	1.159	3.185	24.171
2.24	1.30	2.91	1.069	3.091	22.003
2.24	1.47	3.29	1.192	3.220	25.019
2.20	1.20	2.64	0.971	2.989	19.859
2.19	1.40	3.07	1.120	3.145	23.221
2.28	1.38	3.15	1.146	3.172	23.858
2.29	1.36	3.11	1.136	3.161	23.604
2.12	1.30	2.76	1.014	3.034	20.772
2.16	1.25	2.70	0.993	3.012	20.331
2.39	1.52	3.63	1.290	3.322	27.726
2.20	1.32	2.90	1.066	3.088	21.940
2.27	1.37	3.11	1.135	3.160	23.568
2.41	1.39	3.35	1.209	3.238	25.473
2.13	1.29	2.75	1.011	3.030	20.707
2.21	1.28	2.83	1.040	3.061	21.346
2.29	1.20	2.75	1.011	3.031	20.709
2.30	1.37	3.15	1.148	3.174	23.894
2.25	1.30	2.93	1.073	3.096	22.105
2.15	1.34	2.88	1.058	3.080	21.758
2.20	1.24	2.73	1.004	3.023	20.551
2.02	1.24	2.50	0.918	2.934	18.797
2.33	1.28	2.98	1.093	3.116	22.559
2.24	1.25	2.80	1.030	3.050	21.119
2.31	1.53	3.53	1.263	3.294	26.941
2.32	1.40	3.25	1.178	3.205	24.663
2.21	1.20	2.65	0.975	2.993	19.953
2.33	1.32	3.08	1.124	3.148	23.297
2.24	1.31	2.93	1.077	3.099	22.180

2.22	1.40	3.11	1.134	3.159	23.553
2.50	1.45	3.63	1.288	3.320	27.664
2.25	1.45	3.26	1.182	3.210	24.779
2.05	1.27	2.60	0.957	2.974	19.572
2.39	1.35	3.23	1.171	3.198	24.493
2.29	1.48	3.39	1.221	3.250	25.785
2.22	1.39	3.09	1.127	3.152	23.377
2.16	1.44	3.11	1.135	3.160	23.572
2.37	1.55	3.67	1.301	3.334	28.051
2.41	1.48	3.57	1.272	3.303	27.200
2.25	1.21	2.72	1.002	3.021	20.508
2.21	1.36	3.01	1.100	3.124	22.743
2.39	1.41	3.37	1.215	3.244	25.632
2.20	1.33	2.93	1.074	3.096	22.113
2.26	1.23	2.78	1.022	3.043	20.960
2.17	1.41	3.06	1.118	3.143	23.171
2.27	1.46	3.31	1.198	3.226	25.189
2.21	1.38	3.05	1.115	3.140	23.092
2.10	1.31	2.75	1.012	3.032	20.733
1.97	1.28	2.52	0.925	2.941	18.929
2.15	1.55	3.33	1.204	3.232	25.335
2.10	1.34	2.81	1.035	3.055	21.229
2.23	1.34	2.99	1.095	3.118	22.605

Table A.11 *Rhinolophus ferrumequinum*, Loutra Almopias Cave A. Reconstructed body mass (in grams) from LAC Ia based on the area of m1 (Piskoulis 2020). The equation used is: ln y = a ln x + ln b (Gunnell et al. 2009). LAC Ia: latest Pleistocene; tld: talonid; y: body mass; x: measurement parameter; a: slope of regression line; b: y-intercept of regression line.

L	W (tld)	Area	Ln	Equation	Body Mass
2.27	1.38	3.13	1.142	3.168	23.748
2.00	1.34	2.68	0.986	3.004	20.174
2.15	1.29	2.77	1.020	3.040	20.910
2.06	1.27	2.62	0.962	2.979	19.672
2.04	1.22	2.49	0.912	2.927	18.671
2.00	1.18	2.36	0.859	2.871	17.663
2.11	1.32	2.79	1.024	3.045	21.002
2.22	1.33	2.95	1.083	3.106	22.324
2.04	1.31	2.67	0.983	3.001	20.114
2.11	1.21	2.55	0.937	2.954	19.176
2.18	1.42	3.10	1.130	3.155	23.455
2.05	1.10	2.26	0.813	2.824	16.842
2.11	1.33	2.81	1.032	3.053	21.168
2.15	1.34	2.88	1.058	3.080	21.758
1.98	1.34	2.65	0.976	2.994	19.963
2.06	1.22	2.51	0.922	2.937	18.863
2.00	1.16	2.32	0.842	2.854	17.350
2.12	1.27	2.69	0.990	3.009	20.271
2.05	1.39	2.85	1.047	3.068	21.509

2.20	1.31	2.88	1.058	3.080	21.766
2.11	1.31	2.76	1.017	3.037	20.836
2.09	1.18	2.47	0.903	2.917	18.494
2.08	1.29	2.68	0.987	3.006	20.199
1.97	1.25	2.46	0.901	2.916	18.465
2.08	1.34	2.79	1.025	3.045	21.018
2.24	1.35	3.02	1.107	3.131	22.888
2.11	1.23	2.60	0.954	2.971	19.508
2.09	1.24	2.59	0.952	2.969	19.478
2.09	1.29	2.70	0.992	3.011	20.300
2.17	1.28	2.78	1.022	3.042	20.942
2.14	1.17	2.50	0.918	2.933	18.789
2.01	1.20	2.41	0.880	2.894	18.070
2.11	1.23	2.60	0.954	2.971	19.508
2.16	1.20	2.59	0.952	2.969	19.482
2.12	1.26	2.67	0.983	3.001	20.104
2.12	1.25	2.65	0.975	2.993	19.938
2.13	1.23	2.62	0.963	2.981	19.701
2.16	1.31	2.83	1.040	3.061	21.352
2.13	1.30	2.77	1.018	3.039	20.874
2.14	1.17	2.50	0.918	2.933	18.789
2.00	1.17	2.34	0.850	2.863	17.506
2.14	1.28	2.74	1.008	3.027	20.640
2.13	1.17	2.49	0.913	2.928	18.697
2.14	1.29	2.76	1.015	3.035	20.808
2.11	1.31	2.76	1.017	3.037	20.836
2.19	1.22	2.67	0.983	3.001	20.109
2.07	1.30	2.69	0.990	3.009	20.260
2.11	1.25	2.64	0.970	2.988	19.839
1.99	1.26	2.51	0.919	2.935	18.817
2.02	1.18	2.38	0.869	2.882	17.847
2.16	1.32	2.85	1.048	3.069	21.523
2.12	1.23	2.61	0.958	2.976	19.604
2.11	1.21	2.55	0.937	2.954	19.176
1.96	1.08	2.12	0.750	2.758	15.764
2.04	1.22	2.49	0.912	2.927	18.671
2.15	1.31	2.82	1.035	3.056	21.249
2.18	1.31	2.86	1.049	3.071	21.559
1.96	1.10	2.16	0.768	2.777	16.070
2.09	1.25	2.61	0.960	2.978	19.643
1.89	1.12	2.12	0.750	2.758	15.764
1.87	1.06	1.98	0.684	2.689	14.718
2.11	1.13	2.38	0.869	2.882	17.853
2.06	1.22	2.51	0.922	2.937	18.863
2.10	1.26	2.65	0.973	2.991	19.906
2.09	1.28	2.68	0.984	3.002	20.136
2.06	1.20	2.47	0.905	2.920	18.540
2.16	1.16	2.51	0.919	2.934	18.803
2.20	1.32	2.90			

2.05	1.22	2.50			
2.10	1.31	2.75			
2.01	1.30	2.61			
2.07	1.23	2.55			
2.15	1.28	2.75			
2.15	1.29	2.77			
2.13	1.26	2.68			
1.97	1.31	2.58			
1.94	1.24	2.41			
2.22	1.30	2.89			
2.17	1.31	2.84			
2.05	1.19	2.44			
2.06	1.23	2.53			
2.16	1.30	2.81			
1.99	1.11	2.21			
2.03	1.09	2.21			
2.11	1.20	2.53			
1.97	1.15	2.27			
2.09	1.32	2.76			
2.16	1.34	2.89			
2.05	1.30	2.67			
2.00	1.16	2.32			
2.09	1.26	2.63			
2.10	1.18	2.48			
2.16	1.24	2.68			
1.92	1.16	2.23			
2.15	1.29	2.77			
2.16	1.25	2.70			
2.14	1.19	2.55			
2.01	1.20	2.41			
2.02	1.21	2.44			
2.14	1.23	2.63			
2.08	1.22	2.54			
2.07	1.20	2.48			
2.17	1.21	2.63			
2.08	1.26	2.62			
2.15	1.35	2.90			
2.23	1.40	3.12			
2.13	1.21	2.58			
2.09	1.27	2.65			
2.15	1.33	2.86			
2.02	1.19	2.40			
2.08	1.26	2.62			
2.06	1.30	2.68			
1.99	1.08	2.15			
2.15	1.31	2.82			

Figure A.1 Box 1.

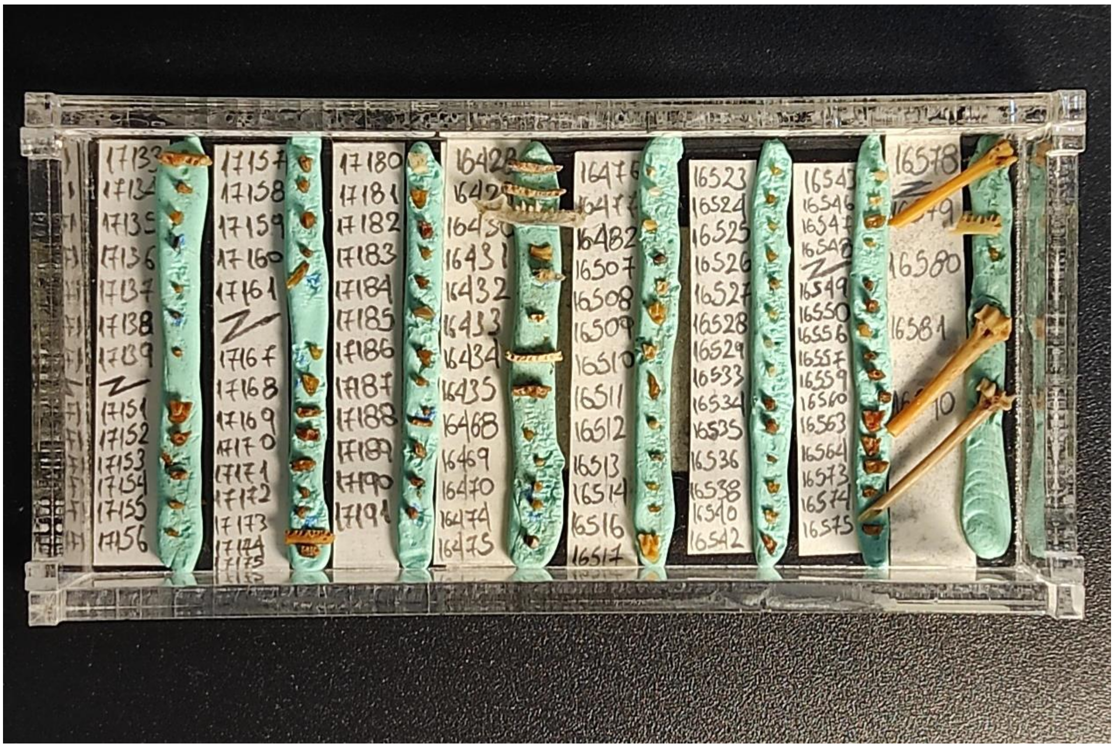

Figure A.2 Box 2.

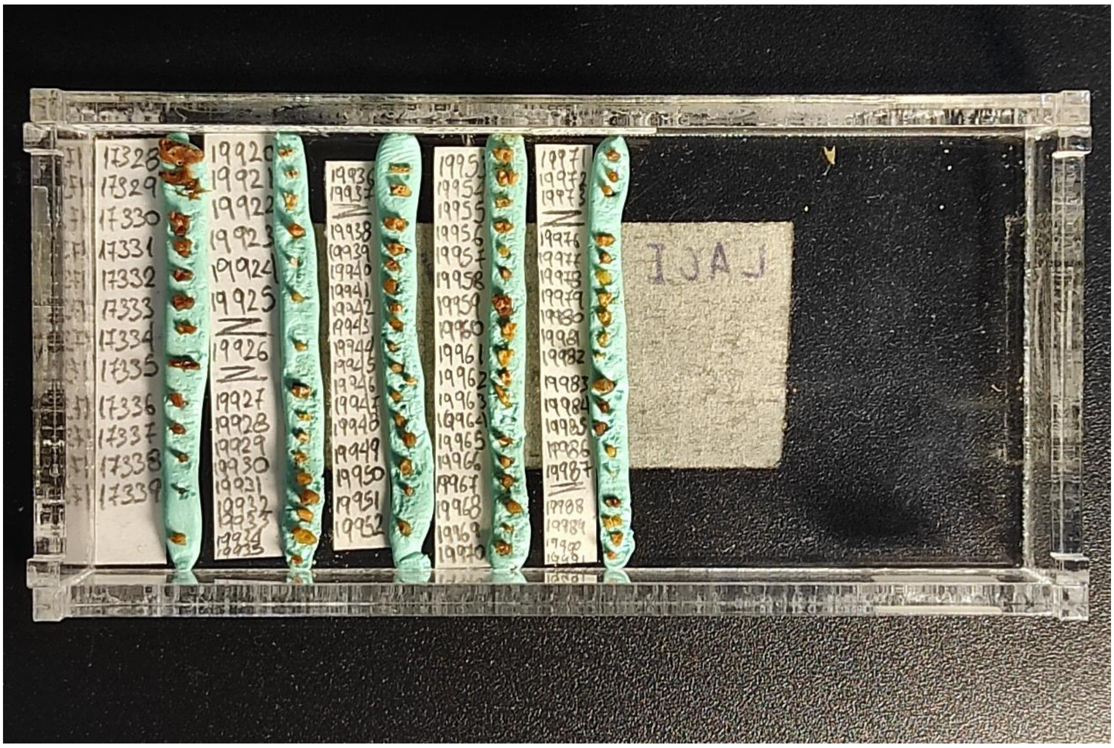

Figure A.3 Box 3.

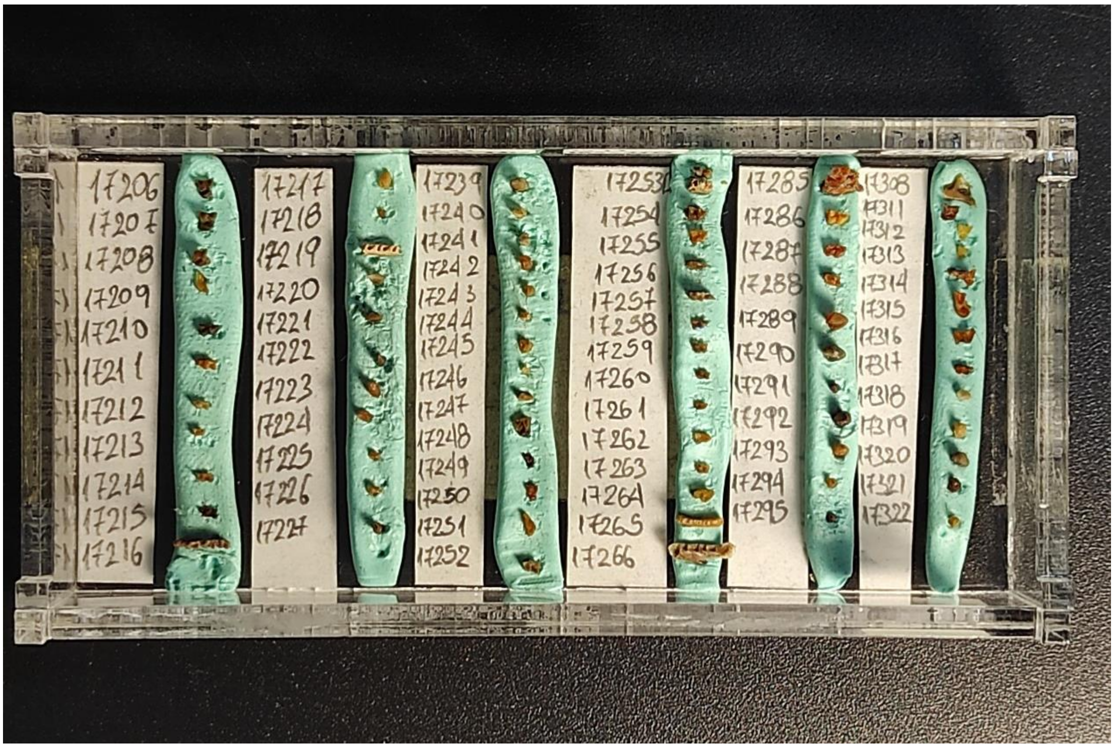

Figure A.4 Box 4.

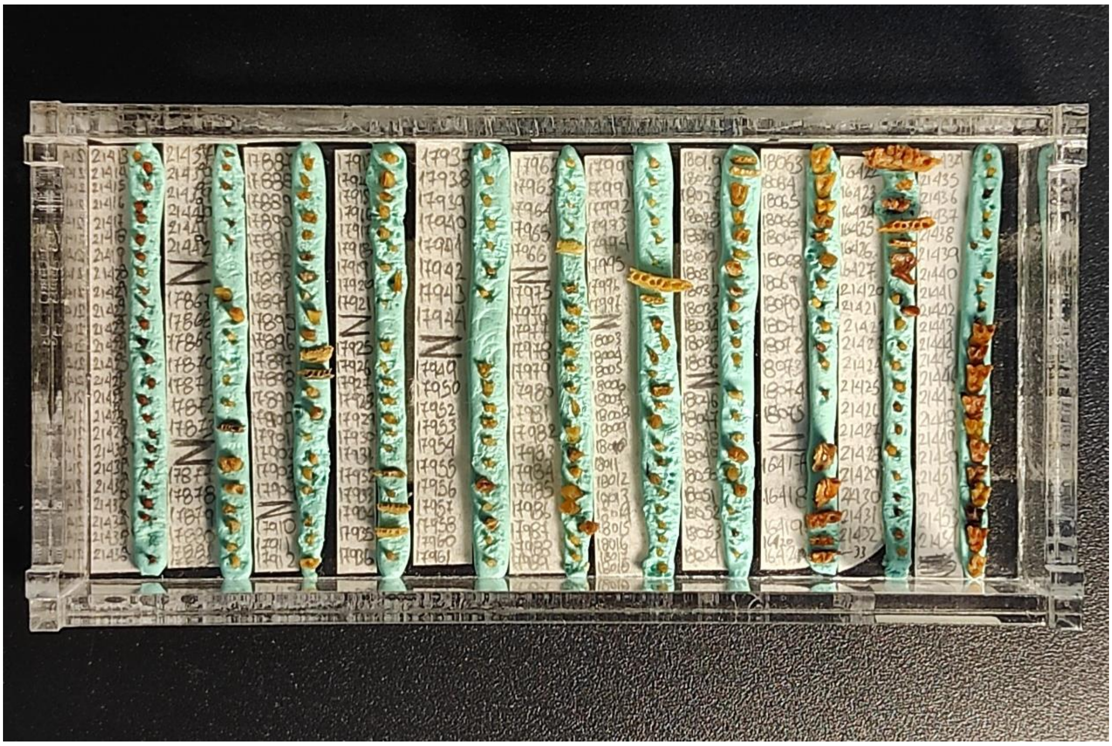

Figure A.5 Box 5.

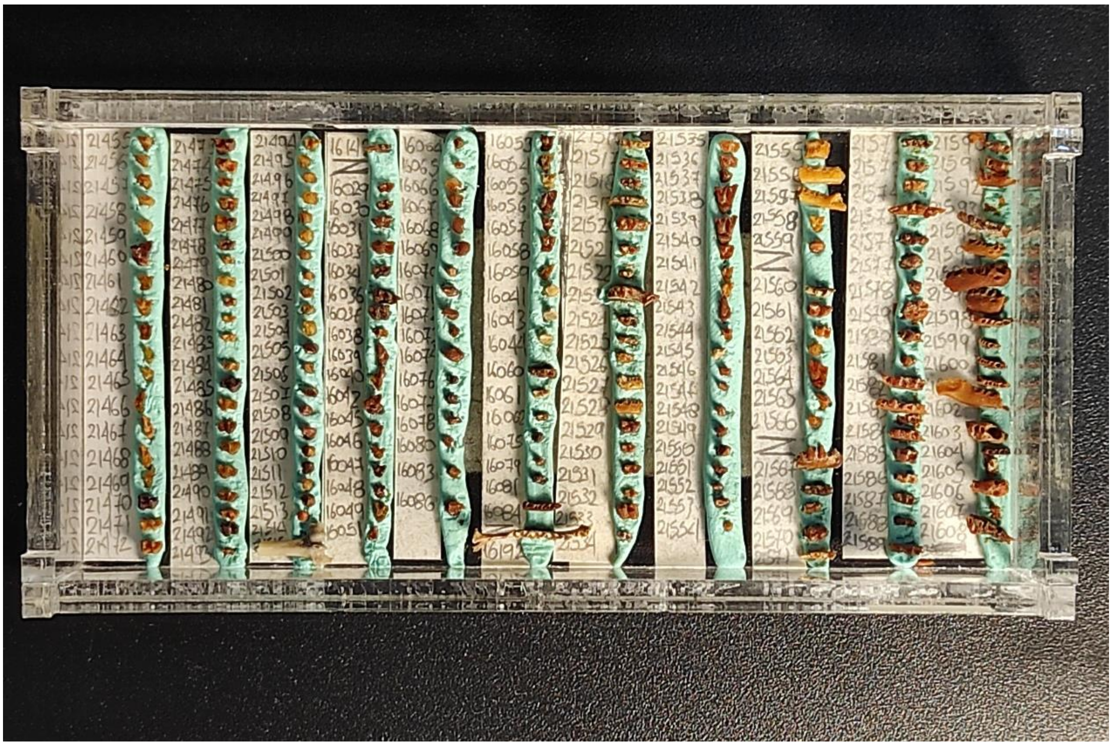

Figure A.6 Box 6.

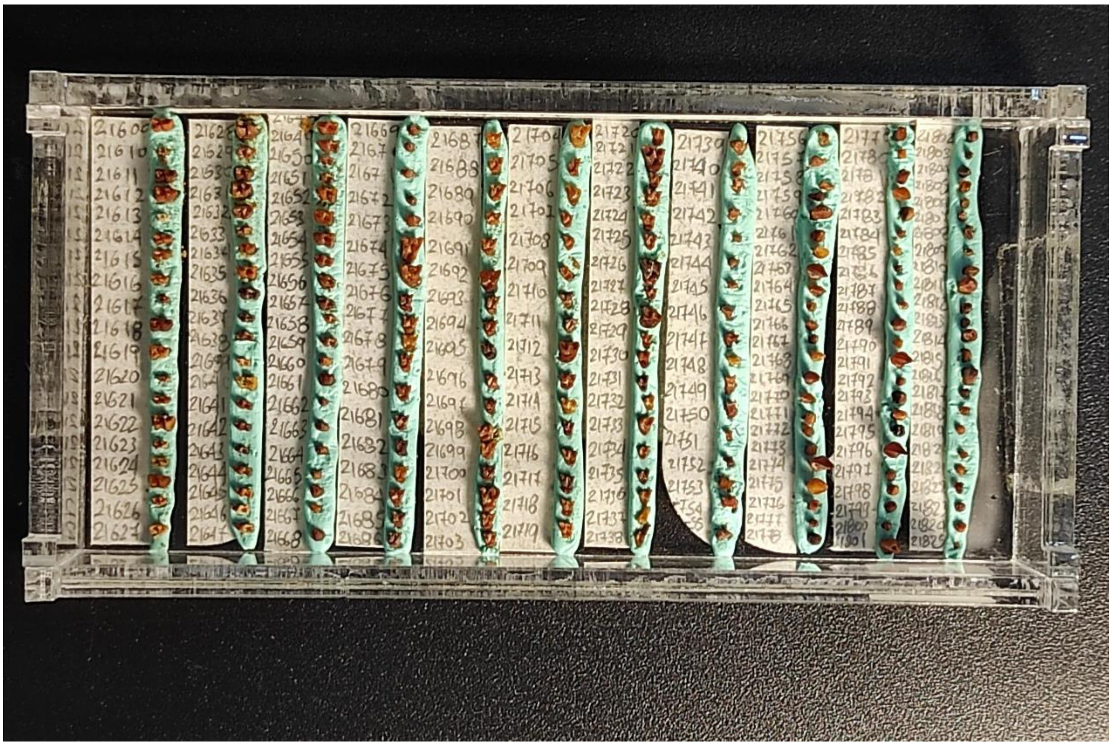

Figure A.7 Box 7.

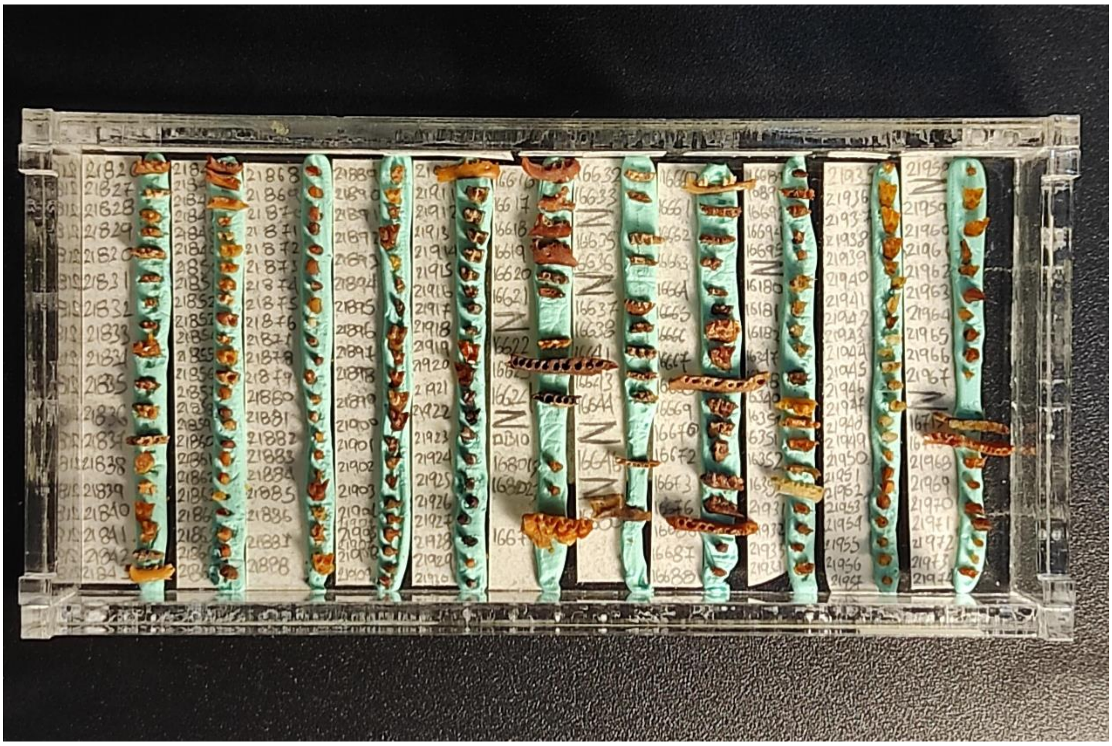

Figure A.8 Box 8.

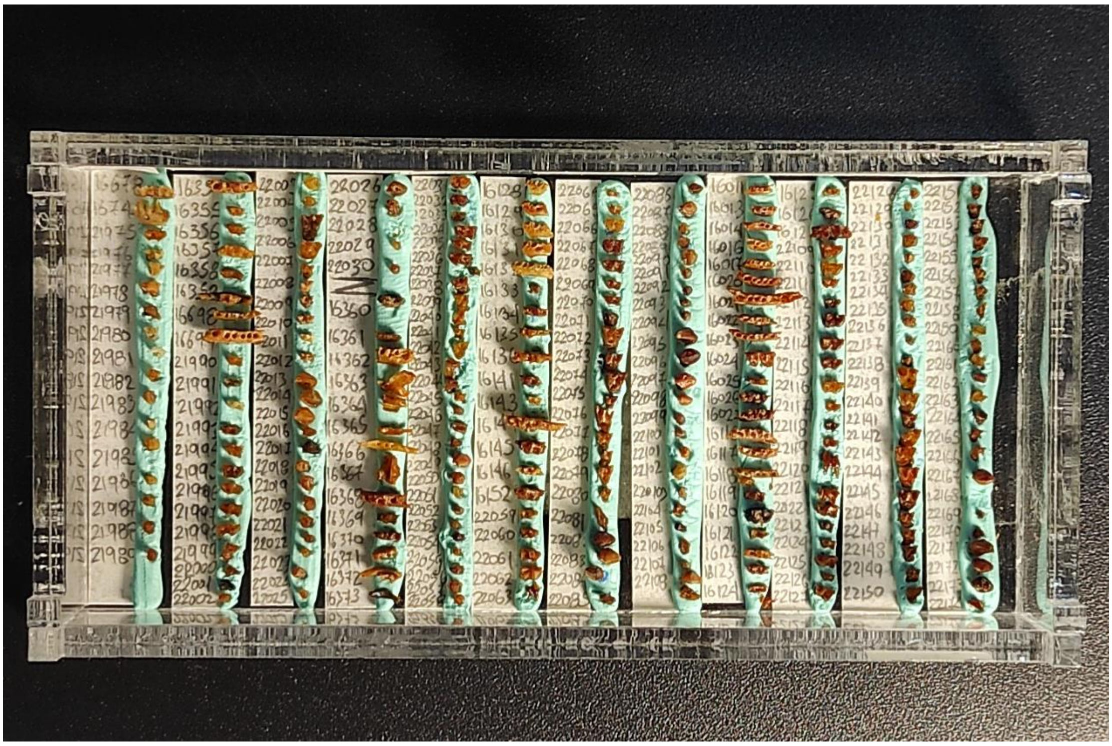

Figure A.9 Box 9.

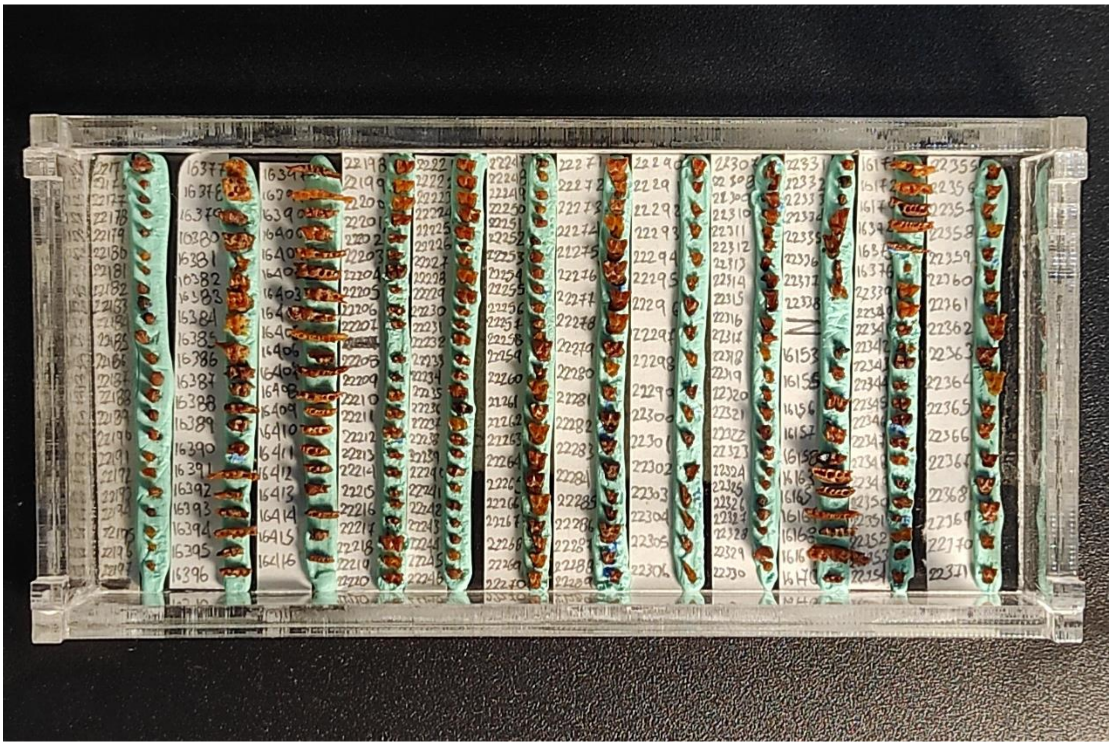

Figure A.10 Box 10.

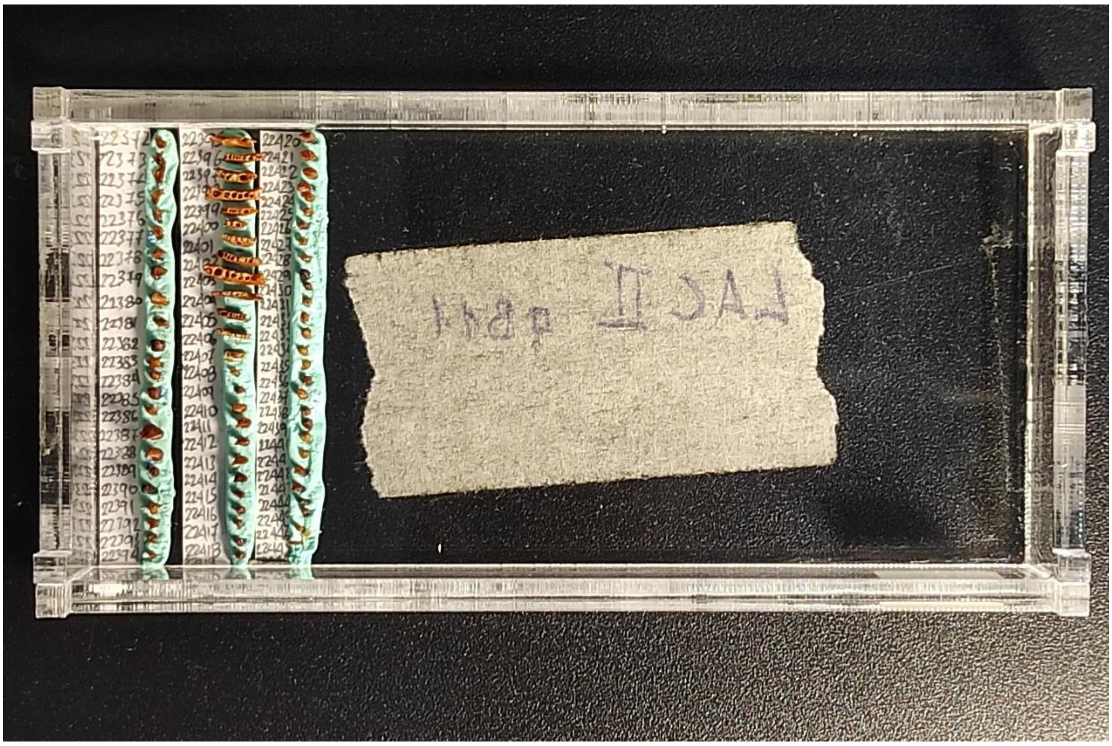

Figure A.11 Box 11.

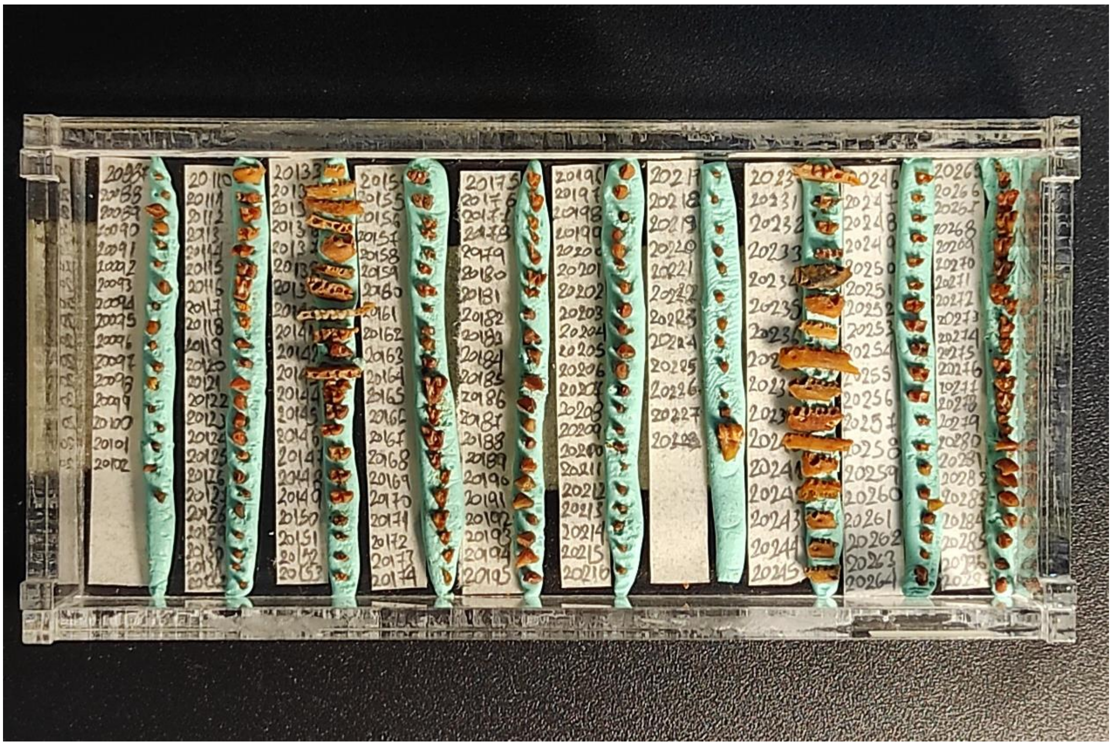

Figure A.12 Box 12.

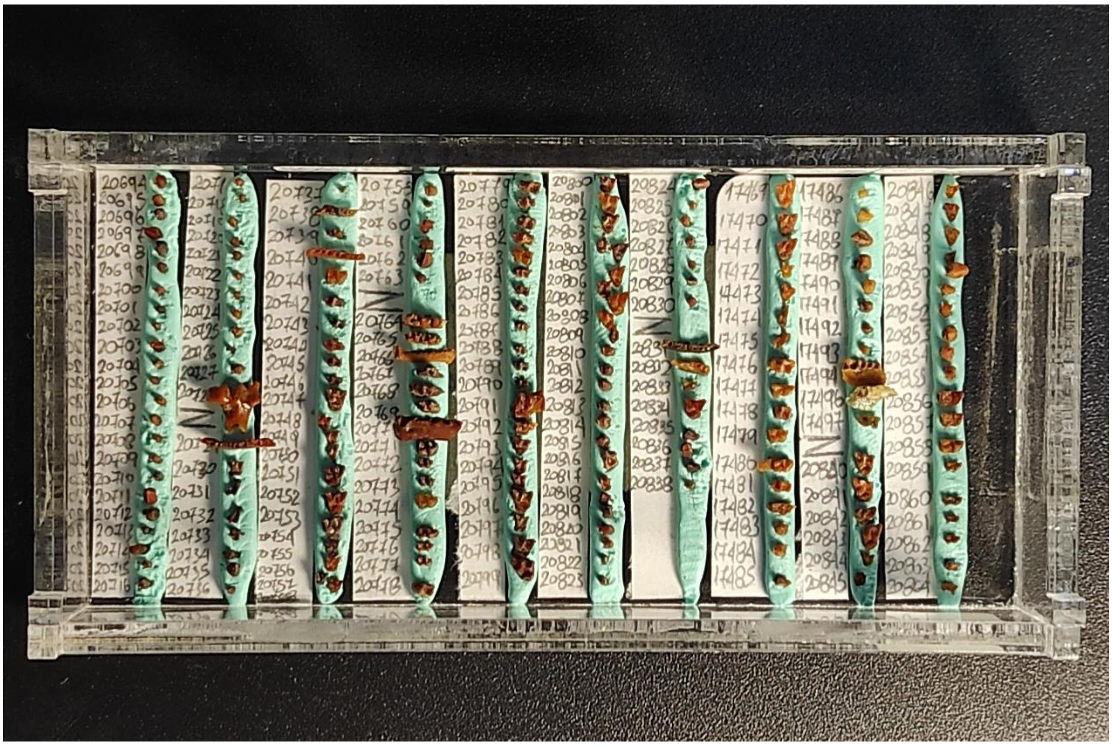

Figure A.13 Box 13.

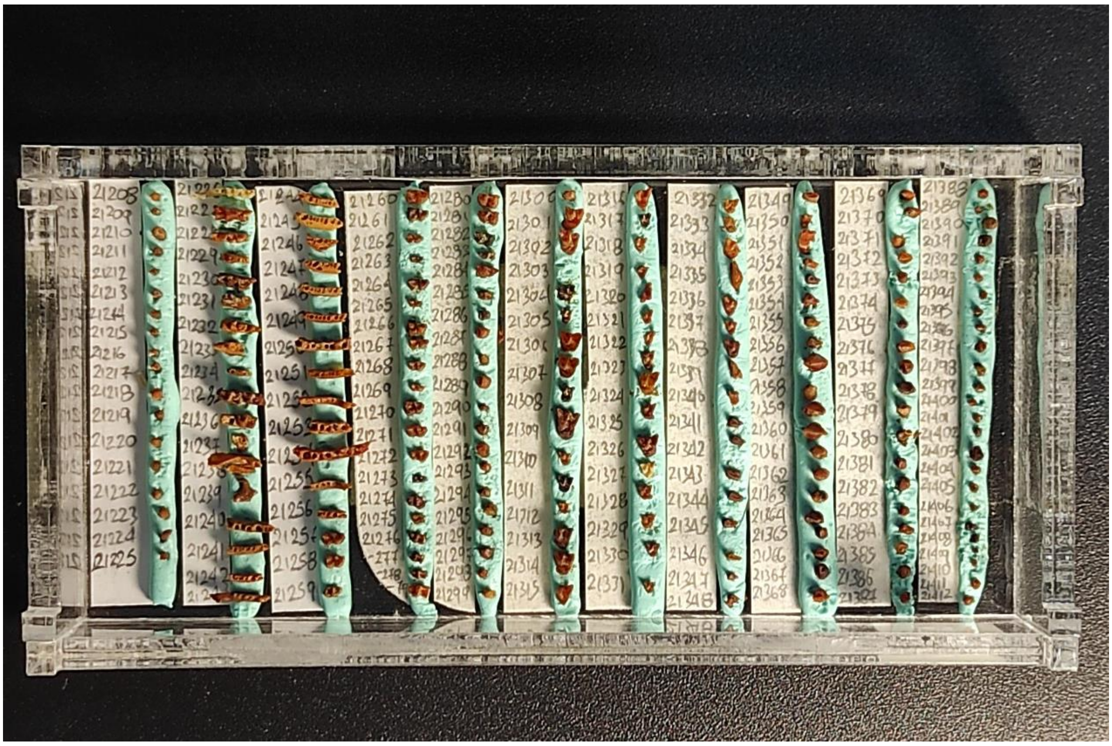

Figure A.14 Box 14.

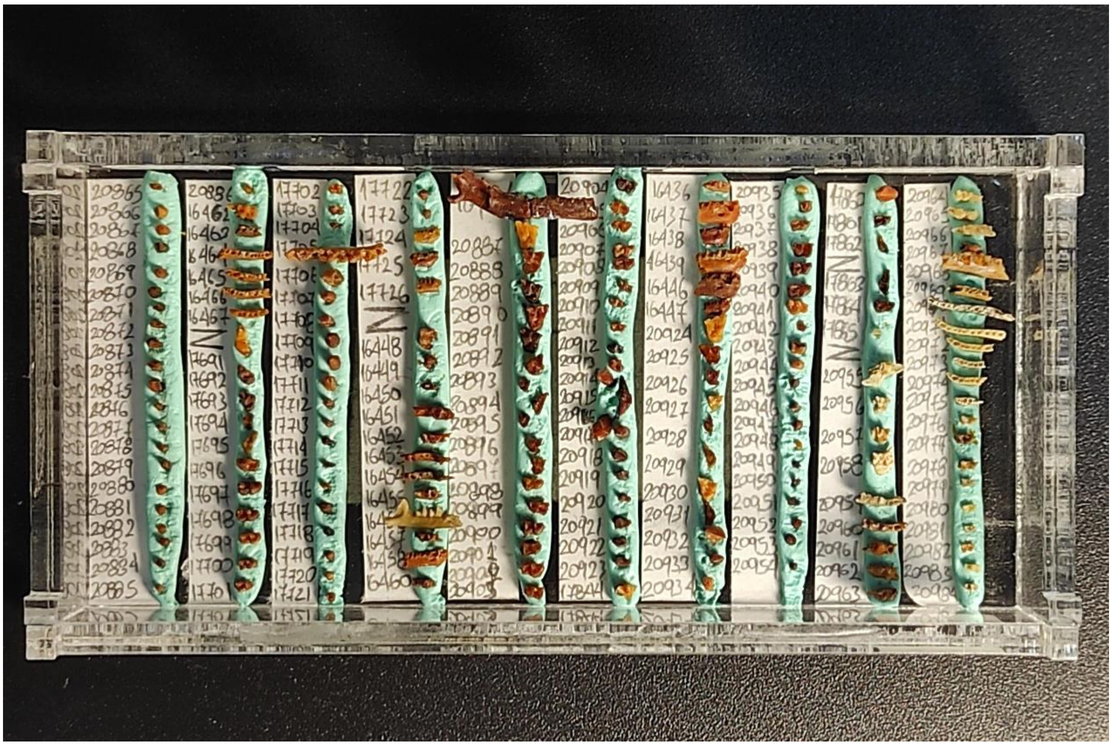

Figure A.15 Box 15.

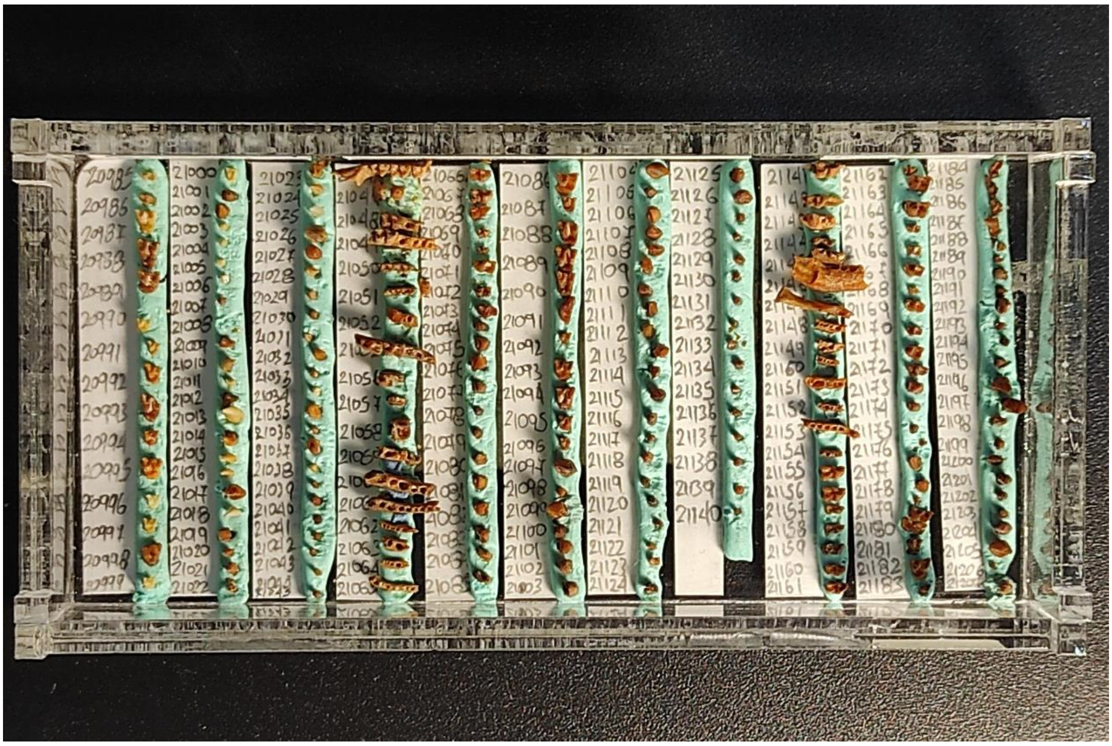

Figure A.16 Box 16.

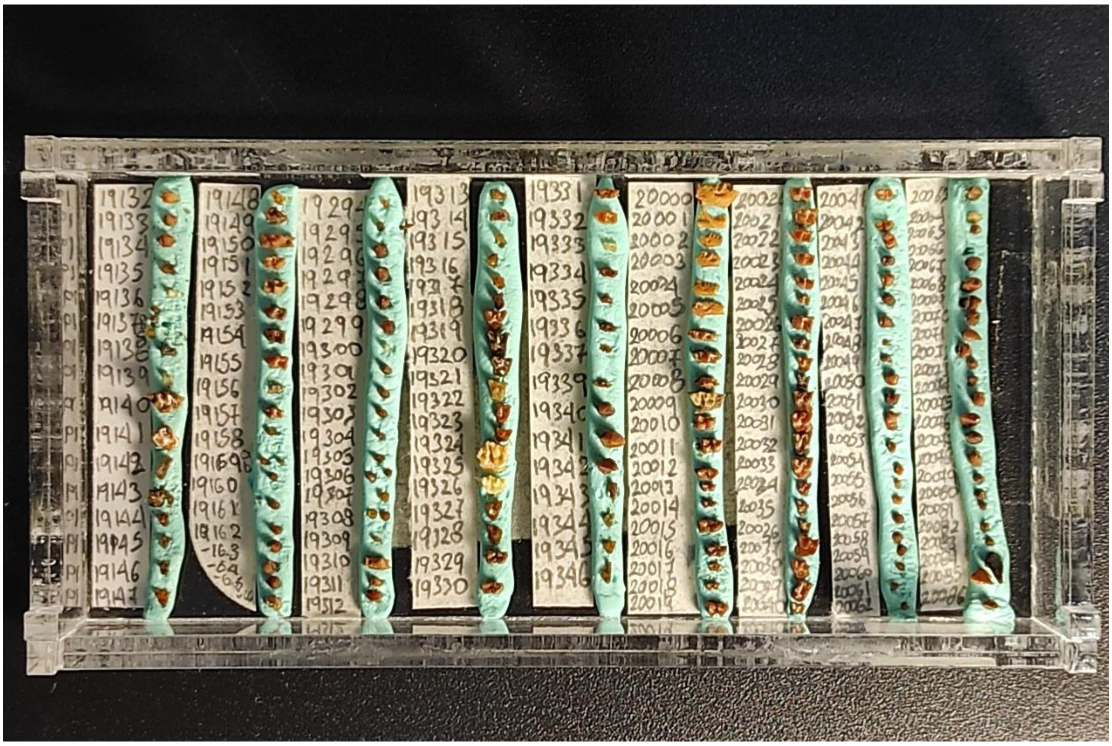

Figure A.17 Box 17.

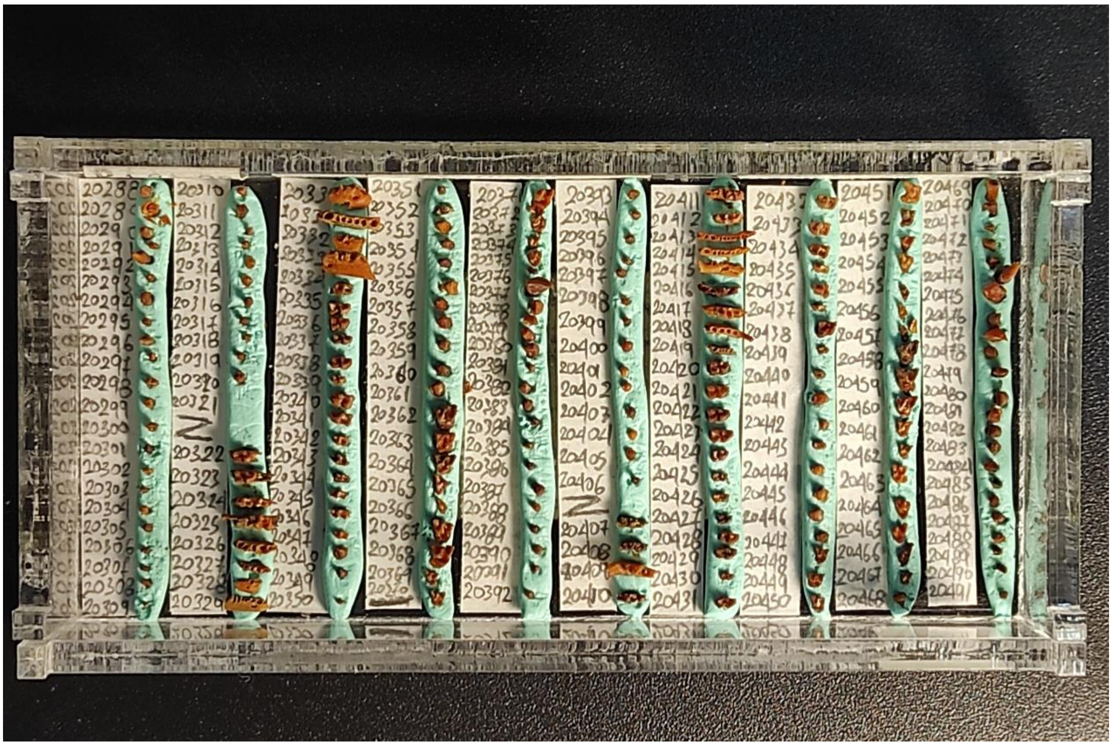

Figure A.18 Box 18.

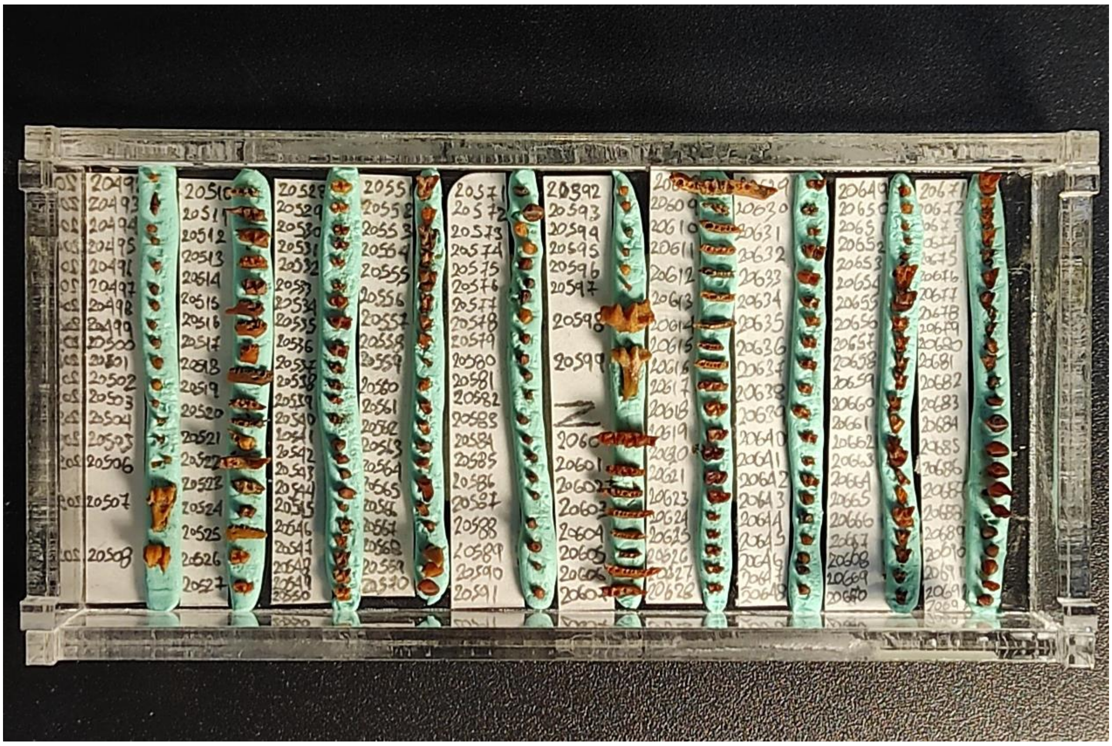

Figure A.19 Box 19.

Figure A.20 Box 20.

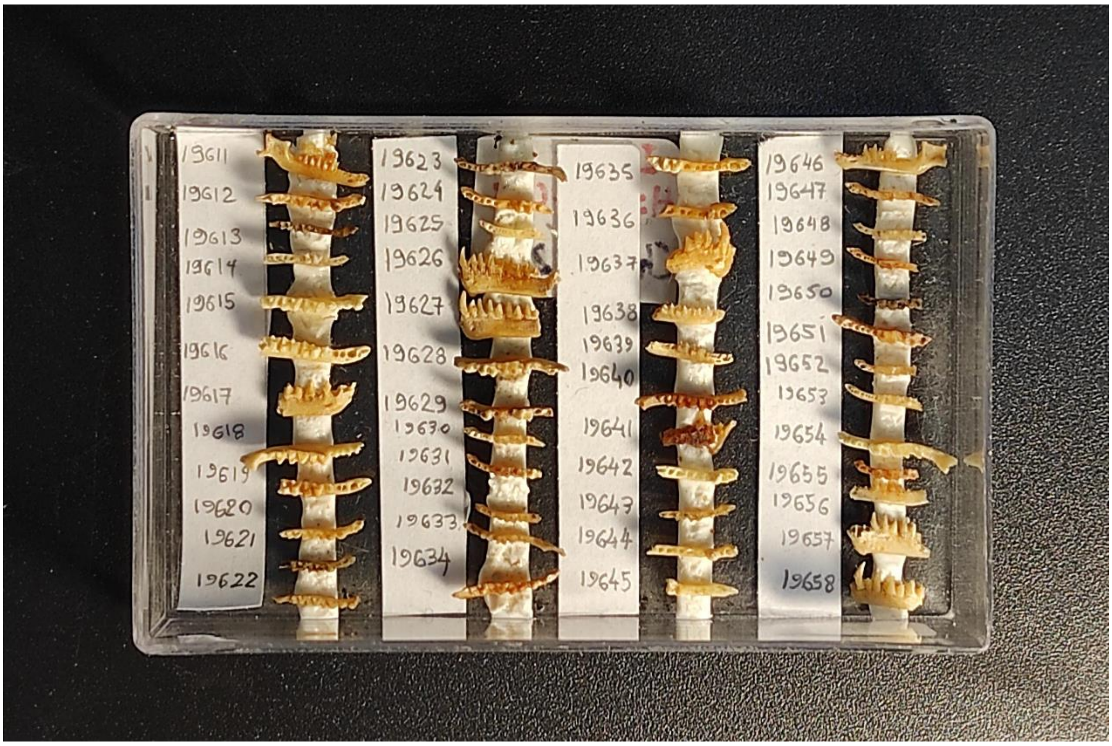

Figure A.21 Box 21.

Figure A.22 Box 22.

Figure A.23 Box 23.

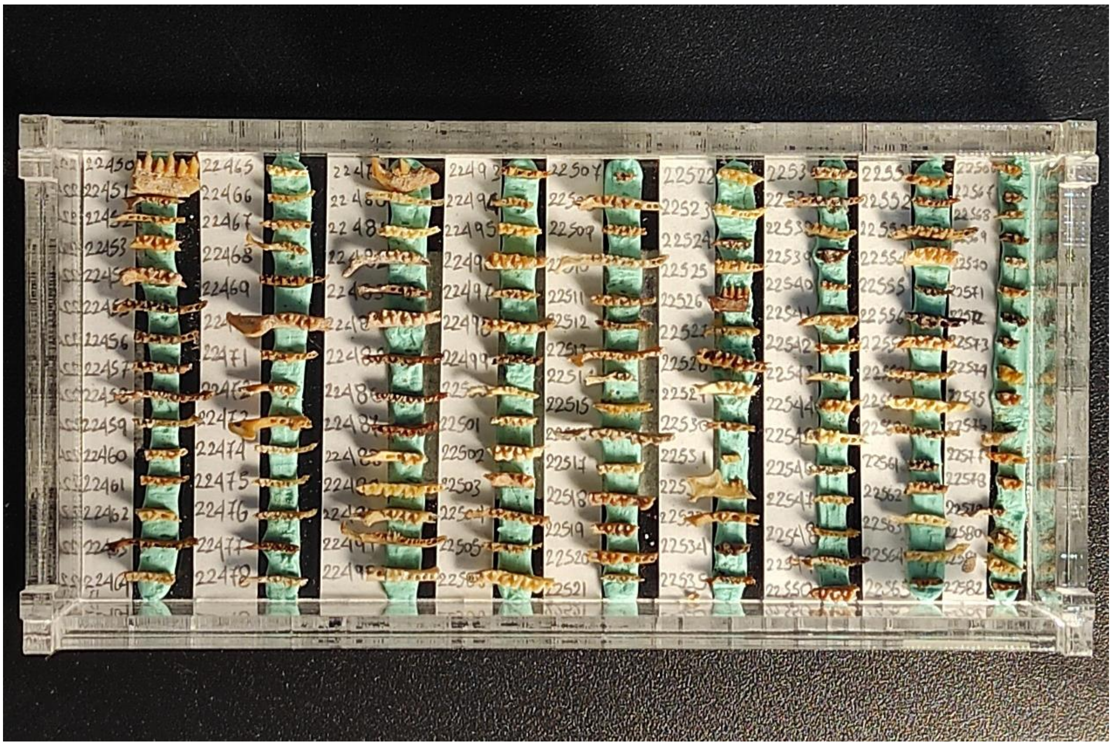

Figure A.24 Box 24.

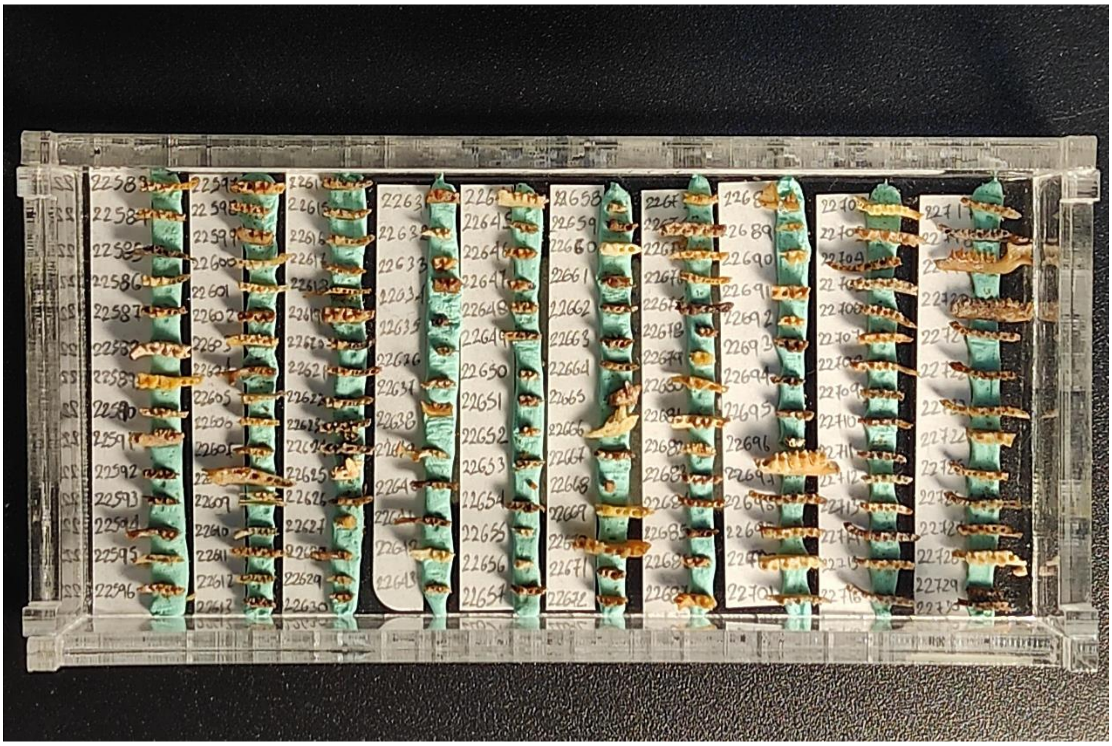

Figure A.25 Box 25.

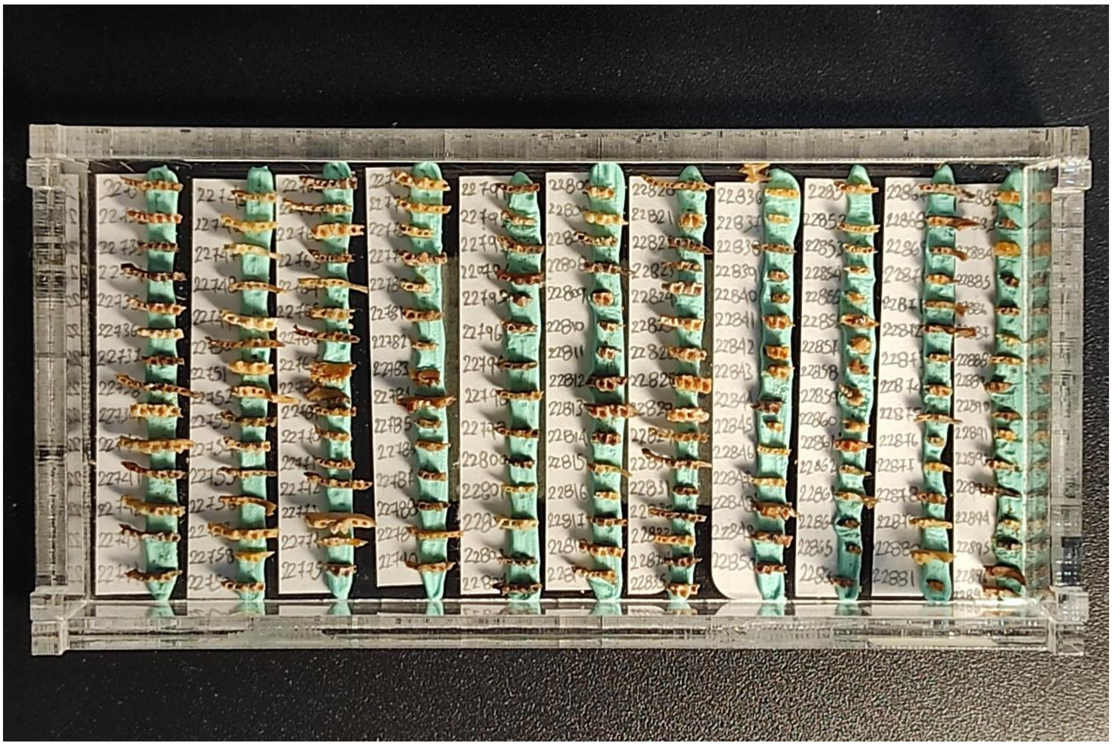

Figure A.26 Box 26.

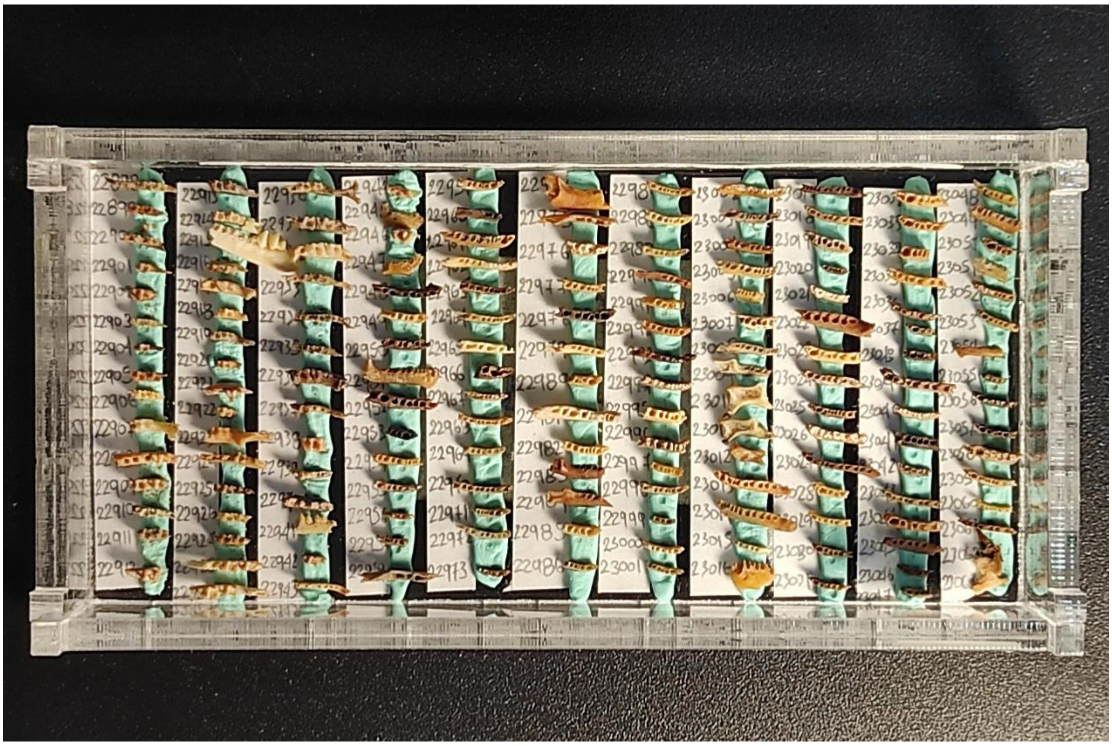

Figure A.27 Box 27.

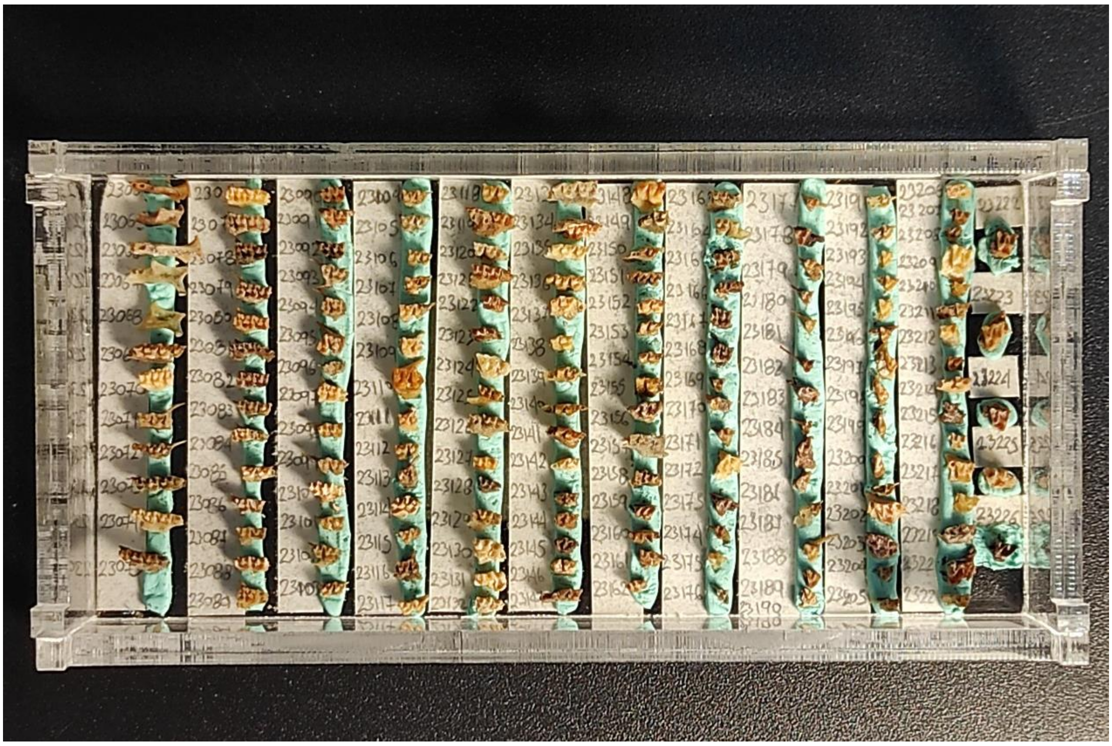

Figure A.28 Box 28.

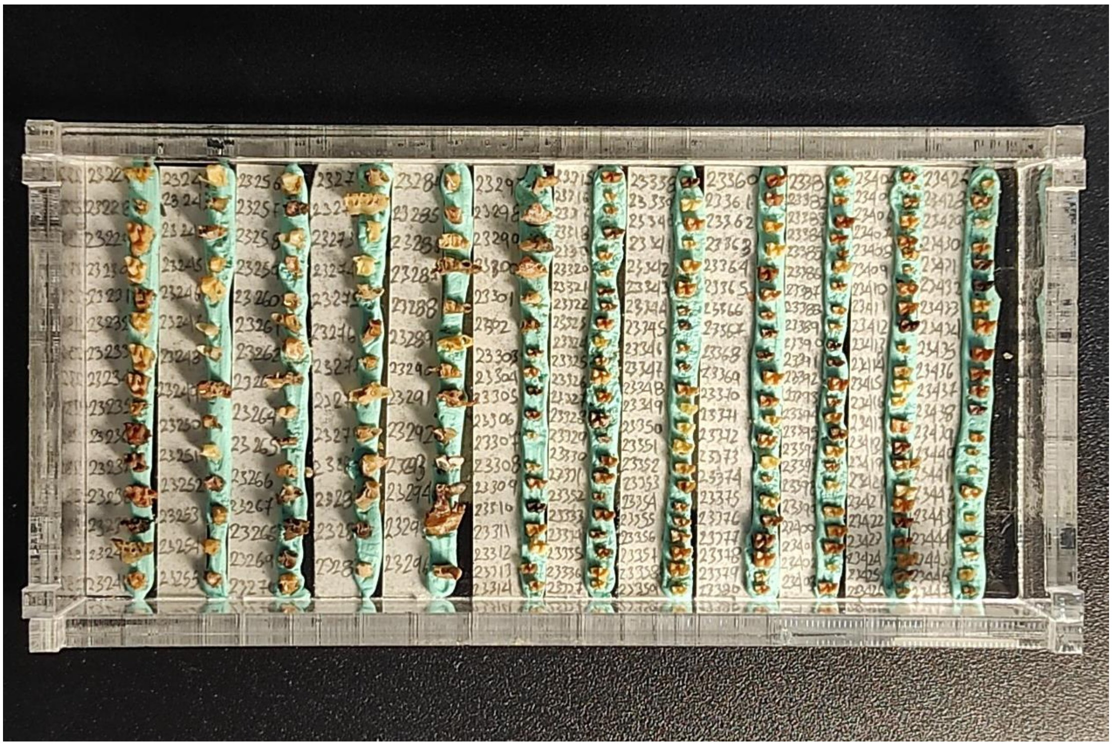

Figure A.29 Box 29.

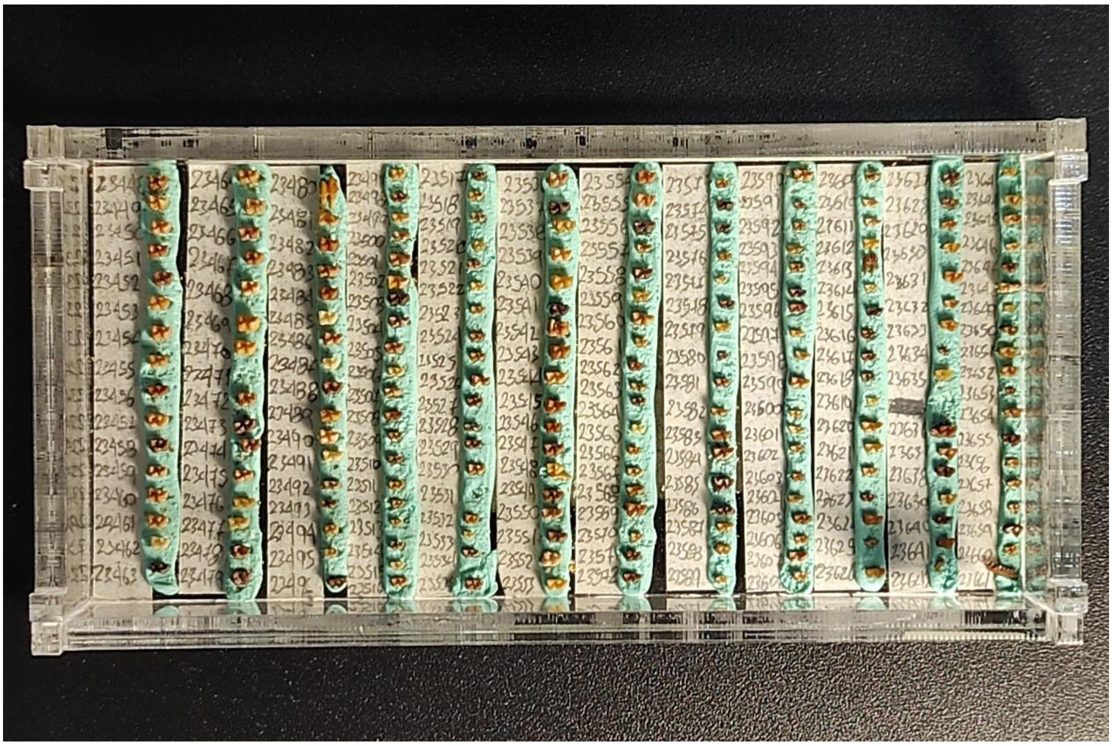

Figure A.30 Box 30.

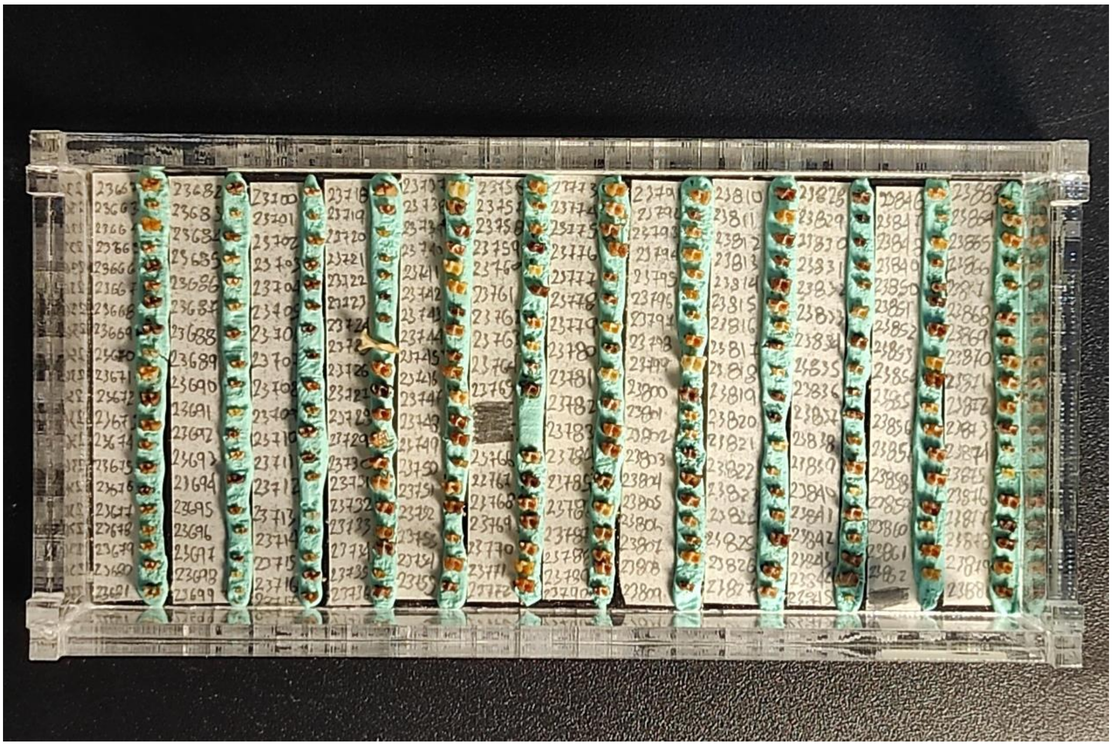

Figure A.31 Box 31.

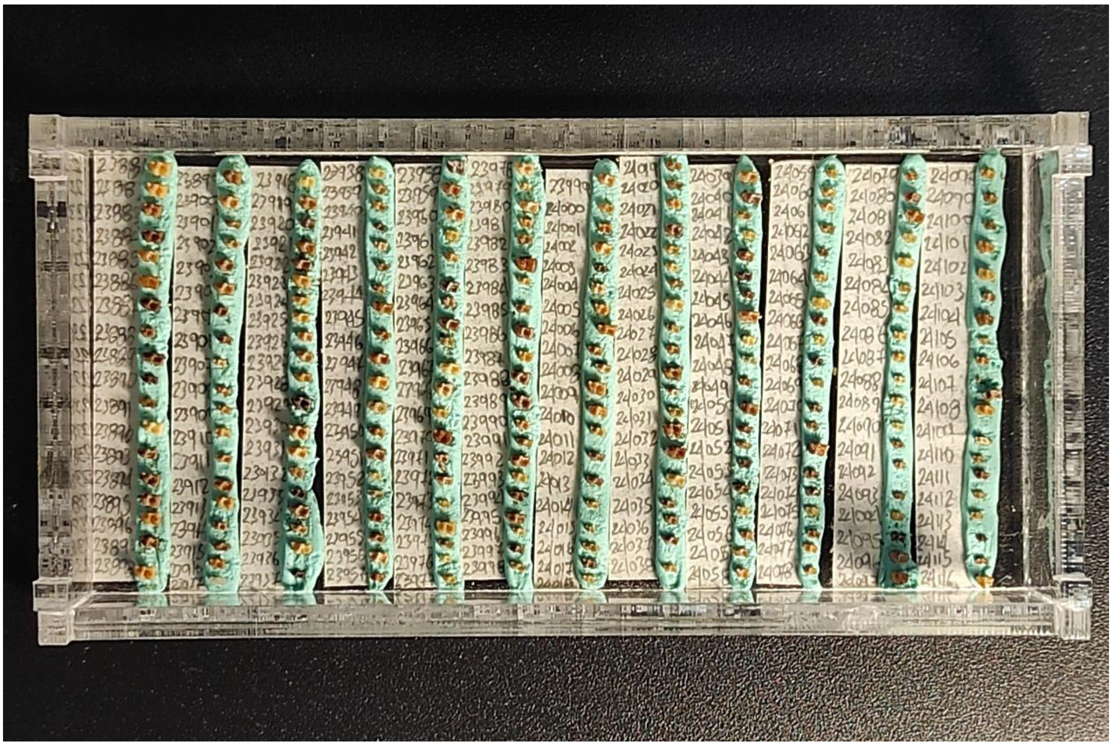

Figure A.32 Box 32.

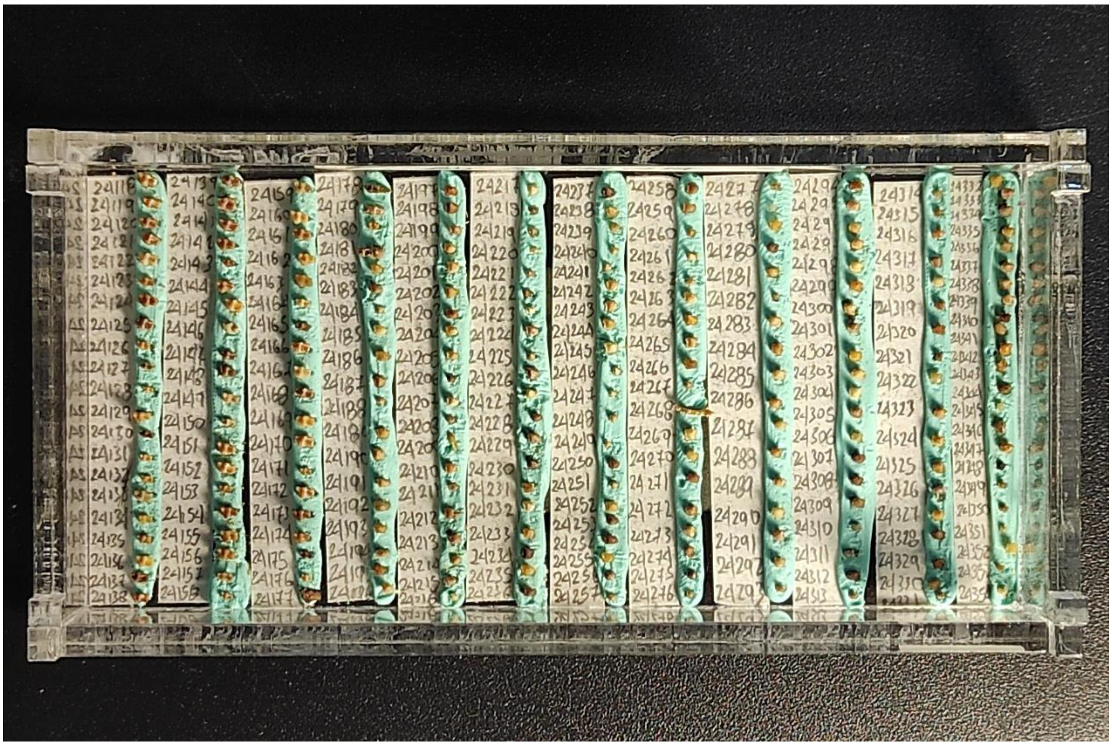

Figure A.33 Box 33.

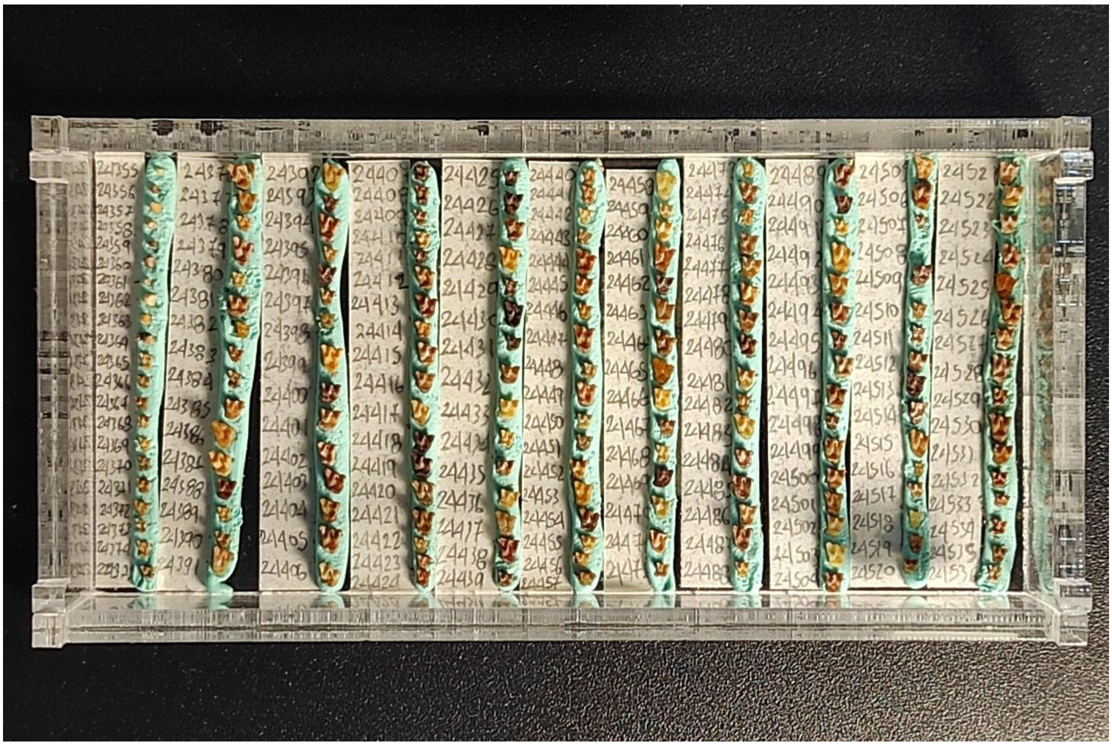

Figure A.34 Box 34.

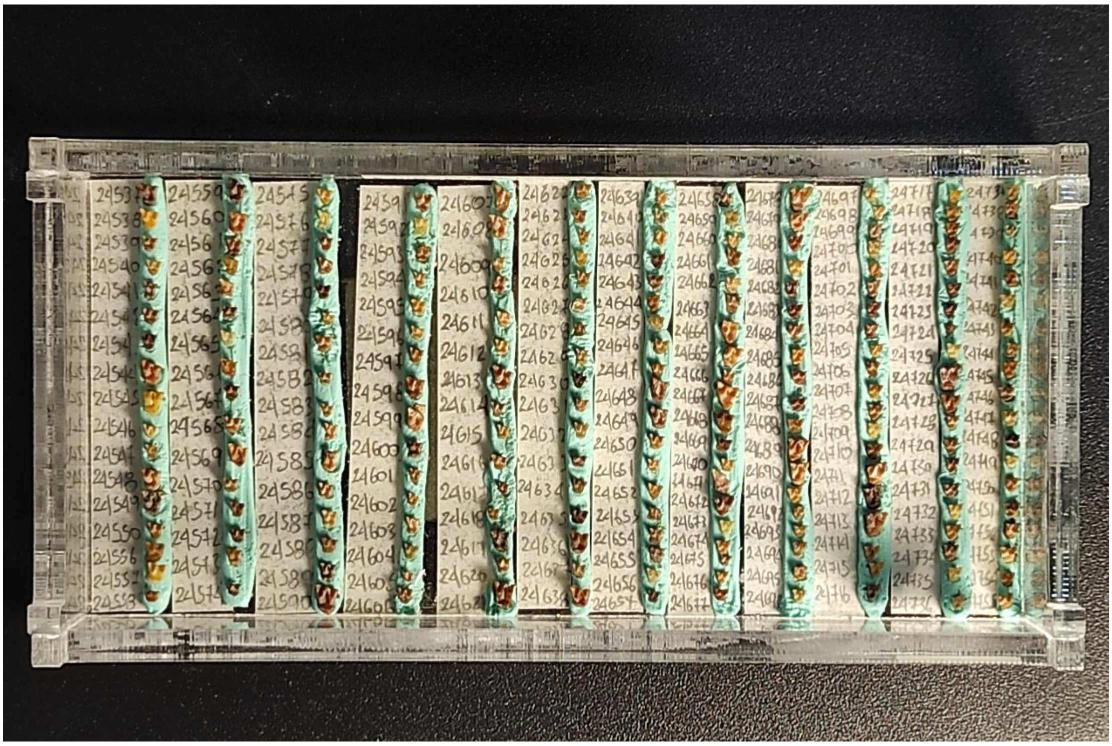

Figure A.35 Box 35.

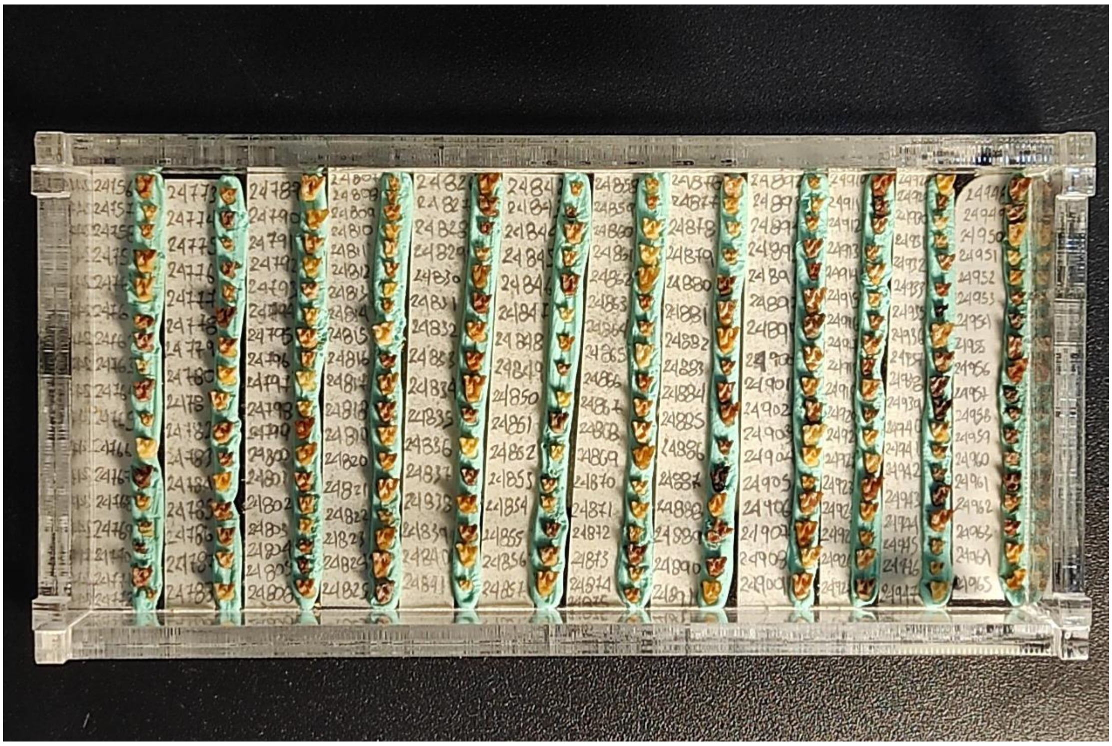

Figure A.36 Box 36.

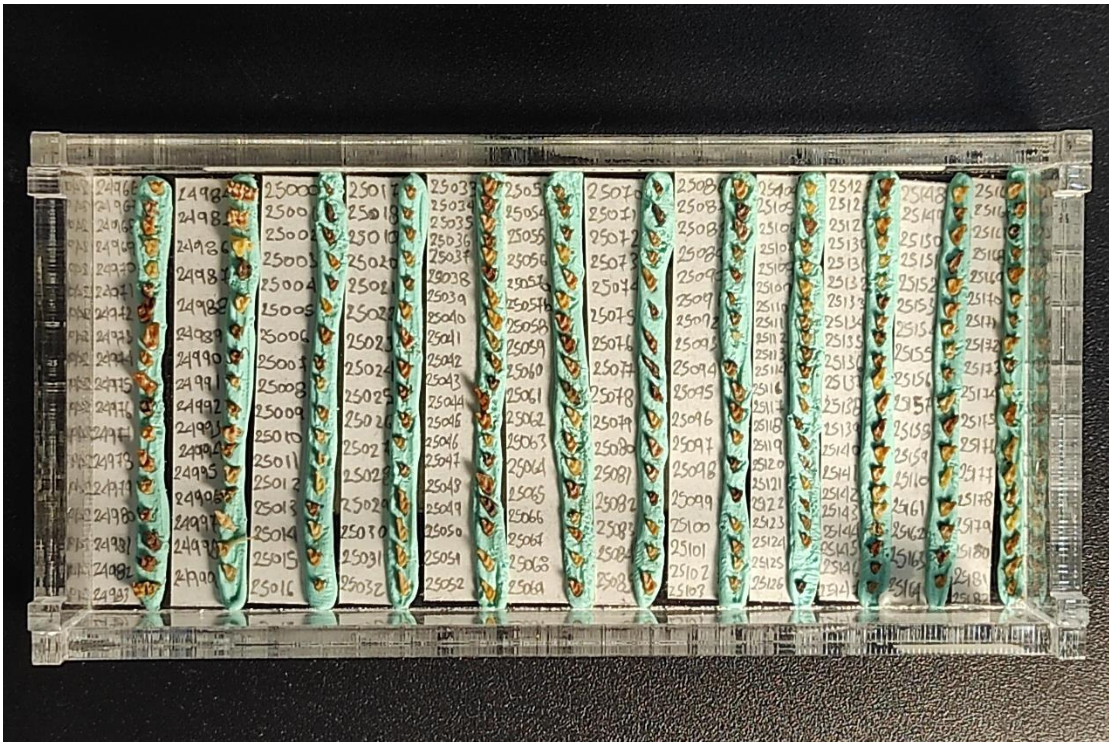

Figure A.37 Box 37.

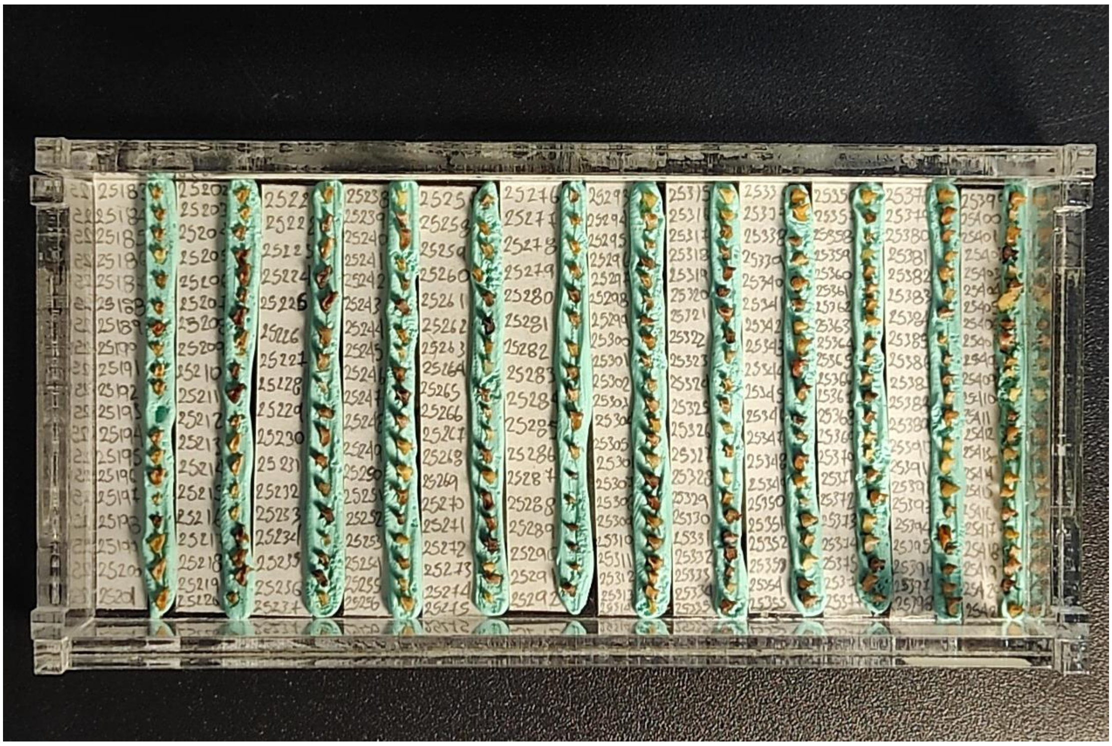

Figure A.38 Box 38.

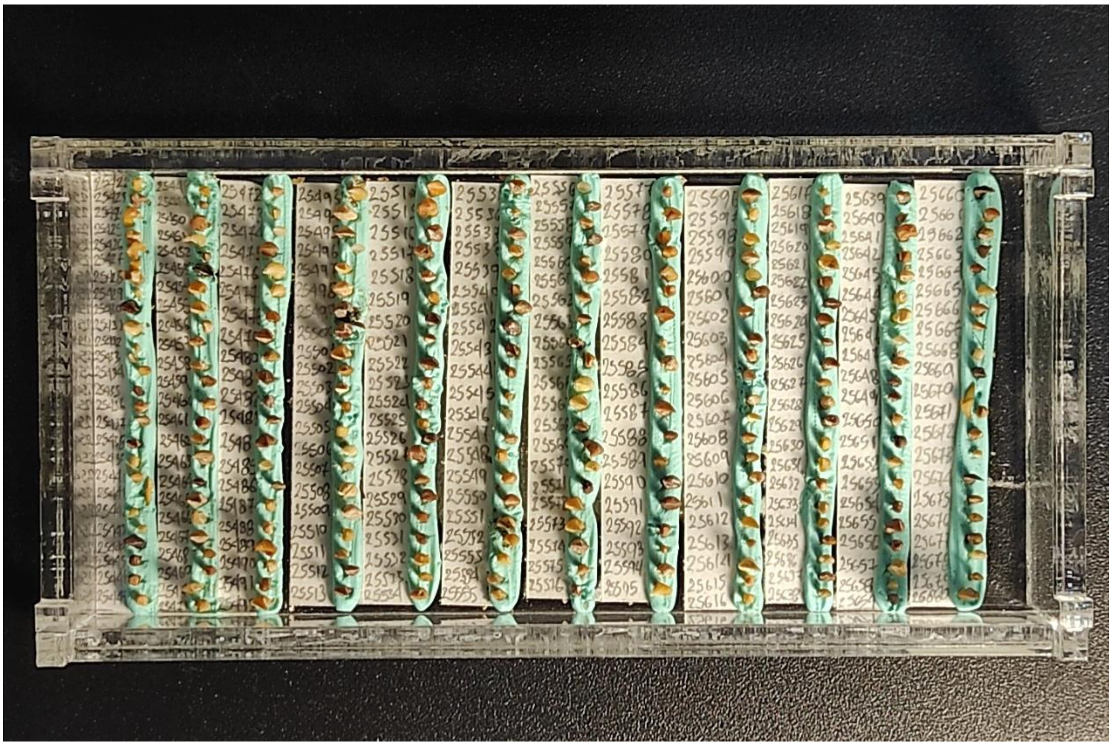

Figure A.39 Box 39.

Figure A.40 Box 40.

Figure A.41 Box 41.

Figure A.42 Box 42.

Figure A.43 Box 43.

Figure A.44 Box 44.

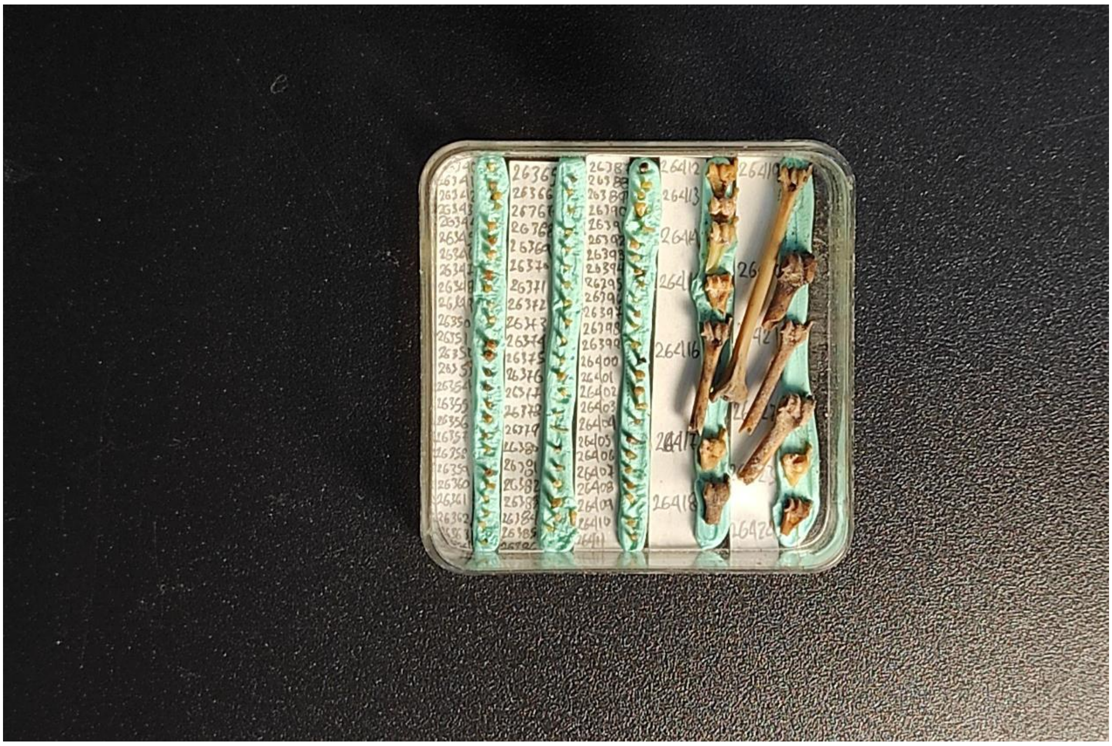

Figure A.45 Box 45.

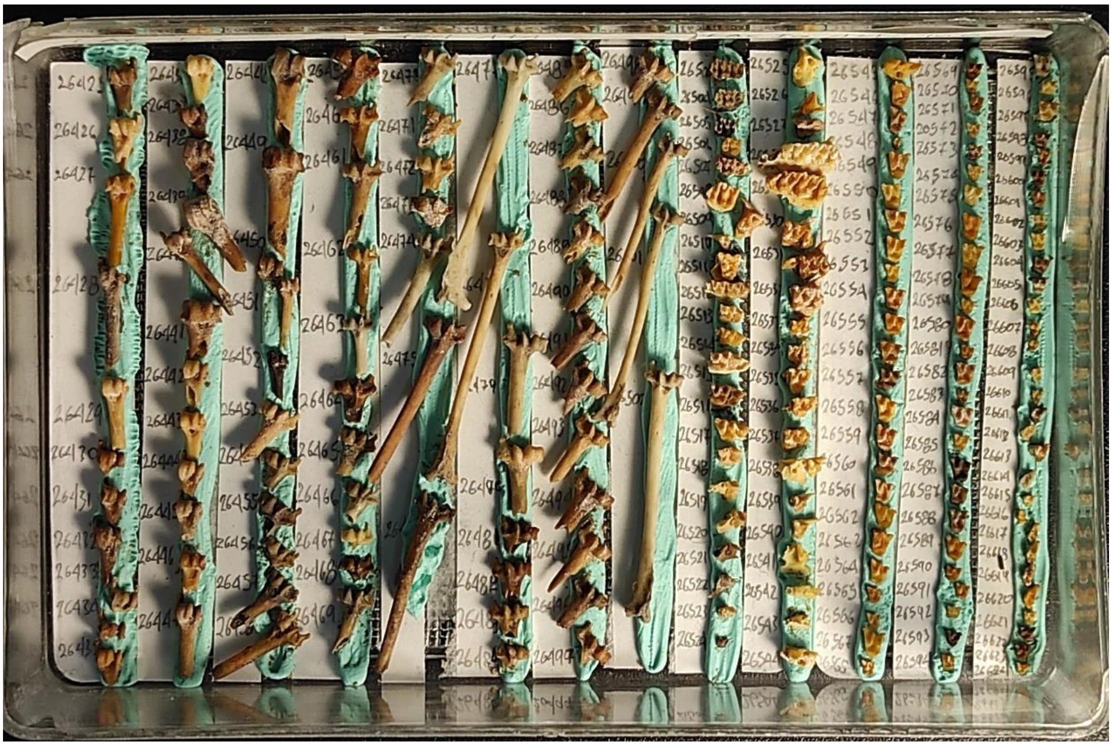

Figure A.46 Box 46.

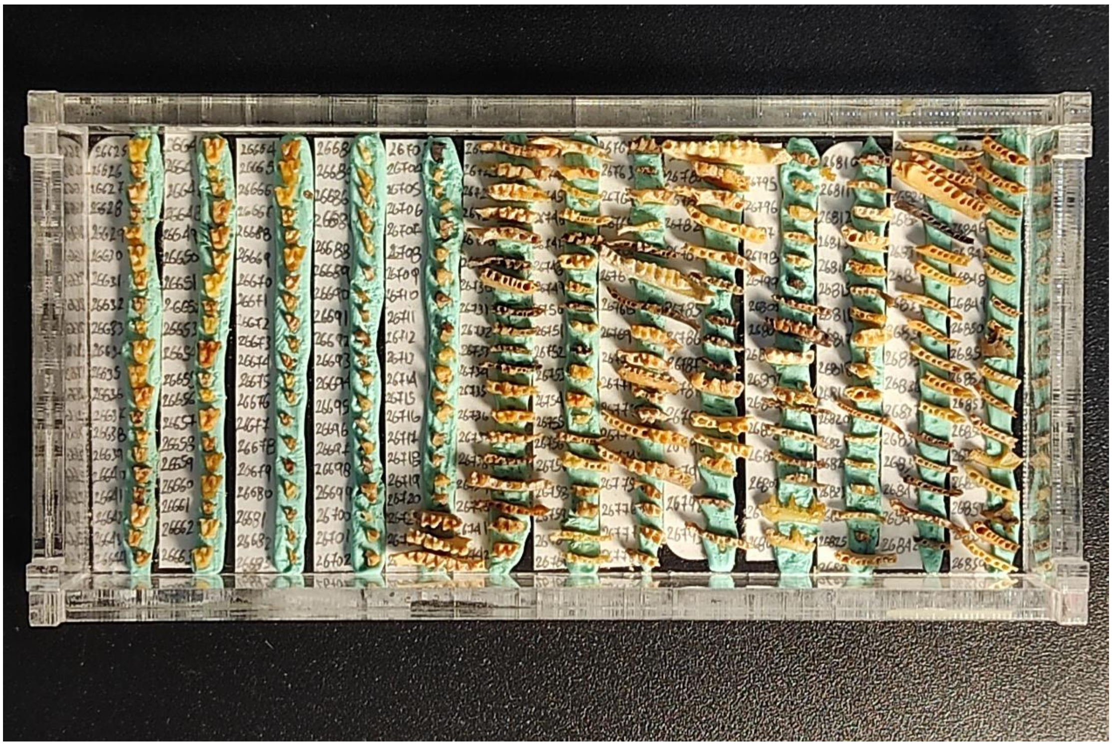

Figure A.47 Box 47.

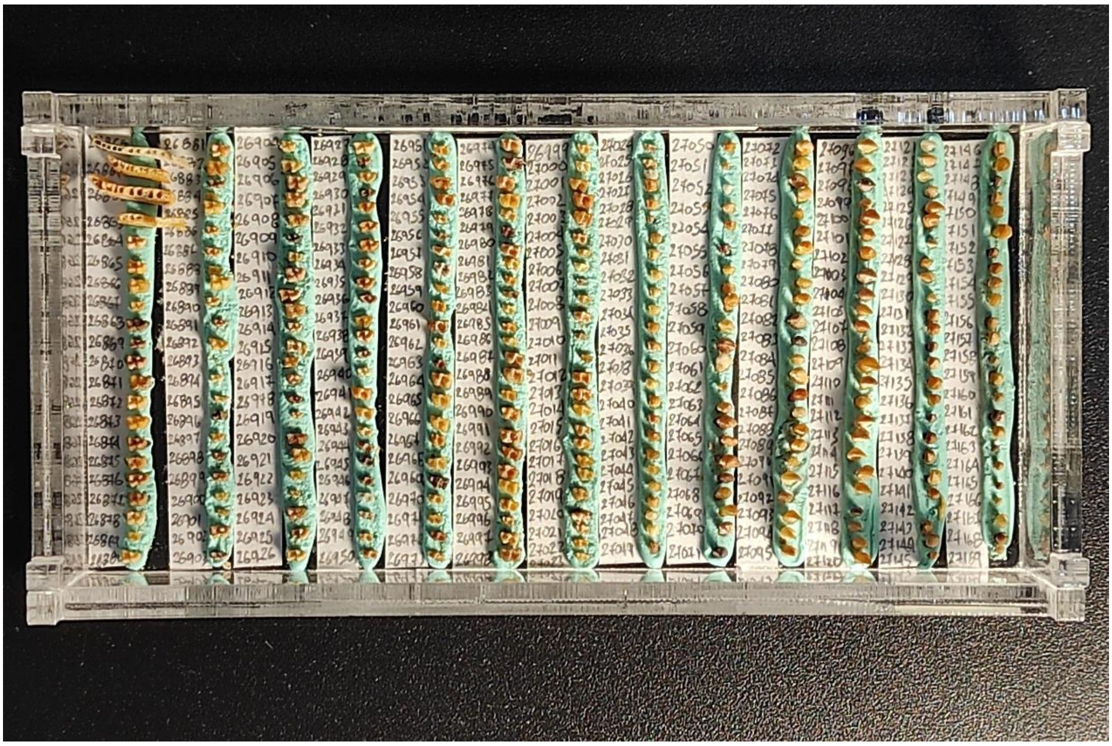

Figure A.48 Box 48.

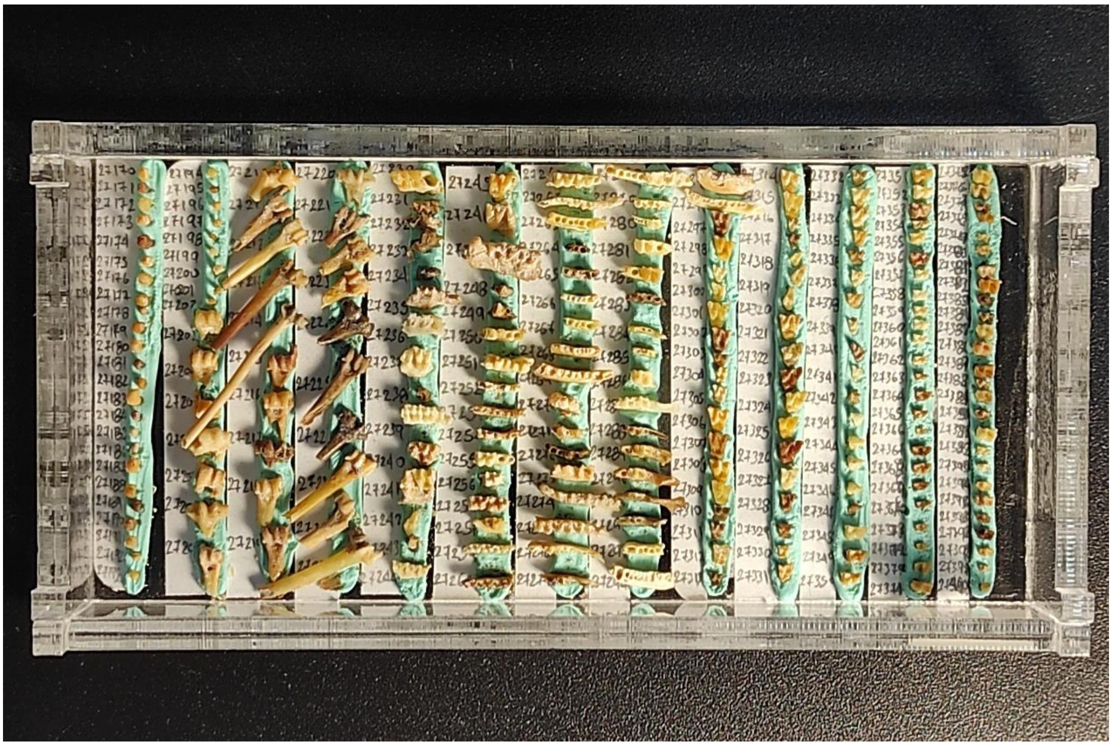

Figure A.49 Box 49.

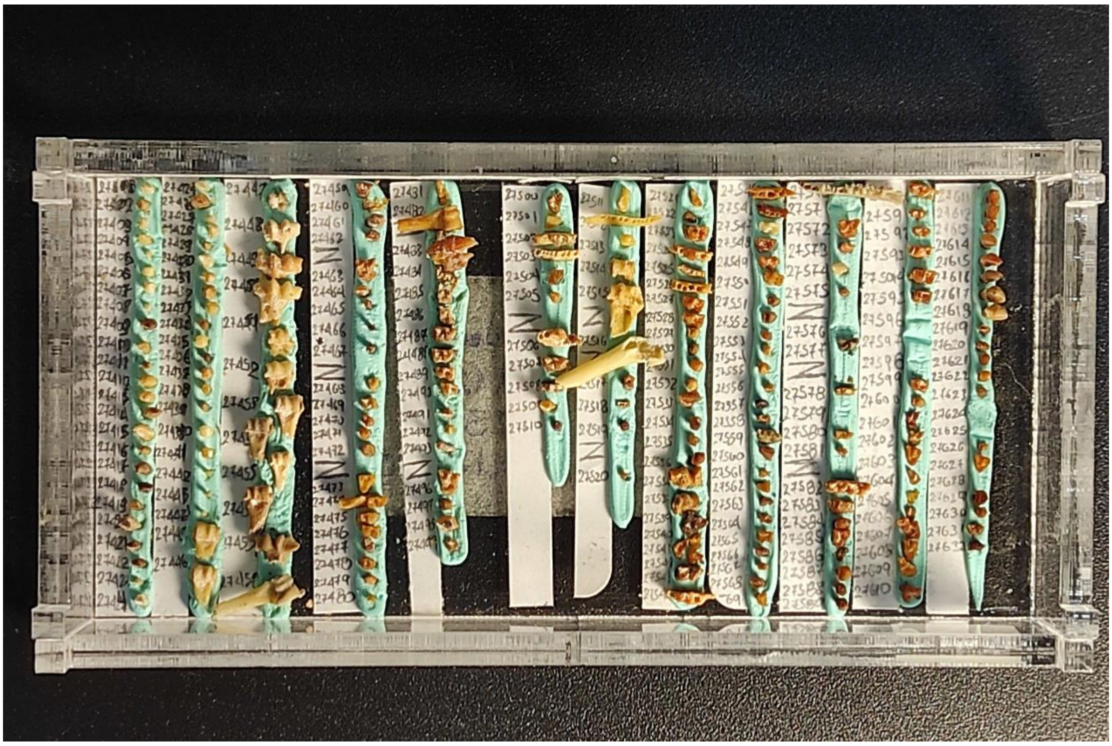

Figure A.50 Box 50.

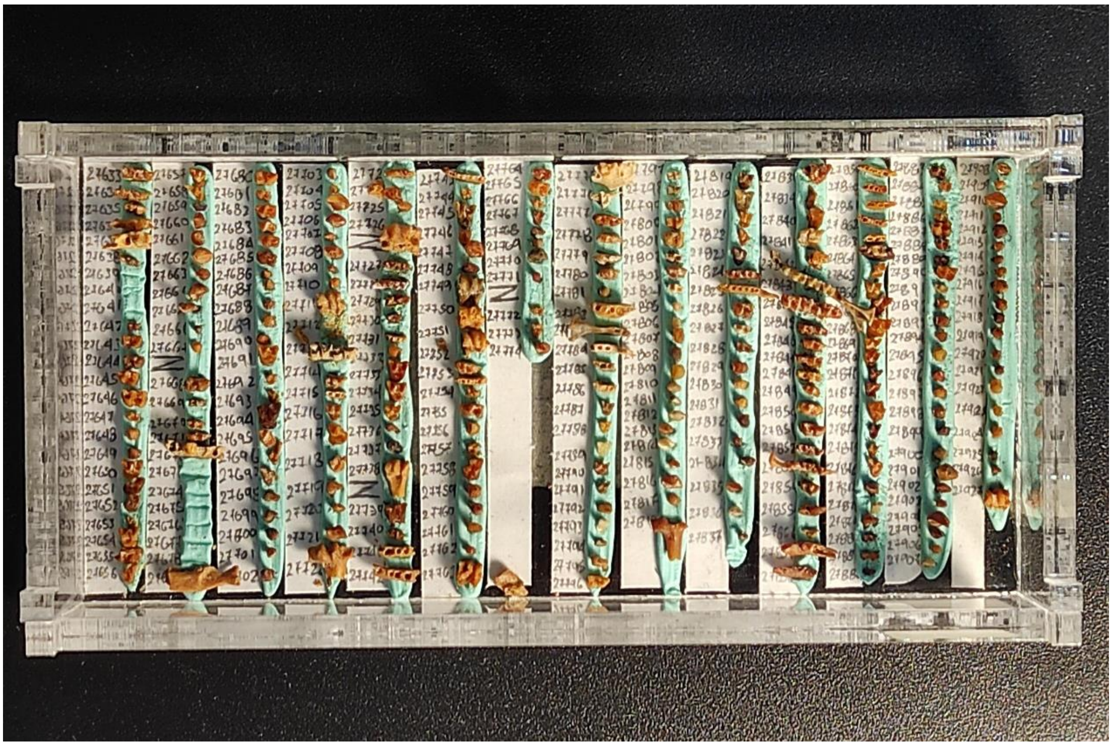

Figure A.51 Box 51.

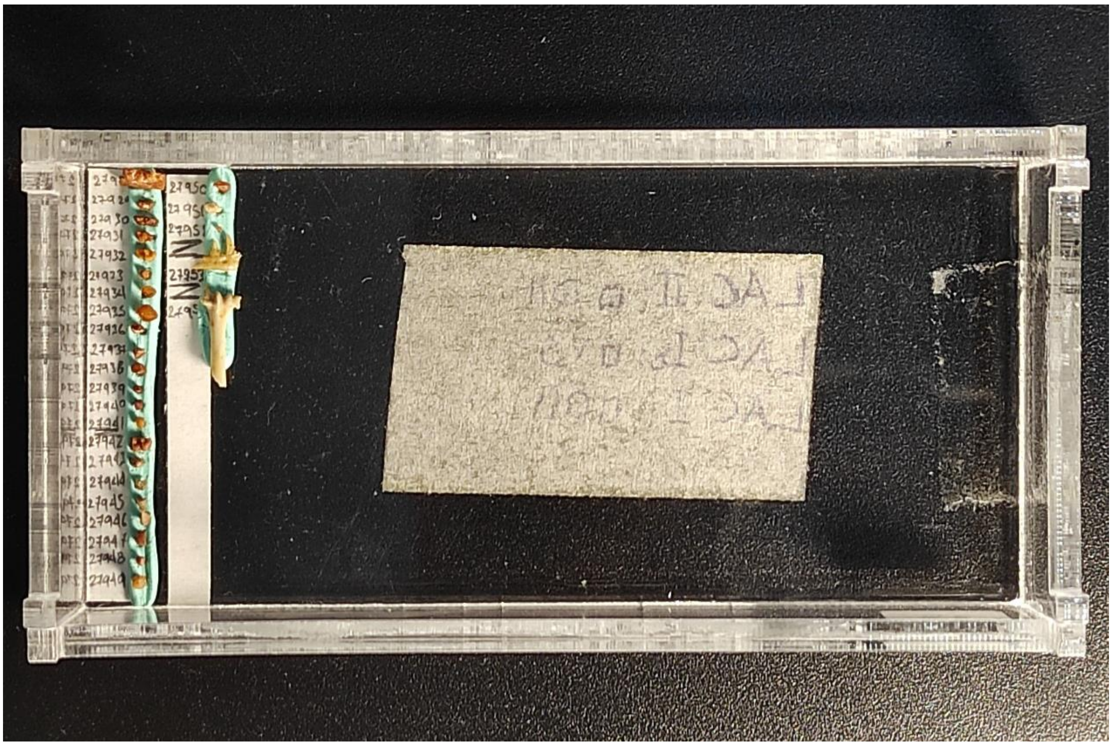

Figure A.52 Box 52.

Figure A.53 *Rhinolophus ferrumequinum*. Photograph by Paulo Barros (UNEP/EUROBATS 2021).

Figure A.54 *Rhinolophus mehelyi*. Photograph by Jens Rydell (UNEP/EUROBATS 2021).

Figure A.55 *Rhinolophus blasii*. Photograph by Mounir Abi-Said (UNEP/EUROBATS 2021).

Figure A.56 *Rhinolophus euryale*. Photograph by Mounir Abi-Said (UNEP/EUROBATS 2021).

Figure A.57 *Rhinolophus hipposideros*. Photograph by Sebastien Krickx (UNEP/EUROBATS 2021).

Figure A.58 *Myotis myotis*. Photograph by Adwan Shehab (UNEP/EUROBATS 2021).

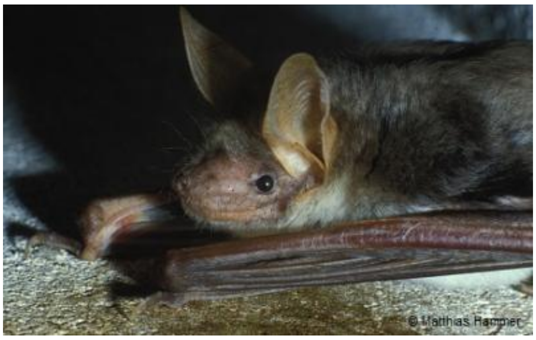

Figure A.59 *Myotis blythii*. Photograph by Matthias Hammer (UNEP/EUROBATS 2021).

Figure A.60 *Myotis bechsteinii*. Photograph by David Garcia (UNEP/EUROBATS 2021).

Figure A.61 *Myotis emarginatus*. Photograph by Panagiotis Georgiakakis (UNEP/EUROBATS 2021).

Figure A.62 *Myotis capaccinii*. Photograph by Boyan Petrov (UNEP/EUROBATS 2021).

Figure A.63 *Myotis mystacinus*. Photograph by Branko Micevski (UNEP/EUROBATS 2021).

Figure A.64 *Nyctalus lasiopterus*. Photograph by Jens Rydell (UNEP/EUROBATS 2021).

Figure A.65 *Nyctalus noctula*. Photograph by Matti Masing (UNEP/EUROBATS 2021).

Figure A.66 *Nyctalus leisleri*. Photograph by Daniela Schmieder (UNEP/EUROBATS 2021).

Figure A.67 *Pipistrellus pipistrellus*. Photograph by Branko Karapandža (UNEP/EUROBATS 2021).

Figure A.68 *Vespertilio murinus*. Photograph by Manuel Ruedi (UNEP/EUROBATS 2021).

Figure A.69 *Eptesicus serotinus*. Photograph by Domingo Trujillo (UNEP/EUROBATS 2021).

Figure A.70 *Plecotus auritus* Photograph by Andreas Zahn (UNEP/EUROBATS 2021).

Figure A.71 *Plecotus austriacus*. Photograph by Branko Karapandža (UNEP/EUROBATS 2021).

Figure A.72 *Barbastella barbastellus*. Photograph by Matthias Hammer (UNEP/EUROBATS 2021).

Figure A.73 *Miniopterus schreibersii*. Photograph by Boyan Petrov (UNEP/EUROBATS 2021).